

**Structural Stability  
Research Council**

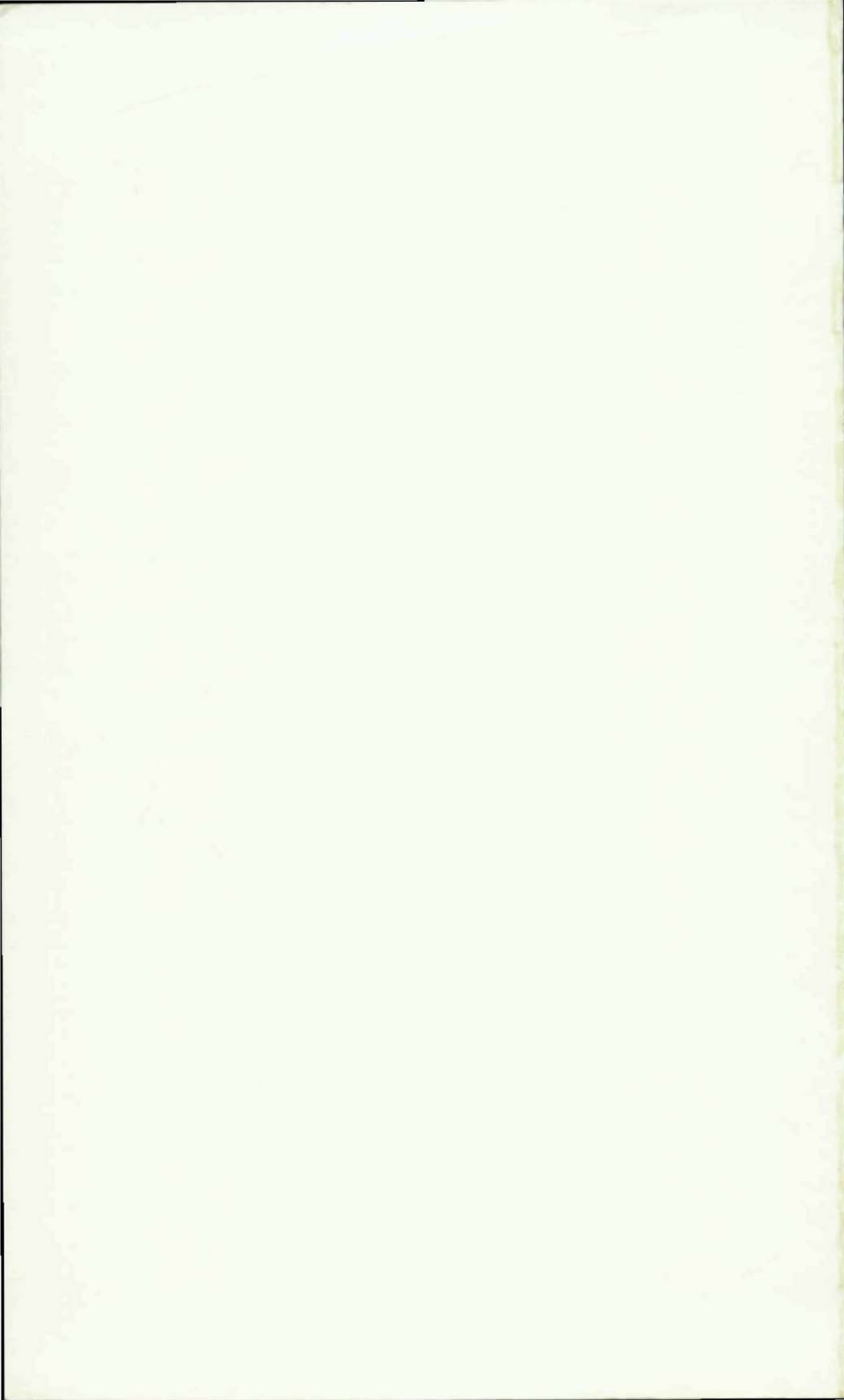
AISC E&R Library



8437

**ANNUAL  
TECHNICAL SESSION  
Proceedings**

**1993**





Structural Stability Research Council

**PROCEEDINGS**  
**1993 ANNUAL**  
**TECHNICAL SESSION**

**Reports on Current Research Activities**

*ORGANIZED BY:*

*Structural Stability Research Council*

*CONFERENCE SPONSORED BY:*

*National Center for Earthquake Engineering Research*

*PROCEEDINGS COMPILED BY:*

*Diana Walsh, SSRC Secretarial Assistant*

**April 5-6, 1993**  
**Milwaukee, Wisconsin**

ISBN 1-879749-54-8

## ACKNOWLEDGEMENTS

THE OPINIONS, FINDINGS, CONCLUSIONS AND RECOMMENDATIONS EXPRESSED HEREIN ARE THOSE OF THE AUTHORS AND DO NOT NECESSARILY REFLECT THE VIEWS OF THE STRUCTURAL STABILITY RESEARCH COUNCIL OR THE CONFERENCE SPONSORS.

Copyright © 1993 by  
Structural Stability Research Council  
All Rights Reserved

Exerpts may be used, except that no portions may be reprinted without permission in writing from the publisher.

### STRUCTURAL STABILITY RESEARCH COUNCIL

Lehigh University  
Fritz Engineering Laboratory  
13 E. Packer Avenue  
Bethlehem, PA 18015-3191 U.S.A.  
PHONE (215) 758-3522  
FAX (215) 758-4522

Printed in the United States of America

## FOREWORD

The 1993 Annual Technical Session of the Structural Stability Research Council was held in the City of Milwaukee, Wisconsin on April 5 and 6. This proved to be a very pleasant venue with good surroundings and eating places. It was the first time the SSRC met in Milwaukee.

Another new venture was a substantial change in the format of the meeting. The presentation of papers for the SSRC meeting took place at Task Group meetings on Monday and at a plenary session on Tuesday morning. The reason for this change was that the traditional half day theme session was expanded to a 1½ day conference with the theme "Is Your Structure Suitably Braced?" Even with the restricted time for the SSRC presentations, a total of 27 presentations were scheduled, with 14 of them in the plenary session. All these papers are contained in these proceedings along with several other papers that were submitted but not presented. The papers were associated with eleven different Task Groups and sincere thanks is due to all the authors for their efforts and participation.

It is not possible to separate the number of participants in the SSRC meeting from the total that also attended the subsequent theme conference. However, the Task group meetings were very well attended and their content was primarily technical in nature. A head count indicated that nearly 100 were in attendance at the plenary session. The combined meetings had over 160 registrants, representing ten different countries. This was the largest attendance ever at an SSRC event. In spite of the initial concerns that the abbreviated SSRC meeting would not be well received, the response of the participants seemed enthusiastic.

A special note of thanks is due to five local sponsors who contributed financially to support the meetings.

CH2M Hill

Computerized Structural Design

Graef Anhalt Schloemer Associates

Howard Needles Tammen & Bergendoff

Society of Iron & Steel Fabricators of Wisconsin

Due to the change in format, considerable extra effort was required in organizing and implementing the SSRC meeting. The Program Committee chaired by Clarence Miller did a commendable job in organizing the technical content of the meeting. The Task Group Chairmen were especially cooperative in integrating technical presentations into their meetings. Lesleigh Federinic, SSRC Administrative Secretary, and her assistant Diana Walsh, did their usual excellent job of insuring that everything went smoothly both before and during the meeting. Thanks for the extra effort this year. Our new Associate Director, Jim Ricles, got a good initiation and we appreciate his contribution to the program and arrangements. Also, thanks to the SSRC Director, Lynn Beedle, for his efforts and overseeing all the details that had to be considered. The students from Marquette University and the University of Wisconsin-Milwaukee deserve recognition for their efficient assistance during the conference. Finally a special thanks to Jerry Iffland Chairman of the Finance Committee, for the idea of the new meeting format and for inspiration to others in making this a successful meeting.

Now we can look forward to next year which will be the 50th Anniversary Meeting of the SSRC. This special and exciting event will be held at Lehigh University, June 19-22, 1994. The theme, "SSRC - Link Between Research and Practice" will be addressed by international experts on all of the various stability topics important to SSRC. We hope to come away from this meeting with a good vision of the future of stability research and design.

*D. R. Sherman*

Donald R. Sherman  
Chairman

Milwaukee, Wisconsin  
April, 1993

## TABLE OF CONTENTS

Foreword .....	i
----------------	---

### TASK GROUP 4 - FRAME STABILITY AND COLUMNS AS FRAME MEMBERS

YOUR BUILDING MAY BE STRONGER THAN YOU THINK; THE BENEFITS OF 3-D ANALYSIS M. Hoit and D. S. Ellifritt .....	1
THE EFFECTIVE LENGTH OF COLUMNS IN PR SWAY FRAMES C. Bernuzzi and R. Zandonini .....	13
OPTIMUM BRACING OF FRAMES SUBJECTED TO TORSIONAL AND FLEXURAL BUCKLING A. Vlahinos and Y. C. Wang .....	29

### TASK GROUP 13 - THIN-WALLED METAL CONSTRUCTION

BEHAVIOR OF GUSSET PLATE CONNECTIONS UNDER COMPRESSIVE MONOTONIC AND CYCLIC LOADINGS J.J. Roger Cheng, J. Rabinovitch, and M.C.H. Yam .....	45
AN EXPERIMENTAL STUDY OF INTERACTIVE BUCKLING OF ROLLED THIN-WALLED H-COLUMNS T. Yamao, T. Aoki, and T. Sakimoto .....	59
RARE DOUBLE-LAYER GRID STRUCTURE: A NEW SOLUTION D. Dubina .....	69
WEB CRIPPLING OF STAINLESS STEEL COLD-FORMED BEAMS S. A. Korvink, G. J. van den Berg, and P. van der Merwe .....	79
SHEAR BEHAVIOR OF WEB ELEMENTS WITH OPENINGS M. Y. Shan, R. A. LaBoube, W. W. Yu .....	103
CAPACITY OF HIGH STRENGTH THIN-WALLED BOX COLUMNS J. M. Ricles, L. W. Lu, P. S. Green, R. Tiberi, A. K. Pang, and R. J. Dexter .....	115

### TASK GROUP 14 - HORIZONTALLY CURVED GIRDERS

STATE-OF-THE-ART ON RESEARCH, DESIGN AND CONSTRUCTION OF HORIZONTALLY CURVED BRIDGES IN JAPAN T. Kitada, H. Nakai, and Y. Murayama .....	141
INTERACTIVE PLASTIC HINGE BASED METHOD FOR ANALYSIS OF STEEL FRAMES M. Ivanyi .....	153

### TASK GROUP 15 - BEAMS

STABILITY OF WEB-TAPERED BEAMS D. Polyzois and L. Qing .....	179
THE PLASTIC STRENGTH OF STAINLESS STEEL BEAMS P. J. Bredenkamp, G. J. van den Berg and P. van der Merwe .....	193

### TASK GROUP 17 - DOUBLY CURVED SHELLS & SHELL-LIKE STRUCTURES

ASYMPTOTIC MODAL ANALYSIS OF LATTICE DOMES R. C. Batista and R. V. Alves .....	211
INTERACTION STABILITY CRITERIA IN COMBINED STATES OF STRESSES FOR METAL PLATES AND SHELLS Z. K. Mendera .....	223

### TASK GROUP 18 - TUBULAR MEMBERS

ON THE STRUCTURAL STABILITY OF LARGE STEEL SPENT NUCLEAR FUEL CANISTERS S. G. Ladkany, and R. Rajagopalan .....	235
STRENGTH ASSESSMENT AND REPAIR OF DAMAGED BRACING IN OFFSHORE PLATFORMS W. A. Salman, P. C. Birkemoe, and J. M. Ricles .....	247

#### TASK GROUP 20 - COMPOSITE MEMBERS AND SYSTEMS

- GROUTED HOLLOW STRUCTURAL STEEL SECTIONS AS SEISMIC  
RETROFIT FOR DEFICIENT BEAM-TO-COLUMN JOINTS  
H.G.L. Prion, T. E. Hoffschild, and S. Cherry . . . . . 259

#### TASK GROUP 24 - STABILITY UNDER SEISMIC LOADING

- P- $\Delta$  EFFECT IN SEISMIC RESISTANT STEEL STRUCTURES  
F. M. Mazzolani and V. Piluso . . . . . 271

#### TASK GROUP 25 - CONNECTION RESTRAINT CHARACTERISTICS

- COLUMN-BASE CONNECTIONS MODELING FOR CYCLIC LOADING  
P. Penserini and A. Colson . . . . . 283

#### TASK GROUP 26 - STABILITY OF ANGLE STRUTS

- ULTIMATE STRENGTH OF GEOMETRICAL IMPERFECT  
ANGLE COLUMNS  
S. L. Chan and S. Kitipornchai . . . . . 295
- FURTHER STUDIES ON COMPRESSIVE STRENGTH OF  
60° EQUAL LEG STEEL ANGLES  
K. K. Sankisa, S.M.R. Adluri, and M.K.S. Madugula . . . . . 309

#### TASK GROUP 29 - 2ND ORDER INELASTIC ANALYSIS FOR FRAME DESIGN

- SECOND ORDER INELASTIC ANALYSIS OF FRAMES  
I. Sohal and L. Cai . . . . . 321
- EFFECTIVE STRATEGIES FOR ELASTO-PLASTIC AND FINITE  
DISPLACEMENT ANALYSIS OF SPATIAL STEEL BRIDGES  
M. Kano, T. Kitada, M. Nibu, and K. Tanaka . . . . . 333
- THE EFFECTS OF THE FRAME GEOMETRICAL IMPERFECTIONS  
ON INELASTIC BUCKLING  
E. D'Amore, A. De Luca, and M. De Stefano . . . . . 345
- ON A COMPUTER PROGRAM, EPASS, TO ANALYZE ULTIMATE LOAD  
CARRYING CAPACITY OF SPATIAL STEEL BRIDGE STRUCTURES  
K. Tanaka, T. Kitada, M. Nibu, and M. Kano . . . . . 357



### OTHER RESEARCH

COMPARATIVE STUDY OF BEAM-COLUMN INTERACTION FORMULAE J. P. Jaspard, Ch. Briquet, and R. Maquoi . . . . .	369
A STUDY ON ULTIMATE STRENGTH OF STIFFENED PLATES IN STEEL BRIDGES SUBJECTED TO BIAXIAL IN-PLANE FORCES T. Furuta, T. Kitada and H. Nakai . . . . .	381
STIFFENING EFFECT OF LATERAL BRACING OF STEEL ARCH BRIDGES ON THEIR IN-PLANE STRENGTH S. Kuranishi . . . . .	393
ATTENDEE ADDRESS LISTING . . . . .	405
NAME INDEX . . . . .	420
SUBJECT INDEX . . . . .	425



## Your Building May be Stronger Than You Think; The Benefits of 3-D Analysis

by Marc Hoit<sup>1</sup> and Duane Ellifritt<sup>2</sup>

### Introduction

Structural engineers are always looking for ways to make more efficient use of materials--for finding secondary uses of members that are already there for another purpose. This is the basis for composite construction; the slab is going to be present anyway so why not make it work as part of a floor beam? Another example is steel deck. In floors its primary function is as a concrete form. However, properly designed shear connectors can make it work as part of a composite slab. In roofs it's there to keep out the weather, but its in-plane shear strength can make it work as bracing for frames and other structural elements.

In metal building systems and other conventional one-story commercial and industrial buildings, some form of X-bracing is usually used in the planes of the roof and wall to provide resistance to wind perpendicular to the main frames. This bracing, too, can serve a secondary function that can only be found through a 3-dimensional analysis of the entire structure.

### Conventional 2-D Analysis

A common method of bracing 1 story framed buildings against wind perpendicular to the frames is shown in Figure 1. The X bracing may be angles, rods, or cables or in very heavy structures may even be W-sections. In most cases, the assumption is made that these members are incapable of resisting compression without buckling elastically and therefore are considered to act as tension members only.

When wind blows against the end wall of this building, loads are transferred through the end wall columns, through struts in the roof, and into the bracing system which, with the assumption mentioned above, becomes a simple Pratt truss. For this case a 3 dimensional analysis would be of little value.

---

<sup>1</sup> Dr. Marc Hoit, Associate Professor of Civil Engineering, University of Florida

<sup>2</sup> Dr. Duane Ellifritt, Professor of Civil Engineering, University of Florida

There are certain types of similar structures, however, where a 3-D analysis can be most beneficial.

### Hangar Buildings

Buildings which are built for large aircraft maintenance facilities generally have large doors in the end walls, as in Figure 2. In these cases, there can be no end wall columns to transfer wind load, so it is common to build a cantilever door support assembly that transfers the load back to an interior frame by means of an inclined compression strut, as shown in Figure 3. This puts an upward force on the frame to which this inclined strut is attached. An upward deflection of this frame means an inward horizontal movement at the top of the sliding doors. Too much movement may cause damage to the doors.

A typical 2-D analysis, modelling the frame stiffness as springs in-plane, may show very large horizontal deflections at the door tracks as seen in Figure 4. This may cause the designer to believe that a heavier frame is needed, but increasing the frame stiffness comes at the cost of dramatically increasing the weight of that frame. A better solution is to utilize something that is already present anyway--the wind bracing. The beneficial effect of this can only be found by performing a 3-D analysis of the entire building.

### 3-Dimensional Analysis

A three dimensional analysis will show that the upward force on the second frame is actually restrained by the roof bracing which transfers some of this force to adjacent frames. For a flat roof building, this effect is negligible, but for a gabled frame building it can be significant. Look at the simplified 2-bay model in Figure 5. In Figure 5(a) the upward force is perpendicular to the plane of the diagonal bracing, so the bracing will not resist much load until large deflections take place. In Figure 5(b), the diagonal bracing is already positioned to provide a vertical component of reaction to the applied upward load.

It should be noted that this works because only one frame is loaded. This comes from having the end wall wind reactions carried back to the first interior frame on an inclined member, producing an upward component of force. The same principle would not work if all frames are equally loaded, as in uniform wind uplift on the roof.

It should also be noted that use of this procedure may result in very large forces in the bracing members and their connections. The designer must insure that these members and their connections are adequate for the increased forces from the door headers. The common practice of using a single rod through a hole in the web may not be sufficient for such forces.

## Analysis Example - Modeling

As an example, the results of a three-dimensional analysis will be compared to the more conventional two-dimensional analysis for a typical hangar building like the one in Figure 2. The dimensions of the building are shown in Figure 6. The building is ten bays long, symmetrical about a vertical plane through the ridge and has sliding doors in both end walls and a door supporting assembly similar to that of Figure 4.

For the analysis, a finite element program called SSTAN will be used. SSTAN is a three dimensional static analysis program that handles trusses, frames, plates, membranes, shells and solid elements. It can also include P-Delta and non-compression member effects.

In order to simplify the modeling and reduce its size, we will model only the first three frames and use symmetry about the peak. In finite elements, symmetry can be handled by modeling only the symmetric portion of the structure and adjusting the boundary conditions to account for the rest of the structure. This method is exact for linear structures subjected to symmetric loading. Generally, symmetry can not be used in a non-linear analysis. This is because as members yield or change properties, the structure becomes non-symmetric. In this case, the only non-linearity being included is non-compression bracing members. The symmetric loading will give symmetric results even with this non-linearity. Therefore the use of symmetry is correct for this case.

By including only the first three frames in the structure, the assumption is made that most of the load is resisted by these frames. If this were not the case, the entire structure would have had to be used. Even though only the first three frames are being modeled, some method must be used to account for the effect of the rest of the structure. The main effect that needs to be represented is the resistance to deflection offered by the other frames. The typical way to account for portions of a structure is to replace it with simple springs. In a linear example, this method can be exact.

In order to model the rest of the structure with springs, the stiffness value to use for these springs must be determined. The exact way is to model the rest of the structure, then apply a load at each node where there is a connection between the first three frames and this model. The load applied divided by the deflection caused by the load is the stiffness value. In a linear model, this load can be a unit load and the stiffness is an exact representation of the structure. In a non-linear problem, the load must be equal to the real load the structure will see. Clearly the real load is not known and either must be found in an iterative manner or the entire structure must be modeled.

This method is useful when replacing a very complex portion of a structure by an accurate simple representation. This replacement allows us to study the rest of the structure without the complexity. Often, an approximate model of the rest of the structure is used since the difference in the approximate and exact models causes only a very small change in the results

of the portion being studied.

In this example, the approximate stiffness is accurate enough since its effect will not change much with more accurate modeling. Therefore, the rest of the structure is modeled by an approximate structure. Fewer nodes and members are used to represent the tapered sections. Only the nodes that connect to the three frames are included. These frames are being loaded about their weak axes so the taper does not effect the moment of inertia. In addition, a unit load is used to calculate the spring stiffness. This is not exact since not all compression members at higher loads will be ignored. In addition, the additional frames do not resist much of the wind load since the bracing transfers most of the load to the first three frames.

Symmetry is also used on the spring evaluation model. Again, only the symmetric portion about the vertical plane along the ridge is used for the spring evaluation. Here, the unit load must be applied as a combination of a symmetric and anti-symmetric part to get the correct displacement. This is because with symmetry, loading is assumed to be the same on the symmetric portion of the structure. *In determining the spring values we only want a single load.* Using anti-symmetric load method (changing the boundary conditions) we can get this effect. The plot of the structure used to determine the spring stiffness is given in Figure 7.

The three rigid frames on the windward end of the building are modeled fairly accurately. Also included in the model are the purlins connecting the frames and the springs calculated for the rest of the structure. The door support assembly is modeled including the diagonal brace used to transfer load back to the interior frame. Two versions of the analysis model were created. The first simulates a two dimensional analysis. This model does not include any roof bracing. The second model adds the full roof bracing to the model.

The no-roof-bracing model will give exactly the same answers as the simplified model shown in Figure 3. The spring values used in the simplified model can be calculated using a two dimensional model of a single rigid frame. A full Three Dimensional model was actually used for the un-braced frame analysis since the model had to be developed for the braced analysis. Figure 8 shows the structure used. If wind load is applied to the un-braced model very large deflections result as shown in Figure 9. The plot shows deflections in an exaggerated form. However, the dramatic shape can only come from extremely large values. Looking at the bottom of the door support assembly at the peak, note that the horizontal deflection is 70". The vertical deflection is 12". These deflections are clearly unacceptable for a connected door.

A plot of the braced model can be seen in Figure 10. Applying the same wind load that was used on the un-braced model, the results are shown in Figure 11. Here the shape is not distorted. At the same support location, a horizontal deflection of 20" and a vertical deflection of 6" can be seen. The bracing added an enormous amount of stiffness to the structure and helped to distribute the force from the door hanger assembly into adjacent frames.

## Conclusions

Any structure is going to behave the way it wants to, regardless of how it is analyzed. A typical two-dimensional analysis, while conservative, may overlook some reserve strength in a structure that can only be revealed in a three-dimensional analysis. This is the case in the example of the aircraft hangar shown. Conventional wind bracing, placed there for alignment during erection and to resist longitudinal wind forces, is in reality performing a third function of distributing the upward force on the first interior frames, due to wind on the hangar door, to adjoining frames. This may require increasing the size of the bracing members found through a two dimensional analysis and improving their connections but at least it is a structural element that is already there. Critical for the gains to occur is having a pitched roof. It is because of this pitch that the bracing offers a vertical stiffness component. Flat roofs do not offer any such advantages.

In summary, a three dimensional analysis does not make a building stronger; it may, however, show that the structure is stronger than you thought it was.



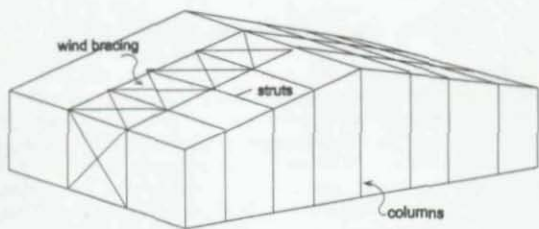


Figure 1 - Conventional Wind Bracing

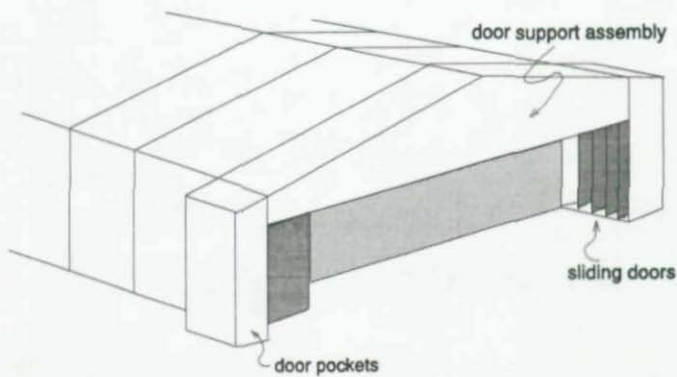


Figure 2 - Typical Hangar

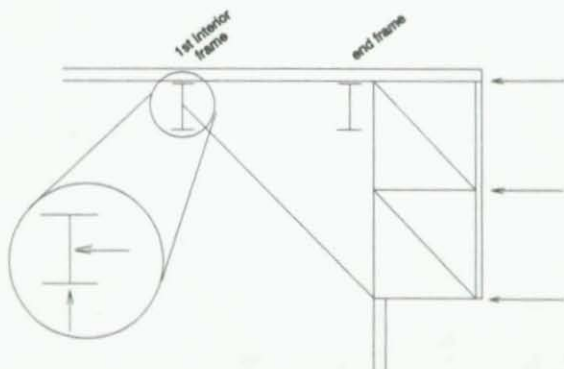


Figure 3 - Wind Loads on Door Support Assembly

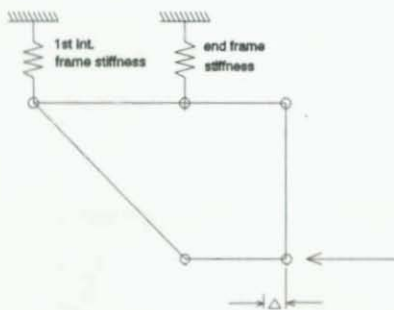
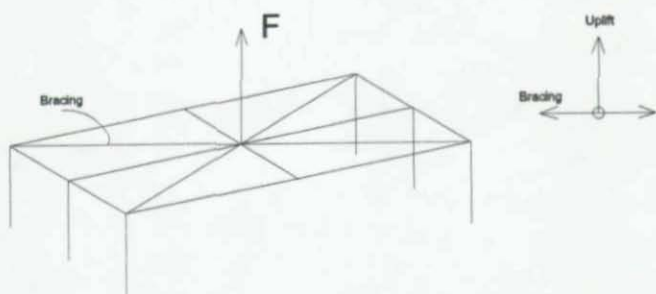
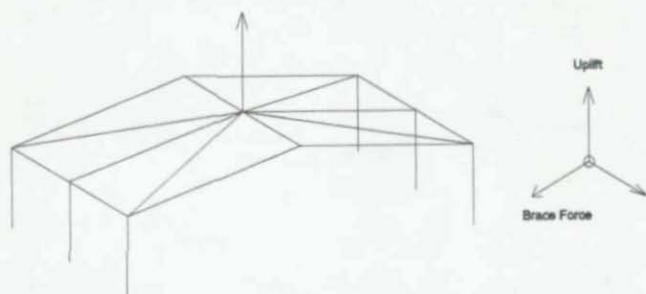


Figure 4 - Schematic of 2-D Deflections In Door Support Assembly



(a) Flat Roof



(b) Gabled Roof

Figure 5 - How Diagonal Bracing Resists Uplift on a Single Frame



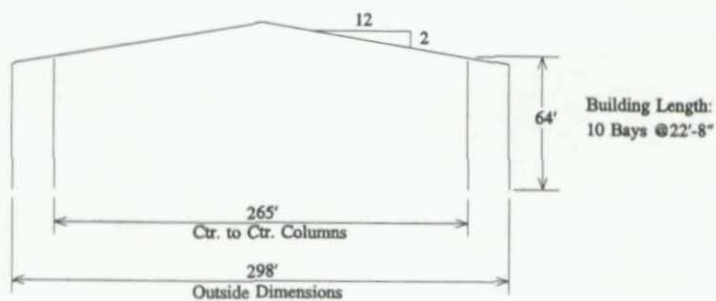


Figure 6 - Building Dimensions

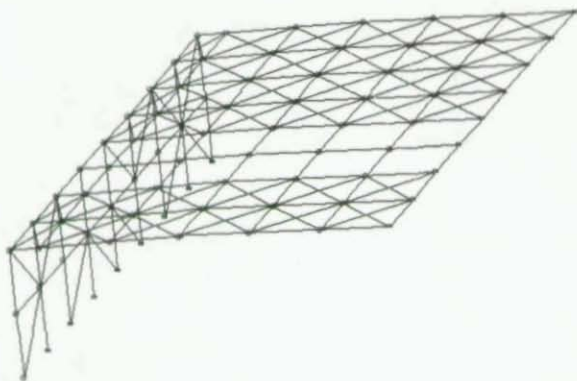


Figure 7 - Frame for Spring Stiffness

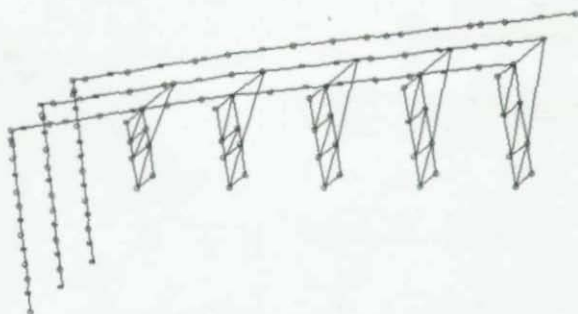


Figure 8 - Unbraced Model

CLICK MOUSE ON NODE FOR NODAL INFORMATION			
NODE FOUND = 140			
DOF = F R F R F F			
X =	1585.98	Y =	981.31 Z = -271.99
Translations are:			
X =	.000000	Y =	26.123066 Z = .000000
Rotations are:			
X =	-.177640	Y =	.000000 Z = .000000
			MENU

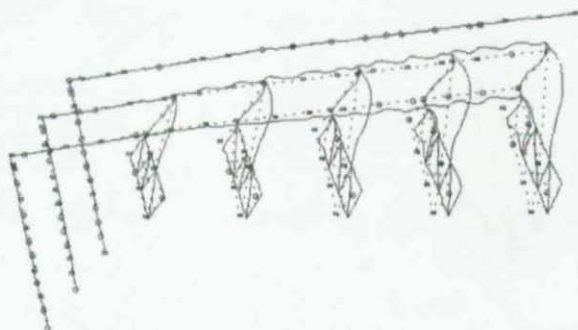


Figure 9 - Deformed Plot  
of Unbraced Model

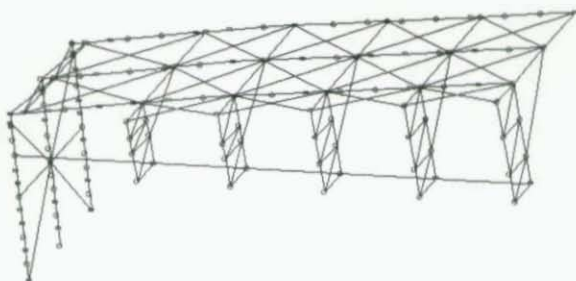


Figure 10 - Braced Model

CLICK MOUSE ON NODE FOR NODAL INFORMATION			
NODE FOUND = 140			
DOF= F R R R F F			
X= 1565.95 Y= 951.31 Z= -271.99			
Translations are:			
Z=	.000000	Y= 5.256244	Z= -.530259
Rotations are:			
X=	.026442	Y= .000000	Z= .000000
			MENU

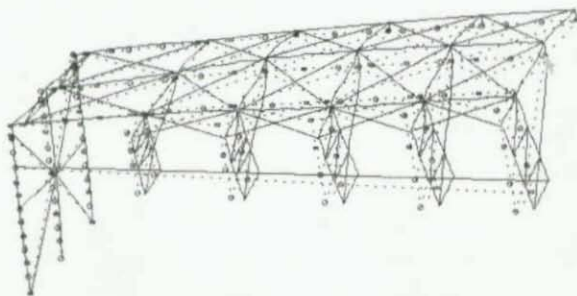


Figure 11 - Deformed Plot  
of Braced Model



## THE EFFECTIVE LENGTH OF COLUMNS IN PR SWAY FRAMES

by

Claudio Bernuzzi and Riccardo Zandonini

Department of Structural Mechanics and Design Automation  
University of Trento - Italy**Abstract**

The paper intends to present some of the results of a project aimed at investigating the stability of semi-rigid sway frames. Attention is focussed in particular on the column effective length, which still is a basic concept of simplified design analysis. The effect of column yielding as well as of initial imperfections and of joint nonlinearity is discussed. The use in design analyses of the effective length based on the elastic critical load, incorporating joint flexibility, is finally considered.

**INTRODUCTION**

Joint behaviour affects significantly the response and stability of steel frames: a number of studies have hence been recently carried out, or are underway, aiming at investigating the behaviour of semi-continuous frames and at developing suitable methods of analysis and design. A complete frame analysis incorporating all sources of nonlinearity (i.e material and joint behaviour as well as second order effects) is now viable also to practitioners, and present computer capabilities make it more and more "affordable" even in everyday design practice. Moreover, full frame analysis represents the most reliable and effective design tool in the case of sway frames. Nonetheless, simplified methods will certainly continue to play an important role in design, at least in the preliminary sizing phases. These methods are generally based on first order elastic analysis, and possibly on simple behavioural models for the whole structure to compute the stress resultants, and make use of a checking procedure by components (columns, beams and joints).

As a part of a research project on the stability of semi-rigid sway frames [1,2], the authors have been investigating some aspects of this type of approaches, concentrating in particular the attention on the "effective length" of partially restrained sway columns. Previous studies of this problem mainly relate to the elastic stability of columns restrained by linear elastic joints [3,4]. The limited knowledge about interaction between member and joint nonlinearities so far hampered the development of specific recommendations for determining the effective length of columns in semi-rigid frames. Eurocode 3 [5] just states that "where a beam has semi-rigid connections, its effective stiffness coefficient (to be used in effective length computations) should be reduced accordingly".

This paper intends to present and discuss some results, obtained via a numerical simulation program validated in a previous phase of the research project [6], which allow a first understanding to be achieved of the effective length problem, and in particular of

(1) the influence of different sources of nonlinearities (responses of beams, columns and joints), (2) the type of geometrical imperfection and (3) the loading condition (i.e. the relative importance of distributed beam loads with respect to concentrated nodal loads). The study considers two limited frames. The first, a column subassemblage, enables investigation of the influence of the column and joint nonlinearity on the stability of individual columns. The second, a storey subassemblage, allows to extend the study to conditions more typical of columns in frame systems, including as well the effect of beam loads. With reference to design analysis, the degree of approximation was then checked inherent in the use of the elastic value of the effective length to determine the ultimate load carrying capacity of a column. The results underline that the use of the elastic effective length may lead to unsafe design. Besides, the need for a consistent definition of the frame imperfections for full frame analysis is pointed out.

#### THE EFFECTIVE SLENDERNESS

When columns are the elements governing the ultimate strength of the system, frame design by components traditionally relies on the concept of effective length to account for the effect of the interaction between the column and the remainder of the structure. The meaning and determination of the effective length of columns in frames are well established [7], when reference is made to the elastic critical load of rigidly jointed systems (Fig. 1). The principal methods enabling determination of the effective buckling length factor  $\beta_e$  for columns in rigid frameworks can be easily extended to the case of columns in PR frames with linear elastic joints [3,4]. However, the attainment of the ultimate load carrying capacity generally involves inelastic frame behaviour, due to member yielding and/or to connection nonlinear response. These factors might affect remarkably column response and column-frame interaction, and hence column ultimate buckling strength. Their influence should therefore be recognized in the design analysis, i.e. in the value of the effective column length  $\beta H$ .

The question then arises of the definition of this parameter allowing for a reliable design of columns in inelastic semi-rigid frames. To this aim, it seems appropriate [8,9] to refer to the maximum strength of an end restrained column and define the "elastic-plastic" value  $\beta_{ep}H$  of the effective length, on the basis of the procedure of equivalence shown in figure 2, i.e. as the value of column length which, when used in conjunction with the stability curve for the pinned-end condition, allows the same strength as for the end-restrained condition to be obtained. Studies were conducted by several authors [8] of the effective slenderness of partially restrained non sway compression members, as affected by material and restraint nonlinearity, which adopted the above definition. A possible procedure for the incorporation of the results in the design of columns in braced frames was also developed [10,11]. The same problem, but for the case of sway frames, received only little attention, and limited to the influence of column yielding [9,12], i.e. no consideration was given to the effect of the nonlinearity of joint and beam responses. Besides, the procedure to evaluate  $\beta_{ep}$  proposed in [12] refers to inelastic buckling by equilibrium bifurcation, hence disregards the effect of geometrical imperfections on the spreading of plasticity in the column and on the effectiveness of the beam-to-column restraint. The appropriate definition of geometrical imperfections

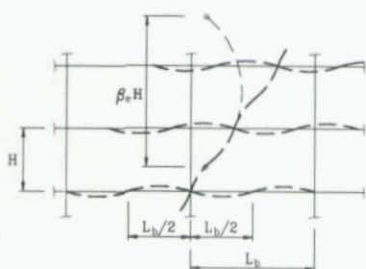


FIGURE 1

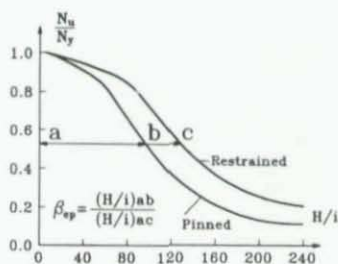


FIGURE 2

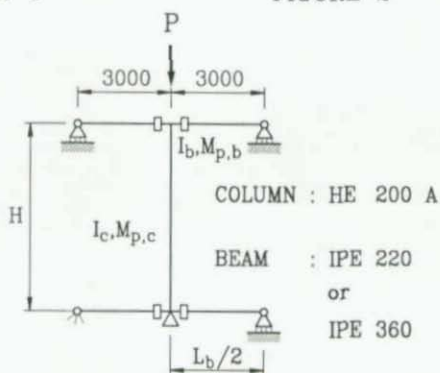


FIGURE 3

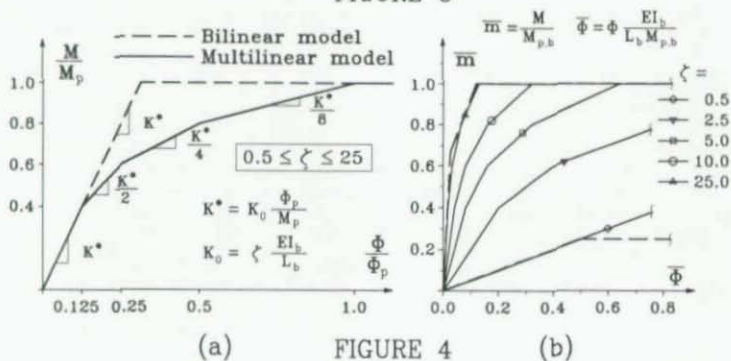


FIGURE 4



to be selected when assessing the  $\beta_{ep}$  factor is a further aspect to be considered.

#### THE STUDY

Two series of analyses were conducted using a finite element formulation previously developed [6], which allows in plane frame analysis to be conducted, taking into account: i) spreading of yielding along both the member cross section and length; ii) second order geometrical effects; iii) joint inelastic response. The method was satisfactorily validated against experimental results related to full scale stability tests on limited and complete frames [11]. The first series considered the column subassembly shown in figure 3, whose geometry is consistent with the traditional assumption [7], as to the buckling configuration, on which the methods for the computation of the elastic effective length are based, i.e. that beams are bent in double curvature. For the sake of simplicity, the effect of column continuity is disregarded. The study considered the main parameters which affect the member inelastic behaviour and the effectiveness of the restraint offered by the joint-beam system: i) the column section, slenderness ratio  $H/i$  and plane of buckling; ii) the ratio between the flexural stiffness ( $\alpha = (I_b/L_b)/(I_c/H)$ ) and the bending plastic strength ( $M_{p,b}/M_{p,c}$ ) of the beam(s) and of the column; iii) the constitutive law of the joints (i.e. initial stiffness, ultimate strength and shape of the  $M-\phi$  curve); iv) the shape and amplitude of the geometrical and mechanical imperfections. With reference to these factors, the following assumptions were made in the study: (1) the column section (an HE200A) and plane of buckling (about the strong axis of inertia) were kept the same throughout all the analyses, whilst the slenderness ratio was varied: values of  $H/i = 50, 100$  and 150 were considered; (2) all the beams were of length 3000 mm (corresponding to a span  $L_b$  of 6000 mm). Two sections were included in the study: the IPE 220 and the IPE 360, allowing the beam to column stiffness ratio  $\alpha$  to range from 0.52 to 9.13. Besides, section IPE 220 has full plastic moment ( $M_{p,b}$ ) equal to 0.67 of the plastic moment of the column  $M_{p,c}$ , whilst for section IPE 360 the ratio  $M_{p,b}/M_{p,c}$  is 2.37. Limited frames with the former beam shape may then be considered as typical of systems designed on the basis of the strong column-weak beam criterion, whilst limited frames with the latter beam section may be considered as typical of weak column-strong beam systems; (3) the beam-to-column joints were assumed to be full strength joints, i.e. to have ultimate moment capacity  $M_{u,j}$  equal to the beam plastic moment  $M_{p,b}$ . To investigate the influence of joint flexibility, a reference piecewise linear moment-rotation relationship was first deduced (fig. 4a), from a  $M-\phi$  curve typical of joints with extended end plate connections [13]. The elastic range, of stiffness  $K_0$ , is assumed to extend up to  $M_j = 0.4 M_{p,b}$ . Different joint responses were then simulated by varying the initial stiffness  $K_0$  from 0.5 to 25 times the flexural stiffness  $EI_b/L_b$  of the connected beam, whilst the stiffness ratios between the branches of the linearized law were kept constant. The  $M-\phi$  laws considered covered the whole semi-rigid range in accordance to Eurocode 3 (Fig. 4b). The ratio between the elastic flexural stiffness  $K_{j,b}$  of the joint-beam system and of the column ranges from 0.25 to 46.0 and, correspondingly, the elastic value of the effective length factor  $\beta_e$  from 1.02 to 3.25, so covering the range of practical interest. In order to point out as well the effect of nonlinearity of joint response, bilinear "elastic plastic" laws



were also assumed. Joint flexibility is the end result of the deformation of a nodal zone of finite dimensions, including the connection and column components. The analysis method concentrate joint flexibility at a specific location along the beam-joint finite element. In order to point out the possible influence of joint "location" in the model the analyses were conducted concentrating joint flexibility either at the column face or at the intersection between the beam and column axes; (4) the four initial deflected shapes in figure 5 were selected: - the first refers to the elastic buckling mode and assumes a member deflection with maximum amplitude equal to  $H/250$  (i.e. to the value given in [14] for the relevant stability curve (curve b)) and shape, cosinusoidal, equal to the critical one of a column with rigid rotational end restraints); - the other three types of imperfection represent different alternatives, which might be adopted in second order frame analysis: type 2 is a sway deflection with sway angle  $1/200$ , i.e. equal to the value specified for a single column by the same document, whilst types 3 and 4 are combinations of the sway and curvature deflection. All sections are considered free of residual stresses, whose effect is however included in the value adopted for the amplitude of the initial deflection; (5) the steel is of grade Fe360 with yield strength  $f_y = 235$  MPa.

The second series of analyses considered the storey subassemblage of figure 6. The main parameters investigated were the same as in the first series, although the results related to the column subassemblage enabled reduction of the cases investigated. A further important parameter was the distribution of the load on the subassemblage. Besides the load case with forces  $P$  applied at the upper nodes, loading conditions were considered, where the ratio  $R$  between the total distributed load  $3ql$  and the total concentrated load  $3P$  was varied from 0 to 2.

Both types of subassemblage were analyzed up the ultimate conditions both in the elastic and elastic-plastic range.

#### THE COLUMN SUBASSEMBLAGE

The study of the column subassemblage (Fig. 3) involved more than 350 analyses under a vertical load  $P$  increased step by step up to the attainment of the buckling strength. On the basis of a preliminary calibration study, five finite elements were used to model the column, while only one joint-beam element was adopted for each "arm" of the subassemblage.

In order to single out the effect of member yielding, the first series of analyses assumed joint behaviour as linear elastic up to the ultimate moment resistance; besides, joints were modelled via springs located at the column face. Numerical results allow the relationship between the ultimate load carrying capacity of the column and the stiffness  $K_{jb}$  of the joint-beam assembly to be obtained. Typical curves are plotted in figures 7a and 7b, where stiffness  $K_{jb}$  and the ultimate buckling load  $N_b$  are normalised with reference to the stiffness  $K_c$  of the column and to the column squash load  $N_y$  respectively. The elastic critical curves are also plotted. As expected on the basis of previous studies [1,2,15,16], the elastic and elastic-plastic curves do have a very similar shape, with a sharp increase of column strength in the field of low end restraint stiffness, and a progressive shallowing as  $K_{jb}$  increases, which makes practically ineffective any further increase of this parameter beyond a value depending on the slenderness ratio and on

the type of column behaviour (elastic or elastic-plastic): elastic-plastic end restrained columns tend to attain the maximum value of the buckling strength compatible with their slenderness ratio  $H/i$  for values of  $K_{bh}/K_c$  lower than for the corresponding elastic case. Inelastic column buckling is attained via a progressive deterioration of the member flexural stiffness consequent to the concurrent increase of axial load and of yielding. In a sway column plastic zones are located at the ends. Hence, unlike for non sway columns, yielding has effects, which are to a certain extent counteractive: on the one hand the associated decrease in member stiffness makes the restraint "stiffer" relatively to the column, on the other hand moment transmission from the joint-beam system is hampered and hence the restraint effectiveness is reduced. Inelastic curvatures at the column ends require an increasingly greater sway for the same increment of restraining moment to be developed. Furthermore, the restraining moment is limited by the plastic moment of the column section, as reduced by the axial thrust. As a consequence, relatively low values of stiffness are sufficient to the restraint system to attain its maximum effectiveness when more significant is the role of yielding, i.e. in the range of low slenderness ratios: for  $H/i = 50$ , the increase of  $N_u$  when  $K_{bh}$  exceeds the value of  $4 K_c$  is negligible (fig. 7a). As the slenderness ratio  $H/i$  increases, yielding becomes less and less important and the shape of the inelastic and elastic curves (i.e. the effect of increments of the restraint stiffness on column stability) tends to be much the same, as it already appears from figure 7b related to  $H/i = 100$ . Such general considerations do not depend upon the type of initial geometrical imperfection, although the assumed deformed configuration for the column varies remarkably both in shape and amplitude (Fig. 5). Imperfections may affect substantially column response: important differences were observed in the load-deflection relationship, and in the bending moment distribution, and hence in the extension and location of the plastic zones in the column and in the stress state of the joints. This leads to non negligible differences in the values of ultimate buckling strength. The lowest value of buckling strength  $N_u$  is associated with the deflected shape type 1, which is the closest to the column elastic buckling mode. Besides, such an imperfection has the greatest amplitude. The highest resistance is associated with the initial configuration type 4. Reference to this latter imperfection entails increments of maximum strength up to 20% (with respect to the deflected shape type 1) for  $H/i = 50$ , 24% for  $H/i = 100$ , and 19% for  $H/i = 150$ . The increments of the buckling resistance associated to imperfection type 2 are more limited. However, they may still be as high as the 17%. In general, the sensitivity to imperfections was found to depend only moderately upon the column slenderness, though it was slightly higher for intermediate values of this parameter. With reference to the combination of the deflections due to sway and to member curvature, the results related to the initial deflected shapes 2 and 3 (based on [14]) seem to indicate that the additional sinusoidal deflection due to column curvature affects only moderately both column response and ultimate load capacity. As to this latter parameter, differences are of 3.2% in average, and never higher than 7%. In the cases studied the sway deflection is the governing component, the curvature imperfection not having enough "weight" relative to the sway imperfection to change the mode of failure from a sway mode to a buckling mode by bending between the supports.

It seems appropriate to appraise these results also from a differ-

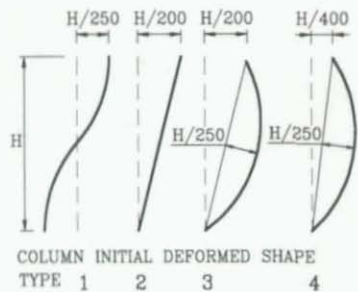
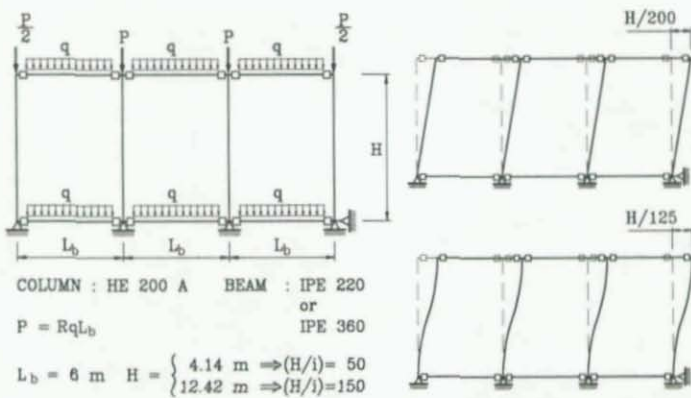


FIGURE 5



(a)

FIGURE 6

(b)

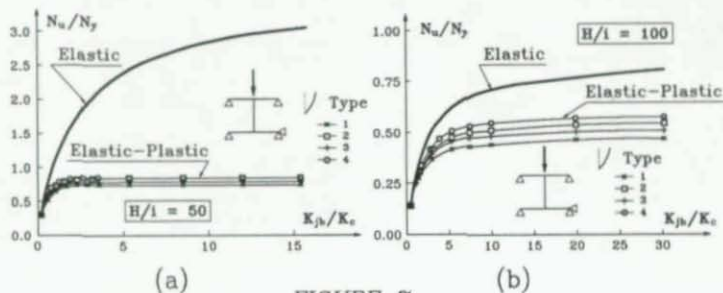


FIGURE 7



ent point of view, i.e. to consider them with reference to design specifications. To this aim, it should be noted that the initial deflected configuration type 1 is the only one making the analysis of a column in a frame consistent with the analysis of an isolated column. This stands not true for the other types of geometrical imperfection. Hence, column buckling analyses aimed at determining the elastic-plastic value of the effective length factor  $\beta_{ep}$  should be based on imperfection type 1, in order to ensure the needed consistency in the stability checks of compression members. Besides, specifications related to design via full frame second order analysis refer to initial column configurations different for shape and amplitude, such as imperfections 2 to 4 [5,14]. This involves a maximum strength for the "framed" column always higher than that determined for the same column on the basis of an appropriate effective length, i.e. methods of sway frame design based on full analysis are not consistent with methods of design by components. It would be certainly desirable to avoid such an inconsistency. This might be a further aspect indicating that reconsideration of the geometrical imperfections to be assumed in frame analysis is appropriate [17].

The elastic-plastic value of the effective length was determined with the procedure illustrated figure 2. This procedure requires the knowledge of a reference stability curve for the pinned-end condition, which was computed numerically adopting an initial sinusoidal deflected shape of amplitude equal to  $H/250$ . As it was already noted, the definition of effective length would require full consistency between the two stability curves (referring to the pinned-end and restrained condition, fig. 1), and hence it strictly allows the value of  $\beta$  to be computed only for the case of imperfection 1. However, for the sake of completeness the effective length factor was determined for all the imperfections considered. Figure 8 compares the effective length factors  $\beta_{ep}$  so obtained for the case  $H/i = 50$  and its elastic value ( $\beta_e$ ). Column yielding appears to have a beneficial effect on the factor  $\beta_e$ : the elastic-plastic value is always lower than the elastic one. The positive effect of column plasticity, due to a consequent increase in the stiffness of the end restraints relative to the column, seems to prevail on the negative effect on the effectiveness of restraining moment transfer. For imperfection type 1, the value of  $\beta_{ep}$  tends to  $\beta_e$ , while it tends to values lower than  $\beta_e$  for the other imperfections, which in effect might entail values of  $\beta_{ep}$  lower than 1.0 (i.e. column effective lengths lower than the storey height). Differences between the elastic and elastic-plastic value of  $\beta$  tends to diminish for all types of imperfection when the slenderness ratio  $H/i$  increases, due to the decreasing importance of the role played by member plasticity: such differences almost vanish for  $H/i = 150$  and imperfection 1.

The value of  $\beta_{ep}$  depends on all the factors affecting member yielding: i.e. slenderness ratio, member shape and axis of bending, presence and magnitude of residual stresses, type and amplitude of geometrical imperfections. An accurate definition of the inelastic effective length factor is beyond the scope of this study. However, the results indicate that the elastic value of  $\beta$  might be conservatively used. In figure 9 the values of  $N_y$  obtained for imperfections 1 and 4 are plotted against the column stability curve, by determining the effective slenderness ratio on the base of  $\beta_e$ . It is apparent that the use of  $\beta_e$  might be acceptable for medium to high values of  $H/i$  if reference is "consistently", and in the opinion

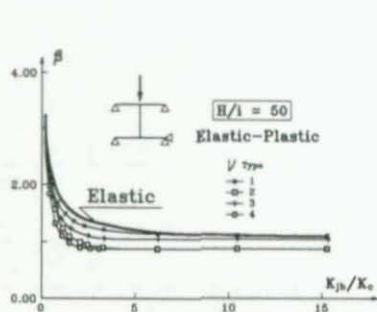


FIGURE 8

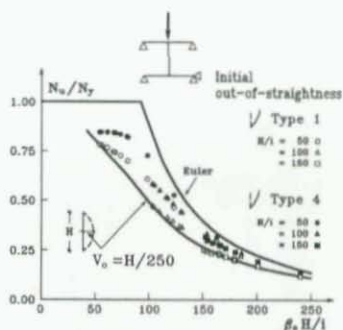
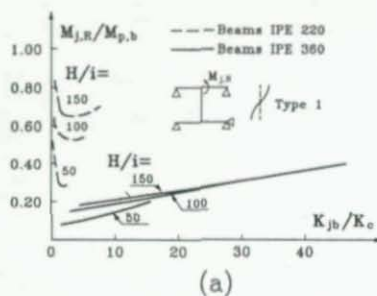
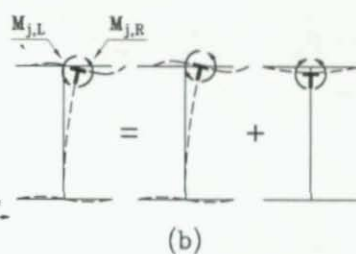


FIGURE 9

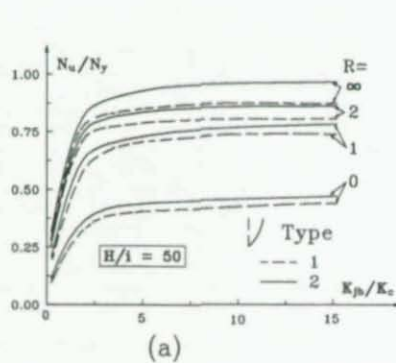


(a)

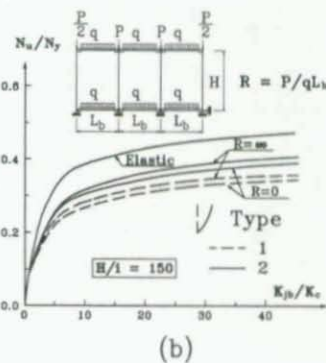


(b)

FIGURE 10



(a)



(b)

FIGURE 11

of the authors correctly, made to imperfection 1. In the range of low  $H/i$ , and if reference is made to other imperfections, the use of  $\beta_c$  might lead to a significant underestimation of the column carrying capacity (up to more than 50% for imperfection 4).

The results so far discussed were obtained under the assumption the behaviour of joints is linear, and then fully defined by its initial stiffness. The maximum moment level in the joints at column collapse is hence a further important parameter, which allows a first appraisal of the possible influence of the nonlinearity of the  $M - \phi$  relationship to be achieved. Figure 10a shows the relationship, obtained by evaluation of the numerical data, between the moment  $M_{j,R}$  acting on the right upper joint (which is the most stressed one) and the restraint stiffness  $K_{j,b}$ ; these parameters are referred to the plastic moment of the beam  $M_{p,b}$  and to the flexural stiffness of the column  $K_c$  respectively. The shape of the curves, which show an initial sharp decrease of moment, the attainment of a minimum and a following steady increase, might be explained if the factors contributing to the joint moment in the subassemblage are singled out. As it is schematically represented in figure 10b, bending moment is induced in the joint due to column bending (which implies joint rotation) and to column shortening (which implies joint translation). These contributions add up at the upper right joint. In the range of low values of  $K_{j,b}/K_c$  (i.e.  $K_{j,b}/K_c < 2$ ), where the column effective slenderness is the highest and so are column sway displacements, the rotation contribution prevails; joint moment therefore decreases with increasing stiffness of the joint-beam system, due to the reduction in column sway flexibility. As  $K_{j,b}/K_c$  increases further on, the contribution of the translation tends to become the most important, and joint moment increases with the joint-beam stiffness. The analysis shows that when the beams have stiffness and strength significantly greater than the column, as in the case of section IPE 360 (strong beam - weak column design) the column sway flexibility is relatively low (the effective slenderness ratio is close to unity), and the maximum joint moment at column buckling tends to remain in the first elastic branch of the  $M - \phi$  curve ( $M_{j,R} < 0.40 M_{p,b}$  in fig. 10a): this indicates that a linear elastic model of the joints is sufficiently accurate. When, on the other hand, the beam has stiffness and strength of the same order of magnitude than the column, or even lower as in the case of section IPE 220 (weak beam - strong column design), the joint state enters well into the nonlinear range of the moment rotation curve (moments up to 85% of  $M_{p,b}$  were attained), and a linear model might hence be no more adequate for a buckling analysis. Therefore all these cases were reanalyzed, for which joint nonlinearity were presumably affecting column stability. The complete  $M - \phi$  relationship was assumed in the simulation, and the ultimate loading capacity recomputed as well as the effective length factor  $\beta$ . The values of both these parameters were found to differ of only few percent from the ones obtained under the assumption of linear joints. This result might have been expected, considering that the value of moment  $M_{j,R}$  at collapse is mostly "built up" in the very vicinity of the ultimate load. Moreover, the stress state in the other joints results to be lower, also significantly, than in the upper right joint, and in many cases still in the elastic range. The results obtained under the assumption of linear joints, and previously discussed, maintain hence their general validity.

Finally, in order to investigate the influence of joint zone



modelling, all the cases were reanalysed, but concentrating connection flexibility at the column axis. Differences in the frame behaviour were found to be modest: with reference to the ultimate carrying capacity, the reduction due to the greater flexibility implied by the model for the joint-beam system didn't attain the 4%. Though a more important influence might be expected for deeper column sections (section HE200A has a depth which only 1/31th of the assumed span), the prediction of column stability behaviour in sway frames seems only modestly sensitive to the location assumed in the numerical model for the elements simulating the rotational flexibility of the joint zone.

#### THE STOREY SUBASSEMBLAGE

The analyses of the storey frame (Fig. 6) under concentrated loads ( $R = \infty$ ) at the upper nodes pointed out that the main features of the general behaviour are consistent with the results obtained for the column subframe, and presented in the previous section. In particular, the relationship between the ultimate load in the most stressed column and the joint relative stiffness as well as the influence of geometrical imperfections are fairly similar, as apparent from figure 11. The uneven distribution of the applied load among the columns implies that the exterior "stronger" columns somewhat brace the interior "weaker" columns, as also indicated by the elastic buckling analysis, which provides buckling loads for the inner columns greater than those obtained for the restrained column of about 20% in average. This favourable interaction affects inelastic instability loads as well, which increase remarkably (columns with imperfection type 2 and  $H/i = 50$  almost attain the squash load when joint stiffness is enhanced). However, the single factor which has the most dramatical influence on frame stability, at least for low slenderness ratios, is the presence of beam load: the values of  $N_u$  for the case of beam loads only ( $R = 0$ ) are up to 63% lower than the values of the corresponding frame loaded at the nodes ( $R = \infty$ , Fig. 11a). The magnitude and spread of plasticity in, and among, the members as well as joints nonlinear response are substantially affected by load distribution, making the failure mode to change from instability of columns with basically elastic restraints to column instability combined with significant stiffness deterioration of the joint-beam system and, finally, to beam plastic collapse (for the frames with weak beams (IPE 220) and stiff semi-rigid joints). Although these last cases were disregarded in the evaluation of the results, the interaction among instability, member plasticity and joint nonlinearity is a fairly complex phenomenon, of which only few aspects were so far appraised. The presence of load on the beams modify frame stress state and deformation, and hence also the restraining mechanism of the columns by the beams changes. With reference to the inner columns, only one beam is effectively providing restraint, whilst the beam on the other side is on the contrary transferring destabilizing moment. External columns are subject to substantial bending, which may induce extensive yielding weakening the member. In the case of strong beams, end plasticity makes the external column in the buckling direction act as a leaning member. It was observed, in general, that: (1) when beam loads are predominant instability is mainly a consequence of the deterioration of the stiffness of the joints and of the beam (which is significantly yielded at midspan): column buckling occurs when the column yielding is still

limited, (2) as the importance of column loads increases, the severity of the stress state of beams and joints reduces, and at the same time columns enter more and more into the inelastic range of the response, (3) moments in the most stressed joints and in the external "leeward" column increase with the joint stiffness. The curves plotted in figure 12 provide the relationships obtained between the maximum joint moment and the stiffness  $K_{jb}$  for the frames with IPE 360 beams. The results related to the concentrated load case ( $R = \infty$ ) confirm that the column subassembly leads to a conservative assessment of the magnitude of joint moments. The more beam loads become important the more the joints are stressed: moments close to the plastic moment of the beam can be achieved. However, due to the particular restraint mechanism and to the fact that these moments are in many instances built up in the vicinity of the ultimate condition, joint nonlinearity was not found to affect remarkably the stability of subframes with strong beams. A series of analyses where joints were modelled as ideally elastic-plastic springs showed that the influence of joint nonlinearity is modest (less than 5% the decrease of  $N_u$  for  $R=0$ ). In frames with beams weaker than the columns joint nonlinearity leads to early plastification of the beam at midspan, and hence may remarkably affect the ultimate frame resistance. Decreases of the value of  $N_u$  up to 20% were hence found for frames with IPE 220 beams and column slenderness ratio  $H/i = 50$ . The rather low values of the ultimate load for  $H/i = 150$  made those frames less sensitive to the beam load.

These type of responses are summarized, for the frames for which column buckling is governing the load carrying capacity, by the  $\beta_{ep}$  values presented in figure 13a for the case of  $H/i = 50$ . Responses under predominant beam loads lead to effective length factors higher, even substantially (up to 140% for  $R = 0$ ), than the values determined via an elastic critical analysis of the subframe. Member plasticity, which is mainly located in the beams, adversely affects frame stability. However, as  $R$  increases, yielding tends to be more and more concentrated in the columns and hence it affects favourably column buckling: it is sufficient that column loads are higher than or equal to twice the beam loads in order to make them play a major role in frame stability behaviour. In the range of high slenderness ratios,  $H/i = 150$ , beam loads do affect moderately the stability of the frame and  $\beta_{ep}$  values depends on the type of imperfection only (Fig. 13b).

The use of the elastic effective length factor  $\beta_e$  in design might imply a dramatic overestimation of column buckling resistance, as shown in figure 14. The load carrying capacity of the column with  $H/i = 50$  is overestimated of more than 40%, and up to 57%, for  $R=0$ . This already reduces to less than 10% in average for  $R = 1$ .

#### SUMMARY AND CONCLUSIONS

The results of a part of a study into the stability of columns in semi-rigid sway frames has been presented. The responses of a series of limited frames were simulated up to collapse: first a subassembly was analysed consisting of an axially loaded column restrained at both ends by two joint-beam systems, then a full storey subassembly was considered. Different aspects were singled out of interest for frame design by components, with reference to the column effective length. Although the study is far from being exhaustive, results allow some interesting conclusions to be drawn:



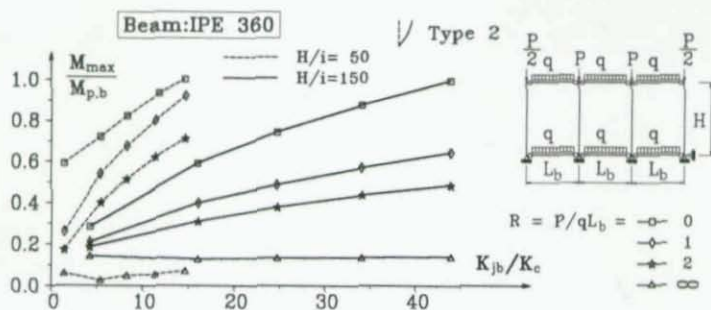


FIGURE 12

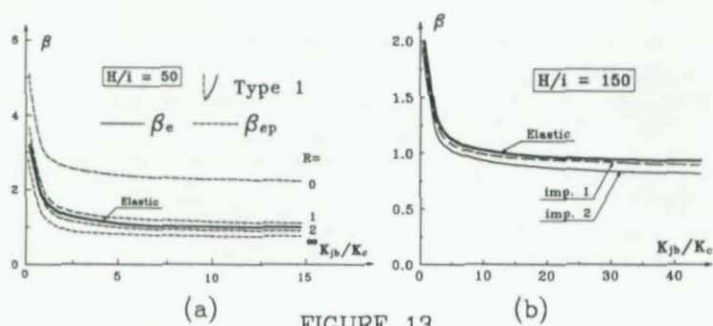


FIGURE 13

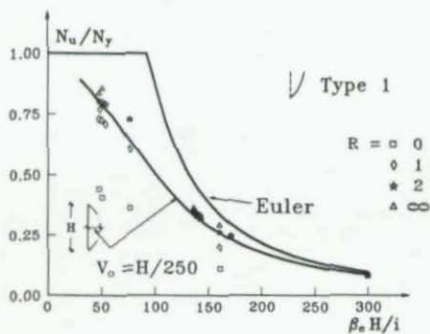


FIGURE 14

- (1) Responses of the column subassemblage and of the storey sub-frame subject to predominant column loads are consistent to each other. The presence of beam loads may influence substantially frame behaviour and stability, when the ratio  $R$  between the column and beam loads is lower than 2.
- (2) Shape and amplitude of the initial column deflection affect substantially column and frame response and load carrying capacity. A sway cosinusoidal imperfection should, in principle, be assumed in order to achieve consistency between the analysis of an isolated column and of a column in a frame. The types of sway imperfections usually adopted in frame analysis entail higher column strength than the cosinusoidal one. This implies that frame design by second order analysis and frame design by components are not fully consistent.
- (3) Column yielding has a "beneficial" effect on the column stability when column loads are predominant: the elastic-plastic value of this parameter is lower than the corresponding elastic one. In frame design by components differences between these two values are limited, and the elastic effective length may be adopted when checking column stability;
- (4) For  $R < 2$ , beam yielding becomes important, and influences significantly column stability. The use of the elastic value of  $\beta$  might entail substantial overestimation of the column load carrying capacity, when it does not account for the deterioration of the beam restraints.
- (5) Joint nonlinearity has only a limited effect on column stability in strong beam - weak column frames. On the other hand, it may play a significant role when beams are weaker than the columns, and  $R < 2$ .

Other aspects of the problem, such as the case of partial strength joints were not considered. They will be investigated in the continuation of the research work, the aim of which is the development of a deeper understanding of the inherent limits and possible application of the effective length concept. However, it should be remarked that beam section IPE 220 has a plastic moment equal to 0.67 times the plastic moment of the column section HE 200 A: the results related to IPE 220 beams with full strength joints may then be considered as indicative, at least for the case of predominant column loads, of the case of joint-beam systems with strong beams, but partial strength joints.

#### ACKNOWLEDGEMENTS

The research was made possible by grants of the Italian Research Council (C.N.R.) and of the Italian Ministry of University and Scientific and Technological Research (M.U.R.S.T.)

#### REFERENCES

- [1] Bernuzzi C, Zandonini R., "Connection Response and Stability of Steel Frames", Second International Workshop: 'Connections in Steel Structures', Pittsburgh, U.S.A., April 1991.
- [2] Bernuzzi C. and Zandonini R., "Stability of Partially restrained Sway Frames", 1991 Annual Technical Session and Meeting S.S.R.C., S.S.R.C., Chicago, U.S.A., April 1991.
- [3] Driscoll G.C., "Effective Length of Columns with Semi-Rigid Connections", Eng. J., AISC, vol. 13, No. 4, 1976.

- [4] Wood R. H., "Effective Lengths of Columns in Multi-Storey Buildings", *The Structural Engineer*, vol. 52, No. 7, July, 1974.
- [5] European Committee for Standardization (CEN), Eurocode 3: Design of Steel Structures - Part 1.1: General Rules and Rules for Buildings, April 1992.
- [6] Poggi C. and Zandonini R., "A Finite Element for the Analysis of Semi-Rigid Frames", State-of-the-Art Workshop on Connections, Strength and Design of Steel Structures, Cachan, May 1987.
- [7] Johnston B.G., editor, SSRC Guide to Stability Design Criteria for Metal Structures, 3rd Edition, John Wiley & Sons, New York, 1976.
- [8] Nethercot D.A. and Chen W.F., "Effect of Connections on Columns", in *Steel Beam-to-Column Connections*, Special Issue, Journal of Constructional Steel Research, 1988.
- [9] Setti P. and Zandonini R., "Stability of Single-Story Unbraced Steel Frames", *Costruzioni Metalliche*, No. 2, 1982.
- [10] Bjorhovde R., "Effect of End Restraint on Column Strength - Practical Applications", *Engineering J.*, AISC, vol. 21, No.1, 1984, pp. 1-13.
- [11] European Convention for Constructional Steelwork - ECCS, Analysis and Design of Steel Frames with Semi-rigid Joints, Technical Committee 8 - Structural Stability, Publication CECM No. 67, 1992.
- [12] Yura J.A., "The effective Length of Columns in Unbraced Frames", *Engineering J.*, AISC, vol. 8, No. 2, 1971.
- [13] Frye M.J. and Morris G.A., "Analysis of Flexibly Connected Steel Frames", *Can. J. Civil Engrs*, vol. 2, 1975, pp. 280-291.
- [14] European Convention for Constructional Steelwork - ECCS, Ultimate limit state calculation of sway frames with rigid joints", Publication CECM No. 33, 1984.
- [15] Cosenza E., De Luca A., Faella C., "Elastic Buckling of Semi-Rigid Sway Frames", in *Stability and Strength series*, vol. 8, Structural Connections (ed. R. Narayanan), Elsevier Applied Science, London, 1988, pp. 253-295.
- [16] Cosenza E., De Luca A., Faella C., "Inelastic Buckling of Semi-Rigid Sway Frames", in *Stability and Strength series*, vol. 8, Structural Connections (ed. R. Narayanan), Elsevier Applied Science, London, 1988, pp. 297-333.
- [17] De Luca A., "Needs for Experimental Measures of Geometrical Frame Imperfections", in *Testing of Metals for Structures*, Proceedings of International RILEM Workshop (ed. F.M. Mazzolani), E & FN SPON, 1992.



## OPTIMUM BRACING OF FRAMES SUBJECTED TO TORSIONAL AND FLEXURAL BUCKLING

by

Andreas S. Vlahinos, Associate Professor  
Yang-Cheng Wang, Graduate Research Assistant  
Department of Civil Engineering,  
University of Colorado at Denver  
1200 Larimer St., Denver, CO 80204

### ABSTRACT

In this paper an elastic stability analysis of three dimensional two story partially braced frames is presented. The dimensions and properties of the frames considered are in a practical range useful to a designer. The flexural as well the torsional buckling are considered.

The effect of each story bracing stiffness on the buckling load is presented in graphical form. Nondimensional interaction surfaces between bracing values and critical loads allow the designer to select the required bracing for a given critical load. In addition curves establishing the minimum total bracing stiffness "critical bracing" required to obtain braced frames critical loads are presented.

### INTRODUCTION

The sway-buckling of an unbraced frame is many times lower than the corresponding buckling load of the same frame with no sway. Thus, it is desirable to increase the total load-carrying capacity of unbraced frames by preventing their sway-buckling mode. Many significant contributions in the topic of bracing requirements of frames have been reported in the last thirty years. Galambos<sup>[1]</sup> presented a simple, practical and conservative method for the evaluation of the lateral support required by the unbraced frames to achieve braced frames buckling strength. Biswas<sup>[2]</sup> presented the concept of threshold bracing stiffness and indicated the feasibility of obtaining required bracing stiffness values for general multi-story multi-bay



structural frames. The concept of "minimum sum stiffness" is introduced and explained by using two story plane frames as examples. Kounadis<sup>[3]</sup> presented the interaction of the joint and of the lateral bracing stiffnesses for the optimum design of unbraced plane frames. It is concluded that the magnitude of the forces required to prevent the sway-buckling of unbraced frames is small and can be established only by using a nonlinear stability analysis. Lee and Basu<sup>[4]</sup> propose some simple relationships for the design of diagonal bracing systems in planar building frames with both fully restrained and partially restrained connections.

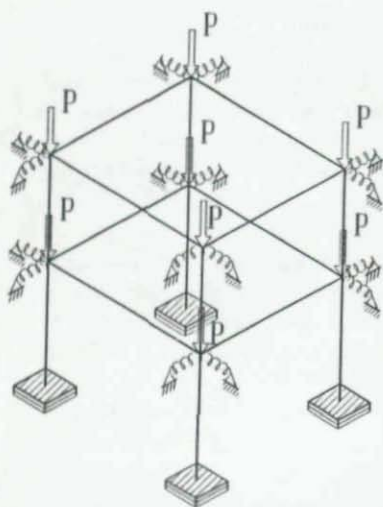


Figure 1. Geometry, Loading and Boundary Conditions of the Two Story Frames.

The analysis of three dimensional frameworks generally presents some difficulties since as a complex three dimensional structure, it may have several modes of failure. Especially in their buckling analysis it is not a priori known which buckling mode controls (i.e. flexural, torsional, torsional-flexural, local etc.). Most of the information available in the literature of the last decades refers to two dimensional analysis, in which the torsional and torsional-flexural buckling is not considered.

In this paper further analytical studies similar to the ones reported by Biswas<sup>[2]</sup> are described. The flexural as well the torsional buckling analysis of three dimensional two story partially braced frames is presented. The effect of each story bracing stiffness on the buckling load is presented.



## MODEL DESCRIPTION AND ANALYSIS

**Assumptions**

The following assumptions were taken into account:

- Members are initially straight and piecewise prismatic;
- The material behavior is linearly elastic and the moduli of elasticity  $E$  in tension and compression are equal;
- Transverse plane section of the members remain plane and normal to the longitudinal fibers before and after bending;
- The structure is loaded by static concentrated axial loads;
- The effect of residual stresses and of geometry imperfections is neglected;
- Local buckling of individual members is ignored.
- The term  $(\frac{\partial u_x}{\partial x})^2$  is small compared to one; where  $u_x$  is axial displacement components at points on the centroidal surface. Thus the strain in the direction of the element axis is:

$$\epsilon_{xx} = \frac{\partial u_x}{\partial x} + \frac{1}{2} \left( \frac{\partial u_x}{\partial x} \right)^2 + \frac{1}{2} \left( \frac{\partial u_k}{\partial x} \right)^2.$$

**Geometry and Loading**

Figure 1 shows the geometry, the loading and the boundary conditions of the two story space frame model considered. The same load  $P$  is applied in all eight joints of the frame, thus the total load applied is  $8 \cdot P$ . The bracing is provided by 16 linear springs attached to all eight nodes in both  $X$  and  $Y$  directions. Figure 2 shows the top, side and isometric views of the considered frame with the dimensions and the cross sectional properties. The first and second story heights are  $h_1$  and  $h_2$ . The horizontal dimensions are  $b_1$  along the  $X$  direction and  $b_2$  along the  $Y$  direction. All springs at the first story have stiffness  $k_1$  and all springs at the second story have stiffness  $k_2$ . The cross sectional area and moment of inertia of the first and second story columns are  $A_1, I_1$  and  $A_2, I_2$  respectively. The cross sectional area and moment of inertia of the first and second story beams are  $A_3, I_3$  and  $A_4, I_4$  respectively. For simplicity in all sections the  $I_{zz}$

was considered equal to  $I_{yy}$ . For the examples considered  $h_1 = 14$  ft,  $I_1 = 40$  in<sup>4</sup>,  $A_1 = 10$  in<sup>2</sup> and modulus of elasticity  $E = 30 \cdot 10^6$  psi. The critical loads are presented in a non-dimensionalized form  $P_{cr} = \frac{P \cdot h_1}{EI_1}$ . The ratios of the moment of inertias, areas and lengths used are:

$$\begin{array}{lll} I_2/I_1 = 0.50 & A_2/A_1 = 0.6 & h_2/h_1 = 12/14 \\ I_3/I_1 = 1.50 & A_3/A_1 = 1.5 & b_1/h_1 = 20/14 \\ I_4/I_1 = 1.25 & A_4/A_1 = 1.2 & b_2/h_1 = 18/14 \end{array}$$

### Solution procedure

According to our assumption the strain energy expression is :

$$U = \frac{AE}{2} \int_0^l \left[ \left( \frac{\partial u_x}{\partial x} \right)^2 + \frac{1}{2} \left( \frac{\partial u_y}{\partial x} \right)^2 + \frac{1}{2} \left( \frac{\partial u_z}{\partial x} \right)^2 \right] dx \quad (1)$$

A three dimensional finite element formulation can be performed by considering the following shape functions for the linear stiffness matrix :

$$\begin{array}{l} u_x(x) = C_1 + C_2x \\ u_y(x) = C_3 + C_4x + C_5x^2 + C_6x^3 \\ u_z(x) = C_7 + C_8x + C_9x^2 + C_{10}x^3 \end{array} \quad (2)$$

The following shape functions were considered for the geometric stiffness matrix:

$$\begin{array}{l} u_x(x) = 0 \\ u_y(x) = C_{11} + C_{12}x + C_{13}x^2 + C_{14}x^3 \\ u_z(x) = C_{15} + C_{16}x + C_{17}x^2 + C_{18}x^3 \end{array} \quad (3)$$

Differentiation of the displacements and integration of the strain energy results in

$$U = \frac{\{d^T\}}{2} [k]_0 \{d\} + \frac{\{d\}^T}{2} \lambda [k]_1 \{d\} \quad (4)$$

where  $[k]_0$  is the linear elastic three dimensional element stiffness matrix

and  $[k]_1$  is the three dimensional initial-stress or geometric element stiffness matrix<sup>[5],[6]</sup>.

The objective is to find the critical intensity  $\lambda_{cr}$  at which buckling occurs. The buckling equation in terms of  $\lambda$  and the global stiffness matrices is:

$$[[K]_0 + \lambda[K]_1]\Phi = 0 \quad (5)$$

where  $\Phi$  is the buckling mode shape. This equation leads to the classic eigenvalue form which can be solved efficiently with the available eigen-solving routines.

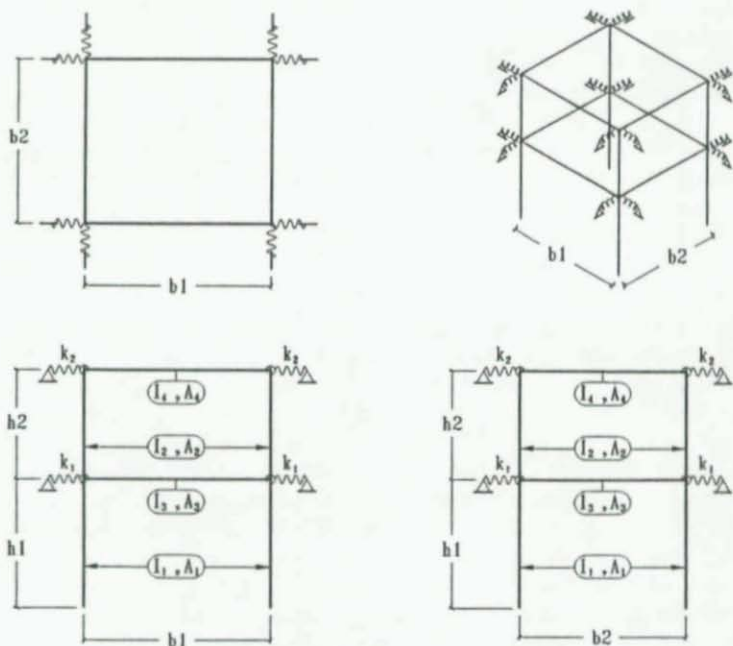


Figure 2. Top, Isometric and side views of the frame with dimensions and cross-sectional properties assignment.

## NUMERICAL RESULTS - CONCLUSIONS

Based on the above mentioned analysis procedure, the critical loads for various values of the considered parameters are computed. The first eight critical loads and their corresponding mode shapes are found. Figure 3 shows as an example the top, isometric and side views of the first side-sway buckling mode shape for the case of the unbraced frame  $k_1 = k_2 = 0$ . The motion of this mode is only observed in the XZ plane and  $P_{cr} = 3.432 h_1^2/EI_1$ . Figure 4 shows the top, isometric and side views of the second side-sway buckling mode shape. The motion of this mode is only observed in the YZ plane and  $P_{cr} = 3.550 h_1^2/EI_1$ . It is observed in this case that both modes could be accurately predicted by two dimensional analysis. Figure 5 shows the top, isometric and side views of the first torsional buckling mode shape. The motion of this mode is observed mainly in the XY plane with the first and second floors turning in same direction, and  $P_{cr} = 4.101 h_1^2/EI_1$ . Figure 6 shows the same views of the third side-sway buckling mode shape. The motion of this mode is observed in the XZ plane and  $P_{cr} = 5.306 h_1^2/EI_1$ . Figure 7 shows the fourth side-sway buckling mode shape. The motion of this mode is observed in the YZ plane and  $P_{cr} = 5.382 h_1^2/EI_1$ . Figure 8 shows the second torsional buckling mode shape. The motion of this mode is observed in the XY plane with the first and second floors turning in opposite directions, and  $P_{cr} = 5.832 h_1^2/EI_1$ . Figure 9 shows the first buckling mode shape in which each floor takes a rhombus shape. Apparently this mode is quite unrealistic since the floor stiffness will not permit that shape. An interesting observation is that this mode has lower critical load than the braced frame. This mode is observed in the XY plane with the diagonals of the first and second floors stretching in opposite directions, and  $P_{cr} = 8.516 h_1^2/EI_1$ . Finally Figure 10 shows the first non-sway buckling mode shape. The motion of this mode is observed in the YZ plane and  $P_{cr} = 11.654 h_1^2/EI_1$ .

Figure 11 shows the effect of the bracing stiffness  $k$  ( $k_1 = k_2 = k$ ) on the critical loads corresponding to all the above mentioned buckling modes. As the bracing stiffness  $k$  increases the critical loads corresponding to the side-sway and torsional modes increase. As one may expect the critical loads corresponding to no-sway modes are not effected by the increase of the bracing stiffness  $k$ . As the bracing stiffness  $k$  increases there is a critical stiffness  $k_{cr}$  at which the the sway-buckling of the unbraced frame is equal to buckling load of the frame with no sway. Any additional increase in the bracing stiffness  $k$  will not result in an additional load carrying capacity. For all examples the principal axes of the columns were oriented



parallel to the X and Y axes. In all these cases the smallest critical load corresponds to the first side-sway mode for bracing stiffness  $k$  less than  $k_{cr}$  and to first sway mode for bracing stiffness  $k$  more than  $k_{cr}$ . In other words the torsional buckling was never the smaller  $P_{cr}$ . If the principal axes of the columns were not parallel to the X and Y axes that may not be the case. When  $k$  is close to zero there is a very drastic increase in the sway and torsional critical loads but for the rest of the range the relationship between bracing stiffness  $k$  and sway critical loads appears to be linear. This observation may be helpful in determining the intersection between the first nonsway and the first sway curves. Figure 12 shows the first nonsway and first sway curves for the case of a) fixed base and rigid connections, b) fixed base and pinned connections and c) pinned base and rigid connections. The critical loads are plotted versus the bracing stiffness  $k$ . The first and second story stiffness was assumed to be the same ( $k_1 = k_2 = k$ ). From this figure one may observe the effect of support fixation and connection rigidity on the critical bracing stiffness.

The minimum critical load  $\min P_{cr}$  versus the second story bracing stiffness  $k_2$  for various values of the first story bracing stiffness  $k_1$  is presented in Figure 13. For a given value of  $k_1$  the  $\min P_{cr}$  increases as  $k_2$  increases and soon reaches a critical value beyond which there is no increase in the  $P_{cr}$ . This indicates that  $k_2$  is sufficiently stiff to restrain the top story and that the critical mode is the side sway of the first floor only. As  $k_1$  increases that critical value increases since it takes more load to sway the first story. As  $k_1$  is sufficiently stiff to restrain the first story the critical mode becomes the nonsway mode (symmetric buckling) as clearly indicated in Figure 13. The minimum critical load  $\min P_{cr}$  versus the first story bracing stiffness  $k_1$  for various values of the second story bracing stiffness  $k_2$  is presented in Figure 14. For a given value of  $k_2$  the  $\min P_{cr}$  increases as  $k_1$  increases and soon reaches a critical value beyond which there is not any increase in the  $P_{cr}$ . This indicates that  $k_1$  is sufficiently stiff to restrain the first story and that the critical mode is the side sway of the top floor only. As  $k_2$  increases that critical value increases since it takes more load to sway the top story. As  $k_2$  is sufficiently stiff to restrain the top story the critical mode becomes again the nonsway mode (symmetric buckling) as clearly indicated in Figure 14.

In order to clarify the results of the last two figures a two dimensional curve fitting technique was employed to generate a surface of the minimum critical load versus  $k_1$  and  $k_2$  and is shown in Figure 15. This interaction

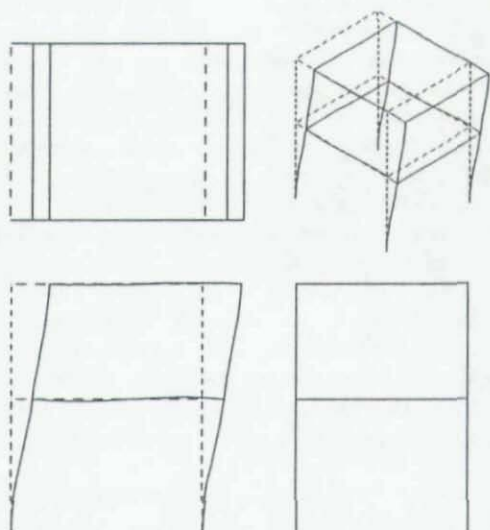


Figure 3. First Side-sway Mode Shape  $P_{cr}=3.432 h_1^2/EI_1$

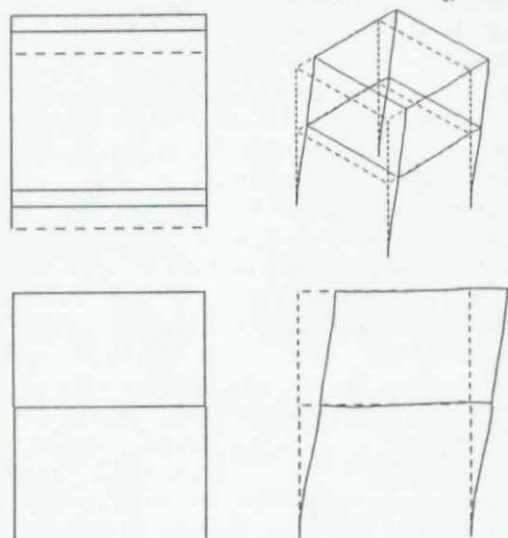


Figure 4. Second Side-sway Mode Shape  $P_{cr}=3.550 h_1^2/EI_1$



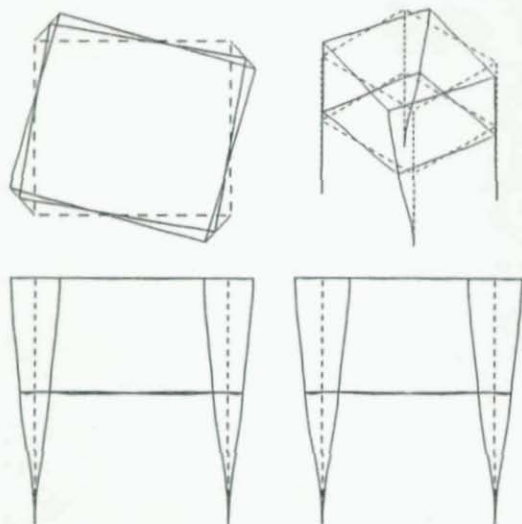


Figure 5. First Torsional Mode Shape  $P_{cr} = 4.101 h_1^2 / EI_1$

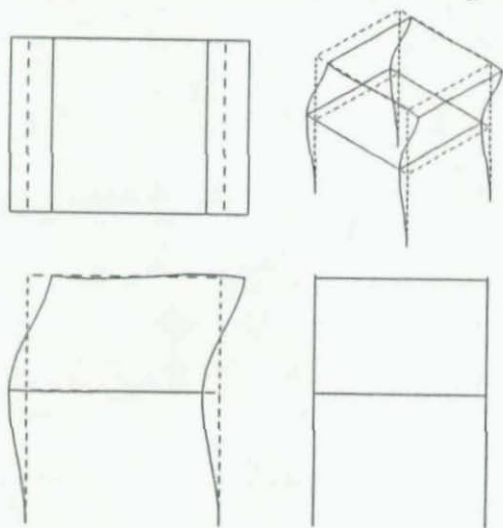


Figure 6. Third Side-sway Mode Shape  $P_{cr} = 5.306 h_1^2 / EI_1$

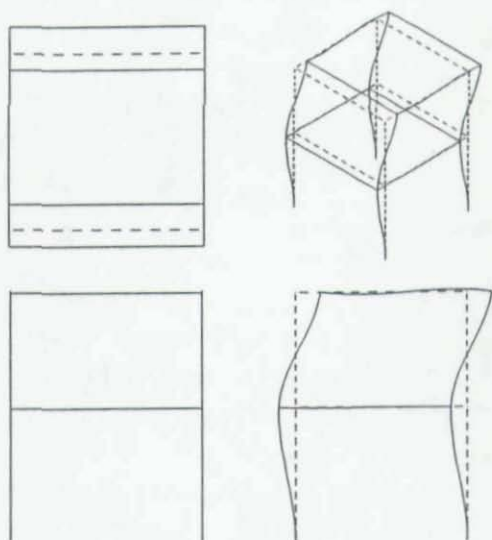


Figure 7. Forth Side-sway Mode Shape  $P_{cr}=5.382 h_1^2/EI_1$

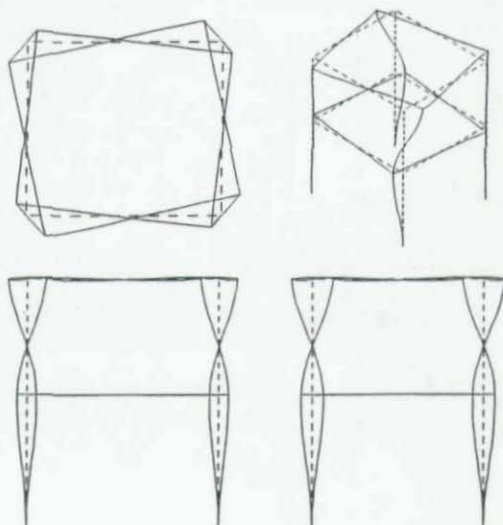


Figure 8. Second Torsional Mode Shape  $P_{cr}=5.832 h_1^2/EI_1$

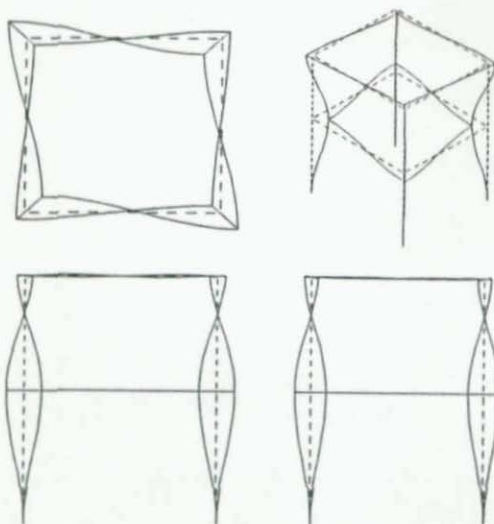


Figure 9. First "Rhombus" Mode Shape  $P_{cr}=8.516 h_1^2/EI_1$

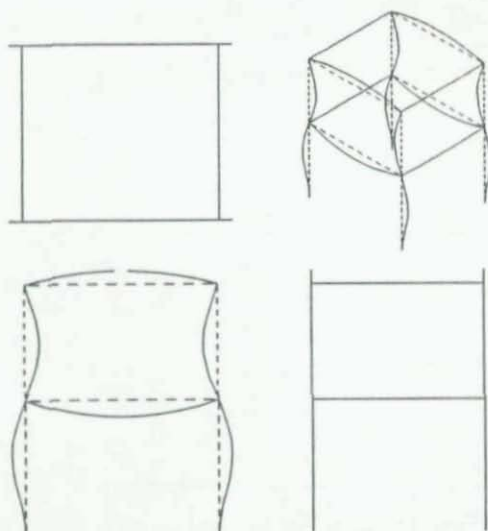


Figure 10 First Non-sway Mode Shape  $P_{cr}=11.654 h_1^2/EI_1$

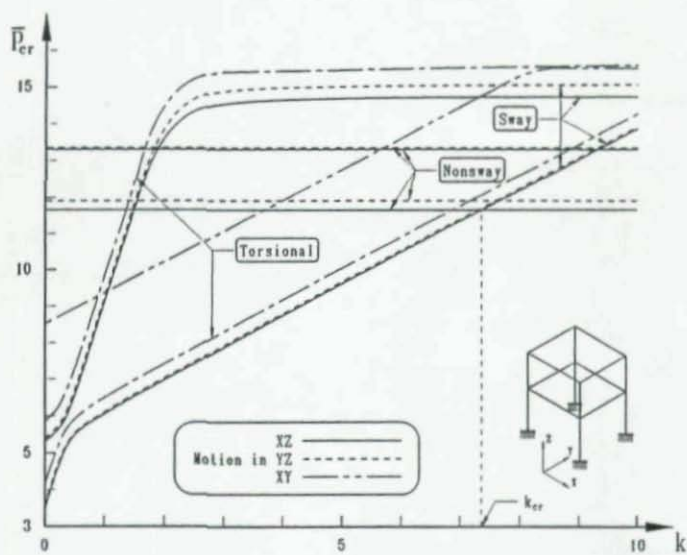


Figure 11. Effect of the Bracing Stiffness  $k$  on the Critical Loads

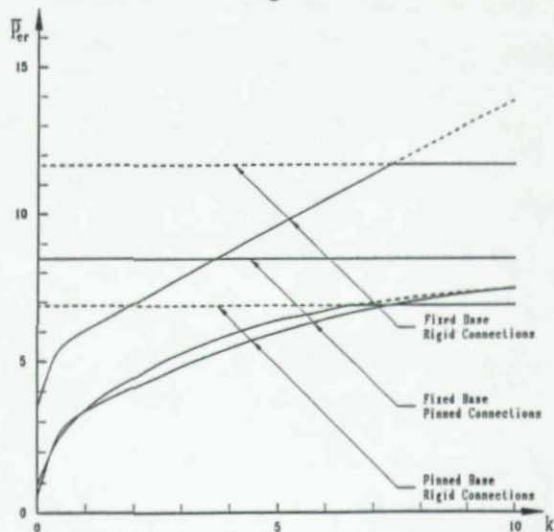


Figure 12. Effect of Support Fixation and Joint rigidity on the Critical Bracing Stiffness

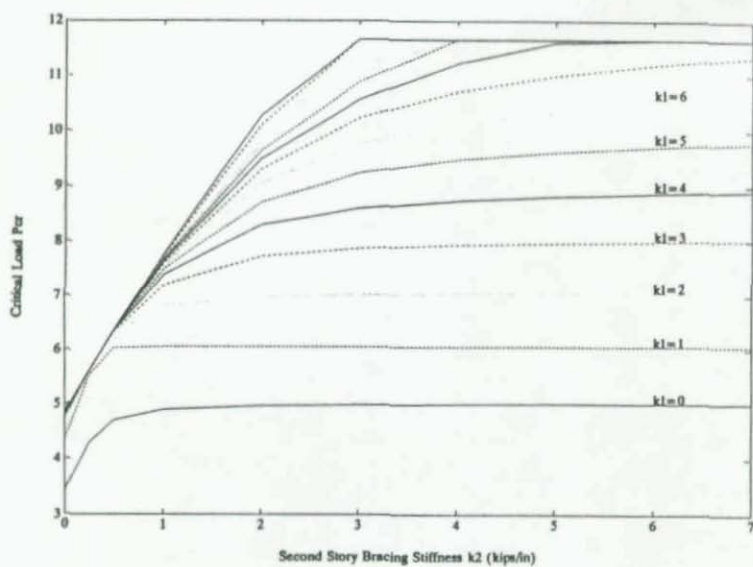


Figure 13. Minimum Critical Load  $\min P_{cr}$  versus  $k_2$

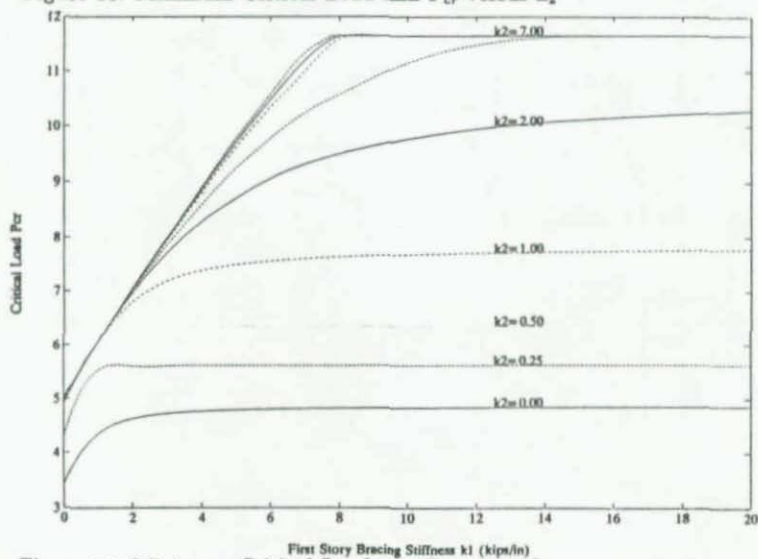


Figure 14. Minimum Critical Load  $\min P_{cr}$  versus  $k_1$

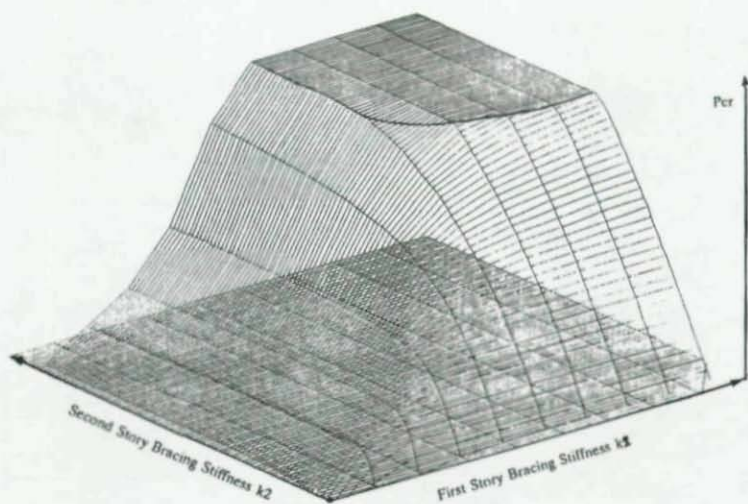


Figure 15. Minimum Critical Load  $\min P_{cr}$  versus  $k_1$  and  $k_2$

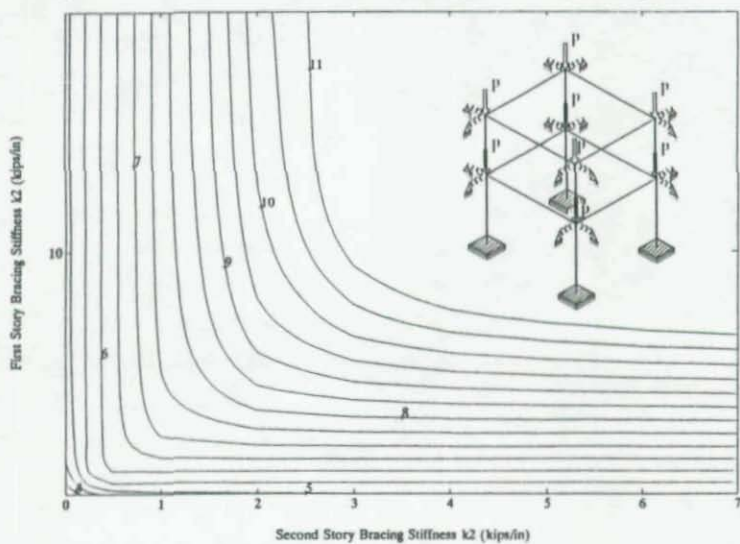


Figure 16. Minimum Critical Load  $\min P_{cr}$  versus  $k_1$  and  $k_2$



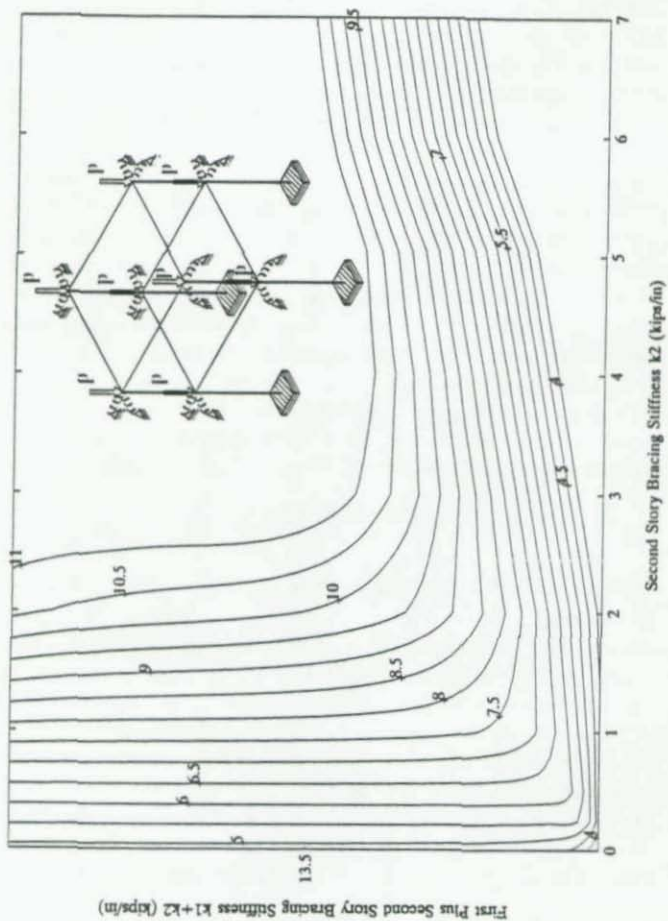


Figure 17. Interaction Curves ( $k_1+k_2$ ) -  $k_2$  for Determining min  $P_{cr}$

surface indicates that the min  $P_{cr}$  increases as  $k_1$  and  $k_2$  increase up to the point they reach the plateau. Figure 16 shows a contour plot of that surface. From this figure one may select the required  $k_1$  and  $k_2$  for the desired  $P_{cr}$ .

Figure 17 presents a surface of the minimum critical load versus  $k_1+k_2$  and  $k_2$  in contour form. Using this figure one may quickly estimate the required  $k_1$  and  $k_2$  for the desired  $P_{cr}$ . Any point on a given  $P_{cr}$  curve will provide adequate bracing. The one point corresponding to the minimum  $k_1+k_2$  can be easily found and is defined as the optimum pair.

In conclusion, the elastic stability analysis of the three dimensional partially braced two story frames shows that either sway or nonsway buckling may control. The torsional buckling is not critical for the range of parameters examined and the orientation of columns considered. For all these cases two dimensional stability analysis would have been sufficient to predict the min  $P_{cr}$ . Use of the presented interaction curves leads to a quick and easy estimation of the minimum total bracing stiffness "optimum critical bracing" required to obtain braced frames critical loads. For all practical purposes the "optimum critical bracing" appears to be close to the case of  $k_1=k_2$ . Further studies need to address the issue of not only the required bracing stiffness but the required bracing force.

#### REFERENCES

- [1] Galambos, T. V., "Lateral Support for Tier Buildings Frames" Engineering Journal, AISC, v. 1, n. 1, January 1964.
- [2] Biswas, M., "Threshold Bracing Stiffness for Two Story Frames" Stability of Metal Structures, Proceeding of Third International Colloquium, May, 1983, pp.389-409.
- [3] A.N. Kounadis, "Interaction of the Joint and of the Lateral Bracing Stiffnesses for the Optimum Design of Unbraced Frames" Acta Mechanica 47, 1983, pp.247-262
- [4] Shyi-Lin Lee and P.K. Basu, "Bracing Requirements of Plane Frames", Proceedings of the 1990 SSRC Annual Technical Session.
- [5] Przemieniecki J. S., "Theory of Matrix Structural Analysis" McGraw- Hill, New York, 1968.
- [6] Vlahinos A. S., Smith C. V. and Simitzes G. J., "A Nonlinear Solution Scheme for Multistory, Multibay Plane Frames", Int. Journal of Computers and Structures, Vol. 22, No.6, 1986, pp. 1035-1045

## BEHAVIOR OF GUSSET PLATE CONNECTIONS UNDER COMPRESSIVE MONOTONIC AND CYCLIC LOADINGS

J.J. Roger Cheng, Jeffrey S. Rabinovitch,  
and Michael C.H. Yam

Department of Civil Engineering, University of Alberta  
Edmonton, Alberta, Canada, T6G 2G7

### ABSTRACT

The behavior of gusset plate connections under compressive monotonic and cyclic loadings were examined by performing full scale tests on diagonal bracing connections. Three different thicknesses with various geometric configurations were used in the testing specimens. The testing program was divided into three phases. The first phase considered the inelastic behavior of gusset plate connections under compression without the effect of frame action. The second phase of the testing program incorporated the effect of frame action by including the beam and column moment and shear. In the third phase, the testing specimens were under cyclic loadings to investigate the energy absorption and ductility performance of the connections.

### INTRODUCTION

Gusset plate connections are frequently used in bridge trusses and braced steel frames. Gusset plates are subjected to either tensile or compressive load from the diagonal bracing member. The load transferred from the diagonal member will produce bending, shear and normal forces in the gusset plate (Gaylord, et al., 1992). Extensive research has been recently conducted into the tensile behavior of gusset plate connections. In particular, Hardash and Bjorhovde (1985) have proposed a block shear tear-out model to determine the ultimate tensile strength of the connection.

When gusset plates are subject to compressive loads, buckling of the gusset plate free edges and local buckling and/or crippling of the gusset plate area near the end of the diagonal member have to be examined. Williams and Richard (1986) performed elastic buckling analysis of gusset plates. They investigated the compressive behavior of gusset plates by excluding the beam and column framing members from the analysis. They also assumed that the bracing member would not buckle and the brace-to-gusset connection was restrained from out-of-plane translations. Cheng and Hu (1987) conducted full-scale tests on gusset plate connections. However, all of the test specimens were designed to fail in elastic buckling. For relatively thick plate, yielding of the plate material may occur prior to the instability failure of the plate. Therefore, inelastic buckling of the gusset plate must be investigated. The most recent experimental investigation of full-scale gusseted connections loaded in compression was performed by Gross (1990). The testing program consisted of three diagonally braced steel subassemblies. However, the test setup did not permit the out-of-plane translation of the bracing member which might have a significant effect on the buckling strength of the gusset plate. The test results showed that the primary failure mode of the gusseted connection loaded in compression was gusset plate buckling. All specimens exhibited yielding before reaching the ultimate load and the first yield load of the specimens agreed well with Whitmore's predictions (1952).

When gusset plates are subject to cyclic loading conditions, reversing cycles of inelastic tension and compression must be investigated. Prior to the present study, no known research has focused on the behavior of gusset plate connections under cyclic loadings.

## TEST PROGRAM

**Specimen Description****1. Monotonic Compression Tests**

A total of fifteen tests were run on thirteen specimens. A 45° brace angle was used for all the tests. When designing the testing program it was assumed that the gusset plate buckled before reaching the failure load of the diagonal bracing member. Hence, rotational restraint was provided by the diagonal member to the gusset plate. Two test series were conducted under monotonic loading. Gusset plate connections were first tested under monotonic loading without the effect of frame action, and then with frame action by including beam and column moments and shears. Two types of test were conducted, namely; the free case and the fixed case. These two loading cases will be defined in the following test setup section. For specimens subject to beam and column moments, only free case tests were performed. However, both types of test were conducted on specimens without the beam and column moments.

A total of thirteen specimens were fabricated using 300W steel. The plate size and thickness used are illustrated in Table 1 and Fig.1. As can be seen in the table, three thicknesses were used for both the GP type (500 x 400) and MGP type (500 x 400) specimens and two thicknesses were used for the CP type (850 x 700) specimens. Both the GP and CP type specimens excluded the effect of frame moments, while the MGP specimens included the frame moments. Two tee sections (WT125x22.5) and two 13.0 mm thick plates were used as the splice member to ensure that the gusset plate buckled before the failure occurred in the spliced section. The specimens were directly welded onto the beam and column.

The ratio of the column moment ( $M_c$ ) to the beam moment ( $M_b$ ) was chosen to be 0.5 in this test series. The beam and column moment magnitudes for the MGP specimens are shown in Table 1. It can be seen from the table that two moment levels were used to investigate the significance of the effects of the beam and column moments.

**2. Cyclic Loading Tests**

In the cyclic testing series, a sequence of five specimens was tested. The three test parameters considered were plate thickness, stiffness of the plate free edge, and the geometry of the plate such that the formation of a plastic hinge is facilitated. A 45° brace angle was used for all tests in this series. In order to simplify the test set-up, the effects of the framing members on the gusset plate were neglected in this phase of the testing program. When designing the testing program, it was assumed that the gusset plate buckles before reaching the failure load of the diagonal bracing member. Hence, the diagonal bracing member provides rotational restraint to the gusset plate. All specimens in this series were tested under the 'free case' condition, which will be defined in the test setup section.

A total of five specimens were tested in this series. The plate size and thickness of the specimens are shown in Table 2 and a typical gusset plate specimen is shown in Fig.2a. All specimens were rectangular in shape with the exception of specimen A-5, which was designed to allow the free formation of a plastic hinge under compressive buckling deformations (Fig. 2b). Stiffeners were welded onto the free edges of specimens A-3 and A-4 in an attempt to increase the energy absorbing capacity of these specimens.

Two tee sections (WT125x22.5) and two 10 mm thick plates were used as a splice member to ensure that the gusset plate failed prior to the splice assembly. The 9.32 mm specimens were connected to the splice member with five rows of ASTM A325 high strength bolts designed for bearing. The 6.18 mm specimens utilized ASTM A490 bolts in order to achieve a slip-critical connection. Due to the loads realized in the connection, all 9.32 mm test specimens underwent major connection slip at some point during the loading history. Since the focus of this paper is the behavior of the individual gusset plates, no further discussion of connection slip will be included in this paper. The specimens were directly welded onto the beam and column.

**Test Setup and Instrumentation**

Two test setups were used in the testing program. For the specimens tested under cyclic



loadings, the test setup as shown in Fig.3 was used. Two W310x129 sections were used as the beam and column. The diagonal bracing member (W250x67) was restricted to translations within the plane of gusset plate by the restraint provided by a pair of lateral bracing assemblies fixed to the frame of the testing machine. In order to allow the set-up to sway out-of-plane under both compressive and tensile loadings, 'free case' condition, the test frame was sandwiched between a set of rollers at each end of the set-up. A guided rod mechanism at each end of the set-up was adjusted throughout the test to prevent a sudden kicking out of the frame. The same general test setup was utilized for the specimens tested under monotonic loading without frame moments. However, since the specimens were tested under compressive loadings, the tensile reaction frame was omitted from the test setup. For the fixed case testing, rollers under the test frame were removed and stoppers were attached to the test frame to prohibit any frame movement. The axial load to the brace member was applied by the MTS testing machine.

For the test setup including the effect of beam and column moments, a separate test frame was constructed to permit the application of axial load from the bracing member and the moments on the beam and column to which the gusset plate is attached. This loading frame is shown schematically in Fig.4. The axial load to the brace is applied by a two loading jack system which is used to resist the secondary moment produced by the out-of-plane displacement of the gusset plate. The beam and column moment is produced by the tension rod as shown in Fig.4.

Linear variable differential transformers (LVDT) were used to measure the buckled shape of the gusset plate and both the in-plane and out-of-plane displacement of the test frame. Strain gauges and rosettes were mounted on the gusset plate to measure the strain distribution and to detect any strain bifurcation. The data recorded from the strain gages, LVDTs, and the MTS testing machine were monitored by a data acquisition system. Whitewash was applied to all specimens to monitor the yielding process.

## **Test Procedure**

### **1. Monotonic Compression Tests**

For the specimens tested without the application of frame moments, the load was applied incrementally to the specimens. Smaller load increments were used once yield lines were observed on the specimen in order to capture the yielding process. After each load increment, the specimens were allowed to stabilize prior to the application of the next load step.

For the specimens with the effect of frame moments included, a similar loading procedure was employed. However, a small axial load (approximately 20% of the Whitmore load of the specimen) was applied prior to the application of the beam and column moments. The test was terminated when the out-of-plane displacements of the gusset plate reached the physical limit of the out-of-plane measuring devices.

### **2. Cyclic Loading Tests**

All specimens were tested under reverse loading conditions. Each test began with a series of cycles in the elastic range. Elastic cycles were conducted at 10% and 50% of the expected tensile yield load based on the Whitmore yield capacity (1952) and nominal material properties. During each cycle, the specimen was initially loaded in tension to the desired maximum cycle load. The specimen was then unloaded from tension, and cycled through to the same load level in compression.

The inelastic loading sequence began with a set of yield cycles at 100% of the expected tensile yield load. Subsequent inelastic cycles were conducted under increasing levels of axial plate deformation. During each cycle, the specimen was initially loaded in tension to a predetermined level of axial deformation. The specimen was unloaded and then deformed in compression to the same axial deformation level, as referenced to the plate deformation level after tension unloading of the same cycle. The level of axial plate deformation was increased sequentially throughout the testing cycles until the tensile failure of the specimen was achieved. Failure in tension was signified by a decrease in specimen load under increasing MTS stroke. The test was concluded by loading the specimen in compression until an excessive level of compressive plate deformation was achieved.

## TEST RESULTS

### 1. MONOTONIC COMPRESSION TESTS

#### Test Specimens Without Beam and Column Moment

##### **Free Case**

The test results of the free case specimens are shown in Table 3. As can be seen from the table, the buckling load of the specimens increased with increasing plate thickness for the same plate size. The curves of applied load versus lateral displacement of the test frame are shown in Fig. 5 for both types of specimens. This figure illustrates that for the same plate thickness, the GP type specimens showed significantly higher ultimate load than the CP type specimens. All the tests showed slight lateral displacement of the test frame before buckling occurred. The CP type specimens exhibited more ductile behavior than the GP type specimens as shown in Fig. 5. The buckled shapes of the free edges and along the centerline of the spliced member of the specimens resembled the buckled shape of a fixed-guided column.

During the tests, extensive yielding was observed for the GP type specimens, except specimen GP3 which showed moderate yielding at the gusset plate region beneath the splice member before reaching the ultimate load. The yield lines for specimens GP1 and GP2 started at the gusset plate region beneath the splice member and subsequently progressed towards the beam and column support boundaries, then to the area about the two sides of the spliced member, and finally to the gusset plate free edges. In addition, yield lines on specimen GP1 spread almost entirely throughout the gusset plate. For specimen CP1, moderate yielding was observed on the gusset plate near the corner of the beam and column support boundaries. Specimen CP2 showed slight yielding in a region about the sides of the splice connection near the base of the splice member. Significant bending strains of the gusset plate were detected from the beginning of loading for the CP type specimens due to the presence of initial imperfections induced by the welding process.

##### **Fixed Case**

Three new GP type specimens were fabricated and tested in the fixed case since excessive permanent deformation was observed in the failed specimens from the free case tests. However, the same CP type specimens were used for both free and fixed case testing. The test results are also shown in Table 3. Again, the buckling load of the specimens increased with increasing plate thickness as illustrated in the table. The load versus lateral deflection at mid-length of the gusset plate long free edge for both types of specimens are shown in Fig. 6. The curves indicated that the GP type specimens remained relatively straight until reaching the buckling load. Specimen CP2 showed a different load deflection behavior due to the initial imperfection induced by the slight permanent deformation developed after the free case test. The buckled shapes of the two free edges and the centerline of the splice member to the support boundary resemble the buckled shape of a fixed column.

For specimen GP1 and GP2, yield lines started at the gusset plate region beneath the splice member; then progressed towards the beam and column support boundary, the area about the sides of the splice member, and finally extended to the free edges. This yield line pattern was very similar to that of the free case tests. On the other hand, moderate yielding was observed in specimen GP3 at the gusset plate region beneath the splice member when the applied load approached the ultimate load. For the CP type specimens, bending of the gusset plate free edges was detected from the beginning of loading due to the presence of initial imperfection in the gusset plate caused by the slight permanent deformation produced after the free case tests and the welding process. The rosette gages and strain gages mounted on the gusset plate indicated that yielding had occurred extensively in specimen CP1 due to the bending effects. However, specimen CP2 only showed yielding in the gusset plate region beneath the splice member and in part of the area about the sides of the splice connection near the end of the splice member.

When comparing the results of the free case and the fixed case, it was found that the increase in buckling load by restraining the out-of-plane movement of the test frame was not significant except for specimen CP2. This may be due to the fact that all the specimens except CP2 experienced reasonable amount of yielding before reaching the buckling load. Hence it can be



seen that the inelastic buckling load of the specimen might be close to its material strength. Therefore, the increase in buckling load of the specimens by providing more restraint might not be significant.

#### **Test Specimens With Beam and Column Moment**

The results of this series of tests are shown in Table 3. The load versus lateral displacement curves for all the MGP type specimens are shown in Fig. 7. It can be seen from this figure that all the specimens deformed laterally when load was applied. After reaching the buckling load, a gradual unloading of the specimens was observed. The beam and column moments also affected the out-of-plane stiffness of the gusset plate. This fact can be realized from the behavior of the MGP3 specimens that the out-of-plane stiffness specimens increased with increasing beam and column moments.

The load versus in-plane deformation of the gusset plate curves for all the specimens, except specimen MGP1, are shown in Fig. 8. Specimen MGP1 was omitted because it has a slightly different arrangement of instrumentation than the other specimens. Fig. 8 shows that the specimens maintained a certain load level after buckling had occurred. However, the drop in load from the buckling load to that particular load level happened without significant in-plane deformation. The effect of beam and column moments on the in-plane stiffness of the gusset plate is also illustrated in this figure. It can be seen from this figure that for specimens MGP3 the in-plane stiffness of the specimens decreased as the beam and column moment increased. This behavior can also be realized from the rosette readings which showed that the higher the beam and column moment, the earlier the yielding at the rosette locations on the gusset plate beneath the splice member.

Although earlier yielding of the gusset plate in the region beneath the splice member was observed for the specimens with beam and column moments, the pattern and process of yielding was very similar to that of the specimens without beam and column moments. Basically, yielding started earlier in the region beneath the splice member, then progressed to the beam and column boundary and the area about the sides of the splice member. As buckling approached, yield lines extended towards the free edges. The theoretical yield load of the specimens is defined as the Whitmore load (1952) which is also shown in Table 3 for all the specimens. Test results show that the ratio of the first yield load (defined as the load level at which first yielding at the rosettes occurred) to the Whitmore load ranges from 0.63 to 0.18. In particular, the ratio changes from 0.33 to 0.18 for specimens MGP3 and MGP3-A, respectively, when the beam and column moment was increased by fifty percent.

It was observed from the strain gages reading that the tensile strain induced by the moments at the boundary of the beam and column decreased rapidly towards the inside corner of the gusset plate, hence, a high stress gradient existed along this boundary. The beam and column moments also initiated tension yielding in the vicinity of the corners of the free edges, near the boundary for the MGP3 specimens. As shown from the failed specimens (MGP3 and MGP3-A), this tension yielding allowed the corner of the free edges to rotate when buckling occurred. Hence, the mode of buckling for these specimens resembled the buckled shape of a pinned-guided column. However, for the other specimens a fixed-guided mode was observed.

#### **Comparison of Specimens With and Without Beam and Column Moment**

In general, the beam and column moment has negligible effects on the buckling strength of the specimens as illustrated in Table 3. Almost identical buckling loads were obtained for all specimens of the same thickness regardless of the existence of the beam and column moments. The in-plane stress distribution in the gusset plate region beneath the splice member was significantly affected by the presence of the beam and column moment. Earlier yielding was observed for the specimens with the beam and column moments. However, for the specimens without the beam and column moment, compression yielding occurred at a load level very close to the corresponding Whitmore load. The buckled shape of the free edges for the 6.5 mm thick specimens was also influenced by the beam and column moment.

## 2. CYCLIC LOADING TESTS

The material properties of the test specimens are shown in Table 2. The ultimate tensile and compressive loads obtained during testing are recorded in Table 4. The ultimate load is defined as the maximum load level reached by a specimen throughout its cyclic loading history.

### **Tensile Behavior**

The ultimate tensile load carrying capacity of the test specimens is recorded in Table 4. The test specimens were well behaved under tensile loading. In all test specimens, tensile yielding began on the gusset plate about the sides of the splice member at mid-height. As the level of tensile axial deformation and corresponding load level increased, the yielding increased upwards and outwards towards the free edge of the plate specimens. In all test specimens, a large level of axial deformation was achieved prior to failure in tension. In addition, it was observed that the tensile behavior of the test specimens was not notably affected by the cyclic loading history and the significant deformations realized during the compressive portion of the loading. The tensile failure mode for all specimens was a fracture of the plate material between the bolts in the bottom row of the splice member connection. A typical load versus axial deformation curve is shown by the tension portion of Fig. 9.

Plate thickness was the primary variable affecting the tensile capacity of the specimens. From the test loads recorded in Table 4, it is evident that the ultimate tensile capacity of the gusset plates tested was not significantly affected by either the addition of plate free edge stiffeners or the plate geometry. It is observed that all specimens with the same plate thickness and the same connection geometry reached approximately the same ultimate load level in tension. Also provided in Table 4 is a comparison of the actual tensile capacities obtained during testing to the *predicted ultimate tensile strength for each specimen. The predicted tensile strengths are based on the block shear tear-out capacity proposed by Hardash and Bjorhovde (1985).* It is shown that the test results are in relatively strong agreement with the predicted capacities, even though Hardash and Bjorhovde's analysis was based on monotonically loaded specimens.

### **Compressive Behavior**

#### **9.32 mm Specimens -**

Specimen A-1 - The compressive buckling load for specimen A-1 is shown in Table 4. During the test, yielding of the specimen was initiated along the welded boundary between the gusset plate and the testing frame. As the axial deformation level increased, yielding was observed on the gusset plate at the base of the splice member, signifying the onset of yielding in the Whitmore (1952) critical region. When overall plate buckling occurred, the long free edge of the gusset plate buckled, allowing the specimen to deform significantly out-of-plane. The load carrying capacity of the specimen dropped significantly after overall plate buckling occurred. The maximum cycle loads reached during the successive post-buckling cycles slowly deteriorated as the level of axial compressive deformation increased.

Specimen A-3 - Plate stiffeners (50 x 9.32 mm) were welded to both free edges of the specimen. During the test, yielding initially progressed in a pattern similar to that of specimen A-1. However, the presence of the plate free edge stiffeners prevented the specimen from undergoing overall plate buckling at the same load level as specimen A-1 (Table 4). The specimen initially buckled locally in a confined region beneath the splice member. Only when the edge stiffeners began to yield was the maximum compressive capacity of the specimen achieved. As the stiffeners continued to yield under cycles of increasing axial deformation, the plate began to buckle in a pattern similar to specimen A-1. In addition, the presence of the edge stiffeners prevented the specimen load carrying capacity from dropping significantly once buckling occurred.

Specimen A-5 - Based on Astaneh's (1985) recommendations, a plastic hinge region of width  $2t$ , where  $t$  is the thickness of the test specimen, was provided for at the base of the splice member (Fig. 2b). Astaneh's study considered the cyclic out-of-plane buckling of double angle bracing and concluded that restraints on the free formation and the rotation of plastic hinges leads to *premature fracture in the gusset plate. In order to accommodate the free formation of a plastic hinge in the specimen geometry, the splice member had to be placed further away from the base*

of the gusset plate. The change in specimen geometry greatly affected the specimen response. Although the specimen yield pattern was not unlike the other specimens of the same plate thickness, yielding and plate buckling occurred at significantly lower load and axial deformation levels. The specimen geometry required to accommodate the plastic hinge region produced a gusset plate that was less stable under cyclic loads. As such, the ultimate compressive capacity of the specimen was sacrificed (Table 4). The specimen initially deformed in a buckled shape similar to that of specimen A-1. However, as the cyclic axial deformations continued, a secondary buckle, extending from the base of the splice member out and upwards towards the plate free edge, began to develop. As the inelastic cycles progressed, the post-buckling load carrying capacity of the specimen continued to deteriorate. Ironically, the geometry of the specimen caused a concentration of out-of-plane deformations at the gusset plate to test frame connection, resulting in a fracture of the weld at this location as the axial deformation level, and the resulting out-of-plane buckling deformations, increased. Therefore, the test results indicate that no benefit was derived from providing for the free formation of a plastic hinge in the geometry of the type of gusset plate investigated in this study.

#### 6.18 mm Specimens -

**Specimen A-2** - The compressive buckling load for specimen A-2 is shown in Table 4. During the testing, yielding was initiated during the elastic cycles at a compressive load of 50% of the expected tensile yield load. Yielding of the specimen plate began in a region beneath the splice member, near the bottom of the specimen. As the loading progressed in the inelastic range, yielding progressed prior to buckling of the specimen. The overall plate buckling of the specimen was accompanied by a significant drop in the load carrying capacity of the specimen. Both plate free edges buckled in order to allow the specimen to undergo significant out-of-plane deformations. The plate buckle extended from the base of the splice member out towards the middle of the plate free edges. As the cyclic axial deformation levels continued to increase, the load carrying capacity of the specimen deteriorated very little from its initial post-buckling level (Fig.9). The relatively stable post-buckling capacity is likely due to the formation of a yield line mechanism within the specimen. With an increasing level of axial compressive deformation, additional buckles developed on the specimen plate and yielding was observed along the welded boundary between the gusset plate and the test frame.

**Specimen A-4** - Plate stiffeners (50 x 6.18 mm) were welded to both free edges of the specimen plate. The dimensions of the plate stiffeners were designed such that the strong axis (out-of-plane) bending stiffness for the stiffeners of specimens A-2 and A-4 was proportional to the thickness of the individual specimen. During the test, yielding was initiated beneath the splice member during the yield cycle at a compressive load equal to 100% of the expected tensile yield load. As the test loading continued into the inelastic region, yielding progressed at the base of the splice member as a localized buckle began to form. Although the ultimate compressive load reached was not significantly different than that obtained during the testing of specimen A-2 (Table 4), the presence of the plate free edge stiffeners greatly affected the post-buckling behavior of the specimen. Initially, as the axial compressive deformation level increased, the plate edge stiffeners prevented the plate from undergoing overall plate buckling. The edge stiffeners yielded to allow the specimen to deform out-of-plane, but the deformations remained localized. However, as the axial deformation level increased, the plate buckle extended outwards towards the plate free edges. Ultimately, the plate free edge stiffeners themselves buckled both in-plane and out-of-plane, allowing overall plate buckling to occur. As the axial deformation level and the out-of-plane buckling deformations increased, the load carrying capacity of the specimen slowly deteriorated from the maximum compressive load reached. Unlike specimen A-2, buckling of the specimen was not immediately followed by a significant drop in specimen load carrying capacity (Fig.10). As such, the energy absorption capacity of the gusset plate was increased by the addition of the plate free edge stiffeners.

#### Comparison of Test Results -

The actual test capacities were compared to predicted capacities based on current design methods. The Whitmore (1952) load ( $P_w$ ) and the Thornton (1984) load ( $P_t$ ) were computed for each specimen using the actual dynamic material properties. The predicted capacities and the ratios of the actual test capacities to the Whitmore load and to the Thornton load are shown in Table 4. In all cases the Thornton load underestimated the cyclic buckling strength of the test



specimens. In addition, the actual test capacities were compared to the load ratios obtained by the authors for similar gusset plates under monotonic loading (GP specimens under free condition - Table 3). It can be observed that cyclic loading significantly reduces the ultimate compressive strength of steel gusset plates. The observed decrease in ultimate compressive capacity under cyclic loading conditions may be partially due to the Baushinger effect.

## SUMMARY AND CONCLUSIONS

### 1. MONOTONIC COMPRESSION TESTS

- 1) The buckling load of the specimens increases with increasing plate thickness regardless of the presence of the beam and column moments.
- 2) Out-of-plane restraint does not significantly affect the buckling load of the GP and CP type specimens.
- 3) For the same plate thickness, specimen buckling load decreases with increasing plate size
- 4) The beam and column moment has a negligible effect of the buckling strength of the specimens tested
- 5) Beam and column moments initiated earlier compression yielding at the Whitmore critical section and tension yielding in the vicinity of the corner of the free edges in the specimens.
- 6) In-plane stiffness of the specimens decreases with increasing beam and column moments.

### 2. CYCLIC LOADING TESTS

- 1) The tensile behavior of gusset plates under cyclic loads is well defined by the block shear tear-out model proposed by Hardash and Bjorhovde (1985)
- 2) All specimens with the same plate thickness and the same connection geometry reached approximately the same ultimate load level in tension
- 3) Ultimate compressive capacities are significantly lower than those obtained during monotonic testing
- 4) The behavior under cyclic loads can be improved by providing stiffeners for the free edges of the gusset plate
- 5) Stiffened specimens yield a more stable post-buckling response, resulting in an increased energy absorption capacity
- 6) When the free formation of a plastic hinge is provided for in the specimen geometry, a significant decrease in cyclic compressive load carrying capacity is observed

## REFERENCES

- Astaneh-Asl, A., S.C. Goel, and R.D. Hanson, "Cyclic Out-of-plane Buckling of Double Angle Bracing," *ASCE Journal of the Structural Division*, Vol. 111, No. 5, May, 1985, pp. 1135-1153.
- Cheng, Roger J.J., and Hu, S.Z., "Compressive Tests of Gusset Plate Connections," *SSRC 1987 Annual Conference*, March 24-25, Houston, Texas.
- Gaylord, E.H., Gaylord C.H., and Stallmeyer, J.E., *Design of Steel Structures*, McGraw-Hill, New York, 3rd edition, 1992.
- Gross, John L., "Experimental Study of Gusseted Connections," *Engineering Journal of the AISC*, Vol. 27, No. 3, 1990, pp. 89-97.
- Hardash, Steve G., and Bjorhovde Reidar, "New Design Criteria for Gusset Plates in Tension," *Engineering Journal of the AISC*, Vol. 22, No. 2, 1985, pp. 77-94.
- Thornton, William A., "Bracing Connections for Heavy Construction," *Engineering Journal of the AISC*, Vol. 21, No. 3, 1984, pp. 139-148.
- Whitmore, R.E., "Experimental Investigation of Stresses in Gusset Plates," *Bulletin No. 16*, Engineering Experiment Station, University of Tennessee, May 1952.
- Williams, George C., and Richard, Ralph M., "Steel Connection Designs Based on Inelastic Finite Element Analysis," *The University of Arizona*, 1986.

Table 1. Specimen Description - Monotonic Series

Beam and Column Moment (kN-m)	Specimen	Plate Size (mmxmm)	Plate Thickness (mm)	Static Yield Strength (MPa)
$M_b=0$	GP1*	500x400	13.3	295
	GP2*	500x400	9.8	305
	GP3*	500x400	6.5	275
$M_c=0$	CP1	850x700	13.3	295
	CP2	850x700	9.8	305
$M_b=250$ $M_c=125$	MGP1	500x400	13.3	295
$M_b=250$ $M_c=125$	MGP2	500x400	9.8	305
$M_b=250$ $M_c=125$	MGP3	500x400	6.5	275
$M_b=375$ $M_c=187.5$	MGP3-A	500x400	6.5	275
$M_b=0$ $M_c=0$	MGP3-B	500x400	6.5	275

\* Separate specimens were fabricated for both the free and fixed cases

Table 2. Specimen Description - Cyclic Series

Specimen	Plate Size (mmxmm)	Plate Thickness (mm)		Material Properties	
				Yield Strength (MPa)	Ultimate Strength (MPa)
A-1	550x450	9.32	-	449	537
A-2	550x450	6.18	-	443	530
A-3	550x450	9.32	Stiffened Free Edge	449	537
A-4	550x450	6.18	Stiffened Free Edge	443	530
A-5	550x450	9.32	Plastic Hinge	449	537

Table 3. Summary and Comparison of Test Results - Monotonic Series

Specimen	Free Case	Fixed Case	Whitmore Load	$\frac{P_{Free}}{P_W}$
	$P_{Free}$ (kN)	$P_{Fixed}$ (kN)	$P_W$ (kN)	
(1)	(2)	(3)	(4)	(5)
GP1	1956	2057	1216	1.61
GP2	1356	1487	930	1.46
GP3	742	790	555	1.34
CP1	1606	1760	1852	0.87
CP2	1010	1477	1416	0.71
MGP1	1933	-	1216	1.59
MGP2	1316	-	930	1.42
MGP3	721	-	555	1.30
MGP3-A	819	-	555	1.48
MGP3-B	821	-	555	1.48

Table 4. Summary and Comparison of Test Results - Cyclic Series

Specimen	Plate Size (mm)	Ultimate Tensile Load (KN)	Bjarhovde Tension Tear-Out (KN)	Ultimate Compressive Load $P_{comp}$ (KN)	Whitmore Load $P_w$ (KN)	Thornton Load $P_t$ (KN) $K = 0.65$	$\frac{P_{comp}}{P_w}$	$\frac{P_{comp}}{P_t}$
A-1	550x450x9.32	1794	1960	1682	1718	1500	0.98	1.12
A-2	550x450x6.18	1340	1282	1128	1122	841	1.01	1.34
A-3	550x450x9.32	1884	1960	2004	1718	1500	1.17	1.34
A-4	550x450x6.18	1265	1282	1149	1122	841	1.02	1.37
A-5	550x450x9.32	1887	1960	907	1718	898	0.53	1.01

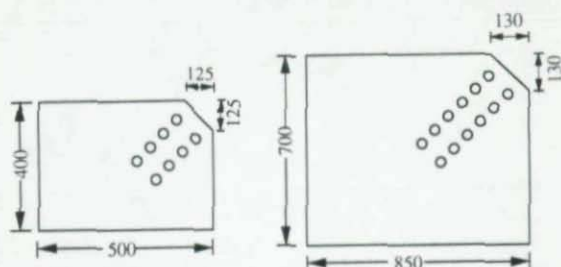


Figure 1. Specimens Description - Monotonic Series

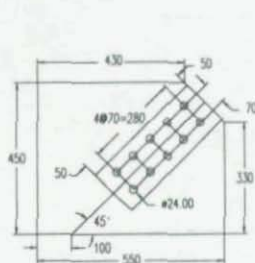


Figure 2a. Typical Specimen Geometry - Cyclic Series

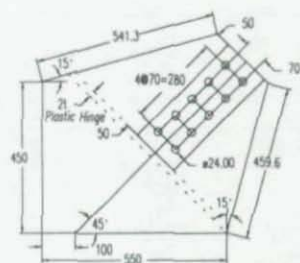


Figure 2b. Plate Configuration of Specimen A-5 - Plastic Hinge



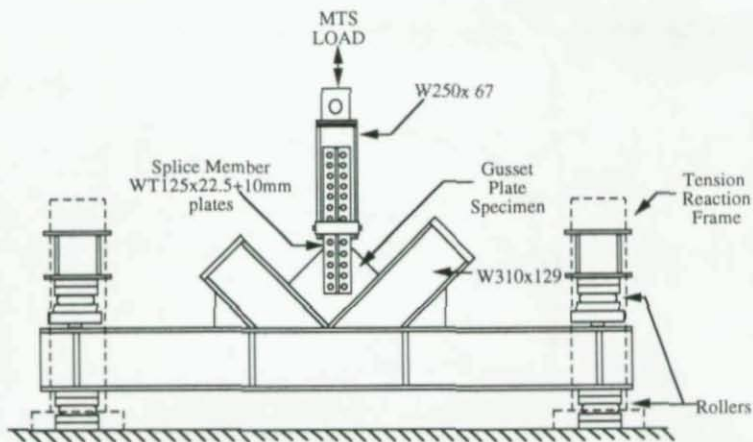


Figure 3. Test Setup - Without Frame Moments

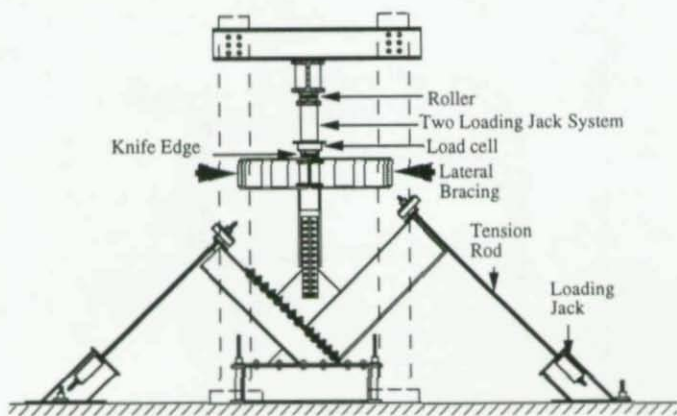


Figure 4. Test Setup - With Frame Moments

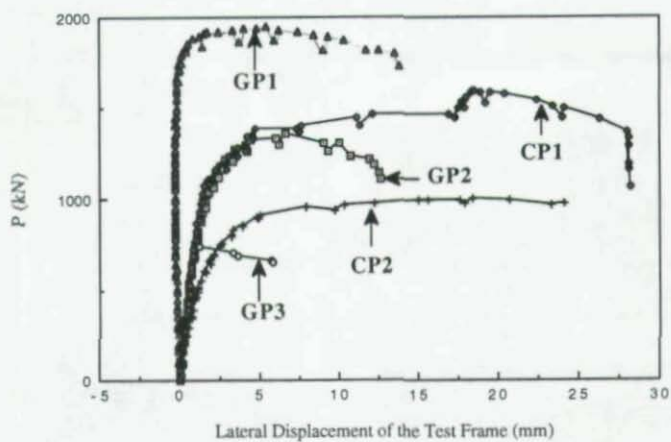


Figure 5. Load Versus Lateral Displacement for Free Case Without Frame Moments

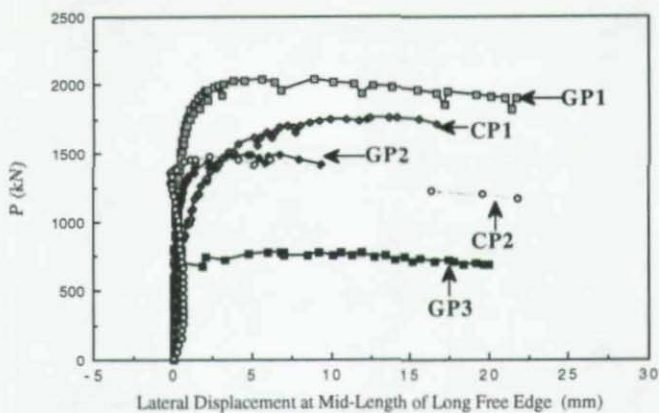


Figure 6. Load Versus Lateral Displacement at Mid-Length of Long Free Edge Without Frame Moments

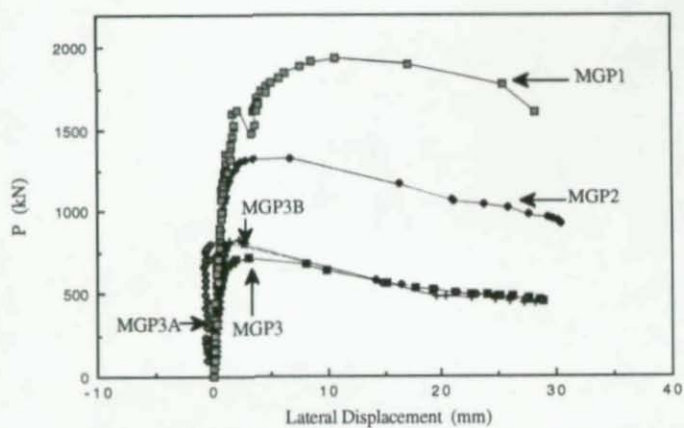


Figure 7. Load Versus Lateral Displacement with Frame Moments

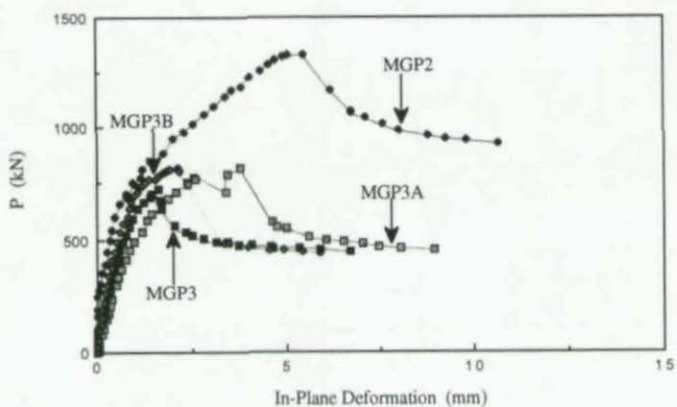


Figure 8. Load Versus In-Plane Deformation for MGP Type Specimens

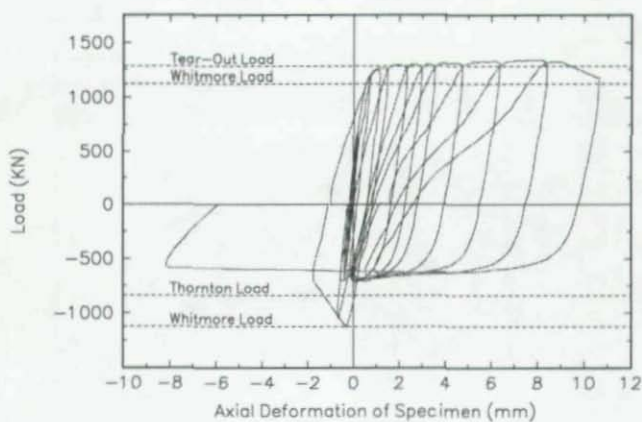


Figure 9. Load versus Axial Deformation - Specimen A-2

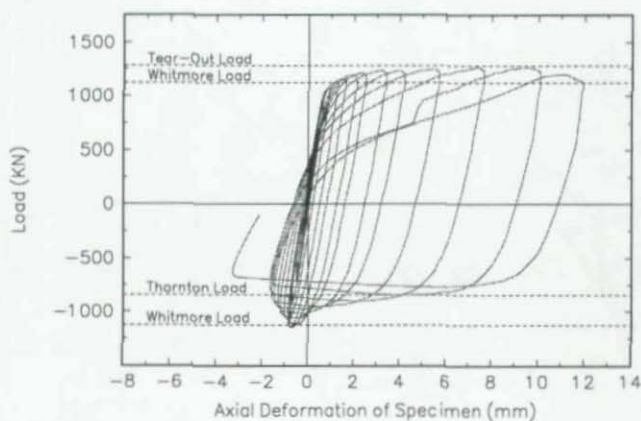


Figure 10. Load versus Axial Deformation - Specimen A-4

AN EXPERIMENTAL STUDY OF INTERACTIVE BUCKLING  
OF ROLLED THIN-WALLED H-COLUMNS

Toshitaka Yamao\*  
Assistant Professor of Civil  
and Environmental Eng.

Tetsuhiko Aoki\*\*  
Professor of Civil Eng.

Tatsuro Sakimoto\*  
Professor of Civil and Environmental Eng.

\* Kumamoto University  
Kurokami Kumamoto, 860 JAPAN

\*\* Aichi Institute of Technology  
Toyota, 470-03 JAPAN

### ABSTRACT

Rolled columns composed of highly thin steel plates are one of the relatively new structural members which fail due to overall and local buckling in usual use condition. An experimental study is carried out to present fundamental data concerning the ultimate strength of rolled thin-walled columns with a relatively large width-to-thickness ratio of the flange and the web plate subjected to concentric and eccentric compression. A total of 36 specimens with various slenderness and width-to-thickness ratios of the component plates was tested. The predictions for the interactive buckling strength of rolled H-section columns by AISC form factor method are found to give fairly accurate results for the columns tested. A simple method to compare the cost performance or to select the minimum weight section profiles is proposed. It is also shown the advantage of this kind thin-walled rolled compression members is clear when they are used in a relatively slender range.

### 1. INTRODUCTION

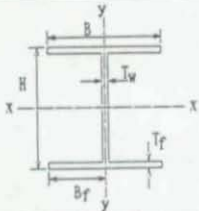
Thin H-section members made by the improved hot rolling process are one of the relatively new structural products. Sections of this type are composed of highly thin and light plates. When thin plates are utilized as component plate element of compression member, the design consideration must be given to the occurrence of the local plate buckling. Though ultimate strength of welded H-section columns has been investigated experimentally and theoretically, few studies have been reported on overall buckling local buckling tests of rolled members[1,2,3,4,5]

This paper presents the results of ultimate strength test for thin-walled columns with rolled H-section which fail by local instability under the interaction between flange and web plate. Since local buckling of the thin component plates may occur before the compressive stress in the plate attained to the yield stress in this region of the ratio, it is important to clarify the ultimate strength of the columns with those large width-to-thickness ratio including the effects of interactive behaviour.

For a thin-walled compression member, the effects of structural imperfections such as residual stresses and initial deflection of the plate have a significant influence on the interactive

Table 1 Measured cross sectional dimensions and properties

Type	H (mm)	B (mm)	T <sub>w</sub> (mm)	T <sub>f</sub> (mm)	A (cm <sup>2</sup> )	I <sub>y</sub> (cm <sup>4</sup> )	r (cm)	H/T <sub>w</sub>	B <sub>f</sub> /T <sub>f</sub>	R <sub>w</sub>	R <sub>f</sub>
A	150.8	100.6	3.36	4.48	13.78	76.0	2.35	42.2	11.1	1.07	0.79
B	200.5	100.7	3.39	4.56	15.77	77.9	2.23	56.6	11.1	1.44	0.80
C	242.5	133.4	3.57	4.58	20.09	151.2	2.74	67.7	13.6	1.60	1.08
D	251.5	150.6	3.43	4.61	22.38	262.7	3.43	70.7	16.3	1.67	1.12



A : Cross sectional area  
I<sub>y</sub> : Geometrical moment of inertia about y  
r : Radius of gyration about weak axis(y)  
R<sub>w</sub>, R<sub>f</sub> : Width-to-thickness ratio parameter

buckling load. It is important to study the interactive behavior and the ultimate strength of thin-walled member experimentally. The AISC form factor method is applied for predicting the ultimate strength of thin rolled H-section columns with large width-to-thickness ratio of plates. The predictions of this method are examined by the test results.

## 2. OUTLINE OF TEST

Four sorts of H-shaped cross section are selected from the manufacture's catalog of H-section, and named A, B, C and D. The measured cross sectional dimensions and properties of test specimens are shown in Table 1. All the test specimens are composed of mild steel SS400 plates and the thickness of flange and web plates are 4.5 mm and 3.2 mm respectively. The test program consists of (1) tensile coupon tests of component plates, (2) measurement of initial deflection of all specimens, (3) measurement of residual stress, for which eight specimens 800 mm in length are prepared, (4) stub-column test, for twelve specimens, (5) buckling test under central load and eccentrical load, (6) pure bending test about weak axis. Specimens with slenderness ratios  $L/r = 50, 75, 100$  ( $L$ : the column length,  $r$ : the radius of gyration about the weak axis of the cross section) and eccentricities  $e/r = 0, 0.15, 0.3$  are chosen in order to investigate the effect of the column length and eccentricities upon the ultimate strength. The length and the number of specimen for each type are given in Table 2. All column tests were conducted in pin-ended condition with respect to the weak axis and in clamped-end condition with respect to the strong axis[4].

Table 2 Length and number of test specimen

Type (HxB) (mm)	Length(mm) and Number of Specimen				Remarks
	L/r=20	L/r=50	L/r=75	L/r=100	
A (150x100)	468(2)	1170(3)	1755(3)	2340(3)	$e=0$
B (200x100)	442(2)	1105(3)	1658(3)	2210(3)	$0.15r$
C (250x125)	552(2)	1380(3)	2070(3)	2760(3)	$0.30r$
D (250x150)	688(2)	1720(3)	2580(3)	3340(3)	

L/r : Slenderness ratio    e : Eccentric distance



The mechanical properties of material obtained from tensile coupon tests are shown in Table 3. The average yield stress  $\sigma_y$  is given by:

$$\sigma_y = (\sigma_{yf} A_f + \sigma_{yw} A_w) / (A_f + A_w) \quad (1)$$

where  $A_f$  and  $A_w$  are cross sectional areas of flange and web plates, respectively. It is noted that the average values of yield stress  $\sigma_y = 379 \text{ N/mm}^2$  exceed the standard values of mild steel. This caused by the repeated rolled process for highly thin plate.

The initial deflection of the column and of the component plates for each specimen were measured by 0.01mm accuracy dial gages at specified grid points. The maximum values of measured initial deflection are shown in Table 4. The values  $\delta_{cw}$  and  $\delta_{cf}$  are the maximum initial deflection of web and flange plates, where  $H$  and  $B_f$  denote the height of the web plate and a half flange width of the flange plate respectively. The value  $\delta_{wa}$  is the maximum initial deflection of a column. These values are very small and within the tolerance for initial geometrical imperfection of the plate and the column specified in JSHB[7].

Table 3 Mechanical properties of material

Type	Yield stress (N/mm <sup>2</sup> )			Young's Modulus E=203 (KN/mm <sup>2</sup> )	Poisson's ratio $\nu=0.277$
	Flange $\sigma_{yf}$	Web $\sigma_{yw}$	Mean $\sigma_y$		
A	384.4	419.0	397.2		
B	316.1	395.5	350.1		
C	370.0	382.1	375.6		
D	384.0	397.5	389.6		
Mean	383.6	398.5	378.6		

Table 4 Initial maximum deflection

Type	Weak axis $\delta_{wa}(xL, \text{mm})$	Circumferential of Flange Plate $\delta_{cf}(xB_f, \text{mm})$	Circumferential of Web Plate $\delta_{cw}(xH, \text{mm})$
A	1/5690	1/329	1/943
B	1/5313	1/306	1/694
C	1/3957	1/312	1/708
D	1/5076	1/105	1/879
Mean	1/4949	1/263	1/806

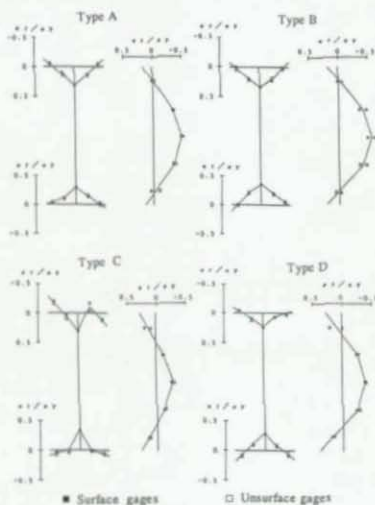


Fig. 1 Measured residual stress distributions

The residual stresses are measured by strain gages attached on both sides of flange and web plates surface in order to remove the effect of the bending residual stresses. The sectioning method was used to measure the released strain. Measured stress patterns were all similar in shape to usual patterns as shown in Fig. 1, i.e., the residual stress distribution is a triangle in the flange plate and the parabola in the web plate. In this figure, residual stresses were nondimensionalized by  $\sigma_y$ . The values of the maximum compressive residual stress of the central part of the web plate were approximately 50% of the yield stress.

A total of 12 stub-column specimens of which cross sections are same with those of column specimens was tested under axial compression[6].

### 3. RESULTS AND DISCUSSIONS

#### (1) Columns Behavior

Typical relations between average stress,  $P/A$ , and deflection,  $\delta/L$ , at the centre of the web plate at the midheight of the column ( $L/r=100$ ) are shown for each type specimens in Fig. 2. Broken lines in those figures represent the solution of the elastic analysis of the eccentric loaded column. The test results correspond to the results of elastic analysis until near the maximum load. The occurrence of the local plate buckling was observed from the stress-strain relations of web and flange plates of column test and the initiation of local buckling are illustrated by a arrow sign on the load-deflection curve in Fig.2. It may be found that the maximum strength is not dominated by the local buckling and the strength increases after the initiation of local buckling in this study.

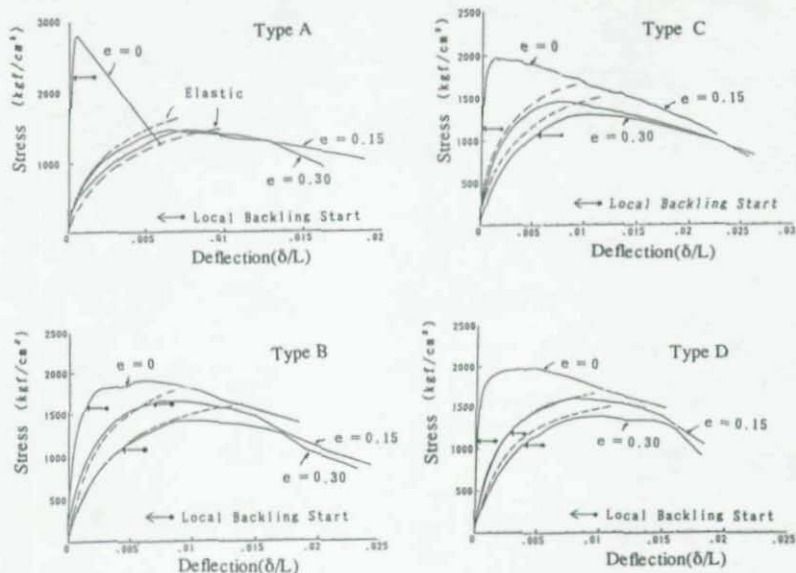


Fig. 2 Load-deflection curves of columns ( $L/r=100$ )

The average stress,  $P/A$ , versus the local strains on flange and web plates at the midheight of the column with  $L/r=50$  subjected to axial load are shown in Fig. 3. Strain gages were attached to the surface of the specimen at the midheight as shown in Fig. 4. For the type A specimen with a small width-to-thickness ratio of flange and web plates, the occurrence of local plate buckling was not observed until near the maximum load, and the maximum load almost attained to the yield thrust. It can be seen, however, that for the type B specimen of which width-to-thickness ratio of the web plate is larger than the type A, the local buckling of the web plate occurred early stage or less than half stress level of the maximum load. Furthermore, it can be recognized from Fig. 3 (b) comparing with Fig. 3 (a) that the strain disturbance in the flange plate of type B is seemed to be triggered by the local buckling. These behavior were also observed in the test for type C and D specimens. From these test results, it may be found that the influence of the interactive effect between the deformation of component plates on the maximum strength of the column seems to be small in this width-to-thickness ratio of the specimen.

## (2) Ultimate strength

The maximum ultimate strengths of central and eccentric loaded columns obtained from the test are summarized in Table 5. In this Table, the column maximum stresses,  $\sigma_u$  were nondimensionalized by yield stress  $\sigma_y$  and specimens of  $L/r=20$  are stub-columns. The maximum ultimate strengths,  $\sigma_u/\sigma_y$  are plotted against the slenderness ratio parameter  $\lambda$  in Fig. 5. For the type D specimens with larger width-to-thickness ratio of component plates, there is very little increase in strength for columns of which slenderness ratio parameter  $\lambda$  is less than 1.0 and the ultimate strengths of them are equal to or less than the maximum stub-column strength, 0.71  $\sigma_y$ . It can be noticed that the same tendency is observed for the type C specimens.

As can be seen from Fig. 5, the test results for the columns with a relatively large width-to-thickness ratio of component plates become fairly lower than JSHB columns strength curve in the smaller  $\lambda$  range. This may be caused by the effects of interaction between the plate buckling and

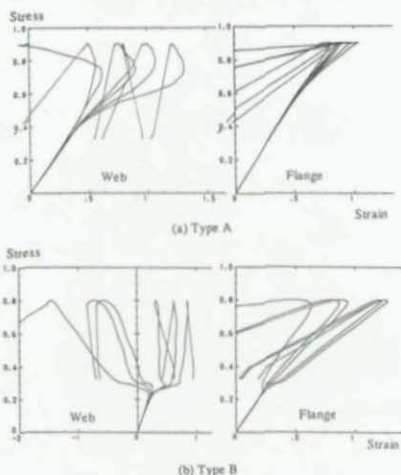


Fig. 3 Stress-strain curves of central loaded column ( $L/r=50$ )

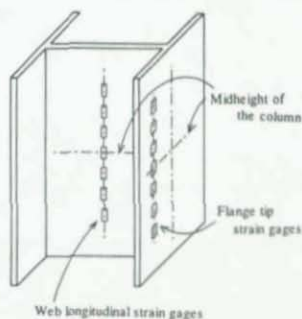


Fig. 4 Location of strain gages at midheight of the column

Table 5 Ultimate strength of test columns

Type	L/r	e (cm)	$\sigma_u$ (N/mm <sup>2</sup> )	$\sigma_u/\sigma_y$	Type	L/r	e (cm)	$\sigma_u$ (N/mm <sup>2</sup> )	$\sigma_u/\sigma_y$
A	20	0	387	—	B	20	0	318	—
		0	346	0.868			0	329	0.861
		0.15r	302	0.755			50	0.15r	278
	50	0	254	0.636		75	0	198	0.567
		0	321	0.824			0	274	0.724
		0.15r	232	0.581			75	0.15r	237
	75	0	206	0.516		100	0	202	0.576
		0	274	0.686			0	187	0.534
		0.15r	144	0.360			100	0.15r	164
	100	0	143	0.357		50	0	256	0.658
		0	316	—			0	277	—
		0	301	0.757			50	0.15r	256
C	20	0	316	—	D	20	0	277	—
		0	301	0.757			0	262	0.687
		0.15r	278	0.741			50	0.15r	256
	50	0	227	0.605		75	0	226	0.580
		0	253	0.637			0	250	0.657
		0.15r	225	0.598			75	0.15r	215
	75	0	186	0.496		100	0	186	0.476
		0	201	0.506			0	195	0.500
		0.15r	148	0.393			100	0.15r	158
	100	0	127	0.339		50	0	158	0.405
		0	127	0.339			0	136	0.349
		0.15r	127	0.339			100	0.30r	136

 $\sigma_y$  : Yield Stress

e : Eccentric distance

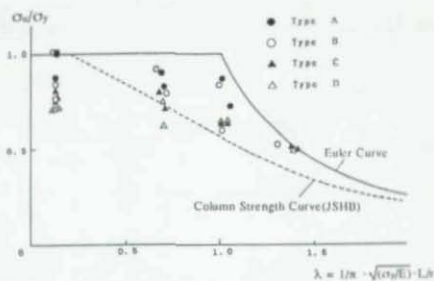


Fig. 5 Ultimate strength of central loaded columns

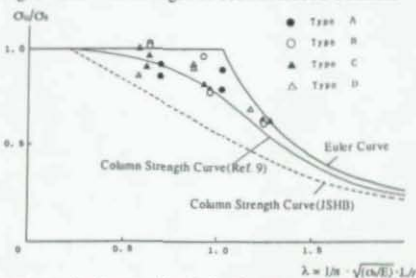


Fig. 6 Ultimate strength of central loaded column reevaluated by stub-column strength

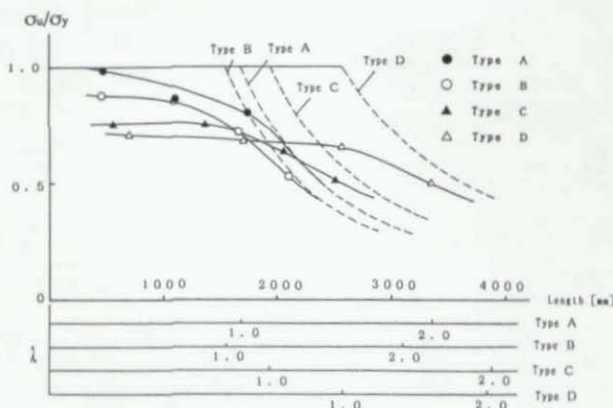


Fig. 7 Comparison of strength between different section profiles under the same member weight

the column buckling. In order to consider the effects of this interaction, the AISC has been proposed so-called form factor method[8]. Fig. 6 shows the comparison of the JSHB columns strength curve and test results that are nondimensionalized by using the stub-column strength  $\sigma_s (= Q \sigma_y$ , where  $Q$  is the form factor), instead of the real material yield stress  $\sigma_y$ . Though test results are scattered somewhat, it is seen from this figure that the JSHB column strength curve seems to be conservative to test results reevaluated by the AISC form factor method. The solid curve in Fig.6 represents the strength curve of rolled column in limit state format proposed in Ref.[9] and is close to the mean strength of test results.

In the examination of the economical column design, the comparison of column strength of per unit area under the same member weight is often adopted. Fig. 7 shows a comparison of the average ultimate strength among different sections under the same member weight. The horizontal axes in Fig.7 describe the length of columns and the slenderness ratio for each type in order to compare the ultimate strength of per unit area, or to examine the cost performance of per unit weight of the column. It can be recognized from this figure that the use of the type A and B members with a small width-to-thickness ratio of plates are useful in the stocky region, but the type C and D members with a relatively large width-to-thickness ratio of plates can be expected the advantage in the slender region. Thus, this figure may be very convenient to select the economical rolled thin section profiles in the compression column design.

The maximum strength of the eccentric loaded column of  $L/r=50$  are shown in Table 5 and Fig.8. In fig. 8, the vertical axis represents the maximum axial load  $P_u$  divided by the yield load  $P_y$  and the horizontal axis shows the maximum bending moment  $M_u (=P_u \times e)$  divided by the plastic bending moment  $M_p (= \sigma_y \times I_y/Bf)$ . The solid curve in this figure is the correlation curve between axial load and moment defined by Eq. (2).

$$\frac{P}{P_{cu}} + \frac{M}{M_p(1-P/P_e)} = 1 \quad (2)$$



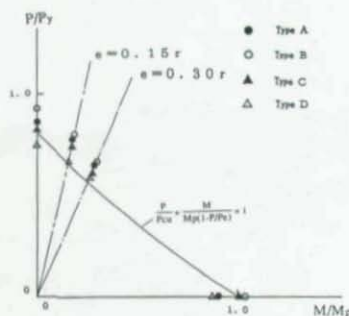


Fig. 8 Correlations between axial load and moment

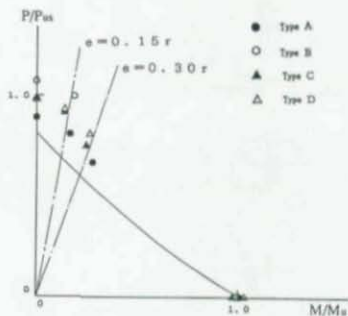


Fig. 9 Correlations between axial load and moment reevaluated by stub-column strength and bending test results

in which  $P_{cu}$  is the axial load obtained from JSHB column strength curve and  $P_e$  denotes the Euler's buckling load. Fig. 9 shows the correlation between axial load and moment nondimensionalized by stub-column strength  $P_{su}$  and maximum bending moment  $M_u$  obtained from the pure bending test (the details are described in the following item) instead of  $P_{cu}$  and  $M_p$  respectively. It can be seen from this figure that the ultimate strength predictions reevaluated by the AISC form factor method is conservative to test results.

### (3) Bending test

Bending test results about weak axis are summarized in Table 6. Typical relations between bending stress and local strain along the flange tip are shown for the type D specimen in Fig. 10. Local buckling stress of bending test in Table 6 is obtained from a bifurcation point of stress-strain curve as shown in Fig. 10. As can be seen, the local buckling of the flange plates occurred early stage or less than half stress level of the maximum bending stress. However, the maximum bending moment  $M_u$  is nearly equal to the plastic bending moment  $M_p$ . It may be found that the post-buckling strength of the flange plates can be expected for the H-section member subjected to bending about weak axis.

Table 6 Results of bending test

Type	$M_u$ (KN·cm)	$M_p$ (KN·cm)	$M_u/M_p$	$\sigma_{mu}$ ( $N/mm^2$ )	$\sigma_{nl}/\sigma_{mu}$
A	795	869	0.92	365	
B	1003	972	1.03	433	0.84
C	1637	1511	1.08	453	0.68
D	1686	1834	0.92	343	0.55

$M_u$  : Maximum Bending Moment  
 $M_p$  : Plastic Bending Moment  
 $\sigma_{mu}$  : Ultimate Bending Stress  
 $\sigma_{nl}$  : Local Buckling Stress of Bending Tests

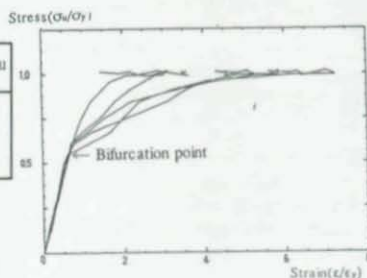


Fig. 10 Relations between bending stress and local strain of flange plate



#### 4. CONCLUSIONS

Ultimate strength and behavior of rolled thin H-section columns subjected to concentric and eccentric compression is studied experimentally. From this study the following conclusions may be drawn.

- 1) The magnitude of the initial deflection were very small compared with usual rolled or welded H-section members.
- 2) It may be found that the maximum strength is not dominated by the local buckling and the strength increases after the initiation of local buckling in this study.
- 3) The figure which is very convenient to select the economical rolled thin section profiles in the compression column design is proposed and also shown the advantage of this kind thin-walled rolled compression members which fail due to overall and local buckling in usual use condition, when they are used in a relatively slender range.
- 4) The AISC form factor method is found to give fairly accurate the ultimate strength predictions for rolled thin H-section members subjected to axial compression, bending or any combination. However, at this stage, this method based on the form factor approach needs to be carried out cumbersome stub-column tests, pure bending tests or numerical analyses to determine the Q-factor.
- 5) The maximum bending moment  $M_u$  is nearly equal to the plastic bending moment  $M_p$ . It may be found that the post-buckling strength of the flange plates can be expected for the H-section member subjected to bending about weak axis.

All the material used in the tests was donated by Kawasaki Steel Company in Japan. We wish to thank Mr. K. Shinoda, a student at Aichi Institute of Technology for his help to do the tests.

#### REFERENCES

1. Davids, A.J. and Hancock, G.J.: Compression tests of long welded I-section columns, *Journal of Structural Engineering*, Vol. 112, No.10, Oct., 1986, pp. 2281-2297.
2. Yamao, T. and Sakimoto, T.: An experimental study on the interaction buckling of thin-walled H-section columns, *Proc., of JSCE*, No. 380/I-7, April, 1987, pp.383-390. (in Japanese)
3. Yamao, T. and Sakimoto, T.: An experimental study on the ultimate strength behavior of thin-walled H-section stub-columns, *Proc. of JSCE*, No.380/I-7, April, 1987. (in Japanese)
4. Aoki, T. and Fukumoto, Y.: An experimental study of local and overall buckling of thin walled H-columns, *ECCS Colloquium on Stability of Plate and Shell Structures*, Ghent University, 6-8 April, 1987
5. Yamao, T., Tuboura, N. and Sakimoto, T.: An analysis and estimations for ultimate strength of thin-walled H-section members subjected to axial compression and bending, *Journal Structural Engineering*, Vol. 36A, March, 1990. (in Japanese)
6. Yamao, T., Aoki, T. and Sakimoto, T.: An experimental study on the ultimate strength of rolled H-section steel stub-columns, *Journal of Structural Engineering*, Vol. 38A, March, 1992, pp. 95-103. (in Japanese)
7. Japan Road Association : Specifications for Highway Bridges, Feb., 1980.
8. AISC : Specification for the Design, Fabrication and Erection of Structural Steel for Buildings, 8th ed., New York, 1980.
9. Fukumoto, Y. etc. : Report of the Funds of Aid for Scientific Researches, Japanese Ministry of Education, Science and Culture. 1990.3 (in Japanese)



## RARE DOUBLE-LAYER GRID STRUCTURE : A NEW SOLUTION

Prof. Dan Dubina, Ph. D.

Technical University of Timisoara  
Civil Engineering Faculty  
Steel Structures Department  
Stadion 1, RO-1900 Timisoara

Space frames are classified as single-, double- or multi-layered structures which may be flat, resulting in grid structures, or may be curved in one or two directions, forming barrel vaults and dome structures. Grid structures can be further categorized into lattice and space grids in which members run in two, three or four main directions.

In double-layer lattice grids, top and bottom grids are identical, with the top layer positioned directly over the bottom layer. Double-layer space grids usually consist in pyramidal units with triangular or square bases resulting in either identical parallel top and bottom grids offset horizontally to each other, or parallel top and bottom grids each with a different configuration interconnected at node points by inclined web members to form a regular stable structure (Ref. 1). Main types of double-layer grids in common use are shown in Fig. 1.

Members in double-layer grids are, as usual, almost entirely subject to axial tensile or compressive forces, whereas structural members proposed in this paper (taking into account the fact that connections are rigid or semirigid) are primarily subject to flexural moments.

Furtheron, some relevant structural details concerning this structure are presented, as well as informations on the experimental program carried out in the Laboratory of the Steel Structures Department of Technical University in Timisoara and numerical results also.

### RARE DOUBLE-LAYER GRID STRUCTURE (RDLG)

RDLG structure is built from standardized pyramidal units joined together by means of square frame units to form upper chord, or independent bars to form bottom chord (Fig. 2a) The jointing system must provide rigid or semirigid connections, lest the structure turn into a mechanism. Fig. 2b shows the author's solution for a bottom chord connection. Prestressed high tensile bolts could be used in order to increase nodal rigidity on rotation. The layer bars can be made of U or C section while diagonals are made in square or circular hollow section.

The jointing solution involving a cross-shaped central connector is a version of a jointing system patented by the author (Ref. 2 and 3)

### EXPERIMENTAL RESEARCH

Between 1989 and 1991, a research program was developed in the Laboratory of the Steel Structures Department in Timisoara, concerning three new types of space grids and also

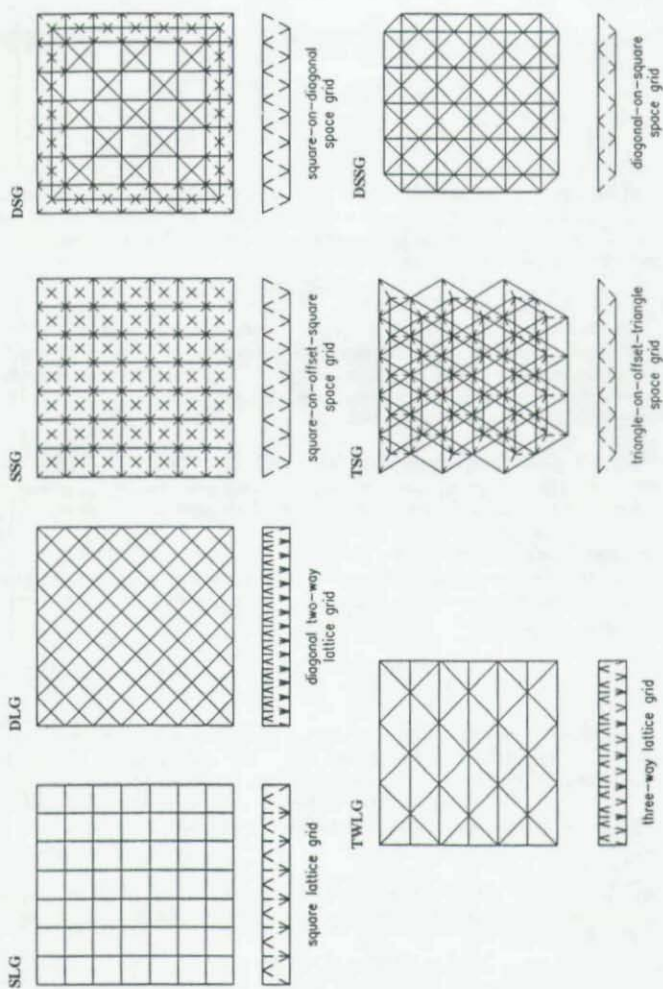


Fig. 1 Lattice and Space Grids

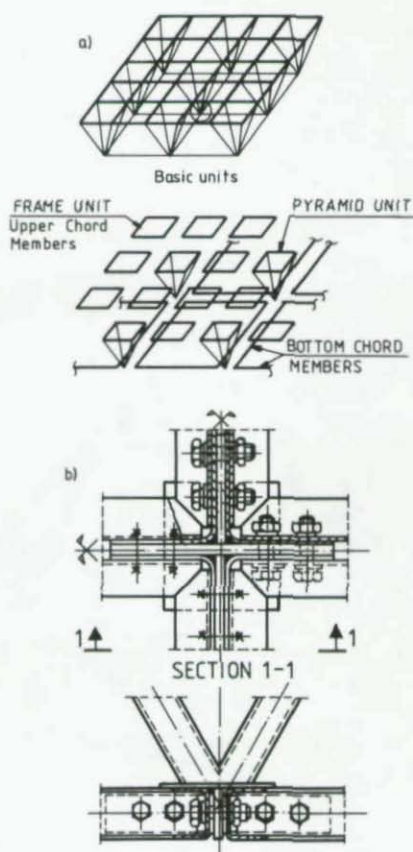


Fig. 2 Rare Double-Layer Grid Structure (RDLG)

- a) Structure geometry  
b) Bottom Chord Connection



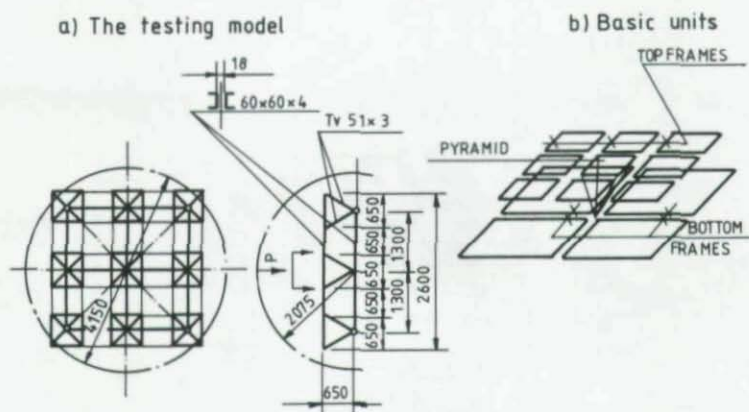


Fig. 3 Testing model dimensions

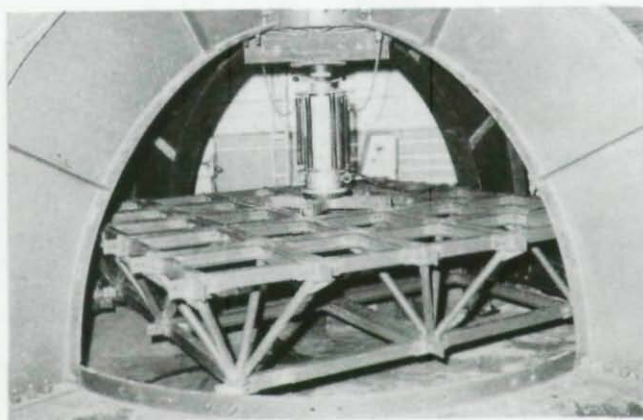


Fig. 4 Testing model



Fig. 5 Basic units of RDLG model

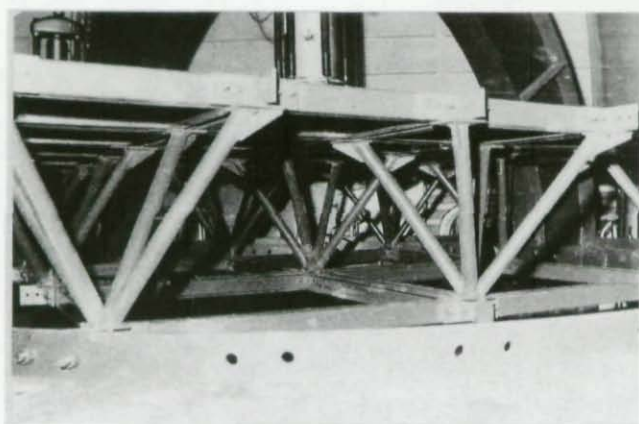


Fig. 6 Front view of RDLG model

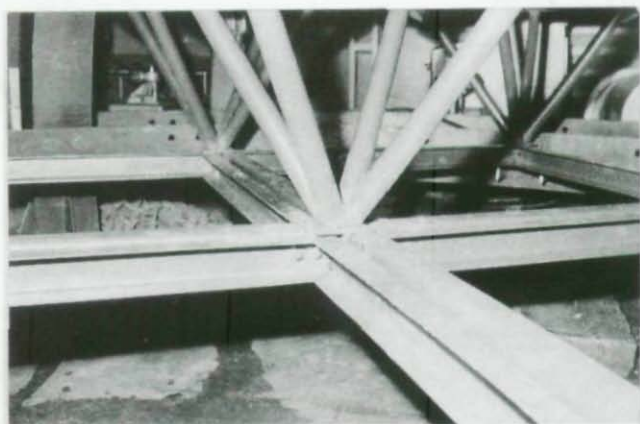


Fig. 7 Bottom Chord Central Node

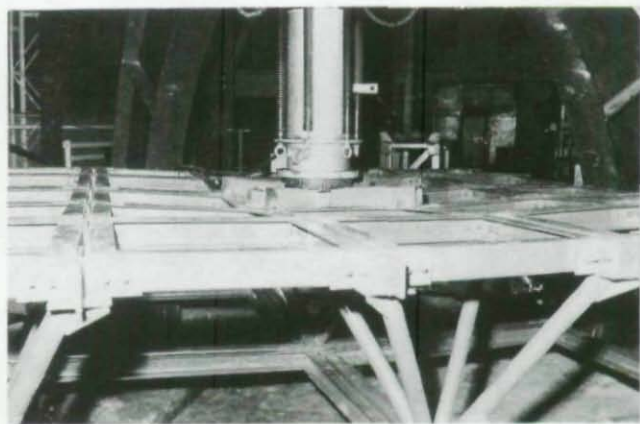


Fig. 8 Feature of RDLG Model

connection systems for single-layered grids. The results of this program were already published in scientific events (Ref. 4, 5, 6).

We will resume now only some aspects concerning experimental research on RDLG structure.

The experimental investigations carried out in our Laboratory aimed first of all to obtain qualitative and quantitative confirmation of the new structural solution. To this end, structural modules were tested, which had been obtained by assembling several basic units, making possible the obtention of valuable data concerning overall behaviour of the structure as well as its connections.

RDLG structure model is shown in (Fig. 3). Chords are made in U section members and diagonals in CHS members. (Fig. 4) presents RDLG model inside the testing machine while (Fig. 5) presents the basic units for this model. Pictures in Figs.6 and 7 show a frontal view of the model and a bottom chord node. An intermediate solution was adopted for building the nodes: each basic unit is connected into the node by means of two tensile bolts, but without taking measures to machine the contact surfaces. Under these conditions structure failure was due to bars sliding and rolling in the nodes. The structure was not destroyed, exhibiting a high carrying capacity, but it underwent large deformations. Practically, while the maximum allowed deflection was not exceeded, the experimental ultimate load was about 10% lower than the computed ultimate load associated with a rigid connection computation model. Picture in Fig.8 presnts the failure of the experimental model and Fig.9 shows the numerical simulation of the structure deformation in the middle span of testing model. If an second order plastic analysis is performed, the failure yields by a plasting hinge mechanism configuration: the hinges appear in the first diagonals, near support nodes (bars 9 and 12 in Fig.9).

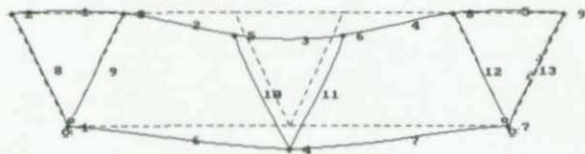


Fig.9 : Failure configuration of RDLG Model in the middle span section.

#### NUMERICAL RESULTS

In order to perfect the baylength and height values for a 30 meters square RDLG structure, under a  $150 \text{ daN/m}^2$  load, an elastic first order analysis was performed. Denoting the upper chord baylength by  $b_1$  and the bottom chord one by  $b_2$ , three cases were analysed :

- $b_1 = 2500.0 \text{ mm}$  ;  $b_2 = 5000.0 \text{ mm}$
- $b_1 = 1875.0 \text{ mm}$  ;  $b_2 = 3750.0 \text{ mm}$
- $b_1 = 1500.0 \text{ mm}$  ;  $b_2 = 3000.0 \text{ mm}$

with the corresponding height values given in Table 1, which contains, also, the results of this analysis. The optimum configurations seems to be in the b case with a height of 1200.0 mm, and also, of 1500.0 mm.

(Tab. 1) - Numerical Results for RDLG Structures

Type of structure	Height h [mm]	Design loads ( N - daN ; $M_y$ - daNcm ; $M_x$ - daNcm )						Maxim. deflect., $U_z$ [cm]	Steel consumption, [kg/m <sup>3</sup> ]
		Bottom chord		Upper chord		Diagonal members			
		N	$M_y$	N	$M_y$	N	$M_y$		
			$M_x$		$M_x$		$M_x$		
a	1,200	-12,019	0	-4,210	12,030	-7,430	65,462	-11.56	23.16
			160,972		334,670		2,676		
	1,500	-10,014	0	-3,512	11,129	-6,700	63,306	-11.36	24.18
			160,000		334,600		2,070		
	2,100	-8,581	0	-3,011	10,105	-6,196	60,694	-11.27	25.49
			158,700		334,540		1,584		
	2,400	-7,508	0	-2,634	9,090	-5,851	53,401	-11.23	26.40
			158,170		334,480		1,046		
b	1,200	-13,578	0	-3,194	7,560	-5,513	36,540	-10.45	27.78
			102,212		207,000		1,324		
	1,500	-10,840	0	-2,526	6,736	-4,867	35,981	-10.16	23.20
			100,000		206,700		935		
	2,100	-9,029	0	-2,137	5,870	-4,483	34,424	-10.02	24.40
			98,000		190,200		670		
c	1,200	-12,102	0	-2,136	4,664	-3,966	23,616	-7.63	25.56
			71,062		140,020		609		
	1,500	-9,539	0	-1,715	3,950	-3,592	22,518	-7.36	25.90
			71,020		140,015		406		

In order to compare the performances of RDLG structure with the structures in (Fig. 1), the same square surface and load were considered, with a baylength of 3.0 m and a height of 2.0 m. Results are presented in Table 2.



(Tab. 2) - Numerical Results for Space Grid Structures in Fig. 1

Type of Structure	$N_{max}^+$ [daN]	$N_{max}^-$ [daN]	Maximum Deflection [cm]	Cross - section Dimensions : (All members)	Weight : [kg / m <sup>2</sup> ]
DLG	9.480	9.310	6.91	CHS $\phi$ 71.6 $\times$ 3.2	31.28
SSG	19.480	19.180	7.16	CHS $\phi$ 114.3 $\times$ 3.2	39.67
DSG	35.710	20.440	10.42	CHS $\phi$ 114.3 $\times$ 5	35.21
TWLG	8.870	9.300	5.43	CHS $\phi$ 88.7 $\times$ 4	29.30
TSG	9.550	11.070	5.61	CHS $\phi$ 88.7 $\times$ 4	26.40
DSSG	9.480	10.000	7.29	CHS $\phi$ 71.6 $\times$ 3.2	38.10

## CONCLUDING REMARKS

Comparing the results in Tables 1 and 2, it shows they are practically of the same order of magnitude for deflections, but with a lower steel consumption for the RDLG structure. What needs to be however emphasized, is the fact that assembly manpower requirements are markedly lower in the case of the new solution, which involves fewer standardized subassemblies and are structurally simpler.

## REFERENCES

1. Steel Designer's Manual, 5th Ed. The Steel Construction Institute, 1992
2. Dubina D. and Colcea E., - Structura metalica reticulata planara pentru acoperis. Brevet RO nr. 87969
3. Dubina D. and Pacoste C. - New Types of Bolted Joints for Reticulated Steel Grids. Proc. of Int. Coll. on Bolted and Special Structural Connections, Vol. 4, Moscow, May 15-20, 1989
4. Dubina D. - New Structural Systems for Double-Layered Grids with Bolted Joints. Proc. of Int. Conf. on Steel and Aluminium Structures, ICSAS' 91, Vol. Steel Structures, pp. 898-907. Singapore May 22-24, 1991
5. Dubina D. - Numerical and Experimental Research Concerning Two New Systems for Double-Layer Grids. Proc. of the Int. IASS Symposium, Vol. 3 pp. 213-220. Copenhagen, September 2-6, 1991
6. Dubina D. - New Structural Solution for Double and Single-Layered Grids. Proc. of Int. Congress IASS-CSCE on Innovative Large Span Structures, Vol.2, pp. 256-270. Toronto, June 1992



## WEB CRIPPLING OF STAINLESS STEEL COLD-FORMED BEAMS

by

S. A. Korvink<sup>1</sup> ; G. J. van den Berg<sup>2</sup> ; P. van der Merwe<sup>3</sup>

### SYNOPSIS

The results of an investigation on the web crippling strength of cold-formed stainless steel channel sections are presented in this paper. The stainless steels under consideration are AISI Types 304, 430 and a modified Type 409, designated Type 3CR12 corrosion resisting steel.

The lipped channel sections were manufactured by a press braking process. Beams were tested in pairs, lips facing, in an end-one-flange loading configuration.

Experimental results were compared with the theoretical predictions given in the 1991 edition of the Specification for the Design of Cold-Formed Stainless Steel Structural Members<sup>1</sup>. It was concluded in this study that the experimental results compare reasonably well with the theoretical predictions. For longer bearing lengths the theoretical strengths show to be conservative.

### GENERAL REMARKS

The usefulness of cold-formed structural members lies basically in its high strength-to-weight ratio compared with structural materials such as concrete and timber.

Local instability can occur where members have high width-to-thickness and high height-to-thickness ratios so that, in designing such members, care should be taken where stresses are

- 
1. Lecturer of Civil Engineering in the Faculty of Engineering at the Rand Afrikaans University, Republic of South Africa.
  2. Associate Professor of Civil Engineering, Chairman of Civil Engineering and Chairman of the Materials Laboratory of the Faculty of Engineering at the Rand Afrikaans University, Republic of South Africa.
  3. Professor of Mechanical Engineering and Dean of the Faculty of Engineering at the Rand Afrikaans University, Republic of South Africa.

excessive.

Such excessive stresses are often induced by point loads, either applied or as reactions. The use of stiffeners in these cold-formed steel members is more often than not impractical<sup>2</sup>. Where such loads are applied to channel sections and other sections with large web depths, web buckling, web crippling and often a combination of web buckling and web crippling can occur.

#### OBJECTIVE OF THE INVESTIGATION

The 1991 ASCE Specification for the Design of Cold-Formed Stainless Steel Structural Members<sup>1</sup> makes provision for the design of flexural members against web crippling based on the 1986 AISI Specification for the Design of Cold-Formed Steel Structural Members with Commentary<sup>3</sup>. The 1986 AISI Specification for the Design of Cold-Formed Steel Structural Members<sup>3</sup> is a specification which may not be directly applicable to stainless steel structural members. The 1991 ASCE Specification for the Design of Cold-Formed Stainless Steel Structural Members<sup>1</sup>, however, uses the equations for the evaluation of web crippling loads from the 1986 AISI design specification. The validity of the 1991 ASCE Specification needed to be researched.

It is clear that<sup>4</sup>, no matter which design specification one refers to for the calculation of web crippling loads, the calculations tend to be loaded with constants that need to be precalculated resulting in a tedious design procedure. To assist designers it is therefore necessary to develop equations that provide a reasonably fast and efficient web crippling check for a small but important part in the design of cold formed structural flexural members.

#### THEORETICAL BACKGROUND

The theoretical analysis of web crippling under concentrated loading conditions is very complex. This can clearly be seen in the literature available on web crippling. Most research and therefore predictions as well as recommendations have been based on experimental results resulting in empirical solutions<sup>5,6,7,8</sup>. These solutions have been generated over a number of years, initially with the investigations of plates that buckle under in-plane loading conditions. Further development led to research in the buckling of beam webs and progressed further into investigations of web crippling as well as the combined effects of web crippling and bending of flexural members.

Beams with large plate width-to-thickness ratios are used more generally in the structural steel industry. When designing for flexure it is more economical to minimise the material in the web. Because of this trend in the reduction of web material the designer has to focus more thoroughly on checks for web buckling, web crippling, buckling due to shear, vertical

buckling of the compression flange into the web as well as buckling due to the linear flexural stress distribution<sup>9</sup>.

Because of the high strength-to-weight ratio, cold-formed steel sections are ideally suited where lightweight is of primary importance. This implies the use of thinner sections. The thinness of sections leads to local instability and therefore web crippling as a general problem.

The use of cold-formed steel members has increased due to the high strength-to-width ratio and stiffness-to-weight ratio of cold-formed steel compared to concrete, masonry and timber<sup>10</sup>. The analysis of cold-formed steel requires different attention because of high width-to-thickness ratios that exhibit local instability at relatively low loads, for example loads transferred from purlins to girders and rafters. Where loads are not transferred evenly into webs, web crippling failure, either bearing failure or buckling failure, can occur. Web crippling is caused by high localised stress concentrations, which in turn are caused by concentrated loads or reactions applied on a short length of beam. This condition can reduce the load carrying capacity of flexural members<sup>8</sup> as the bearing capacity of a beam on a support is governed by the web crippling resistance of such a beam<sup>5</sup>. The use of stiffeners is not always possible due to section geometry such as shape and thickness.

Buckling of such cold-formed members does not necessarily imply failure and the designer can make economic advantageous use of post buckling strength<sup>10</sup>.

In 1986 Santaputra, Parks and Yu<sup>8</sup> investigated web crippling of high strength steel beams. Tests were carried out to determine the web crippling strength of webs of cold-formed steel beams fabricated from high strength sheet steels commonly used in the automotive industry. The high strength steels used in this investigation have yield strengths of 414 Mpa to 1138 Mpa (60 ksi to 165 ksi). The sections under consideration were hat sections as well as I-beams.

The investigation covered the following four loading conditions:  
(refer to Figure 1)

- \* Interior one flange loading (IOF);
- \* End one flange loading (EOF);
- \* Interior two flange loading (ITF);
- \* End two flange loading (ETF).

In developing new equations the authors used data from the following sources<sup>6</sup>:

- \* Cornell and UMR data
- \* UMR tests by Lin
- \* Their own data



Santaputra et al<sup>8</sup> developed a set of non-dimensional imperial equations based on bearing failure and plate buckling. Bearing failure is expressed as a function of  $N$ ,  $t$  and  $R$ , buckling failure is based on a flat plate under partial edge loading. A nonlinear least squares iteration technique was used to determine the empirical constants.

With the new equations a beam could be analyzed for ultimate concentrated loads and reactions. The equations are valid for beams of which:

$$\begin{aligned} F_y &\leq 1310 \text{ MPa (190 ksi)} \\ h/t &\leq 200 \\ N/t &\leq 100 \\ N/h &\leq 2,5 \\ R/t &\leq 10 \end{aligned}$$

where

- $F_y$  yield strength of material
- $h$  clear distance between flanges measured in the plane of the web
- $N$  bearing length
- $R$  inside bend radius
- $t$  web thickness

The equation that would be valid for EOF loading (refer to Figure 1) of stainless steel channel sections has the following two additional conditions:

$$\begin{aligned} z &= 0,0 \text{ mm} \\ e &\geq 0,5h \text{ mm} \end{aligned}$$

where

- $e$  clear distance between edges of the adjacent opposite bearing plates
- $z$  distance between the edge of the bearing plate to the far end of the beam

The ultimate concentrated load  $P_u$  is the lesser of  $P_{cy}$  and  $P_{cb}$  where (in imperial units):

$$P_{cy} = 9,9 t^2 F_y C_{11} C_{21} (\sin \theta) \quad (1)$$

$$P_{cb} = 0,047 E_0 t^2 C_{41} C_{51} \sin(\theta) \quad (2)$$

$$c_{11} = 1 + 0,0122 \left( \frac{N}{t} \right) \leq 2,22 \quad (3)$$

$$c_{21} = 1 - 0,247 \left( \frac{R}{t} \right) \geq 0,32 \quad (4)$$

$$c_{41} = 1 - 0,00348 \left( \frac{h}{t} \right) \geq 0,32 \quad (5)$$

$$c_{51} = 1 - 0,298 \left( \frac{\theta}{h} \right) \geq 0,52 \quad (6)$$

where

- $c_{11}$  dimensionless function of  $(N,t)$
- $c_{21}$  dimensionless function of  $(R,t)$
- $c_{41}$  dimensionless function of  $(h,t)$
- $c_{51}$  dimensionless function of  $(e,h)$
- $E_0$  initial elastic modulus
- $e$  clear distance between edges of the adjacent opposite bearing plates
- $F_y$  yield strength of material
- $h$  clear distance between flanges measured in the plane of the web
- $N$  bearing length
- $P_{cb}$  ultimate web crippling load as a result of buckling failure
- $P_{cy}$  ultimate web crippling load as a result of bearing failure
- $R$  inside bend radius
- $t$  web thickness
- $\theta$  angle between plane of web and plane of bearing surface

Santaputra et al<sup>8</sup> observed the following failure mechanisms:

- \* Bearing failure or overstressing which occurs just under the bearing plates with small lateral deformations of the webs of the hat sections. I-sections show no lateral movement of the webs before ultimate loads are reached. The bearing plate penetrates the web as the load increases to ultimate and remains there.
- \* Buckling failure: The load increases steadily until the ultimate load is reached. At the ultimate load the web becomes unstable and buckles, the load dropping suddenly thereafter.

These mechanisms are concurrent with those stated by Packer<sup>6</sup> and is consistent with those

observed in this investigation of the web crippling of stainless steel channel sections.

#### ANSI/ASCE-8-90<sup>1</sup> DESIGN SPECIFICATION PROVISIONS

The 1991 Specification for the Design of Cold-Formed Stainless Steel Structural Members<sup>1</sup> published by the American Society for Civil Engineers (ASCE) covers web crippling of flexural members based on the 1986 Specification for the Design of Cold-Formed Steel Structural Members<sup>3</sup> published by the American Iron and Steel Institute (AISI). The design specifications in the AISI Specification are for the design of cold-formed carbon steel sections.

The conditions for application as well as the equations given in the 1991 ASCE Specification<sup>1</sup> pertaining to this particular investigation are the following:

For members consisting of single webs, of which opposite loads are spaced at a distance greater than 1.5 of the clear distance between flanges measured in the plane of the web,  $h$ , and of which the end reactions are the concentrated loads, the nominal strength,  $P_n$ , for a concentrated load or reaction for one solid web connecting top and bottom flanges is given by Equation 9:

$$P_c = t^2 c_3 c_4 c_5 \left( 2.28 - 0.0042 \left( \frac{h}{t} \right) \right) \left( 1 + 0.01 \left( \frac{N}{t} \right) \right) \quad (7)$$

For  $F_y \leq 495$  Mpa

$$c_3 = (1.33 - 0.33k)k \quad (8)$$

For  $F_y > 495$  MPa

$$c_3 = 1.34 \quad (9)$$

$$0.50 < \left[ c_4 = \left( 1.15 - 0.15 \frac{R}{t} \right) \right] \leq 1.0 \quad (10)$$

$$c_{\theta} = 0,7 + 0,3 \left( \frac{\theta}{90} \right)^2 \quad (11)$$

$$45^{\circ} \leq \theta \leq 90^{\circ} \quad (12)$$

where

- $F_y$  longitudinal compressive yield strength of the material
- $h$  clear distance between flanges measured in the plane of the web
- $k$   $F_y/228$
- $N$  bearing length
- $P_i$  ultimate web crippling load
- $R$  inside bend radius
- $t$  web thickness
- $\theta$  angle between plane of web and plane of bearing surface

The following limitations are applicable to Equations 7 to 12:

- $h/t \leq 200$
- $N/t \leq 210$
- $N/h \leq 3,5$
- $R/t \leq 6$

In the above-mentioned equations the value of  $F_y$  adopted by both the 1974<sup>11</sup> and 1991<sup>1</sup> specifications is that of longitudinal compression. The 1974 Specification<sup>11</sup> states that: "...Since no research work has been done in the Cornell project to study the problem of web crippling of beams made of high yield strength steels, a conservative approach has been taken by using the longitudinal compressive yield strength of the stainless steel which is the lowest value of the four yield strengths..".

The 1991 Specification<sup>1</sup> suggests the use of the longitudinal compression value without any particular reason. It is therefore assumed that the reason is as quoted above.

#### EXPERIMENTAL PROGRAM

The literature on cold formed stainless steel design<sup>1</sup> is very clear on the lack of experimental data available for the evaluation of web crippling of stainless steel structural members. It was therefore decided to research three different types of stainless steels, AISI Type 304, 430 and a modified Type 409 designated Type 3CR12 corrosion resisting steel in order to gain more knowledge on the behaviour of such steels under web crippling loading conditions.

### **Mechanical Properties**

Uniaxial tensile and compression tests were carried out to determine the mechanical properties of the steels. Two specimens were taken from each plate from which the beams were fabricated, in both the longitudinal and transverse rolling directions. Therefore the specimens and results are designated longitudinal tension, LT, longitudinal compression, LC, transverse compression, TC, and transverse tension, TT.

All specimens were tested using an INSTRON 1195 Universal Testing Machine<sup>4</sup>.

### **Results**

The initial modulus,  $E_0$ , the proportional limit  $F_p$ , defined as the 0,01 % offset strength, the yield strength,  $F_y$ , defined as the 0,2 % offset strength, were calculated for each specimen and the statistical data is given in Table 1. Refer to Figures 2, 3 and 4 for tensile and compression test results of AISI Type 430 and AISI Type 304 stainless steels as well as Type 3CR12 corrosion resisting steel respectively.

### **WEB CRIPPLING TESTS**

#### **Preparation of test specimens**

Channel sections were fabricated using stainless steels Type 304, 430 and Type 3CR12 sheet steel. The channels were fabricated by the press brake method. Web heights varied from 90 mm to 315 mm at increments of approximately 25 mm. Five specimen sets were prepared for each steel type, and each set was tested on a constant bearing length. The bearing lengths varied from 20 mm to 100 mm, at increments of 20 mm. Flange widths and lip widths were kept constant at 50 mm and 20 mm respectively.

The beams were tested in pairs as shown in Figure 5, open ends facing. The beam lengths were chosen such that the distance between the load application and the reaction areas were greater than  $1,5h$ . The load was applied to the webs of the beams by means of 20 mm plates bolted by four or six bolts (depending on the web depth) to the webs. Angles were bolted to the top flanges at quarter lengths to prevent lateral instability. Small plates were bolted to the bottom flanges at half distances between bearing plates and loading plates to prevent the bottom flanges from buckling outwards. Bearing plates were bolted to the beam flanges and were simply supported on rollers.

#### **Experimental Procedure**

The beams were tested using an Avery-Denison loading apparatus. The loading rate was kept



constant at 5 kN/min and the failure load was recorded digitally by the Avery-Denison.

All four beam webs buckled at the reaction points before failure. At failure a large and sudden deformation occurred. This last deformation was also permanent.

A statistical average of 2,464 mm was calculated from 300 measurements and used as the inside bending radius throughout the calculations that followed<sup>4</sup>.

### Web Crippling Test Results

Experimental crippling loads,  $P_e$ , for each of Type 304 and Type 430 stainless steels as well as Type 3CR12 corrosion resisting steel are tabulated in Tables 2, 3 and 4 respectively, where

- h clear distance between flanges measured in the plane of the web
- N bearing length
- $P_e$  experimental web crippling load
- $P_u$  ultimate web crippling load
- t web thickness

### ANSI/ASCE-8-90

In the calculation of web crippling loads according to the 1991 Specification for the Design of Cold-Formed Stainless Steel Structural Members, ANSI/ASCE-8-90<sup>1</sup> the following parameters and equations have been used:

- \* Longitudinal compression yield strength,  $F_y$  (LC) as given in Table 1.
- \* Average web thicknesses, average web heights as well as an average inside bend radius.
- \* Bearing lengths as given in Tables 2 to 4.
- \* Equations 7 to 12.

The web crippling loads,  $P_u$ , obtained by applying the equations of ANSI/ASCE-8-90<sup>1</sup> as well as the ratio of the experimental web crippling loads,  $P_e$ , to the web crippling loads,  $P_u$ , obtained by applying the equations of ANSI/ASCE-8-90<sup>1</sup> are given in Tables 2 to 4. Figures 6, 7 and 8 present the web crippling loads,  $P_u$ , obtained by applying the equations of ANSI/ASCE-8-90<sup>1</sup> as solid lines. Figures 6, 7 and 8 present the experimental web crippling loads,  $P_e$ , as symbols.

### \* ANSI/ASCE-8-90

The calculation of web crippling loads according to ANSI/ASCE-8-90<sup>1</sup> has been repeated

using the transverse compression yield strength,  $F_y$ , (TC). All other parameters were kept constant as before.

The web crippling loads,  $P_u$ , obtained by applying the equations of ANSI/ASCE-8-90<sup>1</sup> as well as the ratio of the experimental web crippling loads,  $P_{e,u}$ , to the web crippling loads,  $P_u$ , obtained by applying the equations of ANSI/ASCE-8-90<sup>1</sup> are given in Tables 2 to 4. Figures 9, 10 and 11 present the web crippling loads,  $P_u$ , obtained by applying the equations of ANSI/ASCE-8-90<sup>1</sup> as solid lines. Figures 9, 10 and 11 present the experimental web crippling loads,  $P_{e,u}$ , as symbols.

#### SANTAPUTRA OVERSTRESSING AND WEB BUCKLING LOADS

In the calculation of overstressing loads and web buckling loads according to Santaputra et al<sup>8</sup> the following parameters and equations have been used:

- \* Longitudinal compression yield strength,  $F_y$  (LC) as given in Table 1.
- \* Average web thicknesses, average web heights as well as an average inside bend radius.
- \* Bearing lengths as given in Tables 2 to 4.
- \* Equations 1 to 6.

The lesser of the overstressing loads and the web buckling loads,  $P_u$ , obtained by applying the equations of Santaputra et al<sup>8</sup> as well as the ratio of the experimental web crippling loads,  $P_{e,u}$ , to the web crippling loads,  $P_u$ , obtained by applying the equations of Santaputra et al<sup>8</sup> are given in Tables 2 to 4. Figures 12, 13 and 14 present the web crippling loads,  $P_u$ , obtained by applying the equations of Santaputra<sup>8</sup> as solid lines and present the experimental web crippling loads,  $P_{e,u}$ , as symbols.

#### DISCUSSION OF RESULTS

It was clearly observed that different failure mechanisms exist when channel sections are subjected to web crippling loading conditions. The smaller channel sections with smaller web heights tend to fail because of flange failure. In this kind of failure mechanism the bearing plate is clearly imprinted in the flange.

The channel sections with larger web heights tend to fail as a result of web buckling, causing overall instability and resulting in a failure which displays a large deformation (buckle) of the web.

A clear transition between these two mechanisms could not be observed so that there is a gradual transition between bearing failure and buckling failure.

These observations are concurrent with those of Santaputra et al<sup>8</sup>.

The ratio of the experimental web crippling loads,  $P_e$ , to the web crippling loads,  $P_t$ , obtained by applying the equations of ANSI/ASCE-8-90<sup>1</sup> are within a  $\pm 20\%$  accuracy range except the values obtained for stainless steel Type 430. The web crippling loads tend to be less conservative with an increase in web slenderness ratio as well as an increase in bearing length. Refer to Figures 6 to 8.

By using the transverse compression yield strength better values are obtained from this specification. The improvement can be seen in Tables 2 to 4 where the statistics for the average experimental-to-theoretical web crippling load ratios are given in the last row of each of Tables 2 to 4.

## CONCLUSIONS

The literature reveals different approaches in the theoretical analysis of the web crippling of flexural members. The literature also reveals the difficulty associated with the theoretical analysis of the web crippling of flexural members. Most of the studies rely on experimental evidence for the verification of a certain idea or approach.

The direct improvement a substitute yield strength brings about shows that the web crippling resistance of a stainless steel channel section is in some way or another dependant on the transverse compression yield strength of the material. The general increase in accuracy of prediction loads with an increase in web slenderness shows that, in the equations of ANSI/ASCE-8-90<sup>1</sup> more emphasis should be placed on the web slenderness section of the equation.

The web crippling modes observed in the experimental part of this study are in accordance with those observed by Santaputra<sup>8</sup> and include the following:

- \* Bearing failure or overstressing which occurs in the sections with smaller web slenderness ratios. The bearing plates are imprinted in the flanges of the beams and small lateral deformations can be observed in the section of the beam webs adjacent to the position of the bearing plates.
- \* Buckling failure where the bearing plates do not become imprinted in the flanges of the beams. The web of a beam subjected to the crippling load buckles and this instability leads to the resultant failure of the beam web.

The transition between the two failure mechanisms can not be distinguished clearly enough to draw a definite conclusion.

## REFERENCES

1. American Society of Civil Engineers. Specification for the Design of Cold-Formed Stainless Steel Structural Members. ANSI/AISI-8-90. ANSI Approved March 5, 1991. ASCE, NY.
2. Yu, W.W.; Cold-Formed Steel Design; John Wiley and Sons, 1985.
3. American Iron and Steel Institute. Specification for the Design of Cold-Formed Steel Structural Members with Commentary. August 1986.
4. Korvink, S.A.; Web Crippling of Stainless Steel Cold-Formed C-Section Beams. M.Eng. Dissertation, Rand Afrikaans University, Johannesburg, South Africa.
5. Hetrakul, N.; Yu, W.W.; Webs for Cold-Formed Steel Flexural Members: Structural Behaviour of Beam Webs Subjected to Web Crippling and a Combination of Web Crippling and Bending. Final Report: Civil Engineering Study 78-4, Structural Series, Department of Civil Engineering, University of Missouri-Rolla, Rolla, Missouri, June 1978.
6. Packer, J.A.; Web Crippling of Rectangular Hollow Sections. Journal of Structural Engineering, Vol. 110, No. 10, October 1984.
7. Wing, B.A.; Web Crippling and the Interaction of Bending and Web Crippling of Unreinforced Multi-Web Cold-Formed Steel Sections. Vol. 1 Text, Vol. 2 Tables. Ph.D. Thesis, University of Waterloo, Waterloo, Ontario, Canada, 1981.
8. Santaputra, C.; Parks, M.B.; Yu, W.W.; Web Crippling Strength of High Strength Steel Beams. Eighth International Specialty Conference on Cold-Formed Steel Structures, St. Louis, Missouri, U.S.A., November 11 - 12, 1986.
9. Dewolf, J.T.; Gladding, C.J.; Post-Buckling Behaviour of Beam Webs in Flexure. Journal of the Structural Division, Proceedings of the American Society of Civil Engineers, Vol. 104, No. ST7. July, 1978.
10. Sivakumaran, K.S.; Analysis for Web Crippling Behaviour of Cold-Formed Steel Members. Computers and Structures, Vol. 32, No. 3 - 4, pp 707 - 719, 1989.
11. American Iron and Steel Institute. Cold-Formed Structural Design Manual. 1974 Edition.





TABLE 2 WEB CRIPPLING LOAD RATIOS  $P_u/P_c$  FOR TYPE 430 STEEL

N/t	h (mm)	$P_c$ (kN)	ANSI/ASCE-80-90 <sup>1</sup>		*ANSI/ASCE-80-90 <sup>1</sup>		SANTAPUTRA <sup>*</sup>	
			$P_c$ (kN)	$P_u/P_c$	$P_c$ (kN)	$P_u/P_c$	$P_c$ (kN)	$P_u/P_c$
10,26	90,0	11,225	10,1	1,110	10,6	1,063	8,9	1,258
	115,5	10,325	9,4	1,102	9,8	1,055	8,5	1,218
	142,1	9,725	9,9	0,985	10,3	0,943	9,2	1,055
	166,2	10,200	9,5	1,076	9,9	1,030	9,1	1,123
	190,5	10,125	8,5	1,195	8,9	1,144	8,3	1,213
	215,9	9,975	9,2	1,084	9,6	1,038	9,3	1,069
	241,4	8,925	8,6	1,034	9,0	0,990	9,0	0,988
	266,7	9,625	8,4	1,143	8,8	1,094	9,1	1,059
	291,1	8,700	8,1	1,076	8,4	1,030	9,0	0,966
	317,7	8,675	8,1	1,073	8,4	1,027	9,0	0,965
20,38	90,9	13,950	11,1	1,254	11,6	1,200	10,0	1,395
	114,7	13,825	10,5	1,320	10,9	1,264	9,6	1,436
	166,8	12,475	11,0	1,135	11,5	1,086	10,7	1,163
	191,2	12,225	10,2	1,201	10,6	1,150	10,2	1,198
	216,2	11,525	10,4	1,104	10,9	1,057	10,8	1,071
	241,1	11,225	9,6	1,169	10,0	1,119	10,2	1,100
	265,3	11,175	9,0	1,243	9,4	1,190	9,9	1,134
	290,8	10,725	8,8	1,221	9,2	1,169	9,4	1,141
316,5	9,950	8,4	1,187	8,8	1,136	8,4	1,186	
29,80	90,6	16,950	13,2	1,280	13,8	1,225	12,1	1,398
	115,6	15,350	12,2	1,254	12,8	1,201	11,5	1,339
	140,4	13,275	11,6	1,143	12,1	1,094	11,2	1,190
	167,7	13,850	11,1	1,249	11,6	1,196	11,0	1,263
	191,4	12,450	10,2	1,217	10,7	1,165	10,4	1,198
	240,9	12,325	10,0	1,230	10,5	1,177	10,8	1,141
	264,6	11,825	9,7	1,221	10,1	1,169	10,1	1,175
	290,7	11,750	9,6	1,225	10,0	1,172	9,5	1,236
316,1	11,150	9,6	1,162	10,0	1,113	9,0	1,234	
39,50	89,3	19,650	13,9	1,412	14,5	1,352	12,8	1,530
	115,1	14,025	12,8	1,099	13,3	1,053	12,1	1,164
	140,6	16,525	12,5	1,321	13,1	1,264	12,1	1,360
	165,3	15,650	11,9	1,316	12,4	1,260	11,9	1,320
	191,4	14,475	11,9	1,220	12,4	1,168	12,2	1,188
	215,2	14,600	11,3	1,289	11,8	1,234	12,0	1,221
	240,0	13,200	10,9	1,207	11,4	1,156	11,1	1,185
	266,7	13,150	10,7	1,225	11,2	1,173	10,5	1,255
	290,4	12,525	10,5	1,196	10,9	1,145	9,7	1,291
315,1	11,700	10,0	1,167	10,5	1,117	8,7	1,345	
49,23	90,5	21,125	16,3	1,294	17,1	1,239	15,3	1,380
	114,9	19,300	14,4	1,340	15,0	1,283	13,8	1,402
	140,3	18,400	12,8	1,441	13,3	1,380	12,5	1,472
	165,6	17,025	12,9	1,322	13,4	1,266	13,0	1,312
	193,2	16,275	13,2	1,234	13,8	1,182	13,7	1,188
	216,1	15,025	12,4	1,210	13,0	1,159	12,4	1,212
	240,7	14,525	11,6	1,251	12,1	1,198	11,0	1,321
	266,9	13,400	11,2	1,120	11,7	1,149	10,1	1,331
	291,4	13,575	11,4	1,192	11,9	1,141	9,9	1,373
315,8	12,225	11,1	1,101	11,6	1,054	9,1	1,344	
MEAN				1,203		1,151		1,231
C.O.V.				7,746		7,746		10,486

Refer to text for symbols and \*.

TABLE 3 WEB CRIPPLING LOAD RATIOS  $P_u/P_c$  FOR TYPE 304 STEEL

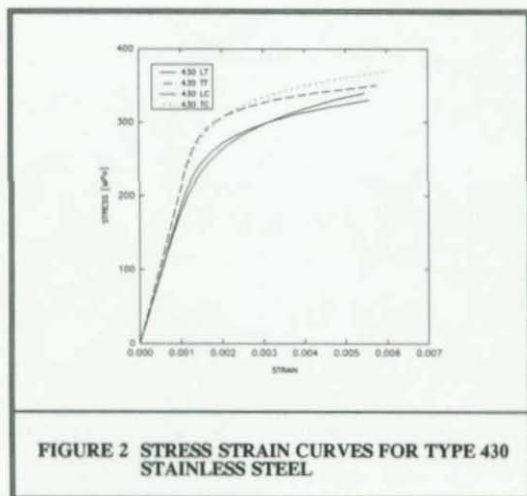
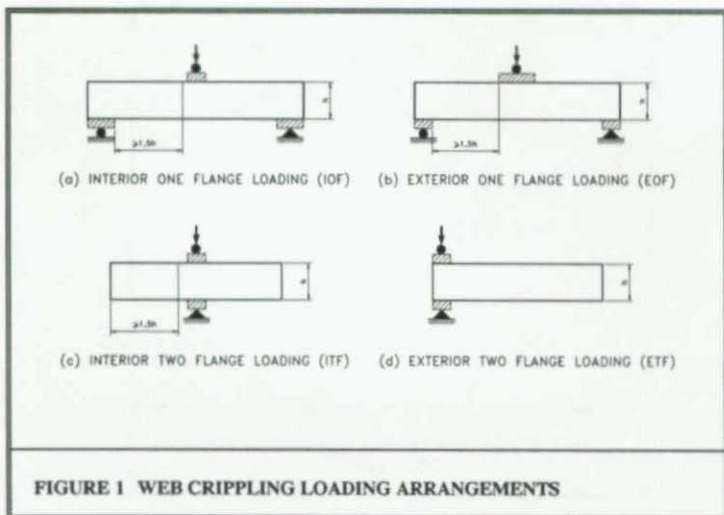
N/t	h (mm)	$P_c$ (kN)	ANSI/ASCE-80-90 <sup>1</sup>		*ANSI/ASCE-80-90 <sup>2</sup>		SANTAPUTRA <sup>3</sup>	
			$P_c$ (kN)	$P_u/P_c$	$P_c$ (kN)	$P_u/P_c$	$P_c$ (kN)	$P_u/P_c$
10,26	90,5	9,125	9,4	0,967	9,8	0,936	9,1	0,998
	115,7	9,200	9,4	0,981	9,7	0,949	9,3	0,986
	165,4	8,600	8,6	1,001	8,9	0,969	9,0	0,955
	190,7	8,325	8,4	0,995	8,7	0,962	9,0	0,922
	215,3	8,100	8,1	1,002	8,4	0,969	9,0	0,902
	241,4	7,825	8,1	0,972	8,3	0,940	9,2	0,849
	265,6	8,175	7,6	1,082	7,8	1,046	8,9	0,916
	291,3	8,525	7,4	1,155	7,6	1,117	9,0	0,947
20,38	89,8	11,350	10,0	1,134	10,3	1,097	9,8	1,155
	115,1	11,350	10,2	1,118	10,5	1,081	10,3	1,106
	139,7	10,000	9,5	1,054	9,8	1,019	9,8	1,017
	164,9	10,275	9,4	1,095	9,7	1,059	10,0	1,028
	190,9	9,750	9,2	1,061	9,5	1,026	10,1	0,967
	215,6	9,225	8,8	1,054	9,0	1,019	9,9	0,933
	242,2	8,900	8,5	1,050	8,8	1,016	9,9	0,900
	266,2	8,750	8,0	1,097	8,2	1,061	9,6	0,911
	291,4	7,925	8,4	0,939	8,7	0,908	10,0	0,790
	315,7	8,075	7,8	1,037	8,0	1,003	8,9	0,910
	317,3	8,000	7,9	1,017	8,1	0,984	8,7	0,919
29,80	90,1	13,300	11,3	1,181	11,6	1,142	11,2	1,183
	115,0	12,025	11,0	1,092	11,4	1,056	11,3	1,066
	139,9	11,400	10,4	1,101	10,7	1,065	10,9	1,048
	166,0	10,675	10,0	1,073	10,3	1,038	10,8	0,993
	191,1	9,975	10,1	0,987	10,5	0,954	11,2	0,887
	216,8	10,475	9,5	1,107	9,8	1,071	10,8	0,966
	241,1	9,600	9,3	1,027	9,7	0,993	11,0	0,870
	267,8	9,925	9,0	1,097	9,4	1,061	10,4	0,955
	291,7	9,100	8,7	1,043	9,0	1,009	9,5	0,962
	315,4	8,575	8,6	0,996	8,9	0,963	8,8	0,972
39,50	90,5	14,525	12,6	1,150	13,1	1,113	12,8	1,137
	115,0	13,875	11,6	1,200	12,0	1,161	12,0	1,161
	139,8	12,600	11,4	1,105	11,8	1,068	12,1	1,040
	165,6	11,975	10,9	1,103	11,2	1,067	11,9	1,010
	191,7	10,900	10,7	1,023	11,0	0,989	12,0	0,909
	214,7	10,755	10,3	1,046	10,6	1,012	11,9	0,898
	242,4	10,000	10,0	0,996	10,4	0,964	11,3	0,888
	265,6	9,900	9,8	1,006	10,2	0,973	10,5	0,941
	291,0	8,925	9,3	0,951	9,6	0,920	9,3	0,946
	315,2	9,250	7,3	1,272	7,5	1,230	6,2	1,483
49,23	89,9	16,675	12,6	1,325	13,0	1,281	12,8	1,302
	116,1	15,375	12,4	1,243	12,8	1,202	12,9	1,188
	140,2	14,450	12,1	1,192	12,5	1,153	13,0	1,111
	165,7	12,950	11,5	1,122	11,9	1,085	12,7	1,017
	191,0	11,850	11,2	1,062	11,5	1,028	12,5	0,945
	241,6	10,925	10,6	1,020	10,9	0,987	12,0	0,900
	246,0	10,800	10,5	1,038	10,9	1,004	10,9	1,001
	265,4	10,975	10,3	1,062	10,7	1,027	10,2	1,073
	291,4	10,425	10,3	1,016	10,6	0,983	9,7	1,075
	315,4	9,700	9,2	1,060	9,5	1,025	7,9	1,236
MEAN				1,072		1,037		1,006
C.O.V.				7,575		7,499		12,527

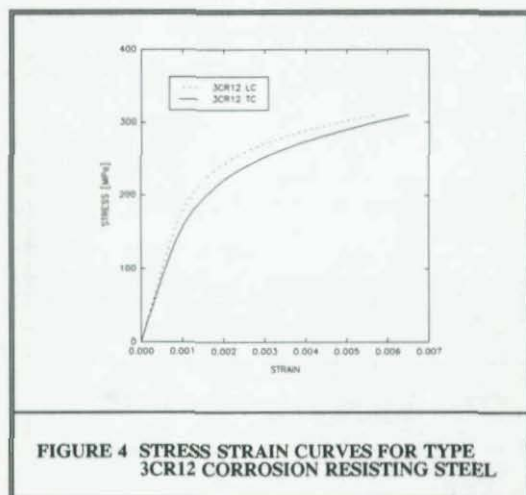
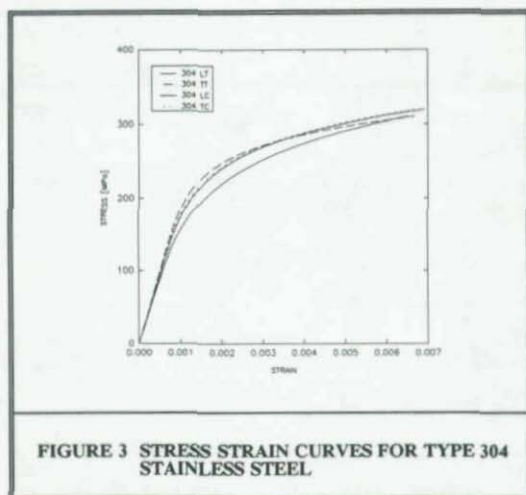
Refer to text for symbols and \*.

TABLE 4 WEB CRIPPLING LOAD RATIOS  $P_u/P_c$  FOR TYPE 3CR12 STEEL

N/t	h (mm)	$P_c$ (kN)	ANSI/ASCE-80-90 <sup>1</sup>		*ANSI/ASCE-80-90 <sup>1</sup>		SANTAPUTRA <sup>4</sup>	
			$P_c$ (kN)	$P_u/P_c$	$P_c$ (kN)	$P_u/P_c$	$P_c$ (kN)	$P_u/P_c$
10,26	48,37	9,28	9,8	0,946	10,0	0,926	9,5	0,980
	60,33	8,63	9,6	0,902	9,8	0,883	9,5	0,911
	75,41	8,23	9,3	0,888	9,5	0,869	9,5	0,869
	90,16	8,23	9,0	0,916	9,2	0,897	9,5	0,869
	103,26	8,00	8,7	0,917	8,9	0,898	9,5	0,845
	116,30	7,88	8,5	0,931	8,6	0,912	9,5	0,832
	127,13	8,23	8,2	0,998	8,4	0,977	9,5	0,869
	153,72	8,35	7,7	1,082	7,9	1,059	9,5	0,882
	163,49	7,73	7,5	1,027	7,7	1,006	9,1	0,851
20,38	47,54	11,45	10,7	1,069	10,9	1,046	10,5	1,091
	59,47	12,25	10,5	1,171	10,7	1,147	10,5	1,167
	75,00	10,23	10,1	1,011	10,3	0,990	10,5	0,975
	88,52	10,05	9,8	1,022	10,0	1,001	10,5	0,958
	102,72	9,75	9,5	1,024	9,7	1,002	10,5	0,929
	116,94	9,65	9,2	1,047	9,4	1,025	10,5	0,920
	127,81	10,30	9,0	1,147	9,2	1,123	10,5	0,982
	157,61	8,88	8,3	1,065	8,5	1,043	9,8	0,902
	167,55	9,93	8,1	1,223	8,3	1,197	9,0	1,109
29,80	48,09	13,00	11,6	1,124	11,8	1,100	11,5	1,131
	62,30	12,53	11,2	1,115	11,5	1,092	11,5	1,090
	75,41	12,85	10,9	1,176	11,2	1,151	11,5	1,118
	89,07	11,88	10,6	1,120	10,8	1,096	11,5	1,034
	103,28	11,28	10,3	1,097	10,5	1,074	11,5	0,981
	116,94	12,13	10,0	1,218	10,2	1,192	11,5	1,055
	127,27	11,73	9,7	1,207	9,9	1,182	11,5	1,021
	139,68	11,68	9,4	1,239	9,6	1,213	10,9	1,069
	166,85	9,93	8,8	1,129	9,0	1,106	9,0	1,107
39,50	47,59	14,53	12,4	1,171	12,7	1,147	12,4	1,168
	61,54	13,70	12,1	1,136	12,3	1,112	12,4	1,101
	75,96	13,43	11,7	1,148	11,9	1,124	12,4	1,079
	89,13	11,75	11,4	1,034	11,6	1,012	12,4	0,944
	103,30	12,88	11,0	1,170	11,2	1,145	12,4	1,035
	116,94	12,98	10,7	1,217	10,9	1,191	12,4	1,043
	127,13	12,55	10,4	1,205	10,6	1,180	11,8	1,060
	156,83	10,90	9,7	1,127	9,9	1,104	9,8	1,109
	166,84	10,80	9,4	1,147	9,6	1,123	8,9	1,207
49,23	75,82	14,63	12,6	1,165	12,8	1,141	13,5	1,084
	103,83	14,45	11,8	1,224	12,1	1,199	13,5	1,071
	117,03	13,85	11,4	1,210	11,7	1,185	12,8	1,080
	126,74	13,83	11,2	1,236	11,4	1,210	11,9	1,167
	158,24	12,15	10,3	1,175	10,6	1,150	9,8	1,241
	168,45	12,45	10,1	1,237	10,3	1,211	8,9	1,399
MEAN				1,105		1,082		1,032
C.O.V.				8,969		9,246		11,686

Refer to text for symbols and \*.







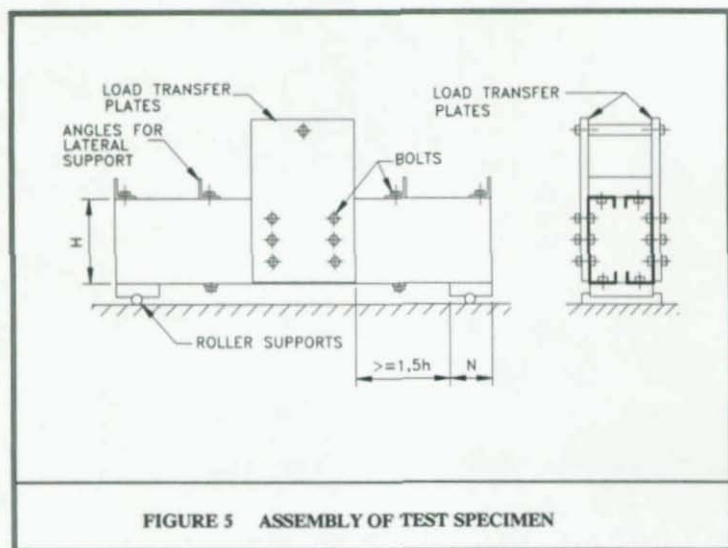


FIGURE 5 ASSEMBLY OF TEST SPECIMEN

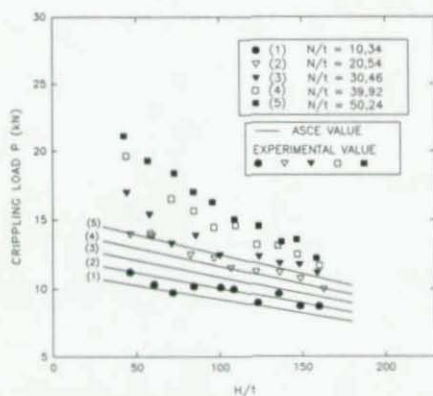


FIGURE 6 STEEL TYPE 430. EXPERIMENTAL and ANSI/ASCE-8-90<sup>1</sup> WEB CRIPPLING LOADS vs WEB SLENDERNESS.

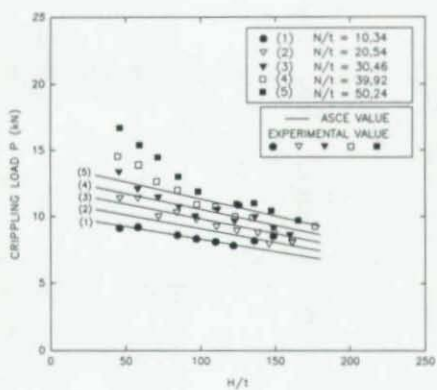


FIGURE 7 STEEL TYPE 304. EXPERIMENTAL and ANSI/ASCE-8-90<sup>1</sup> WEB CRIPPLING LOADS vs WEB SLENDERNESS.

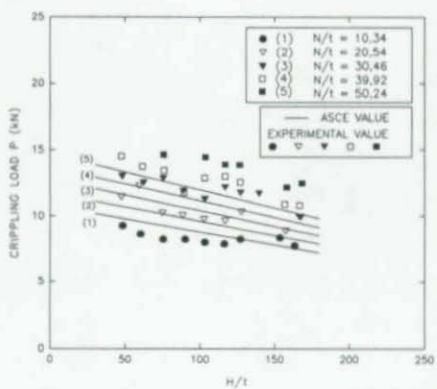


FIGURE 8 STEEL TYPE 3CR12. EXPERIMENTAL and ANSI/ASCE-8-90<sup>1</sup> WEB CRIPPLING LOADS vs WEB SLENDERNESS.

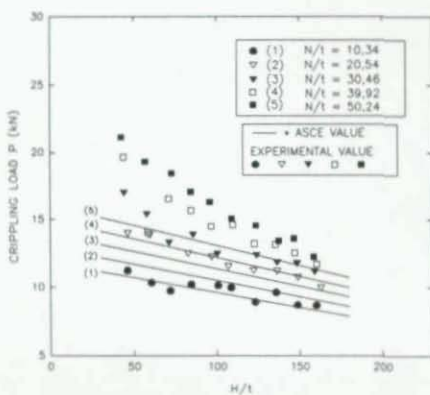


FIGURE 9 STEEL TYPE 430. EXPERIMENTAL and \*ANSI/ASCE-8-90<sup>1</sup> WEB CRIPPLING LOADS vs WEB SLENDERNESS.

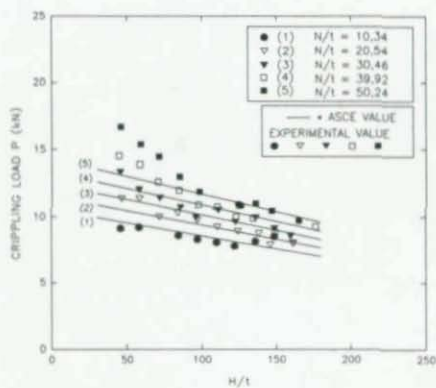


FIGURE 10 STEEL TYPE 304. EXPERIMENTAL and \*ANSI/ASCE-8-90<sup>1</sup> WEB CRIPPLING LOADS vs WEB SLENDERNESS.

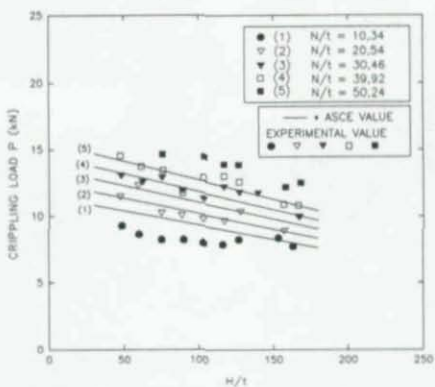


FIGURE 11 STEEL TYPE 3CR12. EXPERIMENTAL and \*ANSI/ASCE-8-90<sup>1</sup> WEB CRIPPLING LOADS vs WEB SLENDERNESS.

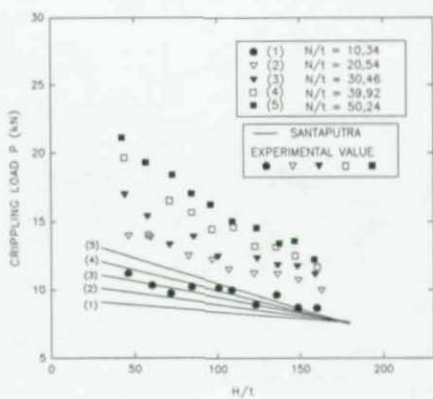


FIGURE 12 STEEL TYPE 430. EXPERIMENTAL and SANTAPUTRA<sup>8</sup> WEB CRIPPLING LOADS vs WEB SLENDERNESS.

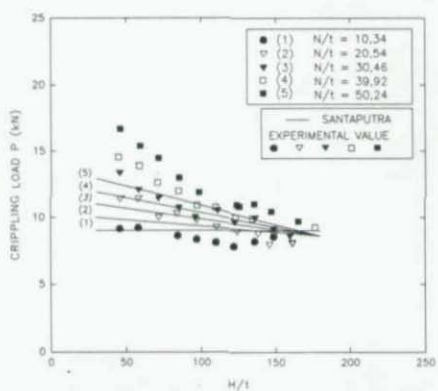


FIGURE 13 STEEL TYPE 304. EXPERIMENTAL and SANTAPUTRA<sup>®</sup> WEB CRIPPLING LOADS vs WEB SLENDERNESS.

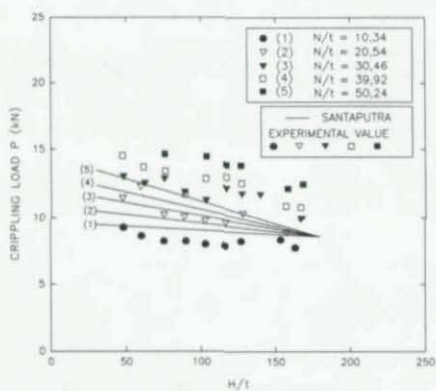


FIGURE 14 STEEL TYPE 3CR12. EXPERIMENTAL and SANTAPUTRA<sup>®</sup> WEB CRIPPLING LOADS vs WEB SLENDERNESS.





## SHEAR BEHAVIOR OF WEB ELEMENTS WITH OPENINGS

M.Y. Shan<sup>1</sup>, R.A. LaBoube<sup>2</sup>, and W.W. Yu<sup>3</sup>

## INTRODUCTION

The light-steel framing industry commonly uses cold-formed steel C-sections for structural members. Cold-formed steel sections are used because of their excellent strength-to-weight ratio, ease of fabrication, and ease of erection. These sections are routinely manufactured with openings, or punchouts, in the web. These web openings facilitate the installation of necessary utility service, i.e., electrical wiring and plumbing. However, generally accepted design guidelines for web openings do not exist in the United States. Thus, the objective for the research reported herein was to investigate experimentally the web shear strength. Based on the experimental findings, appropriate design recommendations have been formulated, and are presented.

## TEST SPECIMENS

Industry standard C-sections were tested. The cross-section dimensions, thickness and geometric parameters of each test specimen are recorded in Table 1.

The material properties of the steel, for each test specimen, were established by standard tensile coupon specimens cut from the web of the section. Table 2 lists the tensile test data for thickness, yield strength, ultimate tensile strength and percent elongation in 2-in. gage length.

## TEST SETUP

Each test specimen was subjected to a concentrated load at midspan (Fig. 2) until the ultimate shear strength of the member was obtained. To prevent lateral-torsional buckling, each test specimen consisted of two C-shaped beams connected together using 3/4 x 3/4 x 1/8 inch angles and self-drilling screws (Figs. 2 and 3).

When thin steel members with web openings are subjected to concentrated loads, three failure modes may occur: (1) bending, (2) shear, or (3) web crippling. To preclude web crippling at midspan, stiffeners were attached vertically to the webs at midspan. The influence of bending was minimized by using members with short span lengths.

---

<sup>1</sup> Research Assistant, Dept. of Civil Eng., University of Missouri-Rolla, Rolla, MO 65401.

<sup>2</sup> Associate Professor, Dept. of Civil Eng., University of Missouri-Rolla, Rolla, MO 65401.

<sup>3</sup> Curator's Professor Emeritus, Dept. of Civil Eng., University of Missouri-Rolla, Rolla, MO 65401.

### TEST RESULTS

Twenty-six tests of beams with web openings were conducted in this experimental investigation. It has been determined that the shear strength of the beam web was influenced primarily by the depth-to-thickness ratio of the web,  $h/t$ , and the ratio of web opening depth to flat web depth,  $a/h$ . For the twenty-six tests reported herein,  $h/t$  ranged from 34.0 to 210.0, and the  $a/h$  ratios varied from 0.13 to 0.74.

The shear failure load per web,  $P_{u(web)}$ , is taken as 1/4 of the ultimate midspan load. Table 3 tabulates the test results.

### SHEAR CAPACITY CALCULATION

For solid web elements, i.e., without web openings, subjected to shear only, the design strength can be estimated by applying the equations from Section C3.2 of AISI LRFD Specification (1991). These nominal equations also serve as the basis for the shear strength equations given in the AISI ASD Specification (1989). The equations are as follows:

$$(a) \text{ For } h/t \leq \sqrt{E k_v / F_y} : \quad V_n = 0.577 F_y h t \quad (\text{Eq. 1})$$

$$(b) \text{ For } \sqrt{E k_v / F_y} < h/t \leq 1.415 \sqrt{E k_v / F_y} : \quad V_n = 0.64 t^2 \sqrt{k_v F_y E} \quad (\text{Eq. 2})$$

$$(c) \text{ For } h/t > 1.415 \sqrt{E k_v / F_y} : \quad V_n = 0.905 E k_v t^3 / h \quad (\text{Eq. 3})$$

where

$V_n$  = Nominal shear strength of beams

$t$  = Web thickness

$h$  = Depth of the flat portion of the web measured along the plane of the web

$k_v$  = Shear buckling coefficient determined as follows:

1. For unreinforced webs,  $k_v = 5.34$

2. For beam webs with adequate stiffeners

when  $a'/h \leq 1.0$

$$k_v = 4.00 + 5.34 / (a' + h)^2$$

when  $a'/h > 1.0$

$$k_v = 5.34 + 4.00 / (a' + h)^2$$

where

$a'$  = the shear panel length for unreinforced web element

= distance between transverse stiffeners for reinforced web elements

Based on the above equations, the nominal shear strength,  $V_n$ , for each test specimen was calculated and is listed in Table 4.

### ANALYSIS OF TEST RESULTS

The influence of a web opening on the ultimate shear strength is not accounted for by the current Specifications (AISI 1989, 1991). Based on the AISI Specification for shear strength of the solid webs, the ratio of  $P_{u(web)}/V_n$  (Table 4) shows the reduction of the shear strength of a C-section with a web opening.

Based on a plot of the test data, Fig. 4, and using a regression analysis, both linear and non-linear shear strength reduction factors  $q_s$  ( $q_s = P_{u50}/V_n$ ) have been developed. Equations 4 and 5 are the linear relationships.

$$\begin{aligned} \text{when } a/h \leq 0.383 : \\ q_s = -3.699(a/h) + 1.722 \end{aligned} \quad (\text{Eq. 4})$$

$$\begin{aligned} \text{when } 0.383 \leq a/h \leq 1.00 : \\ q_s = -0.353(a/h) + 0.439 \end{aligned} \quad (\text{Eq. 5})$$

Equation 6 represents the non-linear strength reduction relationship.

$$q_s = 1.506 * 10^{[-1.33 * (a/h)]} \quad (\text{Eq. 6})$$

#### SUMMARY

An investigation was conducted to study the behavior of C-shaped members with web openings subjected primarily to shear. Based on the results from 26 beam specimen tests, equations were developed to estimate the strength of a web element with an opening centered at mid-depth of the web.

#### ACKNOWLEDGEMENTS

The research reported herein was co-funded by the American Iron and Steel Institute, and the Metal Lath/Steel Framing Association. The financial assistance given, and the technical guidance provided, are gratefully acknowledged.

#### REFERENCES

"Specification For the Design of Cold-Formed Steel Structural Members Design", August 19, 1986, with December 11, 1989 Addendum, American Iron and Steel Institute, Washington, D.C.

"Load and Resistance Factor Design Specification for Cold-Formed Steel Structural Members", March 16, 1991. American Iron and Steel Institute, Washington, D.C.

TABLE 1  
DIMENSIONS OF TEST SPECIMENS  
SUBJECTED TO SHEAR

Beam Specimen No.	Cross-Section Dimensions (inches)											Opening Geom. (in.)	
	Thick.	D1	D2	B1	B2	B3	B4	d1	d2	d3	d4	b	a
SU-4	0.071	3.65	3.63	1.63	1.64	1.63	1.63	0.54	0.51	0.49	0.52	4	1.50
SU-5	0.059	2.47	2.46	1.63	1.63	1.62	1.62	0.47	0.49	0.52	0.49	4	1.50
SU-6	0.033	2.42	2.43	1.63	1.64	1.63	1.62	0.42	0.42	0.50	0.50	4	1.50
SU-8	0.039	2.51	2.50	1.60	1.61	1.59	1.60	0.39	0.42	0.45	0.41	2	0.75
SU-9	0.044	3.70	3.65	1.56	1.57	1.57	1.58	0.57	0.57	0.56	0.50	4	1.50
SU-10	0.077	3.69	3.69	1.64	1.63	1.64	1.63	0.55	0.54	0.59	0.54	4	1.50
SR-12	0.055	12.02	11.97	1.57	1.57	1.57	1.57	0.46	0.57	0.55	0.48	4	1.50
SR-13	0.045	7.95	7.94	1.59	1.58	1.58	1.58	0.47	0.47	0.48	0.47	4	1.50
SR-14	0.046	6.06	6.04	1.62	1.62	1.55	1.55	0.47	0.48	0.50	0.51	4	1.50
SR-15	0.046	8.00	8.00	2.42	2.45	2.45	2.43	0.61	0.70	0.70	0.61	4	1.50

- Notes: 1. See Fig. 1 for the symbols used for dimensions.  
 2. See Fig. 2 for the symbols used for the hole geometry.  
 3. SU: Single Unreinforced (Web)  
 4. SR: Single Reinforced (Web)



TABLE 2  
MATERIAL PROPERTIES  
FOR SHEAR TEST SPECIMENS

Specimen No.	Thickness (in.)	$F_V$ (ksi)	$F_u$ (ksi)	Elongation (%)
SU-4	0.071	81	104	22
SU-5	0.059	54	75	39
SU-6	0.033	67	72	35
SU-8	0.039	34	48	44
SU-9	0.044	47	60	31
SU-10	0.077	64	78	23
SR-12	0.055	49	57	32
SR-13	0.045	72	74	30
SR-14	0.046	47	67	41
SR-15	0.046	22	59	55

- Notes: 1. SU: Single Unreinforced (Web)  
2. SR: Single Reinforced (Web)

TABLE 3  
EXPERIMENTAL DATA FOR SHEAR TEST SPECIMENS

Specimen No.	L (in.)	N (in.)	h/t	a/h	$P_u$ (test) (lbs)
SU-4-7	26.54	3.0	45	0.47	2760
SU-5-3	19.10	1.0	34	0.74	801
SU-5-4	19.10	1.0	34	0.74	778
SU-5-5	19.10	1.0	34	0.74	775
SU-5-6	19.10	1.0	34	0.74	775
SU-5-7	19.10	1.0	34	0.74	756
SU-6-3	19.16	1.0	62	0.73	338
SU-6-4	19.16	1.0	62	0.73	341
SU-6-5	19.16	1.0	62	0.73	328
SU-6-6	19.16	1.0	62	0.73	325
SU-6-7	19.16	3.0	62	0.73	344
SU-8-8	22.11	6.0	54	0.35	550
SU-8-9	22.11	6.0	54	0.35	438
SU-9-10	27.54	5.0	74	0.46	1125
SU-9-11	27.54	6.0	74	0.46	929
SU-10-5	34.81	6.0	42	0.46	2406
SU-10-6	34.81	6.0	42	0.46	2750
SU-10-7	34.81	6.0	42	0.46	2556
SR-12-1	40.56	1.0	210	0.13	2563
SR-12-2	40.56	1.0	210	0.13	3500
SR-13-1	38.00	6.0	168	0.20	2263
SR-13-2	38.00	6.0	168	0.20	2313
SR-14-1	32.00	6.0	123	0.27	2494
SR-14-2	32.00	6.0	123	0.27	2594
SR-15-1	38.00	6.0	165	0.20	2075
SR-15-2	38.00	6.0	165	0.20	2044

Notes: 1. SU: Single Unreinforced (Web)  
2. SR: Single Reinforced (Web)

TABLE 4  
THE EVALUATION OF SHEAR TEST DATA

Specimen No.	h/t	a/h	$P_{u(test)}$ (lbs)	$V_n$ (lbs)	$P_{u(test)}/V_n$
SU-4-7	45	0.47	2760	11524	0.240
SU-5-3	34	0.74	801	3732	0.215
SU-5-4	34	0.74	778	3732	0.208
SU-5-5	34	0.74	775	3732	0.208
SU-5-6	34	0.74	775	3732	0.208
SU-5-7	34	0.74	756	3732	0.203
SU-6-3	62	0.73	338	2264	0.149
SU-6-4	62	0.73	341	2264	0.151
SU-6-5	62	0.73	328	2264	0.145
SU-6-6	62	0.73	325	2264	0.144
SU-6-7	62	0.73	344	2264	0.152
SU-8-8	54	0.35	550	1614	0.341
SU-8-9	54	0.35	438	1614	0.271
SU-9-10	74	0.46	1125	3371	0.334
SU-9-11	74	0.46	929	3371	0.276
SU-10-5	42	0.46	2406	9213	0.261
SU-10-6	42	0.46	2750	9213	0.298
SU-10-7	42	0.46	2556	9213	0.277
SR-12-1	210	0.13	2563	2700	0.949
SR-12-2	210	0.13	3500	2700	1.296
SR-13-1	168	0.20	2263	2010	1.125
SR-13-2	168	0.20	2313	2010	1.151
SR-14-1	123	0.27	2494	2943	0.847
SR-14-2	123	0.27	2594	2943	0.881
SR-15-1	165	0.20	2075	2230	0.931
SR-15-2	165	0.20	2044	2230	0.917

Notes: 1. SU: Single Unreinforced (Web)  
2. SR: Single Reinforced (Web)

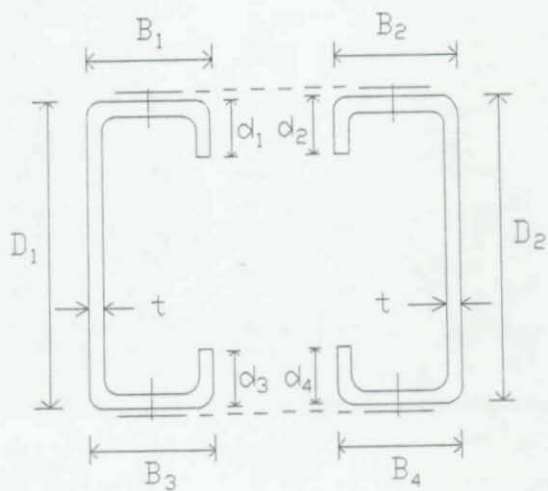


Figure 1. Beam Cross-Section

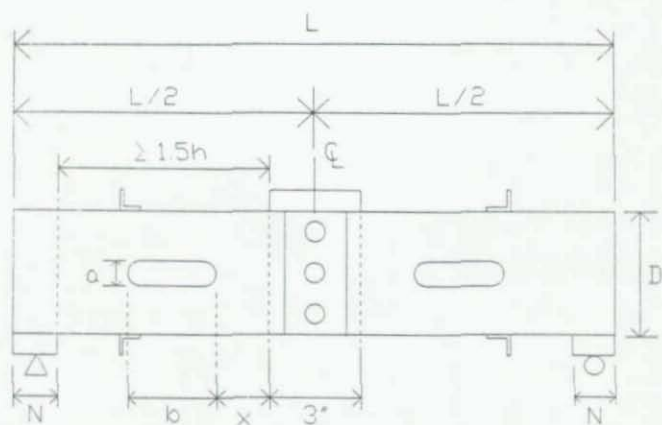


Figure 2. Test Setup



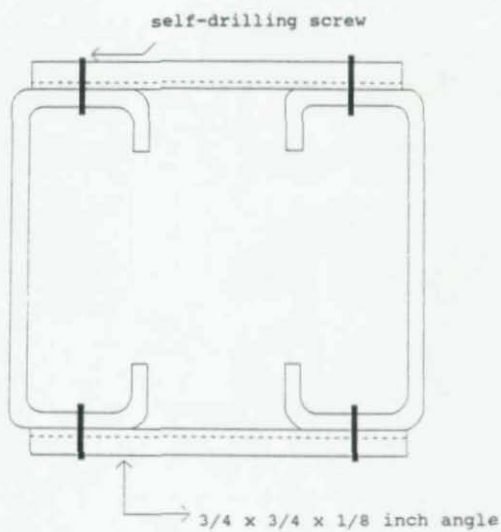


Figure 3. Cross Section of Test Specimen

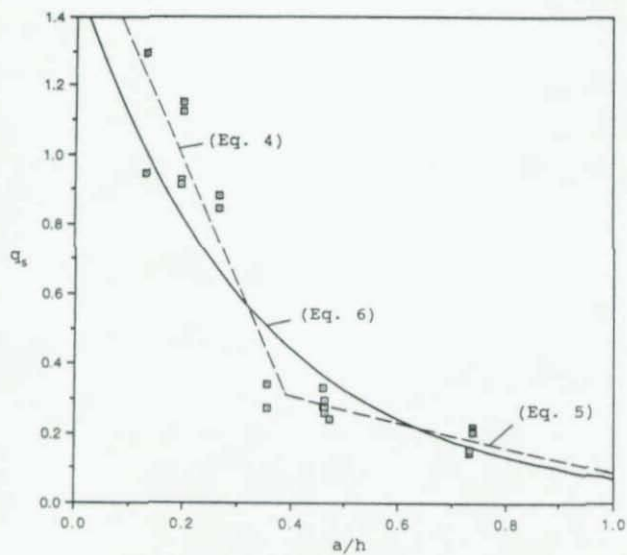


Figure 4. Relationship between the Shear Strength Reduction Factor  $q_s$  and  $a/h$  Ratio



## CAPACITY OF HIGH STRENGTH THIN-WALLED BOX COLUMNS

James M. Ricles<sup>1</sup>, Le-Wu Lu<sup>2</sup>, Perry S. Green<sup>3</sup>, Robert Tiberi<sup>3</sup>  
Alan A. Pang<sup>3</sup>, and Robert J. Dexter<sup>4</sup>

### ABSTRACT

An analytical and experimental program was conducted to investigate the instability failure modes of single and multi-cellular box sections with plate width-to-thickness ( $b/t$ ) ratios ranging from 48 to 96. In each test specimen a loss of stiffness and significant transverse deflections of the cell's plates were observed to occur near the theoretical elastic buckling stress. The failure mode consisted of locally buckled sections, leading to flexural instability. The plate  $b/t$  ratio was found to be the main parameter affecting specimen local buckling and capacity. Nonlinear finite element analysis of the specimens produced good agreement with test results. Cell interaction effects in the multi-cellular specimens was shown experimentally and analytically not to significantly affect their capacity. The specimen strength was found to be well predicted by simple methods that included empirical plate strength equations, tangent modulus, and interaction equations.

### INTRODUCTION

Current conventional ship hull construction consists of a single skin of steel plating which is stiffened in orthogonal directions by stiffeners and transverse members. The U.S. Navy is currently considering an advanced (unidirectional) double-hull design [Beach, 1990] in its fleet of the future program. The advanced double-hull is an unstiffened cellular structure formed by twin skins of steel plating, separated by longitudinal girders that span between transverse bulkheads spaced at 11 meters (36 feet). The arrangement of the plates in the double-hull results in cellular sections. Figure 1 shows sections of a conventional and the advanced double-hull.

The advanced double-hull concept offers several advantages over the conventional hull, including: (1) the unidirectional girder system in the double hull represents a simplified design which facilitates automated welding and fabrication techniques; (2) fewer structural discontinuities and complex weld details exist which could lead to fatigue and fracture problems; and (3) improved structural redundancy and therefore survivability in the event of a collision. The Navy double-hull ships are likely to be fabricated from high-strength low-alloy (HSLA) steels, which offer increased yield and ultimate tensile strength relative to conventional steels as well as increased weldability and toughness. If the allowable primary stress is increased in order to take advantage of high-strength steel then compressive instability is more likely to become a governing consideration in double-hull design. Figure 2 shows the three basic modes of compression instability that need to be considered for the advanced double-hull: (1) local plate instability; (2) beam-column instability; and (3) cellular grillage instability.

Plate components of the cells of double hulls may undergo local instability if the plate slenderness ratios (width-to-thickness,  $b/t$ ) are large. Beam-column instability involves overall buckling of the cells between bulkheads, and is usually coupled with local plate instability

<sup>1</sup>Associate Professor of Civil Engineering, SSRC Associate Director, <sup>2</sup>Professor of Civil Engineering, <sup>3</sup>Research Assistant, <sup>4</sup>Senior Research Engineer

effects, as plate buckling will occur first at relatively low levels of load for typical  $b/t$  ratios used in design. Such interaction is important, especially in the more slender cellular beam-columns, because of the loss of plate stiffness and strength under local buckling leading to a reduction in beam-column stiffness and strength. The third type of instability, cellular grillage, is defined as the instability behavior of a panel of box cells supported of four edges.

To develop a better understanding of the instability behavior of HSLA advanced double-hull components, a research study was conducted at Lehigh University. The objectives of this study were: (1) experimentally investigate the strength and overall load-deformation characteristics of double-hull cellular components fabricated from HSLA steel plating under axial and combined loading; (2) assess the use of existing Naval empirical single hull plate equations for predicting the strength of double-hull cells; and (3) provide a data base for verification of mathematical and numerical models of instability failure modes of advanced double-hull components. In this paper the experimental and analytical program is described and results presented and discussed related to the objectives of the study.

### EXPERIMENTAL PROGRAM

**Test Specimens** - The experimental program involved the testing of nine large scale specimens of various cross-sections (single, double or triple cells), lengths, and end boundary conditions. Details are shown in the specimen test matrix of Table 1. The nomenclature for each specimen is based upon the identification of its number of cells, cell dimensions, and the overall length. Thus Specimen 1-3636-10 represents a specimen with one cell, 914.4 by 914.4 mm (36 by 36 in.) in cross-section and 3.05 m (10 ft.) in length. All specimens were fabricated from 9.5 mm (3/8 in.) thick steel plate that was fillet welded together. High-strength low-alloy (HSLA 80) steel was used which had a nominal yield strength of 551.6 MPa (80 ksi). Seven of the specimens were full scale specimens cut from a prototype double-hull module that was fabricated by Ingalls Shipbuilding located in Pascagoula, Mississippi. The remaining two specimens (3-1818-6 and 3-1818-18) were half-scale models fabricated separately. The 1.83 m (6 ft.) and 3.11 m (10 ft.) long specimens were stub columns, while Specimens 1-3636-18 and 1-3636-35 were pin-ended columns and Specimens 3-1818-18 and 3-3636-36 were beam-columns.

Twelve and six representative tensile coupons were tested in order to obtain the material properties for the full scale and half-scale specimens, respectively. The coupons were extracted from both the longitudinal and transverse (i.e. perpendicular to the direction of rolling) directions. A summary of the material properties is given in Tables 2 and 3. The coupon tests show that the strength in the transverse direction is somewhat lower compared to the longitudinal direction for the full scale specimens, and vice-versa for the half-scale specimens. For the full scale specimens the average measured yield stress,  $\sigma_y$ , was 602 MPa (87.3 ksi) with an average ultimate stress,  $\sigma_u$ , of 676 MPa (98.1 ksi). The average measured strain,  $\epsilon_u$ , corresponding to ultimate stress  $\sigma_u$  was 7.1 percent, with an elongation  $\Delta\%$  of 14.5 percent at fracture. The half-scale specimens had average values of  $\sigma_y$  and  $\sigma_u$  equal to 558 MPa (80.9 ksi) and 634 MPa (91.9 ksi), respectively, with  $\epsilon_u$  equal to 6.2 percent and  $\Delta\%$  equal to 13.5 percent.

Welding residual stress measurements were made on a 914.4 by 914.4 mm (36 by 36 in.) cell using a 254 mm (10 in.) long Whittemore gage. Shown in Figure 3 are the longitudinal residual stresses on the external surface of the cell. The pattern is similar to the well known pattern for welded plates, consisting of a wide middle band of nearly constant compressive stress with narrow bands of high tensile stresses at the plate's junctions. Idealized patterns of the plate's longitudinal residual stresses were developed based on the measurements, consisting of a residual stress block of width  $\eta t$  and magnitude  $\sigma_y$  adjacent to the weld (see Figure 4), where  $t$  is the



plate thickness. The remaining plate width of  $b-2\eta t$  has a stress block with magnitude  $\sigma_{rc}$ , representing the average of a plate's measured compressive longitudinal residual stresses, where the factor  $\eta$  is calculated from equilibrium. Table 4 presents a summary of the values for  $\sigma_{rc}$  and  $\eta$  for the four plates of the cell. The average values of  $\sigma_{rc}$  and  $\eta$  among the four plates were 53.8 MPa (7.8 ksi) and 3.83, respectively. Values of  $\eta$  reported by Faulkner [1975a] for plates made of carbon or manganese steel ranged from 3.0 to 4.0.

Specimen initial geometric imperfections were also measured. Initial out-of-flatness of the component plates was measured by using a series of dial gages mounted on a steel frame. The frame had magnetic pads at its ends to secure it to the edges of the members when readings were taken. Maximum plate out-of-flatness ranged from 3 to 12 mm (0.12 to 0.47 in.) and were within the maximum values proposed by several researchers (see Figure 5). In addition, initial out-of-straightness was also measured for the column and beam-column specimens by means of a level. Maximum out-of-straightness  $\delta_0$  values for the longer specimens are summarized in Table 5 in terms of  $\delta_0/L$ , where  $L$  is the overall specimen length. The average measured maximum out-of-straightness of these specimens was  $L/1626$ .

**Test Set Up and Procedure** - The stub and beam-column specimens were tested under flat ended conditions while the pin-ended columns had a specially hardened cylindrical bearing placed at each end of the specimen. Since the hinged action was in one direction, the column's axis which contained the largest initial crookedness was aligned such that bending occurred about this axis. Lateral pressure was applied to the beam-column specimens by means of air pressure in a bladder which was confined between the specimen and a strongback restraint system, see Figure 6. The ends of the specimens were milled and end plates welded on.

Strain gages were placed around the cross-section at midheight as well as several other locations. Axial shortening and lateral deflections were monitored using LVDTs. The pressure in the air bladders was measured using pressure transducers and calibrated load cells inserted into the bladder restraint system to measure the reactions from the strongback frame. The loading sequence for each test involved initial alignment load followed by monotonically increasing cycles of axial load to failure. In the beam-column tests, initial cycles of lower axial load were applied without applying any lateral pressure. With a low constant axial load being maintained, the air bladders were then inflated to the pressure of 138 kPa (20 psi) or 13.6 m (45 ft.) of seawater for the half-scale specimen and 62 kPa (9 psi) or 6.2 m (20 ft.) of seawater for the full scale specimen. The axial load was then increased monotonically until a prescribed axial deformation beyond the peak load was reached. After this an unload/reload cycle was usually performed to check the residual stiffness of the specimen.

## RESULTS AND DISCUSSION

A typical normalized axial load - shortening response ( $P/P_y - \Delta/\Delta_y$ ) for Specimen 1-3636-18 is shown in Figure 7. Local plate buckling occurred in all of the specimens leading to a reduction in their axial stiffness. The initial local buckling was elastic, with each specimen possessing a post-buckling reserve strength. At large strains, corresponding to specimen capacity and beyond, buckling became more pronounced and was concentrated at the midheight location, as shown in Figure 8.

The initial local buckling strength was deduced from a plot of the load versus transverse plate displacements. Examples of such plots are shown in Figure 9 for three different  $b/t$  ratios. Elastic local buckling is defined as the point where a change in slope occurs. The initial local buckling was found to occur at an axial load  $P$  of 4 to 12 percent of the axial yield strength  $P_y$ .



for specimens with  $b/t = 96$ , and 37 to 50 percent of the axial yield strength for specimens with  $b/t = 48$ . After initial local buckling occurred the longitudinal strain distribution was found to become nonuniform in the specimens. This is evident in Figures 10 and 11, where the strain is shown to be nonuniform at 18 percent in single cell Specimen 1-3636-10 and 16 percent in triple cell Specimen 3-2430-6. Due to the local outward plate's movement causing bending curvature, tensile strains are shown in Figure 11 to develop on the outside of the plates near the middle of Panels 1 and 3 of Specimen 3-2430-6.

Because insufficient strain measurement data was available for each specimen, the initial buckling loads were based on plate transverse displacements. This load was compared to available strain measurements for some of the specimens, using the separation of strain readings of strain gages placed on opposite surfaces at a point on a plate to define initial local buckling. Figure 12 shows a typical plot of strain separation occurring at the middle of a plate at the initial buckling load of  $0.043P_y$  for Specimen 1-3636-10. It was determined that this method resulted in an initial buckling load that was 70 to 85 percent of the initial buckling load based on transverse plate displacement.

The margin of reserve strength beyond initial local buckling in addition to the capacity  $P_{max}$  of the specimens was found to be highly dependent on the  $b/t$  ratio of the cell's plates. Table 6 provides a summary of specimen capacity. The ultimate strength of the specimens with nominal ratios of  $b/t = 96$  ranged from 35 to 42 percent of their yield strength  $P_y$ . Specimen 3-2430-6, having  $b/t = 80$ , had a strength of 48 percent of its yield strength with half-scale Specimens 3-1818-6 and 3-1818-18 ( $b/t = 48$ ) having a capacity of 75 to 70 percent of their yield strength, respectively. An illustration of the margin of reserve strength beyond the initial buckling load  $P_{cr}$  based on plate transverse displacement is given in Figure 13, where the ratio  $P_{max} / P_{cr}$  has been plotted as a function of the parameter:

$$\beta = b/t \sqrt{\sigma_y E} \quad (1)$$

where  $E =$  Young's Modulus. A summary of the  $\beta$  values for each specimen is included in Table 6. For specimens with  $b/t = 48$  ( $\beta = 2.4$ ) the ratio of  $P_{max} / P_{cr}$  was equal to 1.4 and 2.0, whereas for  $b/t = 96$  ( $\beta = 5.0$ ),  $P_{max} / P_{cr}$  ranged from 4.5 to 10 (see Figure 13). Figure 13 indicates a greater scatter in the results for  $P_{max} / P_{cr}$  for specimens having higher values of  $\beta$ . This phenomenon is explained by the fact that while  $P_{max}$  was rather consistent for a given  $\beta$ ,  $P_{cr}$  for large  $\beta$  was more variable because of the greater differences in the out-of-flatness for the specimens with  $b/t = 96$  (see Figure 5).

Current Naval design criteria makes use of the Frankland [1940] equation for plate strength  $P_{max}$  in single hull ships, where

$$\frac{P_{max}}{P_y} = \frac{2.25}{\beta} - \frac{1.25}{\beta^2} \quad (2)$$

A similar empirical based equation has been developed by Faulkner [1975b]:

$$\frac{P_{max}}{P_y} = \frac{2.0}{\beta} - \frac{1.0}{\beta^2} \quad (3)$$

Figure 14 shows the specimen experimental capacity to be well predicted by these empirical plate strength equations. Numerical comparisons with these equations are given in the last two columns of Table 6. The experimental data in Figure 14 shows also the significance of the parameter which governs specimen strength to be the  $b/t$  ratio of a cell's plates. Specimen capacity was determined not to be significantly affected by end boundary conditions, length, number of cells, or the lateral load.

### ANALYTICAL PROGRAM

The analytical program involved analyzing the test specimens using several methods, namely: the nonlinear finite element method, empirical plate strength equations (Frankland and Faulkner), tangent modulus method, and beam-column analysis in conjunction with an interaction equation.

**Finite Element Analysis** - The program ADINA [ADINA R & D, 1990] was employed for the analytical studies of the test specimens and their component plates. Geometric nonlinearity was modeled using the large displacement, small strain feature of the program. A plastic material model with the von Mises yield criterion was used. Residual stresses were easily included using the initial strain/strain gradient feature. The solution method adopted was Newton-Raphson with full stiffness reformulation and equilibrium iterations at each load step. If the load step was too large for convergence the program automatically subdivided it into smaller steps until convergence was reached or the solution terminated after a specified maximum number of subdivisions.

Rectangular shell elements were used to model the test specimens. The elements adjacent to the plate intersections are more narrow in order to model the thin edge strip of residual tensile stress, assuming the idealized rectangular stress pattern of two thin edge strips with a tensile stress equal to the measured yield strength  $\sigma_y$  and a wide middle strip with the balancing compressive stress  $\sigma_{rc}$ . The width of the tensile strip was taken to be four times the nominal plate thickness (e.g.  $\eta = 4$ ) which is based on Faulkner's analysis of a large data base of plating [1975a], and close to the average value of 3.83 from the specimen residual stress measurements. This pattern was assumed to be constant over the length of the specimens except near the ends, where it decays linearly from the full value to zero at the ends, over a distance of one plate width. For multicellular specimens, the residual stresses in the flanges and webs were also assumed to be separately self-equilibrating. The out-of-flatness of the component plates was modeled by direct input of the measured initial geometrical imperfections or using a double sine series surface fit to the measured data [Lu and Pang, 1992]. The measured out-of-straightness was included in the models of the longer specimens.

Based upon the results of the tensile coupon tests, a kinematic hardening material model with the average yield stress of  $\sigma_y = 602$  MPa (87 ksi) and a strain hardening modulus  $E_{sh} = 1207$  MPa (175 ksi) was used for the full scale specimens; for the half-scale specimens the average yield stress of  $\sigma_y = 558$  MPa (81 ksi) and  $E_{sh} = 1937$  MPa (281 ksi) was used. The ends of the fixed-ended specimens were taken to be fixed against lateral translation and rotation. Loading was applied in the form of displacement increments up to and beyond the ultimate load, and the complete load-deflection behavior was obtained for the specimens.

Table 7 summarizes the analytical (see FEM Unit) and experimental maximum strengths of the specimens while Figure 15 shows the experimental normalized average stress versus average strain curves along with the response predicted using ADINA for several specimens. In general the stiffness and ultimate strengths of the specimens are reasonably predicted by the finite element models. The predicted ultimate loads of the fixed-ended stub specimens are higher than

the experimental values. The higher values can be attributed to the assumption of fixed boundary conditions at the ends of the specimens; in practice the conditions will be intermediate between fully fixed and simply supported. For the pinned column tests (Specimens 1-3636-18 and 1-3636-35), the slopes of the analytical curves were smaller compared to that of the experimental curves. This may be due to uncertainties in the values of the actual measured plate thicknesses as well as some friction in the cylindrical bearings. Figure 16 shows the deformed profiles of two specimens, 3-2430-6 and 1-3636-18, at deformations beyond the peak load. It can be seen that in the case of the multi-cellular specimen that the buckles tended to localize at the midheight location, which agrees with observed specimen behavior.

Since the cells are interconnected, rotational restraint along the plate junctions can be expected to increase the strength of the plates and hence, the specimens. To investigate the effect of such rotational restraint, the component plates of the stub specimens were analyzed separately using the same residual stresses and initial deflections as in the complete model, with simply supported conditions along the unloaded edges. The in-plane restraint condition along the unloaded edges was the unrestrained condition, i.e., free to take up any position under load. The analysis results are summarized in Table 7 (see FEM Plates). In all five stub specimens, as expected, the sum of the plate strengths gives lower values for maximum strength compared to the unit strength. However, the results from the two methods differ by a maximum of only about 7 percent (for Specimen 3-3630-6). Moreover, for Specimens 1-3636-10 and 3-1818-6, whose cells each have plates of equal width-to-thickness ( $b/t$ ) ratios, the difference between the strengths predicted by the two methods is less than 1 percent. The other three specimens show bigger differences but a simply supported plate boundary condition still seems to be reasonable. The maximum loads of the individual plates occur at about the same strain level such that the aggregate of the maximum is a fair approximation to the strength of the whole specimen. In general, the specimen strength predicted by the sum of its plates agrees with test results to within about  $\pm 7$  percent. A scatter plot of the predicted and experimental results from the empirical Frankland and Faulkner equations and from the finite element analyses is shown in Figure 17. Ironically, the best agreement is found with the simple empirical equations, followed by the plate analyses, and finally the full three-dimensional nonlinear finite element analyses. Not shown are relatively poor results predicted using the AISC  $Q$ -factor for the effective width as well as modifications of this approach, e.g. Usami and Fukumoto [1982 and 1985].

**Column Strength by Tangent Modulus Method** - In this method, the average stress-average strain of the stub column specimen is used to obtain the capacity of a long column of the same cross-section. The method is well established [Galambos, 1968], and the stub column test has been standardized internationally. The test basically accounts for the effect of residual stresses in a section. For the double-hull cells, where local buckling occurs, it also accounts for the loss of stiffness due to the local buckling. It is assumed that the deflected surface profiles of the long column is similar to that of the stub column.

The method was applied to Specimens 1-3636-18, 1-3636-35, 3-1818-18, and 3-3636-36. Specimen 1-3636-10 was taken to be the stub for the full scale specimens, while Specimen 3-1818-6 was the stub column for the half-scale specimen. The tangent modulus load (in stress form) of a column is given by:

$$\sigma_t = \frac{\pi^2 E_t}{(kL/r)^2} \quad (4)$$

or in normalized form,

$$\frac{\sigma_t}{\sigma_y} = \frac{\pi^2 E_t}{\sigma_y (kL/r)^2} \quad (5)$$

The analytical expression for the stress-strain curve is of the form

$$\frac{\sigma}{\sigma_y} = \sum_{i=0}^n C_i (\epsilon/\epsilon_y)^i \quad (6)$$

where  $C_i$  represents constant coefficients. The exponent  $i$  may be fractional. Equation (6) can be differentiated to get  $E_t$  for any stress level, where

$$\frac{E_t}{\sigma_y} = \frac{1}{\sigma_y} \frac{d\sigma}{d\epsilon} = \frac{d}{d\epsilon} \left( \sum_{i=0}^n C_i (\epsilon/\epsilon_y)^i \right) \quad (7)$$

Thus, upon substituting Equation (7) into (5)

$$\frac{\sigma_t}{\sigma_y} = \frac{\pi^2}{(kL/r)^2} \frac{d}{d\epsilon} \left( \sum_{i=0}^n C_i (\epsilon/\epsilon_y)^i \right) \quad (8)$$

The tangent modulus stress  $\sigma_t$  is that which corresponds to the strain  $\epsilon$  which equates Equations (6) and (8), e.g.

$$\sum_{i=0}^n C_i (\epsilon/\epsilon_y)^i = \frac{\pi^2}{(kL/r)^2} \frac{d}{d\epsilon} \left( \sum_{i=0}^n C_i (\epsilon/\epsilon_y)^i \right) \quad (9)$$

The strain  $\epsilon$  is found by a trial and error iterative procedure and then used in Equation (8) to obtain  $\sigma_t$ . To facilitate the differentiation analytical expressions for Equation (6) were fitted to the numerical results of the stub columns, see Figure 18.

Results for the two pin-ended columns (Specimens 1-3636-18 and 1-3636-35) are shown in Column 3 of Table 8. The method overestimates the experimental maximum loads of these specimens by about 8 and 11 percent, respectively. The difference can be explained by the following reasons. Firstly, the tangent modulus method does not account for initial crookedness of the column. Secondly, the stub column average thickness was slightly larger than that of the columns. The corresponding stub curve is thus stiffer and gives a higher value of the tangent modulus load. However, considering the simplicity of the method, the results are good predictions for the actual strengths.



**Beam Column Interaction Equation** - An interaction equation of the form

$$\frac{P}{P_u} + \frac{C_m M}{[M_u(1 - P/P_e)]} = 1 \quad (10)$$

represents a state of combined axial and flexural loading for which the beam-column is on the verge of failure.  $P_u$  and  $M_u$  are the member strengths when acting solely as a column and as a beam, respectively,  $P_e$  is the Euler buckling load and  $C_m$  is an equivalent uniform moment factor to be applied when the loading is other than equal end moment causing single curvature. The term in the brackets is a factor by which the primary moment is multiplied to account for *moment amplification*. The use of Equation (10) for double-hull cells with high b/t plates is complicated by the fact that the cross-section experiences local buckling.  $P_u$  can therefore be estimated using the tangent modulus method as discussed above. The ultimate bending strength,  $M_u$ , is defined to be the flexural strength when the average stress of the effective compression flange is at yield. For pure bending only, the compression flange is assumed to buckle and the effective widths are obtained from the AISC Specification [1986]. Okamoto et al [1985] have presented interaction curves for the longitudinal girders of a double hulled product oil carrier.

Equation (10) was used to predict the ultimate strength of the beam-column Specimens 3-1818-18 and 3-3636-36. They were first analyzed as a fixed-ended column to get the value of  $P_e$  using the tangent modulus method, and secondly as a beam-column using Equation (10). Table 8 summarizes the results and shows that the interaction equation predicts the ultimate strength of the cellular beam-columns fairly well and on the conservative side. Calculated loads for both specimens were about 90 percent of the experimental values. Comparison of the column with the beam-column strengths for the specimens (see Table 8, columns 3 and 4) indicate about a 10 to 15 percent reduction in strength due to the applied lateral load.

#### CONCLUSIONS AND RECOMMENDATIONS

Compressive instability failure modes of double-hull cells affect the overall longitudinal strength of the ship hull. A large scale experimental study involving cellular components was conducted to investigate the failure modes. Specimens were analyzed by numerical models using the nonlinear finite element method, empirical and beam-column equations, and tangent modulus method, respectively, to predict their capacity. The main conclusions from the study are as follows:

- (1) Local plate instability occurs prior to overall flexural instability for the range of plate b/t ratios used in the specimens. This was particularly observed in the testing of the long specimens. The effect of the locally buckled plates must be taken into consideration in assessing beam-column strength of the double-hull cells.
- (2) For b/t ratios of 96, initial local plate buckling occurs between 4 and 12 percent of the yield strength, whereas for b/t ratios of 48 the initial local buckling occurs at about 38 to 50 percent of the yield strength. For cells having b/t = 96, local buckling could occur for severe wave loading which could lead to fatigue.
- (3) For the specimens tested, the initial buckling strength and ultimate capacity were not sensitive to length, number of cells, boundary conditions, or lateral load. The

cross-section of the cellular structure is therefore apparently stiff enough that column buckling and beam-column interaction are not of concern for lengths between bulkheads of about 11 meters (36 feet).

- (4) The local buckling, ultimate capacity, and post-ultimate behavior of the specimens was reasonably simulated using the finite element method, provided the residual stresses, initial imperfections, large displacements, and plasticity were included in the analyses.
- (5) The simple empirical design equations of Frankland and Faulkner both gave a good prediction of the specimen ultimate load capacity.
- (6) Box column strength can be well predicted by the tangent modulus approach in conjunction with stub column stress-strain properties.
- (7) The interaction equation approach can predict the ultimate strength of the beam-columns. However, to obtain the complete load-deformation behavior, numerical methods must be used.

Based on the above findings, the following recommendations are made:

- (i) Simply supported conditions along the unloaded edges can be assumed in analyzing the behavior of the unstiffened component plates of the double-hull cell if the difference of the plate's  $b/t$  ratio meeting at the junction is not too large;
- (ii) The tangent modulus method, after modification for the effect of local buckling, can be used to predict box column strength;
- (iii) For beam-columns, the interaction equation with reduced strengths due to local buckling can be used to obtain beam-column strength predictions under various combinations of axial compression and lateral loads.

Work is currently being conducted to develop beam-column models for the box sections using numerical integration techniques. It is anticipated that interaction graphs and design charts can then be produced for design of these sections.

#### ACKNOWLEDGEMENTS

This study was funded by the U.S. Navy under U.S. Navy-Lehigh University Cooperative Agreement N00014-91-CA-0001. The support is gratefully acknowledged. The study was carried out at the National Science Foundation Engineering Research Center for Advanced Technology for Large Structural Systems at Lehigh University, U.S.A. Dr. John W. Fisher is the Director.

#### REFERENCES

- ADINA R & D, Inc. (1990) ADINA-IN for ADINA Users Manual, ADINA R & D, Inc., Watertown, MA.



- AISC (1986) Manual of Steel Construction: Load & Resistance Factor Design, 1st Ed., American Institute of Steel Construction, Chicago.
- Antoniou, A.C. (1980) 'On the Maximum Deflection of Plating in New Ships,' J. Ship Research, Vol. 24, No. 1, 31-39.
- Beach, J.E. (1990) 'Advanced Surface Ship Technology - Cluster B' ASNE Symposium 1990, 89-112.
- Carlsen, C.A. and Czujko, J. (1978) 'The Specification of Post-Welding Distortion Tolerances for Stiffened Plates in Compression,' The Structural Engineer, Vol. 56A, No. 5, 133-141.
- Faulkner, D. (1975a) 'Compressive Strength of Welded Grillages,' in Ship Structural Design Concepts, J.H. Evans, ed., Cornell Maritime Press, Cambridge, MD.
- Faulkner, D. (1975) 'A Review of Effective Plating for Use in the Analysis of Stiffened Plating in Bending and Compression,' J. Ship Research, Vol. 19, No. 1, 1-17.
- Frankland, J.M. (1940) Strength of Ship Plating under Edge Compression, David Taylor Model Basin Report No. 469.
- Galambos, T. V. (1968) Structural Members and Frames, Prentice-Hall, Englewood Cliffs, N.J.
- Lu, L.W. and Pang, A.A. (1992) 'Structural Instability Failure Modes: Design Recommendations,' Final Report for TDL 91-01, ATLSS Volume 1, Lehigh University, Bethlehem, PA.
- Okamoto, T., Hori, T., Tateishi, M., Rashed, S.M.H., and Miwa, S. (1985) 'Strength Evaluation of Novel Unidirectional-Girder-System Product Oil Carrier by Reliability Analysis,' Trans. SNAME, Vol. 93, 1-18.
- Paik, J.K., Kim, D.H., Bong, H.S., Kim, M.S., and Han, S.K. (1992) Deterministic and Probabilistic Safety Evaluation for a New Double-Hull Tanker with Transverseless System, Paper No. 6, Annual Meeting of the SNAME, October 28-31.
- Usami, T. and Fukumoto, Y. (1982) Local and Overall Buckling of Welded Box Columns, J. Struct. Div, ASCE, Vol. 108, No. ST3, 525-542.
- Usami, T. and Fukumoto, Y. (1985) Welded Box Compression Members, J. Struct. Eng., ASCE, Vol 110, No. 10, 2457-2470.

Table 1 Test Specimen Matrix

Specimen Number	Number of Cells	Length (feet)	b/t Ratio	Test Configuration
1-3636-10	1	10	96	Fix-ended Column
1-3636-18	1	18	96	Pin-ended Column
1-3636-35	1	35	96	Pin-ended Column
2-3036-6	2	6	96	Fix-ended Column
3-1818-6	3	6	48	Fix-ended Column
3-1818-18	3	18	48	Fix-ended Beam-Column
3-2430-6	3	6	80	Fix-ended Column
3-3036-6	3	6	96	Fix-ended Column
3-3636-36	3	36	96	Fix-ended Beam-Column

Table 2 Tensile Coupon Material Tests, Full Scale Specimens

Orientation	Yield Strength, $\sigma_y$ (MPa)	Ultimate Strength, $\sigma_u$ (MPa)	Strain at Ultimate Strength, $\epsilon_u$ (%)	Elongation, $\Delta\%$ (%)
Longitudinal	623.3	692.3	7.4	15.2
Transverse	579.9	660.5	6.7	13.9
Average	601.9	676.4	7.1	14.5

Table 3 Tensile Coupon Material Tests, One-Half Scale Specimens

Orientation	Yield Strength, $\sigma_y$ (MPa)	Ultimate Strength, $\sigma_u$ (MPa)	Strain at Ultimate Strength, $\epsilon_u$ (%)	Elongation, $\Delta\%$ (%)
Longitudinal	552.8	633.5	7.4	14.9
Transverse	562.2	634.3	5.0	11.9
Average	557.5	633.9	6.2	13.5

Table 4 Longitudinal Residual Stress Distribution Parameters  $\sigma_m$  and  $\eta$ 

Plate	Average $\sigma_m$ (MPa)	$\eta$
A	48.3	3.46
B	52.5	3.74
C	64.7	4.53
D	49.5	3.54

Table 5 Maximum Measured Specimen Out-of-Straightness

Specimen	Out-of-Straightness, $\delta_y/L$
1-3636-18	0.00058
1-3636-35	0.00061
3-1818-18	0.00056
3-3636-36	0.00071

Table 6 Specimen Capacity and Comparisons with Theory

Specimen	b/t	$\beta$	$P_{max}$ (KN)	$P_{max}/P_y$	$P_{max}/P_{TH,1}$	$P_{max}/P_{TH,2}$
1-3636-10	96	5.04	8389	0.369	0.930	1.033
1-3636-18	96	5.07	8038	0.358	0.906	1.007
1-3636-35	96	5.04	7922	0.353	0.890	0.989
2-3036-6	96	5.05	15061	0.420	1.060	1.178
3-1818-6	48	2.49	19678	0.752	1.071	1.172
3-1818-18	48	2.39	18935	0.696	0.962	1.050
3-2430-6	80	4.15	19398	0.479	1.020	1.130
3-3036-6	96	5.16	20496	0.403	1.035	1.151
3-3636-36	96	4.88	20661	0.376	0.922	1.024

$P_{TH,1}$  = Capacity per Frankland, Equation (1)

$P_{TH,2}$  = Capacity per Faulkner, Equation (2)

Table 7 Comparison of Specimen Capacity with Finite Element Analysis

Specimen	$P_{max}$			Strength Ratio	
	Experimental (KN)	FEM Unit (KN)	FEM Plates (KN)	Experimental Unit	Experimental Plates
1-3636-10	8389	9007	8989	0.931	0.933
1-3636-18	8038	8215	---	0.978	---
1-3636-35	7922	7695	---	1.029	---
2-3036-6	15061	16591	15777	0.908	0.955
3-1818-6	19678	18539	18424	1.061	1.068
3-1818-18	18935	18183	---	1.041	---
3-2430-6	19398	21515	20621	0.902	0.941
3-3036-6	20496	23783	22178	0.862	0.924
3-3636-36	20661	20016	---	1.032	---

Mean : 0.97 0.96  
 Coefficient of Variation : 0.04 0.02

Table 8 Comparison of Experimental Strengths with Tangent Modulus and Interaction Equation Predicted Maximum Strengths

Specimen	$P_{max}/P_y$		
	Experimental	Tangent Modulus	
		Column	Beam Column
1-3636-18	0.358	0.398	----
1-3636-35	0.353	0.382	----
3-1818-18	0.696	0.725	0.660 *
3-3636-36	0.376	0.406	0.346 *

\* Based on AISC Interaction Formula

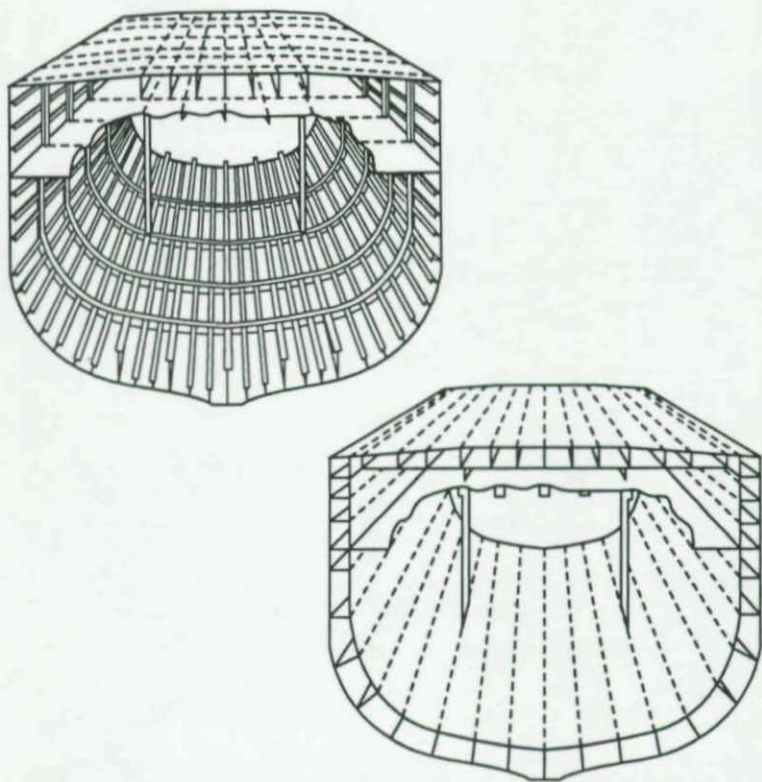
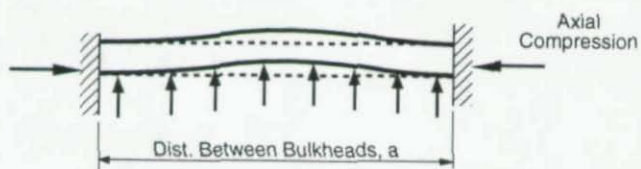
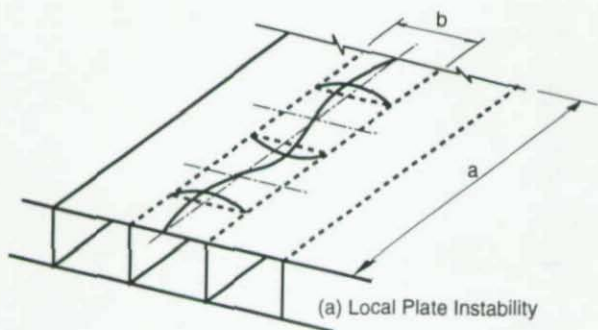
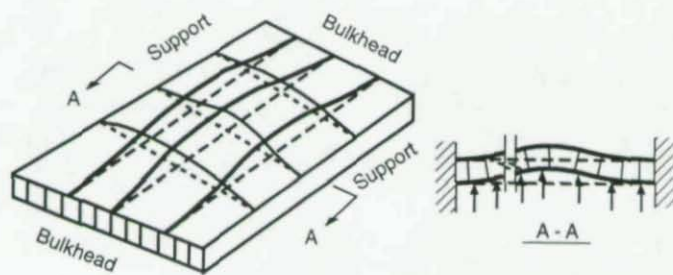


Figure 1 Conventional and Advanced Double Hull Designs  
(after Beach, 1990)





(b) Box Beam-Column Instability



(c) Cellular Grillage Instability

Figure 2 Compressive Instability Failure Modes of Advanced Double Hull

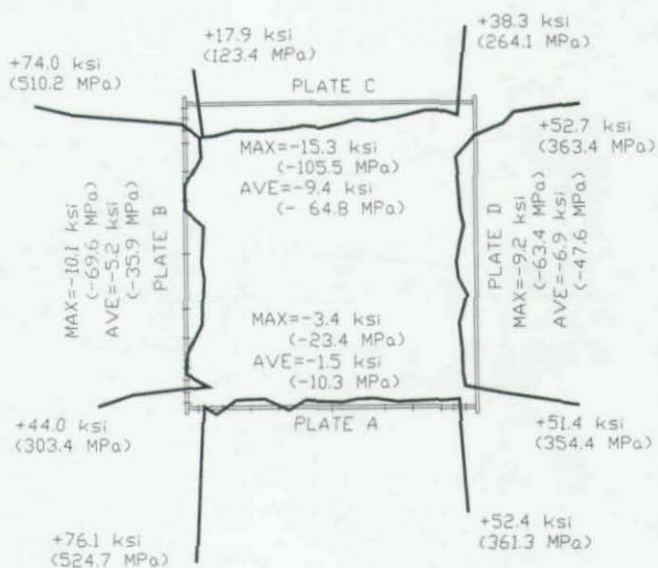


Figure 3 External Surface Longitudinal Residual Stress Distributions, Whittmore Gage Readings

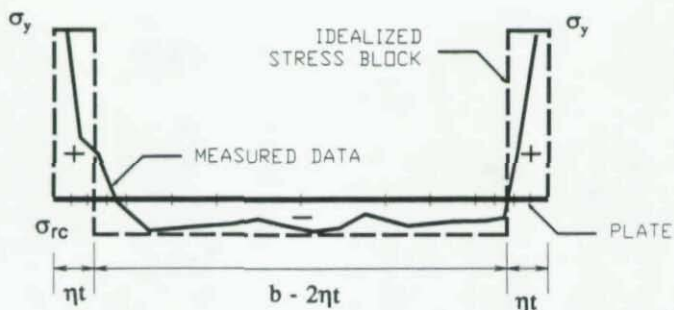


Figure 4 Idealized Longitudinal Residual Stress Distribution

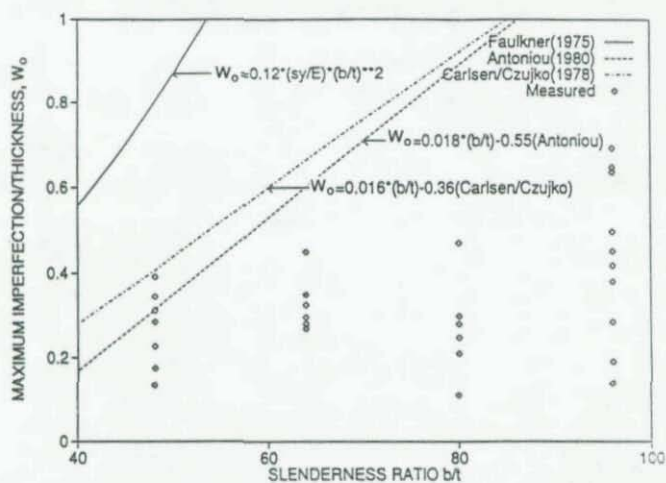


Figure 5 Measured Plate Out-of-Flatness Compared with Faulkner's, Carlsen and Czujko's and Antoniou's Proposed Equations



Figure 6 Test Set-up for Beam Column Test  
(Air bladder on right side of specimen)

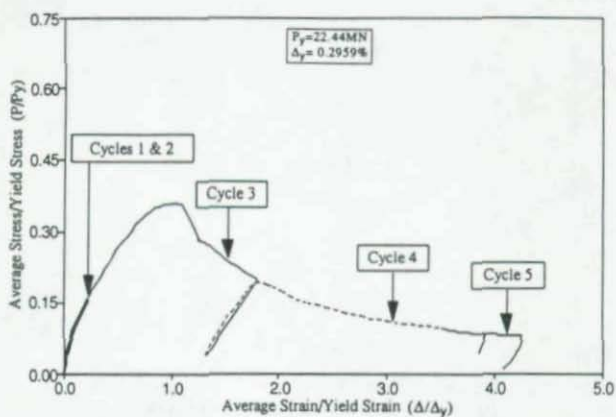


Figure 7 Load Shortening Relationship for Specimen 1-3636-18

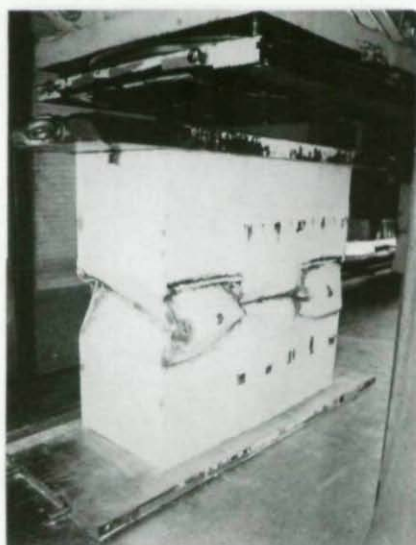


Figure 8 Specimen 3-2430-6 after 100mm of Axial Compression Showing Development of Plastic Hinges in the Whitewash Coating

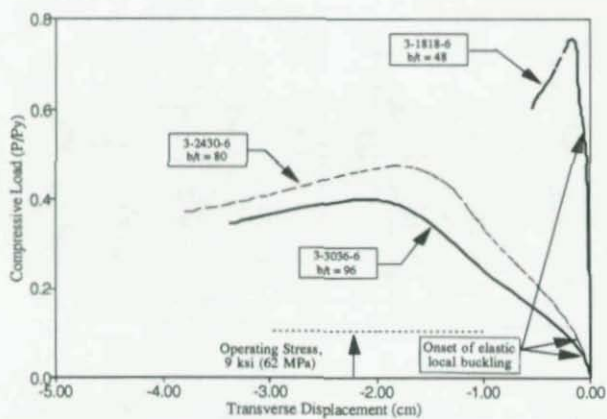


Figure 9 Local Out-of-Plane Panel Displacement-Axial Load Relationship, Selected Triple Cell Specimens



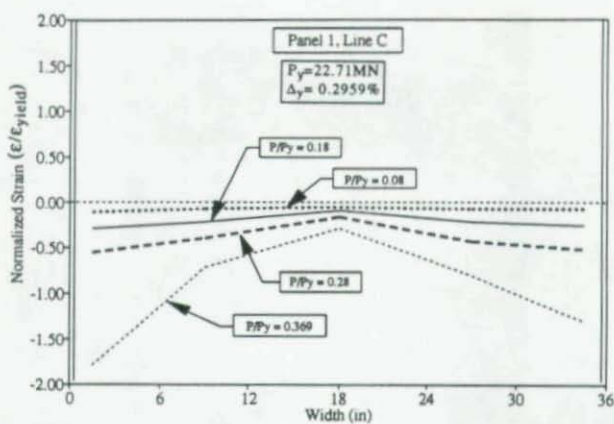


Figure 10 Measured Longitudinal Strains for Specimen 1-3636-10, Panel 1

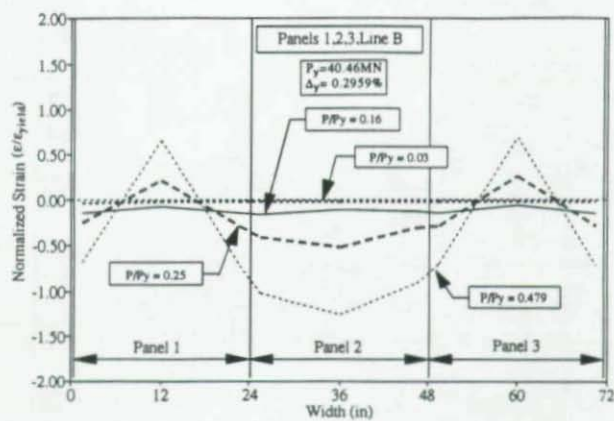


Figure 11 Measured Longitudinal Strains for Specimen 3-2430-6, Panels 1, 2 and 3

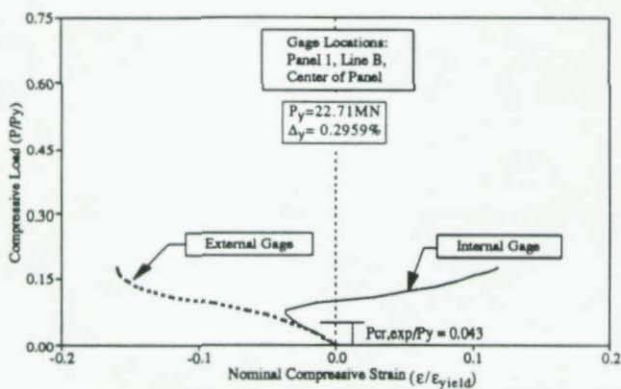


Figure 12 Strain Separation for Specimen 1-36-10, Panel 1

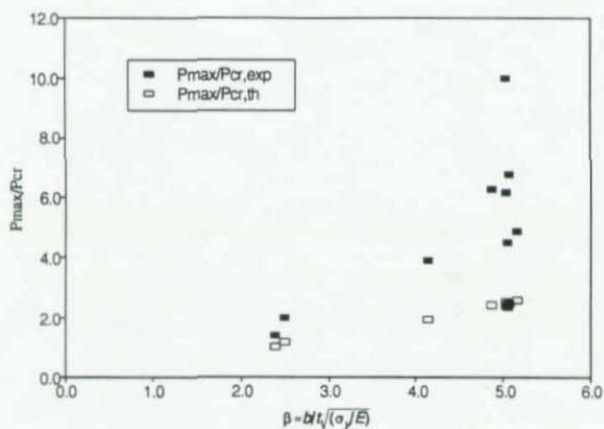


Figure 13 Post-Buckling Strength Ratios for Specimens

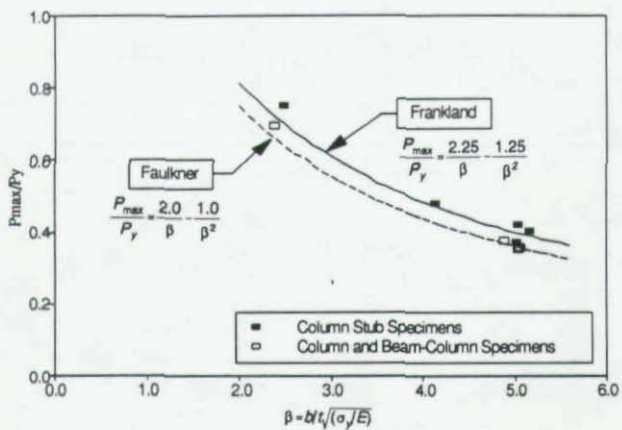


Figure 14 Comparison of Maximum Load Predicted with Frankland and Faulkner Design Equations to Experimental Data

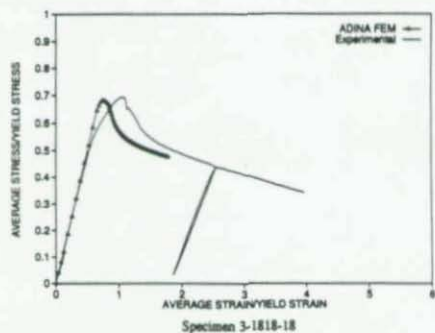
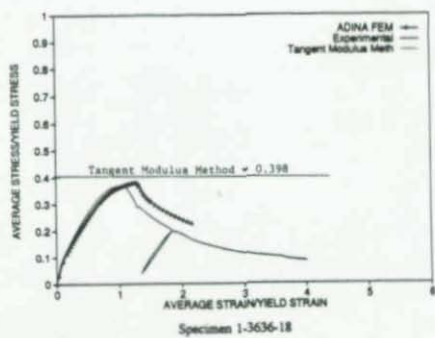
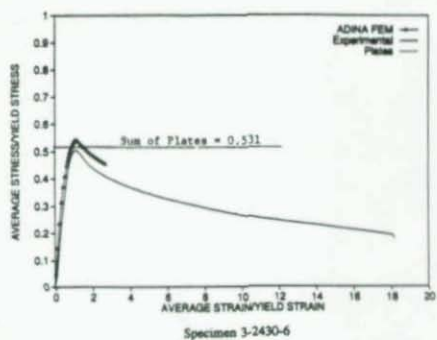
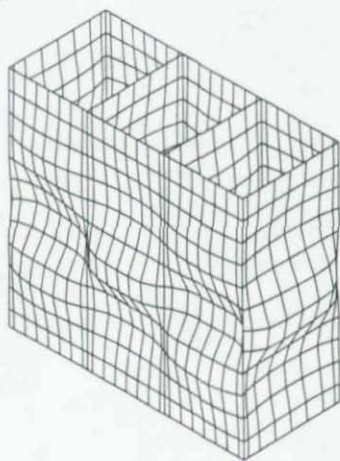


Figure 15 Analytical and Experimental Normalized Load Deformation Curves for Several Test Specimens



(a) Specimen 1-3636-18



(b) Specimen 3-2430-6

Figure 16 Deformed Profiles of Two Test Specimens from FEM Analysis



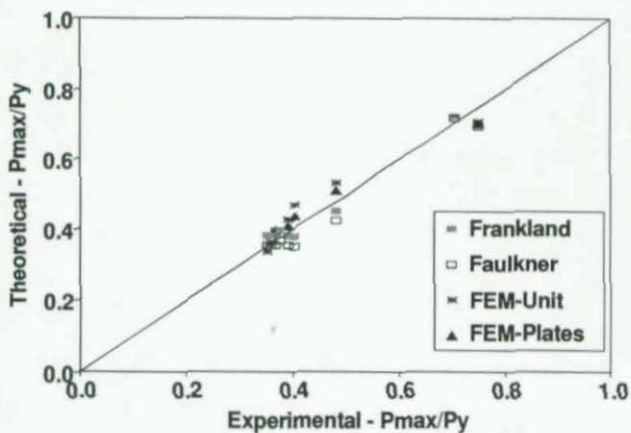


Figure 17 Comparison of Maximum Load Predicted with Various Methods to Experimental Results

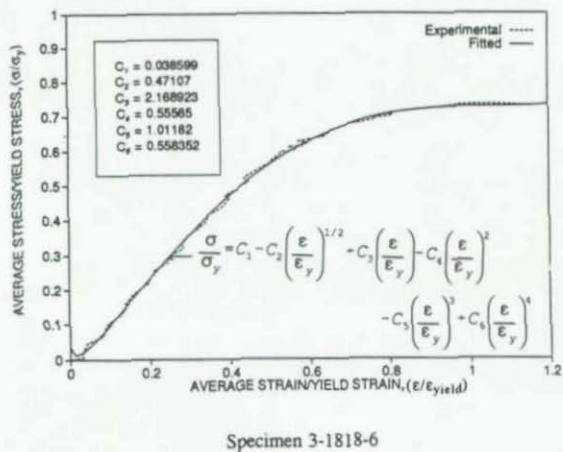


Figure 18 Fitted Analytical Expression for Stress Strain Curve of Specimen 3-1818-6



State-of-the-Art on Research, Design and  
Construction of Horizontally Curved Bridges in Japan

by

Toshiyuki KITADA\*, Hiroshi NAKAI\*\* and Yasuo MURAYAMA\*\*\*

SUMMARY

This paper emphasizes the necessity of research study on the ultimate strength concerning the horizontally curved plate and box girders through a survey of references published in Japan since 1977. Then, the outline of a latest draft design method for curved plate girders is presented herewith. Next, the applicable ranges of parameters on buckling stability of the curved box girders are shown on the basis of a questionnaire for about 260 curved box girder bridges. Finally, a special curved continuous spiral girder bridge under construction is also introduced together with a few numerical results based on the elasto-plastic and finite displacement analysis for this bridge under seismic load.

INTRODUCTION

In metropolitan districts in Japan, numerous horizontally curved bridges have been constructed and will be constructed, because of tight right-of-way of circumferential conditions. For this reason, various researches on curved bridges have been active<sup>1)</sup> in Japan, in comparison with in other foreign countries. Thus, it becomes also possible to construct the curved cable-stayed bridges such as the Katsusika Harp Bridge (spans: 40.5+ 134.0+ 220.0+ 60.5 in m, 1987), and continuous spiral girder bridges such as the approach bridges of the Senbonmatsu Bridge (spans:  $6 \times 38.587$  in m, 1979).

First of all, this paper summarizes theoretical and experimental investigations<sup>2)-26)</sup> on the buckling stability of horizontally curved plate and box girders which have been carried out in Japan since 1977, because the state-of-the-art on curved bridges before 1976 had been already reported by one of the authors as a work of the Task Committee on Curved Box Girders of the ASCE-AASHTO<sup>27),28)</sup>.

Secondly, this paper introduces the outline of the buckling stability criteria in the draft

---

\* Associate Professor, Department of Civil Engineering, Osaka City University, Osaka, JAPAN, Member-at-Large of SSRC

\*\* Professor, Department of Civil Engineering, Osaka City University

\*\*\* Chief Engineer, Design Section, Division of Steel Bridge Design, Kurimoto Ltd.

guidelines<sup>29)</sup> for the horizontally curved girder bridges in the Hanshin Expressway Public Corporation (HEPC).

Then, statistical data with respect to cross-sectional dimensions and span lengths of box girder bridges as well as buckling parameters of compression flanges and web plates are shown on the basis of a questionnaire for about 260 horizontally curved box girder bridges which had been already constructed in Japan.

Finally, the north approach bridge of the River Kizu Bridge under construction, a continuous spiral box girder bridge with seventeen spans connected rigidly to six steel piers of rigid frame, is introduced. Also reported in this paper are a few results of the elasto-plastic and finite displacement analysis executed to investigate the ultimate load carrying capacity of this bridge<sup>30)</sup>.

### RECENT RESEARCH WORKS ON BUCKLING STABILITY OF CURVED PLATE AND BOX GIRDERS

Recent Japanese research works<sup>23)-26)</sup> concerning the buckling stability of curved plate and box girders are summarized in Table 1. This table reveals that it is necessary to research the ultimate strength of horizontally curved box girders much more actively, because almost all the research studies have been carried out only in the author's group<sup>23),26)</sup> in Japan.

Table.1 Recent research works on buckling study in Japan (since 1977)

Type	①Lateral buckling		②Local buckling (Bending)		③Local buckling (Shear)		④Combination (②+③)	
	Theory	Experiment	Theory	Experiment	Theory	Experiment	Theory	Experiment
Plate Girders	#Nakai-Kotoguchi (1983) #Maekawa-Yoshida (1981)	#Nakai-Kotoguchi (1983)	#Fuji-Ohura (1985, 1987, 1989) #Nakai-Kitada-Ohnami (1986) #Sustake-Hirashima-Yoda (1981, 1984, 1985) #Mikami-Furunishi-Yonezawa (1980)	#Fuji-Pujieda-Sakaoka (1992) #Nakai-Kitada-Ohnami (1983)	#Nakai-Kitada-Ohnami (1983, 1985, 1986)	#Nakai-Kitada-Ohnami-Fukamoto (1986)	#Imai-Ohta (1987) #Nakai-Kitada-Ohnami (1985)	#Nakai-Kitada-Ohnami (1985)
Box Girders			#Oote-Hirashima-Yoda (1989) #Imai-Tajima-Ohta (1988)	#Nakai-Murayama-Kitada (1990, 1992)	#Oote-Hirashima-Yoda (1989) #Imai-Tajima-Ohta (1988)	#Nakai-Murayama-Kitada (1990, 1992)	#Oote-Hirashima-Yoda (1989) #Imai-Tajima-	#Nakai-Murayama-Kitada (1990, 1992)
Imperfection	#Nakai-Kitada-Ohnami (1988)							

## EXPERIMENTAL RESEARCH ON BOX GIRDERS

Fig.1 shows a test apparatus developed in Osaka City University<sup>24)</sup>, which applies bending and torsional moments simultaneously to a box girder specimen. The cross section of box girder specimens, illustrated in Fig.2, is designed as an asymmetric one to realize the non-uniform distribution of normal stress in the compression flange due to warping and superelevation of the top flange. The test results are plotted in Fig.3 together with an interaction curve of ultimate bending moment,  $M_u$  and torsional moment,  $T_u$ , of which

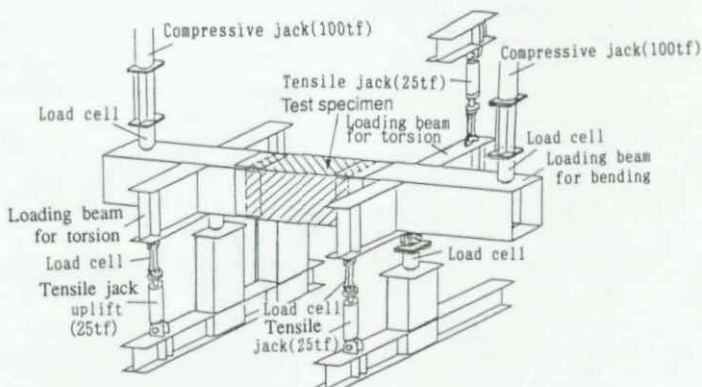


Fig.1 Test apparatus applying bending and torsion to specimens<sup>26)</sup>

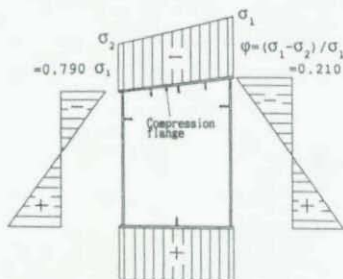


Fig.2 Cross section of test specimen and normal stress distribution

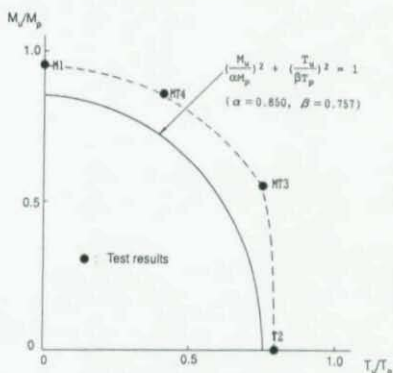


Fig.3 Interaction curve for combined action of bending and torsion at ultimate state<sup>26)</sup>

formula has been proposed by the authors<sup>26)</sup>. In this figure  $M_p$  and  $T_p$  are the fully plastic bending and torsional moments, respectively,  $\alpha M_p$  and  $\beta T_p$  being the ultimate bending and torsional moments of cross section under bending and torsion separately. The shape of the proposed interaction curve has similar tendency to the dotted curve enveloping the test results, with the exception of slight error in the ultimate bending strength,  $\alpha M_p$ .

### GEOMETRY OF CURVED BOX GIRDER BRIDGES IN JAPAN

A questionnaire was carried out to examine the applicable ranges of the cross-sectional dimensions, span lengths, radii of curvature and various parameters on plate buckling of horizontally curved box girder bridges constructed in Japan. Data of 260 curved box girder bridges have been collected from this questionnaire. A few histograms of important factors are depicted in Figs. 4~7.

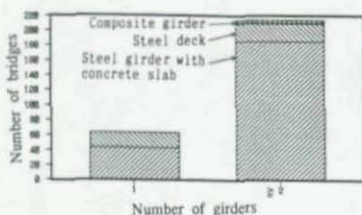


Fig.4 Histogram of type of box girders

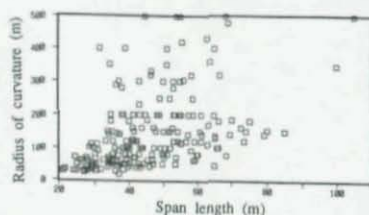


Fig.5 Relationship between radius of curvature and span length (steel girder with concrete slab)

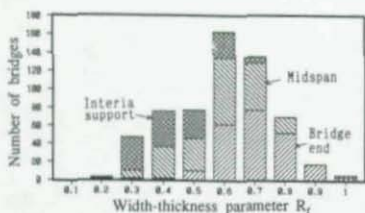


Fig.6 Histogram of width-thickness parameter,  $R_f$

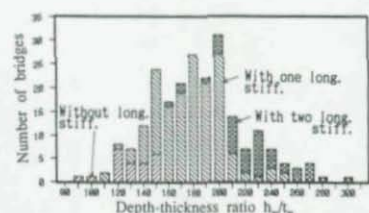


Fig.7 Histogram of depth-thickness ratio



From these figures, the following features can be clarified:

- (1) Curved bridges consisting of two box girders and a concrete slab are popular and common.
- (2) Radius of curvature is larger than 20 m .
- (3) Radius of curvature has a tendency to increase in accordance with the increase of span length.
- (4) The width-thickness parameter,  $R_f = \sqrt{\sigma_y / \sigma_{cr}}$ ,  $\sigma_y$ : yield stress,  $\sigma_{cr}$ : elastic buckling stress) of plate panels between longitudinal stiffeners in the compression flanges varies within the ranges from 0.3 to 0.9 .
- (5) The width-thickness parameter,  $R_f$  near bridge ends is generally larger than that of near midspan and interior supports.
- (6) The depth-thickness ratio,  $h_w / t_w$  of the web plates falls within the ranges from 130 to 210 and from 200 to 270 for web plates with single and two longitudinal stiffeners, respectively.

#### DRAFT GUIDELINE FOR DESIGN OF HORIZONTALLY CURVED GIRDER BRIDGES IN HEPC<sup>29)</sup>

Fig.8 shows the difference of lateral buckling mode between curved and straight I-girder bridges. An I-girder between floor beams buckles with the boundary conditions similar to restrained supports in bending. The ultimate stress of flange plate in curved I-girders due to the lateral buckling can be evaluated by the ultimate stress of straight I-girders<sup>31)</sup> multiplied by the factor,  $\beta$  given by:

$$\beta = 1.0 - 1.05\sqrt{\alpha(\phi + 4.52\phi^2)} \quad (0.02 \leq \phi \leq 0.2) \quad (1)$$

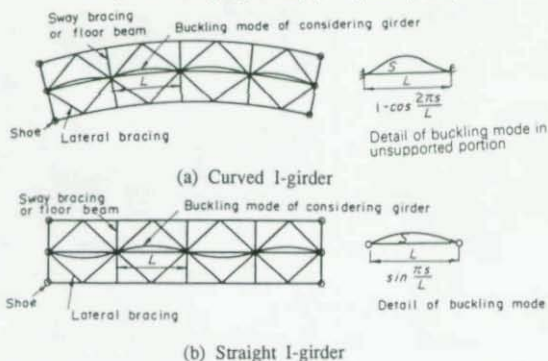


Fig.8 Difference of buckling modes<sup>1)</sup>

in which

$\phi$ : central angle of I-girder between floor beams

and

$$\alpha = \frac{2}{\pi} \sqrt{3 + \frac{A_w}{2A_c} \left(\frac{l}{b}\right)} \sqrt{\frac{E}{\sigma_Y}}; \text{ buckling parameter of I-girder} \quad (2)$$

where

$A_w$  : cross-sectional area of web  
 $A_c$  : cross-sectional area of compression flange  
 $l$  : effective lateral buckling length  
 $b$  : width of compression flange  
 $E$  : Young's modulus  
 $\sigma_Y$  : yield stress

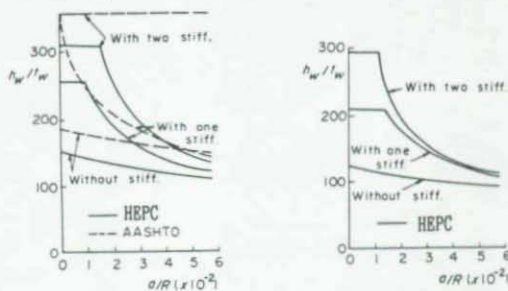
However, the following effective lateral buckling length should be adopted to calculate the ultimate stress of the corresponding straight I-girder.

$$l = \gamma L \quad (3)$$

where  $L$  is the span length of curved I-girder between floor beams,  
 and

$$\gamma = 1 - 1.97\phi^{1/3} + 4.25\phi - 2.63\phi^3 \quad (4)$$

The upper limits of width-thickness ratio,  $h_w/t_w$  for curved web plates, shown in Fig.9, are proposed on the basis of the conditions where the maximum out-of-plane bending stress of curved web plates should be nearly equal to that of straight web plates<sup>1)</sup>. In this figure,  $a$  is the spacing of transverse stiffeners.



(a) SM400 ( $\sigma_Y = 2,400 \text{ kgf/cm}^2$ )      (b) SM490Y ( $\sigma_Y = 3,200 \text{ kgf/cm}^2$ )

Fig.9 Proposed slenderness ratio for curved web plate:

The width-thickness parameter,  $R_f$  for the compression flange plate of a curved plate girder is recommended to be less than 0.5 to avoid the local buckling before reaching the fully plastic state of the flange plate as follows:

$$R_f = \frac{b}{t} \sqrt{\frac{\sigma_Y 12(1-\mu^2)}{E 0.43\pi^2}} \leq 0.5 \quad (5)$$

where  $b$  is half the flange width,  $t$  is the thickness of flange plate, and  $\mu$  is the Poisson's ratio.

### STIFFNESS OF LONGITUDINAL AND TRANSVERSE STIFFENERS

The required minimum stiffness of longitudinal and transverse stiffeners of curved plate girders can be determined as the corresponding value of straight curved plate girders<sup>31)</sup> multiplied by the factors,  $\beta_L$  and  $\beta_T$ , which can be estimated from Figs.10 and 11, respectively.

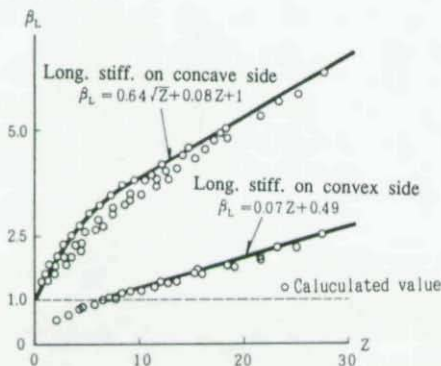


Fig.10 Variation of  $\beta_L$  due to curvature parameter,  $Z^{29)}$

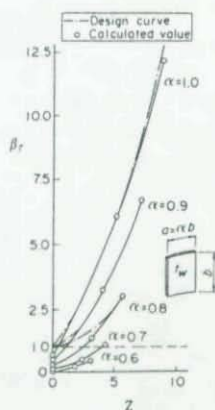


Fig.11 Variation of  $\beta_T$  due to curvature parameter,  $Z^{1)}$

In these figures,  $Z$  is the curvature parameter given by :

$$Z = \left(\frac{a}{R}\right) \left(\frac{a}{r_w}\right) \sqrt{1 - \mu^2} \quad (6)$$

The above coefficients,  $\beta_L$  and  $\beta_T$  are derived according to the ultimate strength of these stiffeners regarding as the beam-column models.

### A RECENT BIG CONSTRUCTION

Fig.12 shows a side elevation of the River Kizu Bridge and its north approach bridge is now under construction. The approach bridge is a continuous spiral box girder bridge with seventeen spans (span length: 41.95 + 52.66 + 14 × 52.36 + 53.31 in m) connected rigidly to six steel piers of rigid frame. In designing this approach bridge, the elasto-plastic and finite displacement analyses were executed to investigate the behavior up to the ultimate state and the ultimate load carrying capacity of the bridge subjected to live load or seismic load<sup>29)</sup>.

The analytical model for the approach bridge is illustrated in Fig.13. The number of nodal points and finite elements are resulted in 1,128 and 939, respectively. The computer program, EPASS<sup>32)</sup>, for the elasto-plastic and finite displacement analysis of spatial steel bridge structures was used for this analysis. A few numerical results are shown in Fig.14.

Seismic load ( $\alpha E_q$ ) is gradually increased up to the ultimate state in the condition where the dead load is kept to be constant. The behavior of the analytical model is almost linear in the region where  $\alpha$  is less than 3, although the factor of safety against the seismic load is 1.15 in JSHB<sup>31)</sup>.

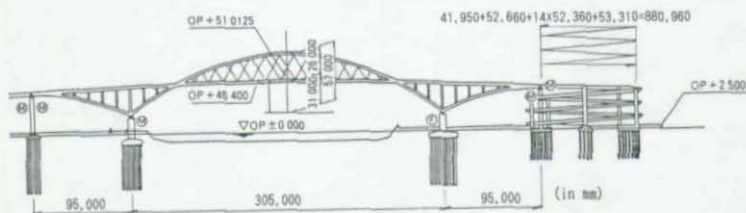


Fig.12 Side elevation of River Kizu Bridge and its approach spiral box girder bridge (in mm)

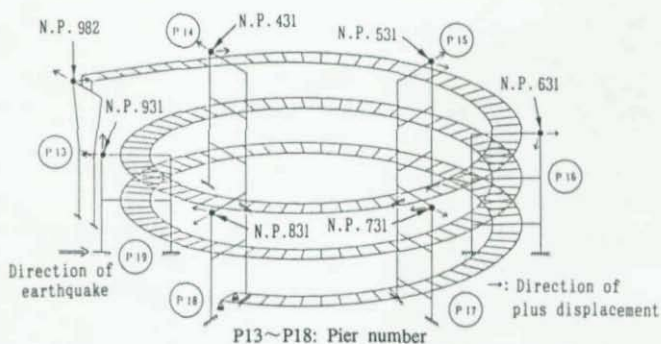


Fig.13 Analytical model and nodal points (N.P.) of spiral girder bridge

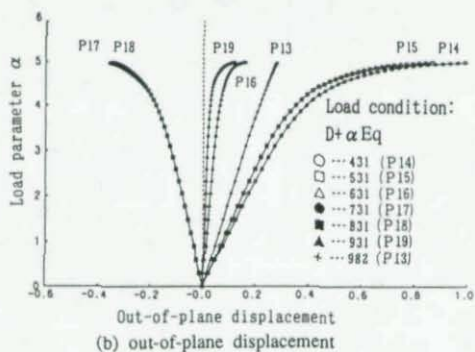
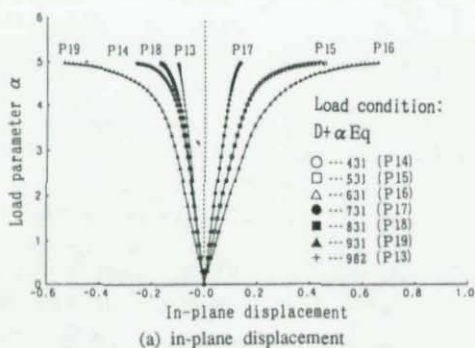


Fig.14 Load-Displacement curves

## CONCLUSION

In this paper, the following conclusions have been obtained:

- (1) A state-of-the-art for research on the buckling of horizontally curved girder bridges in Japan has briefly predicted.
- (2) Necessity of the research on the ultimate strength of curved box girders has been emphasized.
- (3) The applicable ranges of representative dimensions and buckling parameters of curved box girder bridges have been shown through a questionnaire.
- (4) A new draft design method for curved plate girders and a big special spiral bridge under construction have been introduced.

## REFERENCES

- 1) Nakai, H. and C.H.Yoo: Analysis and Design of Curved Steel Bridges, McGraw-Hill, 1988.
- 2) Mikami, I., K. Furunishi and H. Yonezawa : Nonlinear behavior of cylindrical web panels under bending, Proc. of JSCE (Japan Society of Civil Engineering), No.299, pp.23-34, July 1980 (in Japanese).
- 3) Maegawa, K. and H. Yoshida : Ultimate strength analysis of curved I-beams by transfer matrix method, Proc. of JSCE, No.312, pp.27-37, August 1981 (in Japanese).
- 4) Kuranishi, S. and S. Hiwatashi : Elastic behavior of web plates of curved plate girders in bending, Proc. of JSCE, No.315, pp.1-11, November 1981 (in Japanese).
- 5) Nakai, H. and H. Kotoguchi : A study on lateral buckling strength and design aid for horizontally curved I-girder bridges, Proc. of JSCE, No.339, pp.195-204, November 1983.
- 6) Nakai, H., T. Kitada and R. Ohminami : Experimental study on bending strength of web plate of horizontally curved girder bridges, Proc. of JSCE, No.340, pp.19-28, December 1983 (in Japanese).
- 7) Hiwatashi, S. and S. Kuranishi : The finite displacement behavior of horizontally curved elastic I-section plate girders under bending, Proc. of JSCE, Structural Eng./Earthquake Eng., Vol.1, No.2, pp.59-69, October 1984.
- 8) Nakai, H., T. Kitada, R. Ohminami and K. Fukumoto : Experimental study on shear strength of horizontally curved plate girders, Proc. of JSCE, No.350/1-2, pp.281-290, October 1984 (in Japanese).
- 9) Hiwatashi, S. and S. Kuranishi : On the elastic finite displacement behavior of horizontally curved I-section plate girders under bending, *Journal of Structural*



- Engineering, JSCE, Vol.31A, pp.197-207, March 1985 (in Japanese).
- 10) Nakai, H., T. Kitada and R. Ohminami : Experimental study on buckling and ultimate strength of curved girders subjected to combined loads of bending and shear, Proc. of JSCE, No.356, pp.445-454, April 1985 (in Japanese).
  - 11) Fujii, K. and H. Ohmura : Nonlinear behavior of curved girder-web considered flange rigidities : Proc. of JSCE, Structural Eng./Earthquake Eng., Vol.2, No.1, pp.69-79, April 1985.
  - 12) Nakai, H., T. Kitada and R. Ohminami : A proposition for designing intermediate transverse stiffeners in web plate of horizontally curved girders, Proc. of JSCE, No. 362/I-4, pp.249-257, October 1985 (in Japanese).
  - 13) Nakai, H., T. Kitada, R. Ohminami and T. Kawai : A study on analysis and design of web plate in curved girder bridges subjected to bending : Proc. of JSCE, No.368/I-5, pp.235-244, April 1986 (in Japanese).
  - 14) Kitada, T., R. Ohminami and H. Nakai : Criteria for designing web and flange plates of horizontally curved plate girders, Proc. of Annual Technical Session, SSRC (Structural Stability Research Council), pp.119-130, April 1986.
  - 15) Suetake, Y., M. Hirashima and T. Yoda : Geometrical nonlinear analysis of curved I-girders under bending using mixed finite element method, Proc. of JSCE, Structural Eng./Earthquake Eng., Vol.3, No.2, pp.39-46, October 1986.
  - 16) Fujii, K. and H. Ohmura : Elasto-plastic behavior of cross-sectional deformations of curved I-girders in bending, Journal of Structural Engineering, JSCE, Vol.33A, pp. 83-92, March 1987 (in Japanese).
  - 17) Imai, F. and T. Ohta : Investigation on yield surface equation of curved I-beams, Proc. of JSCE, No.380/I-7, pp.349-354, April 1987 (in Japanese).
  - 18) Fujii, K. and H. Ohmura : Local buckling and width-thickness ratio in flange of curved I-girders : Proc. of JSCE, No.386/I-8, pp.339-347, October 1987 (in Japanese).
  - 19) Imai, F., T. Tajima and T. Ohta : A study on the optimal elastic-plastic design of curved box girder bridges, Journal of Structural Engineering, JSCE, Vol.34A, pp. 657-666, March 1988 (in Japanese).
  - 20) Kitada, T., R. Ohminami and H. Nakai : Initial deflection and residual stress in horizontally curved plate girders, Proc. of Annual Technical Session, SSRC, pp.129-139, April 1988.
  - 21) Fujii, K. and H. Ohmura : Nonlinear bending behavior of curved girder-web with initial deflections, Journal of Structural Engineering, JSCE, Vol.34A, pp.117-126, March 1988 (in Japanese).
  - 22) Omote, T., M. Hirashima and T. Yoda : Finite displacement theory of curved and twisted thin-walled box girders, Proc. of JSCE, No.404/I-11, pp.239-248, April 1989

- (in Japanese).
- 23) Nakai, H., Y. Murayama, T. Kitada and Y. Takada : An experimental study on ultimate strength of thin-walled box beams subjected to bending and torsion, *Journal of Structural Engineering, JSCE, Vol.36A, pp.63-70, March 1990* (in Japanese).
  - 24) Nakai, H., Y. Murayama and T. Kitada : An experimental study on ultimate strength of thin-walled box beams with longitudinal stiffeners subjected to bending and torsion, *Journal of Structural Engineering, JSCE, Vol.38A, pp.155-165, March 1992* (in Japanese).
  - 25) Nakaoka, T., K. Fujii and Y. Fujieda : The ultimate behavior and strength of horizontally curved plate girders under bending, *Proc. of JSCE Annual Conference, Vol.I-8, pp.192-193, September 1993* (in Japanese).
  - 26) Nakai, H., T. Kitada and Y. Murayama : On ultimate strength of horizontally curved box girders, *Proc. of 1st World Conference on Constructional Steel Design, Acapulco, Mexico, pp.108-117, December 1992*.
  - 27) Task Committee on Curved Box Girders of the ASCE-AASHTO : Curved steel box-girder bridges: A survey, *Journal of the Structural Division, ASCE, Vol.104, No.ST11, pp.1697-1718, November 1978*.
  - 28) Task Committee on Curved Box Girders of the ASCE-AASHTO : Curved steel box-girder bridges : State-of-the-art, *Journal of the Structural Division, ASCE, Vol.104, No.ST11, pp.1719-1739, November 1978*.
  - 29) Hanshin Expressway Public Corporation : Guidelines for design of horizontally curved girder bridges (draft), October 1988 (in Japanese).
  - 30) Nakai, H., T.Kitada, T.Yokota and T.Yasui: Ultimate Load-carrying capacity of a three-dimensional rigid-frame bridge, *Proc. of Fourth East Asian Conference of Structural Eng. & Construction, Seoul, Korea, September 1993* (to be published).
  - 31) Japan Road Association : Specifications for highway bridges, Part 2. Steel bridges, February 1990.
  - 32) Kitada, T., R. Ohminami, M. Nibu and K. Tanaka : Exploitation of computer program to analyze ultimate strength of steel bridges using cable members, *Proc. of Symposium on Computational Methods in Structural Engineering and Related Fields, JSCE, Vol. 13, pp.89-94, July 1989* (in Japanese).

## INTERACTIVE PLASTIC HINGE BASED METHOD FOR ANALYSIS OF STEEL FRAMES

Prof. Miklós, IVÁNYI  
Department of Steel Structures  
Technical University of Budapest, Hungary

### ABSTRACT

Limit design of steel structures is based on the model of the plastic hinge. In its traditional form it is usually combined with rigid-plastic constitutive law. The model of "interactive plastic hinge" is suggested, which can take into account several phenomena (as residual stresses, strain-hardening, plate buckling, lateral buckling).

### 1. INTRODUCTION

The traditional concept of plastic design of steel structures is based on the assumption that under gradually increasing static loads plastic zones develop and grow in size and number, and eventually cause unstricted, increasing deflections; thus loading to the onset of ultimate limit state of the structure. The concept was first introduced by KAZINCZY (1914) by establishing concept of the "plastic hinge". Some basic questions are still discussed. Among them are the effects of the difference between ideal-plastic constitutive law and actual behaviour of steel material and the consequence of local instability (plate buckling; lateral buckling). The element of the bar is considered to be built up of plate elements (following the pattern of steel structures) instead of a compact section. Then the behaviour of the "plastic hinge" can be characterized by tests with simple supported beam (Figure 1.). Based on these tests a yield-mechanism for the bar-element can be introduced, giving basis for a mechanism curve: defining thus the descending branch of the moment-rotation diagram. We introduce the concept of "interactive plastic hinge" which can substitute the classical concept of plastic hinge in the traditional methods of limit design, but can reflect the effect of phenomena like strain-hardening, residual stresses, plate buckling and lateral buckling (IVÁNYI 1985).

Local and lateral bucklings are so diverse and so complex that large amounts of experimental and analytical data must be collected and systematized thus reliable frame analysis can become common practice (IVÁNYI 1992).

## 2. THE MODEL OF "INTERACTIVE PLASTIC HINGE"

### 2.1. DIFFICULTIES IN PREDICTING FAILURE

The increasingly powerful experimental and computational tools of structural design require a well-defined design philosophy. As its basis generally the concept of limit states is accepted in many countries.

Limit states are usually divided into the two following groups:

- limit states of carrying capacity /ultimate limit states/
- limit states of serviceability.

Checking serviceability at working load level the traditional and well tried out methods of structural analysis are used. The quite frequent tests on original structures show as a rule a relatively good accordance with calculated stress patterns or even better with predicted deflections apart from the occasional effect of lack of fit connections.

On the other hand the analysis of structural response in the vicinity of peak load proved to be extremely complicated, due not only (and even not mainly) to inelastic behaviour, but to the fact, that in the vicinity of peak load

- change in geometry (geometrical non-linearity) gains in importance among others because of magnifying the effect of initial geometrical imperfections (often negligible at lower load levels),
- residual stresses (remaining latent at lower loads) interact with growing active stresses resulting in premature plastic zones, and last but not least
- usual and widely accepted tools of analysis — as beam theory based on the Bernoulli-Navier theorem; small deflection theory of plates etc. — restricting the actual degree of freedom of the structure cannot describe exactly enough its real response at failure.

These difficulties can be overcome in case of simple structural elements (separated compression members, parts of plate girders, etc.) by using more refined (e.g. finite element) methods, allowing degrees of freedom (e.g. distortion of cross sections) excluded in traditional analysis, etc., or even in case of statically non-redundant structures, where the above indicated complex behaviour is usually confined to a limited section of the whole structure.

If the simplified model is not elaborate enough to reflect real structural behaviour, a secondary, more detailed local model is inserted to depict the mostly critical part of the structure, by which more realistic quality parameters (and limit surface) can be deduced from the already known primary parameters (HALÁSZ, IVÁNYI 1985).

Because of the interaction of local and global behaviour this pattern cannot be followed in case of hyperstatic structures, as the additional information gained by the secondary, local model is to be fed back to the computation of primary parameters as well. For this purpose, if — as very often — the secondary model can be analysed by numerical methods or only experimentally, the results have either be re-interpreted to gain mathematically treatable, simple enough rules, or the secondary model has to be simplified to furnish digestible results. In both cases the validity or accuracy has to be proved by (usually very expensive) failure tests with full-scale structures. The same applies for directly non or hardly measurable quantities, as residual stresses.



The traditional concept of plastic design of steel structures is based on the assumption that, under gradually increasing static loads, plastic zones develop and grow in size and number, and eventually cause unrestricted, increasing deflections; thus loading until the onset of ultimate limit state of the structure. The concept was first introduced by KAZINCZY (1914) by establishing the concept of "plastic hinge". Some basic questions are still discussed. Among them are the effects of the difference between ideal-plastic constitutive law and actual behaviour of steel material and the consequence of local instability (plate buckling; lateral buckling). Joining into the international research in this field we tried to introduce the concept of "interactive plastic hinge", which can be substitute the classic concept of plastic hinge in the traditional methods of limit design, but can reflect the effect of phenomena like strain-hardening, residual stresses, plate buckling and lateral buckling (IVÁNYI 1983).

## 2.2. BASIC METHOD AND A SIMPLE EXAMPLE

In the course of plate experiments, if the width-to-thickness ratio is high, the plate does not lose its load bearing capacity with the development of plastic deformations but is able to take the load causing yield until a deformation characteristic of the plate occurs and is even able to take a small increase in load. In the course of the process "crumplings" (bucklings) can be observed on the plate surface. These "crumplings" form a yield mechanism with the plastic moments acting in the linear plastic hinges (peaks of waves) not constant but ever increasing due to strain-hardening. The yield mechanism formed by the "crumplings" extends to the component plates of the bar. The description of its behaviour is obtained, from among the extreme values theorems of plasticity, with the aid of the *theorem of kinematics*.

Thus, in the course of our investigations an upper limit of the load bearing has been determined, however, to be able to assess the results, the following have to be taken into consideration: on one hand the yield mechanisms are taken into account through the "crumpling" forms determined by experimental results and on the other hand, the results of theoretical investigations are compared with those of the experimental investigations.

Thus, a yield mechanism will be adopted such as to correspond to the geometrical conditions and the assumed yield criterion. In addition to BEN KATO (1965), this method has been applied by CLIMENHAGA and JOHNSON (1972) for the analysis of buckling due to the negative moment of the steel beam component of composite beams.

The method will be illustrated by a simple example (Figure 2.1). Let us take a bar of an isotropic, incompressible, rigid-plastic material (Figure 2.2), subject to the Tresca yield condition. Rigid and plastic zones include an angle of  $45^\circ$  with the bar axis. For a small rotation  $\Theta$ , in the plastic hinge (yield mechanism) deformations of identical magnitude but opposite sign develop in directions  $x$  and  $y$ , while incompressibility requires zero strain in direction  $z$  ( $\epsilon_z = 0$ ). According to the yield criterion, stresses in directions  $y$  and  $z$  are zero ( $\sigma_y = \sigma_z = 0$ ) while in direction  $x$  they are equal to the yield point ( $\sigma_x = \pm\sigma_Y$ ).

Centre of rotation  $C$  is located as a function of depth  $h$ .

Writing deformation energy of the plastic hinge (yield mechanism):

$$W_a = V \int_{(\epsilon)} \sigma d\epsilon = \left( \frac{2\eta^2 h^2}{2} + \frac{2(1-\eta)^2 h^2}{2} \right) a \int_{(\epsilon)} \sigma d\epsilon$$

$V = \text{minimum for } \eta = 0.5$ , hence

$$V = \frac{ah^2}{2}$$

For a small rotation  $\Theta$ , because of the  $45^\circ$  limit, the strain becomes

$$\epsilon_x = \pm \frac{\Theta}{2}$$

$$W_a = V \int_0^{\epsilon_x} \sigma_x d\epsilon = \frac{ah^2}{2} \int_0^{\Theta/2} \sigma_Y d\epsilon = \frac{ah^2}{2} \cdot \Theta \cdot \frac{\sigma_Y}{2}$$

The potential energy is equating deformation energy of the plastic hinge:

$$W_h = \int_{\Theta} M d\Theta = \frac{ah^2}{4} \sigma_Y \Theta$$

Deriving this equation with respect to  $\Theta$ :

$$M = \frac{ah^2}{4} \sigma_Y$$

In case of a strain-hardening material (Figure 2.2):

$$M = \frac{ah^2}{4} \left( \sigma_Y + \frac{1}{2} \Theta E_s \right)$$

The presented method suits also more complicated cases.

## 2.3. YIELD MECHANISM OF STRUCTURAL MEMBERS

### 2.31. Yield Mechanism Forms Based on Experimental Results

The different form of yield mechanisms can be determined on the basis of experimental results.

Experimental investigations are essentially expected partly to supply physical background (often inspiration) needed to establish models for theoretical examinations, and partly to delimit the range of validity.

Our experiments involved measurements to determine (IVÁNYI 1983):

- plastic material characteristics of steel;
- residual deformations;



- c) load carrying capacities of members in compression, bending and eccentric compression.

The yield mechanism forms of an I-section bar can be classified according to the following criteria:

- a.) according to the manner of loading,  
 b.) according to the positions of the intersecting lines of the web and the flanges, the so-called "throat-lines", thus  
 bi.) the evolving formation is called a planar yield mechanism if the two "throat-lines" are in the same plane also after the development of the yield mechanism.  
 bii.) the evolving formation is called a spatial yield mechanism if the two "throat-lines" are not in the same plane after the development of the yield mechanism.

#### 2.311. Yield mechanism of compression members

##### (i) Planar yield mechanism

The buckled form of the compression member and the formation of the chosen yield mechanism is shown in Figure 2.3.

Plastic deformation occurs in the shaded regions.

As an effect of compressive force  $N$  a compression part develops.

The symbol of the yield mechanism is  $(N)_P$  where  $P$  stands for the planar yield mechanism formation.

##### (ii) Spatial yield mechanism

The formation of the spatial yield mechanism for a compression member is shown in Figure 2.4. The ends of the member are assumed to be hinge-supported in both main inertia directions. The yield mechanism that has occurred is called spatial, the phenomenon models the planar buckling of the compression member or the buckling of the component plates in the course of buckling.

The symbol of the yield mechanism is  $(N)_S$  where  $S$  stands for the spatial yield mechanism formation.

#### 2.312. Yield mechanisms of bent members

- a.) In case of a bending moment constant along the members axis:

##### ai) Planar yield mechanism

The buckled form of the bent specimen and the chosen yield mechanism formation is shown in Figure 2.5. As an effect of moment  $M$  a rotation  $\Theta$  develops.

As an effect  $M$ , tension and compression parts develop.

The symbol of the yield mechanism is  $(MC)_P$ , where  $C$  stands for the constant bending moment.

##### aii) Spatial yield mechanism

The form of the spatial yield mechanism in the case of a bent rod is indicated in Figure 2.6. The rod ends are assumed to be hinge-supported in both main inertia directions. The yield mechanism models the buckling of the component plates of the bent member, the lateral buckling of the beams as well as their interaction.

The buckled formation of a simple-supported beam specimen and the chosen yield mechanism is shown in Figure 2.7.

In case of the yield mechanism formations in Figure 2.7 the effect of neighbouring supports (the effect of ribs) has also been taken into account. As an effect of the moment, a rotation  $\Theta$  develops.

The symbol of the yield mechanism is  $(MC)_S$ .

b.) In case of a bending moment varying along the rod axis.

In case of a varying bending moment along the member axis it is assumed that the "crack" of the web plate of the I-section in the cross section of the concentrated force is hindered by the suitable thickness of the web plate or by the ribs.

CLIMENHAGA and JOHNSON (1972) assumed yield mechanism forms similar to those introduced in point (b) for the investigation of bucklings occurring at the steel beam parts of composite steel-concrete construction.

bi) Planar yield mechanism

The buckled form of a bent specimen and the selected yield mechanism is shown in Figure 2.8. As an effect of the moment a rotation  $\Theta$  develops.

Because of the clamping of the cross-section  $EC$ , the yield mechanism loses its symmetric character.

The symbol of the yield mechanism is  $(MV)_P$  where  $V$  stands for the varying moment.

bii) Spatial yield mechanism

The form of the spatial yield mechanism in case of a bending moment varying along the rod axis is shown in Figure 2.9.

As an effect of the moment a rotation  $\Theta$  develops.

The symbol of the yield mechanism is  $(MV)_S$ .

### 2.32. Yield Mechanism of the Component Plates of an I-section Member

Yield mechanism formations have been determined for different stresses. On the basis of the experimental results it is expedient to decompose these yield mechanism formations to the yield mechanism formations of the component plates of an I-section rod as certain component plate formations appear in other yield mechanism, too.

To classify the yield mechanisms of component plates, the following division has been used:

- a.) flange plate, if the plate is supported along the central line,
- b.) web plate, if the plate is supported at the unloaded ends.

Figure 2.10 shows the yield mechanisms of the component plates where  $F$  is the flange plate,  $W$  is the web plate, the odd numbers refer to the planar yield mechanisms while the even ones to the spatial yield mechanisms.

### 2.33. "Joining" the Yield Mechanisms of Component Plates

The "joining" of the yield mechanisms of component plates depends on the positions of the so-called "throat-lines" of the yield mechanism chosen on the basis of the experimental results.

In cases pertaining to planar yield mechanisms this "joining" is to be realized in a linear way, with a linear plastic hinge: the length of the linear plastic hinge is governed — due to the properties of the chosen yield mechanism — by the length of the yield mechanism of the compression flange plate (F-1). In case of spatial yield mechanisms the "joining" should be realized in one point or more points.

The relationships of the component plate yield mechanisms and the "joining" of the component plates have been given by IVÁNYI (1983); IVÁNYI (1979a and 1979b) show the basic relationships of partial cases.

#### 2.4. MODEL OF THE INTERACTIVE HINGE

The plastic load-bearing investigation assumes the development of rigid-ideally plastic hinges, however, the model describes the inelastic behaviour of steel structures but with major constraints and approximations. There are some effects with the consideration of which the behaviour of the steel material and the I-section member can be taken into account in a more realistic way.

- i) When determining the load-displacement relationship of an I-section member, the symbol of the elastic state is  $E$  and if the so-called "rigid" state is assumed instead of the elastic one, the symbol of the rigid state is  $R$ .
- ii) The effect of residual stress and deformation is characterized by a straight line for the sake of ease of handling. The symbol used when taking the residual stress and deformation into consideration is  $O$ .
- iii) Strain-hardening is one of the important features of the steel material,  $S$  indicates that it had been accounted for.
- iv) The effect of buckling of the I-section member component plates on the rod element load-displacement relationship has been investigated, this is indicated by  $L$ .

The models that take the above effects into consideration at the investigation of load-displacement (relative displacement) relationship of I-section are called "interactive" ones.

The model of the interactive plastic hinge taking into consideration the effect of rigid — residual stress — strain hardening — plate bucklings can be described with the aid of the "equivalent beam length" suggested by HORNE (1960) (Figure 2.11a). The material model employed at the investigations is shown in Figure 2.11b. The effect of the residual stresses and deformations is substituted by a straight line. The effect of strain-hardening can be determined with the help of the rigid-hardening ( $R-S$ ) model. The buckling of the I-section member component plates is described by the yield mechanism curve which is substituted by a straight line.

Figure 2.11c indicates the load-displacement relationship belonging to the ( $R-O-S-L$ ) interactive plastic hinge. The substitution by straight lines is justified to simplify the investigations. In the ( $R-O-S$ ) sections the intersections are connected while in section  $L$  the moment-rotation relationship is substituted by a tangent that can be drawn at the apex.

### 3. PREDICTION OF ULTIMATE LOAD OF STEEL FRAMES

#### 3.1. INTRODUCTION

Questions relating to the effects of the plastic properties of steel material on the load bearing capacity of steel structures have long been of interest to researchers, a number of problems have been solved. The application of the theory of plasticity to designing has been enabled by the introduction of plastic load capacity investigations. These take into account that in steel structures an increasing number of extensive plastic zones are brought about by gradually increasing so-called "static" load until in the end, at the limit of load bearing, the structure, without further increase in load, is able to undertake continuous displacements. Calculations of plastic load bearing capacity are based on the research work of Gábor KAZINCZY.

Several questions remained unanswered in connection with plastic load bearing capacity investigations. Thus, for instance, the difference between the behaviour of the ideally plastic model and of real steel material, as well as problems connected with loss of stability (plate buckling, flexural-torsional buckling). Extensive research, especially in the experimental field, tried to answer these questions determining the conditions the adherence to which allows the maintenance of the validity of plastic load bearing capacity investigations.

#### 3.2. EFFECT OF LOCAL INSTABILITY

The final collapse of steel structures is mostly caused by instability phenomena (THÜRLIMANN 1960). These instability phenomena may be:

- disadvantageous change in the steel structure geometry,
- disadvantageous change in the cross section geometry.

The effect of disadvantageous change in structure geometry can be — traditionally — grouped in the field of plastic instability. It was Ottó HALÁSZ (1976) who treated the problem in a doctoral thesis and, over and above theoretical studies, he also introduced a method suitable for practical design work.

The disadvantageous changes in cross section geometry are mainly plate bucklings. Plate buckling causes a change in the behaviour of the plastic hinge, too, and thus for the plastic investigations of statically indeterminate steel structures, methods have to be elaborated that take also the effect of plate buckling into consideration.

The case of ideally plastic material is an assumed case and it should be taken while investigating the effects of the evolving plastic hinges, lest the previously formed plastic hinges should "close".

Studying the effect of strain-hardening and plate buckling one should keep in mind that the load-displacement diagram of the structure may be of an ascending type even if the characteristic curves of the given member section or sections are of a descending type in individual cross sections because of the effect of plate buckling.



In the theory of plasticity, when deriving the condition of plasticity or some other physical relationships, Drucker's postulate for stability is applied, by assuming stable materials (DRUCKER 1951).

MAIER (1961) was the first to treat the problem of the effect of the unstable state of certain members on the behaviour of a triangulated structure. Again it was Maier who in 1966 re-introduced the subject and investigated a structure consisting of compressed members and rigid beams where the load-displacement diagram of individual members contained stable and unstable parts.

MAIER and DRUCKER (1966) re-examined the original Drucker postulate applied when determining the condition of plasticity since the original postulate is suitable for the determination of the convexity and normality of the condition of plasticity in case of stable materials only.

When studying the load bearing capacity of steel structures, the problem of unstable material or softening material, according to Drucker's postulate does not appear since the strain-hardening of the steel material may increase in a major way the plastic load bearing capacity of steel structure. However, as it has been known for a long time, the final collapse of steel structures is caused — in a high percentage of cases — by instability (plate buckling, flexural-torsional buckling) phenomena that may occur in the cross section or in a structural unit. (Figure 3.1)

Concerning steel structures the properties of plastic hinges over and above the usual elastic-ideally plastic-hardening behaviour may be complemented with the effect of instability (flexural-torsional buckling) developing in the given structural unit (environment of the plastic hinge).

This type of inelastic or interactive hinge describes the behaviour of the structural unit and at the same time, also satisfies the criteria of unstable or softening structural unit, according to Maier-Drucker's postulate.

When determining the plastic load bearing capacity of steel structures the interactive hinge of softening has so far not been considered or applied. The effects of the stability phenomena causing the softening character (flexural-torsional buckling, plate buckling) can be taken into account indirectly with the aid of construction rules. In principle, mathematical programming allows the investigation of more complex steel structures, too, however, it is less suitable for designing practice. The author (IVÁNYI 1980) has suggested a procedure that is taking into account the softening character of the inelastic hinge in the form of an interactive zone. The softening character of the interactive zone is caused by the buckling of the component plates, a phenomenon that can be studied with the help of the yield mechanism.

### 3.3. ANALYSIS OF STEEL FRAMES WITH CONDITIONAL JOINTS

In the theory of structures the wide application of matrix calculation was introduced by SZABÓ and ROLLER (1971). It gave the possibility to treat the theoretical and computational investigations of rod structures in a uniform way, allowed the application of computer technique. The results most important for our investigations are those concerned with the application of kinematic load. In their work Kaliszky, S. and Kurutz,

M. elaborated in detail the computerized computation of structures containing conditional joints with the kinematic load (KALISZKY 1978), (KURUTZ 1975). The procedure was based on the solution of structures by the displacement method. The investigation imitates the effect of the hinges with a rigidity changing stepwise as a kinematic load without alternating the original rigidity matrix of the structure continually softening due to the gradually developing interactive hinges.

The investigation of the change of state of the frame structure is carried out by matching two model-parts:

- a.) an ideal linearly elastic member
- b.) an interactive hinge: *R-O-S-L* model containing the effects of rigid — residual stress — strain hardening — plate buckling.

The ideally elastic member was studied by usual methods (SZABÓ, ROLLER 1971).

### 3.31. The interactive hinge

(i) In Chapter 2. a description of the interactive hinge has been introduced that takes into consideration the effects of rigid — residual stress — strain-hardening — plate buckling and is called a *R-O-S-L* hinge. The model of the *R-O-S-L* hinge can be described with the aid of the "equivalent beam length". In the course of the investigations, the length "h" of the "equivalent beam" was determined from the moment diagram established during plastic load bearing investigations and this length *h* does not change — according to assumptions — with the increase of the load.

Figure 3.2 shows the model of the *R-O-S-L* hinge. Rigidity of the hinge for different phases is expressed by the rigidity factor,  $c = \Delta M / \Delta \theta$ .

Figure 3.2 also shows the kinematic loads valid for different rotation phases.

Compatibility relations of rotation sections:

*R* section:

$$c = \infty; \quad 0 \leq M \leq M_1; \quad \theta = 0$$

$$\text{kinematic load : } t = 0$$

*O* section:

$$c = c_0; \quad M_1 \leq M \leq M_2; \quad 0 \leq \theta \leq \theta_2$$

$$\theta = \frac{1}{c_0}(M - M_1); \quad 0 = -\theta + \frac{1}{c_0}M + \left(-\frac{1}{c_0}M_1\right);$$

$$\text{kinematic load : } t = -\frac{1}{c_0}M_1$$

*S* section:

$$c = c_s; \quad M_2 \leq M \leq M_3; \quad \theta_2 \leq \theta \leq \theta_3$$

$$\theta - \theta_2 = \frac{1}{c_s}(M - M_2); \quad 0 = -\theta + \frac{1}{c_s}M + \left(\theta_2 - \frac{1}{c_s}M_2\right)$$

$$\text{kinematic load : } t = \theta_2 - \frac{1}{c_s}M_2$$



*L* section:

$$c = c_L; \quad M > M_3; \quad \Theta \geq \Theta_3$$

$$\Theta - \Theta_3 = \frac{1}{c_L}(M - M_3); \quad 0 = -\Theta + \frac{1}{c_L}M + \left(\Theta_3 - \frac{1}{c_L}M_3\right)$$

$$\text{kinematic load : } t = \Theta_3 - \frac{1}{c_L}M_3$$

It was assumed that interactive hinges do not "close" with an increase in load, no elastic-type unloading occurs (MAJID 1972).

(ii) Anchoring of the columns has not been developed in the form of a mechanical hinge or of complete clamping and therefore, primarily on the basis of experimental results, a "hinge" has been assumed in the cross sections of the anchoring of the columns where an increase in moment involves a rotation increasing in a changing measure (Figure 3.3).

### 3.32. Model of planar frame structures

The analysis of the Conder-system frame structure figuring in the experimental program has been selected as basis for our investigations. The selected model is shown in Figure 3.4.

A potentially occurring interactive hinge has been assumed in the cross section of possible maximal moment. Interactive hinges 1 through 7 have one degree of freedom while elastic members 8 through 17 have three degrees of freedom and thus the number of degrees of freedom of the model is 37. The state equation is:

$$\mathbf{G}^* \cdot \mathbf{s} + \mathbf{q} = 0$$

$$\mathbf{G} \cdot \mathbf{u} + \mathbf{F} \cdot \mathbf{s} + \mathbf{t} = 0$$

where:

- $\mathbf{G}$  — geometric matrix
- $\mathbf{s}$  — vector of load actions
- $\mathbf{q}$  — load vector
- $\mathbf{u}$  — displacement vector
- $\mathbf{t}$  — vector of "kinematic load"
- $\mathbf{F}$  — flexibility matrix

The solution of the equations is possible in the usual form (SZABÓ, ROLLER 1971).

### 3.33. Changes of state with a uni-parameter load system taken into account

The load vector  $q$  is increased by a value  $\Delta q$  from a suitable starting value till the moment  $M$  in the cross section of a potential interactive hinge attains the value  $M_1$ . At this point the relevant kinematic load  $t$  is inserted into the hinge and the hinge rotation rigidity is changed to the new value. Further increasing the amount of  $q$ , the modifications are undertaken until the determinant of the rigidity matrix becomes negative. This means that the size of the further steps is:  $-\Delta q$ .

In the course of the changes of state an interactive hinge may be encountered, where because of a plate buckling development, a descending curve characterizes the hinge behaviour, however, the frame structure can take up further loads.

The computations have been carried out with aid of a PDP 11/34 computer.

### 3.4. A SIMPLE APPROXIMATE METHOD

Numerous approximate engineering methods are introduced in the literature (HORNE, MORRIS 1981) from which as one of the possibilities we are going to deal with the extension of the Mechanism Curve Method. The Mechanism Curve Method — above the determination of the plastic load bearing capacity — can be applied to take the effect of finite deformations and strain hardening of steel into consideration.

#### 3.4.1. Mechanism Curve Method

(i) Plastic collapse loads are idealizations of the failure loads of elastic-plastic structures. In these idealizations the collapse load refers to infinitely small differences from the undeformed states with infinitely small plastic hinge rotations.

Based on previous consideration an adequate yield mechanism (pattern of plastic hinges) is to be chosen (Figure 3.5). Denoting the displacements of the external forces in the yield mechanism by  $u_i$  and the hinge rotations by  $\theta_j$  (Figure 3.5), the virtual work equation furnishes:

$$\lambda \sum_i Q_i u_i = \sum_j M_p \theta_j$$

This gives the collapse mechanism load factor  $\lambda_p$  (Figure 3.5).

(ii) In order to determine the rigid-plastic mechanism line it is necessary to follow the variation in the load factor  $\lambda$  at increasing finite values of the rotation  $\phi$ . At finite deformations, the mechanism itself becomes non-linear, and consideration of the exact geometry changes becomes laborious. HORNE (1960) has shown that a simple treatment gives a value for  $\lambda$  which is correct up to the first power of  $\phi$ . The work equation for the incremental deformation may be written as:

$$\lambda \sum_i Q_i du_i + \sum_k N_k L_k \phi_k d\phi_k = \sum_j M_{pj} d\theta_j$$

The second term of the equation is due to the additional external work arising from finite deformations.

The axial thrusts  $N_k$  may be obtained with sufficient accuracy by proportion from the values they have in the simple collapse state. The axial thrusts are  $\lambda(N_{kp}/\lambda_p)$ . A further approximation is that the total and incremental rotations and displacements are all in the same proportion as those for the same mechanism during an infinitely small deformation from the undeformed state. Hence

$$\frac{du_i}{u_i} = \frac{d\Phi_k}{\Phi_k} = \frac{d\Theta_j}{\Theta_j}$$

and the previous equation becomes

$$\lambda \left( \sum_i Q_i u_i + \sum_k \frac{N_{kp}}{\lambda_p} L_k \phi_k^2 \right) = \sum_j M_{pj} \Theta_j$$

This gives the relationship *AC* shown in Figure 3.5.

(iii) HORNE (1960) proposed the use of the simple rigid-plastic-rigid relationship in order to take into account the effect of strain-hardening on the collapse load of a structure.

Change of geometry due to elastic-plastic deformations tends to decrease the ultimate load bearing capacity of steel frames in comparison with the plastic collapse load. This tendency is counteracted by the strain-hardening properties of steel. The rigid-plastic-rigid theory of structural behaviour is found to be an adequate mean to assess the stiffness of a structure immediately on the formation of the last hinge in a plastic hinge mechanism.

Different strain-hardening theories can be used during the analysis: (Figure 3.6)

- rigid-plastic-rigid (RPR) model (HORNE 1960),
- rigid-plastic-hardening (RPH) model (HORNE, MEDLAND 1966),
- rigid-hardening (RH) model.

This treatment uses the rigid-hardening (RH) hinge model.

Hinge model determines the end moments of cantilevers of the length *h* and the depth *b*, the shape factor *f* of symmetrical I-section, the end moment comes out to be ( $M_p + m$ ) (Figure 3.7)

$$m = M_p \sqrt{\left( \frac{b}{fh} \right) \cdot \frac{E}{K \sigma_Y} \Theta}$$

The summations could be included in the rigid-plastic work equation, which then becomes

$$\lambda \left( \sum_i Q_i u_i + \sum_k N_k L_k \phi_k^2 \right) = \sum_j (M_{pj} + m_j) \Theta_j$$

The slope of the approximately linear relationship between  $\lambda$  and *u* which as a result of equation depends on the relative values of the two extra terms containing the deformations, namely

$$\lambda \sum \frac{N}{\lambda_p} L \phi^2 \quad \text{and} \quad \sum m \Theta.$$

It follows that strain-hardening will predominate over the tendency of instability and the rigid-plastic collapse mechanism will be stable if the "stability ratio" *R* is greater than unit where

$$R = \frac{\sum_j m_j \Theta_j}{\lambda_p \sum_k N_k L_k \phi_k^2}$$

Thus, if  $R > 1$  the rigid-plastic load-deflection relationship is raised from *AC* to *AD* in Figure 3.5. If, however  $R < 1$ , the relationship drops, as shown by *AE*.

### 3.42. Approximate Engineering Method to Take the Effect of Plate Buckling into Consideration (IVÁNYI 1983)

In the field of plastic design of steel structures the effect of plate buckling can be taken into consideration by the so called indirect method. During analysis it should be determined that the ratio of plate element dimensions of the section should be less than the ratio given in the specification; in this case buckling of plate elements do not occur until mechanism formation. Such kind of direct method can be applied to eliminate the disturbing effect of plate buckling, but not to analyze — at least only to predict — the effect of plate buckling in regard with a given structure. We extend the category of hardening plastic hinges by taking the effect of plate buckling into consideration. Such hinge model can be the basis of an Approximate Engineering Method, that — without analyzing the full load history —, with simple methods can directly take the effect of plate buckling into consideration.

Figure 3.8 shows the linear interaction of moment-rotation of interactive hinge that contains the effects of strain hardening and plate buckling. The essence of Approximate Engineering Method is that the two effects are separated and the interactive hinge of the structure is put together from two separate components: (Figure 3.9)

- (1) Strain-hardening component: (S)
- (2) Plate buckling component: (L)

With the assumed two hinge components the values of the load parameter for the chosen mechanism of the framework can be determined as a function of finite deformations.

The expression for (1) strain-hardening component is:

$$\lambda_{(S)} \left( \sum Q_u + \sum NL\phi^2 \right) = \sum M_p\theta + \sum m_S\theta$$

$$\lambda_{(S)} = \frac{\sum M_p\theta + \sum m_S\theta}{\sum Q_u + \sum NL\phi^2}$$

To write down the expression for the (2) plate buckling component it should be assumed that the interactive hinge characteristic curve contains rigid, plate buckling effects, so rigid behaviour goes up to the value of  $M' = M_p + \Delta M$  first, then a linearly decreasing change is taken into consideration due to the effect of plate buckling. Because of the shape of the characteristic curve belonging to the (2) plate buckling component, external and internal capacities and works are written similarly to the (1) strain-hardening component — except the sign of the increment  $m\theta$

$$\lambda_{(L)} \left( \sum Q_u + \sum NL\phi^2 \right) = \sum M'\theta - \sum m_L\theta$$

$$\lambda_{(L)} = \frac{\sum M'\theta - \sum m_L\theta}{\sum Q_u + \sum NL\phi^2}$$



Load parameter  $\lambda_{(S)}$  takes the effect of strain-hardening into consideration, while load parameter  $\lambda_{(L)}$  that of plate buckling.

From the displacement given by the intersection of the two curves; the reduction-like change of state is due to the effect of plate buckling (Figure 3.10). In connection with the results it should be emphasized, that — similarly to plastic load bearing capacity analysis — the expression — taking the two separate components into consideration — assumes the structure motionless till the moments  $M_P$  and  $M'$  in the hinges form.

The axial forces in bars are assumed to be proportional to the external loading. Equivalent cantilever length  $h$  for the interactive hinge can be determined by the moment diagram from plastic load bearing capacity analysis.

## 4. EVALUATION OF LOAD BEARING CAPACITY OF STEEL FRAMES

### 4.1. TEST PROGRAM

The experimental research project was carried out in the Laboratory of the Department of Steel Structures, Technical University, Budapest.

Three main series of experiments were covered by the test program.

The first part of the program contained the additional tests on stub columns, frame corners, plates elements, simple beams (HALÁSZ, IVÁNYI 1979). A brief summary of this serie is given in Figure 4.1.

#### 4.11. Full-scale Tests of Frames

In the second part of the program the full-scale tests of frames have been included. Figure 4.2 gives a brief summary of the full-scale tests and dimensions of the specimens, indicating the loads and the characteristics of the loading process.

#### 4.12. Building Section Test

The third part of the program was a representative part of a multipurpose, pinned, pitched roof industrial hall: a building section consisting of 3 frames, bracings with pinned elements, light gage purlins and wall beams with corrugated steel sheeting (Figure 4.3) (IVÁNYI, KÁLLÓ, TOMKA 1986).

Non-elastic tests (cyclically repeated load, incremental collapse) were carried out on the building section corresponding to stage 6 using load combination composed from dead and meteorological loads.

## 4.2. RESULTS OF THEORETICAL AND EXPERIMENTAL INVESTIGATIONS

### 4.21. Application of Computer Programs

Concerning the experimental frame C-3/2, the relation of load-deflection curve develops according to Figure 4.4. On the side of horizontal load, the first inelastic hinge develops due to the residual stresses and deformations in the cross section beneath the



frame knee and this hinge develops at 52% of the maximal frame load. At 97% of the maximal load, Zone *L* describing the effect of plate buckling develops also in this cross section, i.e. in the frame cross section an "unstable" state — a descending characteristic curve — develops.

For comparison Figure 4.4 introduces the characteristic load-displacement curve of the frame structure in the case, too, when the basis of the computations is the traditional plastic hinge.

The results show well that presence of residual stresses influence in a major way the range of limited plastic deformation, however, mainly because of the cross section geometry of experimental beam, the maximal load bearing capacities computed with the traditional (elastic-ideally plastic) hinge as well as those obtained by the interactive hinge coincide with the experimental results.

#### 4.22. Application of Approximate Engineering Method

The Approximate Engineering Method is presented on test frame *C-3/2*. Column base of test frame was supported by the foundation, but it did not act as fix end, so plastic load bearing capacity of column base was determined by experiments; these values were used in the calculations.

Approximate Engineering Method described in Section 3.4 is suitable for analyses of the strain hardening and the effect of plate buckling. The most important steps of the analysis of frame *C-3/2* given in Figure 4.5 are as follows:

- (i) Plastic load bearing capacity analysis: by mechanism chosen by test results,
- (ii) Analysis of effects of finite deformations with the help of the chosen mechanism,
- (iii) Effect of strain-hardening: moment-rotation relationship of inelastic zones can be replaced by straight lines, therefore rigid-hardening model can be applied to determine  $m_s$ ,
- (iv) Effect of plate buckling: characteristic curves of interactive hinges can be replaced by straight lines too, therefore the rigid-hardening model can be applied to determine  $M'$  and  $m_L$ .

Figure 4.5 compares test result and the results of Approximate Engineering Method taking strain-hardening of steel and the effect of the plate buckling into consideration. The comparison shows that the Approximate Engineering Method gives a satisfactory result for the maximum loads and the unstable equilibrium state path of whole structure as well; and at the same time the analysis can be done at the "desk of the designer".

#### 4.23. Building under Proportional Loading

##### Horizontal and Vertical Bracing System

Load-displacement diagrams of incremental collapse tests are shown in Figure 4.6. Ultimate loads are influenced by local loss of stability, previous loadings and the layout of frame-horizontal and vertical bracing connections.

Analysing the results of the experiments in the different phases of construction and in the fully completed state, the following conclusions can be drawn:

The actual behaviour of hall structures is more favourable than that generally taken into consideration in design practice. In strength analysis, and in stability analysis in

plane of the frame the effects of semi-rigid column bases, roof sheeting and end walls are generally neglected.

The measurement results showed the limit to which these effects advantageously affect both internal forces and the rigidity (mostly that of the horizontal displacement) of the structure.

The actual rigidity of the hall structures, the semi-rigid connection of the structural elements advantageously affect the value of load intensity belonging to the loss of stability perpendicular to the plane of the frame.

It also should be mentioned that, beside advantageous effects, also effects disadvantageously affecting the load-bearing capacity of the structure are occurring. These are the residual stresses due to welding, imperfections due to manufacturing and assembling, eccentricity.

No doubt these effects must be taken into consideration according to their significance. The method and the values of factors (such as fictitious eccentricity) applied in calculations are mostly contained in our present specifications. In cases not regulated or not adequately known, the decision of the designer governs. It should be mentioned that economic design can not be imagined such as taking the disadvantageous circumstances, practically in full, into consideration, and totally neglecting the advantageous ones, or taking effects into considerably underestimated.

## 5. CONCLUSION

Experimental and theoretical investigations have been carried out in connection with the elastic and the plastic load-bearing study of frame and hall structures, with strain-hardening of steel material, the residual stresses and plate buckling taken into account.

A method has been presented for the investigation of frame structures applying the steps of known, traditional methods so that the structural behaviour can be analyzed during the entire loading process. Certain effects determining the structural behaviour (e.g. residual deformation, steel material strain-hardening and plate buckling) have been taken into consideration with the aid of the interactive plastic hinge. The interactive hinge was incorporated into an investigation method operating with the structure matrix-calculation method. The results of the elaborated method has been compared with the *experimental investigation of full-scale structures*.

## ACKNOWLEDGEMENT

This contribution has been supported by the "Hungarian National Science Foundation" under the theme number 598/1991., titled "Theoretical and Practical Problems of Up-to-Date Stability Analysis of Steel Structures".

## REFERENCES

- BAKSAI, R. 1983.  
Plastic analysis by theoretical methods of the state change of steel frameworks. Diploma work, TUB, Budapest, (In Hungarian)
- BAKSAI, R. - IVÁNYI, M. - PAPP, F. 1985.  
Computer program for steel frames taking initial imperfections and local buckling into consideration, *Periodica Polytechnica, Civil Engineering*, Vol. 29. No. 3-4. pp. 171-185.
- BEN KATO, 1965.  
Buckling strength of plates in the plastic range, *Publications of IABSE*, Vol. 25.
- CLIMENHAGA, J. J. - JOHNSON, P. 1972.  
Moment-rotation curves for locally buckling beams. *Jrnl. of Struct. Div. ASCE*, Vol. 98 ST6.
- DRUCKER, D. C. 1951.  
A more fundamental approach to plastic stress-strain relations. *Proceedings, 1st U. S. Natl. Congress of Applied Mechanics, ASME*, 487
- HAAIJER, G. 1957.  
Plastic buckling in the strain-hardening range, *Jrnl. ASCE*, Vol. 83. EM2
- HALÁSZ, O. 1976.  
Limit design of steel structures. Second-order problems (In Hungarian). DSc. Thesis, Budapest
- HALÁSZ, O. - IVÁNYI, M. 1979.  
Tests with simple elastic-plastic frames. *Periodica Polytechnica, Civil Engineering*, Vol. 23, 157
- HALÁSZ, O. - IVÁNYI, M. 1985.  
Some lessons drawn from tests with steel structures, *Periodica Polytechnica, Civil Engineering*, Vol. 29. No. 3-4. pp. 113-122.
- HOFF, N. J. 1956.  
The analysis of structures, John Wiley and Sons, New York
- HORNE, M. R. 1960.  
Instability and the plastic theory of structures. *Transactions of the EIC*, 4, 31
- HORNE, M. R. - MEDLAND, J. C. 1966.  
Collapse loads of steel frameworks allowing for the effect of strain-hardening, *Proc. of Inst. of Civil Engineers*, Vol. 33. pp. 381-402.
- HORNE, M. R. - MERCHANT, W. 1965.  
The stability of frames, Pergamon Press
- HORNE, M. R. - MORRIS, L. J. 1981.  
Plastic design of low-rise frames, Granada, *Constrado Monographs*
- IVÁNYI, M. 1979a.  
Yield mechanism curves for local buckling of axially compressed members, *Periodica Polytechnica, Civil Engineering*, Vol. 23. No 3-4. pp. 203-216.

- IVÁNYI, M. 1979b.  
Moment-rotation characteristics of locally buckling beams, *Periodica Polytechnica, Civil Engineering*, Vol. 23. No 3-4. pp. 217-230.
- IVÁNYI, M. 1980.  
Effect of plate buckling on the plastic load carrying capacity of frames. IABSE 11th Congress, Vienna
- IVÁNYI, M. 1983.  
Interaction of stability and strength phenomena in the load carrying capacity of steel structures. Role of plate buckling. (In Hungarian). DSc. Thesis, Hung. Ac. Sci., Budapest
- IVÁNYI, M. 1985.  
The model of "interactive plastic hinge" *Periodica Politechnica*, Vol. 29. No. 3-4. pp. 121-146.
- IVÁNYI, M. - KÁLLÓ, M. - TOMKA, P. 1986.  
Experimental investigation of full-scale industrial building section, Second Regional Colloquium on Stability of Steel Structures, Hungary, Final Report, pp. 163-170.
- KALISZKY, S. 1978.  
The analysis of structures with conditional joints, *Jrnl. of Structural Mechanics*, 6., 195.
- KAZINCZY, G. 1914.  
Experiments with fixed-end beams. (In Hungarian). *Betonszemle*, 2, 68
- KURUTZ, M. 1975.  
Mechanical computation of structures containing conditional joints under kinematic loads (In Hungarian), *Magyar Építőipar* 24, 455.
- LAY, M. G. 1965.  
Flange local buckling in wide-flange shapes, *Jrnl. ASCE*, Vol. 91. ST6.
- MAIER, G. 1961.  
Sull'equilibrio elastoplastico delle strutture reticolari in presenza di diagrammi forze-elongazioni a tratti desrescenti. *Rendiconti, Istituto Lombardo di Scienze e Lettere, Casse di Scienze A, Milano* 95, 177
- MAIER, G. - DRUCKER, D. C. 1966.  
Elastic-plastic continua containing unstable elements obeying normality and convexity relations. *Schweizerische Bauzeitung* 84, No. 23., Juni. 1
- MAJID, K. 1972.  
Non-linear structures. Matrix methods of analysis and design by computers. Butterworths, London
- SZABÓ, J. - ROLLER, B. 1971.  
Theory and analysis of bar systems. (In Hungarian) *Műszaki Könyvkiadó, Budapest*
- THÜRLIMANN, B. 1960.  
New aspects concerning the inelastic instability of steel structures. *Journal of the Structural Division, ASCE*, 86, ST1, Jan.
- IVÁNYI, M. 1992.  
Ultimate load behaviour of steel-framed structures. *Journal of Constructional Steel Research*, Vol. 21. Nos 1-3. pp. 5-42.



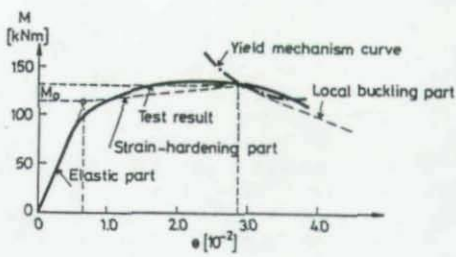
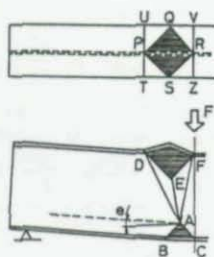
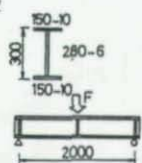


Figure 1.

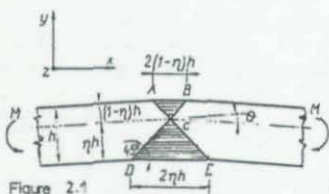


Figure 2.1

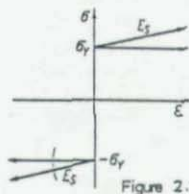


Figure 2.2

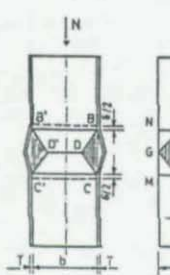


Figure 2.3

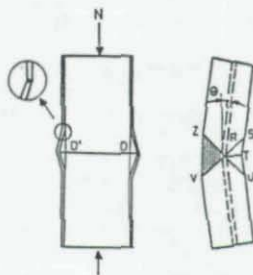


Figure 2.4

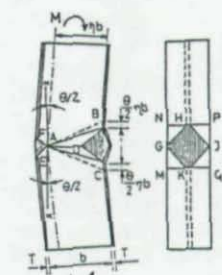


Figure 2.5

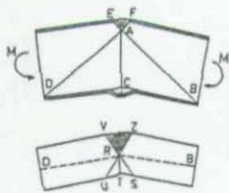


Figure 2.6

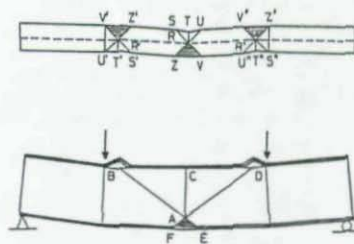


Figure 2.7



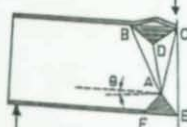
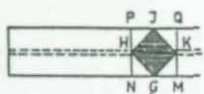


Figure 2.9

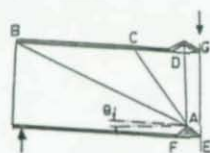
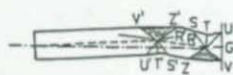
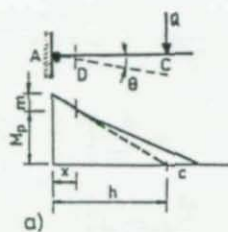


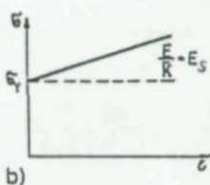
Figure 2.9

Flange plate yield mechanism	Web plate yield mechanism
Tension flange plate	Sign (W-1)
Sign (F-1)	
	Sign (W-2)
Compressed flange plate	
Sign (F-2)	Sign (W-3)
Sign (F-3)	Sign (W-4)
	Sign (W-5)
	Sign (W-6)

Figure 2.10

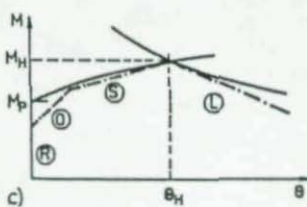


a)



b)

Figure 2.11



c)

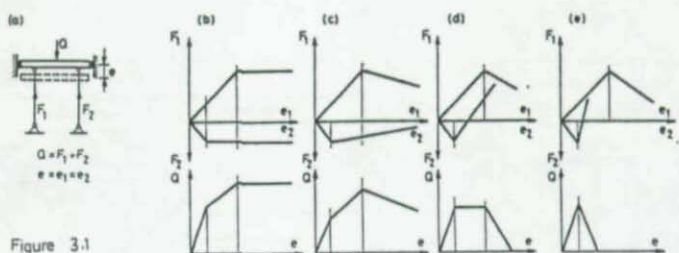


Figure 3.1

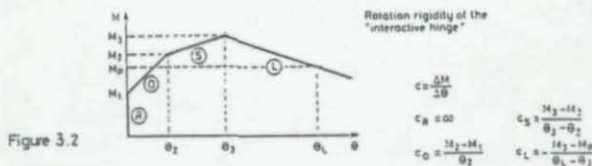


Figure 3.2

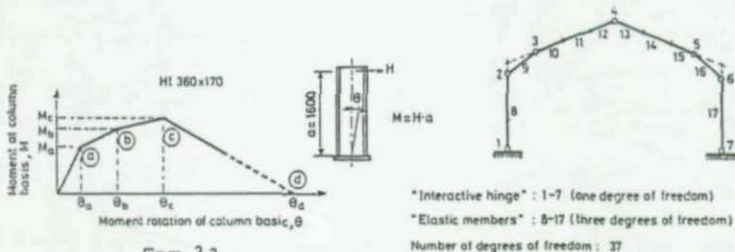


Figure 3.3

Figure 3.4

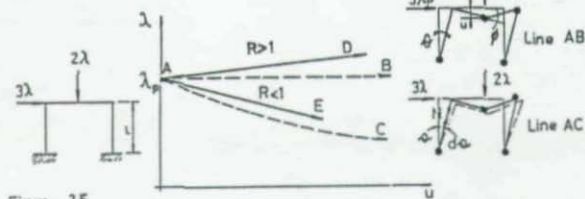


Figure 3.5

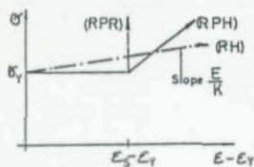


Figure 3.5

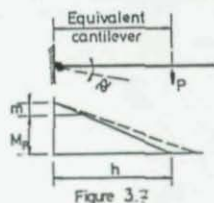


Figure 3.7

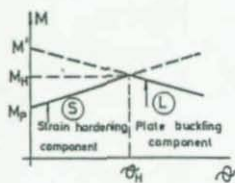


Figure 3.8

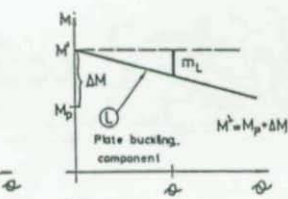
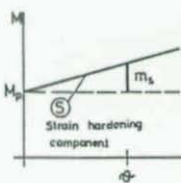


Figure 3.9

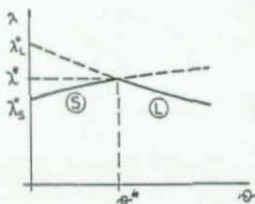


Figure 3.10

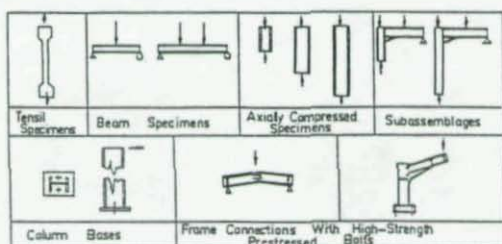


Figure 4.1

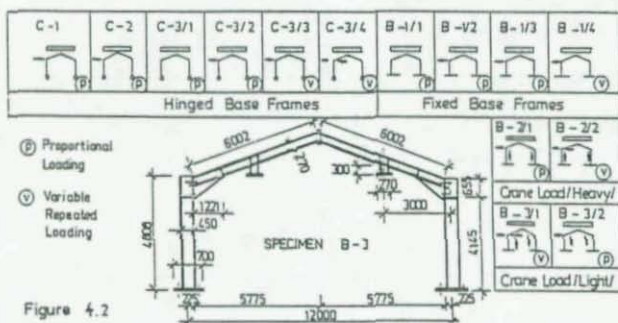


Figure 4.2

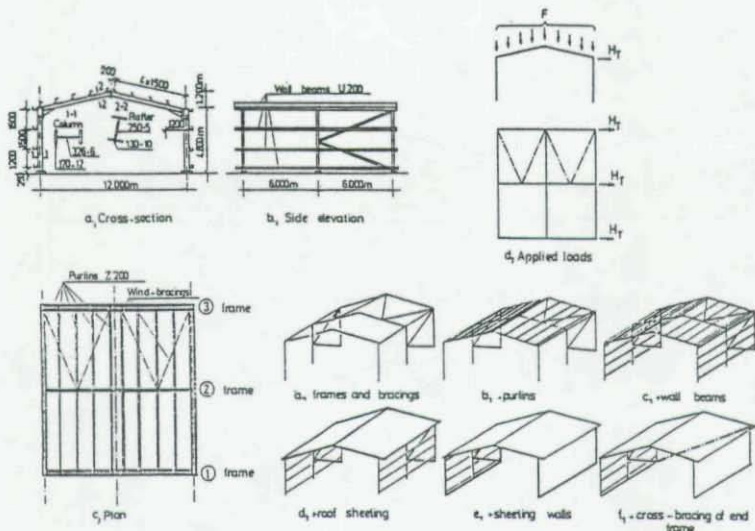


Figure 4.3

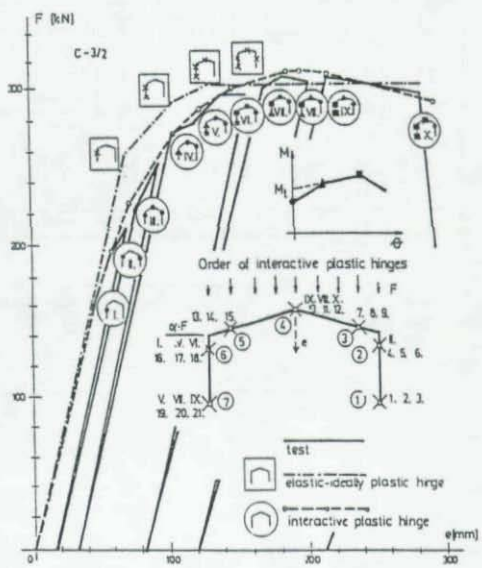


Figure 4.4

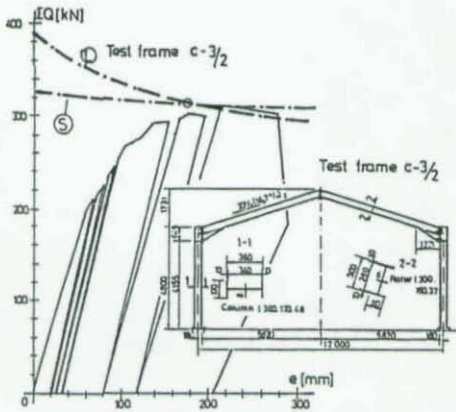


Figure 4.5

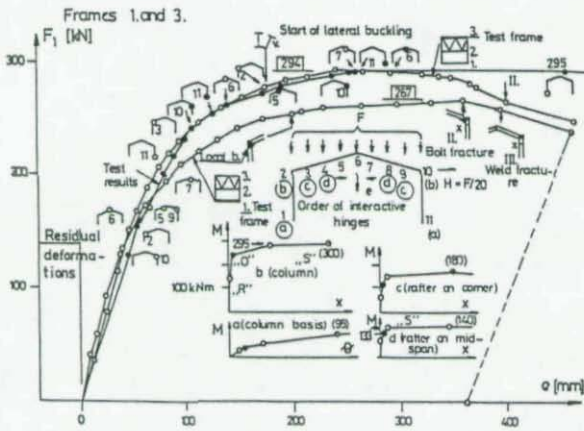


Figure 4.5





## STABILITY OF WEB-TAPERED BEAMS

by  
Dimos Polyzois<sup>1</sup> and Li Qing<sup>2</sup>

**ABSTRACT:** According to current design guidelines, a tapered member is replaced by an equivalent prismatic member with a different length and a cross section identical to that of the smaller end of the tapered member. Length modification factors are used to obtain the length of the equivalent prismatic members. To account for the moment gradient within the unbraced length and also for the restraining effect of adjacent spans in laterally braced members modification factors have been incorporated in the expression used for computing their buckling stress. In this paper, the current design guidelines for laterally unbraced web tapered beams are examined, and modifications to these guidelines are proposed.

(Key Words: steel, beams, web-tapered, buckling, stability, braced)

## INTRODUCTION

The current design guidelines for web-tapered beams are covered in Appendix F of the AISC Specification (AISC, 1986). These are based on work conducted by Lee, Morrell and Ketter in the early seventies (Lee et al, 1972; Morrell and Lee, 1974; Lee and Morrell, 1975). While the design of braced prismatic members accounts only for the moment gradient within the unbraced length, the design of tapered members accounts for both the moment (or stress) gradient and the restraining effect of adjacent segments. Four specific cases of loading and restraining conditions are presented. The current design procedure, however, is limited and may lead to misinterpretation. For the case of prismatic members, which may be considered as tapered members with a taper ratio of zero, the design criteria are not consistent with those corresponding to prismatic members. In the following sections, the current background to the current AISC design criteria is examined and modifications based on an extensive theoretical analysis are proposed.

## REVIEW OF CURRENT AISC DESIGN CRITERIA

The approach of designing tapered beams in the current AISC Specification (1986) is based on the concept that the critical moment,  $M_{cr}$ , for a tapered beam subjected to end moments, is the same as the critical moment of a prismatic beam of a different length, but with the same cross-section as the small end of the tapered beam, as shown in Fig. 1. The factored bending resistance of tapered beams is defined in Appendix F as

$$M_r = \phi_b \left(\frac{5}{3}\right) S_x' F_{by} \quad (1)$$

where  $S_x'$  is the section modulus of the tapered member at the point of maximum stress,  $\phi_b$  is the bending resistance factor, equal to 0.85,  $F_{by}$  is the allowable lateral torsional buckling stress, and the factor  $(5/3)$  is used to change the allowable stress to a limit states stress.  $F_{by}$  is defined as follows:

$$\text{when } F_{by} \leq \frac{F_y}{3} \quad F_{by} = B\sqrt{F_{sy}^2 + F_{wy}^2} \quad (2)$$

$$\text{when } F_{by} > \frac{F_y}{3} \quad F_{by} = \frac{2}{3} \left[ 1 - \frac{F_y}{6B\sqrt{F_{sy}^2 + F_{wy}^2}} \right] F_y \leq 0.60 F_y \quad (3)$$

1 Associate Professor, Department of Civil Engineering, University of Manitoba, Winnipeg, Canada

2 Graduate Student, Department of Civil Engineering, University of Manitoba, Winnipeg, Canada

where  $F_y$  is the yield stress (ksi),  $F_{sY}$  is the allowable St. Venant's torsional resistance (ksi), and  $F_{wY}$  is the allowable warping resistance of the equivalent prismatic member (ksi), defined as follows:

$$F_{sY} = \frac{12 \times 10^3}{h_s L d_o / A_f} \quad (4)$$

$$F_{wY} = \frac{170 \times 10^3}{(h_w L / r_{T0})^2} \quad (5)$$

where 
$$h_s = 1.0 + 0.0230 \gamma \sqrt{L d_o / A_f} \quad (6)$$

$$h_w = 1.0 + 0.0385 \gamma \sqrt{L / r_{T0}} \quad (7)$$

$r_{T0}$  is the radius of gyration of the section at the small end, considering only the compression flange plus one third of the compression web area, taken about an axis in the plane of the web, (in), and  $A_f$  is the area of the compression flange, (in<sup>2</sup>).

The term  $B$  in Eqs. 2 and 3 is a modification factor which accounts for the moment (or stress) gradient and/or the restraining effect of adjacent spans when a member is continuous over lateral supports. There are four cases covered in Appendix F. These cases are summarized below:

Case (a): When the maximum moment  $M_2$  in three adjacent segments of approximately equal unbraced length is located within the central segment and  $M_1$  is the larger moment at one end of the three-segment portion of a member, as shown in Fig. 2,

$$B = 1.0 + 0.37 \left( 1.0 + \frac{M_1}{M_2} \right) + 0.50 \gamma \left( 1.0 + \frac{M_1}{M_2} \right) \geq 1.0 \quad (8)$$

$M_1/M_2$  is considered negative when the critical segment is bent in single curvature. If  $M_1/M_2$  is positive, the specification recommends this ratio be taken as zero.

Case (b): When the largest computed bending stress  $f_{b2}$  occurs at the large end of two adjacent segments of approximately equal unbraced lengths and  $f_{b1}$  is the computed bending stress at the smaller end of the two-segment portion of the member, as shown in Fig. 3,

$$B = 1.0 + 0.58 \left( 1.0 + \frac{f_{b1}}{f_{b2}} \right) - 0.70 \gamma \left( 1.0 + \frac{f_{b1}}{f_{b2}} \right) \geq 1.0 \quad (9)$$

$f_{b1}/f_{b2}$  is considered negative when the two segment portion of the member is bent in single curvature. The ratio  $f_{b1}/f_{b2} \neq 0$ . The taper ratio,  $\gamma$ , is defined as  $\gamma = (d_L - d_o)/d_o$ , where  $d_o$  and  $d_L$  are shown in Fig. 3.

Case (c): When the largest computed bending stress  $f_{b2}$  occurs at the smaller end of two adjacent segments of approximately equal unbraced length and  $f_{b1}$  is the computed bending stress at the larger end of the two-segment portion of a member, as shown in Fig. 4,

$$B = 1.0 + 0.55 \left( 1.0 + \frac{f_{b1}}{f_{b2}} \right) + 2.20 \gamma \left( 1.0 + \frac{f_{b1}}{f_{b2}} \right) \geq 1.0 \quad (10)$$

The stress ratio  $f_{b1}/f_{b2}$  and the taper ratio  $\gamma$  are defined in Case (b). The dimensions  $d_0$  and  $d_L$  required to compute  $\gamma$ , are shown in Fig. 4.

Case (d): When the computed bending stress at the smaller end of a tapered member or segment thereof is equal to zero, as shown in Fig. 5,

$$B = \frac{1.75}{1.0 + 0.25\sqrt{\gamma}} \quad (11)$$

Where  $\gamma$  is calculated for the unbraced length adjacent to the point of zero bending stress.

The current AISC design criteria for doubly symmetric web-tapered beams assume that the flanges have equal and constant area and the depth varies linearly as:

$$d_z = d_0 \left( 1 + \gamma \frac{z}{L} \right) \quad (12)$$

where  $\gamma$  is the taper ratio of the tapered beam and is defined as follows:

$$\gamma = \frac{d_L - d_0}{d_0} \leq 0.268 \frac{L}{d_0} \leq 6.0 \quad (13)$$

#### BACKGROUND TO THE AISC DESIGN CRITERIA

Equations 8 to 11 were developed by researchers at the State University of New York at Buffalo (Lee et al, 1972; Lee and Morrell, 1974 and 1975). In their original work, these investigators referred to the term B in Eqs. 8, 9, and 10, as  $R_\gamma$ , a factor which accounted for both the stress gradient and the restraint provided by adjacent spans on the critical section, shown in Figs. 2, 3, and 4. They defined this term as:

$$R_\gamma = \frac{(\sigma_\gamma)_{LR}}{(\sigma_\gamma)_{SS} |_{\alpha=k}} \quad (14)$$

where  $(\sigma_\gamma)_{LR}$  is the elastic buckling stress of the critical section in a laterally restrained tapered beam, and  $(\sigma_\gamma)_{SS}$  is the elastic buckling stress of a simply supported tapered beam whose dimensions are identical to those of the critical section and loaded with end moments which produce a nearly uniform stress in the critical section.  $\alpha$  is the ratio between the minimum and maximum moments, and  $k$  is the ratio between the section modulus at the small end and the section modulus at the large end. Thus,  $\alpha = k$  implies a constant stress whereas  $\alpha \neq k$  implies a stress gradient.

Thus, except for Eq. 11 in Case (d), where the factor B accounts for only the moment gradient, the factor B in all other cases includes the effect of restraint provided by adjacent spans to the critical span. The effect of continuity over lateral supports has been well documented in the literature (Nethercot, 1983; Hartmann, 1967; Trahair, 1977) and methods for evaluating the buckling capacity of laterally restrained prismatic beams have been developed. The degree of restraint provided by adjacent spans to the critical segment in a member continuous over a number of lateral supports depends on the stress level in those spans and the stiffness of the lateral supports. The higher the stress level, the lower the restraining contribution. In the design of prismatic beams a conservative

critical load is computed ignoring the restraining contribution of adjacent spans, thus, assuming each unbraced segment is laterally and torsionally simply supported.

To investigate the buckling behaviour of tapered members and the effect of adjacent unbraced segments on the buckling capacity of a critical segment, Morrell and Lee (1974) used the moment diagram shown in Fig. 6. This moment distribution was chosen so that the center span would be critical and the stress would be nearly uniform in this span. The computed ratio of the critical stress of the laterally restrained member to the critical stress of the unrestrained segment was almost constant for the range of taper ratios investigated. The increase in the buckling capacity of the critical segment due to the restraints provided by adjacent segments was about 35%. The authors then proceeded to develop relationships between the buckling capacity of laterally restrained tapered members with various moment gradients and the taper ratio. These relationships have been incorporated in Appendix F of the current AISC Specification (1986).

Since the expressions for the modification factor B include both the effect of stress gradient and the effect of continuity, it is desirable to access the level of importance of each one. Use of the recommended AISC values of B, implies that both of these factors are equally important. There may be situations in practice, however, where the effect of continuity is drastically diminished, especially when the lateral supports have insufficient stiffness and/or are improperly applied to the tapered member. In this case, it may be wise to ignore the effect of continuity.

In this paper, separate expressions for the stress gradient factor B and the restraining factor  $R_\gamma$  are proposed and recommendations for design are made.

#### DEVELOPMENT OF STRESS GRADIENT AND RESTRAINT FACTORS

In developing expressions for the stress gradient factor B and the restraint factor  $R_\gamma$  for tapered members, six cases of loading and restraint conditions were investigated using the finite element program BASP (Akay et al., 1977). The cross sectional properties of the members used in this investigation are shown in Fig. 7. In the first three cases (Cases 1(a), 1(b) and 1(c)), the beams were simply supported and laterally unbraced. Three loading conditions were studied, as shown in Table 1. They were used to develop the stress gradient factor. The remaining three cases (Cases 2(a), 2(b) and 2(c)) also involved simply supported beams but these were laterally braced at equal intervals. These cases were used to develop only the restraint factor  $R_\gamma$ .

For cases 1(a) to 1(c), the stress gradient factor was defined as follows:

$$B = \frac{(\sigma_\gamma)_{SS} |_{\alpha \neq k}}{(\sigma_\gamma)_{SS} |_{\alpha = k}} \quad (15)$$

where  $(\sigma_\gamma)_{SS} |_{\alpha \neq k}$  is the elastic critical buckling stress of the simply supported member under a stress gradient, and  $(\sigma_\gamma)_{SS} |_{\alpha = k}$  is the elastic critical buckling stress of the same member but with a stress gradient equal to zero. The results from the finite element analysis were plotted and expressions for the stress gradient factor B were developed using curve fitting techniques. Examples of this factor are plotted in Figs. 8 to 10. The expressions for the factor B are listed in Table 1 as Eqs. 16, 17 and 18.

A special loading condition develops when the stress in Case 1(b) at the small end of the tapered member is zero. This case is identified in the current AISC Specification as Case (d). The finite element results, along with the results predicted by the AISC procedure and the results obtained from Eq. 17, are shown in Fig. 11.

For Cases 2(a), 2(b), and 2(c), the restraint factor,  $R_\gamma$ , was defined as,



$$F\gamma = \frac{(\sigma_\gamma)_{LR} |_{\alpha=k}}{(\sigma_\gamma)_{SS} |_{\alpha=k}} \quad (19)$$

where  $(\sigma_\gamma)_{LR} |_{\alpha=k}$  is the elastic critical buckling stress of the critical segment in the laterally braced beam with a stress gradient equal to zero and  $(\sigma_\gamma)_{SS}$  is the elastic critical buckling stress of the same segment assuming it to be simply supported and also subject to zero stress gradient. Examples of the restraint factor  $R_\gamma$  for Cases 2(a), 2(b) and 2(c) obtained from the finite element analysis of the section shown in Fig. 7, are plotted in Figs. 12, 13 and 14, respectively. The expressions developed for  $R_\gamma$  are listed in Table 2 as Eqs. 20, 21 and 22.

#### CONCLUSIONS AND RECOMMENDATIONS

In this paper, the current design guidelines for tapered beams were reviewed and the background to these guidelines was investigated. The use of one modification factor to account for both the moment (or stress) gradient and the restraint provided by adjacent segments in laterally braced beams, was questioned. Based on the results from an extensive finite element analysis, separate factors were developed and presented in this paper. The restraint factor is a function of the stress level in the segments that provide the restraint and the type and location of the lateral supports. Because of the uncertainty over its magnitude, a restraint factor of  $R_\gamma = 1.0$  is recommended for design. Moment (or stress) gradient factors,  $B$ , were presented in the paper which cover most of the loading conditions encountered in practice.

#### REFERENCES

- American Institute of Steel Construction (AISC) (1986), "Manual of Steel Construction - LRFD," Chicago, Ill.
- Lee, G.C., Morrell, M.L., and Ketter, R.L. (1972), "Design of Tapered Members," Welding Research Council Bulletin, No. 173, June.
- Morrell, M.L., and Lee, G.C. (1974), "Allowable Stress for Web-Tapered Beams with Lateral Restraints," Welding Research Council Bulletin, No. 172, February.
- Lee, G.C., and Morrell, M.L. (1975), "Application of AISC Design Provisions for Tapered Members," AISC Engineering Journal, Vol. 12, No. 1, January.
- Nethercot, D. A. (1983), "Elastic Lateral Buckling of Beams," in Beams and Beam Columns-Stability in Strength (ed. R. Narayanan), Applied Science Publishers, Barking, Essex, England
- Hartmann, A. J. (1967), "Elastic Lateral Buckling of Continuous Beams," ASCE J. Struct. Div., Vol. 93, No. ST4, pp. 11-28.
- Trahair, N. S. (1977), "Lateral Buckling of Beams and Beam-Columns," in Theory of Beam-Columns, Vol. 2, W. F. Chen and T. Atsuta, McGraw-Hill, New York, Chap. 3.
- Akay, H. U., Johnson, C. P., and Will, K. M. (1977), "Lateral and Local Buckling of Beams and Frames," ASCE J. Struct. Div., Vol. 103, No. ST9, p 1821.

Table I. Moment (Stress) Gradient Factor  $R_\gamma$ 

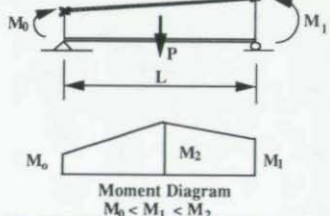
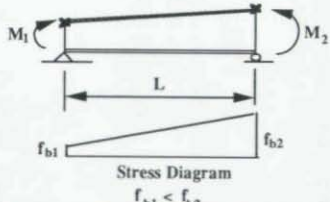
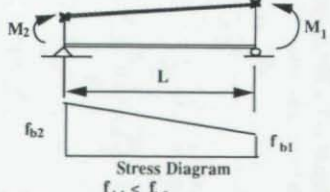
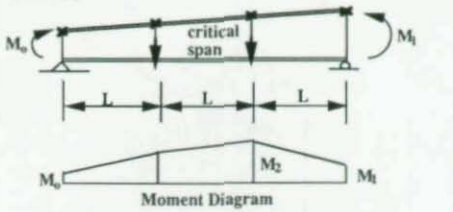
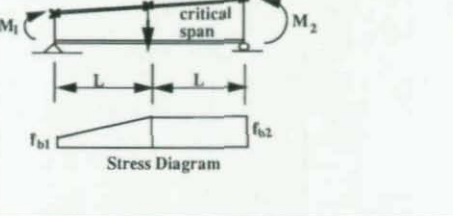
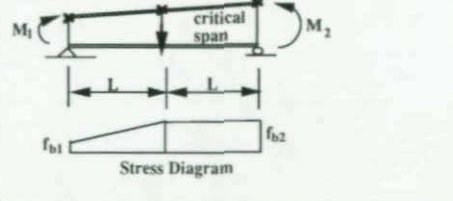
<p>Case I(a)</p>  <p>Moment Diagram <math>M_0 &lt; M_1 &lt; M_2</math></p>	$B = 1.0 \quad \dots (16)$
<p>Case I(b)</p>  <p>Stress Diagram <math>f_{b1} &lt; f_{b2}</math></p>	$B = 1.0 + 0.64 C_r - 0.3823 C_r \gamma + 0.066 C_r \gamma^2 \geq 1.0 \quad \dots (17)$ $C_r = 1 + f_{b1} / f_{b2}$ <p><math>f_{b1} / f_{b2}</math> is negative if member is bent in single curvature</p>
<p>Case I(c)</p>  <p>Stress Diagram <math>f_{b1} &lt; f_{b2}</math></p>	$B = 1.0 + 0.550 C_r + (0.175 + 0.454 \gamma) C_r^2 - 0.0425 C_r \gamma^2 \geq 1.0 \quad \dots (18)$ $C_r = 1 + f_{b1} / f_{b2}$ <p><math>f_{b1} / f_{b2}</math> is negative if member is bent in single curvature</p>

Table 2. Restraint Factor  $R_{\gamma}$ 

<p>Case 2(a)</p>  <p>Moment Diagram</p>	$R_{\gamma} = 1.0 + 0.403 D_f + (0.300 - 0.223 D_f) \gamma - 0.331 D_f \gamma^2 \geq 1 \quad \dots (20)$ $\alpha = M_1 / M_2$ $D_f = 1 + \alpha$ <p><math>\alpha</math> is negative when member is bent in single curvature If <math>\alpha &gt; 0</math>, then <math>D_f = 1</math></p>
<p>Case 2(b)</p>  <p>Stress Diagram</p>	$R_{\gamma} = 1.0 + 0.162 C_f + (0.619 - 0.383 C_f) C_f \gamma + (-0.430 + 0.263 C_f) C_f \gamma^2 \geq 1 \quad \dots (21)$ $C_f = 1 + f_{b1} / f_{b2}$ <p><math>f_{b1} / f_{b2}</math> is negative when member is bent in single curvature</p>
<p>Case 2(c)</p>  <p>Stress Diagram</p>	$R_{\gamma} = 1.0 + 0.162 C_f + (-0.070 + 0.039 C_f) C_f \gamma + 0.0175 C_f \gamma^2 \geq 1 \quad \dots (22)$ $C_f = 1 + f_{b1} / f_{b2}$ <p><math>f_{b1} / f_{b2}</math> is negative when member is bent in single curvature</p>

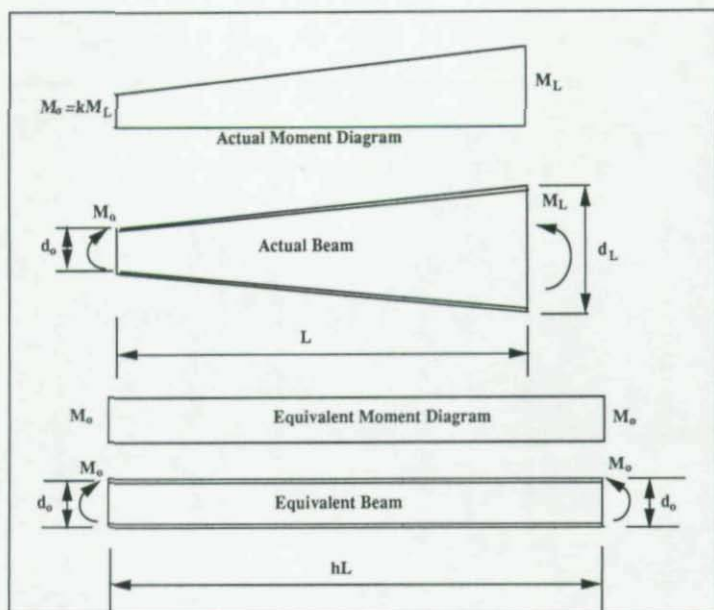


Fig. 1. Prismatic Beam Equivalent to Tapered beam

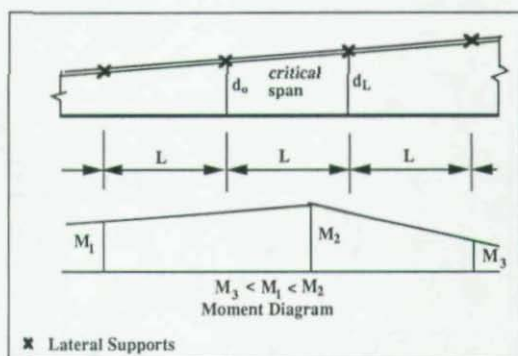


Fig. 2. Laterally Restrained Tapered Beam: AISC - Case (a)

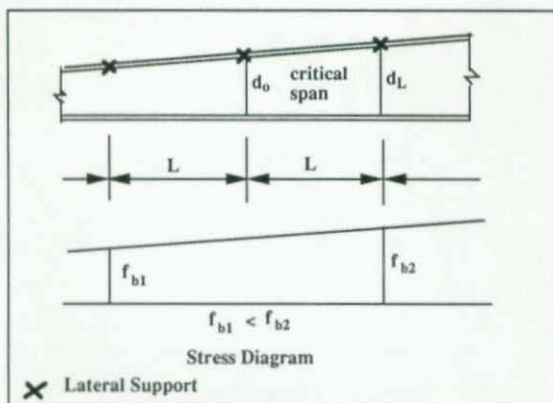


Fig. 3. Laterally Restrained Tapered Beam: AISC - Case (b)

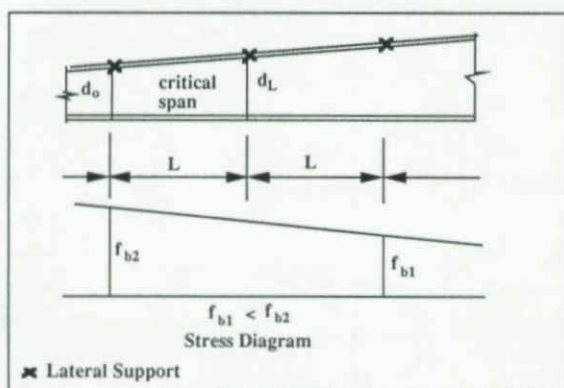


Fig. 4. Laterally Restrained Tapered Beam: AISC - Case (c)



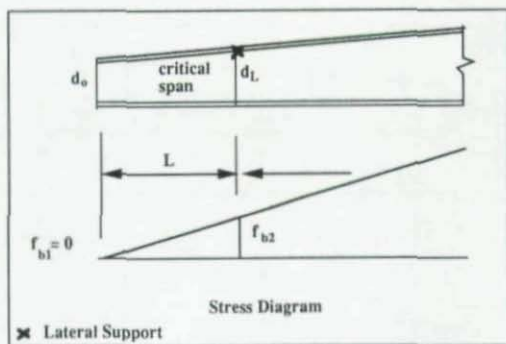


Fig. 5. Laterally Restrained Tapered Beam: AISC - Case (d)

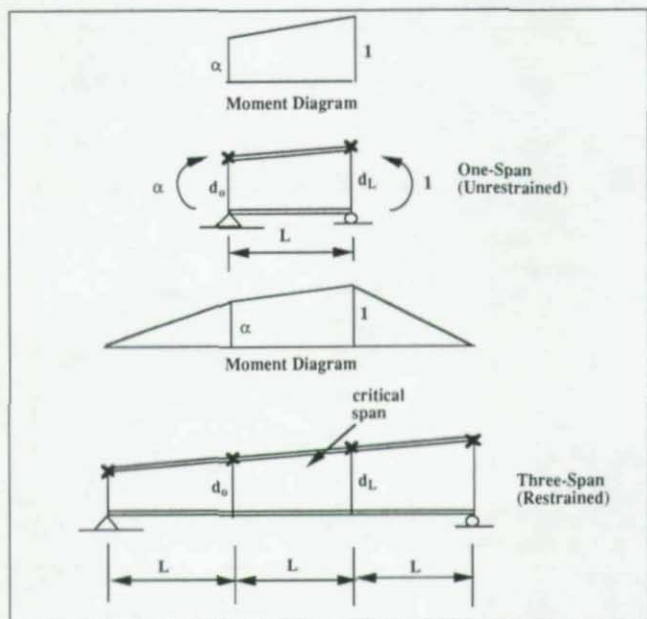


Fig. 6. Effect of Adjacent Spans in Laterally Braced Beams

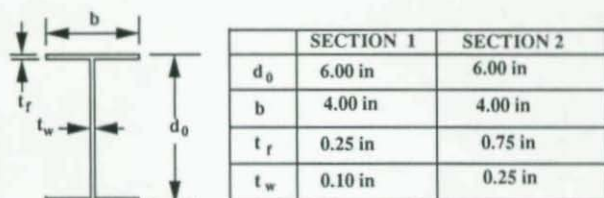


Fig. 7 Sections Used in the Finite Element Analysis

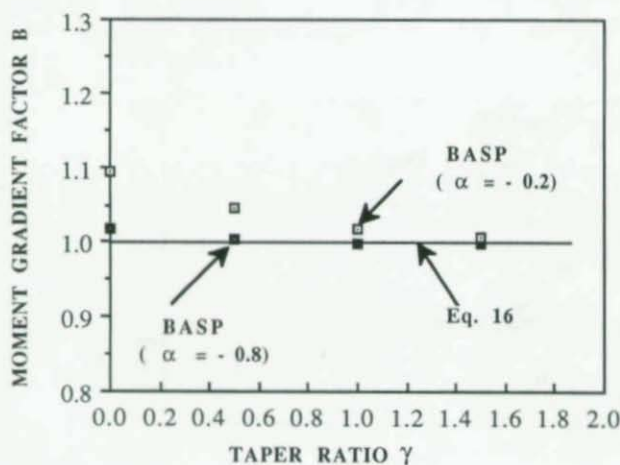


Fig. 8 Moment Gradient Factor B: Case 1(a)

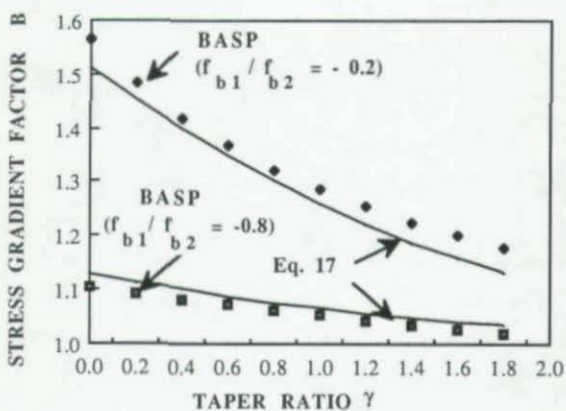


Fig. 9 Stress Gradient Factor B for Case 1(b)

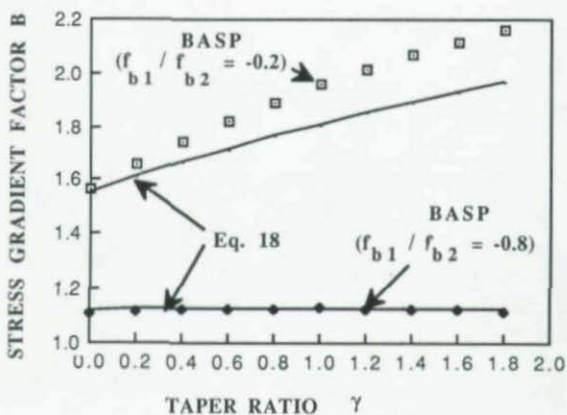


Fig. 10. Stress Gradient Factor B: Case 1(c)

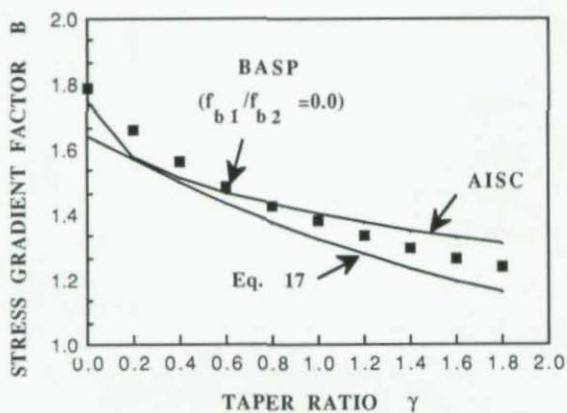
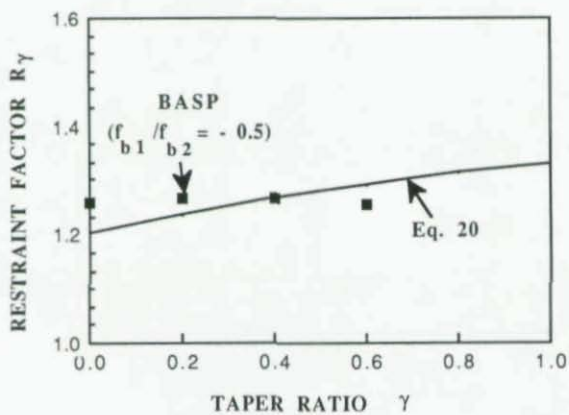
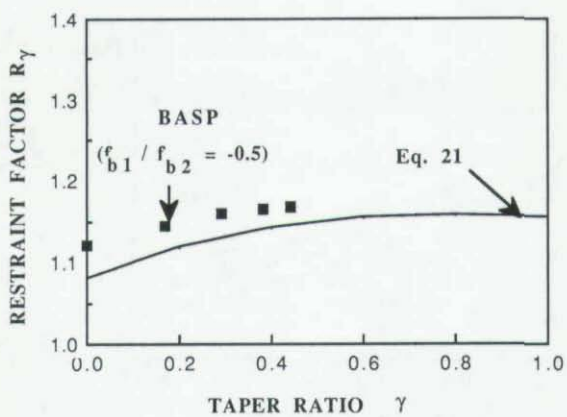
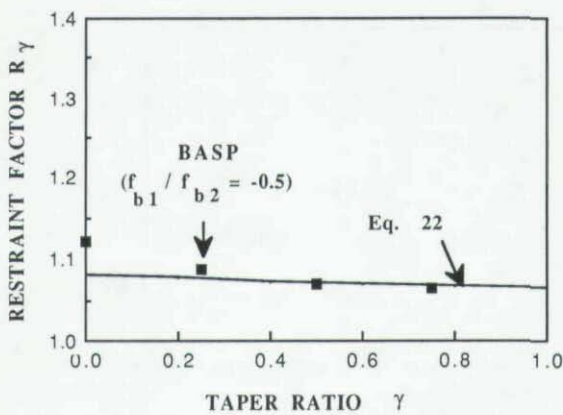


Fig. 11 Stress Gradient Factor B: Case 1(d)

Fig. 12 Restraint Factor  $R_\gamma$  : Case 2(a)

Fig. 13 Restraint Factor  $R_\gamma$  : Case 2(b)Fig. 14 Restraint Factor  $R_\gamma$  : Case 2(c)



## THE PLASTIC STRENGTH OF STAINLESS STEEL BEAMS

by

P.J. BREDENKAMP<sup>1</sup>, G.J. VAN DEN BERG<sup>2</sup>, P. VAN DER MERWE<sup>3</sup>.

### ABSTRACT

The findings of an investigation into the yield and plastic moment resistance as well as the plastic rotational capacity of hot-rolled stainless steel beams are reported in this study. This study is motivated in that stainless steel is an anisotropic and gradual yielding material. The hot-rolled stainless steel beams used in this study were fabricated from a modified AISI stainless steel Type 409, designated 3CR12, a ferritic corrosion resisting steel.

Three beam sizes were tested comprising of two I-sections and an H-section. These section sizes were similar to carbon steel sections commonly produced in South Africa. The experimental setup consisted of a beam being loaded by a concentrated point load in the centre of the beam span and were laterally restrained at bearing points. The beam spans were chosen to fall within the unbraced lengths set for plastic analysis of carbon steel beams. Lateral and rotational deflections were measured.

It is concluded from this investigation that because the I-sections were not annealed after hot-rolling, it resulted in very high yield strengths. High yield strengths, due to work hardening, greatly reduce the ductility of the material and tend to exceed the limiting flange width-to-thickness ratio necessary for plastic analysis. The annealed H-section is a non compact section, as defined in SABS 0162-1:1992<sup>1</sup>, and is unsuitable for plastic analysis. Although one of the sections tested gave a satisfactory rotational capacity necessary for plastic analysis large deflections can limit the use of stainless steels for such design. It is suggested by the authors that the I-sections be annealed which would result in sections suitable for plastic design. This will be done in future tests.

### GENERAL REMARKS

The hot-rolled Type 3CR12 corrosion resisting steel sections tested in this study were the first hot-rolled stainless steel sections ever to be produced in South Africa. It is thus expected that some problems will be encountered at first, such as the problems found for not heat treating the sections after hot-rolling.

- 
1. Lecturer of Civil Engineering in the Faculty of Engineering at the Rand Afrikaans University. Johannesburg, Republic of South Africa.
  2. Associated Professor, Chairman of Civil Engineering and Chairman of the Materials Laboratory in the Faculty of Engineering at the Rand Afrikaans University. Johannesburg, Republic of South Africa.
  3. Professor of Mechanical Engineering and Dean of the faculty of Engineering at the Rand Afrikaans University. Johannesburg, Republic of South Africa.

## MECHANICAL PROPERTIES

### Testing Procedure

Two I-sections and one H-section were tested in this study. The dimensions of these sections are given in Table 1. A portion, 220 mm long, was cold sawn from each section and were used to determine the mechanical properties. The remainder of the sections were used to prepare the beam tests.

Uniaxial tensile and compression test specimens were prepared from each 220 mm long section. Figure 1 shows the position from where these tensile and compression tests were taken. The mechanical properties were only determined in the longitudinal direction, that is the direction parallel to the rolling direction of the section.

The uniaxial tensile and compression tests were carried out generally in accordance with the procedures outlined by the ASTM Standard A370-77<sup>2</sup>. Average strain was measured by two strain gauges mounted on either side of the specimen in a full bridge configuration with temperature compensation. Compression test specimens were mounted in a specially manufactured compression test fixture which prevents overall buckling of the specimen about the minor axis.

### Results

*Type 3CR12 corrosion resisting steel yields gradually under load. In order to compute the initial modulus,  $E_0$ , and subsequently the proportional limit,  $F_p$ , defined as the 0,01% offset strength, and the yield strength,  $F_y$ , defined as the 0,2% offset strength from experimental data, a computer program has been developed. This program enables the computation of the best fit straight line for the initial part of the stress-strain curve through a process of iterative linear regression. The slope of the best fit straight line is considered to be the initial modulus,  $E_0$ .*

The mean values of the mechanical properties given in Table 2 were used together with Equation 1, attributed to Ramberg and Osgood<sup>3</sup> and revised by Van der Merwe<sup>4</sup>, to produce the analytical stress-strain curves shown in Figures 2, 3 and 4.

$$\epsilon = \frac{\sigma}{E_0} + 0,002 \left( \frac{\sigma}{F_y} \right)^n \quad (1)$$

where

$$n = \frac{\log \left( \frac{\epsilon_y}{\epsilon_p} \right)}{\log \left( \frac{F_y}{F_p} \right)}$$

and

- $\epsilon$  = strain
- $\sigma$  = stress
- $E_0$  = initial modulus
- $F_y$  = yield strength
- $F_p$  = proportional limit
- $\epsilon_y$  = yield offset strain
- $\epsilon_p$  = proportional offset strain

### THEORETICAL BACKGROUND

Before plastic analysis of a structure can be considered a structural element must have adequate lateral stability to ensure failure in pure bending only. The plastic moment resistance of a structural element must be attained and be able to withhold this resistance through a nominal rotation capacity of 2,5 as suggested by Lurkey and Adams<sup>5</sup> although AISC<sup>6</sup> requires a rotational capacity of 3,0 in order to form a plastic mechanism. Figure 5 shows how the rotational capacity is determined. A structural material should therefore be very ductile and the structural element should be so proportioned as not to fail prematurely in local buckling.

To determine the plastic strength of beams, two quantities, the yield moment resistance and the plastic moment resistance of the section must first be determined.

In order to determine the yield moment resistance of a stainless steel section in pure bending a new equation need to be developed as it is not possible to use the elastic flexure formula, derived in most strength of materials text books such as Popov<sup>7</sup>, due to the gradual yielding properties of stainless steel. However since the beam acts in pure bending the same equations of statics will be used here as were used in establishing the elastic flexure formula.

In order to determine the centroid of a section in pure bending Equation 2 may be used.

$$\int_A \sigma dA = 0 \quad (2)$$

Once the centroid of the section has been determined the moment resistance of a section in pure bending may be obtained by Equation 3.

$$\int_A \sigma y dA = M \quad (3)$$

Equations 2 and 3 result in a laborious iteration procedure involving numerical analysis when

considering gradual yielding materials. However this process may be simplified by some degree in using the revised Ramberg-Osgood equation, Equation 1, where strain is given as a function of stress. The yield moment resistance can be derived in the following manner.

Consider a rectangular stainless steel section, height,  $d$ , and width unity, in pure bending as shown in Figure 6. Assuming a linear strain distribution through the cross section of the beam, that is assuming plane sections remain plain after bending, the stress distribution in the cross section of the beam can be found by calculating the stress at each value of strain using Equation 1. This would once again result in a laborious iteration procedure as it is not possible to rewrite the stress in Equation 1 as a function of strain.

Note further that in inelastic flexure the neutral axis of a beam may not coincide with the centroidal axis of the cross-sectional area. It does so only if the cross-sectional area has two axis of symmetry and the stress-strain diagram is identical in tension and compression which is not the case when considering an anisotropic material such as stainless steel.

Thus the analysis is made in the following manner as the neutral axis of the beam is initially unknown. By arbitrarily selecting a neutral axis and using Equation 3 the total sum of the forces on the compressive side of the beam is determined which in turn should be balanced by the total sum of tensile forces acting on the tensile side of the beam. Note that the smaller of the tensile or compressive yield strength should be reached at the outer fibre of the section in order to calculate the yield moment resistance of the section.

In order to determine the total sum of forces on either the tensile or compressive side of the beam, the area of the stress distribution diagram of Figure 6 must be determined. This is done by integrating Equation 1 with respect to stress determining the hatched area. The area of the stress distribution is then determined by subtracting the area of the rectangle included under the stress-strain diagram by the hatched area as shown in Figure 6. The force is then obtained by multiplying this area by the distance between the arbitrarily chosen neutral axis and the extreme fibre divided by the yield strain. Mathematically this is shown in Equations 4, 5 and 6.

The hatched area is determined by.

$$A' = \int_0^a f(\sigma) d\sigma \quad (4)$$

where

$$f(\sigma) = \frac{\sigma}{E_0} + 0,002 \left( \frac{\sigma}{F_y} \right)^n$$

$a$  = maximum stress for determining the yield moment resistance

The area of the stress distribution is then determined by.

$$A = ab - A' \quad (5)$$

where

$b$  = corresponding strain, determined by Equation 1, to the stress used in Equation 4

The force is then calculated as.

$$P = \frac{c}{\epsilon_y} A \quad (6)$$

where

$c$  = the distance from the neutral axis to the extreme fibre of the beam section

When the tensile force is balanced by the compressive force the position of the neutral axis is determined.

The yield moment resistance can now be calculated by Equation 3 that is multiplying either the compressive force or the tensile force with the distance between the line of action between these forces. The line of action of the tensile and compression forces work through the centroid of each stress distribution diagram and can be calculated by the following procedure. For notations refer to Figure 6.

The centroid of the hatched area is calculated by Equation 7.

$$y' = \frac{1}{A'} \int_0^a \frac{1}{2} [f(\sigma)]^2 d\sigma \quad (7)$$

where

$$f(\sigma) = \frac{\sigma}{E_0} + 0,002 \left( \frac{\sigma}{F_y} \right)^n$$

$y'$  = strain distance from the neutral axis to the centroid of the hatched area

The centroid of the rectangle included under the stress-strain diagram is half the distance from the neutral axis to the extreme fibre. Therefore the centroid of the stress distribution diagram can be calculated by taking moments about the neutral axis. This results in the following equation.

$$y = \frac{\frac{ab^2}{2} - A'y'}{A} \quad (8)$$

This procedure should be performed on both the compressive and tensile side of the beam.

The distance  $y$  in Equation 8 is given in terms of a strain. In order to compute this distance in units of length Equation 8 is multiplied by the same factor as was used in Equation 6.



$$y_l = \frac{c}{\epsilon_y} y_s \quad (9)$$

where

- $y_l$  = distance from the neutral axis to the centroid of the stress distribution diagram in units of length  
 $y_s$  = distance from the neutral axis to the centroid of the stress distribution diagram in units of strain

The yield moment resistance is then calculated by Equation 10.

$$M_y = P (y_B + y_C) \quad (10)$$

where

- $y_B$  = distance from the neutral axis to the centroid of the tensile stress distribution diagram in units of length  
 $y_C$  = distance from the neutral axis to the centroid of the compressive stress distribution diagram in units of length

In calculating the plastic moment resistance of the above rectangular beam in pure bending a procedure similar to the above mentioned is followed. Some assumptions are however made. It is assumed that the beam is in a fully plastic state when the fibres of the web material has yielded at the neutral axis. Due to the gradual yielding characteristics of stainless steel the stress in the material increases directly beyond the yield strength until the plastic strain at the extreme fibre is reached. This is shown in Figure 7.

The plastic strain at the extreme fibre is assumed to be.

$$\epsilon_p = 12 \epsilon_y \quad (11)$$

Galambos<sup>8</sup> found this to be a typical value for carbon steel. It is further assumed that Equation 1 is valid up to the plastic strain calculated in Equation 11. Van der Merwe<sup>7</sup> only validated this equation up to the yield strength however Parks<sup>9</sup> have shown this assumption to be conservative. Care should however be taken not to exceed the ultimate strength of the material.

The area of the stress distribution diagram is then calculated by subtracting the hatched area from the rectangular plastic stress distribution diagram. The hatched area in Figure 7 is determined by.

$$A_p' = \int_a^d f(\sigma) d\sigma \quad (12)$$

where

- $a$  = maximum stress for determining the yield moment resistance  
 $d$  = the stress, determined by Equation 1, at the plastic strain calculated in Equation 11

$$f(\sigma) = \frac{\sigma}{E_0} + 0,002 \left( \frac{\sigma}{F_y} \right)^n$$

The area of the plastic stress distribution diagram is then calculated as.

$$A_p = db - A_p' \quad (13)$$

where

$b$  = plastic strain, determined by Equation 11

The plastic force is then determined by Equation 14.

$$P_p = \frac{c}{\epsilon_p} A_p \quad (14)$$

where

$c$  = the distance from the neutral axis to the extreme plastic fibre of the beam section

The neutral axis is determined as before by balancing the tensile force and the compressive force. The plastic moment resistance is now calculated similarly as before by multiplying either the compressive force or the tensile force with the distance between the line of action between these forces. One again the line of action of these forces work through the centroid of the stress distribution diagram which is calculated by the following procedure.

The centroid of the hatched area of Figure 7 is determined by.

$$y' = \frac{1}{A_p'} \int_a^d \frac{1}{2} [f(\sigma)]^2 d\sigma \quad (15)$$

where

$$f(\sigma) = \frac{\sigma}{E_0} + 0,002 \left( \frac{\sigma}{F_y} \right)^n$$

$y'$  = strain distance from the neutral axis to the centroid of the hatched area

The centroid of the plastic stress distribution diagram is now calculated by Equation 16 by taking moments about the neutral axis.

$$y = \frac{\frac{db^2}{2} - A_p' y'}{A_p} \quad (16)$$

The distance  $y$  in Equation 16 is given in terms of a strain. In order to compute this distance in units of length Equation 16 is multiplied by a similar factor as was used in Equation 6.

$$y_{pl} = \frac{c}{\epsilon_p} y_{ps} \quad (17)$$

where

$y_{pl}$  = distance from neutral axis to the centroid of the plastic stress distribution diagram in units of length

$y_{ps}$  = distance from neutral axis to the centroid of the plastic stress distribution diagram in units of strain

The plastic moment resistance is then calculated by Equation 18.

$$M_p = P_p (y_{plt} + y_{plc}) \quad (18)$$

where

$y_{plt}$  = distance from neutral axis to the centroid of the tensile plastic stress distribution diagram in units of length

$y_{plc}$  = distance from neutral axis to the centroid of the compressive plastic stress distribution diagram in units of length

In the above derivation of the yield moment resistance and plastic moment resistance a rectangular beam was used. This theory can also be made applicable to other types of sections such as I-sections.

Making use of superposition the moment resistance of the web is separated from the moment resistance attributed to the flanges. The moment resistance of the web is similar to that previously derived for a rectangular beam. The moment resistance of the flanges are then added. The stress distribution in the flanges are taken constant on the assumption that the ratio of the sum of the web thicknesses to the section depth is small and only a small error is made considering that the material yields gradually. It should however be noted that the difference in the compression force and tensile force in the flanges should be brought into account when determining the neutral axis.

Once the neutral axis has been determined for an I-section in inelastic flexure the yield moment resistance can be calculated by Equation 19.

$$M_y = P t_w (y_k + y_c) + \sigma t_f (b - t_w) (h - t_f) \quad (19)$$

where

$\sigma$  = the maximum allowable yield stress in the flanges

Similarly can the plastic moment resistance be calculated by Equation 20.

$$M_p = P_p t_w (y_{plt} + y_{plc}) + \sigma_p t_f (b - t_w) (h - t_f) \quad (20)$$

where

$\sigma_p$  = the maximum allowable plastic stress in the flanges

## EXPERIMENTAL SETUP AND PROCEDURE

The experimental setup consisted of a simply supported beam loaded in the centre of the span by a concentrated point load. The beam was laterally restrained in the centre of the span and laterally fixed at the end bearing points. The beam spans were chosen to correspond to work done by Lay, Maxwell and Galambos<sup>10</sup> and Lurkey and Adams<sup>5</sup>. The spans were  $72 r_y$ , or  $36 r_y$  between lateral restraints thus preventing the occurrence of lateral instability resulting in a beam failing in pure bending. Web stiffeners were welded onto the beams at bearing points in order to prevent web crushing or web crippling occurring.

The end rotations on either side of the beam were measured with an LVDT via lever arms bolted to the beam through the centroid of the web. The lever arms were used in order to amplify this deflection, later converted to radians. Lateral displacements were measured with two dial gauges, a distance  $18 r_y$  to either side of the concentrated point load on the compression flange. These measurements were taken in order to ensure that no lateral displacement occurred ensuring that the beam failed in pure bending. No strain readings were taken since the order of strains expected in the beams were beyond the capabilities of strain gauges.

The concentrated point load was applied to the beam via a hydraulic Instron actuator with a displacement rate of 1 mm per minute. Load and deflection readings were taken at 30 second intervals and stored on computer diskette to facilitate further data processing.

## RESULTS

In general, beams can be categorized as one of four types i.e. a plastic section, compact section, non-compact section and a slender section. The results of the different section types tested are given in Table 3.

The yield moment and plastic moment resistances were calculated for the beams by using the mechanical properties of the sections, given in Table 2, and these results are given in Table 4. Moment-rotation curves were drawn for each of the beams tested. These curves are shown in Figures 8 to 10 from where the rotation capacity of the beams were obtained and are given in Table 4. In Table 5 a comparison is drawn between the yield moment resistance and plastic moment resistance of carbon steel and stainless steel beams.

The lateral deflections of the beams were negligible and it is concluded thereby that the beams failed in pure bending. These deflections are not shown.

## CONCLUSIONS

It can clearly be seen from comparing Tables 4 and 5 that by using the above analysis for determining the yield and plastic moment resistance for a stainless steel section that, however laborious, there is some advantage to be gained in the strength of such a section. It should be pointed out however that the deflection at which these strengths occur is much larger than that obtained for carbon steel sections.

It was further concluded from this investigation that because the I-sections were not annealed after hot-rolling, it resulted in very high yield strengths due to work hardening through the rolling process. The result of these high yield strengths in the I-sections was that the IPE<sub>AA</sub> 100 section, although still classified as a plastic section, gave a barely satisfactory rotation capacity due to a significant decrease in the ductility of the material. The 203x133x25 I-section however was reduced from a plastic section to a slender section according to the definition in SABS 0162-1:1992<sup>1</sup> giving an unsatisfactory rotational capacity.

The 152x152x23 H-section was annealed after rolling. According to the definition in SABS 0162-1:1992<sup>1</sup> this is a non-compact section meaning that this section is able to attain the yield moment resistance but not the plastic moment resistance. This section can therefore not be used for plastic analysis, as was expected.

It is suggested by the authors that the I-sections be annealed which would result in sections suitable for plastic design and retested.

#### REFERENCES

- 1 South African Bureau of Standards. Code of Practice for the Structural Use of Steel. SABS 0162-1:1992.
- 2 American Society for Testing and Materials. Standard Methods and Definitions for Mechanical Testing of Steel Products. ASTM A370-77. Annual Book of ASTM Standards. 1981.
- 3 Ramberg, W; Osgood, W.R; Determination of Stress-Strain Curves by Three Parameters. National Advisory Committee on Aeronautics. Technical Note No. 503.
- 4 Van der Merwe, P; Development of Design Criteria for Ferritic Stainless Steel Cold-formed Structural Members and Connections. Ph.D. Thesis. University of Missouri-Rolla. 1987.
- 5 Lurkey, A.F; Adams, A.M; Rotation Capacity of Beams Under Moment Gradient. Journal of the Structural Division, ASCE, ST6. June 1969.
- 6 American Institute of Steel Construction. Manual of Steel Construction. Load and Resistance Factor Design. Chicago Illinois. 1986.
- 7 Popov, E.P; Mechanics of Materials. Prentice Hall. Second Edition. 1987.
- 8 Galambos, T.V; Structural Members and Frames. Prentice Hall. 1968.
- 9 Parks, M.B; Design of Automotive Structural Components using High Strength Sheet Steels. Second Progress Report. Civil Engineering Study 83-3. University of Missouri-Rolla. August 1983.
- 10 Lay, M.G; Maxwell, G; Galambos, T.V; Inelastic Beams Under Moment Gradient. Journal of the Structural Division, ASCE, ST1. February 1967.



TABLE 1 Dimensions of Sections

Beam Designation (mm x mm x kg/m)	h (mm)	b (mm)	$t_w$ (mm)	$t_f$ (mm)
IPE <sub>AA</sub> 100	99	55	3,45	4,45
203x133x25	203	133	5,80	7,00
152x152x23	152	152	6,50	7,00

TABLE 2 Mechanical Properties of the Sections

Property	Tensile	Compression
<b>Initial Elastic Modulus <math>E_s</math> (GPa)</b>		
IPE <sub>AA</sub> 100	198,00	199,65
203x133x25	195,33	206,19
152x152x23	196,33	209,92
<b>Yield Strength <math>F_y</math> (MPa)</b>		
IPE <sub>AA</sub> 100	476,75	520,91
203x133x25	504,51	536,74
152x152x23	301,22	306,80
<b>Proportional Limit <math>F_p</math> (MPa)</b>		
IPE <sub>AA</sub> 100	208,19	236,92
203x133x25	333,57	330,56
152x152x23	238,35	244,56
<b>Ultimate Strength <math>F_u</math> (MPa)</b>		
IPE <sub>AA</sub> 100	700	-
203x133x25	615	-
152x152x23	468	-
<b>Elongation (%)</b>		
IPE <sub>AA</sub> 100	18,5	-
203x133x25	21,56	-
152x152x23	34,63	-

TABLE 3 Width to Thickness Ratio Classification of Beam Flanges

Beam Size	Class 1	Class 2	Class 3	$b_f/t_f$	Resulting Type
	$\frac{145}{\sqrt{F_y}}$	$\frac{170}{\sqrt{F_y}}$	$\frac{200}{\sqrt{F_y}}$		
IPE <sub>AA</sub> 100	6,35	7,45	8,76	6,19	Class 1
203x133x25	6,26	7,34	8,63	9,70	Class 4
152x152x23	8,28	9,71	11,42	10,85	Class 3

Class 4 beams are classified as slender beams.

$b_f$  is half the distance of the total flange width.

All the beam webs tested are classified as Class 1.

TABLE 4 Results of Beam Tests

Beam Size	$M_{yt}$ (kN.m)	$M_{pr}$ (kN.m)	$M_{pe}$ (kN.m)	$\frac{M_{pe}}{M_{pr}}$	Rotation Capacity
IPE <sub>AA</sub> 100	13,503	20,518	21,71	1,058	5,00
			23,29	1,135	5,89
203x133x25	112,538	141,808	143,33	1,011	1,80
			144,58	1,019	2,78
152x152x23	52,247	69,820	63,49	0,909	-

$M_{yt}$  = theoretical yield moment resistance for Type 3CR12 steel.

$M_{pr}$  = theoretical plastic moment resistance for Type 3CR12 steel.

$M_{pe}$  = experimental plastic moment.

TABLE 5 Comparison between Stainless Steel and Carbon Steel Beams

Beam Size	$M_{yc}$ (kN.m)	$M_{yt}$ (kN.m)	$M_{pic}$ (kN.m)	$M_{pt}$ (kN.m)	$\frac{M_{yt}}{M_{yc}}$	$\frac{M_{pt}}{M_{pic}}$
IPE <sub>AA</sub> 100	13,232	13,503	15,208	20,518	1,020	1,349
203x133x25	106,332	112,538	130,668	141,808	1,058	1,085
152x152x23	49,939	52,247	55,424	69,820	1,046	1,260

$M_{yc}$  = theoretical elastic moment resistance for carbon steel.

$M_{pic}$  = theoretical plastic moment resistance for carbon steel.

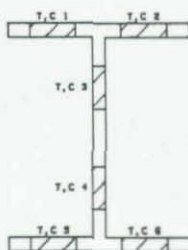


FIGURE 1 POSITION OF TENSILE AND COMPRESSION TEST SPECIMENS ON SECTIONS

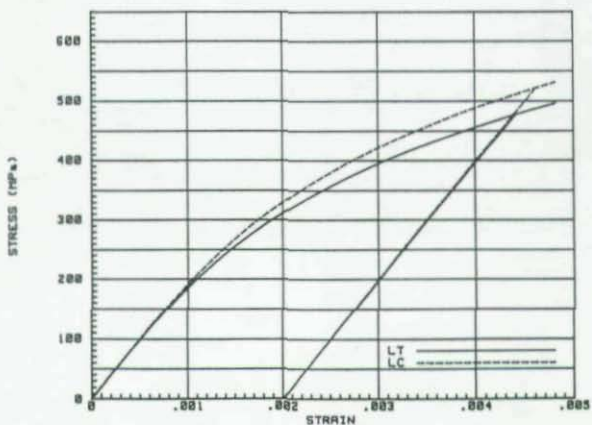


FIGURE 2 ANALYTICAL STRESS-STRAIN CURVES FOR SECTION IPE<sub>M</sub> 180

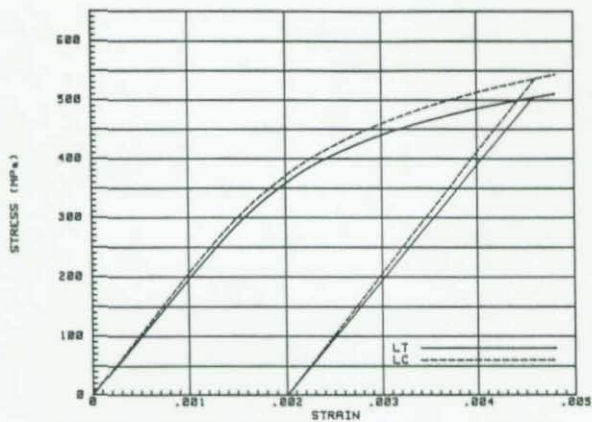


FIGURE 3 ANALYTICAL STRESS-STRAIN CURVES  
FOR SECTION 203x133x25

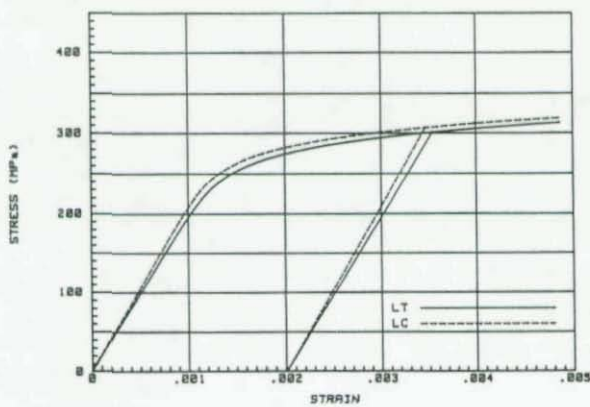


FIGURE 4 ANALYTICAL STRESS-STRAIN CURVES  
FOR SECTION 152x152x23



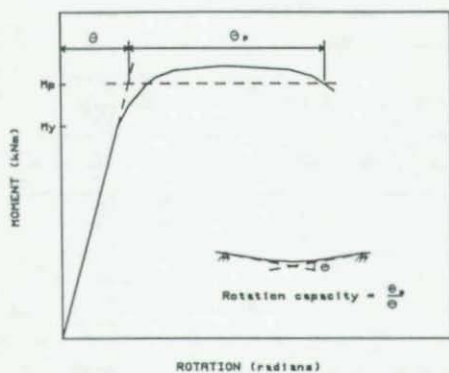


FIGURE 5 DETERMINATION OF ROTATION CAPACITY

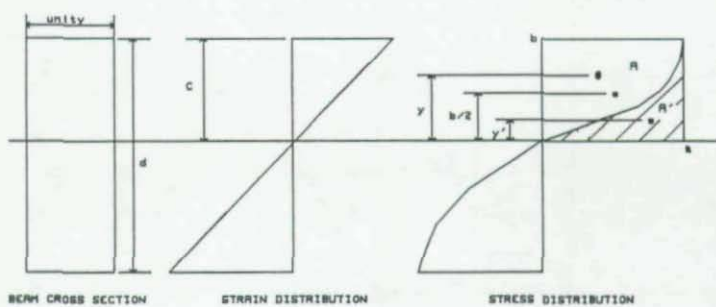


FIGURE 6 DETERMINATION OF YIELD MOMENT RESISTANCE

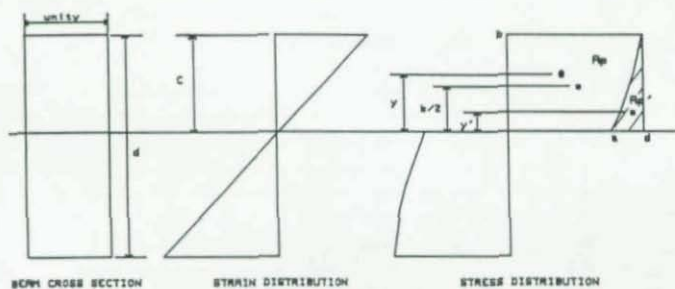


FIGURE 7 DETERMINATION OF PLASTIC MOMENT RESISTANCE

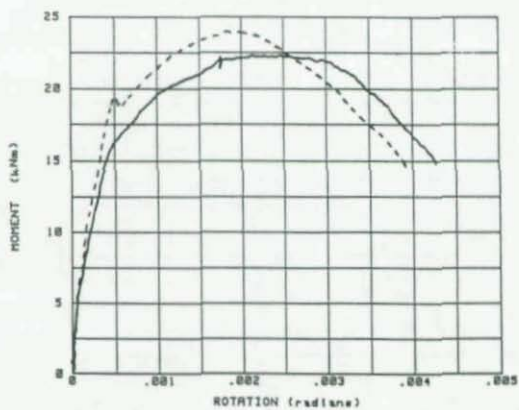


FIGURE 8 MOMENT-ROTATION CURVES FOR SECTION IPE 180

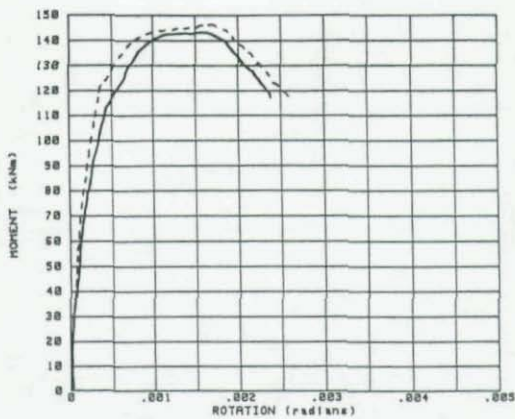


FIGURE 9 MOMENT-ROTATION CURVES FOR SECTION 283x133x25



FIGURE 10 MOMENT-ROTATION CURVE FOR SECTION 152x152x23

## ASYMPTOTIC MODAL ANALYSIS OF LATTICE DOMES

by Ronaldo C. Batista and Ricardo V. Alves  
COPPE - Universidade Federal, Rio de Janeiro  
CEP 21945 - 970, C. Postal 68506

### ABSTRACT

The nonlinear behavior and structural elastic instability of a lattice dome is analyzed through an asymptotic modal method. It is shown that by using the proposed method bifurcation and limit loads of an idealized geometrically perfect structure or buckling loads of its imperfect counterpart can be calculated, initial post-critical paths can be traced and imperfection sensitivity if any can be estimated. These main features are demonstrated through application to stability analysis of a classical example and of a hemispherical lattice dome whose structural behavior and stability are discussed.

### 1. INTRODUCTION

Lattice domes are reticulated light-weight space frames which are generally fabricated from an assemblage of many truss-shaped triangulated plane frames. Their overall geometry may approximate a shell surface by employing a large number of members and nodes, although their nonlinear buckling behavior may differ considerably from the continuum shell structure.

Their integrity is usually based on the resistance of the slender members to local buckling collapse under axial compression, and as they are interconnected at joints having some degree of fixity, local buckling calculations have to take into account in-plane and out-of-plane rotational stiffnesses. In any case the load at which these local buckles may occur can be predicted from simple flexural/torsional column buckling approaches, based upon the axial member forces obtained from classical linear analyses of space frames. Hence, if properly designed and sized in accordance with adequate detailing of joints fixity and stiffness, local buckling of these slender members can be eliminated from controlling collapse. Then for members beyond their needed critical size it is the overall critical modes that may dominate the structural behavior, becoming the controlling design constraint of buckling collapse of lattice domes. These overall modes may be potentially sensitive to the form of loading system and magnitude of certain unavoidable initial geometric imperfections inherent to fabrication, assemblage and erection procedures. It is therefore toward this overall buckling behavior and instabilities that attention is focused in this paper. The structural nonlinear elastic behavior is analyzed through an asymptotic modal method, which can detect bifurcation and limit loads and trace initial post-critical paths and estimate imperfection sensitivity.

## 2. ASYMPTOTIC MODAL ANALYSIS

An asymptotic modal approach to nonlinear instability analysis of perfect and imperfect structures has been recently proposed and reported in references [1, 2]. This approach makes use simultaneously of the perturbation, incremental/iterative, nonlinear modal coupling and finite element methods. Having been developed within the main framework of the general asymptotic theory of elastic stability, it can detect distinct bifurcation or limit loads along the nonlinear fundamental path. Moreover it can trace automatically the associated initial post-critical responses and the corresponding imperfection paths, and therefore estimate imperfection sensitivity.

In relation to the apparent disadvantage of the small range of imperfection amplitudes allowed for in such asymptotic analysis, it can be argued that it is the up-dated spectrum of critical loads and associated modes together with small imperfections sensitivity estimates that will assist in any comprehensive simulation and interpretation of large imperfection/large displacement structural responses to be obtained by a full nonlinear numerical analysis, whenever this becomes a practical imposition.

In the following a very brief account of the used mathematical model is presented. The interested reader can find in references [1, 2] the basis of the theoretical formulation at a level of detail which hopefully will allow him to grasp the most relevant points of the proposed approach.

In the nonlinear asymptotic modal analysis of a structure discretized by using displacement finite element models, the state vector of modal unknowns is written as

$$\mathbf{U} = \lambda \mathbf{U}_0 + a_i \bar{\Phi}_i + \bar{\mathbf{U}} \quad ; \quad i = 1, \dots, 4. \quad (1)$$

where  $\lambda$  is a scalar control parameter (e.g. load),  $\mathbf{U}_0$  the vector of fundamental displacements,  $a_i \bar{\Phi}_i$  is a linear combination of a reduced number of four normalized modes  $\bar{\Phi}_i$  with unknown amplitudes  $a_i$ , and  $\bar{\mathbf{U}}$  is the vector of nodal initial imperfections in the form of retained modes  $\bar{\Phi}_i$ , or in any other given random form.

The nonlinear pre-critical and post-critical equilibrium paths are obtained by applying the stationary principle onto the reduced energy functional

$$\delta V^* = V^*(\lambda \mathbf{U}_0 + a_i \bar{\Phi}_i ; \bar{\mathbf{U}}) \delta a_i \bar{\Phi}_i = 0 \quad (2)$$

resulting in a system of nonlinear modal equations.

An incremental approach combined together with a Newton-Raphson iterative scheme is used as the numerical strategy to solve the nonlinear equations. Because the modal combination is derived through a perturbation scheme it is loading dependent and there is no requirement for correction vectors to trace the nonlinear equilibrium paths. Only initial post-critical (e.g. post bifurcation or post-limit) paths are traced automatically and therefore no use is made of any other numerical strategy (e.g. arc-length continuation) to overcome convergence problems beyond these deformation stages.

Limit loads occurring along perfect or imperfect paths are detected by singularity of the tangent stiffness matrix



$$\mathbf{K}_T = \left[ \mathbf{K}_0 + \mathbf{K}_1(\mathbf{U}^E) + \frac{1}{2} \mathbf{K}_2(\mathbf{U}^E; \mathbf{U}^E) \right] \quad (3)$$

in which  $\mathbf{K}_0$ ,  $\mathbf{K}_1$  and  $\mathbf{K}_2$  are, respectively, the linear stiffness matrix and the first and second order incremental stiffness matrices, and where superscript E stands for any regular equilibrium point.

Bifurcation loads are detected either by equation (2) or by the up-dated linearized eigenvalue problem

$$\left\{ \mathbf{K}_T^E + \Lambda^C \left[ \mathbf{K}_1(\mathbf{U}_0^E) + \mathbf{K}_2(\mathbf{U}^E; \mathbf{U}_0^E) \right] \right\} \Phi^C = 0 \quad (4)$$

$$\Lambda^C = (\lambda^C - \lambda^E)$$

where the superscript C stands for a critical point,  $\mathbf{K}_T^E$  is given by equation (3) and  $\mathbf{U}_0^E$  is the vector of fundamental displacement at the equilibrium point E.

For mildly nonlinear fundamental paths bifurcations may be detected approximately by the linearized modified eigenvalue problem

$$\left[ \mathbf{K}_0 + \lambda^C \mathbf{K}_1(\mathbf{U}_0) \right] \Phi^C = 0 \quad (5)$$

which although referred to the path tangent at the point  $(\mathbf{U}_0, \lambda) = (\mathbf{0}, 0)$ , takes into account pre-critical rotations.

For quasi-linear fundamental paths critical points may be detected by the classical eigenvalue problem, constructed with the geometric stiffness matrix  $\mathbf{K}_G$

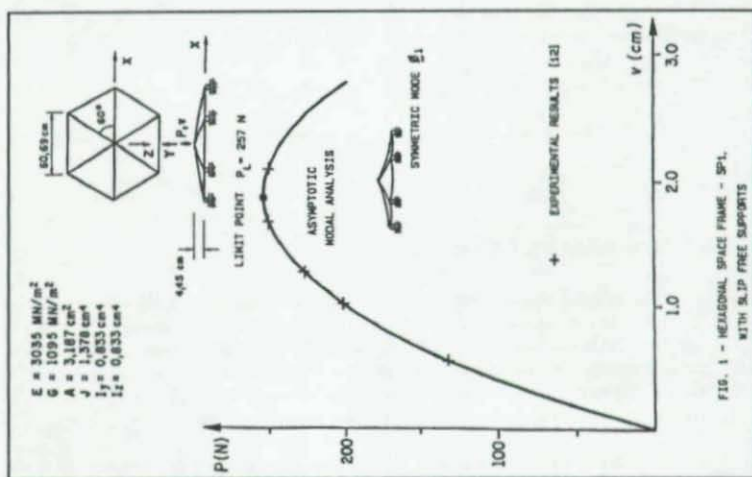
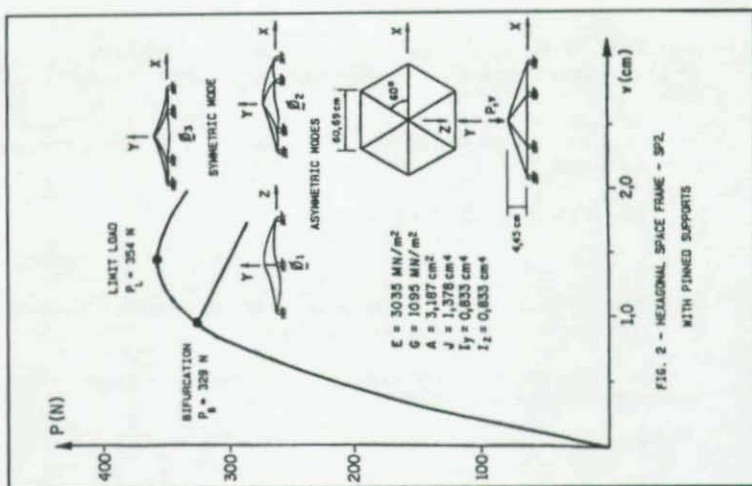
$$\left[ \mathbf{K}_0 + \lambda^C \mathbf{K}_G \right] \Phi^C = 0 \quad (6)$$

which gives upper-bound estimates for the bifurcation loads  $\lambda^C$  in the associated critical modes  $\Phi^C$ .

### 3. BENCHMARK EXAMPLE

Numerical examples of classical problems of elastic stability of space frames have been used [2, 3] both to compare with past solutions and experiments and to demonstrate that the proposed approach can detect both limit and bifurcation loads, trace the nonlinear fundamental and post-critical responses and estimate the corresponding imperfection sensitivity. Herein, we recall one of these examples and reconsider it with minor modifications in order to bring together new and past results and discuss the changes in overall buckling behavior and stability.

Figures 1, 2 and 3 show, respectively, three distinct behaviors of a simple hexagonal space frame subjected to a vertical load applied to its top joint. All structural joints are of rigid type and the space frame was discretized by using 72 elements, six for each member whose characteristics are shown inset these figures.



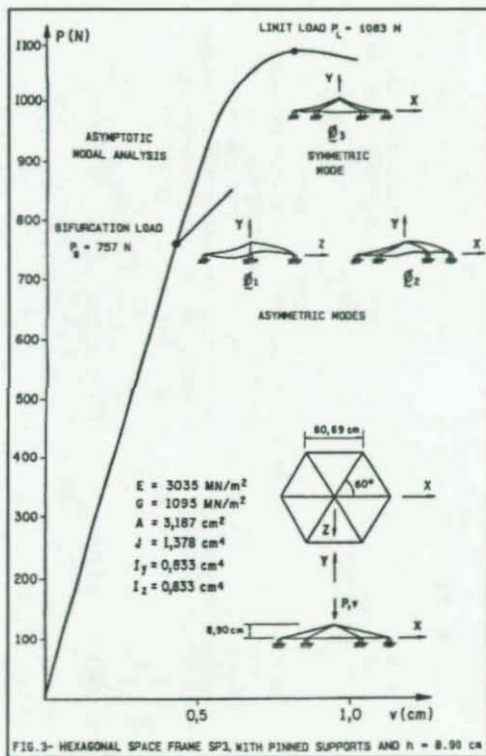


Table 1 - Critical Loads and Modes for Space Frame SP1

Approach	Critical Load $P_{CR}$ (N)	Critical Mode
Classical, eqn (6)	428	} fictitious bifurcation Asymmetric
Modified, eqn (5)	325	
Up-dated, eqn (4)	275	} limit point Symmetric
Asymptotic Modal, eqn (3)	257	

Table 2 - Critical Loads and Modes for Space Frame SP2

Approach	Bifurcation Load, $P_B$ (N) in Asymmetric Modes	Limit Load, $P_L$ (N) in Symmetric Modes
Classical, eqn (6)	428	549
Modified, eqn (5)	373	501
Up-dated, eqn (4)	337	396
Asymptotic Modal, eqn (3)	329	354

Table 3 - Critical Loads and Modes for Space Frame SP3

Approach	Bifurcation Load, $P_B$ (N) in Asymmetric Modes	Limit Load, $P_L$ (N) in Symmetric Modes
Classical, eqn (6)	802	1223
Modified, eqn (5)	772	1169
Up-dated, eqn (4)	763	1083
Asymptotic Modal, eqn (3)	757	1083

### Space Frame SP1

In figure 1 the computed nonlinear response of the space frame SP1 with slip free supports is compared with the experimental response reported in [4,5]. In this case the space frame resists the load by combined extensional and bending forces and displays a strong nonlinear response dominated by a radially symmetric mode. Its behavior is characterized by an elastic limit point instability occurring at the load level equal to 257.0 N, which is very close to the experimental buckling load. As expected for this type of behavior, the existing initial geometric imperfections in the experimental model did not play any important role in the nonlinear response. Furthermore no bifurcation loads occurring prior to the limit load were detected by the present analysis. Table 1 presents the numerical results obtained for the example SP1 of figure 1 by using different approaches as given by equations (3-6). What can be readily noted from this table is that both classical and modified linearized eigenvalue approaches give highly non-conservative results for the critical load and indicate misleading asymmetric critical modes which would be associated with non-existing bifurcations. Alternatively, the up-dated linearized eigenvalue approach yielded, with lower computational effort than the asymptotic modal approach, a critical load in the same symmetric mode associated with the limit point instability, which is very close to both the experimental buckling load and the limit load predicted by the asymptotic modal approach, being only 7% higher than the latter.

### Space Frame SP2

Figure 2 shows the moderate nonlinear fundamental response and the initial post-bifurcation path displayed by the same hexagonal space frame when its supports are fully restrained against translation. In this case the shallow space frame resists the applied load predominantly by extensional forces in its members and therefore is liable to lose its stability at a bifurcation point which occurs at a load level  $P_B = 329.0$  N. This unstable bifurcation in any one of the critical modes  $\Phi_1$  or  $\Phi_2$  illustrated in figure 2 occurs prior to the unstable limit point at a load level  $P_L$  close to 490.0 N, associated with the radially symmetric critical mode  $\Phi_3$ . Table 2 presents the numerical results for critical loads and modes of the space frame SP2 obtained from different approach, as given by equations (3-6). What can be noted once more with these results is that both the classical and modified linearized eigenvalue approaches give non-conservative results for bifurcation and limits loads as compared to those computed by the asymptotic modal approach. It is important to note here that the classical approach yields sometimes misleading results: it yields the same value for critical loads associated with an asymmetric mode for both SP2 and SP1 (see Tables 1 and 2) despite their distinct support conditions. The second thing that can be noted from the results in Table 2 is that the up-dated linearized eigenvalue approach yields critical loads that are close upper bounds of bifurcation and limit loads predicted by the asymptotic approach, being, respectively 2.5% and 12% higher than those given by the latter approach. It is also worth noting that SP2 has a somewhat sharper limit point than SP1, and that is why a slightly larger difference between up-dated and asymptotic limit loads is found for SP2 as compared to SP1.

### Space Frame SP3

Figure 3 shows the quasi-linear fundamental response and the initial post-bifurcation path displayed by the hexagonal space frame with the modification that the rise is now twice higher than in SP2. This modification allowed the structure to resist the applied load almost entirely by



extensional force in its upper members up to load levels above the bifurcation load,  $P_B = 757.0$  N. This bifurcation in any one of the asymmetric modes  $\Phi_1$  or  $\Phi_2$  seems to derive its stability from torsional and bending forces in the lower horizontal members, which is driven by larger initial post-bifurcation rotations of the rigid structural joints. A limit point instability in a radially symmetric mode is reached at load level  $P_L = 1083.0$  N, much higher than for SP2. Table 3 presents the critical loads and modes obtained for SP3 from different approaches. Now, because of the quasi-linear or quasi-extensional fundamental behavior of the space frame all the critical loads obtained with classical, modified an up-dated eigenvalue approaches are close upper bounds of the bifurcation and limit loads predicted by the asymptotic modal approach. One case exception is made for the classical approach as none of the three first required eigenvalues corresponded to a limit point associated with a symmetric mode. The ratios between these critical loads to the asymptotic modal predictions are now 0.8% to 0.6% for bifurcation and 8% to 13% for limits points; the latter occurring along a strongly nonlinear final patch response.

### Summary of Results

The results shown in figures 1-3 and Tables 1-3 for the analyzed hexagonal space frame may be summarized by the following assertions:

- critical loads given by the classical eigenvalue approach are in general too non-conservative and sometimes misleading as far as critical modes are concerned. Bifurcation predictions may be reasonable only when pre-critical responses are almost purely extensional.
- by taking into account small pre-critical rotations the modified eigenvalue approach can lead to close upper bounds of bifurcation loads, whenever the fundamental responses are quasi-linear or quasi-extensional. Limit loads are otherwise badly approached.
- the up-dated eigenvalues are in general close upper bounds of bifurcation and limit loads predicted by the asymptotic modal approach.
- this latter approach has the further advantage of tracing the fundamental and initial post-critical (bifurcation or limit) paths, making it possible to investigate the degrees of nonlinearity and imperfection sensitivity of the structure.

### 4. ANALYSIS OF A LATTICE DOME

To demonstrate the potentiality of the asymptotic modal approach, application is made to stability analysis of a hemispherical lattice dome (Schwedler dome) illustrated in figure 4. This dome is the same reported in reference [6] with the modification that all structural joints are now considered of a rigid type. The dome was discretized by using 264 space frame elements and all joints lie on the spherical surface, and all base nodes are assumed to be fully restrained against translation. The physical and cross section geometric characteristics are the same for all members, and although this may not be realistic for an actual dome it is maintained herein so as to compare present and past results, respectively for space frame and space truss modeling.

A typical design uniform vertical pressure load  $p_D = 2,900$  N/m<sup>2</sup> is applied to the dome surface and the resulting nodal forces along each latitudinal ring together with the top nodal force are presented in Table 4.



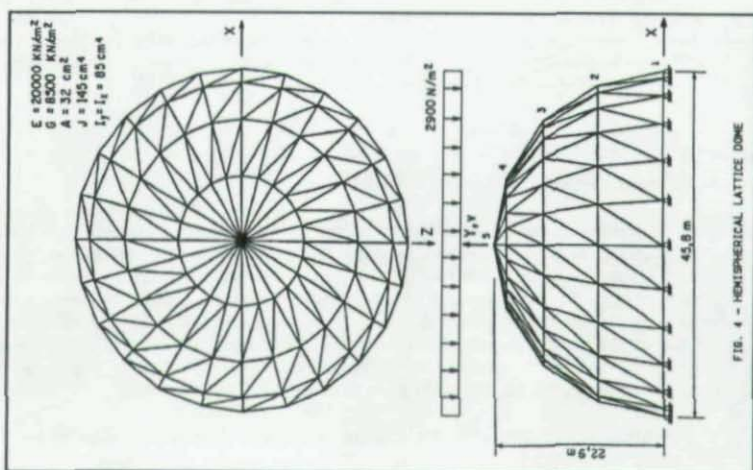


FIG. 4 - HEMISPHERICAL LATTICE DOME

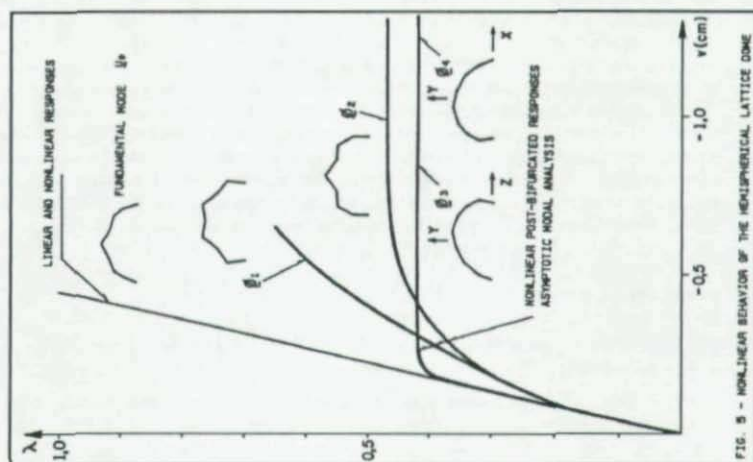


FIG. 5 - NONLINEAR BEHAVIOR OF THE HEMISPHERICAL LATTICE DOME

Table 4 - Joint Loads due to uniform vertical pressure,  $p_D$ 

Ring	2	3	4	5 (top)
Load (kN)	137.46	105.20	56.92	174.13

Figure 4 shows the structural responses obtained from past [12] and present analyses and Table 5 presents the critical load parameters  $\lambda = p/p_D$  and critical modes obtained from distinct approaches as given by equations (3-6); for the scalar control parameter  $\lambda = 1.0$ ,  $p = 2,900 \text{ N/m}^2$ . The first thing that deserves attention in figure 4 is the extensional behavior of the fundamental path of this hemispherical dome subjected to the uniform vertical pressure. The linear and nonlinear fundamental responses yielded by either truss or frame modeling are practically the same, and due to the particular arrangement of diagonals the dome twists in a counter-clockwise direction under uniform vertical pressure. A complete account of member stresses and joint displacements is given in reference [6] for the space truss model, and do not differ appreciably from the present results for the space frame model. With regard to the nonlinear results it is worthwhile mentioning that under this symmetric loading the diagonals suffer minor stresses and the latitudinal members in ring 2 closest to the base are set in tension. This latter result could be obviously expected from the almost upright arrangement of the lowest meridional and diagonal members.

The second and most important thing that can be readily noted in figure 4 is the post-bifurcation behavior displayed by this dome, which can only be found when a nonlinear asymptotic modal analysis is performed. As it can be observed from the results presented in Table 5, any one of the eigenvalue approaches gives a cluster of bifurcation loads which do not differ appreciably from one approach to any other. The main differences lie on the shapes of these bifurcation modes.

Table 5 - Bifurcation Load Parameters  $\lambda$  for Hemispherical Dome

Eigenvalue Approach	$\lambda_B = p_B/p_D$	Bifurcation Mode, $\Phi$
Classical, eqn (6) and Modified, eqn (5)	$\lambda_1 = 0.2002$ $\lambda_2 = \lambda_3 = 0.2036$ $\lambda_4 = 0.2151$	$\Phi_1$ , Twisting, clockwise $\Phi_2, \Phi_3$ , Asymmetric $\Phi_4$ , Asymmetric
Up-dated, eqn (4)	$\lambda_1 = 0.1974$ $\lambda_2 = 0.2006$ $\lambda_3 = \lambda_4 = 0.2030$	$\Phi_1$ , Twisting, counter-clockwise $\Phi_2$ , Twisting, clockwise $\Phi_3, \Phi_4$ , Asymmetric

The post-bifurcation responses associated with each of these modes demonstrate that this dome may display stable and near unstable behaviors and multiple asymmetric bifurcations. The stable path occurs for a twisting counter clockwise mode  $\Phi_1$ . But the most relevant results for this dome are the near unstable bifurcation paths in the twisting clockwise mode  $\Phi_2$  and in the asymmetric sway-type mode  $\Phi_3$  or  $\Phi_4$ , reaching, respectively, load levels  $p_L = 1,363 \text{ N/m}^2$  ( $\lambda = 0.47$ ) and  $p_N = 1,218 \text{ N/m}^2$  ( $\lambda = 0.42$ ) associated with limit point and quasi-neutral equilibriums. The near unstable equilibrium path may be explained by the role played by the tensioned

latitudinal members in ring 2, which allowed the radial expansion of joints and led to a strong nonlinear behavior similar to that occurred for the hexagonal space frame of figure 1. The quasi-neutral equilibrium path may otherwise be explained simply by the combined effect of the tensioned ring 2 and the upright arrangement of the lowest meridional and diagonal members, which led to a sway-type frame behavior.

## 5. FINAL COMMENTS ON OVERALL BEHAVIOR AND STABILITY PREDICTIONS.

From the present and previously reported analyses [2,7,8], and many other results reported elsewhere as cited in these references, it can be stated that the structural behavior and overall stability of lattice domes are very much dependent on the following factors:

- geometric rise to span ratios.
- spatial distribution of loads applied to the nodes.
- type of members (pipes, tubulars or flanges) and their arrangements, degree of fixity and rotational stiffness of joints.
- dome support conditions and extensional stiffness of latitudinal circles (rings).
- number of elements and nodes, whenever a lattice dome is intended to close approximate a shell continuum surface.
- and of course initial geometric and other imperfections.

Prediction of their behavior and determination of buckling loads are on the other hand very much dependent on:

- the adopted instability approach,
- structural and loading modelling
- and numerical algorithms used for nonlinear analyses.

A lattice dome should not be modelled as a space truss because the resulting nonlinear behavior and load carrying capacity may be far apart from a space frame behavior [7]. In general the overall buckling of a lattice dome can be said to be resisted by a combination of extensional and bending resistance within the members and joints, as radial deformations of nodes may develop over the entire dome surface. Even if it is idealized as geometrically perfect, bending resistance may be arrested by initial pre-buckling rotations at joints, induced by concentrated forces applied directly to these joints. That is why a classical eigenvalue analysis - based on a linear extensional pre-critical path emerging from the unloaded state - provides non-conservative estimates of buckling loads. Depending on the geometric rise to span ratio and on the number of members, joints and also on the number of nodes used in the structural modelling, this classical linear eigenvalue analysis may provide critical loads which sometimes are overwhelmingly non-conservative buckling estimates, or even worse misleading fictitious bifurcation loads. This is particularly true for a single layer shallow lattice dome having a small number of members and subjected to vertical loads concentrated around its apex, for which a highly nonlinear behavior is expected. Conversely, for lattice domes with larger rise to span ratios, or otherwise having many members and joints on to which gravity and other vertical loads are applied, an extensional pre-buckling behavior is expected. In these cases the classical eigenvalue analysis may provide upper bounds for bifurcation and sharp limit loads, although no distinction can be made between the two and stability of associated critical and post-critical states remain unknown. On the other hand lattice domes subjected to unsymmetrical (e.g. snow or wind) loads deserve special attention as

their behavior are much affected by this sort of load imperfection and should be always investigated by a nonlinear analysis. But it is mainly in cases of ever existing gravity symmetrical loads that the alternative of a full nonlinear numerical analysis suffers from serious drawback. Conventional nonlinear elastic analysis associated with commonly-used incremental/iterative techniques fails to detect bifurcation branching and therefore it is not really adequate for reliable nonlinear instability analysis of structures. Nonlinear analysis of the geometrically imperfect structure is another usual technique that also suffers from a serious drawback as some insight is always required into both the nonlinear behavior of the perfect system and the relevant imperfection modes. For these reasons the seemingly potential advantages of a combined classical eigenvalue and full conventional nonlinear analyses can in fact constitute pitfalls for one designing a lattice dome against instabilities.

## 6. CONCLUSIONS

It has been demonstrated that buckling of lattice domes and space frames may be properly analyzed by using a nonlinear asymptotic approach, which can overcome the main deficiencies of usual methods for buckling analysis. The approach can detect both limit and bifurcation loads, trace nonlinear fundamental perfect or slightly imperfect responses and initial post-critical paths and therefore estimate imperfection sensitivity. As such it can assist the designer to interpret the buckling behavior and load carrying capacity of these structures without resorting to shell analogy and related ultra conservative knockdown factors. In regard to this latter aspect the proposed approach can, in one step, also assist the designer in any comprehensive and reliable simulation of large imperfection-large displacement nonlinear response analysis.

## 7. REFERENCES

- 1 - Batista, R.C., *An asymptotic modal analysis of nonlinear structural systems*. Proc. 1988 Annual Tech. Session, SSRC, Minneapolis, MN, 1988.
- 2 - Batista, R.C.; Antonini, R.C. and Alves R.V., *An asymptotic modal approach to nonlinear structural elastic instability*. Computer & Structures, Vol. 38, No. 4, pp. 475-484, 1991.
- 3 - Alves, R.V., *Stability analysis of space frames by an asymptotic modal approach* (in Portuguese). M.Sc. thesis, COPPE / Federal University, Rio de Janeiro, 1989.
- 4 - Griggs, H.P., *Experimental study of instability in elements of shallow space frames*. Research Report, Dept. of Civil Engng., MIT, Cambridge, Mass., Sept., 1966.
- 5 - Connor, J.J.; Logcher, R.D. and Chan S.-C., *Nonlinear analysis of elastic framed structures*. J. of the Structural Division, ASCE, Vol. 94, No. ST6, pp 1525-1547, June, 1968.
- 6 - Jagannathan, D.S.; Epstein, H.I. and Christiano, P., *Nonlinear analysis of reticulated space truss*. J. of the Structural Division, ASCE, Vol. 101, No. ST12, pp. 2641-2658, Dec., 1975.
- 7 - Morris, N.F., *Computer computation of lattice dome knockdown factors*. Proc. 1991 Annual Tech. Session, SSRC, Chicago, Ill., 1991.
- 8 - Kashami, M. and Croll, J.G.A., *Non-linear buckling response of spherical space domes*. 30 th anniversary of IASS, Madrid, Sept., 1989.







INTERACTION STABILITY CRITERIA IN COMBINED STATES OF STRESSES  
FOR METAL PLATES AND SHELLS

Zbigniew K. MENDERA  
Professor of Civil Engineering  
Cracow University of Technology  
Cracow, Poland

ABSTRACT

Plates and shells are often used in civil and mechanical engineering as structural elements. In metal structures there are thin-walled elements, then the definition of their stability criteria is one of the essential safety condition.

The stability criteria of plates and shells in simple states of stress have already been worked out and confirmed in experiments and codified. However, in combined states of stress it is necessary to have interaction formulae as hypotheses which should next be tested on the basis of running research and further experiments. The formulae existing so far are not satisfactory and rather conservative.

In this paper suggestions of general interaction formulae in combined states of stress and with various forms of instability of plates and cylindrical shells are presented in non-dimensional limit states conditions, which will be useful in structure design standards.

The partial factors of safety are defined on the design values level in the sense of limit states format. Comparisons between the DIN 18800 (1990) approach and new proposals are presented.

LOCAL STABILITY OF PLATES IN SIMPLE AND COMBINED STRESSES

The stability condition of plate in simple state of stress can be written in the form:

- for longitudinal compression

$$\frac{\sigma_x}{\phi_x f_{lx}} \leq 1 \quad (1)$$

- for transverse compression

$$\frac{\sigma_y}{\phi_y f_{ly}} \leq 1, \quad (2)$$

- for shear

$$\left( \frac{\tau_{xy} \sqrt{3}}{\phi_{xy} f_{lxy}} \right) \leq 1, \quad (3)$$

where:

$\sigma_x, \sigma_y, \tau_{xy}$  - design stresses of plate,

$f_d$  - design strength of steel (material),

$\varphi_i$  - buckling factor of plate,  $i = x, y, s$ .

Buckling factor of plate can be formulated in the general form (Mendera, 1991):

$$\varphi_i = (1 + \Lambda_i^{2/u})^{-u}, \quad (4)$$

where:

$$\Lambda_i = \frac{\lambda}{0.95\sqrt{k_i}} \left(\frac{f_d}{E}\right)^{0.5} - \text{slenderness parameter of plate,}$$

$$\lambda = \frac{b}{t} - \text{the plate width-to-thickness ratio,}$$

$k_i$  - non-dimensional plate buckling coefficient (Bleich, 1952; Brockenbrough and Johnston, 1968),

$u = 0.5$  - index of imperfections (curve a).

In combined loads of plate the interaction equations have been formulated only for interactions of some states of stress (Brzoska, 1961; Galambos, 1988; SSRC, 1991):

- uniaxial compression and shear

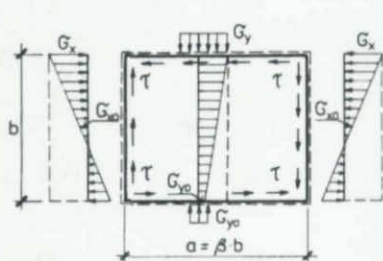
$$\frac{\sigma_x}{\varphi_x f_d} + \left(\frac{\tau_{xy} \sqrt{3}}{\varphi_s f_d}\right)^2 = 1, \quad (5)$$

- bending and shear

$$\left(\frac{\sigma_{xb}}{\varphi_{xb} f_d}\right)^2 + \left(\frac{\tau_{xy} \sqrt{3}}{\varphi_s f_d}\right)^2 = 1, \quad (6)$$

- compression, bending and shear

$$\frac{\sigma_x}{\varphi_x f_d} + \left(\frac{\sigma_{xb}}{\varphi_{xb} f_d}\right)^2 + \left(\frac{\tau_{xy} \sqrt{3}}{\varphi_s f_d}\right)^2 = 1, \quad (7)$$



$$\lambda = \frac{b}{t}, \quad \Lambda_i = \frac{\lambda}{0.95\sqrt{k_i}} \left(\frac{f_d}{E}\right)^{1/2}$$

$$k_i = f(G, \beta, \text{b. cond.})$$

$$\varphi = (1 + \Lambda^4)^{-0.5}$$

$$\alpha_x = \frac{G_{xo}}{G_x}, \quad \alpha_y = \frac{G_{yo}}{G_y}$$

$i / x, y, s$

Fig.1. Combined stresses of flat plate

- biaxial compression (uniform)

$$\frac{\sigma_x}{\varphi_x f_{0x}} + \frac{\sigma_y}{\varphi_y f_{0y}} = 1, \quad (8)$$

but it is pointed-out, that these formulae are conservative.

Murzewski (1973) proposed the plate stability criterion under bending and local pressure on one edge of the plate.

In this paper an interaction stability criterion in the combined states of stress is proposed and discussed. The criterion includes previous cases and satisfies two postulates:

1° - the criterion leads to the Huber-Mises-Hencky yield condition (Huber, 1904) in the pure plastic states (for small slenderness  $\lambda$ , i.e. for  $\varphi_i$  leading to 1):

$$\left(\frac{\sigma_x}{f_x}\right)^2 - \frac{\sigma_x \sigma_y}{f_x^2} + \left(\frac{\sigma_y}{f_y}\right)^2 + \left(\frac{\tau_{xy} \sqrt{3}}{f_s}\right)^2 = 1, \quad (9)$$

2° - the criterion leads to the elastic stability condition in the pure elastic state (for large slenderness  $\lambda$ , i.e. for  $\varphi_i$  leading to 0):

- under biaxial uniform compression and shear

$$\frac{\sigma_x}{\varphi_x f_{0x}} + \frac{\sigma_y}{\varphi_y f_{0y}} + \left(\frac{\tau_{xy} \sqrt{3}}{\varphi_s f_{0s}}\right)^2 = 1, \quad (10a)$$

- under biaxial nonuniform compression (e.g. bending and pressure only on one edge of plate) and shear

$$\left(\frac{\sigma_x}{\varphi_x f_x}\right)^2 + 2 \frac{\sigma_x}{\varphi_x f_x} \frac{\sigma_y}{\varphi_y f_y} + \left(\frac{\sigma_y}{\varphi_y f_y}\right)^2 + \left(\frac{\tau_{xy} \sqrt{3}}{\varphi_s f_s}\right)^2 = 1, \quad (10b)$$

Such a criterion can be formulated as follows:

- lower estimate (conservative)

$$\sqrt{\left(\frac{\sigma_x}{\varphi_x f_x}\right)^2 + C \frac{\sigma_x}{\varphi_x f_x} \frac{\sigma_y}{\varphi_y f_y} + \left(\frac{\sigma_y}{\varphi_y f_y}\right)^2 + \left(\frac{\tau_{xy} \sqrt{3}}{\varphi_s f_s}\right)^2} = 1, \quad (11a)$$

- realistic estimate (but based on incomplete tests)

$$\left(\frac{\sigma_x}{\varphi_x f_x}\right)^2 + C \frac{\sigma_x}{\varphi_x f_x} \frac{\sigma_y}{\varphi_y f_y} + \left(\frac{\sigma_y}{\varphi_y f_y}\right)^2 + \left(\frac{\tau_{xy} \sqrt{3}}{\varphi_s f_s}\right)^2 = 1, \quad (11b)$$

in which parameter  $C = 2-3\varphi^n$ , and  $\varphi = \min(\varphi_x, \varphi_y)$ ,

$n$  - exponent, which takes into considerations the distribution

of stresses  $\sigma_x, \sigma_y$  on the plate height, specified as follows:

$n = 4$  - for biaxial uniform compression,

$n = 3$  - for longitudinal compression and transverse pressure only on one edge of plate,

$n = 2$  - for bending and transverse pressure only on one edge of plate.

In general:  $n = 2 + \chi_x + \chi_y$ ,

where  $\chi_x = \frac{\sigma_{ax}}{\sigma_x}$  and  $\chi_y = \frac{\sigma_{ay}}{\sigma_y}$  (see Fig.1).

The graphical interpretation of stability criterion (11) (for  $\tau_{xy} = 0$ , Eq.(11a) and Eq.(11b) being identical) is shown

in Fig.2, in the system of co-ordinates  $(\frac{\sigma_x}{f_a}, \frac{\sigma_y}{f_a} \frac{\varphi_x}{\varphi_y})$ , after transformation of Eq.(11b) to the form:

$$\left(\frac{\sigma_x}{f_a}\right)^2 + C \frac{\sigma_x}{f_a} \frac{\sigma_y}{f_a} \frac{\varphi_x}{\varphi_y} + \left(\frac{\sigma_y}{f_a} \frac{\varphi_x}{\varphi_y}\right)^2 = \varphi_x^2, \quad (11c)$$

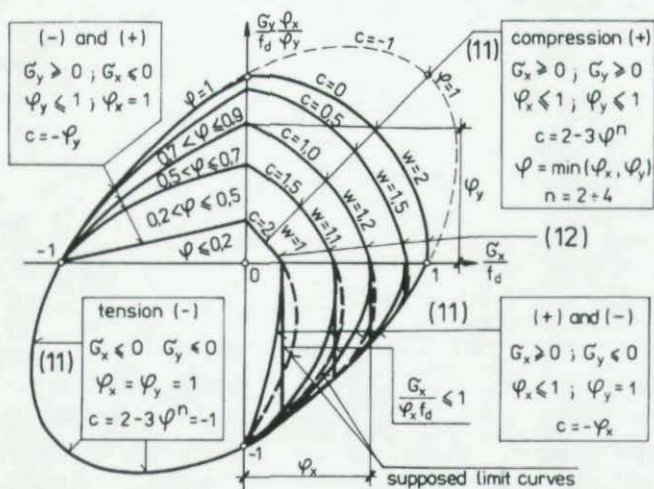


Fig.2. Interaction curves for buckling under combined states of stress (for  $\sigma_x = \sigma_1$ ,  $\sigma_y = \sigma_2$ ,  $\tau_{xy} = 0$ )

As is known, the yield condition depends only on state of stress and yield strength of the material, therefore it is a local problem, while the stability condition of an element (structure) is an integral problem and depends not only on state of stress in the point and mechanical properties of material but also on stresses distribution in the element, geometry of the element and boundary conditions - through buckling factors  $\varphi_x$ ,

$\varphi_y$ ,  $\varphi_x$  and exponent  $n$ , which regulates the interaction character of Eq.(11).

The proposal of defining the interaction stability criterion according to Eq.(11) is a hypothesis based, however, on rational postulates 1° and 2° and non discordant with partial formulae Eq.(5) to Eq.(8).

From the point of view of engineering applications, the most important are states of biaxial compression and shear, therefore they will be discussed in detail.

In Fig.3 limit curves after Eq.(11) have been shown (with  $\tau_{xy}=0$ ) depending on parameter  $C$  (solid lines). It can be seen that when buckling factor  $\varphi$  leading to 0, the limit line leads to straight line, while when  $\varphi$  leads to 1, the limit line leads to Huber-Mises-Hencky ellipsis.

The problem becomes slightly complicated when besides normal stresses  $\sigma_x$ ,  $\sigma_y$  there are shear stresses  $\tau_{xy}$ , because it would be necessary to interpolate the limit curve from parabolic Eq.(11a) and elliptic Eq.(11b). After a brief analysis, however, it turned out that an interpolation formula is useful and simple in the form:

$$\left(\frac{\sigma_x}{\varphi_x f_d}\right)^w + \left(\frac{\sigma_y}{\varphi_y f_d}\right)^w + \left(\frac{\tau_{xy} \sqrt{3}}{\varphi_s f_d}\right)^2 = 1, \quad (12)$$

where:  $w \equiv 1 + \varphi^n$  and  $\varphi = \min(\varphi_x, \varphi_y)$  which well matches Eq.(11a) and Eq.(11b), when  $C \geq -0.5$ , i.e. when  $\varphi^n \leq 0.833$ , which has been illustrated by broken lines in Fig.3.

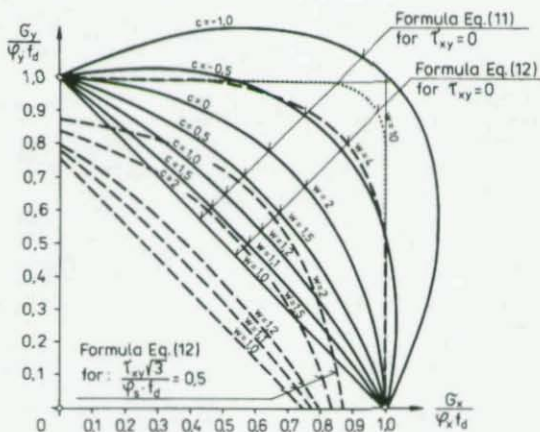


Fig.3. Limit curves of stability according to Eqs (11) and (12)



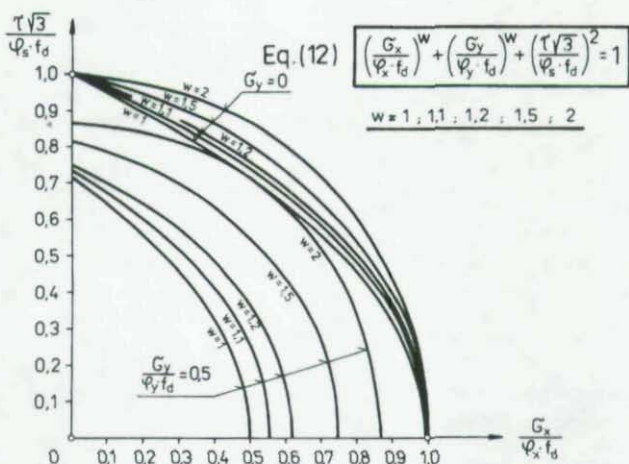


Fig.4. Interaction buckling curves under shear and compression

Limit curves after Eq.(12) have been shown in Fig.4, for buckling under shear and biaxial compression.

The Polish code (PN-90/B-03200, 1990) recommends checking web stability in combined state of stress after a formula which can be written in the stress form as follows:

$$\left(\frac{\sigma_x}{\phi_x f_d} + \frac{\sigma_{xb}}{\phi_{xb} f_d} + \frac{\sigma_y}{\phi_y f_d}\right)^2 - 3\phi_p \left(\frac{\sigma_x}{\phi_x f_d} + \frac{\sigma_{xb}}{\phi_{xb} f_d}\right) \frac{\sigma_y}{\phi_y f_d} + \left(\frac{\tau_{xy} \sqrt{3}}{\phi_s f_d}\right)^2 = 1, \quad (13)$$

where indices xb denote bending and  $\phi_p$  is an buckling factor under unaxial compression of plate. This formula seems too optimistic, particularly when compared with very cautious formula of a new German code (DIN 18800, 1990):

$$\left(\frac{\sigma_x}{\phi_x f_d}\right)^{e_1} - V \frac{|\sigma_x \sigma_y|}{\phi_x f_d \phi_y f_d} + \left(\frac{\sigma_y}{\phi_y f_d}\right)^{e_2} + \left(\frac{\tau_{xy} \sqrt{3}}{\phi_s f_d}\right)^{e_3} = 1, \quad (14)$$

where:  $e_1 = 1 + \phi_x^4$ ,  $e_2 = 1 + \phi_y^4$ ,  $e_3 = 1 + \phi_x \phi_y \phi_s^8$ , and the value of V under biaxial compression  $\sigma_x, \sigma_y$  is  $V = (\phi_x \phi_y)^8$ , but in the other

cases it is  $V = \frac{\sigma_x \sigma_y}{|\sigma_x \sigma_y|}$ .

As mentioned before, formula (14) seems to cautions, especially in case of the effect of shear stresses, and when one of the normal stresses is tension, it gives even restricting

estimates, which do not result from either theoretical considerations or experimental data.

The comparison between formulae (11), (13) and (14) is shown in Fig.5 and Fig.6.

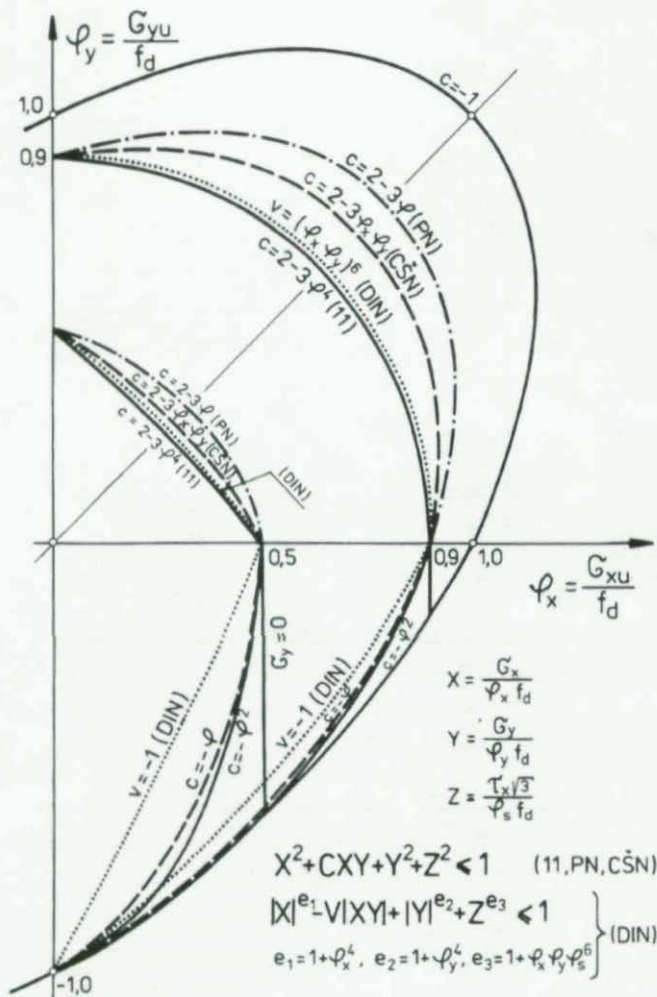
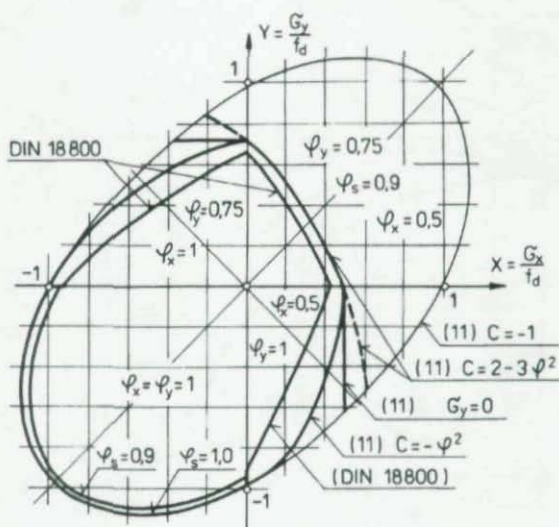


Fig.5. A comparison between Eqs.(11), (13) and (14).

Design example:

$$\varphi_x = 0.5 \quad \varphi_y = 0.75 \quad \varphi_s = 0.9 \quad Z = \frac{\tau_{xy}}{f_d \sqrt{3}} = 0.2$$



$$\left( \frac{G_x}{\varphi_x f_d} \right)^2 + C \frac{G_x}{\varphi_x f_d} \frac{G_y}{\varphi_y f_d} + \left( \frac{G_y}{\varphi_y f_d} \right)^2 + \left( \frac{\tau_{xy} \sqrt{3}}{\varphi_s f_d} \right)^2 < 1 \quad (11)$$

$$C = 2 - 3\varphi^2 \rightarrow (+\pm), \quad \varphi = \min(\varphi_x, \varphi_y);$$

$$C = -\varphi^2 \rightarrow (+-),$$

$$\left( \frac{|G_x|}{\varphi_x f_d} \right)^{W_x} - V \frac{|G_x G_y|}{\varphi_x f_d \varphi_y f_d} + \left( \frac{|G_y|}{\varphi_y f_d} \right)^{W_y} + \left( \frac{\tau_{xy} \sqrt{3}}{\varphi_s f_d} \right)^{W_\tau} < 1 \quad (14)$$

$$W_x = 1 + \varphi_x^4; \quad W_y = 1 + \varphi_y^4; \quad W_\tau = 1 + \varphi_x \cdot \varphi_y \cdot \varphi_s^6$$

$$V = (\varphi_x \cdot \varphi_y)^6 \rightarrow (++)$$

$$V = \frac{G_x G_y}{|G_x G_y|} \rightarrow (--)$$

Fig. 6. A design example and comparison between formulae of Eqs. (11) and (14).

STABILITY OF CYLINDRICAL SHELLS OF MEDIUM LENGTH IN SIMPLE AND COMBINED STATES OF STRESS

In Fig.7 a cylindrical shell has been shown schematically together with explanations and typical loading.

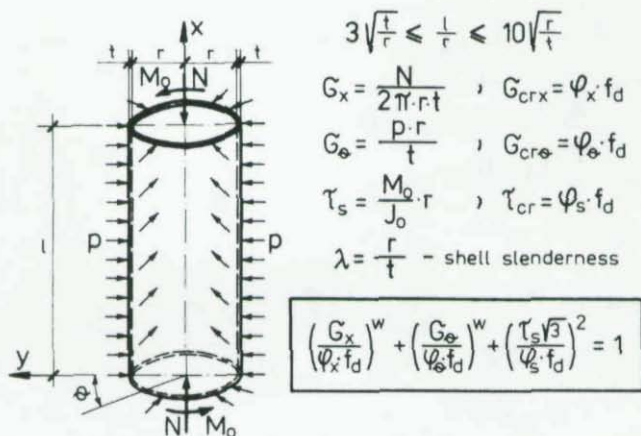


Fig.7. Combined state of loads of cylindrical shell

Longitudinal Compression

Stability condition after (Mendera, 1986):

$$\frac{\sigma_x}{\varphi_x \cdot f_u} \leq 1, \quad (15)$$

where:

$$\varphi_x = (1 + \Lambda_x^{1/2u})^{-u} \quad - \text{buckling factor,}$$

$$\Lambda_x = \frac{\lambda}{1.59} \left(\frac{f_u}{E}\right)^{2/3} \quad - \text{slenderness parameter,}$$

$$\lambda = \frac{r}{t} \quad - \text{slenderness of shell (the shell radius-to-thickness ratio),}$$

$$u = 0.5 \text{ to } 1.0 \quad - \text{parameter of imperfections.}$$

External Pressure

Stability condition after (Grigoliuk and Kabanov, 1969; DAST 013, 1980; SNIP II-23; 1981; Mendera, 1991):

$$\frac{\sigma_0}{\varphi_0 f_{01}} \leq 1, \quad (16)$$

where:

$$\varphi_0 = (1 + \Lambda_0^2)^{-0.5} - \text{buckling factor,}$$

$$\Lambda_0 = \frac{\lambda}{0.67 \left(\frac{r}{1}\right)^{2/5}} \left(\frac{f_{01}}{E}\right)^{2/3} - \text{slenderness parameter,}$$

$$\lambda = \frac{r}{t} - \text{slenderness of shell.}$$

### Torsion

Stability condition after (Grigoliuk and Kabanov, 1969; DAST 013, 1980; SNIP II-23; 1981; Mendera, 1991):

$$\frac{\tau_s \sqrt{3}}{\varphi_s f_{s1}} \leq 1, \quad (17)$$

where:

$$\varphi_s = (1 + \Lambda_s^2)^{-0.5} - \text{buckling factor,}$$

$$\Lambda_s = \frac{\lambda}{0.89 \left(\frac{r}{1}\right)^{2/3}} \left(\frac{f_{s1}}{E}\right)^{2/3} - \text{slenderness parameter,}$$

$$\lambda = \frac{r}{t} - \text{slenderness of shell.}$$

### Interaction Between Longitudinal Compression, External Pressure and Torsion of Shell

As an interaction stability criterion, Eq.(11b) has been proposed:

$$\left(\frac{\sigma_x}{\varphi_x f_{x1}}\right)^2 + C \frac{\sigma_x}{\varphi_x f_{x1}} \frac{\sigma_0}{\varphi_0 f_{01}} + \left(\frac{\sigma_0}{\varphi_0 f_{01}}\right)^2 + \left(\frac{\tau_s \sqrt{3}}{\varphi_s f_{s1}}\right)^2 = 1,$$

where:

$$C = 2 - 3\varphi^n,$$

$$\varphi = \min(\varphi_x, \varphi_0),$$

$n = 4$  - for axial compression and external pressure,

$n = 3$  - for bending and external pressure,

or Eq.(12) with modified exponent  $w$ , i.e.:

$$\left(\frac{\sigma_x}{\varphi_x f_{x1}}\right)^w + \left(\frac{\sigma_0}{\varphi_0 f_{01}}\right)^w + \left(\frac{\tau_s \sqrt{3}}{\varphi_s f_{s1}}\right)^2 = 1,$$

where:  $w = 1 + \varphi^5$ , and  $\varphi = \min(\varphi_x, \varphi_0)$ .



For standardisation purposes (design) it is proposed to evaluate exponent  $w$ , as follows:

$$w = \begin{cases} 1.0 & \text{for } \varphi \leq 0.2 \\ 1.05 & \text{for } 0.2 < \varphi \leq 0.5 \\ 1.1 & \text{for } 0.5 < \varphi \leq 0.6 \\ 1.25 & \text{for } 0.6 < \varphi \leq 0.75 \\ 1.5 & \text{for } 0.75 < \varphi \leq 0.9 \\ 2.0 & \text{for } \varphi > 0.9 \end{cases}, \varphi = \min(\varphi_x, \varphi_s).$$

In German codes (DAST 013, 1980; DIN 18800, 1990) it is recommended to adopt  $w=1.1$  or  $w=1.25$ , independent of the value of buckling factors  $\varphi_x, \varphi_s$ , which is generally a conservative approach, but with very low values of  $\varphi$ , it can be too optimistic (unsafe).

In Fig.8 the stability limit surface after Eq.(12) has been presented.

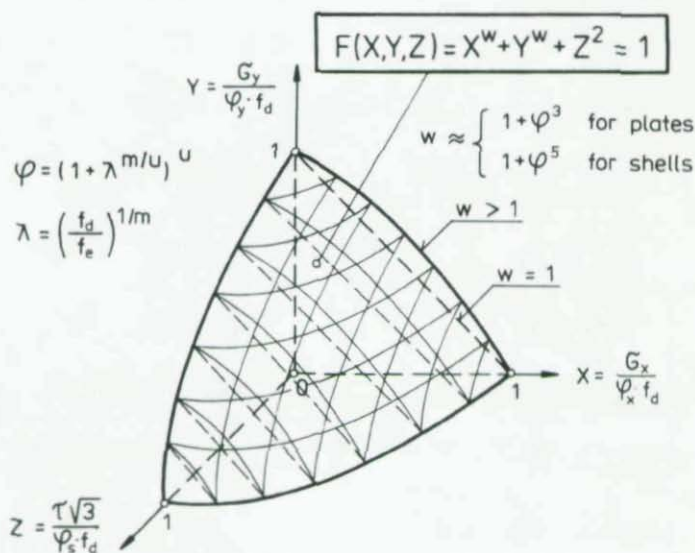


Fig.8. Limit surface of stability

## REFERENCES

- Bleich, F., 1952, Buckling Strength of Metal Structures, McGraw Hill, New York.
- Brockenbrough, R.L. and Johnson, B.G., 1968, USS Steel Design Manual, US Steel Corporation, Pittsburgh, pp.70-82.
- Brzoska, Z., 1961, Statistics and Stability of Bar and Thin-Walled Structures (In Polish), Warszawa, pp.560-576.
- DAST 013, Deutscher Ausschus für Stahlbau, 1980, Beulsich erheitnachweise für Schalen, Köln.
- DIN 18800, 1990, German Standard, Steel Structures, Design and Construction, Part 4, Berlin.
- Galambos, T.V., Editor, 1988, Guide to Stability Criteria for Metal Structures, J.Wiley and Sons, New York, pp.90-112 and 208-219.
- Grigoliuk, E.J. and Kabanov, V.V., 1969, Stability of Circular Cylindrical Shells, Mechanics of Solid Bodies, Series Mechanics, (In Russian), Itogi Nauki, Moscow.
- Huber, M.T., 1904, Specific Work of Deformation as Measure of an Effort of the Material (In Polish), Czasopismo Techniczne, No 22, Lwow, p.81.
- Mendera, Z., 1986, Interaction of Elastic and Plastic Instability in Cylindrical Shells with Imperfections, IASS Symposium: SHELLS, MEMBRANES AND SPACE FRAMES, Osaka, Ed. Heki, Elsevier, Tokyo, Vol.1, pp.17-24.
- Mendera, Z., 1991, Uniform Approach to Metal Stability Design, Journal of Constructional Steel Research, 19, 1991 Elsevier, England, pp.69-78.
- Murzewski, J., 1973, Lokal Stability Criterion Based on Unified Table of Coefficients (In Polish), Bulletin of MOSTOSPAL, Konstrukcje Metalowe, Nr 1/2, 1973, Warszawa, pp.136-148.
- PN-90/B-03200, 1990, Polish Standard, Steel Structures, Design Rules, Warszawa.
- SNIP II-23-81, 1981, Soviet Union Standard, Steel Structures, Design Rules, Moscow.
- SSRC, 1991, Stability of Metal Structures, A World View, 2nd Edition, Structural Stability Research Council, Bethlehem, PA, U.S.A.

ON THE STRUCTURAL STABILITY OF LARGE STEEL  
SPENT NUCLEAR FUEL CANISTERS

Samaan G. Ladkany\*, Ph.D., P.E., Professor of Engineering,  
Rajkumar Rajagopalan, Ph.D. Candidate

Civil Engineering Department, University of Nevada, Las Vegas  
4505, Maryland Parkway, Las Vegas, NV 89154  
(702)-895-4328 / FAX (702)-895-3936

**ABSTRACT**

Linear and non-linear stresses and buckling loads in the pintle, top head, canister shell and top plate of two high-level spent nuclear fuel canister models are evaluated under a variety of static and dynamic loading conditions resulting from normal handling. The proposed canister designs are made of 304L stainless steel, having a yield strength of 220 Mpa (32000 psi), an ultimate tensile strength of 586 Mpa (85000 psi) and a high resistance to crack initiation. The canisters are 0.0095m (0.375 in) thick, 0.7m (28 in) in diameter and 4.2m (165 in) long. Finite element analysis is used in the stress and stability analysis. Four node thin shell elements and 3-D isoparametric four node thick shell elements are used in modeling the weldment, tophead, pintle, bottom plate and the canister shell. Results obtained from the various types of analysis and the two finite element models, compare favorably within the limitation and applicability of each element type. Results are also compared with theory for some canister loading conditions when a theoretical analysis is possible. Results show that these proposed container models are not adequate to handle stresses and some local and global instabilities resulting from accidental drops, impact between canisters and sudden slippage of the crane cable, during the process of lifting and handling of the nuclear fuel containers.

**I. INTRODUCTION**

The University of Nevada, Las Vegas, is under contract to the U.S. Department of Energy [1] to study the long term storage of high level nuclear waste in geological rock formations. The commercial waste, which consists of reactor core units containing the spent fuel rods [2], is placed in long thin walled 304L stainless steel canisters, 4.2 m (15 ft) long, 0.7 m (28 inches) in diameter and 0.0095 m (3/8 inch) thick. The canisters are sealed at the plant site with welded bottom plates, 0.0508 m (2 inch) thick and a top plate varying in thickness from 0.375 inch to 2 inch. A pintle, which is a shell-type structure with variable or constant thickness, is welded to the tophead of the canister models and is used for carrying and handling the canister [3]. Two types of pintles are considered [4,5], a variable thickness pintle 0.2 m (7.88 inches) long and 0.158 m (6.255 inches) in diameter cylindrical structure welded to the center of a 2 inch thick top plate (Fig.1a), and a doubly curved ASME flanged and dished

\* Director, US-DOE Nuclear Waste Package Project, UNLV

pintle-tophead combination welded to a 3/8 inch top plate and edge of the canister (Fig.1b).

Nuclear spent fuel containers weighing 64.5 kN (14500 lb.) are placed in shipping casks, transported to a long-term storage site, removed from the casks then transported to underground storage drifts [3]. Various scenarios are being considered for the canister permanent placement in the rock, which include stacking in horizontal position along the drift or vertical position in deep boreholes or in individual placement inside vertical boreholes [6]. Since several accident scenarios may be possible during normal handling or transportation of the spent fuel, the canisters may be subjected to a variety of compressive loading conditions, in the axial and radial directions [7]. During the monitored and retrievable stage of storage which may last between 80 and several hundred years, a canister may get slightly wedged in a placement hole due to the collapsed rock around it. Under such conditions, the canister may experience non-linear radial compressive buckling with the stresses beyond yield, during an attempted remote control retrieval. Accident scenarios also include various modes of canister impact [7] with ground or other canisters at different angles of contact. Since buckling of the canister shell may occur in the yield zone of the stainless steel, this may translate into a appreciable deflection, the thin fuel rods inside may be severely damaged and may disintegrate into powderous form upon impact with the canister shell. Therefore, it is imperative to attempt an accurate determination of the various modes of canister buckling and the long term effect they may have on the integrity of the stored nuclear fuel.

## II. MATERIAL CONSIDERATIONS

The yield strength of the selected container material (304L stainless steel) is 220 Mpa (32,000 psi.); the ultimate strength is 586 Mpa (85,000 psi.). These high strength values delineate the selection of 304L stainless steel for the long term storage of nuclear waste, in part because 304L displays high ductility and a high resistance to crack initiation [8], since crack initiation may lead to stress corrosion cracking over long period of time.

## III. ELASTIC STRESS AND STABILITY ANALYSIS OF WASTE CONTAINERS

Finite element analysis is being used for the stability analysis of the canister [9]. Two models are analyzed (Fig.1a,1b) and two shell element types are used in the analysis, a 3-D isoparametric 4 node shell element model and a 2-D thin shell element model. Both shell element types have 4 nodes with 6 degrees of freedom per node, three translations and three rotations [10]. Linear and non-linear analyses have been performed and the results obtained using different models are compared with each other and with theory [11,12] whenever possible.

### A. Load and Stability Case Study

Canister stress and stability scenarios are presented in this paper with emphasis on the elastic and the inelastic post buckling behavior of the canisters. Critical stress analysis of the nuclear fuel canisters under normal handling conditions were presented in a separate publication [13]. The following is a study of various canister buckling conditions.



1. Thin shell element model of the canister with an applied radial line load along its full length.

Figure 2a shows an exaggerated deflection pattern for the canister under a line load applied radially outward. Figure 2b shows the circumferential buckling mode for the canister under a line load applied radially inward, thus causing compressive stresses. Such loading conditions may occur if horizontal stacking of the empty canisters is used prior to loading or if loaded canisters are placed on stands in the horizontal position during storage. Compressive loading conditions may also occur when two loaded canisters impact each other during normal handling. The buckling load of  $7.607 \text{ E}+05 \text{ kN}$  ( $1.71 \text{ E}+06 \text{ lbs}$ ) is far above the actual strength of the canister and indicates that the canister will yield and crush before it achieves elastic buckling conditions in this mode.

The models used for this study consist of 2272 4-node thin shell elements and 2243 nodes.

2. Thin shell element model of a simply supported canister under two eccentric radial load, symmetric and unsymmetric support conditions around the lip of the pintle.

This loading condition may occur due to the impact of the canister while being carried from the pintle by the crane. This partial model of the canister which has the ASME flanged and dished shell structure for a pintle consists of 1360 four node thin shell elements and 1346 nodes. Figure 3a shows the positions of the two eccentrically placed radial buckling loads. Figure 3b shows the buckling mode for this loading condition if the pintle is symmetrically supported around the lip. The mode shape shown indicates a prevailing bending condition in the ASME flanged and dished pintle and in the top plate cover of the pintle. The low buckling load of  $62.3 \text{ kN}$  ( $14,000 \text{ lbs}$ ) indicates that the ASME pintle would buckle elastically if a canister gets impacted in the shell or pulled up abruptly by a crane from a horizontal position. Figure 3c shows an asymmetrical canister buckling mode in the shell due to two adjacently placed eccentric radial buckling loads. This loading condition may occur due to the impact of the bottom plate of a canister with the shell of another. The elastic buckling load for this case is  $2380 \text{ kN}$  ( $5.35 \text{ E}+05 \text{ lbs}$ ), which indicates that the canister shell would yield before it buckles elastically. Inelastic buckling will be discussed later in this paper.

Figure 4 shows a twist buckling mode in the ASME shell pintle due to concentrated radial loading in the canister and eccentric support conditions around the lip of the canister. This condition may occur if the crane grippers did not grab the pintle lip adequately while the canister is abruptly lifted from horizontal position or while under impact in its shell. This elastic twisting mode is the lowest that we encountered in our studies and demonstrates an inherent instability in a  $0.0095 \text{ m}$  ( $0.375 \text{ inch}$ ) thick pintle shell.

3. Canister shell model subjected to uniform axial loads.

The canister was subjected to uniform axial load applied to the lip of the pintle and to the top of the circumference of the cylindrical shell. These loads represent lifting of the canister



by the crane or vertical stacking of canisters.

Figure 5a shows buckling mode of the 0.7 m (28 inches) top plate of the canister due to uniform axial tensile lifting load applied to the lip of the pintle. This unusual buckling mode results from the radial compression and bending applied to the top plate by the ASME pintle shell. This mode of loading was used to check the adequacy of the finite element models to predict complex buckling conditions. Using analytical expressions for shell structures provided by references [12 and 14], the radial displacements of the cylindrical shell due to axial tensile stresses, transverse shear stresses and bending moments were equated to the displacement resulting from the outward radial buckling forces of the top plate. The tensile lifting load that caused the buckling in the plate was predicted by finite element to be 3541 kN (7.96 E+05 lbs) and by the approximate theoretical analysis discussed above to be 2891 kN (6.5 E+05 lbs).

Figure 5b shows the buckling mode of the pintle top plate due to uniform axial tensile lifting load applied to the circumference of the pintle. This mode of buckling predicted a higher buckling load of 5338 kN (1.2 E+06 lbs). Both buckling loads predicted are within the elastic range of the canisters.

Figure 5c represents a compressive axial buckling load of the canister shell due to uniform axial load applied to the top circumference of the cylinder. This classical buckling mode was also used to check the ability of the finite element models to accurately predict the buckling loads. Finite element analysis predicted an axial buckling load of 5338 kN (1.2 E+06 lbs) and theoretical analysis provided by reference [11] predicted a load of 6627 kN (1.4 E+06 lbs). The finite element model representing one fourth of the length of the cylinder used for the previous analysis consisted of 1360 thin shell elements and 1346 nodes.

#### 4. Effect of mesh refinement and change in element type.

Stresses due to radial concentrated loads applied to the canister shell were compared when a partial model of the canister having 1360 elements was replaced by a model having 5440 elements. Maximum Von Mises stresses under the load increased from 507 MPa (73,800 psi) to 852 MPa (124,000 psi) for the thin shell element model and from 275 MPa (40,100 psi) to 549 MPa (80,000 psi) for the thick shell element model.

In the elasto-plastic analysis only the thick shell elements were used for the models.

#### IV. ELASTO-PLASTIC POST BUCKLING OF CANISTER SHELL

A finite element model using four node thick shell elements, representing a quadrant of the canister shell, was subjected to concentrated radial load 0.5 m (20 in.) below the top plate.

Elasto-plastic stress and buckling analysis are shown. Figure 6 shows the idealized material property curve for 304L stainless steel used in the non-linear analysis. Figure 7 shows the applied radial load versus time curve used in applying the concentrated load in six time steps each of 0.05 seconds. This loading rate was deemed reasonable to describe the impact of one canister dropping at an angle from a small height of few inches

over horizontally placed canister.

Figure 8 shows the displacement values in inches under the applied radial load as function of time resulting from the non-linear elasto-plastic stress analysis. The Von Mises stresses resulting from the same loading condition are shown in Figure 9 for the six time steps used in the analysis. The spread of the yield zone at the different time steps is shown for a maximum radial force of 119 kN (27,000 lbs) which is approximately twice the weight of the canister. The membrane circumferential stresses were found to remain in the compressive range throughout the shell and no snap through buckling mode was considered for this level of loading. The finite element model was modified at every time step to include the changes in the material property due to the spread of the yield zone. Finite element and experimental analysis of steel cylinders were discussed in ref. [15,16]. Buckling analysis was then performed at that time step. Figure 10 shows the various buckling modes due to the applied radial load. The light colored elements shown in the figure represent the yield zone at the appropriate time step.

The predicted buckling loads were plotted against the applied radial loads as shown in Figure 11 and the elasto-plastic buckling load was graphically predicted at 86 kN (19,500 lbs). Further increase in the radial load would result eventually in snap through buckling.

## V. CONCLUSIONS

Stress analysis along with elastic and plastic buckling analysis was performed on a 0.0095 m (0.375 in.) thick. Results indicate the need for thicker, more robust and preferably multi-layer canister design to protect the inner shell from accidental overloading and potential crack initiation.

## ACKNOWLEDGEMENT

Shashidhar Channarayapatna and Yuping Huang, Graduate Students in Civil Engineering at UNLV are hereby acknowledged for their help in typing and preparation of this manuscript.

## REFERENCES

1. U.S. Department of Energy Grant #DE-FC08-90NV10872 to Waste Package Project, UNLV, April 1990 - 1991 -1992.
2. Office of Civilian Radioactive Waste Management, "Characteristics of Spent Fuel, High level Waste and Other Radioactive Wastes Which May Require Long Term Isolation", DOE/RWW-0184, USDOE, December (1987).
3. Nuclear Regulatory Commission, "Packing of Radioactive Material for Transport and Transportation of Radioactive Material Under Certain Conditions," 10CFR part 71, Federal Regulations, (1982).
4. S.G. Ladkany and B.R. Kniss " Critical stresses in pintle, weldment and tophead of nuclear waste container", High Level Radioactive Waste Management, Proceedings of the 3<sup>rd</sup> International Conference, Las Vegas, Nevada (1992).

5. S.G. Ladkany and B.R. Kniss, "A Study of a Container for Long Term Storage of High Level Waste Using Finite Elements." Report to the U.S. Department of Energy, University of Nevada, Las Vegas, June (1991).
6. L. B. Ballou, "Current Status of Waste Package Project Designs for the Yucca Mountain Project," UCID-100790, Lawrence Livermore National Laboratories, July (1989).
7. C.L. Wu, J. Lee, D.L. Wu, and L.J. Jardine, Bechtel National, Inc., "Effects of a Potential Drop of a Shipping Cask, a Waste Container and a Bare Fuel Assembly during Waste-Handling Operations," SAND87-8082 Sandia National Laboratory, May (1990).
8. D.W. Gregg and W.C. O'Neal, "Initial Specifications for Nuclear Waste Package External Dimensions and Materials," UCID-19926, Lawrence Livermore National Laboratory, September (1983).
9. M. Lashkari, Cosmos/M User Guide, Volume II, release 1.65, Structural Research and Analysis Corp., California (1991).
10. O. C. Zienkiewicz, The Finite Element Method, Third Edition, McGraw Hill, Inc., New York (1985).
11. S.P. Timoshenko and J.M. Gere, "Theory of Elastic Stability", Second Edition, McGraw-Hill Book Company, Inc., New York (1961).
12. R.J. Roark and W.C. Young, "Formulas for Stress and Strain", Fifth Edition, McGraw-Hill Book Company, Inc., New York
13. S.G. Ladkany, et.al., "Critical Stresses in Nuclear Waste Container under Normal Handling Conditions", High Level Radioactive Waste Management, Proceedings of the 4<sup>th</sup> International Conference, Las Vegas, Nevada (1993).
14. S. Timoshenko and Goodyear, Theory of Plates and Shells, Second Edition, McGraw Hill, Inc., New York (1959).
15. P.C. Birkemoe et.al., "Non-linear Finite Element Analysis of Fabricated Steel Tubes", Structural Stability Research Council, Proceedings of the Annual Technical Session, Chicago, IL, April (1991).
16. K.H. Obaia et.al., "Tests of Fabricated Steel Cylinders Subjected to Transverse Loading", Structural Stability Research Council, Proceedings of the Annual Technical Session, Chicago, IL, April (1991).

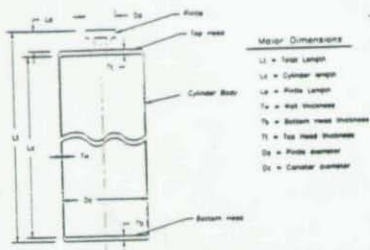


Figure 1a. Basic Geometry and Dimensions of Canister with Flat Tophead

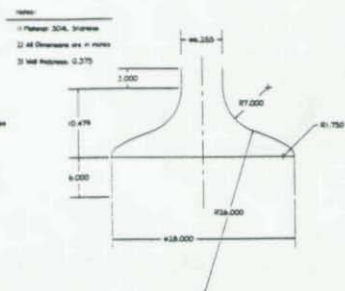


Figure 1b. Geometry of ASME Flanged a Dished Canister Tophead



Figure 2a. Four Node Thin Shell Element Model Showing Exaggerated Deflection Patterns Under a Radial Live Load Along its Length

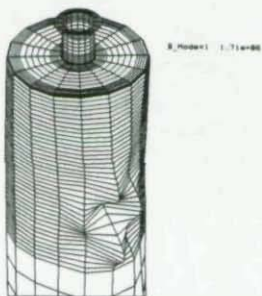


Figure 2b. Circumferential Buckling Mode Due to a Radial Live Load Placed Along the Length of the Canister



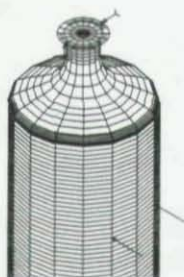


Figure 3a. Two Eccentrically Placed Radial Buckling Loads 10.6 in. Apart Circumferentially and 2 in. Apart Axially

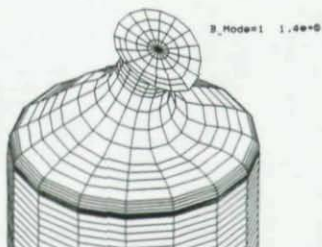


Figure 3b. Buckling Under Two Diagonally Eccentric Loads and Three Symmetrical Support Conditions 120 Degree Apart around the Lip of the Canister

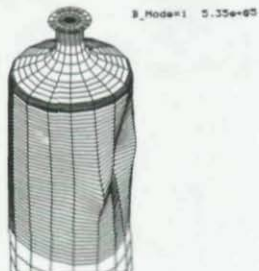


Figure 3c. Asymmetrical Canister Buckling Mode in the Shell Due to Eccentrically Placed Radial Buckling Loads

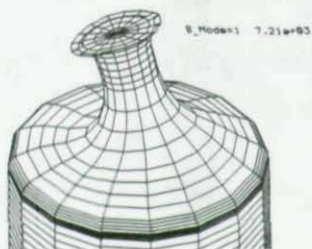


Figure 4. Twist Mode Buckling in the Pintle Shell due to Concentrated Radial Loading in the Canister with Two Eccentric Support Conditions around the Lip of the Canister



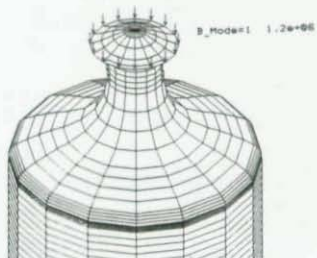
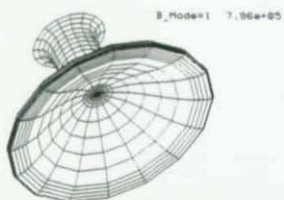


Figure 5a. Buckling Mode of the Canister Top Plate Due to Uniform Axial Tensile Lifting Load Applied to the Lip of the Pintle

Figure 5b. Buckling Mode of Pintle Top Plate Due to Uniform Axial Tensile Lifting Load Applied to the Lip of the Pintle

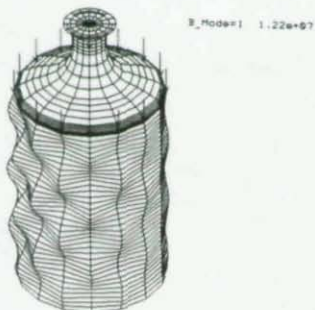


Figure 5c. Axial Buckling Mode of the Canister Shell Due to Uniform Axial Compressive Load Applied to the Top Circumference of the Shell

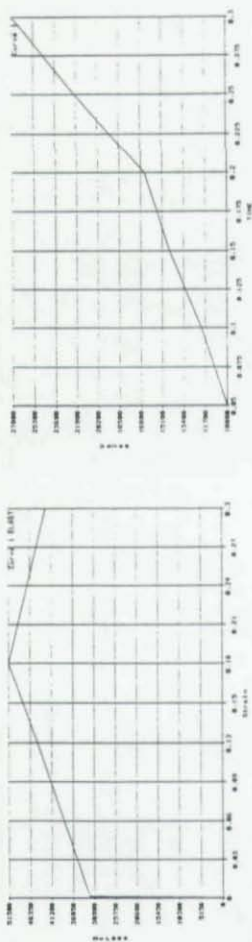


Figure 6. Idealized Elasto-Plastic Material Property Curve for 304L Stainless Steel Used in the Non-linear Analysis of Canister

Figure 7. Applied Radial Load (lbs) Versus Time (sec) Curve Used in the Non-linear Analysis of the Canister

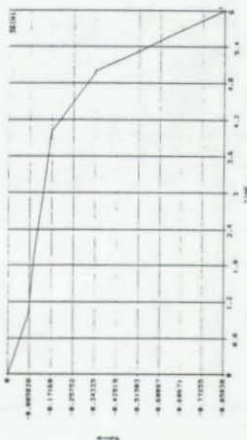


Figure 8. Displacement Values in Inches Under an Applied Radial Load versus Time in Seconds Used in the Non-linear Analysis of the Canister

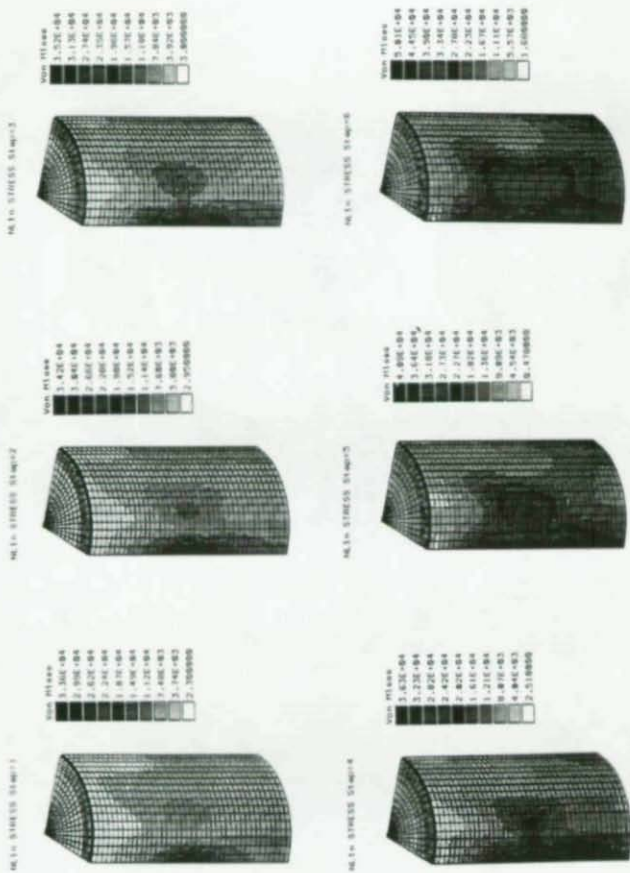


Figure 9. plots Showing the Von Mises Stresses Due to Increasing Radial Loads Applied to the Canister in Time Steps of 0.05 secs Shown in Figure 7

$P_{Mode}=1$   $3.28e+04$     
  $P_{Mode}=1$   $2.31e+04$     
  $P_{Mode}=1$   $1.66e+04$     
  $P_{Mode}=1$   $1.59e+04$

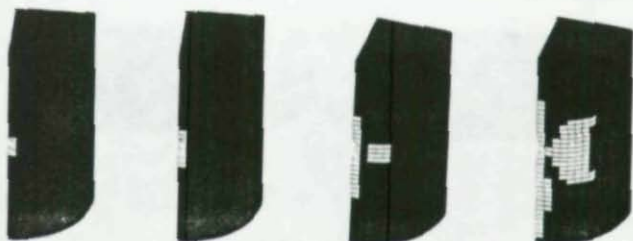


Figure 10. Plots Showing the Buckling Modes Due to Increasing Radial Loads Applied to the Canister Under Elasto-Plastic State of Stress. Light Colored Elements Represent the Yield Zone

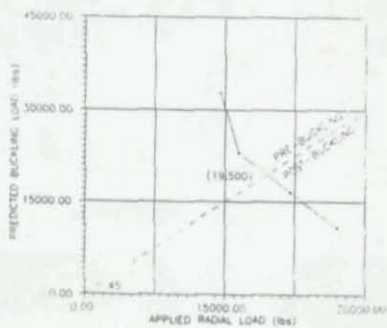


Figure 11. Predicted Buckling Load Versus Applied Radial Load for the Steel Canister with Progressive Elasto-Plastic State of Stress

## STRENGTH ASSESSMENT AND REPAIR OF DAMAGED BRACING IN OFFSHORE PLATFORMS

Walid A. Salman<sup>1</sup> Peter C. Birkemoe<sup>2</sup> James M. Ricles<sup>3</sup>

### Abstract

This paper presents results of current experimental and analytical research studies related to the residual strength of dent damaged offshore tubular steel bracing. Large scale specimens of various diameter-to-thickness ratios ( $D/t$ ) were tested in the laboratory to demonstrate the relationship between dent depth,  $D/t$  ratio, and residual strength. Nonlinear finite element techniques were used to produce damage and to model the behaviour of the dented members. A parametric study was conducted to assess the effects of  $D/t$  ratio, damaged induced residual stresses, and other related parameters on residual strength.

Under applied axial loading, the dent was found to cause a local instability, where the dent depth grows, leading to a reduced strength of the member. To avoid this local instability, dented specimens were repaired by internal grouting and were subsequently tested in the laboratory. The results from these tests indicate that this repair method is successful in increasing the strength of a damaged member. Analytical methods are now being studied to replicate the observed response and to study the nature of the composite behaviour.

The results from the research studies provide essential knowledge for incorporation into a maintenance and repair program. With an assessment of damaged member strength, and its effect on the platform strength and stability, decisions can be made related to the nature and effectiveness of a repair.

<sup>1</sup>Graduate Student, Department of Civil Engineering, University of Toronto, 35 St. George St., Toronto, Canada M5S 1A4

<sup>2</sup>Professor, Department of Civil Engineering, University of Toronto, 35 St. George St., Toronto, Canada M5S 1A4

<sup>3</sup>Associate Director, Structural Stability Research Council, Lehigh University, Fritz Engineering Laboratory, 13 E. Packer Ave., Bethlehem, PA 18015



## Introduction

Most offshore platforms are diagonally braced structures constructed of steel tubular members. These structures are subjected to a variety of environmental loadings, including wave, current, wind, and seismic. Structural inspections of offshore platforms indicate that a majority of them have members that have been damaged from impact with either marine vessels or dropped objects. The degree of dent damage resulting from these collisions varies, however, a dent depth of 10% of the member's diameter is common and is prevalent in the braces located near the ocean water surface. Dent damage, both local and global, reduces the load carrying capacity of the braces such that the strength and stability of the structural system may be jeopardized.

An experimental study on two-thirds to full scale models of fabricated tubes was conducted to assess the effects of damage on the strength and behaviour of tubular members [3]. Tubes with nominal  $D/t$  ratios of 34.5, 46 and 64 and local dent depths equal to 10% of their diameter were tested under axial compression including both concentrically and eccentrically applied loads. The study also included axial compression tests on dented specimens that were repaired by internal grouting.

This paper presents a finite element modeling approach using commercially available software to investigate the problem of damage to tubular members. The results of the experimental study in comparison with the numerical method are also discussed. From the thirteen specimens tested and analyzed, three are selected for the purpose of this report, Specimens A1, A2 and A3. These specimens all had a nominal diameter to thickness ratio of 34.5. A1 and A2 were unrepaired damaged tubes, while A3 was first damaged and subsequently repaired by internal grouting prior to loading. All specimens were loaded with simply supported end conditions.

## Experimental Program

Specimens A1, A2 and A3 each had a nominal diameter of 8.625 inches, a nominal wall thickness of 0.25 inches ( $D/t=34.5$ ), and a length equal to 178.8 inches. They were each fabricated from hot rolled electric resistance welded (ERW) carbon steel pipe of ASTM A53 Grade B material. The weld was oriented along the longitudinal axis of the pipes. From the average of three coupon tests performed on this series of pipes, with a  $D/t$  ratio of 34.5, a tensile yield stress of 34.8 ksi was obtained. The ultimate stress of the material was found to be equal to 46.5 ksi with a Young's Modulus of 29000 ksi and a strain hardening modulus of 518 ksi.

The specimens were each damaged by applying a lateral load at their midspan through a solid knife-edge indenter. The tubes were supported opposite the indenter to reduce the amount of global bending experienced by the tubes during the denting process. A 48 inch long support used for this purpose was centered about the dent section [See Fig. 1]. The resulting damage consisted of a local dent with a depth equal to 10% of the diameter of the tubes and slight overall bending resulting from lifting of the unsupported ends.

Specimen A1 was then subjected to a concentric axial load in a 500 kip self-reacting test frame as shown in Fig. 2. This frame was used in testing all the specimens, since it also enabled the axial load to be applied at an end eccentricity by means of load collars located at the ends of the simply supported specimens. The compressive axial load was applied by a 150 ton capacity hollow plunger hydraulic cylinder attached to each tension rod. Load control was used until the ultimate capacity of the tube was attained, beyond which displacement control was employed. Specimen A2 was eccentrically loaded through an end eccentricity equal to 20% of the tube diameter, resulting in a state of combined axial compression and bending along the axis of the specimen.

Prior to applying the axial load, Specimen A3 was repaired by complete internal grouting. It was then mounted in the test frame and subjected to axial compression at an end eccentricity of 20% of its diameter. The internal grout was shown to arrest the growth in the dent depth that occurred in the previously tested unrepaired specimens and resulted in a considerable increase in the ultimate strength of the specimen. The experimental parameters and the axial load results for the three specimens discussed above are summarized in Table 1.

### Finite Element Modeling

*The finite element modeling and analysis was performed using the general purpose commercial program ABAQUS [1]. The numerical model included the effects of large displacements and material non-linearities. Symmetry of the loading and boundary conditions, both during the denting and loading phases of the analysis, permitted modeling a quarter of the tube. The finite element model used is shown in Fig. 3.*

Eight noded doubly curved isoparametric quadrilateral shell elements known as ABAQUS S8R5 elements were used to model the surface of the shell. These elements have five degrees of freedom per node: three displacement components and two in-plane rotation components. Moreover, a sixth degree of freedom, the out-of-plane rotation, is activated for any node with a boundary condition on a rotational degree of freedom, for a node involved in a constraint equation using rotational degrees of freedom, for a node attached

to a beam or shell element that uses six degrees of freedom at all nodes, or for nodes common to elements that have different surface normals. The nodal displacements and nodal rotations are interpolated independently. Numerical integration to obtain the stiffness coefficients are carried out using four Gauss points over the surface of the shell. In addition, nine through thickness integration points using Simpson's rule were specified in order to model the non-linear behaviour through the thickness of the shell. The S8R5 elements account for the out-of-plane shear deformations of the shell using reduced integration for the associated shear stiffness.

As seen in Fig. 3 a relatively finer mesh was used in the vicinity of the dented zone. The transition between the fine and coarse mesh was carried out using multi-point constraint equations. The material behaviour was assumed to be isotropic and homogeneous. Yielding was governed by the von Mises criterion with the "associated" plastic flow theory used to account for the material non-linearities. In addition, isotropic hardening was assumed.

To include the damage induced residual stresses in the finite element models, the denting of the specimens was simulated analytically, prior to axial loading. Uni-directional gap elements, GAPUNI, available in the ABAQUS element library, were used to model the contact between the edge of the indenter and the surface of the tube. These elements possess no stiffness when the gap between the two connected nodes (one on the edge of the indenter, the other on the top surface of the tube) is open, but are infinitely stiff when the gap is closed, that is, when the edge of the indenter comes into contact with the tube. The support opposite the indenter was modeled by assuming that the nodes at the midspan of the tube opposite the indenter were pinned. The pinned nodes spanned an arc equal to one-third of the circumference of the tube. Although the actual support in the experimental setup had a finite length of 48 inches along the tube axis as shown in Fig. 1, only a line support (zero length) was assumed in the numerical model. Preliminary analyses had indicated that extending the support through a finite distance along the tube axis, although adding to the solution time and complexity of the model, had little effect on the denting behaviour, and even less effect on the subsequent behaviour of the model under loading. In addition, the tendency of the tube to lift off the support during denting was found to be minimal for the given degree of denting. This allowed the support conditions to be simplified during the creation of the dent for all the damaged models. The required dent depth was attained by applying a prescribed lateral displacement to the nodes representing the edge of the knife indenter. Fig. 4 shows a portion of the finite element model around the dented region for Specimen A1 after completion of the denting cycle.

After denting, the analysis was continued by modifying the boundary conditions and applying the appropriate loading. Simple supported ends were simulated by restricting the lateral displacements of the nodes at the end of the model. Applying an eccentric load to the model was carried out by first introducing a dummy node in the plane of the end cross-section. Constraint equations were then written to relate the longitudinal displacements of the end nodes on the surface of the shell to the longitudinal displacement of the dummy node and its rotation about the global Y axis [See Fig. 3]. The applied axial load was simulated by prescribing incremental longitudinal displacements to the dummy node. This technique allowed the axial load for a given specimen to be applied at any required eccentricity by appropriately locating the dummy node. For example, in the case of Specimens A2 and A3, the dummy node was introduced at an eccentricity equal to 20% of the tube diameter.

Results from the axial compression test on A3, indicated that the internal grouting of the specimen was able to restore, and in certain cases exceed, the undamaged strength of the tube. A finite element model that would closely simulate the behaviour of the repaired specimen requires detailed modeling of the internal grouting. This could be carried out by means of three dimensional solid elements, representing the grout, coupled with interface elements to model the interaction between the solid elements and the shell elements forming the surface of the tube. However, based on the experimental observations of the repaired specimen, no bond was found to develop between the grout and the tube wall, implying that the full composite strength of the member was not developed. A part of the increase in the strength provided by the grout is mainly attributed to the ability of the grout to stop the growth of the local dent, and prevent the resulting local instability in the dented region. This suggests, as a first approximation of the repair effect, that a simplified model of the repair process based on arresting the inward collapse of the cross-section could be adopted.

Based on the above, the modeling of the repair process was carried out by introducing very stiff truss elements at the dented cross-section of the model at the end of the denting cycle and prior to the application of the axial load. These elements coupled the relative lateral displacement at the top and bottom of the dented section, thus preventing the increase in the local dent depth throughout the axial loading process. Although the effectiveness of the internal grout is not thought to be restricted to the midspan of the tube where the dent depth is greatest, this initial model was based on this assumption.



## Analytical Results

Results from the numerical analysis of Specimen A1 are shown in Fig. 5 in the form of applied axial load  $P$ , normalized with respect to the cross-sectional yield strength of the tube  $P_y$ , versus the overall axial shortening, normalized by the original length of the member. The experimental results, also presented in the figure, indicate that the behaviour exhibited by the analytical model agrees well with the experimental behaviour. The pre-buckling responses, which are almost identical at the start of loading, diverge slightly prior to attaining the ultimate load, with the experimental curve showing more softening in its behaviour as yielding progresses. The analytical model, on the other hand, shows little loss in stiffness and consequently fails at a higher ultimate load. The post-buckling behaviour of the experimental specimen is very well simulated by the numerical model as the two corresponding curves are seen to converge following failure.

Two additional curves are also shown in Fig. 5. to investigate the influences of the damage induced residual stresses and the modeling of the material strain-hardening characteristics on the strength and behaviour of the damaged tube. For the finite element model that did not include the damage induced residual stresses in the analysis, the tube failed at a lower ultimate load as indicated by the corresponding curve. This behaviour is explained by the presence of residual tensile stresses in the dent zone that develop as a result of the imposed local damage. These stresses, by acting opposite to the compressive stresses produced by the axial loading of the tube, result in the observed higher capacity. The post-buckling strength and behaviour of the tube remain unaffected by the residual stresses as seen in Fig. 5. MacIntyre [2] arrived at similar conclusions in his earlier study. However, for the tubes he analyzed with  $D/t$  ratios and dent depths comparable to those of Specimen A1, the residual stresses had a more significant effect on the ultimate strength of the tubes. Since the magnitude and distribution of the residual stresses is a function of the boundary conditions imposed on the tube during denting, the effects of these stresses might have been mitigated in the case of Specimen A1 as a result of supporting the tube opposite the indenter during the denting cycle. This aspect remains to be verified. The other curve in Fig. 5 describes the load-displacement behaviour corresponding to a finite element model with an assumed elastic-perfectly plastic material response. In addition to a reduced ultimate strength compared to the model that included strain-hardening, the post buckling strength is also underestimated.

The load-deformation curves for Specimen A2 are shown in Fig. 6. Good agreement between the analytical and experimental behaviour is again observed. Similar to the results seen for Specimen A1, the finite element model appears to lose very little stiffness prior to failure while the effects of pre-ultimate yielding of the tube are more apparent in



the experimental specimen as demonstrated by the corresponding curve. The numerical analysis consequently slightly overestimates the capacity of the specimen. The post-buckling behaviour however, is seen to converge.

Analysis results from the finite element model corresponding to Specimen A3 are presented in Fig. 7. To show the effects of the repair procedures, experimental and analytical, load-deformation curves for Specimen A2 are also shown on the figure. The effect of introducing stiff elements at the dented cross-section prior to axial loading only leads to a modest gain of 14 % in the ultimate strength of the tube when compared to the corresponding unrepaired Specimen A2. On the other hand, internal grouting of the experimental specimen results in a considerable gain in the strength, exceeding twice the failure load of the damaged tube.

A summary of the axial load results,  $P/P_y$ , from the analytical solutions are presented in Table 2 where they are compared with the experimental values. Results for the dent depth values  $D_d$  and the overall out-of-straightness  $\delta_p/L$  for the three specimens are also given.

## Conclusions

Results from the finite element analysis of the damaged unrepaired specimens indicate that the numerical model is capable of reproducing the experimental load-deformation behaviour with relatively good accuracy, particularly with regards to the pre-buckling response and the post-ultimate strength and behaviour. For the tubes analyzed, and the parameters considered, the finite element model generally exhibits a stiffer response in the pre-buckling zone as the failure load is approached. The earlier yielding demonstrated by the experimental specimens might have resulted from the residual stresses created during manufacturing which were not included in the numerical analysis.

Neglecting the damage induced residual stresses in the loading phase of the analysis is shown to result in a conservative estimate of the ultimate axial strength. By referring to previous analyses not presented in this paper, the degree of conservatism appears to be a function of the dent depth, the diameter to thickness ratio of the tube, and the boundary conditions imposed on the tube as the damage is created.

Including the material strain-hardening characteristics in the analysis is necessary if the post-buckling strength and behaviour of the member is to be correctly modeled. Results based on an elastic-perfectly plastic model generally lead to conservative estimates of the strength.

Finally, modeling of the internally grouted repaired specimens by restricting the deformations at the dented cross-section fails to reproduce the large gain in strength exhibited by the experiment, indicating that the effect of the internal grout extends beyond the dent location. Revised modeling techniques have to be considered.

### Acknowledgements

The support of the Natural Sciences and Engineering Research Council of Canada and the Department of Civil Engineering at the University of Toronto is gratefully acknowledged. The experimental study was sponsored by the National Science Foundation, Chevron Oil Field Research Company, Unocal 76 Corporation, and California State Lands Commission. This work is also a result of research sponsored in part by NOAA, National Sea Grant College Program, Department of Commerce under Grant No. NA89AA-D-SG138, Project No. R/OE-16, through the California Sea Grant College, and in part by the California State Resources Agency. The U.S. government is authorized to reproduce and distribute for governmental purposes. Their support is gratefully acknowledged. The opinions expressed herein are those of the authors and do not necessarily reflect the views of the sponsors.

### References

- [1] ABAQUS User's Manual, Volumes I and II (Version 5.2), Hibbit, Karlsson and Sorensen, Inc., 1080 Main Street, Pawtucket, Rhode Island, 1992.
- [2] MacIntyre, J., "An Analytical Study of Damaged Tubular Member Behaviour", Ph.D. Thesis, University of Toronto, Toronto, Canada, 1991.
- [3] Ricles, J., Gillum, T. and Lampert, W., "Residual Strength and Grout Repair of Dented Offshore Tubular Bracing - Phase 1 Study", ATLSS Report No. 92-14, ATLSS Engineering Research Center, Lehigh University, Bethlehem, October 1992.

Specimen No.	Description of Specimen	End Eccent.	$\frac{D_d}{D}$	Exp. Pmax (kips)
A1	Damaged, Non-repaired	0	0.1	141
A2	Damaged, Non-repaired	0.2	0.1	91
A3	Damaged, Internal Grout Repair	0.2	0.1	191

Table 1: Experimental parameters and axial load results

Specimen No.	Exp.		FE		Exp.	FE	$\frac{P_{Exp}}{P_{FE}}$
	$\frac{\delta_P}{L}$	$D_d$ (in)	$\frac{\delta_P}{L}$	$D_d$ (in)	$\frac{P}{P_y}$	$\frac{P}{P_y}$	
A1	0.0007	0.868	0.0014	0.862	0.61	0.64	0.95
A2	0.0006	0.861	0.0014	0.854	0.40	0.42	0.95
A3	0.0006	0.857	0.0014	0.854	0.84	0.48	1.75

Table 2: Comparison between experimental and numerical results for the damage cycle and ultimate loads

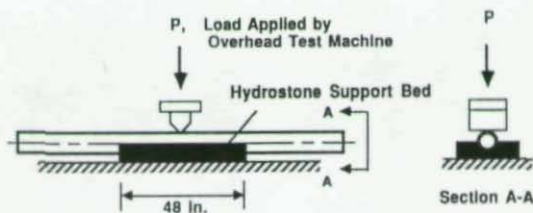


Figure 1: Experimental device used for the denting of the specimens

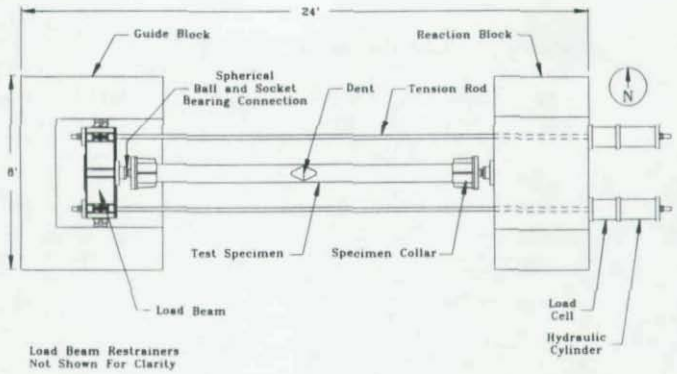


Figure 2: Plan view of test frame

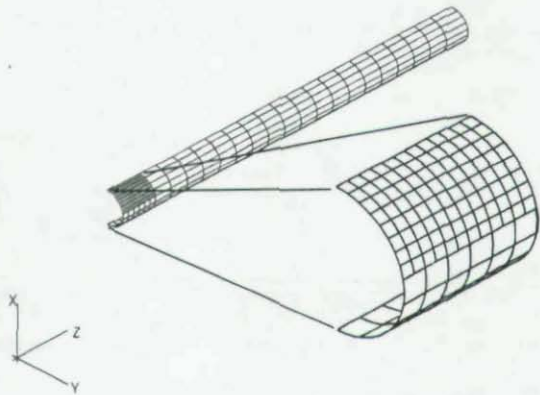


Figure 3: Finite element model employed in the analysis

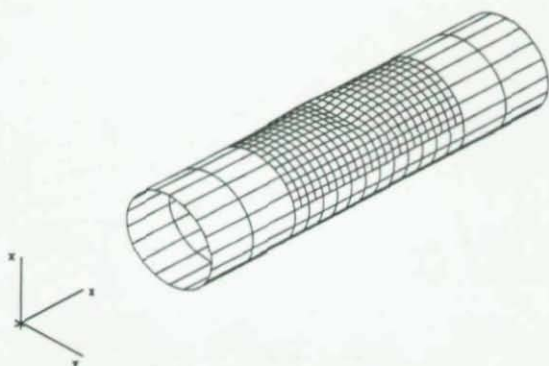


Figure 4: Specimen A1 - Dented zone of finite element model at the end of the denting cycle

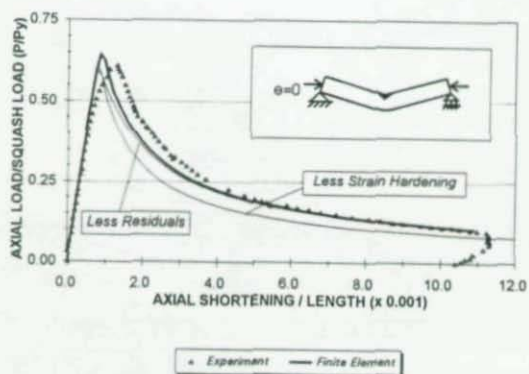


Figure 5: Axial load - axial strain relationship for Specimen A1



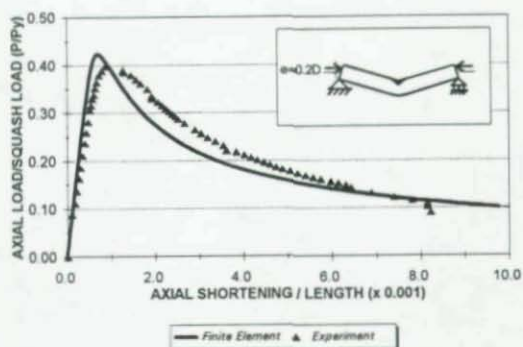


Figure 6: Axial load – axial strain relationship for Specimen A2

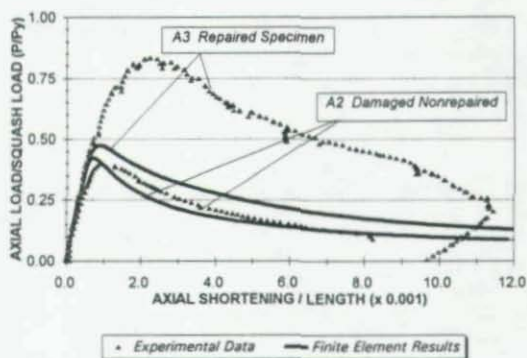


Figure 7: Load – displacement relations for unrepaired and repaired tubes. Experimental and analytical solutions

# GROUTED HOLLOW STRUCTURAL STEEL SECTIONS AS SEISMIC RETROFIT FOR DEFICIENT BEAM-TO-COLUMN JOINTS

Helmut G.L. Prion<sup>1</sup>, Thomas E. Hoffschild<sup>2</sup> and Sheldon Cherry<sup>1</sup>

## ABSTRACT

This paper presents the findings of an experimental study to evaluate a method of retrofit which addresses a deficiency in strength and ductility in reinforced concrete frames caused by the lack of sufficient reinforcement in and around beam-to-column joints.

The proposed retrofit method consists of encasing the reinforced concrete joint with a grouted steel jacket. In this study, two styles of retrofit jacket were tested: circular and rectangular tubular casing. Both methods provided the necessary strength to the joint area, although the circular tube proved to be more efficient in confining the concrete. In the paper, the two jacket styles are evaluated for strength, stiffness and ductility, and their relative merits are discussed.

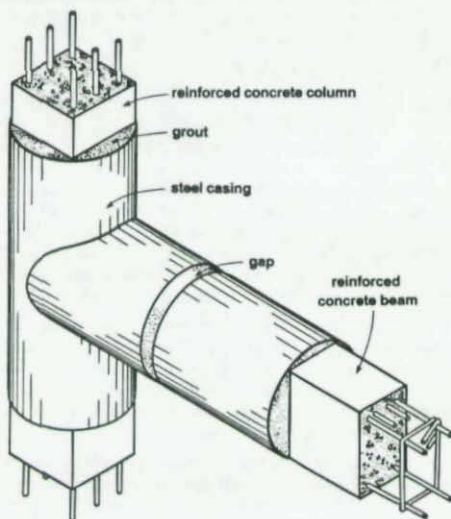


Figure 1: Beam-to-column joint retrofit

<sup>1</sup> Department of Civil Engineering, University of British Columbia, Vancouver, B.C., Canada

<sup>2</sup> Westmar Consultants, North Vancouver, B.C., Canada

## INTRODUCTION

The benefits of concrete-filled tubes have been realized in applications such as columns in new construction and as a means of retrofitting deficient bridge columns (Priestley et al 1990). The major advantage is the efficient use of relatively thin steel tubes combined with an inexpensive and brittle material such as concrete to create a strong and ductile framing member. The function of the steel tubing is twofold, namely to contribute to the load resistance, especially under bending, and to provide lateral confinement to the concrete. In columns the latter is the most important and special measures are often taken to prevent the steel tube from attracting compressive forces. When bending constitutes a significant load component, however, the steel tube is called upon to provide tension resistance in the longitudinal direction, especially when no concrete reinforcement is present. Because the load carrying mechanism of concrete-filled tubes is largely independent of the ingredients of the inside components and relies mainly on the direct interface between the concrete and the exterior shell, this construction method is particularly suitable for the rehabilitation or repair of deficient structural components.

The relatively minimal requirements for transverse reinforcement prevalent in the pre-1971 reinforced concrete design codes have resulted in a large number of moment resisting frames that, under today's standards, would be considered prone to shear failures in the columns and beam-to-column joints, thus exhibiting a low level of ductility in a seismic event. This study deals specifically with the retrofit of beam-to-column joints in such moment-resisting frames. The purpose was to investigate the application of concrete-filled steel tubes as a suitable method of retrofit that can be applied to strengthen the beam-to-column joint region. Deficient (or damaged) reinforced concrete members and joints were retrofitted by encasing the joints with a steel jacket and filling the void between the jacket and the joint members with concrete grout (Fig. 1). This is an elegant and simple solution; the steel provides both lateral confinement and shear reinforcement, thereby adding strength and ductility to the joint.

## PREVIOUS RESEARCH

A large amount of research has been directed towards the enhancement of ductility of reinforced concrete members and joints. The usual method is to provide confinement to the concrete through transverse reinforcement in the form of hoops or spirals. An alternate method of providing confinement by encasing the concrete core within a steel shell was found to be very effective for columns (Priestley et al, 1990; Priestley and Park, 1984, 1985). When reinforced concrete columns need to be retrofitted, it was found to be preferable that the steel jacketing provide confinement only, and not directly carry any axial load. In reality, however, the structural separation of steel tube and concrete was difficult to achieve since chemical bond and friction are usually sufficient to assure strain compatibility (Prion and Boehme, 1993).

Joint performance appears to be a function of the joint shear stress and confinement level (Alameddine and Ehsani 1991). High joint shear stresses were found to reduce the energy absorption capacity and cause a rapid loss of load-carrying capacity. The primary role of transverse joint reinforcement is thus one of confinement (Ehsani and Wight 1990, Leon 1990). Other recommendations for the improvement of joint behaviour are the avoidance of large plastic deformations within the joint, the concentration of hinging to prescribed sections, and the avoidance of brittle failures.

Based on previous research, the object of the beam-to-column connection retrofit/repair program was thus to address the problems associated with joint shear failure (yield hinges within the joint, and insufficient confinement and anchorage) by the use of steel jackets. The forces within the joint region are much more complicated than in the isolated column retrofit case and it was not clear at the onset of this study whether adequate confinement could be provided, and whether circular tubes were required or if rectangular ones would also be sufficient. The relative merits of both jacket types were therefore investigated. The objectives were thus twofold: to strengthen the joint region while at the same time increase the ductility of the system by developing a plastic hinge within the beam adjacent to the joint.

## EXPERIMENTAL STUDY

Six cyclic loading tests were performed on a total of four reinforced concrete specimens built according to typical 1960's design specifications. The testing program included two preliminary tests on unretrofitted specimens, causing some initial damage and intended as a likely scenario after an earthquake. The subsequent four tests were performed on the two damaged and the two undamaged specimens after retrofitting them with grouted steel jackets: two with a circular jacket, and two with a rectangular jacket (Fig.2).

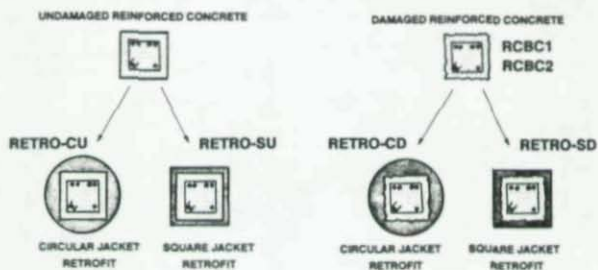


Figure 2: Test program

### Test Specimen Design

As a basis for the experimental work, a two-storey office structure situated in Vancouver, B.C., was designed in accordance with the requirements of the 1970 National Building Code of Canada (National 1970), and primarily satisfied the CAN3-A23.3-M66 (1966) code for reinforced concrete structures (Canadian 1966) (Fig. 3). A typical beam-to-column joint sub-assembly was scaled down for testing and modified by omitting all the transverse reinforcement from the joint region. This was common practice at the time due to ambiguities in the interpretation of the code; the 1966 code did not explicitly state that the joint region should be considered part of the column, with specific transverse reinforcement requirements. Consequently, ties or hoops were typically left out of the joint, mainly to avoid congestion of reinforcement which often led to honeycomb voids.

### Retrofit Design

Steel jackets were provided as a substitute for the lateral reinforcement steel that was left out in the original design. They were intended to provide confinement and shear strength to the joints, without unduly increasing the moment capacity of the specimens. The required volume of reinforcement, based on modern design codes, was replaced by the steel jackets, resulting in a plate thickness of 2.86 mm (0.110 in). The lengths of the retrofit were made equal to the member depth along the columns and twice the member depth along the beam,

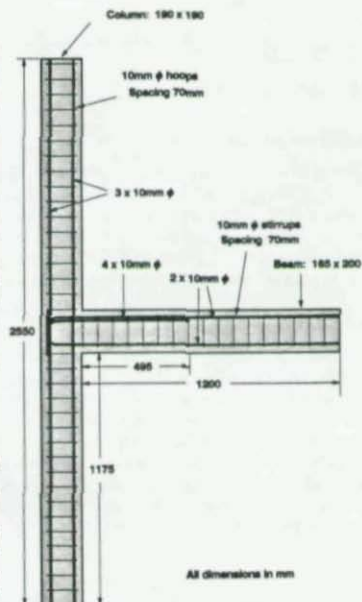


Figure 3: Reinforced concrete specimen



measured from the beam-to-column interface. A gap of 20mm (3/4 in) was left halfway along the length of the beam jacket, to create a flexural hinge at that point (Fig. 4). Despite the discontinuity in the steel tube at the gap, an increase in the overall moment resistance of about one-third was expected due to the added concrete. The size of the steel jackets was kept to a minimum to reduce the amount of disruption to the structure during the retrofit process, and also to limit the increase in strength of the frame members, which could force a failure elsewhere in the structure.

As testing progressed, changes were made to the retrofit schemes because the strength increases of the retrofit sections exceeded expectations and caused failures in the beam and column outside the retrofit regions. These changes are detailed in a later section.

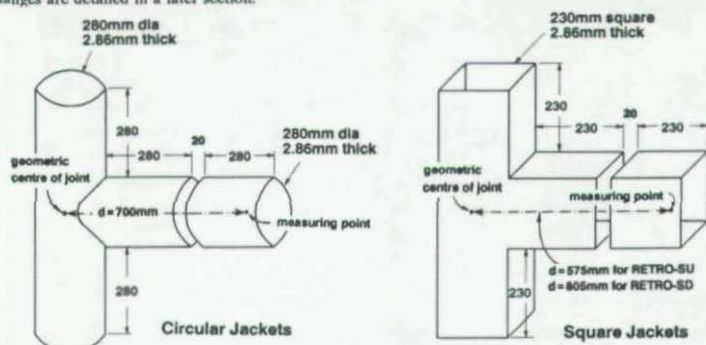


Figure 4: Jacket geometry

### Experimental Apparatus and Procedure

A testing frame in the Civil Engineering Structures Laboratory at the University of British Columbia was used to apply cyclic displacements to the beam while maintaining a constant axial load in the column (Fig.5). Data from load cells, displacement transducers and strain gauges were recorded by an automatic computer controlled data acquisition system. Strain gauges on the retrofit tubes were used to determine the behaviour of the steel jackets during cyclic loading. They were concentrated within the joint area and were intended to provide an insight into the complicated stress pattern of the steel jacket in that area.

### Testing Procedure

First, the axial load was applied to the column, which was maintained constant throughout the test. A moment was then applied to the joint by displacing the end of the beam in an upward (positive) direction. The load was steadily increased until the yield moment was reached, which, due to the non-linear response of the specimen, depended somewhat on judgment. A ductility factor of  $\theta=1$  was associated with this displacement. This same displacement was then applied in the opposite (negative) direction. For the unretrofitted specimens the full cycle was repeated a second time, followed by two complete cycles at double amplitude. These four cycles of loading caused enough distress in the joint that it could be considered damaged, but repairable. The retrofitted specimens were subjected to a greater number of load cycles with increasing amplitude.



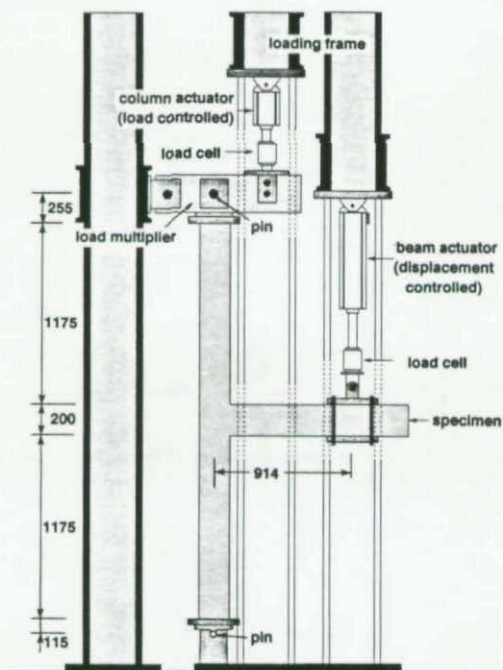


Figure 5: Test arrangement

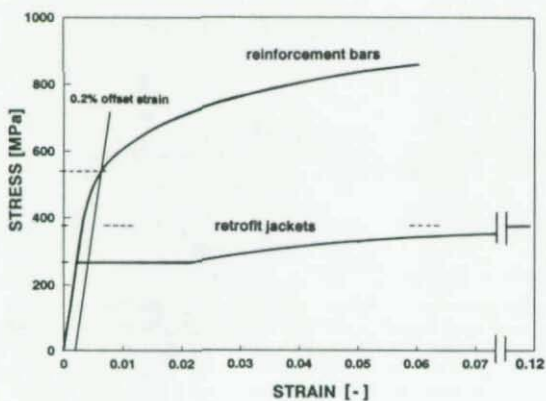


Figure 6: Steel properties

## TEST RESULTS

### Material Properties

The reinforcing steel had an average yield strength of 566 MPa; the ultimate strength was approximately 800 MPa. The stress strain curves did not feature a marked yield plateau and the stress at 0.2% offset strain was used to define the tensile yield stress (Fig. 6). The retrofit jackets were fabricated from hot-rolled plate having a yield stress of 267 MPa and ultimate stress of approximately 370 MPa.

The compressive strength of the concrete, determined from standard 300mm cylinders, was 26.3 MPa at the time of the unretrofitted tests, and 30.3 MPa when the retrofitted specimens were tested. The average compressive strength of the grout was 31.3 MPa.

### Unretrofitted Specimens

The unretrofitted reinforced concrete specimens behaved as expected, that is, they disclosed lack of shear strength and ductility in the joint area. The virtually identical hysteresis curves of the applied moment versus the joint rotation for specimens RCBC1 and RCBC2 (Fig. 7) exhibit a rapid degradation in stiffness and strength with progressive cycling. The characteristic pinching effect, typical for reinforced concrete members without special detailing, is clearly evident. Extensive damage occurred within the joint region with minor flexural cracking in the beam and column. A large amount of concrete cover spalled off the column and concrete crushing took place within the hinge area at the interface of the column and the beam. Failure within the joint occurred essentially due to bond failure of the longitudinal reinforcement and shear failure of the concrete in the joint area.

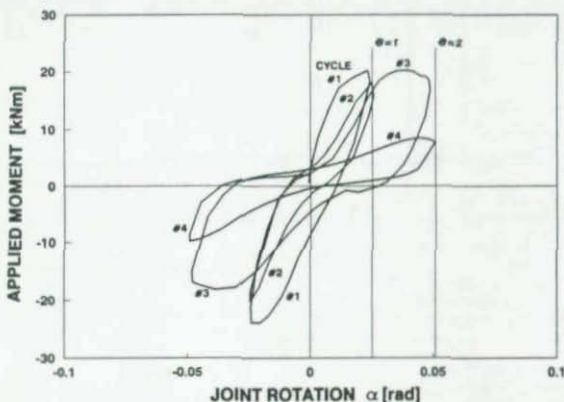


Figure 7: Hysteresis curve for unretrofitted specimen RCBC1

### Retrofitted Specimens

A total of four retrofitted specimens was tested. Each had its own peculiarities and will be discussed individually. Although some of the original specimens had been damaged previously, this did not affect the behaviour of the retrofitted specimens. Nevertheless, the designation "undamaged" or "previously damaged" is used to distinguish the different tests. Test results are tabulated in Table 1. The moment  $M_s$  is derived from a section analysis at the particular location listed, corresponding to the 2% offset stress in the reinforcement. This moment is then scaled linearly to the centre of the joint ( $M_c$ ). The experimental moment ( $M_e$ ) also corresponds to "first yield" and is calculated with respect to the centre of the joint. For the sake of uniformity, the hysteresis curves are plotted for the moment at the centre of the joint ( $M$  = vertical load

x 914 mm) against the average rotation of the beam with respect to a horizontal plane (rotation =  $1/d$  x vertical displacement at the measuring point, where  $d$  is shown in Fig.4).

#### RETRO-SU: Undamaged specimen with square jacket

This specimen developed two modes of failure, depending on the direction of load application. With positive (upward) loading, a flexural hinge formed at the gap between the two sections of steel jacket in the beam. During negative (downward) loading, a flexural hinge formed in the reinforced concrete, just outside the retrofit area. With repeated cycling this flexural hinge deteriorated into a shear failure resulting in a drastic drop in load-carrying capacity in both directions. The flexural hinge in the gap area thus ceased to undergo further yielding.

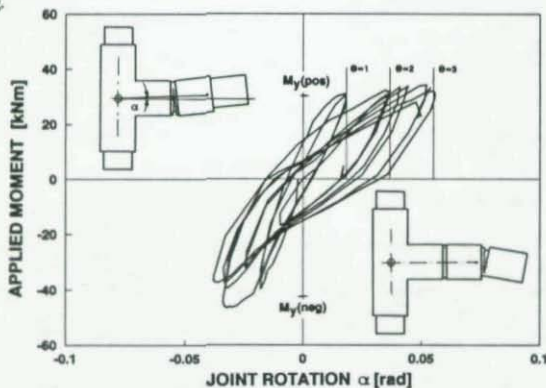


Figure 8: Hysteresis curve of specimen RETRO-SU

The hysteresis plot of the joint (Fig. 8) shows the progressive development of the plastic hinge at the bottom of the gap during positive loading. Since hinging during negative loading was outside the gap, the top layer of steel in the gap never reached yield stress, and hence little or no plastic action was observed for this portion of the loading cycle. Not much strength loss was recorded during the progression of the experiment, although the stiffness deteriorated significantly. Shear deformation within the joint area was negligible.

#### RETRO-CU: Undamaged specimen with circular jacket

This specimen also developed two modes of failure: with positive loading, a flexural hinge developed at the retrofit gap in the beam; under negative loading, a flexural hinge once again formed outside the retrofitted region, this time in the upper portion of the column. To avoid a catastrophic buckling failure of the column, negative loading past a ductility factor of  $\theta=1.5$  was avoided, since it was deemed more important to observe the development of the plastic hinge within the retrofitted zone. The flexural hinge was concentrated over a very short distance, due to the confinement of the core concrete. A maximum ductility of  $\theta=5$  was reached in the fourth cycle.

During positive loading, when the flexural hinge developed within the retrofit gap, no significant loss of bending strength was detected. During negative loading, however, gradual deterioration in load capacity occurred, mainly due to second order effects resulting from the column deflection. The hysteresis curve (Fig. 9) shows the progression of the plastic hinge within the bottom layer of steel during positive loading. The top layer of steel never reached the yield stress under negative loading, since the flexural hinge under negative loading formed within the column.

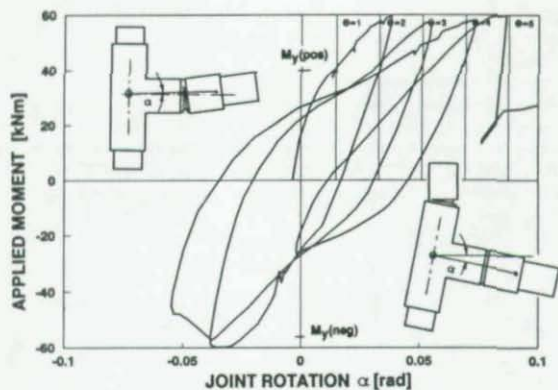


Figure 9: Hysteresis curve for specimen RETRO-CU

**RETRO-SD: Previously damaged specimen with square jacket**

Based on the results from RETRO-SU, it was decided to extend the steel jacket along the beam by 250mm. The critical section for both positive and negative loading directions was now within the gap region and the specimen developed the desired flexural hinge.

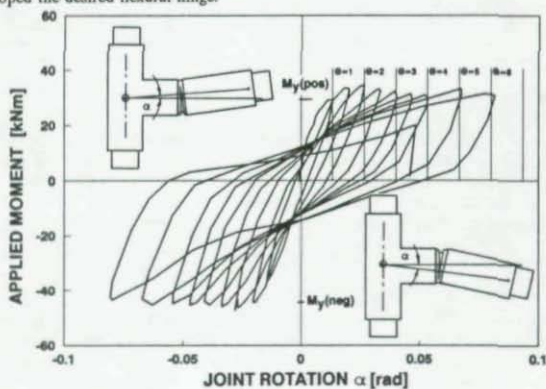


Figure 10: Hysteresis curve for specimen RETRO-SD

Failure of the specimen was caused by tensile rupture of the bottom layer of steel. The hysteresis loop of the plastic hinge zone (Fig. 10) shows that a maximum ductility factor of  $\theta=6$  was reached during the ninth cycle. Only a marginal loss of strength was recorded during cycles four to seven, but that strength was regained during cycles eight and nine, which can be attributed to strain hardening in the reinforcement steel. In this specimen, a small amount of hysteretic loop pinching occurred during negative loading. This can be explained by the fact that the bending stiffness under positive loading was mainly due to the reinforcing steel (tension and compression), whereas the concrete in compression contributed significantly to the stiffness under negative loading.

#### RETRO-CD: Previously Damaged Specimen with Circular Jacket

Based on the behaviour of specimen RETRO-CU a modification of the retrofit was undertaken to avoid development of a flexural hinge in the column. An extra pair of equidistant gaps, 25mm wide, were cut between the originally designed gap and the column face. This was to reduce the moment capacity in the beam, and hence move the critical section for negative loading from the column into the beam area. This specimen's failure mode was as expected with a plastic hinge forming within the gap region of the retrofit under both positive and negative loading. The extra gaps helped to increase the spread of yielding in the reinforcing bars while the remaining steel rings provide sufficient confinement for the concrete to prevent spalling. The bottom layer of steel failed in tension during the positive loading portion of the eleventh cycle with an overall hinge ductility ratio of  $\theta=7$  (Fig. 11). Most of the bending strain after yielding was concentrated in the first gap (closest to the column), with some deformation in the other two gaps. There was no evidence of loss of bond and the strain gauges indicated confinement stresses of up to 50% of the yield stress.

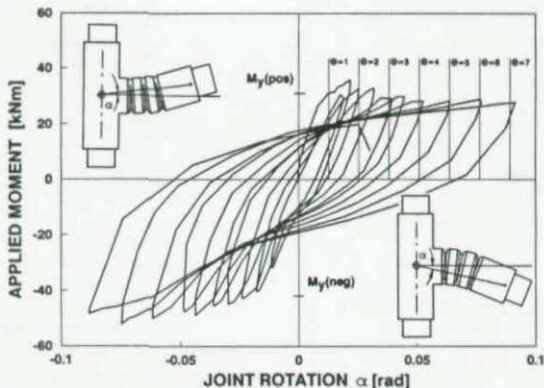


Figure 11: Hysteresis curve for specimen RETRO-CD

There was some concern that the close proximity of the gap to the joint area might unduly affect the integrity of the joint. Since the joint area was not confined by the steel jacket on all sides, it was felt that the bond and confinement might have been compromised in this region. The measured levels and distribution of strain in this area suggest, however, that this concern was unwarranted.

#### Summary of Retrofit Testing

The testing program of the four retrofitted specimens highlighted typical mistakes that occur in the design of retrofit schemes. Flexural failure in the beam or column outside the retrofitted area necessitated changes in the retrofit design of subsequent specimens. This was accomplished by either extending the retrofit along the beam or by cutting the two extra gaps into the jacket of the beam, adjacent to the joint.

Some deterioration of the bond between the steel tube and the grout occurred in the two square specimens; no significant bond failure occurred in the two circular specimens. All the specimens developed tensile strains in their jackets during testing. However, only the circular jackets were effective in causing significant confinement stress on the core concrete, leading to a generally superior behaviour with regard to pinching.



SPECIMEN	Failure Location	Positive Loading			Negative Loading		
		$M_x$ [kNm]	$M_z$ [kNm]	$M_y$ [kNm]	$M_x$ [kNm]	$M_z$ [kNm]	$M_y$ [kNm]
RETRO -SU	Beam - End of Retrofit	16.8	46.5	----	16.8	46.5	42.7
	Beam - Gap Region	18.7	29.9	27.4	35.8	57.3	----
	Column	22.9	59.0	----	22.9	59.0	----
RETRO -CU	Beam - End of Retrofit	16.8	75.6	----	16.8	75.6	----
	Beam - Gap Region	21.4	37.6	39.6	38.9	68.3	----
	Column	22.9	63.2	----	22.9	63.2	56.4
RETRO -SD	Beam - End of Retrofit	16.8	151.2	----	16.8	151.2	----
	Beam - Gap Region	18.7	29.9	29.0	35.8	57.3	44.3
	Column	20.7	59.0	----	20.7	59.0	----
RETRO -CD	Beam - End of Retrofit	16.8	75.6	----	16.8	75.6	----
	Beam - Gap Region	21.4	28.5	29.8	38.9	51.9	44.3
	Column	22.9	63.2	----	22.9	63.2	----

Table 1: Retrofit Test Results

## EVALUATION OF RETROFIT SCHEMES

Before considering the advantages and disadvantages of the different retrofit schemes studied, it is useful to summarize what was actually achieved in the retrofit process under evaluation. First and foremost, the retrofit strengthened the deficient or damaged reinforced concrete joint area to such an extent that hinging or failure was deflected to adjacent areas: to the beam or column outside the retrofit, or to the beam within the intentionally weakened "hinge section". Any comparisons of "before" and "after" are thus somewhat misleading because the "problem" was shifted from the most critical link to the next one in line. It is thus useful to consider the retrofit process in its entirety, which involves not only assessment of strengthening measures, but also the behaviour of the critical failure zone after retrofit.

### Reliability of bond between grout and steel casing

In the design of the retrofit jacket, the possibility of developing considerable bond between the concrete and the retrofit steel was considered. To break the continuity of the tubes in the longitudinal direction, circumferential gaps were provided in the casing. Ideally, the steel casing should act only as confinement for the concrete, and should not increase the moment capacity of the specimen; no longitudinal bond or interaction should exist between the concrete and the retrofit steel. It is, however, impossible to expect lateral confinement of the concrete, resulting from a biaxial stress state in the jacket, without experiencing some amount of mechanical interaction (friction) in the longitudinal direction. This interaction, of course, would increase the moment capacity, perhaps significantly, particularly where the beam jacket is physically connected to the column jacket.

The chemical bond between the concrete and the steel did not appear to be very consistent, as was evidenced in certain areas of the square jacket retrofits, where bond failure occurred early in the tests. A more likely scenario would be the development of a more reliable mechanism through friction or mechanical bond between the concrete and the retrofit steel.

### Positioning the gap for plastic hinge development

The gap in the beam retrofit was initially incorporated in the design concept in response to the anticipated increase in the moment capacity from chemical and/or mechanical bond between the steel casing and the grout. The gap was intended to contain failure within the retrofitted zone of the specimen, and also to limit the resulting increase in moment capacity. It was placed a reasonable distance away from the joint area to avoid

any risk of a repeated joint failure. Since the joint area was not entirely surrounded by a continuous steel jacket, a gap very close to the beam-to-column interface would remove some of the confinement protection provided by the jacket. This was of particular concern with the square jackets which, because of their geometry, were not expected to act as efficiently as the circular tubes.

Two major considerations thus governed the positioning of gaps: reduction of the moment capacity, which would be most effective with a gap close to the joint, and preservation of the integrity of the joint zone, which called for an uninterrupted casing close to the joint. A third consideration entered at a later stage, namely the placement of multiple gaps to provide an extended hinge zone.

### Improvement in ductility

The overall improvement in ductility of the specimens was substantial, regardless of the jacket shape used in the retrofit, provided that failure occurred within the retrofitted zone.

### Dimensions of the retrofit jacket

The thickness of the steel jacket was found to be sufficient for the purposes of this particular study. The basis of design was to replace the missing transverse steel in the joint area, on a volume basis, with an equivalent amount of steel in the form of a steel jacket. A major consideration dictating the use of a steel jacket was ease of fabrication. Weldability of the casing required a minimum thickness to avoid excessive distortions and burn-through when joining the component parts of the steel jacket. The weld needed to be able to withstand the high stress concentrations that would occur in the beam-to-column joint area; this could be a severe requirement, especially under repeated yield cycles.

The length of the jacket sleeves and the placement of the gaps were the critical dimensions affecting the behaviour of the retrofit. Two possibilities arose: extend the jackets sufficiently to force a failure in the joint itself, or provide a weakened hinge zone in a non-critical area. In both the square and circular jacket cases, the length of the retrofit was sufficient, provided the gaps were close to the column face. The confinement effect of the steel jacket was mainly to prevent spalling of the concrete, both within the enclosed zones and the narrow gaps in the plastic hinge zones.

### Confinement effects

In general it may be stated that the increase in concrete compressive strength due to confinement is only an issue in heavily loaded columns. In beams, the increase in bond and shear strength are of greater importance. The confinement of the concrete was maintained throughout the loading sequence; even in the gap area the arching effect was sufficient to contain the concrete. With the aid of mechanical bond (friction), the failure zone was concentrated in the gap zone. There was no evidence of an increase in compressive strength of the concrete due to triaxial confinement. The measured moments at yield were generally consistent with predictions based on the conventional unconfined strength of the concrete.

### Rating the retrofit schemes

Considering the efficiency of the retrofit schemes, all the specimens behaved satisfactorily, with a slightly better performance being exhibited by the circular retrofits. The square retrofits did, however, behave well enough to merit consideration as a reasonable retrofit scheme. Evidently, the increase in the moment capacity provided by the concrete-to-steel bond, and the containment provided by the jacket, regardless of its geometric shape, were the overriding factors in the improvement of ductility. Placing the gap closer to the joint helped the effectiveness of the jacket as designed.

RETRO-CD provided the greatest retrofit improvement, with RETRO-SD a close runner-up. Failure was observed to be entirely within the retrofit region of these two specimens. RETRO-SU and RETRO-CU were affected by failure modes outside the retrofit region, and their performances should thus not be compared to RETRO-CD and RETRO-SD. RETRO-CU developed a larger ductility than RETRO-SU, but the increase in ductility was limited by the failure in the column under negative loading. RETRO-SU developed reasonable ductility under positive loading, until flexural and shear failure took place outside the retrofit zone under negative loading.

## CONCLUSIONS

An effective retrofit method has been studied for deficient or damaged beam-to-column joints in reinforced concrete frames. Grouted steel tubes provided the necessary strength and confinement to avoid distress of the joint region. Circular tubes, which are more costly to fabricate and install, proved to be more effective than rectangular tubes, although the latter also met the general expectations.

A side effect of this retrofit method was the increase in moment capacity of the sections, which should be minimized to avoid undue distress in other regions of the structure that have not been designed to carry additional loads. To limit the increase in moment capacity of the joint area, it is recommended that gaps be placed in the steel casing, close to the beam-to-column joint area. A number of gaps may be advisable to avoid concentrated yielding and reduced ductility of the reinforcement bars within the gap areas. When using square jackets, care should be taken to avoid placing the gaps too close to the joint area. The joint area has been shown to be weak, and without the added benefit of the radial confinement provided by a circular retrofit jacket, this joint area, which is effectively within the column, can be significantly affected by a plastic hinge forming too close to it.

A jacket thickness designed to replace the missing transverse steel, on a volume basis, was found to be sufficient. For practical reasons during construction (e.g. welding) a minimum thickness would be advisable. Since none of the retrofitted specimens failed in the same manner as the unretrofitted ones, no conclusions can be drawn pertaining to the effectiveness of the proposed retrofit method in the immediate joint area. Follow-up tests are necessary to determine the amount of strengthening and added ductility needed in that region.

## ACKNOWLEDGEMENTS

The direct and indirect support of the Natural Sciences and Engineering Research Council of Canada and the Department of Civil Engineering at the University of British Columbia is gratefully acknowledged.

## REFERENCES

- Alameddine, Fadel; Ehsani, Mohammed R., (1991), "High Strength RC Connections Subjected to Inelastic Cyclic Loading", *Journal of Structural Engineering, ASCE* Vol 117, No 3, pp 829-850
- Canadian Standards Association (CSA), (1966), "Code for the Design of Plain or Reinforced Concrete Structures", CSA Standard A23.3-1966, Canadian Standards Association, Ottawa ON
- Ehsani, Mohammed R.; Wight, J.K., (1990), "Confinement Steel Requirements for Connections in Ductile Frames", *Journal of Structural Engineering, ASCE* Vol 116, No 3, pp 751-767
- Leon, Roberto T., (1990), "Shear Strength and Hysteretic Behavior of Interior Beam-Column Joints", *ACI Structural Journal*, Vol 87, No 1, pp 3-11
- National Building Code of Canada (NBCC), (1970), National Research Council, Ottawa ON
- Priestley, M.J.N.; Park, R., (1984), "Strength and Ductility of Bridge Substructures", Road Research Unit Bulletin 71, New Zealand National Roads Board Wellington, NZ
- Priestley, M.J.N.; Park, R., (1985), "Concrete Filled Steel Tubular Piles Under Seismic Loading", International Specialty Conference on Concrete Filled Steel Tubular Structures Harbin, China Proceedings, pp 96-103
- Priestley, M.J.N.; Seible, F.; Chai, Y.H.; Sun, Z.L., (1990), "Steel Jacketing of Bridge Columns for Enhanced Flexural Performance", Second Workshop on Bridge Engineering Research in Progress, National Science Foundation and Civil Engineering Department, University of Nevada, Reno.
- Prión, H.G.L., Boehme, J., (1989), "Beam-Column Behaviour of Steel Tubes Filled with High Strength Concrete", Proc. 4th International Colloquium of the Structural Stability Research Council, New York, April 1989, pp. 439-450.



## P- $\Delta$ EFFECT IN SEISMIC RESISTANT STEEL STRUCTURES

*Federico M. Mazzolani*

*Istituto di Tecnica delle Costruzioni  
Università di Napoli, Italia*

*Vincenzo Piluso*

*Istituto di Ingegneria Civile  
Università di Salerno, Italia*

### ABSTRACT

In this paper the state of the Italian research activity regarding the influence of second order effects on the seismic behaviour of steel structures is presented.

A simplified model for predicting geometrical nonlinearity effects in steel structures under seismic loads is analysed. The method is based on the statistical analysis of the seismic inelastic response of a SDOF model including P- $\Delta$  effect. The equivalence between actual MDOF structures and the SDOF model is established through the lateral loads versus top sway displacement behavioural curve.

The method allows to define a reduction coefficient of the q-factor which has to be considered in design. This reduction factor, which is related to the magnitude of vertical loads, the available ductility and the collapse mechanism, takes into account the amplification of the structural damage, under severe earthquakes, due to P- $\Delta$  effect.

Numerical simulations of MDOF structures subjected to earthquake action have been performed in order to check the reliability of the proposed method.

Finally, the future activities of the Italian research group, in the field of overall stability effects under seismic loads, are briefly presented.

### 1 - INTRODUCTION

The term P- $\Delta$  effect is referred to the action of gravity loads acting on a structure in its deformed configuration. In case of structures stressed in elastic range and subjected to static loads, this effect produces an amplification of the internal actions with respect to the ones computed by means of a first order analysis.

In spite of second order analyses can be nowadays easily performed, the effects deriving from the geometric non-linearity are usually taken into account by means of amplification formulae in which both P- $\delta$  effect at member level and P- $\Delta$  effect at structure level are considered [1].

In case of structures subjected to dynamic loads, geometric non-linearity gives rise to an increase of the natural period of vibration so that, depending on the loading features, improvement or worsening of the structural response can arise. This is a fundamental difference with respect to the case of static loading conditions where, the P- $\Delta$  effect always determines an increase of the internal actions. Within the elastic range, P- $\Delta$  effects are not always significant; on the contrary they cannot be neglected in the seismic design of structures [2,3,4,5,6,7,8]: in particular, this is the case of steel structures [9,10].

The ultimate conditions of steel frames under seismic loads are mainly related to the rotational capacity of members, which value is limited by the overall stability phenomena of the member as a whole and by the local buckling of the compressed parts of its cross section [11,12]. In addition, from the global point of view, vertical loads influence the shape of the horizontal forces versus deflection curve. In fact the slopes both of the increasing elastic branch and of the softening plastic one are affected by the magnitude of the ratio between vertical and critical load of columns. Both aspects, local and global, play an important role on the dynamic inelastic behaviour of structures.

Geometrical non-linearity interacts with the mechanical non-linearity, due to the yielding of dissipative zones, leading to an increase of the required ductility in order to prevent collapse [6,7,8,10,13].

In addition, it is very important to forecast the collapse mechanism in order to correctly foresee not only the damage concentration, but also the amplification of the ductility demand due to P- $\Delta$  effect. In order to obtain a collapse mechanism of the global type, modern seismic codes

provide simple design rules based on the amplification of the stresses for which columns must be dimensioned. As it has been pointed out in [14,15], the use of these simple «Column Overstrength Factors» (COF) seems to be unsatisfactory. It has been observed that the control of the failure mode is very important in order to limit the values of the slope of the softening branch of the multiplier of horizontal forces versus top displacement curve, which is related to the influence of P- $\Delta$  effects.

In spite of the problem of evaluating the overall stability effects in steel structures under seismic loads has attracted significant attention and the research efforts have provided a great amount of informations, a very small part of these results has been codified. In fact, in seismic codes the provisions regarding the influence of the geometric non-linearity are insufficient, because they are based on the extension of static elastic results.

This paper is devoted to the presentation of the results obtained by the italian research group in analysing the influence of the overall stability phenomena on the inelastic response of steel frames under seismic loads.

In particular, the attention is focused on the possibility to take into account the increase of the structural damage under seismic loads, due to second order effects, by reducing the q-factor of the examined structural type by means of a coefficient  $\phi$ , which depends on the level of geometric non linearity. This approach has been introduced in [10] and a statistical evaluation of the reduction factor  $\phi$  has been performed in [13] for the SDOF system.

The comparison between the values of the reduction factor  $\phi$  obtained from the SDOF analysis and the ones computed by means of the numerical simulation of the seismic response of MDOF systems has proved that the above approach can be usefully adopted for estimating second order effects in actual steel frames.

After some conclusive remarks, the last part of the paper is devoted to the presentation of the future activities of the italian research group.

## 2 - SEISMIC CODE PROVISIONS FOR SECOND ORDER EFFECTS

It has already evidenced that the existing seismic codes have adopted just a small part of the research results which have been obtained in analysing the overall stability effects in seismic resistant steel frames. This is mainly due to the fact that the most rational way for taking into account the influence of the second order effects consists on their inclusion in the definition of the q-factor design value, but this procedure is not directly provided in seismic codes and no mention is made for its rational evaluation.

At the moment, the provisions are mainly limited to the extension of the rules for non-seismic zones. In fact, the only check provided in EC8 [16] regarding second order effects states that P- $\Delta$  effect can be neglected when, for each floor, the following relation is satisfied:

$$\Delta_e < \frac{V h}{10 N} \quad (1)$$

being:

- $\Delta_e$  the elastic interstorey drift;
- h the distance between the floors;
- V the total shear force acting above the considered floor;
- N the total axial force acting above the considered floor.

This provision is coincident with the one provided in Eurocode 3 [17] and it is the same given in UBC91 [18].

The above recommendation is substantially equivalent to state that P- $\Delta$  effects have to be taken into account when the critical elastic multiplier of the vertical loads  $\alpha_{cr}$  is less than 10.

A more severe provision is given in ECCS Recommendations [19] where the relation (1) is applied with reference to the inelastic displacements. The inelastic displacements can be estimated from the elastic ones by means of the relation:



$$\Delta_p = q \Delta_e \quad (2)$$

being  $\Delta_p$  and  $\Delta_e$  the inelastic and elastic drifts respectively and  $q$  the design value of the  $q$ -factor. This relation is based on the so-called «theory of ductility factor».

As a consequence according to ECCS, P- $\Delta$  effects can be neglected when, for each floor, the following relation is verified:

$$\Delta_e < \frac{V h}{10 q N} \quad (3)$$

which is substantially equivalent to state that  $\alpha_{cr}$  has to be greater than  $10q$ .

A different approach is provided in the Mexican Seismic Code [20] where, in order to take into account the overall stability effects, the design forces have to be amplified by means of a coefficient depending on the magnitude of vertical loads. The amplification coefficient is given by:

$$\alpha = \frac{1}{1 - \mu \gamma} \quad (4)$$

being  $\mu$  the available ductility and  $\gamma$  the stability coefficient (see par.3).

### 3 - OVERALL STABILITY EFFECTS IN SDOF SYSTEMS

#### Mechanical model

The simplified model adopted for numerical analyses consists on the SDOF system with geometrical degradation (fig.1).

The hysteretic model is the elastic-perfectly plastic one. Due to geometrical and mechanical non-linearities, the lateral strength depends upon the horizontal displacement  $x$  and it is influenced by the vertical load  $N$ . The stiffness corresponding to the elastic increasing branch is given by:

$$K = K_0 (1 - \gamma) \quad (5)$$

being  $K_0$  the value the elastic stiffness in absence of vertical loads. The parameter  $\gamma$ , known as «stability coefficient», takes into account the level of vertical loads. In particular, for frames failing in global mode, the stability coefficient  $\gamma$  can be approximatively evaluated by the simplified relation:

$$\gamma = \frac{1}{\alpha_{cr}} \quad (6)$$

The slope of the softening plastic branch is  $-K_0\gamma$ .

Denoting with  $\omega$  and  $\nu$ , respectively, the frequency and the viscous damping of the system, the motion equation for the elastic branch is given by:

$$\ddot{x} + 2\nu\omega\dot{x} + \omega^2(1-\gamma)(x - x_{y,j}) = -a(t) \quad (7)$$

while for the plastic branch it becomes:

$$\ddot{x} + 2\nu\omega\dot{x} + \omega^2(x_y - \gamma x) = -a(t) \quad (8)$$

being  $a(t)$  the considered accelerogram,  $x_y$  the first yielding displacement and  $x_{y,j}$  the intersection between the elastic branch and the displacement axis (initially  $x_{y,j}=0$ ).

#### Numerical analyses

Numerical analyses have been carried out by using a computer program specifically developed [10,13]. In a first stage of the research, ten artificial accelerograms have been considered; they have been generated from the elastic design response spectrum which corresponds to the one given in EC8 with the numerical parameters of the new italian code GNDT. Thirty different values, appropriately selected, of the design level ( $F_y/Ma$ ) have been considered and the ductility demand  $x_{max}/x_y$  has been computed by varying the period of vibration from 0.1 to 2.0 sec. The

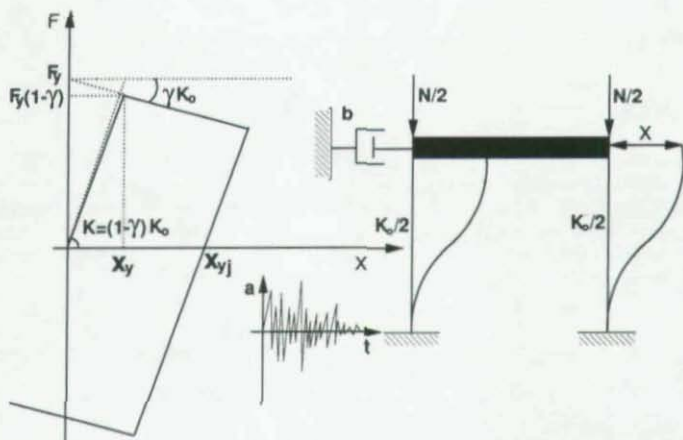


Fig.1 - The mechanical model adopted for numerical analyses

analyses have been repeated for values of the stability coefficient  $\gamma$  equal to 0, 0.025, 0.05, 0.075, 0.1, 0.15 and 0.20.

The outcome of the analyses [13] is the reduction factor  $\phi$  given as the ratio between the inelastic response spectrum in absence of geometrical non-linearity ( $\gamma=0$ ), for a given value of the ductility demand, and the one computed including P- $\Delta$  effect ( $\gamma \neq 0$ ). This approach, therefore, allows the evaluation of the q-factor  $q(\gamma)$ , including P- $\Delta$  effect, from the one  $q(\gamma=0)$  computed neglecting geometrical non-linearity as stated by the following relation:

$$q(\gamma) = \frac{q(\gamma=0)}{\phi} \quad (9)$$

The reduction spectra, computed for a given value of the available ductility and averaged for the ten considered accelerograms, are plotted in fig.2 for some values of the stability coefficient  $\gamma$ . These spectra are characterized by the presence of a period range corresponding to a peak response, probably related to the shape of the elastic response spectrum adopted in earthquake generation, and by the existence of a period range ( $T \geq 0.5$ sec) where the reduction factor  $\phi$  can be practically considered independent from T.

Therefore, in this range which is of particular importance for steel structures, the following relation can be adopted:

$$\phi = \phi(\mu, \gamma) \quad (10)$$

According to Cosenza, Faella and Piluso [13] the investigation on the quantitative assessment of the relation (10) led to the following formulation:

$$\phi = \frac{1 + \psi_1(\mu - 1)\psi_2\gamma}{1 - \gamma} \quad (11)$$

where the coefficients  $\psi_1$  and  $\psi_2$  can be obtained from the analysis of results by means of numerical regression. The mathematical structure of equation (11) has been chosen so that  $\phi$  tends to infinity in the case  $\gamma=1$ , which represents the case of static instability. Moreover eq.(11) provides  $\phi = 1$  for  $\gamma = 0$ , which corresponds to the absence of geometric non-linearity, and

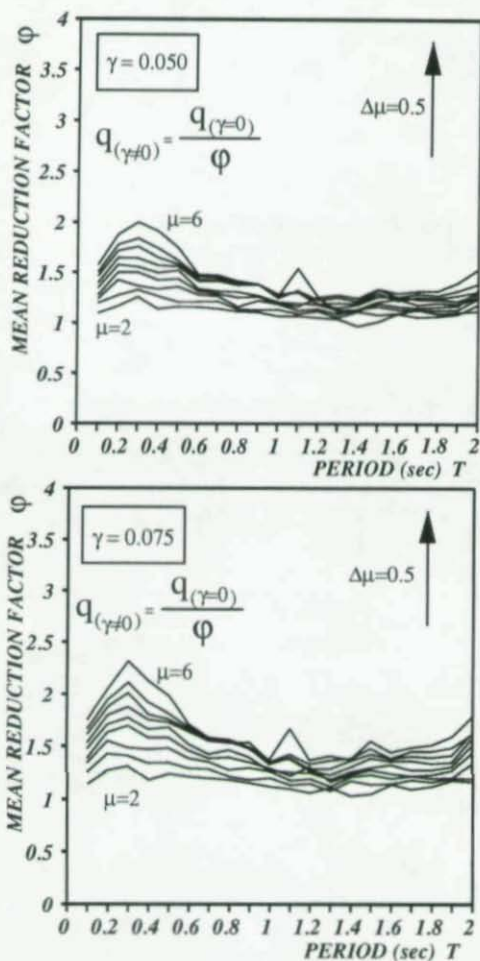


Fig.2 - Reduction factor spectra

$\phi = \nu(1-\gamma)$  for  $\mu = 1$ . This last result corresponds to the reduction of the yield level, due to P- $\Delta$  effect, from  $F_y$  to  $F_y\phi = F_y(1-\gamma)$  (fig.1).

It has to be pointed out that the range of applicability of eq.(11) is defined by the condition:

$$\mu\gamma < 1 \quad (12)$$

which assures the absence of dynamic instability [9].

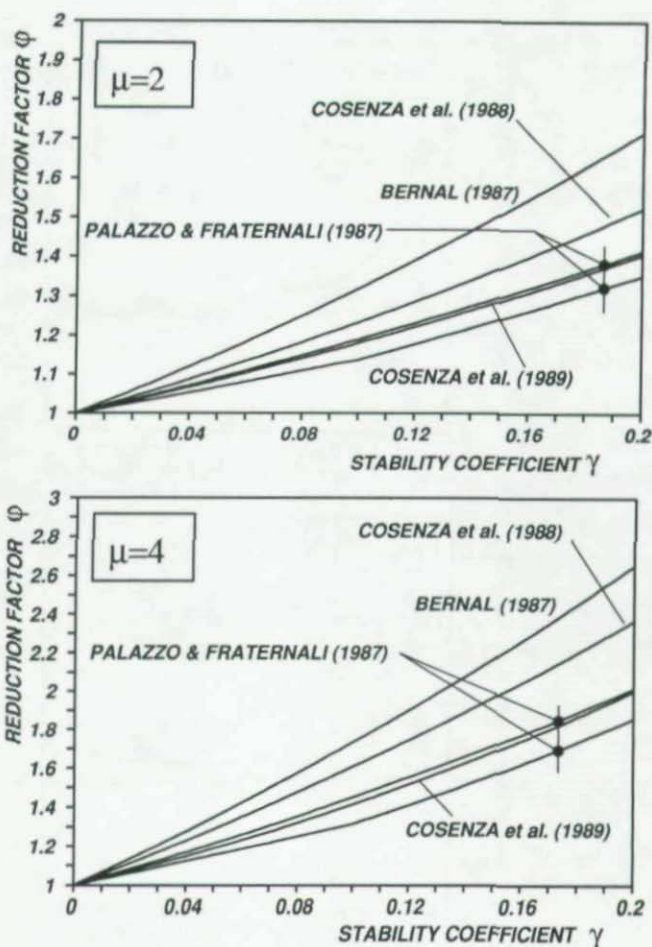


Fig.4 - Comparison among different formulations

A regression analysis [13] has shown that, for  $T=0.5$  sec, the mean values of  $\phi$  can be obtained from equation (11) by adopting  $\psi_1=0.62$  and  $\psi_2=1.45$ . The corresponding curves are represented in fig.3a, where the condition leading to dynamic instability is also pointed out. With reference to the characteristic values of  $\phi$ , the regression analysis has provided  $\psi_1=3.79$  and  $\psi_2=0.75$  and the corresponding representation is given in fig.3b.

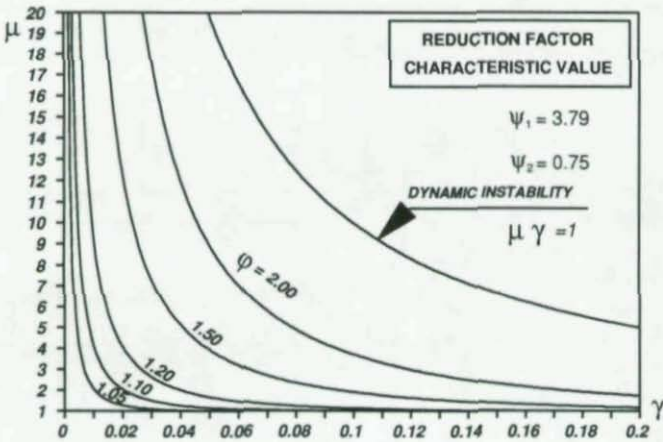
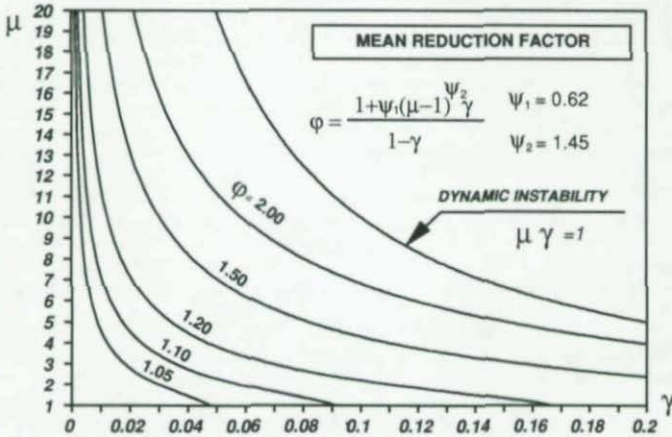


Fig.3 - Representation of the proposed formulation for the evaluation of the reduction factor  $\varphi$



#### Comparison among different formulations

The mean values of the reduction factor  $\phi$  evaluated according to the proposal of Cosenza, Faella and Piluso (1989) [13] by means of eq.(11), with the coefficient previously given, are compared in fig.4 with the formulations proposed by various Authors [7,8,10].

We observe that the above results are less onerous than the ones obtained in [10] by the same Authors, because a more accurate consideration of the period influence has been successively introduced. The results are in good agreement with the ones provided in [8], where the study of the dependence of the q-factor upon  $\mu$ ,  $\gamma$  and  $T$  is faced. These curves cover the period range between 0.35 sec (upper curve) and 2.0 sec (lower curve), excluding, therefore, the lowest periods where some peak amplifications can arise. The small width of this band representing the period influence seems to confirm that  $\phi$  can be considered with good approximation independent upon  $T$ .

Finally, with reference to the formulations given in [7], it has to be pointed out that they have been obtained exclusively from the analysis of historical earthquake records and without introducing limitations regarding the period range and, as a consequence, including the effects of critical values of the period leading to peak amplifications of the ductility demand and, therefore, to a larger reduction of the q-factor. The reasons explained above justify the more onerous result obtained by Bernal.

Other comparisons between the outcome of the analyses carried out both for historical and generated earthquakes have confirmed that the second order effects in seismic resistant steel frames can be conveniently taken into account by means of the reduction factor  $\phi$  [13].

#### 4 - OVERALL STABILITY EFFECTS IN MDOF SYSTEMS

Mazzolani, Guerra and Piluso [21] have investigated the possibility to extend the results obtained for the SDOF system to multistory frames. Dynamic inelastic analyses, which have been carried out by means of the computer program DRAIN-2D [22], have been performed in order to analyze the seismic response of the frames shown in fig.5 taking into account the P- $\Delta$

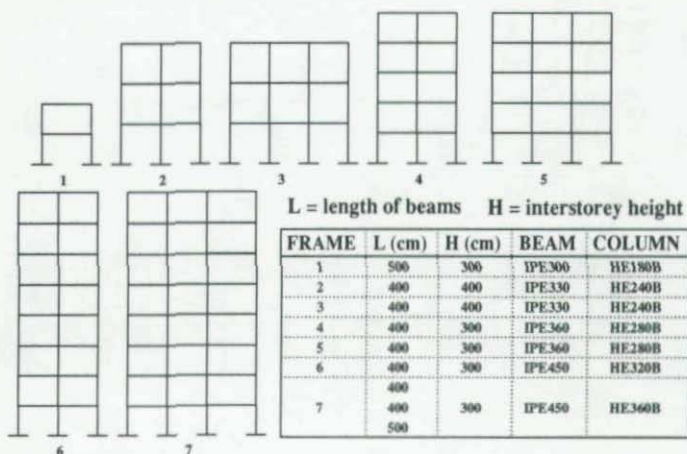


Fig.5 - Analysed frames

effect. Three simulated accelerograms have been used. Each of them has been amplified until collapse, so that the ultimate peak ground acceleration has been evaluated. Successively, with the same amplified earthquake accelerogram, the structures have been analysed again by neglecting geometric non-linearity. As a consequence, a new value of the multiplier of the peak ground acceleration leading to collapse (which is greater than the previous one) has been evaluated for each frame.

The comparison with the previous values, obtained taking into account geometrical non-linearity, provides the reduction factor  $\phi$  of the structural factor  $q$ , due to the effect of vertical loads. These values  $\phi_c$  are provided in tab.1 where are compared with the mean values  $\phi_m$  and the characteristic values  $\phi_k$  provided by eq.(11). In the same table the values of the available

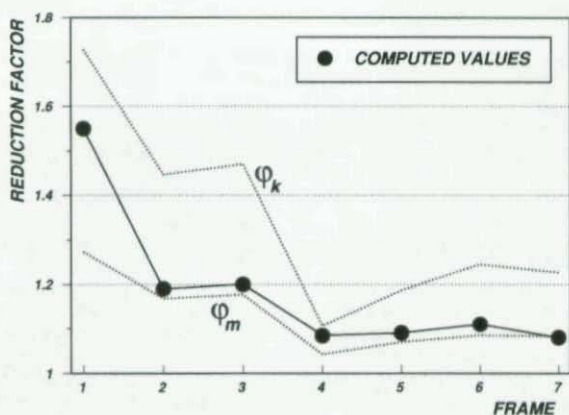


Fig.6 - Comparison between predicted values and computed values of the reduction factor  $\phi$  of the  $q$ -factor

FRAME	$\gamma$	$\mu$	$\phi_m$	$\phi_k$	$\phi_c$
1	0.0853	3.185	1.273	1.728	1.550
2	0.0534	3.233	1.168	1.447	1.190
3	0.0560	3.236	1.177	1.470	1.200
4	0.0117	3.703	1.043	1.106	1.085
5	0.0223	3.331	1.071	1.186	1.091
6	0.0372	2.581	1.085	1.245	1.110
7	0.0321	2.771	1.083	1.226	1.080

Tab.1 - Comparison between predicted values and computed values of the reduction factor  $\phi$  of the  $q$ -factor

$\mu$	$\varphi_{lim}=1.05$	$\varphi_{lim}=1.10$	$\varphi_{lim}=1.20$
2	0.030	0.058	0.110
4	0.012	0.024	0.047
6	0.007	0.013	0.026

**Tab.2 - Maximum values of the stability coefficient  $\gamma$  for different values of the available ductility  $\mu$  with respect to a given limit value  $\varphi_{lim}$**

global ductility  $\mu$  of the equivalent SDOF system and the slope  $\gamma$  of the softening branch of the  $\alpha$ - $\delta$  curve, which have been obtained by means of static inelastic analyses, are also shown.

The comparison between the actual values of the reduction factor  $\varphi_c$  with the ones provided by equation (11) is given in fig.6. A very good agreement with the forecasts based on the SDOF (relation 11) can be observed for all the examined frames (MDOF systems). In fact, the computed reduction factor values fall within the interval between  $\varphi_k$  and  $\varphi_m$  and are mainly close to the lower bound. The width of

this interval increases as far as the value of  $\gamma$  increases (see table 1).

### 5 - THE INFLUENCE OF GEOMETRIC NON-LINEARITY

From the design point of view, it is important to find out in which cases the geometrical non-linearity is negligible. We can use the definition of a limit value of the reduction factor. We define  $\varphi_{lim}$  as the mean value of the reduction factor, which separates cases in which P- $\Delta$  effects can be neglected ( $\varphi < \varphi_{lim}$ ) from cases in which geometrical non-linearity has to be included into the analysis ( $\varphi > \varphi_{lim}$ ).

Equation (11) provides the maximum values of the stability coefficient  $\gamma$ , for any given value of the available ductility  $\mu$  and with respect to a given limit value  $\varphi = \varphi_{lim}$ . These maximum values of  $\gamma$  are given in tab.2 for a limit level of the q-factor reduction equal to 1.05, 1.10 and 1.20, respectively.

Therefore, it can be pointed out that, even if a 20% q-factor reduction is considered negligible then, by assuming as an example the value 6 for the available ductility, the maximum value which can be reached by the stability coefficient  $\gamma$  is 0.026 (tab.2) and, therefore, according to eq.(6) a value about of 40 is required for the critical elastic multiplier of vertical loads.

In other words the effects of geometrical non-linearity are, in general, not negligible. Exception is made for cases in which the ratio between the value of the design vertical loads and the one corresponding to their critical value is very small. With reference to this problem it is useful to point out that EC8 and UBC91 provide, as already mentioned, the value  $\alpha_{cr}=10$  as the upper limit which defines cases in which P- $\Delta$  effects have to be investigated. The corresponding value of  $\gamma$  is 0.1 which provides, for  $\mu=6$ , a reduction factor about of 1.80 (fig.3a). It seems that 45% reduction (1/1.80) of the q-factor, due to overall stability effects, is not at all negligible!

A more rational provision is given by ECCS Recommendations, where the control of the P- $\Delta$  effects is made on the base of the estimate of the inelastic displacements. In case of moment-resisting frames, taking into account that  $q=5\alpha_w/\alpha_y=5 \times 1.2=6$ , second order effects have to be taken into account when  $\alpha_{cr}$  is approximately less than 60, which corresponds to  $\gamma$  approximately greater than 0.017. This last value, by approximately assuming  $q=\mu=6$  (according to the theory of ductility factor) corresponds to a reduction of the q-factor of about 10% (1/1.13, see tab.2). Therefore, it can be concluded that the provision given by ECCS Recommendations allows a more correct prediction of cases for which P- $\Delta$  effects can be neglected.

### 6 - CONCLUSIVE REMARKS

The quantitative evaluation of the reduction of the q-factor in order to take into account P- $\Delta$  effects due to vertical loads can be provided by means of the formulation obtained for the SDOF system, which has been proved to give a good approximation also in the case of multistory frames.



In addition, this formulation is suitable to grasp cases in which geometrical non-linearity must be taken into account. In fact the formulation herein explained also provides, for a given limit value of the reduction factor  $\phi_{lim}$  of the structural coefficient  $q$  and for a given ductility  $\mu$ , the upper bound of  $\gamma$  and, therefore, the lower bound of the limit elastic multiplier  $\alpha_{cr}$  of the frame.

Among the provisions given by different seismic codes, the ones of the ECCS Recommendations seem to allow the most correct prediction, even if particularly severe, of cases in which P- $\Delta$  effect can be neglected.

We also point out that the collapse mechanism type plays an important role affecting the value of the stability coefficient  $\gamma$  and, therefore, the magnitude of the reduction of the  $q$ -factor due to geometrical non-linearity.

## 7 - FUTURE ACTIVITIES

In many cases, the ductility demand does not represent a sufficient parameter to characterize the structural damage, because it doesn't take into account neither the number of load reversals nor the plastic engage required by each cycle. For this reason, new parameters have been proposed in order to evaluate the structural damage under seismic loadings.

As the interpretation of the structural failure can require different damage index depending on the type of loading history and on the structural typology, it is necessary to examine how the above mentioned reduction factor  $\phi$  could be influenced by the choice of the damage index to be assumed for the damage characterization. Therefore, the future activities will be focused on the evaluation of the influence of the P- $\Delta$  effect on the most commonly used parameters for the damage characterization such as: cinematic ductility, cyclic ductility, hysteretic ductility, Park & Ang damage index [23] and low cycle fatigue index [24]. The purpose of this new analysis is represented by the formulation of a general validity relation for the reduction factor  $\phi$  in the form  $\phi = \phi(D, \gamma)$ , where  $D$  represents a generic damage parameter which has to be assumed on the base of the structural material and the structural typology [25].

It is well known that among the steel structural typologies there are some of them in which second order effects can represent the dominant design problem; this is the case of semi-rigid sway frames. In fact, in this typology, the connection deformability leads to a reduction of the lateral stiffness which determines, on one hand, an increase of the geometric non-linearity effects and, on the other hand, an increase of the period of vibration. These variations, taking into account the spectral shapes given in seismic codes, which are characterized by a softening branch where the spectral amplitude decreases as far as the period of vibration increases, lead to effects which are opposite in sign and the corresponding magnitude has to be evaluated in order to understand the essence of the seismic performance of semirigid sway frames [26].

Therefore, it is clear that there is a strong interaction between the research activities dealing with the influence of the P- $\Delta$  effect on the seismic behaviour of steel structures and the ones referring to the overall seismic behaviour of semirigid sway frames.

## 8 - REFERENCES

- [1] *A. De Luca, C. Faella, V. Piluso*: «Stability of Sway Frames: Different Approaches Around the World», ICSAS91, International Conference on Steel and Aluminium Structures, Singapore, 22-24 May, 1991.
- [2] *R. Husid*: «The Effect of Gravity on the Collapse of Yielding Structures with Earthquake Excitation», IV WCEE, Santiago, Chile, 1969.
- [3] *C.K. Sun, G.V. Berg, R.D. Hanson*: «Gravity Effect on Single Degree Inelastic System», Journal of Mechanical Division, ASCE, February, 1973.
- [4] *F. Braga, A. Parducci*: «Plastic Deformations Required to R/C Structures During Strong Earthquakes - Influence of the Mechanical Decay by Taking into Account P- $\Delta$  Effect», VI ECEE, Dubrovnik, Yugoslavia, September 18-22, 1978.

- [5] **S. Mahin, V. Bertero**: «An evaluation of inelastic seismic design spectra», Journal of the Structural Division, ASCE, September, 1981.
- [6] **G. Al Sulaimami, J.M. Roesset**: «Design Spectra for Degrading Systems», ASCE, Journal of Structural Engineering, Vol.115, 1985
- [7] **D. Bernal**: «Amplification Factors for the Inelastic Dynamic P- $\Delta$  Effects in Earthquake Analysis», Earthquake Engineering and Structural Dynamics, Vol.15, 1987.
- [8] **B. Palazzo, F. Fraternali**: «L'Influenza dell' Effetto P- $\Delta$  sulla Risposta Sismica di Sistemi a Comportamento Elastoplastico: Proposta di una Diversa Formulazione del Coefficiente di Struttura», Giornate Italiane della Costruzione in Acciaio, CTA, Trieste, Ottobre, 1987.
- [9] **E. Cosenza**: «Duttilità Globale delle Strutture Sismoresistenti in Acciaio», Ph.D. Thesis, Napoli, Aprile, 1987.
- [10] **E. Cosenza, A. De Luca, C. Faella, V. Piluso**: «A Rational Formulation for the q-factor in Steel Structures», paper 8-4-11, Vol.V, IX WCEE, Tokyo-Kyoto, August 2-9, 1988.
- [11] **I.Mitani, M.Makino**: «Post Local Buckling Behaviour and Plastic Rotation Capacity of Steel Beam-Columns», 7th. WCEE, Istanbul, 1980.
- [12] **H.Akiyama**: «Earthquake-Resistant Limit State Design for Buildings», University of Tokyo Press, 1985.
- [13] **E. Cosenza, C. Faella, V. Piluso**: «Effetto del Degrado Geometrico sul Coefficiente di Struttura», IV Convegno Nazionale, L'Ingegneria Sismica in Italia, Milano, Ottobre, 1989
- [14] **R. Landolfo, F.M. Mazzolani, M. Perneti**: «L'influenza dei criteri di dimensionamento sul comportamento sismico dei telai in acciaio», IV Convegno Nazionale, L'Ingegneria Sismica in Italia, Milano, Ottobre, 1989
- [15] **R. Landolfo, F.M. Mazzolani**: «The consequence of the design criteria on the seismic behaviour of steel frames», 9th ECEE, Moscow, 11-16 September 1990.
- [16] **Commission of the European Communities**: «Eurocode 8: European Code for Seismic Regions», 1988.
- [17] **Commission of the European Communities**: «Eurocode 3: Design of Steel Structures», 1992.
- [18] **UBC91**: «Uniform Building Code», International Conference of Building Officials, Edition 1991.
- [19] **ECCS (European Convention for Constructional Steelwork)**: «European Recommendations for Steel Structures in Seismic Zones», 1988.
- [20] **IAEE**: «Earthquake Resistant Regulations: A World List», compiled by the International Association for Earthquake Engineering, 1984.
- [21] **C.A. Guerra, F.M. Mazzolani, V. Piluso**: «Overall Stability Effects in Steel Structures Under Seismic Loads», 9th ECEE, Moscow, 11-16 September 1990.
- [22] **G.H. Powell**: «Drain-2D User's Guide», Earthquake Engineering Research Center, University of California, Berkeley, September 1973.
- [23] **Y.J. Park, A.H.S. Ang**: «Mechanic Seismic Damage Model for Reinforced Concrete», ASCE, April 1985.
- [24] **H. Krawinkler, M. Zohrei**: «Cumulative Damage in Steel Structures Subjected to Earthquake Ground Motion», Computer & Structures, Vol.16, n.1-4, 1983.
- [25] **C. Faella, O. Mazarella, V. Piluso**: «L'influenza della non-linearità geometrica sul danneggiamento strutturale sotto azioni sismiche», VI Convegno Nazionale, L'Ingegneria Sismica in Italia, Perugia 13-15 Ottobre 1993 (in press).
- [26] **C. Faella, V. Piluso, G. Rizzano**: «Sul comportamento sismico inelastico dei telai in acciaio a nodi semirigidi», VI Convegno Nazionale, L'Ingegneria Sismica in Italia, Perugia 13-15 Ottobre 1993 (in press).



## Column - base connections modeling for cyclic loading

Paul	PENSERINI	Electricite de France, Research and Development Division
André	COLSON	Ecole Nationale Supérieure des Arts et Industries de Strasbourg ( France )

### ABSTRACT

This paper summarizes the principal features of the behavior of usual column base connections tested for various loading conditions. The influence of the normal force-moment interaction is pointed out and evaluated.

An original approach for modeling, based on the concept of behavior mechanism is presented and applied to the column-base connections. The proposed model shows to be in good accordance with experimental results.

Finally, the influence of the column-base end-restraint is evaluated in the case of an isolated column. The results are given in terms of buckling effective length.

### INTRODUCTION

The behavior of column-base connections is not at the moment really well-known. Tests are seldom and show quite different responses for various loading conditions. An investigation for columns subjected to buckling [1] emphasizes the high end restraint capacity of the usual and simple connection with two anchor-bolts. On the opposite ( for cyclic loading ), the same connections act more likely as quasi-pinned [2].

In the first case, the existence of a high normal force (  $N$  ) enables a moment (  $M$  ) to develop at the column footing. In the second case, the lack of stiffness appears for  $M=0$  and  $N=0$  since the loading path is generally obtained by one eccentrically actuator ( fig. 1 ).

In fact, the behavior of column-base connections is greatly influenced by the N-M interaction. In the real structure, the dead loads induce  $N \neq 0$ , therefore the connection should be able of end-restraint capacity

## EXPERIMENTAL DEVICE

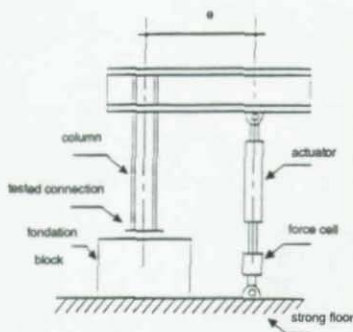


Fig. 1 : single parameter device used by MELCHERS [2]  
This type of testing device leads to a quasi-proportional loading path.

Confronted with this lack of experimental results, it was decided to carry out some tests with two independent actuators ( fig. 2 ) . It is thus possible to obtain any controlled loading path in the  $M - N$  diagram (for example  $N$  constant and cyclic moment paths which are representative of usual loading conditions ). The testing device is fully controlled by a real time computerized synchro-system [3].

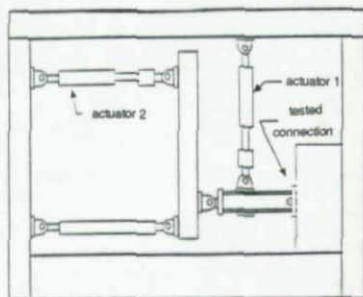


Fig. 2 : view of the device used by PENSERINI and COLSON [4]



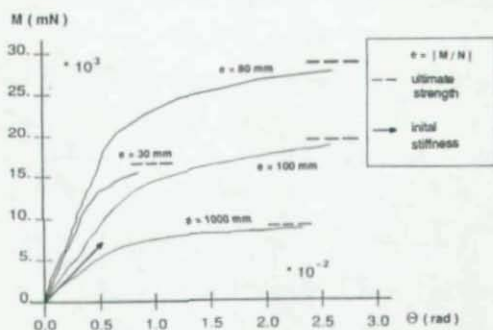


Fig 5 : pinned connection : monotonic loading results

For cyclic loading, the most important feature is the drop of the tangent stiffness, since it can change the stability conditions of the frame. The threshold corresponding to this drop depends on the normal force value (compare Fig. 6 and Fig. 7, see also Fig. 8).

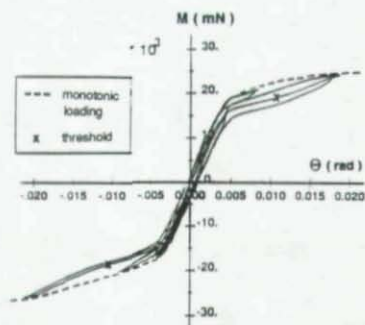


Fig 6 : pinned connection : moment cyclic loading with constant compressive normal force  $N = -233 \text{ kN}$  ( $0.3 N_p$ )

Furthermore, the energy dissipation is very small for the tested specimen since it is due to the plastification of the bolts during the first loading. A clearance is created between the nuts and the plate. This gap resumes when the rotation reaches the threshold value, then the bolts are stressed again and the tangent stiffness increases. This behavior is emphasized in the case of a tensile normal-force (Fig. 7) but it appears also for a compressive normal force (Fig. 6). Under the threshold the behavior of the connections is controlled by the contact behavior of the plate on the concrete block.

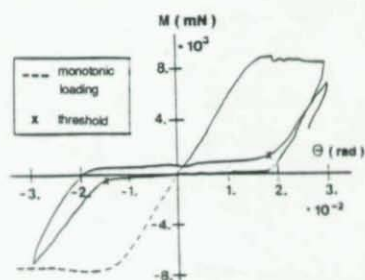


Fig 7 : pinned connection : moment cyclic loading with constant tensile normal force  $N = 9.1 \text{ kN}$

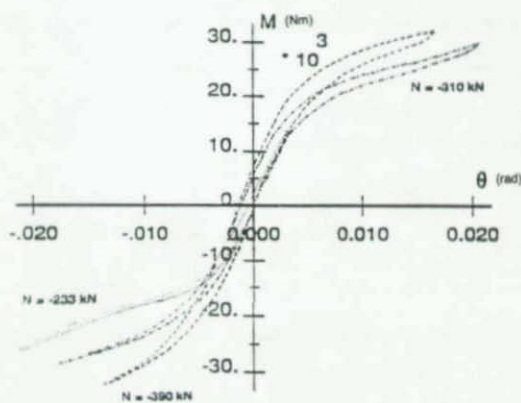


Fig 8 : pinned connection : behavior for cyclic loading.

#### FIXED COLUMN-BASE CONNECTIONS

The behavior of the fixed column-base connection is qualitatively the same as for the pinned connection either for monotonic or cyclic loading ( Fig. 9 )



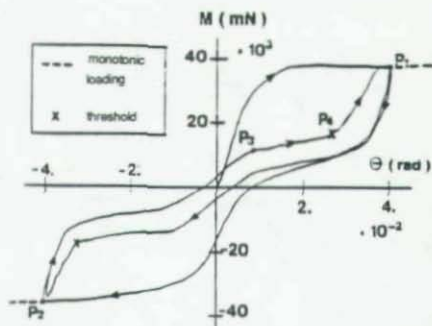


Fig. 9 : fixed connection : moment cyclic loading with constant compressive normal force  $N = -148 \text{ kN}$

For the tested specimen, the threshold phenomenon is due to the plastification of the anchor-bolts.

## CONCLUSION

The monotonic loading tests show that the behavior of column-base connections, either pinned or fixed is typically semi-rigid. The behavior is non linear at the beginning of loading, with an initial tangent stiffness and asymptotic before failure at the ultimate strength. The values of the initial stiffness and of the ultimate strength are strongly dependent of the normal force value.

The cyclic loading tests show that the energy dissipation is negligible ( for the tested specimen ) and point out a zone of the  $M-\phi$  curve where the tangent stiffness is quasi zero. This zone is followed by a sharp increase of the tangent stiffness when the contact between the nuts and the plate resumes.

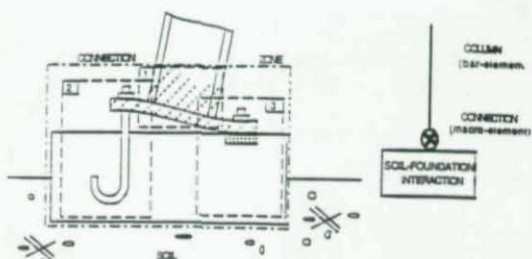
## MODELING

For modeling, the overall connection is replaced by a macro-element. This concept is consistent with frame analysis computer programs since the behavior of the connection zone is concentrated at a punctual node ( Fig. 10 ).

A new approach for modeling is proposed. It is based on the concept of behavior mechanism.

The aim is to divide the connection in some elementary groups of components, the behavior of which is independent.

Each mechanism is the association of the relevant physical phenomena with a group of connection components. The application of the method to column-base connections exhibits three different mechanisms ( Fig. 10 ).



Mechanism	1	2	3
Connection components	Plate Column Welding	Plate Anchor-bolts Concrete surrounding the anchor-bolts	Concrete under the plate-concrete contact area
Physical phenomena	Elasticity Plasticity	Elasticity Plasticity Damage of concrete	Elasticity Damage of concrete
	Residual stresses Stress concentration	Residual stresses Stress concentration	Contact behavior

Fig. 10 : proposed approach for modeling of column-base connections.

### MODELING OF THE MECHANISMS

Each mechanism is modelled in a global manner using the initial tangent stiffness ( $E$ ), ultimate limit strength (ULS) and non linearity ( $a$ ) parameters. The proposed models are therefore simple and describe the main physical features of the mechanism behavior ( Fig. 11 ).

The first mechanism, which contains only steel components, is modelled using an isotropic plasticity theory adapted to solicitations ( $N, M$ ) and displacements ( $u_1, \theta_1$ ). The influence of simultaneous plasticity and damage in the second mechanism is described for the unloading behavior by a unique scalar parameter,  $\alpha$ . The non linearities in the third mechanism due to damage and contact behavior are treated as a whole ( scalar  $a_3$ ). The unloading behavior depends on the loading level reached by the first loading and on the sensitivity of the concrete and of the contact zone to damage (scalar  $r_3$ ). The behavior of the connection is obtained by a statically admissible assembling of the mechanisms behaviors. The analytical formulations of the models are detailed in reference[4]

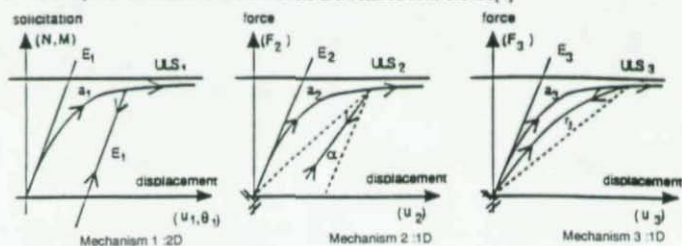


Fig.11 : modeling of mechanism's behaviors

The formulations for mechanisms 1 and 2 are reported here for example. For a moment monotonic loading with  $N=0$ , the displacements of mechanism 1 are :

$$u_1 = 0 \quad \Theta = \frac{M}{E_M \left[ 1 - \left( \frac{eM}{M_u} \right)^{\alpha_1} \right]}$$

for mechanism 2, the displacement for loading and unloading is respectively :

$$s_2 \geq \bar{s}_2 \quad u_2 = \frac{F_{u2}}{E_2} \left[ \frac{s_2}{1 - s_2^2} \right] \quad s_2 < \bar{s}_2 \quad u_2 = \frac{F_{u2}}{E_2} \left[ \frac{\alpha s_2^2 (\bar{s}_2 - s_2) + s_2}{1 - s_2^2} \right]$$

with  $s_2 = \frac{F_2}{F_{u2}} \quad \bar{s}_2 = \frac{\bar{F}_2}{F_{u2}}$

**ASSEMBLING : ULS of the connections**

The assembling of the three mechanisms is presented to define the Ultimate Limit Strength of the connection. The ULS of the connection without the bolts that is also when there is a gap between the nuts and the plate is calculated by a limit analysis approach [5]. The stress field associated with the statical theorem is shown in Fig. 12 :

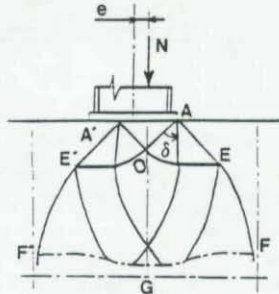


Fig 12 : Stress field for statical limit analysis approach

To explain the influence of anchor-bolts, we consider Fig. 13. For a pinned connection,  $da=0$ , and for a fixed connection,  $da \neq 0$ . The column is in compression. The equilibrium conditions are :

$$N_a + F_b = N_c$$

$$F_b * d_a + N_c * e' = N_a * e$$

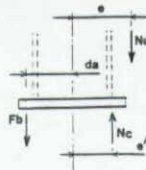


Fig 13 : Equilibrium for column in compression.

$F_b$  : action of the bolts  
 $N_c$  : action of the concrete block  
 $d_a$  : position of the bolts

In the diagram, the point  $(N_c, e', N_c)$  belongs to the ULS curve of the "connection without the bolts". So, to get the highest value of  $M_u = N_c e$ ,  $F_b$  must take its highest value. This value is related to the plastification of the bolts under pure tension or to the failure of the plate. The plate ultimate limit strength is calculated by a yield line method. The previous relations are shown in Fig.14. For decreasing eccentricity, AC becomes tangential to the ULS curve of the "connection without the bolts". So, for eccentricities smaller than that at this point of contact, the anchor-bolts are not loaded.

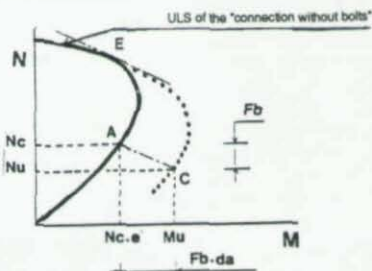


Fig14 : influence of the anchor-bolts.

The ULS of the column ( interaction M-N curve ) is well-known and it is modeled by a parabola taking into account the influence of the welded plate at the column footing. Finally the modeled ULS of the tested pinned connection is obtained ( Fig.15 ). The test results from cyclic moment and constant normal force are reported to the estimated ULS curve.

The experimental threshold values (M, N) corresponding to an important drop in connection stiffness are reported too. We note that these points are near the ULS curve of the "connection without bolts".

Finally, the threshold phenomenon is related to the "connection without bolts" ULS curve, and then can only occur for large eccentricity. These remarks imply that cyclic loading must stay inside the "connection without bolts" ULS curve in order to keep an effective end-restraint capacity and avoid instability phenomena.

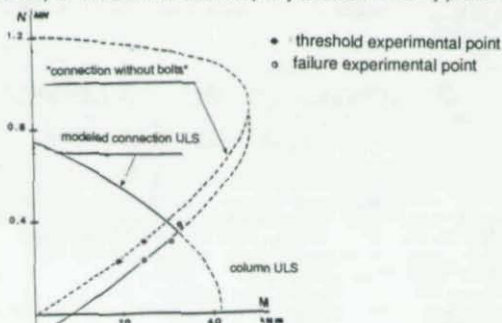


Fig 15 : modeled ULS of the tested pinned connection

The assembling of the mechanisms fulfills the equilibrium equations at each step of loading. The analytical formulation of the assembling is detailed in reference [4].

### COMPARISON WITH CYCLIC TEST RESULTS

The ultimate limit strength parameter are obtained in a predictable way by limit analysis methods [5]. The other parameters are either deduced from material properties or identified from basic tests. This set of values allows the computer simulation of the connection behavior (pinned or fixed) for different loading paths. One simulation result is presented for constant normal force and cyclic moment ( $N = -233$  kN i.e.  $\approx 0.3 N_p$  of the column) and compared with the test result ( Fig 16 ). The predicted behavior describes quite accurately the real behavior. The model describes the N-u (N normal force, u associated displacement) behavior too, but, for practical purpose, only the M- $\theta$  curve is required.

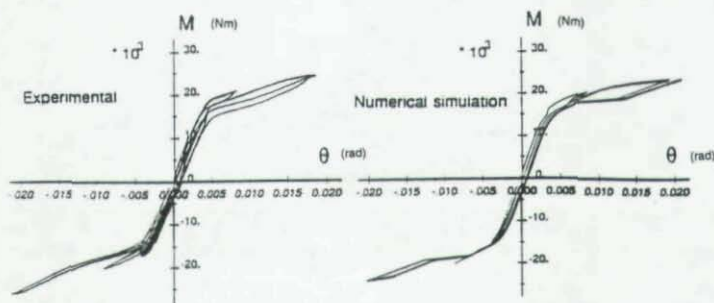


Fig 16 : pinned connection : comparison with test result :  $N = -233$  kN ( compression )

### INFLUENCE OF THE COLUMN-BASE END-RESTRAINT : BUCKLING OF THE COLUMN.

An "academic" example is proposed to show the influence of the column-base end-restraint on the buckling strength of the column ( Fig. 17 ). The problem has been calculated with the PEP-micro program of the CTICM [6] [7]. The column is a normalised HEA 140 profile bent with respect to his strong inertia axis. It is divided in twenty sections of equal length ( 21 nodes ) and its initial imperfection is a sine curve. The connection at the top is a perfect articulation. The connection at the bottom is either perfectly pinned or perfectly fixed or semi-rigid ( Fig. 18 ).

Two semi-rigid base connections are used in order to define the bounds of the connection behavior measured by the tests. We must notice that for small excentricities the monotonic behavior of the "fixed" or the "pinned" connection is bounded by the behavior of connection 1 and connection 2 since the bolts are not activated.



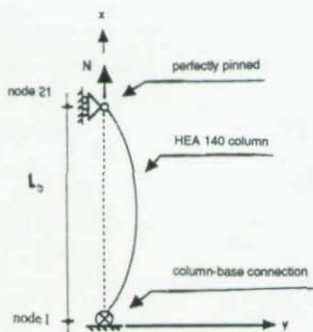


Fig 17 : Proposed buckling problem

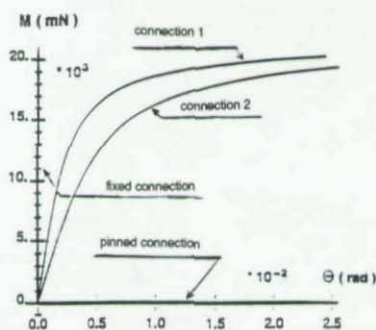


Fig 18 : Column-base models used in calculus

The initial stiffness  $R_0$  is respectively for connections 1 and 2 equal to  $6 \cdot 10^3$  mkN/rad and  $3 \cdot 10^3$  mkN/rad. The semi-rigid behavior is modeled in the PEP program by :

$$\theta = \frac{M}{R_0} \frac{1}{1 - \left(\frac{M}{Mu}\right)^a}$$

with  $M_u$  : ULS moment equal to 21 mkN  
and  $a$  : non linearity parameter equal to 3

The numerical results are reported in Table 1 using the concept of buckling effective length coefficient  $C_{eff}$ ; i.e. the ratio of the buckling effective length to the column length  $L_0$ .

initial imperfection	length of the column	column-base connection			
		perfectly pinned	perfectly fixed	connection 1	connection 2
$L_0/1000$	3	1.00	0.71	0.71	0.77
	5	1.00	0.71	0.71	0.74
	6	1.00	0.70	0.71	0.78
	7	1.00	0.70	0.74	0.77
$L_0/500$	3	1.00	0.71	0.71	0.80
	5	1.00	0.71	0.71	0.74
	6	1.00	0.71	0.72	0.78
	7	1.00	0.70	0.75	0.79
$L_0/250$	3	1.00	0.72	0.72	0.78
	5	1.00	0.72	0.72	0.75
	6	1.00	0.73	0.75	0.78
	7	1.00	0.73	0.78	0.80

Table 1 : buckling effective length coefficient :  $C_{eff}$ 

The maximum loading eccentricity at the semi-rigid column-base connection is 43 mm; Showing that buckling takes place before the loading of the anchor-bolts. So, the initial hypothesis associated with the column-base behavior used for calculation is satisfied.

The results show that  $C_{eff}=0.8$  should be conservative for the "pinned" connection. Furthermore,  $C_{eff}=0.7$  (theoretical value) for the "fixed" condition may be unsafe since the "fixed" connection does not provide more restraint than the "pinned" one. On the other hand the  $C_{eff}$  value is fairly not dependant on the initial imperfection of the column: showing that the effective length concept is consistent to describe the influence of the base end-restraint.

These results are coarse since the influence of the soil-foundation block interaction is not taken into account. The validity is obviously limited by the reduced slope of the proposed problem.

### CONCLUSION

The behavior of the tested column-base connection for a monotonic loading is really semi-rigid. The  $M-\theta$  behavior is however strongly dependent on the normal force interaction.

An example of buckling problem, shows that for braced frames, the real end-restraint of the "pinned" type connection should be considered since it is the same as that of the "fixed" type. For cyclic loading, the behavior of the column-base connection is far more complicated due to the appearance of unilateral contact phenomena as soon as the excentricity of the load increases.

A model of behaviour, based on the understanding of the physical phenomena involved has been proposed. It has the capability to describe the overall connection behavior and in particular to define the zone of quasi zero tangent stiffness related with the unilateral contact phenomena. The latter point is of peculiar importance since it can modify the stability of the frame. The presented model is implemented for PC computer to simulate the behavior of the usual column base connections.

### REFERENCES

- [1] Beaulieu D.,Picard A., "Contribution des assemblages avec plaque d'assise à la stabilité des poteaux", Construction Métallique, N°2, 1985
- [2] Melchers R. E., "Modeling of column-base behavior", Connections in Steel Structures : behavior, strength and design., Elsevier Applied Science, 1988.
- [3] Colson A., Penserini P., Pilvin P., "Pour une utilisation optimale des interfaces structures métalliques-fondations : méthode d'essai, modélisation", RILEM, 1er congrès international, 1987.
- [4] Penserini P., "Caractérisation et modélisation du comportement des liaisons structure métallique-fondation", Thèse de doctorat de l'Université Paris 6, 1991.
- [5] Penserini P., Colson A., "Ultimate limit strength of column-base connections" J. of Construct. Steel Research, Vol 14, 1989
- [6] Galéa Y., "Programme d'analyse élasto-plastique non linéaire de structures planes à barre" Construction Métallique, N°4, 1978.
- [7] Galéa Y., Colson A., Pilvin P., "Programme d'analyse de structures planes à barres avec liaisons semi-rigides à comportement non linéaire" Construction Métallique, N°2, 1986.

ULTIMATE STRENGTH OF GEOMETRICALLY  
IMPERFECT ANGLE COLUMNS

S.L. Chan

Department of Civil & Structural Engineering  
Hong Kong Polytechnic, Hong Kong

S. Kitipornchai

Department of Civil Engineering  
The University of Queensland, Australia

## 1. INTRODUCTION

The ultimate strength of a column is influenced by factors such as geometrical imperfection or initial out-of-straightness, residual stress, load eccentricity and end restraint. The first two factors are normally incorporated through the use of appropriate column design curves as specified in various codes [1,3], while the last two factors are normally accounted for in design calculations. Design curves for columns of different cross-sectional shapes and methods of manufacture have been established, based on extensive experimental data. As such, the influences of residual stress and initial out-of-straightness, provided they are within normal bounds, are incorporated empirically in the column design curves.

The angle is one of the most common structural shapes, used widely in light trusses, transmission towers and bracing systems providing lateral support in many structural frames. The failure of an angle compression member is complex, even in the elastic range [2,4-7]. A general angle beam-column may buckle in a flexural, a torsional, or a combined flexural-torsional mode. An accurate method of determining the ultimate load of a structure incorporating angle members must therefore consider all of these buckling modes, taking into account the spread of plasticity across the section and along the member length.

Due to the asymmetrical nature of the angle cross-section, the effects of the initial out-of-straightness in angle columns cannot easily be quantified. The ultimate strengths are not only dependent on the magnitude and the shape of the initial out-of-straightness, but also on its orientation with respect to the section principal axes. The latter effect has not been studied previously.

Fig. 1 shows test results for a series of hot-rolled equal and unequal, concentrically loaded, pin-ended angle columns [6]. The test data show significant variations in the ultimate loads of the tested angle columns. The nature of the geometrical imperfection inherent in angle members might have been one of the main reasons for this. In practice, however, it is difficult to measure imperfections accurately or to quantify the effect experimentally, particularly in angle columns. On the basis of experimental data, Kitipornchai and Lee [6] recommended that SSRC [2] Curve 2 be adopted to provide a lower bound estimate of the ultimate strength of single angle columns.

Based on the geometric stiffness matrix for an angle element previously derived by the authors [7], this paper presents a numerical procedure for geometric and material nonlinear analysis of geometrically imperfect angle columns. This method accounts for the change in the member geometry during

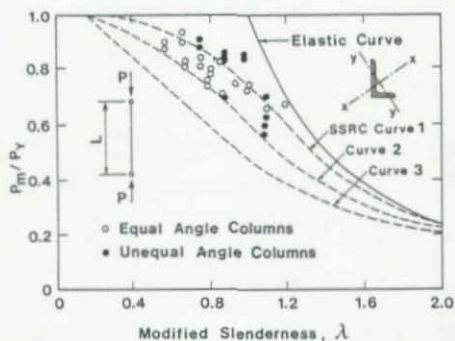


Fig. 1: Experimental ultimate loads for single angle columns

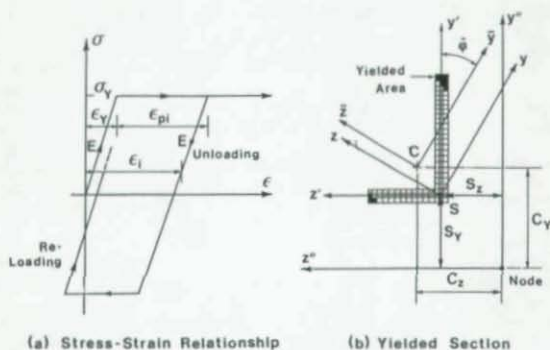


Fig. 2: Stress-strain relationship and yielding of angle section

deformation, the shift in the centroids of the remaining elastic core and the influence of strain-unloading. The method is applied to study the influence of initial out-of-straightness on the ultimate behaviour of single angle columns.

## 2. ANALYTICAL MODELLING

The geometrically nonlinear motion of a deforming member can be described either in an updated or in a total Lagrangian framework. The former has been found efficient [8] because of the ease of including large deflection effects via a continuous updating process for the geometry [9], and the convenience of formulating the rate material tensor.

Basically, there are two main approaches to considering the effects of material yielding in a member [10]. The first model assumes the formation of a plastic hinge when the combined forces in a member exceed a certain yield function. This technique has been used successfully by a number of researchers for the analysis of axisymmetric tubular, symmetric I and other



sections (see, for examples, Refs 11-13). Recently, this approach has been used [14-15] to analyse asymmetric angle member structures. A comparison with experimental results has also been made to validate the theory.

In the second approach, referred to as a mesh or layered idealization, the section of an element is divided into a mesh of a finite number of sub-areas (see Fig. 2). The section properties and resisting forces and moments are calculated by summing up the properties and stresses in these areas. This somewhat more rigorous and accurate technique has been employed successfully by a number of investigators for studies of the nonlinear behaviour of beam-columns (e.g. Refs 15-17) but at the expense of longer computer time. This is because the mesh model reflects more closely the actual behaviour of the member, since the failure of a member usually occurs when the cross-section is partially yielded.

In this paper, the layer or mesh type of idealization is adopted in conjunction with the updated Lagrangian formulation for the member to account for the effect of partial yielding across the section of an element. The material model proposed by the authors [7, 15] allowing for strain-unloading (see Fig. 2(a)) is employed for the consideration of material nonlinearity. The set of nonlinear simultaneous equations is then solved by an incremental-iterative technique. However, to prevent shift of the real path for this type of path-dependent nonlinear problem, the numerical procedure is converted to the pure incremental method once yielding is detected.

Numerical examples are given to validate the present theory against the experiments by Kitipornchai and Lee [6] and to study the influence of the magnitude and orientation of initial out-of-straightness on the ultimate strength of angle columns.

### 3. THEORETICAL DEVELOPMENT

#### 3.1 Assumptions

The following assumptions are made in the theory.

1. Bernoulli's assumption of plane sections before deformation remain plane after deformation occurs.
2. The idealized elastic-perfectly plastic stress versus strain relation shown in Fig. 2(a) is assumed. Strain hardening is neglected and the stress versus strain curve is symmetric in compression and in tension.
3. Yielding is governed entirely by direct stress.
4. Strain is small but displacements and rotations can be moderately large.
5. The torsional rigidity,  $GJ$ , is unchanged by yielding.
6. Local plate buckling and cross-sectional distortion are not considered.

#### 3.2 Material modelling and constitutive relationship

From the first two assumptions, the stress on an elementary area of a cross-section shown in Fig. 2(b) can be expressed as,

$$\sigma_1 = E\epsilon_1 \quad \text{for } |\epsilon_{1\max}| < \epsilon_y \quad (1)$$

$$\sigma_1 = E(\epsilon_1 - \epsilon_{p1}) \quad \text{for } |\epsilon_{1\max}| \geq \epsilon_y \quad (2)$$

In which  $\sigma_1$  and  $\epsilon_1$  are the stress and strain of a sub-area respectively;  $\epsilon_y$



is the tensile yield strain of the material and  $\epsilon_{pl}^c$  is the irreversible plastic strain of the elementary area given by,

$$\epsilon_{pl} = \epsilon_{imax} - \epsilon_y \quad (3)$$

Eqns (1)-(3) are the secant relations between stress and strain to be used in the evaluation of resisting forces and moments. To determine the incremental or the tangential relationship between the stress and the strain increments for the formulation of the tangent stiffness matrix, a variation (see Fig. 2(a)) can be taken on the equations to obtain the rate constitutive relationship as,

$$\delta\sigma_1 = E \delta\epsilon_1 \quad \text{for } |\epsilon_{imax}| < \epsilon_y \text{ or } \epsilon_{pl} \neq 0 \quad (4)$$

$$= 0 \quad \text{for } |\epsilon_{imax}| \geq \epsilon_y \text{ and } \epsilon_{pl} = 0 \quad (5)$$

### 3.3 Tangent stiffness matrix and incremental equilibrium equations

The incremental virtual work equation is utilized to formulate the incremental equilibrium equation. Thus,

$$\begin{aligned} \sum_V^n \left[ [\epsilon_L] [D_T] \delta[\epsilon_L] + [\sigma] \delta[\epsilon_N] + [\sigma] \delta[\epsilon_L] \right] dV \\ = \int_V [\bar{F}_V] \delta[\Delta u] dV + \int_A [\bar{F}_A] \delta[\Delta u] dA \end{aligned} \quad (6)$$

in which  $[\bar{F}_V]$  is the body force per unit volume;  $[\bar{F}_A]$  is the surface traction per unit area;  $[\epsilon_L]$  and  $[\epsilon_N]$  are the linear and nonlinear components of the incremental Green strain tensor;  $[\sigma]$  is the Cauchy stress tensor;  $[D_T]$  is the rate constitutive tensor;  $V$  and  $A$  are the volume and the surface area of the continuum under consideration,  $[\Delta u]$  is the incremental displacement vector and  $n$  is the number of elements. As implied in the updated Lagrangian framework, all the variables are referenced in the last known configuration.

Substituting the cubic Hermite function for the lateral deflection and a linear function for the twist and the axial deformation, the following equation is obtained

$$\sum_V^n [k_L + k_G] [\Delta u] = [F] - \int_V [B]^T [\sigma] dV \quad (7)$$

in which  $k_L$  and  $k_G$  are the linear and geometric stiffness matrices;  $[F]$  is the transformed nodal applied force vector and  $[B]$  is the strain versus displacement transformation mapping.

The linear and geometric stiffness matrices of a general thin-walled beam-column, capable of predicting flexural, torsional and flexural-torsional failure modes, have been derived previously [7, 18] and will not be repeated. It should be noted, however, that a series of

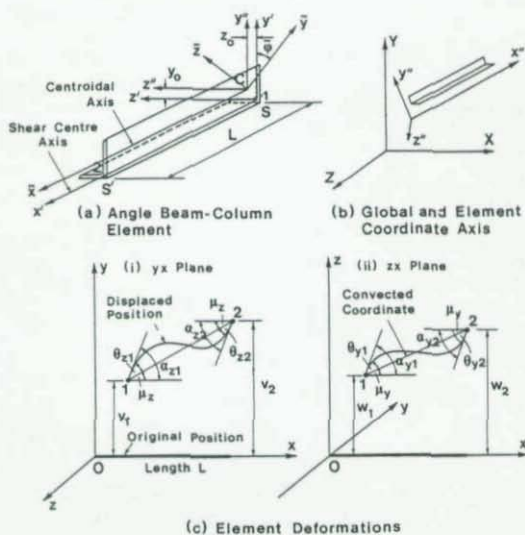


Fig. 3: Angle element and coordinate axes

transformations from local to global axes is necessary in order to account for the effects of eccentric connection and inclined principal axes for the angle member (see Fig. 3). Mathematically, this process can be summarized as,

$$\sum^n \left\{ [L_1] [L_2] [L_3] [k_L + k_G] [L_3]^T [L_2]^T [L_1]^T \right\} \{ \Delta u \} = \{ \Delta F \} \quad (8)$$

in which  $[L_1]$ ,  $[L_2]$  and  $[L_3]$  are the transformation matrices for the inclined principal planes, the eccentric connection and the local to global mapping respectively (see Fig. 3). All of these matrices must be updated continuously as the element deforms.

To account for the effects of material yielding across the section, the effective section properties of the member must be modified and updated according to the state of stress in the sub-areas. Thus, the effective flexural and axial rigidities used in formulating the linear element stiffness matrix in eqn (3) can be evaluated as,

$$\{ EI_y \}_{\text{eff}} = \sum^m E_t z_1^2 \Delta A_1 \quad (9)$$

$$\{ EI_z \}_{\text{eff}} = \sum^m E_t y_1^2 \Delta A_1 \quad (10)$$

$$\{ EA \}_{\text{eff}} = \sum^m E_t \Delta A_1 \quad (11)$$

in which  $\bar{y}_1, \bar{z}_1$  are coordinates of the centroid of the elementary area  $\Delta A_1$  and  $m$  is the number of elementary areas.

### 3.4 Total equilibrium equation and secant stiffness relations

The linearised incremental equilibrium condition in eqn (8) introduces an accumulative numerical error in tracing the nonlinear load versus deflection path. The magnitude of this error can be reduced by using smaller load steps, at the expense of longer computer time, or the error can be eliminated using an iterative process. In the elastic range, the incremental-iterative method is used in the present study to improve the efficiency of the numerical procedure without reducing the accuracy of the solution. To facilitate this, the resistance of the structure, represented by the last integral of eqn (7), must be calculated to determine the unbalanced forces for dissipation through the iterative process.

Using the total secant stiffness relations given elsewhere by the authors [7, 10, 18], the chordal relative rotations at the two ends of an element ( $\theta_{y1}$  and  $\theta_{z1}$ , see Fig. 3) about the principal coordinate axes can be calculated by subtracting the rigid body rotations ( $\mu_y$  and  $\mu_z$ ) from the total rotations ( $\alpha_{y1}$  and  $\alpha_{z1}$ ) as,

$$\theta_{z1} = \alpha_{z1} - \mu_z \quad (12)$$

$$\theta_{z2} = \alpha_{z2} - \mu_z \quad (13)$$

$$\theta_{y1} = \alpha_{y1} + \mu_y \quad (14)$$

$$\theta_{y2} = \alpha_{y2} + \mu_y \quad (15)$$

The rigid body rotations ( $\mu_y$  and  $\mu_z$ ) in eqns (12)-(15) can be determined by simple geometry shown in Fig. 3 as,

$$\mu_z = \sin^{-1} \left( \frac{v_2 - v_1}{L} \right) \quad (16)$$

$$\mu_y = \sin^{-1} \left( \frac{w_2 - w_1}{L} \right) \quad (17)$$

in which ( $w_1, w_2$ ) and ( $v_1, v_2$ ) are the transverse displacements along the principal axes of the element.

With the value of axial stretching obtained by the difference between the old and the new lengths and the rotation given in eqns (12)-(15), the strain of an elementary area can be calculated as,

$$e_1 = \frac{\Delta u}{L} + \phi_y \bar{z}_1 + \phi_z \bar{y}_1 \quad (18)$$

in which  $\Delta u$  is the axial stretching about the centroidal axis;  $\bar{y}_1$  and  $\bar{z}_1$

are the coordinates of the centroid of the elementary area about the principal axes;  $\phi_y$  and  $\phi_z$  are average curvatures of the element given by

$$\phi_y = -\frac{(\theta_{y2} - \theta_{y1})}{L} \quad (19)$$

$$\phi_z = \frac{(\theta_{z2} - \theta_{z1})}{L} \quad (20)$$

Using the idealized stress versus strain relationship given in eqns (1)-(3), the stress  $\sigma_1$  and thus the axial force and moments can be determined as,

$$P = \sum \sigma_1 \Delta A_1 \quad (21)$$

$$M_y = \sum \sigma_1 \bar{z}_1 \Delta A_1 \quad (22)$$

$$M_z = \sum \sigma_1 \bar{y}_1 \Delta A_1 \quad (23)$$

in which  $P$  is the resisting axial force;  $M_y$  and  $M_z$  are the average moments of the element about the principal  $\bar{y}$  and  $\bar{z}$ -axes respectively. To calculate the nodal resisting moments, the assumption that the curvature is proportional to the moment in a prismatic element is used, thus

$$\begin{aligned} \phi_{y1} &= \frac{\left[ \frac{\partial^2 f}{\partial x^2} \right]_{x=0}}{\left[ \frac{\partial^2 f}{\partial x^2} \right]_{x=L}} \left[ (w_1 \quad \theta_{y1} \quad w_2 \quad \theta_{y2})^T \right] \\ \phi_{y2} &= \frac{\left[ \frac{\partial^2 f}{\partial x^2} \right]_{x=L}}{\left[ \frac{\partial^2 f}{\partial x^2} \right]_{x=0}} \left[ (w_1 \quad \theta_{y1} \quad w_2 \quad \theta_{y2})^T \right] \\ &= \frac{2\theta_{y1} + \theta_{y2}}{\theta_{y1} + 2\theta_{y2}} \quad (24) \end{aligned}$$

in which  $f$  is the Hermite cubic function for lateral deflections given by,

$$\begin{aligned} f = \left( 1 - \frac{3x^2}{L^2} + \frac{2x^3}{L^3} \right) & x - \frac{2x^2}{L} + \frac{x^3}{L^2} \\ & \left( \frac{3x^2}{L^2} - \frac{2x^3}{L^3} \right) \left( \frac{-x^2}{L} + \frac{x^3}{L^2} \right) \quad (25) \end{aligned}$$

Similarly, curvature about the z-axis can be written as,

$$\begin{aligned} \phi_{z1} &= \frac{2\theta_{z1} + \theta_{z2}}{\theta_{z1} + 2\theta_{z2}} \quad (26) \\ \phi_{z2} &= \frac{\theta_{z1} + 2\theta_{z2}}{2\theta_{z1} + \theta_{z2}} \end{aligned}$$

Solving eqns (21)-(25), the nodal moments at the two ends of an element can

be determined. Transforming the internal forces and moments from local to global coordinate axes, the resisting forces and moments of an element and thus the structure can be obtained. Mathematically, this process can be written as,

$$[F]_R = \sum^n [L_1][L_2][L_3][T][P] \quad (27)$$

in which [P] is the element nodal resisting force given by,

$$[P]^T = [P \quad M_{y1} \quad M_{z1} \quad M_x \quad M_{y2} \quad M_{z2}] \quad (28)$$

and [T] is the 12x6 transformation matrix relating the 6 internal forces and moments to the 12 nodal forces and moments at the two end nodes of an element. This transformation matrix can be obtained by consideration of the equilibrium condition in an element [19]

### 3.5 Numerical method

The conventional Newton-Raphson method and its modified form diverge near the limit point because of the ill-conditioning of the tangent stiffness matrix. A number of methods have been suggested over the past decade to circumvent this divergence problem. Among these methods are the single displacement control method by Batoz and Dhatt [20], the method of current stiffness parameter by Bergan et al. [21], the constant work method by Powell and Simons [22], the arc-length method by Riks [23], Ramm [24] and Crisfield [25] and more recently the minimum residual displacement method by Chan [26].

In the present study, the arc-length method of the version suggested by Crisfield [25] is used. However, the incremental-iterative method will be converted to the pure incremental method with reduced load increments once yielding is detected. This is because the iterative process will alter the real path for the plasticity in the member and thus affect the accuracy of the solution and may eventually cause the iterative process to diverge.

## 4. NUMERICAL STUDIES

### 4.1 Comparison of ultimate strengths of angle columns with experiments

Tests on single and double angle and tee columns have been conducted by Kitipornchai and Lee [7]. Of these, 13 pairs (a;b - see Table 1) of equal and unequal single angle, pin-ended columns were tested to failure with loads applied concentrically. The end supports of the test columns were free to rotate about the major and minor principal axes but were prevented from twisting about the longitudinal axis. The modified slenderness,  $\lambda$  ( $=\sqrt{P_Y/P_E}$ ) of the test columns ranged from 0.57 to 1.07. Measurements were made of cross-sectional dimension, yield stress and failure load. No initial out-of-straightness in the columns was measured, however. Fig. 1 shows scatter of test results confirming that SSRC Curve 2 is the appropriate lower bound column design curve for single angle columns [2].

The proposed formulation has been used to predict the ultimate strength of tested single angle columns. A half-sine wave initial out-of-straightness in the positive z-direction (i.e. bending about minor axis) is assumed, using maximum mid-height initial out-of-straightness  $\delta_0$  values of 0, L/1000



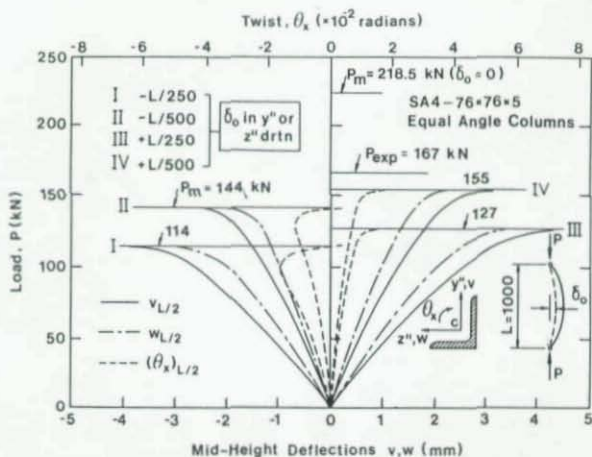


Fig. 4: Load-deflection curves for an equal angle column (SA4) with initial out-of-straightness in direction parallel to leg

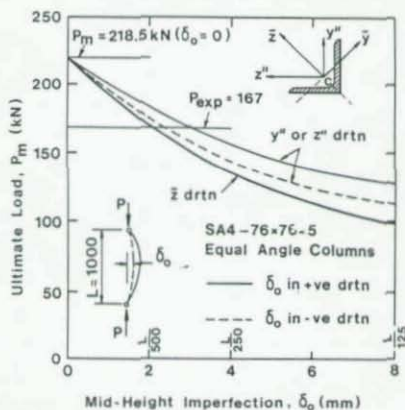


Fig. 5: Influence of magnitude and direction of initial out-of-straightness on the ultimate strength of equal angle columns (SA4)

and  $L/500$ , respectively. Experimental and predicted failure loads are compared in Table 1. The results indicate that the ultimate strength of angle columns is highly sensitive to the magnitude of the initial out-of-straightness assigned. The mean differences between the experimental and predicted failure loads assuming  $\delta_0$  of 0,  $L/1000$  and  $L/500$  are 19.6%, 0.95% and -9.6% with corresponding standard deviations of 8.95, 9.13 and 10.24 kN, respectively. In practice, it is difficult to measure initial geometrical imperfection accurately in angle members. This study shows that

Table 1 : Comparison of Predicted Results with Tests

Strut	Nominal Dimensions (mm)	Effective Length (mm)	Test Load (kN)	Predicted Failure Load (kN)		
				$\delta_0 = 0$	$\delta_0 =$	$\delta_0 =$
					L/1000	L/500
SA1-a;b	64x64x5	600	163	182.7	176.4	166.0
SA2-a;b	64x64x5	700	169	182.2	171.0	157.8
SA3-a;b	76x76x5	850	182	218.9	199.0	184.7
SA4-a;b	76x76x5	1000	167	218.5	186.3	169.8
SA5-a;b	76x76x5	1100	161	218.6	177.8	157.9
SA6-a;b	102x102x6.5	1310	295	353.0	307.9	279.1
SA7-a;b	102x102x6.5	1400	283	345.7	299.4	268.7
SA8-a;b	64x51x5	700	141	156.1	138.0	123.3
SA9-a;b	64x51x5	900	135	154.0	115.0	99.9
SA10-a;b	76x51x5	800	143	173.4	125.3	104.9
SA11-a;b	76x51x5	1000	123	133.6	113.2	99.1
SA12-a;b	102x76x6.5	1200	277	331.5	253.9	223.1
SA13-a;b	102x76x6.5	1500	190	269.4	203.3	177.8

Note that the assumed maximum mid-height initial out-of-straightness,  $\delta_0$ , is in the positive z-direction (i.e. bending about the minor axis).

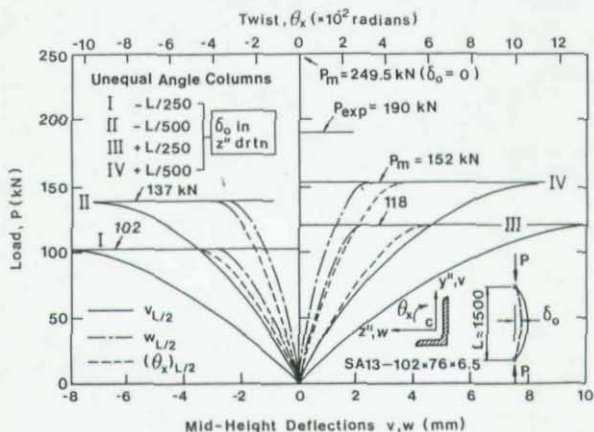


Fig. 6: Load-deflection curves for an unequal angle column (SA13) with initial out-of-straightness in direction parallel to long leg

an initial mid-height out-of-straightness  $\delta_0$  of close to  $L/1000$  must have existed in these tested single angle columns.

#### 4.2 Influence of magnitude and orientation of initial out-of-straightness on ultimate strength of angle columns

Design codes [1-3] normally specify a maximum limit of  $L/1000$  for the initial out-of-straightness in compression members. Because a general unequal angle section is asymmetric, the ultimate strength of an angle column will depend not only on the magnitude but also on the orientation of the initial out-of-straightness in the member.

For the purpose of the present study, the SA4 (76x76x5) equal angle and the SA13 (102x76x5) unequal angle columns tested by Kitipornchai and Lee [7] are selected. The initial out-of-straightness is taken to be in the direction parallel to the outstanding leg, since most angle members are connected by one leg only.

Fig. 4 shows load versus deflection curves for the SA4 equal angle column with  $\delta_0 = 0$ ,  $L/500$  and  $L/250$  in the positive or negative  $y''$  (or  $z''$ ) direction (i.e. parallel to legs). Fig. 5 shows the variation of the ultimate strength of the SA4 equal angle column with varying magnitudes of  $\delta_0$  in the direction parallel to the legs, as well as in the positive  $z$ -direction (i.e. bending about the minor axis). It is seen that the ultimate strength of angle columns is highly dependent on both the magnitude and the orientation of the initial out-of-straightness. As expected, columns with initial out-of-straightness bending about the minor axis have the lowest ultimate capacity.

Figs 6 and 7 show load versus deflection curves for the SA13 unequal angle column. Because the unequal angle has no axis of symmetry, the ultimate strength of unequal angle columns is more complicated. Fig. 6 shows load versus deflection curves for the SA13 column in which the initial out-of-straightness is in the  $z''$ -direction (short leg), while in Fig. 7 the initial out-of-straightness is in the  $y''$ -direction (long leg). Fig. 8

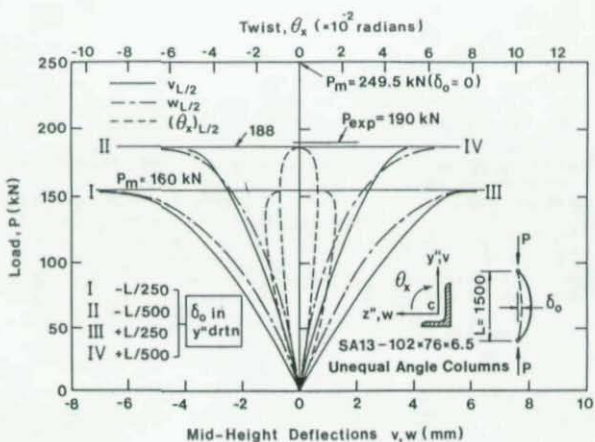


Fig. 7: Load-deflection curves for an unequal angle column (SA13) with initial out-of-straightness in direction parallel to short leg

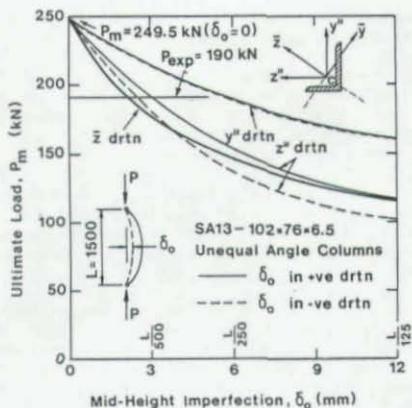


Fig. 8: Influence of magnitude and direction of initial out-of-straightness on the ultimate strength of unequal angle columns (SA13)

shows the variation of ultimate load with varying values of  $\delta$  for different orientations of initial out-of-straightness. Results obtained reveal that for unequal angle columns, the ultimate strength is even more sensitive to the orientation of the initial out-of-straightness when compared to the equal angle columns.

## 5. CONCLUSION

The paper investigates the influence of initial out-of-straightness on the ultimate behaviour of single angle columns. An incremental-iterative numerical procedure has been used for the geometric and material nonlinear analysis of geometrically imperfect angle columns. The method accounts for the change in geometry during deformation, the shift in the centroid of the remaining elastic core and the influence of strain-unloading.

The analytical technique has been used to predict the failure loads for a member of a series of equal and unequal angle column experiments conducted by Kitipornchai and Lee [7]. Results confirm that an initial out-of-straightness of  $L/1000$  as recommended by most codes is appropriate for angle columns. The study highlights the sensitivity to geometrical imperfection of the ultimate strength of single angle columns. It shows that the ultimate strength of an angle column is highly dependent on the orientation of the initial out-of-straightness in the member.

## REFERENCES

1. *Specification for the design, fabrication and erection of standard steel for buildings*. American Institute of Steel Construction, New York, N.Y., 1978.
2. Galambos, I.V. ed., *Guide to design criteria for metal structures*. 4th edn, Structural Stability Research Council, New York, USA, John Wiley and



3. Standards Association. *AS4100-1990 SA Steel Structures Code*. SA, Sydney, Australia, 1990.
4. Kitipornchai, S., Torsional-flexural buckling of angles: a parametric study. *J. Const. Steel Res.*, 3(3) (1983) 27-31.
5. Kitipornchai, S. and Lee, H.W., Inelastic buckling of single angle, tee and double angle struts. *J. Const. Steel Res.*, 6(1) (1986) 3-20.
6. Kitipornchai, S. and Lee, H.W., Inelastic experiments on angle and tee struts. *J. Const. Steel Res.*, 6(3) (1986) 219-236.
7. Kitipornchai, S. and Chan, S.L., Nonlinear finite element analysis of angle and tee beam-columns. *J. Struct. Engrg.*, ASCE, 113(4) (1987) 721-239.
8. Bathe, K.J. and Bolourchi, S., Large displacement analysis of three-dimensional beam structures. *Int. J. Numer. Methods Engrg.*, 14 (1979) 961-986.
9. Zienkiewicz, O.C. *The finite element method*. 3rd edn, McGraw-Hill Book Co., New York, N.Y. 1977.
10. Kitipornchai, S., Al-Bermani, F.G.A. and Chan, S.L., Geometric and material nonlinear analysis of structures comprising rectangular hollow sections. *Engrg. Struct.*, 10(1) (1988) 13-23.
11. Chen, W.F. and Atsuta, T. *Theory of beam-columns - Space behaviour and design*, Vol. 2, McGraw-Hill Book Co., New York, N.Y., 1977.
12. Orbison, J.G., McGuire, W. and Abel, J.F., Yield surface applications in nonlinear steel frame analysis. *Comput. Methods Appl. Mech. Engrg.*, 33 (1982) 557-573.
13. Ueda, T. and Yao, T., The plastic node method: a new method of plastic analysis. *Compt. Methods Appl. Mech. Engrg.*, 34 (1982) 1089-1104.
14. Al-Bermani, F.G.A. and Kitipornchai, S., Elasto-plastic large deformation analysis of thin-walled structures. *Engrg. Struct.*, 12(1) (1990) 28-36.
15. Kitipornchai, S., Al-Bermani, F.G.A. and Chan, S.L., Elasto-plastic finite element models for angle steel frames. *J. Struct. Engrg.*, ASCE, 116(10) (1990) 2567-2581.
16. Harstead, G.A., Birnstiel, C. and Leu, K.C., Inelastic H-columns under biaxial bending. *J. Struct. Div.*, ASCE, 94(ST10) (1968) 2371-2397.
17. Vinnakota, S. and Aoshima, Y., Inelastic behaviour of rotationally restrained columns under biaxial bending. *The Struct. Engrg.*, 52(7) (1974) 235-255.
18. Chan, S.L. and Kitipornchai, S., Geometric nonlinear analysis of asymmetric thin-walled beam-columns. *Engrg. Struct.*, 9(4) (1987) 243-254.
19. Meek, J.L. *Matrix structural analysis*. McGraw-Hill, Inc., New York, N.Y., 1971.
20. Batoz, J.L. and Dhatt, G., Incremental displacement algorithms for nonlinear problems. *Int. J. Numer. Methods Engrg.*, 14 (1979) 1262-1266.



21. Bergan, P.G., Hottigmo, G., Krakeland, B. and Soreide, T.H. Solution techniques for nonlinear finite element problems. *Int. J. Numer. Methods Engrg.*, 12 (1978) 1677-1696.
22. Powell, G. and Simmons, J., Improved iteration strategy for nonlinear structures. *Int. J. Numer. Methods Engrg.*, 17 (1981) 1455-1467.
23. Riks, E., An incremental approach to the solution of snapping and buckling problems. *Int. J. Solids Struct.*, 15 (1979) 529-551.
24. Ramm, E., Strategies for tracing the nonlinear response near limit points. *Nonlinear Finite Element Analysis in Structural Mechanics*, W. Wunderlich, E. Stein and K.J. Bathe, eds., Springer-Verlag, Berlin, Germany, (1981) 63-89.
25. Crisfield, M.A., A fast incremental/iterative solution procedure that handles snap-through. *Comp. Struct.*, 13 (1981) 55-62.
26. Chan, S.L., Geometric and material nonlinear analysis of beam-columns and frames using the minimum residual displacement method. *Int. J. Numer. Methods Engrg.*, 26 (1988) 2657-2669.

## FURTHER STUDIES ON THE COMPRESSIVE STRENGTH OF 60° EQUAL LEG STEEL ANGLES

Krishna K. Sankisa, Seshu Madhava Rao Adluri, and Murty K.S. Madugula,  
Department of Civil and Environmental Engineering,  
University of Windsor, Windsor, Ontario, Canada N9B 3P4.

### ABSTRACT

Triangular-base communication and transmission towers in North America are commonly designed using 60° angles as main leg members. These 60° angle members could be either Schifflerized hot-rolled angles or cold formed angles. The 60° angle properties are significantly different from those of the corresponding 90° angles. Until recently, no systematic study of these angles was available in published literature. In light of this, an experimental program was carried out to determine the compressive strength of Schifflerized angles using hinged end conditions. The main conclusions of the study were published in the proceedings of 1991 Annual Technical Session of SSRC. However, since the end conditions of the leg members in an actual tower may not be ideal hinges, the actual capacity of Schifflerized angles could be different from that based on the testing of ideally hinged Schifflerized angles. In addition, the earlier Schifflerized angle study included only nine (out of eighteen) specimens failing in torsional-flexural buckling. Therefore, a further set of buckling tests has been carried out with 19 more Schifflerized angles with a different set of end fixtures to further confirm the earlier conclusions. In addition, nineteen 60° cold formed angles have also been tested with the same end fixtures. The Schifflerized angles are of sizes 4x4x1/4, 3x3x1/4, and 3x3x3/16 in. (102x102x6.4 mm, 76x76x6.4 mm, and 76x76x4.8 mm). The cold formed angles are of sizes 2x2x3/16 and 1 1/2x1 1/2x1/8 in. (51x51x4.8 mm and 38x38x3.2 mm). The lengths of the specimens varied from 369 mm to 2140 mm with  $kl/r$  ratios between 30 and 100. This paper presents the results of these tests in light of the conclusions reported earlier. All the experimental loads further validated the results of a detailed finite element analysis similar to the one reported earlier with certain modifications. The results for Schifflerized angles indicate that the conclusions arrived earlier are acceptable. In addition, the data for 60° cold formed angles indicates that these members can be designed using procedures similar to those recommended for Schifflerized angles.

Key Words : Angle, Buckling, Buckling Tests, Cold Formed 60° Angle, Compression, Design Code, Design Strength, Failure Load, Flat Width, Local Buckling, Schifflerized Angle, Torsional-Flexural Buckling.

## INTRODUCTION

Structural steel angles are widely used in several kinds of structures for a variety of purposes. One of the most common uses of steel angles is in the area of latticed structures. The communication and the electrical transmission industries utilize extensively the advantages offered by the latticed towers. Such towers are usually triangular or rectangular in plan view (cross-section). They are composed of three or four leg members at the corners of an equilateral triangle or a rectangle respectively. In rectangular towers, the main leg members are braced in two different planes at  $90^\circ$  to each other. The leg plates of the main leg members that are orthogonal to each other permit easy connection to the bracing members in the two perpendicular planes. However, in triangular towers, regular  $90^\circ$  steel angles can be used only with bent gusset plates (which are relatively more expensive to fabricate) to facilitate connections with diagonal members whose planes are at  $60^\circ$  to each other. For ease of fabrication, main leg members of triangular towers are usually made of steel angles whose leg plates make an included angle of  $60^\circ$  instead of  $90^\circ$  as is the case with regular rolled steel angles. Such angles are usually manufactured either by Schifflerizing regular hot-rolled  $90^\circ$  angles or by cold-forming.

Schifflerized angles are regular hot-rolled steel angles cold bent to create an included angle of  $60^\circ$  between the leg plates. The cold bending is usually done by brake-pressing or re-rolling. The process of Schifflerization cannot bend the root portion of the original angle because of its high stiffness. Hence every Schifflerized angle contains an original  $90^\circ$  angle root portion and two leg plates at  $60^\circ$  to each other as shown in Fig. 1a. Properties of Schifflerized angles in US customary and SI units are given by Adluri and Madugula [1991a, 1991c]. Cold-formed  $60^\circ$  angles are manufactured in the same manner as regular  $90^\circ$  cold-formed angles as shown in Fig. 1b.

## CURRENT DESIGN PRACTICE

Until recently, very little published literature was available on  $60^\circ$  steel angles. Most leading world codes do not have specific recommendations regarding these angles. Compression design of these angles is usually carried out using the formulas applicable to regular hot-rolled  $90^\circ$  angles without any special modifications. However, it should be noted that the minor axis moment of inertia of these angles is more than that of regular angles by as much as 50%. The major axis moment of inertia on the other hand can be lower by a similar percentage. Consequently,  $60^\circ$  steel angles are stronger in flexural buckling and can be considerably weaker in torsional-flexural buckling when compared to  $90^\circ$  steel angles. This suggests that the existing procedures for calculating the design strength of  $60^\circ$  steel angles should be re-examined. To the best of the authors' knowledge, the first research in this connection was reported by Adluri [1990] (see also Adluri, Madugula, Monforton [1991d, 1991e, 1992]). In that research, a total of eighteen

tests were conducted on Schifferized angles to determine their compressive strength under concentric loading conditions. Pinned end conditions were used at either end of the member. Six of the test specimens failed in torsional-flexural buckling, three of the specimens failed in a combined mode showing flexural and torsional-flexural buckling, while the remaining failed in flexural buckling mode. The members that failed in the combined mode had their flexural and equivalent torsional-flexural buckling radii of gyration close to each other. A detailed non-linear finite element analysis was carried out to predict the capacities of the test specimens [Adluri, Madugula, and Monforton, 1991d]. The results of this study were used to arrive at suitable design recommendations compatible with existing practices. These recommendations can be briefly restated as below:

- Design according to Canadian antenna tower code CAN/CSA-S37-M86: Use existing procedures considering the bent portion of the angle leg as the flat width in the computation of "width-thickness ratio". Since the unbent portion of the angle can vary slightly between different fabricators, for the sake of uniformity, it is recommended that flat width up to the root fillet of the angle be used in the computations. This change involves negligible reduction in the member strength.
- Design according to ASCE Manual No.52 [ASCE, 1988]: Use the existing procedure for design with **one** of the following two modifications:
  1. Use the minimum of the elastic torsional-flexural buckling radius of gyration and flexural buckling radius of gyration for the calculation of slenderness ratio.
  2. Use the full leg width as flat width in the computation of "width-thickness ratio".
- Design according to AISC-LRFD [1986]: Use existing procedures by considering the bent portion of the leg as the flat width, instead of the entire leg width, to compute "width-thickness ratio".

The design recommendations appropriate to the CAN/CSA-S37-M86 (Adluri, [1990]), were approved by the Technical Committee on Antenna Towers (CSA-S37) and were included in Amendment No. 12, May 1990. Since the earlier test program included only nine Schifferized angles failing in torsional-flexural buckling, and no 60° cold-formed angles, a new experimental program was designed to test 60° steel angles (both Schifferized and cold-formed) predominantly failing in torsional-flexural buckling.

#### EXPERIMENTAL INVESTIGATION

The experimental program included buckling tests on 19 Schifferized angles and 19 cold-formed 60° angles under concentric load. Fixed end conditions were chosen for the specimens. The specimens were cut to length and the ends were milled to be parallel



to each other. Tables 1a and 1b show the geometrical properties of the test specimens. The members were mounted vertically on to a Gilmore testing frame (Fig. 2). The load was applied using a 100 kip (445 kN) hydraulic jack. The load was measured using a 100 kip Strainert flat load cell. Load was transmitted to the member through two flat plates bearing on the milled ends of the member. The member centroid was aligned with the line of application of load by first marking the member centroid on the flat plates and then placing the member in proper position. The alignment was secured by adjustable steel blocks on either side of each of the legs at top and bottom. The load was applied in gradual increments. The deflections and rotations at 1/4, 1/2 and 3/4 of the height were measured along the two principal axes. The member lengths were chosen such that all of the specimens failed in torsional-flexural buckling mode. Choosing fixed end conditions also helped in the reduction of effective length thereby forcing the specimens to buckle in torsional-flexural mode. The test results (shown as  $P_i$ ) are given in Tables 2a and 2b. It should be noted that due to practical limitations, the guiding mechanism on top of the loading piston connected to the bottom plate was capable of rotation by up to an angle of approximately  $1^\circ$  under heavy loads.

TABLE 1a. GEOMETRIC PROPERTIES OF SCHIFFLERIZED ANGLE TEST SPECIMENS

Specimen Mark	Nominal Size, in.	Actual d, mm	Actual Size t, mm	a mm	Nominal Length, mm	$r_{min}$ mm	$r_{max}$ mm	$u_c$ mm	$J, 10^3 \text{ mm}^4$
H1-1,2	3x3x1/4	76.04	6.51	24	1220	17.6	24.7	33.3	14.4
H2-1,2	3x3x3/16	75.90	4.76	24	1870	17.7	25.1	32.3	5.87
H3-1,2,3	3x3x3/16	75.97	4.79	24	1530	17.7	25.1	32.3	5.98
H4-1,2,3	3x3x3/16	76.54	4.69	24	732	17.9	25.3	32.5	5.67
H5-1,2,3	4x4x1/4	101.58	6.51	24	2140	24.1	32.1	44.2	19.6
H6-1,2	4x4x1/4	102.66	6.40	24	1960	24.4	32.5	44.6	18.8
H7-1,2,3,4	4x4x1/4	103.05	6.43	24	1520	24.5	32.6	44.8	19.2

Note: For definition of a, d, t and  $u_c$  refer to Fig. 1a.;  $J$  = Torsion constant.

TABLE 1b. GEOMETRIC PROPERTIES OF COLD-FORMED  $60^\circ$  ANGLE TEST SPECIMENS

Specimen Mark	Nominal Size, in.	Actual Size		$R_c$ mm	Nominal Length, mm	$r_{min}$ mm	$r_{max}$ mm	$u_c$ mm	$J \text{ mm}^4$
		d, mm	t, mm						
C1-1,2,3	1 1/2x1 1/2x1/8	37.87	3.13	10	900	8.51	14.4	13.2	754
C2-1,2,3	1 1/2x1 1/2x1/8	38.01	3.01	10	631	8.57	14.5	13.2	674
C3-1,2,3	1 1/2x1 1/2x1/8	38.60	3.00	10	369	8.72	14.6	13.4	685
C4-1,2,3	2x2x3/16	50.85	4.77	11	1350	11.6	18.5	18.6	3550
C5-1,2,3	2x2x3/16	50.93	4.83	11	874	11.6	18.5	18.7	3690
C6-1,2,3,4	2x2x3/16	50.87	4.71	11	404	11.6	18.5	18.6	3420

Note:  $R_c$  is the center line radius of bend,  $J$  = Torsion constant  
For definition of t and  $u_c$  refer to Fig. 1b.



Standard tension tests for each of the specimens were conducted on coupons prepared from the same material as that of the individual specimens. The tension tests produced the yield strength, Young's modulus, and tensile strength of the material of each of the specimens. Material yield strengths are listed in Tables 2a and 2b.

### Finite Element Analysis

Traditionally, column strengths have been theoretically computed using solutions of differential equations governing their behavior in the elastic range. In the inelastic range, the same equations can be solved numerically using various techniques. One of the most versatile techniques to solve such problems has been the finite element method.

Adluri, Madugula and Monforton [1991d] have applied the finite element method to find the strengths of Schifflerized angles for different failure modes. In the present study, similar models appropriately modified to account for the end conditions have been used to compute theoretical failure loads of the test specimens. The angle was divided into several segments along the length of the member. Each segment consisted of four elements on each leg. Eight-node quadrilateral plate/shell elements with reduced integration have been chosen for the analysis. The end plates bearing on the member as well as the end blocks securing the member alignment have been similarly modeled. The angle was given a multipoint constraint at nodes where the alignment blocks touched it. The alignment blocks were secured to the bearing plate through another set of multipoint constraints. The bearing plate was fixed at the top. The bottom bearing plate, resting on top of the hydraulic jack was capable of rotation. The buckling mode was simulated by a trigger load placed at mid-height to induce an initial out-of-straightness. The analysis included both material and geometric non-linearities. Residual stresses and other modeling parameters were similar to those discussed by Adluri, Madugula and Monforton [1991d]. Software package ABAQUS [1989] was used for the computer runs. The failure loads predicted by the finite element analysis are in good agreement with the test results.

### RESULTS

The test results can be used to verify the design strength predicted by the current design codes. Tables 2a and 2b show calculated member capacities as per the method given by Adluri [1990]. These capacities (as per the Canadian standard CSA-S37-M86) are computed by assuming an effective length factor equal to 0.8. This is the same factor traditionally specified by the design codes for columns with one end fixed and the other end hinged. It should be recalled that the member end at the bottom of the specimen was capable of rotation at high loads. This, along with any incidental eccentricity in the application of the load at the bottom would prompt the bottom end of the member to

behave as a hinge. To account for the end fixture at the bottom, the length of test specimen used for calculation purposes is taken as approximately 60 mm larger than the nominal length. The relevant formulas for the member capacity as per CAN/CSA-S37, are given below (these formulas reduce the yield strength to account for local buckling of the angle leg as a plate):

$$(w/t)_{\text{lim}} = 200/\sqrt{F_y} \quad \text{where, } F_y \text{ is in MPa,}$$

$$F_y' = F_y, \quad w/t \leq (w/t)_{\text{lim}} \leq 25$$

$$F_y' = [1.677 - 0.677 \frac{w/t}{(w/t)_{\text{lim}}}] F_y, \quad 25 \geq w/t \geq (w/t)_{\text{lim}}$$

where, "w" is the flat width of the leg of the angle and "t" is the thickness of the leg. In the calculation of the member capacities for Schifflerized angles, flat width = total leg width - leg thickness - root fillet.

However, for cold-formed 60° angles, the flat width was taken as the greater of the unbent flat portion of the leg and the total leg width minus three times the thickness of the leg.

The factored compressive resistance  $C_r$  is given by [CAN/CSA-S16.1-M89],

$$C_r = \phi A F_y', \quad 0 \leq \lambda \leq 0.15$$

$$C_r = \phi A F_y' (1.035 - 0.202\lambda - 0.222\lambda^2), \quad 0.15 < \lambda \leq 1.0$$

$$C_r = \phi A F_y' (-0.111 + 0.636\lambda^{-1} + 0.087\lambda^{-2}), \quad 1.0 < \lambda \leq 2.0$$

$$C_r = \phi A F_y' (0.009 + 0.877\lambda^{-2}), \quad 2.0 < \lambda \leq 3.6$$

$$C_r = \phi A F_y' \lambda^{-2}, \quad 3.6 < \lambda$$

where, slenderness parameter  $\lambda = \frac{kL}{r\pi} \sqrt{\frac{F_y'}{E}}$

Note that these equations are the same as SSRC column curve no.2. These equations are applicable to wide flange sections and other symmetric sections. Although they have not been calibrated specifically for steel angles, they have been in use for angles as well. It can be shown from available test data, that these equations are conservative for steel angle design. From the results in Tables 2a and 2b, it can be seen that computed strengths of Schifflerized angles are less conservative than the computed strengths of cold-formed 60° angles. This may be due to the fact that the Schifflerized angles, which had significantly higher failure loads than the cold-formed angles, forced the bottom end

fixture to rotate on top of the hydraulic jack more than the rotation forced by the smaller sized cold-formed angles.

TABLE 2a. COMPARISON OF FACTORED AXIAL COMPRESSIVE RESISTANCE OF SCHIFFLERIZED ANGLES AS PER CAN/CSA-S37-M86 WITH TEST RESULTS

Specimen Mark	Size in.	a mm	length mm	$F_y$ MPa	$\lambda$	$P_{11}$ kN	$P_1$ kN	Ratio $P_{11}/P_1$
H1-1,2	3x3x1/4	24	1220	360	0.79	252	265	0.95
H2-1,2	3x3x3/16	24	1870	378	1.08	117	144	0.82
H3-1,2,3	3x3x3/16	24	1530	379	0.89	146	146	1.00
H4-1,2,3	3x3x3/16	24	732	378	0.43	186	204	0.91
H5-1,2,3	4x4x1/4	24	2140	367	0.90	260	273	0.95
H6-1,2	4x4x1/4	24	1960	351	0.80	267	261	1.03
H7-1,2,3,4	4x4x1/4	24	1520	358	0.63	306	301	1.02
Mean of ratio : 0.95, Standard deviation of ratio : 0.068								

Note : for definition of "a" refer to Fig. 1a.;

$$\lambda \text{ is the slenderness parameter } \lambda = \frac{kL}{r\pi} \sqrt{\frac{F_y}{E}}$$

TABLE 2b. COMPARISON OF FACTORED AXIAL COMPRESSIVE RESISTANCE OF COLD-FORMED 60° ANGLES AS PER CAN/CSA-S37-M86 WITH TEST RESULTS

Specimen Mark	Size mm	$R_c$ mm	length mm	$F_y$ MPa	$\lambda$	$P_{11}$ kN	$P_1$ kN	Ratio $P_{11}/P_1$
C1-1,2,3	1 1/2x1 1/2x1/8	10	900	310	1.13	37	49	0.76
C2-1,2,3	1 1/2x1 1/2x1/8	10	631	314	0.81	51	61	0.84
C3-1,2,3	1 1/2x1 1/2x1/8	10	369	337	0.51	67	74	0.90
C4-1,2,3	2x2x3/16	11	1350	303	1.21	68	116	0.58
C5-1,2,3	2x2x3/16	11	874	303	0.80	105	136	0.77
C6-1,2,3,4	2x2x3/16	11	404	312	0.40	133	162	0.82
Mean of ratio : 0.78, Standard deviation of ratio : 0.099								

Note :  $R_c$  is the mean radius of bend (Fig. 1b).

## DISCUSSION

The Canadian standard CSA-S37 does not explicitly account for torsional-flexural buckling. However, it can be demonstrated that this mode of failure governs a large number of practical cases of 60° angles. Adluri and Madugula [1991b] have given a design method accounting for the torsional-flexural buckling of Schifflerized angles.

This method involves the inclusion of equivalent torsional-flexural buckling radius of gyration in place of flexural buckling radius of gyration in the column formulas, i.e.,

$$\lambda_{t-f} = \sqrt{\frac{F_y'}{F_{t-f}}}$$

where,  $\lambda_{t-f}$  is the equivalent slenderness parameter in torsional-flexural buckling, and  $F_{t-f}$  is the elastic buckling stress in torsional-flexural buckling.  $F_{t-f}$  can easily be calculated from classical solutions given in standard texts on the subject [Bleich, 1952; Timoshenko and Gere, 1961]. In Tables 3a and 3b, the test results are compared with this method of solution taking the larger of  $\lambda$  and  $\lambda_{t-f}$ . The effective length factor for flexure about major axis is taken as 0.80 (as was the case with minor axis buckling). From the results, it can be seen that for Schifflerized angles as well as for cold-formed angles, the member capacities predicted by this method are well below the corresponding test loads. The degree of conservatism is of the same level as that usually observed for hot-rolled angle capacities predicted by the current design formulas. It should be noted that, the computed strengths using flexural buckling formulas alone, although very close to (and sometimes slightly more than) the test results are justifiable from the designer's point of view. In the computation of the member strengths in Tables 2a and 2b, the resistance factor was taken as 1.0 and  $F_y$  was taken as yield strength obtained from tensile coupon tests. However, for actual designs, the resistance must be computed using a resistance factor  $\phi = 0.90$  and  $F_y = 300$  MPa (specified minimum value and not the mill test certificate).

TABLE 3a. FACTORED AXIAL COMPRESSIVE RESISTANCE OF SCHIFFLERIZED ANGLES INCLUDING THE EFFECTS OF TORSIONAL-FLEXURAL BUCKLING

Specimen Mark	Size mm	a mm	$\lambda$	$\lambda_{t-f}$	$P_{II}$ kN	$P_I$ kN	Ratio $P_{II}/P_I$
H1-1,2	3x3x1/4	24	0.79	0.92	226	265	0.85
H2-1,2	3x3x3/16	24	1.08	1.18	104	144	0.73
H3-1,2,3	3x3x3/16	24	0.89	1.12	114	146	0.78
H4-1,2,3	3x3x3/16	24	0.43	1.03	121	204	0.60
H5-1,2,3	4x4x1/4	24	0.90	1.13	202	273	0.74
H6-1,2	4x4x1/4	24	0.80	1.09	198	261	0.76
H7-1,2,3,4	4x4x1/4	24	0.63	1.05	213	301	0.71
Mean of ratio : 0.74. Standard deviation of ratio : 0.073							

Notes : For definition of "a" refer to Fig. 1a,

$\lambda$  is the slenderness parameter for flexural buckling,

$\lambda_{t-f}$  is the slenderness parameter for torsional-flexural buckling.

TABLE 3b. FACTORED AXIAL COMPRESSIVE RESISTANCE OF COLD-FORMED 60° ANGLES INCLUDING THE EFFECTS OF TORSIONAL-FLEXURAL BUCKLING

Specimen Mark	Size mm	R <sub>c</sub> mm	$\lambda$	$\lambda_{t-f}$	P <sub>11</sub> kN	P <sub>1</sub> kN	Ratio P <sub>11</sub> /P <sub>1</sub>
C1-1,2,3	1 1/2x1 1/2x1/8	10	1.13	0.87	37	49	0.76
C2-1,2,3	1 1/2x1 1/2x1/8	10	0.81	0.81	51	61	0.84
C3-1,2,3	1 1/2x1 1/2x1/8	10	0.51	0.81	55	74	0.75
C4-1,2,3	2x2x3/16	11	1.21	0.88	68	116	0.58
C5-1,2,3	2x2x3/16	11	0.80	0.71	105	136	0.77
C6-1,2,3,4	2x2x3/16	11	0.40	0.65	117	162	0.72
Mean of ratio : 0.74, Standard deviation of ratio : 0.078							

Note : R<sub>c</sub> is the mean radius of bend (Fig. 1b).

### CONCLUSIONS

The results of the present study show that 60° steel angles can be designed by the methods such as those suggested in an earlier paper by Adluri, Madugula and Monforton [1991e]. The degree of conservatism of this method is less than that usually associated with the design of hot-rolled 90° angles. This is due to the fact that 60° angles are highly susceptible to torsional-flexural buckling at lengths well within the ranges practically used. This can be explicitly accounted for using the method given by Adluri and Madugula [1991b]. Present test results indicate that this method predicts member capacities with a degree of conservatism similar to that associated with hot-rolled 90° angles. It may also be noted that it is not over-conservative for the design of 60° steel angles.

### Acknowledgments

This present research is carried out with financial support from Natural Sciences and Engineering Research Council of Canada. The authors wish to acknowledge the contribution of Steve Duncan and Tony Montanino to the experimental program as part of their final year project. Thanks are also due to Mr. D.G. Marshall, Vice-President - Engineering, LeBlanc and Royle Inc., Oakville, Ont. Canada, and Mr. K. Penfold, Manager of Engineering, Trylon Manufacturing Co. Ltd., Elmira, Ont., for supplying the material used in the investigation.

### REFERENCES

ABAQUS Version 4.8, 1989, User's manual, Parts 1, 2, 3 & 4, Hibbitt, Karlsson & Sorensen, Inc., 100 Medway st., Providence, RI 02906-4402, USA.



- Adhuri, Seshu Madhava Rao, 1990. *Ultimate strength of Schifflerized angles*, M.A.Sc. Thesis, University of Windsor, Windsor, Ontario, N9B 3P4, Canada.
- Adhuri, Seshu Madhava Rao and Madugula, Murty K.S. 1991a. "Design strength of Schifflerized angle struts", American Institute of Steel Construction, *Engineering Journal*, Vol. 28, No. 2, Chicago, IL, U.S.A.
- Adhuri, Seshu Madhava Rao and Madugula, Murty K.S. 1991b. "Factored axial compressive resistance of Schifflerized angles", *Canadian Journal of Civil Engineering*, Vol. 18, No.6, pp.926-932, Ottawa, Canada
- Adhuri, Seshu Madhava Rao and Madugula, Murty K.S. 1991c. "Geometric Properties of Schifflerized Angles", *Journal of Constructional Steel Research*, UK., Vol.18, pp.71-83.
- Adhuri, S.M.R, Madugula, M.K.S., Monforton, G.R., 1991d. "Finite element failure analysis of Schifflerized angles", *Computers and Structures*, Pergamon Press, Vol.41, No.5, pp.1087-1093, Great Britain.
- Adhuri, Seshu Madhava Rao , Madugula, Murty K.S., Monforton, G.R. 1991e. "Strength of Schifflerized angles", *Proceedings of Structural Stability Research Council Annual Technical Session*, April 14-17, Chicago, IL, USA.
- Adhuri, Seshu Madhava Rao , Madugula, Murty K.S. and Monforton, G.R. 1992. "Schifflerized angle struts", *Journal of Structural Engineering*, American Society of Civil Engineers, Vol. 118, No.7, July, pp.1920-1936, New York, NY, USA.
- AISC-American Institute of Steel Construction, 1986. *Manual of steel construction -Load and resistance factor design*, First Ed., Chicago, IL., USA.
- ASCE-American Society of Civil Engineers, 1988. *Guide for Design of Steel Transmission Towers*, ASCE Manuals and Reports on Engineering Practice No. 52, Second Ed. New York, NY, USA.
- Bleich, F. and Bleich, H.H. 1952. *Buckling Strength of Metal Structures*, McGraw-Hill Book Co., New York, NY, USA
- Canadian Standards Association, 1986. *CAN/CSA-S37-M86. Antennas, towers, and antenna supporting structures*, National Standard of Canada, Rexdale, Ont., Canada.
- Canadian Standards Association, 1989. *CAN/CSA-S16.1-M89, Limit states design of steel structures*, National Standard of Canada, Rexdale, Ont., Canada.
- Timoshenko, S.P. and Gere, J.M. 1961. *Theory of Elastic Stability*, Second Ed., McGraw-Hill Book Co., New York, NY.

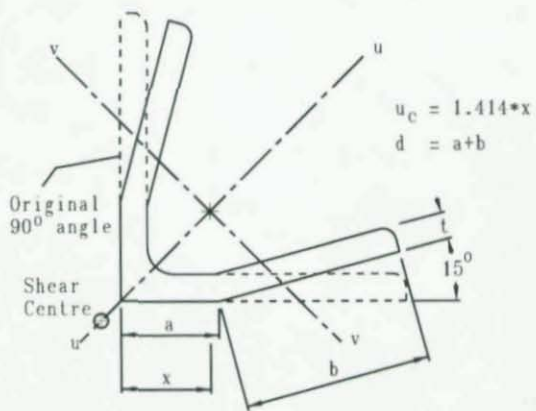


Fig. 1a Schifflerized Hot-Rolled Steel Angle

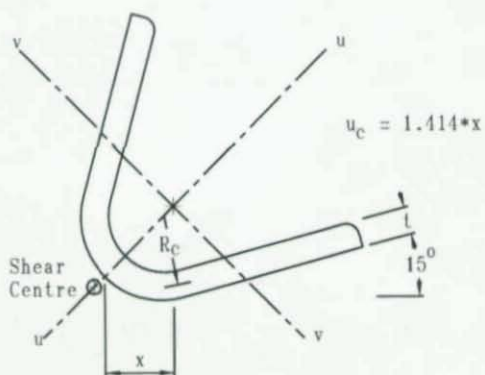


Fig. 1b Cold-Formed 60° Steel Angle

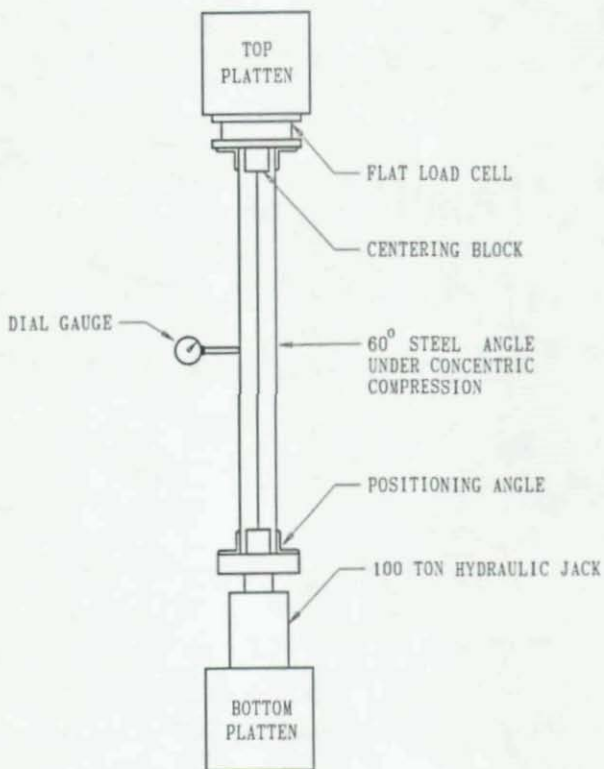


Fig. 2 TEST SET-UP FOR SCHIFFLERIZED AND COLD-FORMED 60° STEEL ANGLES

## Second Order Inelastic Analysis of Frames

by

Iqbal S. Sohal<sup>1</sup> and Liping Cai<sup>2</sup>

### 1. Introduction

The steel structures are being designed on the basis of first order or second order elastic analysis. However, recent developments in computer technology have created a potential for integrating the second order inelastic analysis with the design practice. In the inelastic analysis, the members are usually divided into several segments. However, in order to integrate the analysis and design, the analysis method must be very efficient which can be achieved if each member of the structural system can be modeled by only one beam-column element. To this end, recently, simple hinge by hinge method which utilizes only one element per member, was modified to include the effects of non-linear moment-curvature curve [1,4,8,10 and 11]. In these studies, the tangent stiffness matrix was obtained by stability function approach, but the intermediate yielding in the members was not considered. Thus, for the structural systems with members having uniform lateral load, the method may not give accurate results by using one element per member. Abdel-Ghaffar et. al. [1] derived stiffness matrix for member with intermediate yielding, but without the presence of axial load.

Herein, we present tangent stiffness matrix of a member with axial load and with intermediate plastic hinge derived by stability function approach in slope-deflection co-ordinates [11]. Then, these relationships are transformed into matrix analysis co-ordinates. A computer program based on this stiffness matrix is used to obtain load deflection behaviors of several types of frames which are compared with experimental results and the results from more accurate numerical methods.

### 2. Slope-Deflection Relation of Beam-Columns with Fully Developed Hinges

The slope-deflection relation of a beam-column with an intermediate plastic hinge can be expressed as [11]

$$\begin{bmatrix} M_A \\ M_B \end{bmatrix} = \begin{bmatrix} K_{11}^0 & K_{12}^0 \\ K_{21}^0 & K_{22}^0 \end{bmatrix} \begin{bmatrix} \theta_A \\ \theta_B \end{bmatrix} \quad (1)$$

where  $M_A$  and  $M_B$  are incremental end moments; and  $\theta_A$  and  $\theta_B$  are incremental end rotations; and

$$K_{11}^0 = \left(\frac{EI}{\gamma L}\right) kL \sin ka (kL \cos kb - \sin kb) \quad (2)$$

1. Assistant Professor, Dept. of Civil & Env. Engineering, Rutgers University, Piscataway, NJ, 08855

2. Graduate Student, Dept. of Civil & Env. Engineering, Rutgers University, Piscataway, NJ, 08855

$$K_{12}^0 = K_{21}^0 = \left(\frac{EI}{\gamma L}\right) kL \sin ka \sin kb \quad (3)$$

$$K_{22}^0 = \left(\frac{EI}{\gamma L}\right) kL \sin kb (kL \cos ka - \sin ka) \quad (4)$$

$$\gamma = -kL \cos ka \cos kb + \sin kL \quad (5)$$

Eqs. (2) to (5) represent stability functions for a member with a hinge. These can be simplified by substituting specified number of terms of Taylor's series for sin and cos as previously done for elastic cases [3].

When an additional plastic hinge is developed at an end say A, then  $M_A = 0$ . Now, the solution of Eq. (1) gives

$$\left(K_{21}^0 \left(\frac{K_{12}^0}{K_{11}^0}\right) + K_{22}^0\right) \theta_B = M_B \quad (6)$$

When hinges are developed at both ends, both  $M_A$  and  $M_B$  are zero.

### 3. Slope-Deflection Relationship of Beam-Columns with Hardening Hinges

The relationship presented in the previous section is for elastic-perfectly plastic moment-curvature ( $M-\Phi$ ) relationship. Herein, the stiffness matrix is modified to include the non-linearity in  $M-\Phi$  relationship. It is assumed that the slope of hardening portion of  $M-\Phi$  curve varies linearly from  $EI$  at initial yield moment to zero at the fully plastic state. This assumption has shown good agreement with the actual  $M-\Phi$  relationship of several types of sections [8]. Let  $\rho_i$  be a parameter to denote the stage of hardening at hinge  $i$ , defined by

$$\rho_i = \frac{M_i - M_{yc}}{M_{pc} - M_{yc}} \quad (7)$$

where  $M_i$  is moment at hinge  $i$ ,  $M_{yc}$  is the section yield moment reduced for presence of axial load and  $M_{pc}$  is the section plastic moment reduced for axial load. Now if  $\rho_0$ ,  $\rho_1$  and  $\rho_2$  are the parameters to denote hardening at intermediate point and the end points respectively, then modified stiffness coefficients are obtained from

$$K''_{11} = \left(K'_{11} - K'_{12} \left(\frac{K'_{21}}{K'_{22}}\right) \rho_2\right) (1 - \rho_1) \quad (8)$$

$$K''_{12} = K'_{21} = K'_{12} (1 - \rho_1) (1 - \rho_2) \quad (9)$$



$$K_{22}^n = \left( K_{22}^0 - K_{21}^0 \left( \frac{K_{12}^0}{K_{11}^0} \right) \rho_1 \right) (1 - \rho_2) \quad (10)$$

where

$$K^0 = (K^0 - K^e) \rho_0 + K^e \quad (11)$$

in which  $K^0$  is the stiffness matrix of the beam-column with a fully developed intermediate hinge and  $K^e$  is the elastic stiffness matrix of the beam-column.

#### 4. Transformation of Slope-Deflection Relation to Matrix Analysis Co-ordinate

For analysis of framed structures, it is convenient to use matrix analysis co-ordinates. Therefore, stiffness matrix presented in previous section is needed to be transformed to matrix analysis co-ordinate. Moreover, this stiffness matrix does not include the effects of sway i.e. shear force due to  $P - \Delta$  moment is not included. The transformed matrix including the shear due to  $P - \Delta$  moment is used in the analysis of the frame examples [11].

#### 5. Numerical Procedure in the Analysis Method

Herein, we utilize Arc Length Control Method [3,11] for tracing the load-deflection behavior of structural frames. This method has advantage over usual load control and displacement control methods in that it can be used for tracing load-deflection relationship that exhibit softening, snapthrough and snapback behavior.

#### 6. Numerical Examples

To show the usefulness and to validate the developed computer program, herein, we present solutions of several examples.

##### 6.1 Imperfect Column

A second order inelastic analysis (SOIA) computer program must be able to predict the strength of a member under pure axial loads which is an extreme case of general member in structural systems. The most of SOIA can not achieve this by using only one element for the member. The program developed here has this capability and is demonstrated by analyzing simply supported imperfect columns with several slenderness values  $KL/r_x$ . The imperfection is taken as  $\delta_0 = L/1000$ . The shape factor for the columns is 1.13. The ultimate loads are compared with SSRC Curve 2 [6] in Fig.1. There is reasonably a good agreement.

##### 6.2 Portal Frame with Distributed Horizontal Load

Portal frame shown in Fig. 2 is subjected to an increasing distributed load at the left-side column and two constant concentrated gravity loads applied at the top joints of the frame. The columns are made of  $W8 \times 31$  sections and beam is of  $W10 \times 112$ . An intermediate hinge forms at the left-side column when the uniform load is increased. The results obtained by considering intermediate hinges are compared with those

without intermediate hinges for different values of gravity loads. The difference between the results is significant and it increases as  $P/P_e$  decreases.

### 6.3 El-Zanaty Portal Frame

A portal frame, Fig. 3, originally analyzed by El-Zanaty [5], is analyzed by the developed modified plastic hinge method and results are compared with plastic zone method as well as simple plastic hinge method in Fig. 3. All the members of the frame have  $W8 \times 31$  sections. The yield stress  $\sigma_y$ , Young's modulus  $E$  and the maximum residual stress  $\sigma_{rc}$  are taken as 36 ksi, 29,000 ksi and  $0.3\sigma_y$  respectively. The lateral load  $H$  and two constant concentrated gravity loads of  $0.6P_y$  are applied at the top joints of the frame as shown in the inset of Fig. 3. The developed analysis method uses one element for each member. The simple plastic hinge method gives a highest load-deflection curve, because it uses elastic-perfectly plastic moment-curvature relationship. The modified plastic hinge method considers non-linear moment-curvature relationship which gives a lower load-deflection curve. The presence of residual stresses in the frame results in early yielding of the frame which further lowers the curve. However, there is a good agreement between the modified plastic hinge method with residual stresses and plastic zone method.

### 6.4 Leaned Frame

A leaned portal frame shown in Fig. 4 is analyzed by the proposed modified plastic hinge method and the strength of the right-side beam-column is compared with the LRFD [2] equations using the simplified LeMessurier's K-factor [9] and the results from plastic-zone analysis. In the analysis, yield stress  $\sigma_y$ , Young's modulus  $E$  and the maximum residual stress  $\sigma_{rc}$  are taken as  $250\text{N/mm}^2$ ,  $200,000\text{N/mm}^2$  and  $0.3\sigma_y$  respectively. All the members are assumed to be perfectly straight and in plumb. The columns are made of  $W8 \times 31$  section and the beam is made of  $W8 \times 67$ . The comparisons are made for slenderness ( $L/r_x$ ) values equal to 40, and for  $\alpha$ , the ratio of the axial load applied to the leaned column on the left side of frame to that applied to the lateral-load resisting column on the right side, equal to 0 and 2. The end restraint factors  $G_A$  and  $G_B$  are taken as 4 and  $\infty$  respectively. The strength curves are shown in Fig. 4. The good agreement can be seen between the proposed method and plastic zone analysis.

### 6.5. Two-story Rectangular Frame

A one-quarter scaled two-story frame [12] is analyzed by the developed method and compared with experimental results and plastic zone method. The beams of the frame shown in Fig. 5, have  $H100 \times 50 \times 4 \times 6$  section (section height = 100 mm, section width = 50 mm, web thickness = 4 mm, flange thickness = 6 mm) and the columns have  $H100 \times 100 \times 6 \times 8$  section. The frame is subjected to constant joint vertical loads  $P$  of 20 ton with an increasing horizontal load  $H$  at the left top joint. The connections are welded and stiffened to prevent local buckling in the joint panels. Therefore, in both the present method and the plastic zone method, local buckling and lateral buckling are neglected. The residual stresses are considered in both the

modified plastic hinge method and plastic zone method. The second order effects are neglected in plastic zone method. So the load-deflection curves by the modified plastic hinge method are slightly lower than that by plastic zone method. The analysis methods give conservative peak loads, because they did not consider the effects of strain hardening of the material. The numerical elastic stiffness of the structure is higher than that obtained in experiments, because the column-base is not perfectly-fixed in the tested frame.

## 6.6 Gable Frame

A full sized gable frame [12] is analyzed by the modified second order plastic hinge method and first-order simple plastic hinge method. Their results are compared with the experimental results in Fig. 6. The frame consists of two  $H298 \times 149 \times 5.5 \times 8$  columns and two  $H250 \times 125 \times 6 \times 9$  beams. The columns are hinged to their bases. Four vertical loads are applied on the beams as shown in Fig. 6 with no horizontal load. The total plotted load  $W$  in the ordinate includes the dead load of the frame and the loading apparatus ( $W_D = 1,250\text{kg}$ ). All curves start at this load. It can be seen from Fig. 6 that the simple plastic hinge method, in which the elastic-perfectly plastic type of moment-curvature relationship is used, over predicts the ultimate load and the modified plastic hinge method gives a conservative and very close estimation of the ultimate load. The difference is because, in the modified plastic hinge method, the residual stresses are considered while strain hardening is neglected. Also the hinged ends are not perfectly-hinged in the tested gable frame, so the numerical elastic stiffness of the structure is less than that obtained in experiments. The softening part in the experimental load-deflection curve is due to local buckling of the compression flange of the right hand side column. The local buckling effects are not included in the shown results.

## 7. Summary and Conclusions:

Tangent stiffness matrix of a member with axial load and with intermediate plastic hinge, derived by stability function approach, is presented. Then, the results computed on the basis of the presented stiffness matrix are shown and discussed. To highlight the significance of considering intermediate hinges, two examples were analyzed. First, an imperfect pin-ended column which is an extreme case of general beam-column member of a structural system, is analyzed by using only one element for the entire column and the results are found in reasonably good agreement with SSRC curve-2. Note that without considering intermediate hinge, column strength cannot be predicted accurately by using one element for the entire column. Secondly, the load-deflection behavior of a portal frame under uniformly distributed lateral load is analyzed to show the significance of considering intermediate plastic hinge. The load-deflection behaviors computed by considering intermediate yielding are lower than those computed without considering intermediate yielding. The difference is significant for lower values of axial load.

The computer code is validated by analyzing El-Zanaty frame [5], a leaned frame, a two-story rectangular frame and a gable frame and comparing the results with the experiments and other available numerical methods. The computed results show a

reasonably good agreement with experiments and other more extensive computational analysis methods.

#### **Acknowledgement:**

*The study is supported by National Science Foundation through Grant No. MSM-9010208. The authors wish to thank Program Manager Dr. K.P. Chong for his support.*

#### **References:**

1. Abdel-Ghaffar, M., White, D.W., and Chen, W.F., 'Simplified Second-Order Inelastic Analysis for Steel Frame Design', Structural Engineering Report No. CE-STR-90-34, School of Civil Engineering, Purdue University, West Lafayette, IN, 1990, 16 pages.
2. American Institute of Steel Construction, Load and Resistance Factor Design Specification for Structural Steel Buildings', Chicago, IL, 1986.
3. Chen, W.F. and Lui, E.M., 'Stability Design of Steel Frames', CRC Press Boca Raton, FL, 1991, 380 pages.
4. Chen, W.F. and Sohal, I.S. 'Plastic Design and Advanced Analysis of Steel Structures', Springer Verlag, New York, NY, to be published in 1993.
5. El-Zanaty, M.H., Murray, D.W. and Bjorhovde, R., 'Inelastic Behavior of Multistory Steel Frames', The University of Alberta, Structural Engineering Report No. 83, April, 1980.
6. Galambos, T.V., 'Guide to Stability Design Criteria for Metal Structures', Fourth Edition, John Wiley & Sons, New York, NY, 1988, 786 pages.
7. Kanchanalai, T., 'The Design and Behavior of Beam-columns in Unbraced Steel Frames', AISI Project No. 189, Report No. 2, Civil Engineering/Structures Research Lab., University of Texas at Austin, Texas, 1977, 300 pages.
8. King, W.S., White D.W. and Chen, W.F., 'A modified Plastic Hinge Method for Second Order Inelastic Analysis of Steel Rigid Frames', Structural Engineering Report No. CE-STR-90-13, School of Civil Engineering, Purdue University, West Lafayette, IN, 1990, 34 pages.
9. LeMessurier, W. J., 'A Practical Method of Second-Order Analysis, Part 2-Rigid Frames', Engineering Journal, AISC, 14, 2, 1977, pp.48-67.
10. Liew, J.Y. Richard., White, D.W. and Chen, W.F., 'Second-Order Refined Plastic Hinge Analysis for Frame Design', Structural Engineering Report No. CE-STR-92-14, School of Civil Engineering, Purdue University, West Lafayette, IN, 1992,



40 pages.

11. Sohal, I. S., and Cai, L., 'An Efficient Second Order Inelastic Method', submitted for possible publication in a journal.
12. Toma, S. and Chen, W. F., 'Calibration Frames for Second-order Inelastic Analysis in Japan', Structural Engineering Report No. CE-STR-92-16, Purdue University, West Lafayette, IN, 1992, 34 pp.

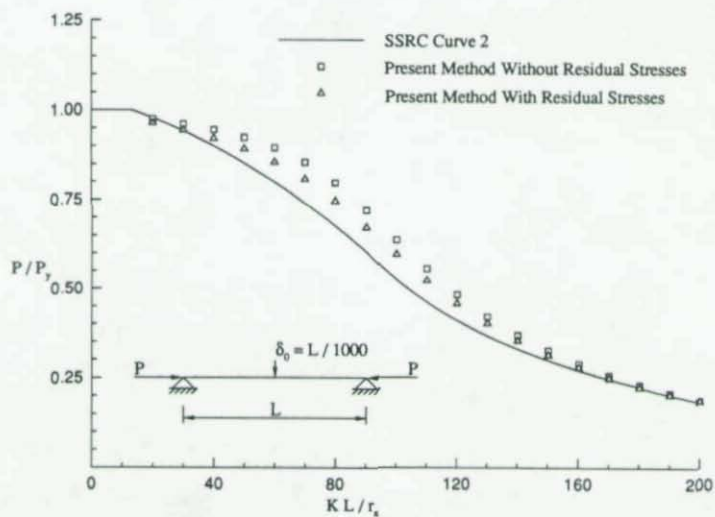


Figure 1 Comparison of Computed Column Strength with a SSRC Curve



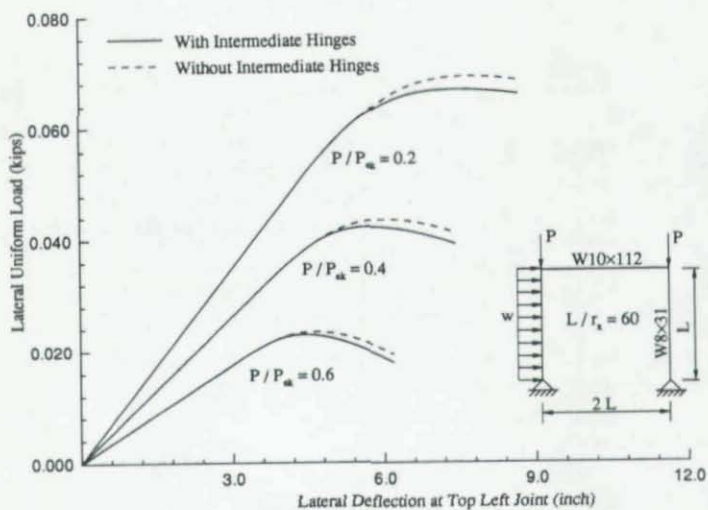


Figure 2 Effects of Considering Intermediate Hinge on Load-Deflection Behavior of a Portal Frame

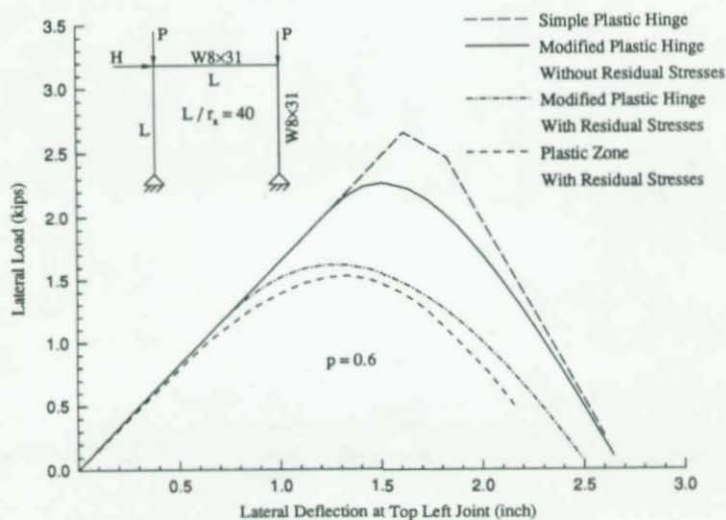


Figure 3 Load-Deflection Behavior of El-Zanaty Portal Frame

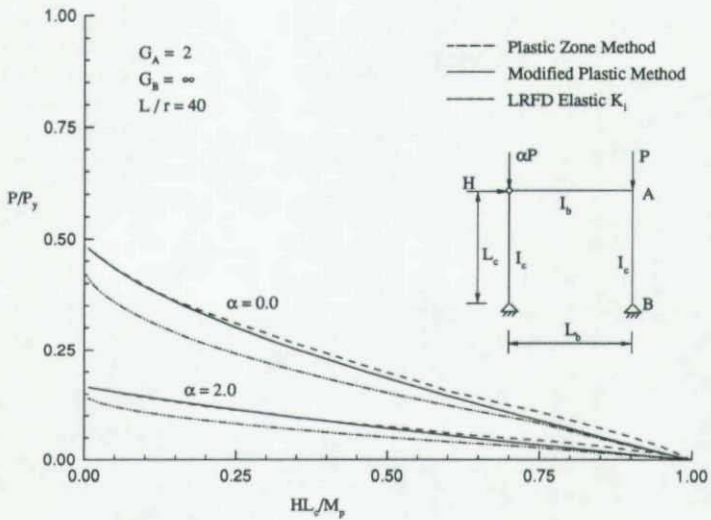


Figure 4 Strength of a Leaned Frame with Member Slenderness ratio of 40

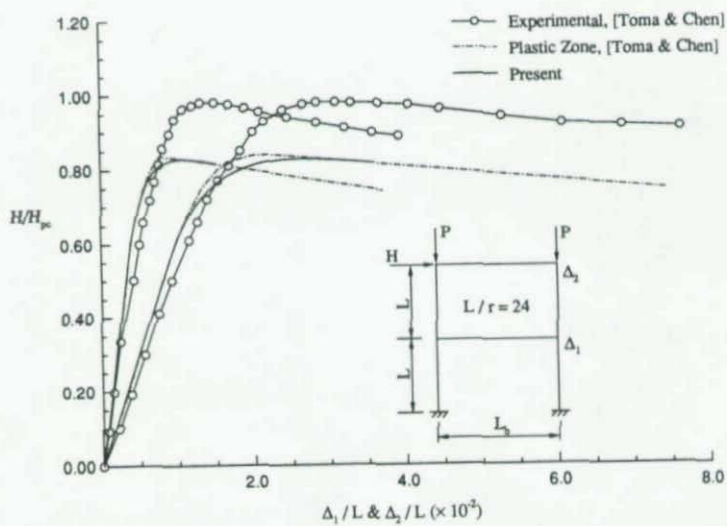


Figure 5 Comparison of Computed and Experimental Load-Deflection Behavior of a Two-story Frame

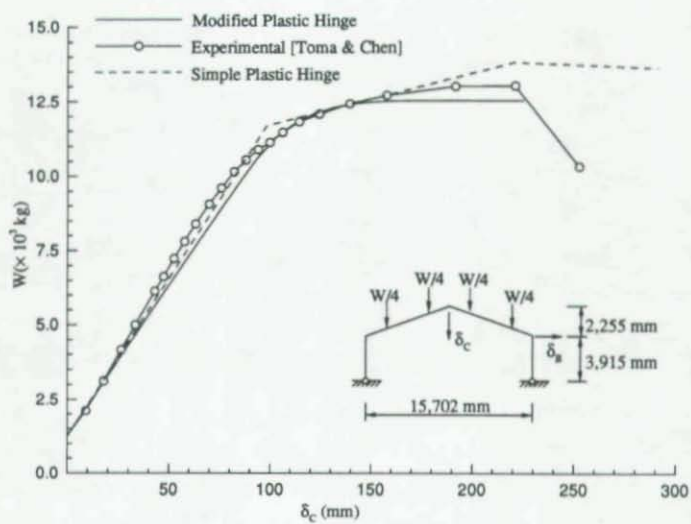


Figure 6 Comparison of Computed and Experimental Load vs. Vertical Displacement Curves of a Gable Frame



## Effective Strategies for Elasto-Plastic and Finite Displacement Analysis of Spatial Steel Bridges

By Masato KANO\*, Toshiyuki KITADA\*\*, Mitsunori NIBU\*\*\* and Katsuhiro TANAKA\*\*\*\*

### SUMMARY

A computer program named EPASS has been developed for the elasto-plastic and finite displacement analysis of spatial steel bridge structures with/without cables. This paper deals with the efficiency of the strategies such as pre-processing analysis, arc-length method, current stiffness parameter, under-relaxation method and post-processing which are used in EPASS for accurate evaluation of ultimate load, labor-saving in making input data and processing output data, as well as reduction of computation time in the elasto-plastic and finite displacement analysis for calculating the load carrying capacity of big and complicated steel bridge structures. A practical example of a cable stayed bridge is analyzed with EPASS to verify the efficiency of the proposed strategies.

### 1. INTRODUCTION

In recent years, a lot of long-span steel bridges with cables such as suspension bridges, cable-stayed bridges and Nielsen-type arch bridges have been constructed and some are now under construction in Japan. It is very important to investigate the load carrying capacity of such a long-span bridge structure and to confirm its safety. There are some computer programs<sup>1)-2)</sup>, which have been developed to cope with the problem. Some programs for comprehensive purpose based on finite element methods, such as MARC and NASTRAN and so forth, can be also used for this purpose. But, these programs are inconveniently big for the analysis of steel bridge structures and a big computer is necessary for these programs. That is the reason we have developed a computer program named EPASS<sup>3)</sup> for the elasto-plastic and finite displacement analysis of spatial steel bridge structures with/without cables.

The following troublesome work and problems occur generally in carrying out elasto-plastic and finite displacement analyses to get the load carrying capacity of big and complicated steel bridge structures:

- 1) Preparation of input data concerning the initial configuration of an analytical model with initial imperfection and residual stress subjected to dead load and prestressing load of cables.
- 2) The prediction of accurate ultimate loads in analyses by a load incremental method and the estimation of proper load increment.
- 3) The accurate and efficient evaluation of ultimate loads.
- 4) Labor-saving in making input data and processing output data.
- 5) The reduction of computation time.

This paper deals with the efficiency of the strategies which are used in EPASS for solving the troublesome work and problems mentioned above.

---

\* Bridge & Computer Engineering Co., Ltd., Osaka, Japan.

\*\* Associate Professor, Department of Civil Engineering, Osaka City University, Osaka, Japan, Member-at-Large of SSRC.

\*\*\* Bridge & Computer Engineering Co., Ltd., Osaka, Japan.

\*\*\*\* Japan Information Processing Service Co., Ltd., Osaka, Japan.

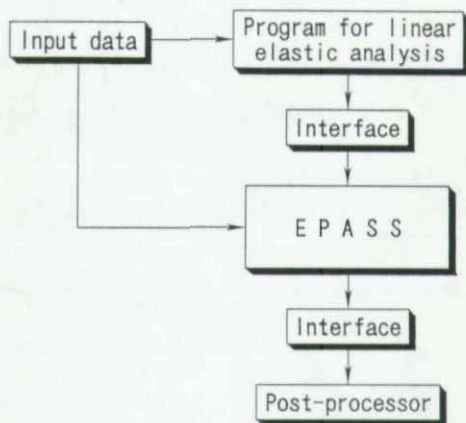


Fig. 1 Constitution of the system

## 2. OUTLINE OF EPASS

A system, containing EPASS, for the elasto-plastic and finite displacement analysis of spatial steel bridge structures is shown in Fig. 1. The program, EPASS, can be connected with both a pre-processor for a linear elastic analysis and a post-processor for representing numerical results diagrammatically. And EPASS itself consists of input, solution and output modules from a functional point of view.

Using the pre-processor, it becomes possible to carry out the following analyses:

1) Evaluation of the expected initial configuration of an analytical model  
 In an analysis of a bridge with cables, such as a cable stayed bridge, the expected initial configuration of its analytical model subjected to dead load and prestressing load has to be evaluated. In this system, a pre-processing linear elastic analysis is carried out previously to calculate stress resultants in all the members of an analytical model subjected to dead load and prestressing load. The expected initial configuration can be generated easily using the stress resultants as initial ones at starting load level.

2) Evaluation of the initial deflection of structure  
 The most adverse initial configuration of a structure can be evaluated using the first buckling mode obtained by a pre-processing eigenvalue analysis.

## 3. EFFECTIVE STRATEGIES FOR ANALYSIS OF REAL BRIDGES

### 3.1 Arc-length method

To accurately evaluate an unknown ultimate load by an ordinary load increment method, it is required but difficult to select an appropriate load increment according to the degree of nonlinearity and using a smaller load increment near the unknown ultimate load which may be predicted after several trials. Moreover, it is also very difficult without adequate knowledge and experience to predict the unknown ultimate load and to select a suitable load increment. Besides,

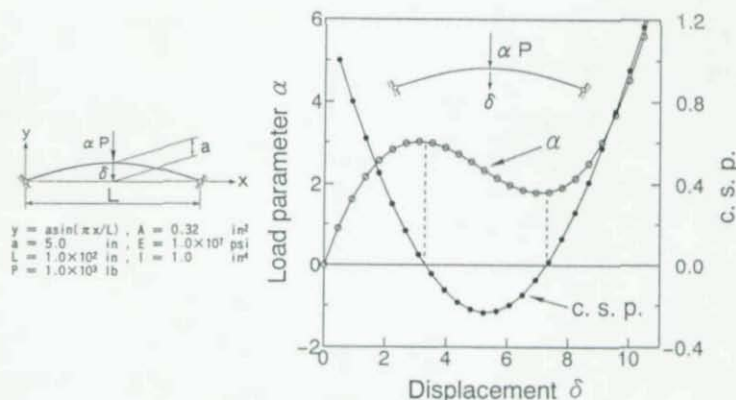


Fig. 2 Current stiffness parameter

it is not necessarily possible to practice several trials in nonlinear analyses of real bridge models because of computation time and cost. For these reasons, an arc-length method has been introduced into this program, based on Refs. 4) and 5). As a result, the ultimate load of an analytical model has been able to be evaluated easily because the equilibrium path of the model after its ultimate load point can be traced using the arc-length method.

### 3.2 Current Stiffness Parameter

In order to obtain the ultimate load effectively, a current stiffness parameter (c.s.p) proposed in Ref. 6) has been adopted. The current stiffness parameter is positive in stable region, negative in unstable region and equal to zero at the stationary points. It can be defined as follows. The incremental load vector of a loading level  $i$ ,  $\Delta \mathbf{R}_i$  and the corresponding incremental displacement vector  $\Delta \mathbf{r}_i$  are standardized by the Euclidean norm of the incremental load vector of loading level  $i$ ,  $|\Delta \mathbf{R}_i|$ . And  $Sp_i^*$  is defined as the reciprocal of the product of these standardized vectors by Eq. (1):

$$Sp_i^* = |\Delta \mathbf{R}_i|^2 / \Delta \mathbf{r}_i^T \Delta \mathbf{R}_i \quad (1)$$

The value of  $Sp_i^*$  becomes small and large when the structure is softening and stiffening respectively. The current stiffness parameter is defined by:

$$Sp_i = Sp_i^* / Sp_1^* \quad (2)$$

in which  $Sp_1^*$  is the value of  $Sp_i^*$  in loading level 1, where the load-displacement relations of a system under consideration are linear.

Fig. 2 shows how the current stiffness parameter changes in accordance with loading levels in the analysis of a 2 hinged arch<sup>7)</sup> as an example. The current stiffness parameter becomes equal to zero at the stationary points on the load-displacement curve, as indicated in the figure.

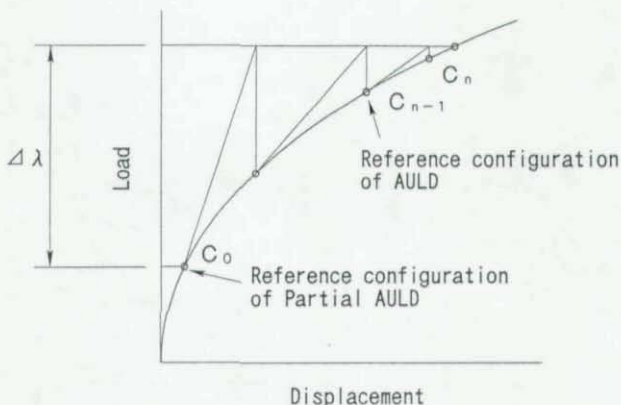


Fig. 3 AULD and Partial AULD

### 3.3 Partial AULD (Approximate Updated Lagrangian Description)

A load-displacement curve with three points is shown in Fig. 3 to explain two kinds of ULD (Updated Lagrangian Description) methods used in EPASS. Point  $C_0$  indicates the converged configuration of a previous load step. Points  $C_{n-1}$  and  $C_n$  correspond two successive configurations until the next converged point of this load step. To describe the incremental strain of element in the configuration  $C_n$ , the AULD (Approximate Updated Lagrangian Description) takes Point  $C_{n-1}$ , which is defined approximately by a rigid body motion of the undeformed body of the element, as a reference configuration<sup>9)</sup>. The PULD (Partially Updated Lagrangian Description) makes use of the concept adopted in the ULD. A major difference of the PULD compared with the ULD is that the coordinates of each element in the PULD are updated once only at the beginning of each load step. The numerical manipulations within each load step are then performed like a TLD manner<sup>9)</sup>.

In this program to evaluate stress accurately, a Partial AULD, a new type of Lagrangian description method, has been adopted improving the AULD with the concept used in the PULD. This description method has two reference configurations. The Partial AULD takes Point  $C_{n-1}$  as a reference configuration to make the stiffness matrix like the AULD. But it takes the converged configuration of the previous load step  $C_0$  as the reference configuration when the strains, stresses and stress resultants of each element are evaluated using the incremental displacement obtained.

It is advantageous to use the AULD in geometrically nonlinear problems and to use the Partial AULD in case that materially nonlinear problems are analyzed by the arc-length method. The Partial AULD is not suitable for problems in which geometrical nonlinearity is predominant. As can be seen in Fig. 4, convergence in the case of the Partial AULD becomes difficult near the critical load in an elastica problem. While plastic area obtained in the case of the AULD tends to spread widely compared with the Partial AULD if larger load increment is used. It is because larger strain could occur at an iterative step than at the final converged one during an incremental load step using the arc-length method in the AULD as shown in Fig. 5. Smaller load increment makes it possible to obtain the accurate plastic area even if the AULD, but it requires much more computation time. Accordingly it is advantageous to use the Partial AULD or under-relaxation method<sup>10)</sup> in the case of elasto-plastic analyses using the arc-length method.

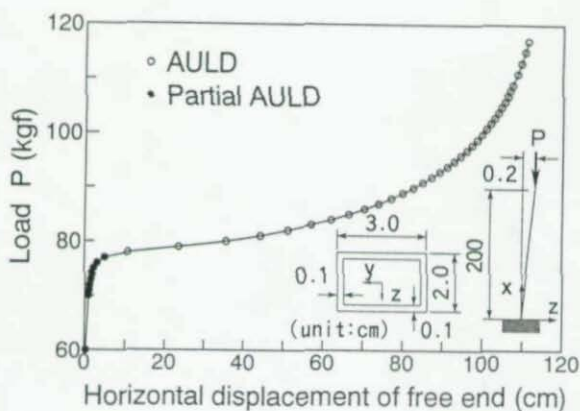


Fig. 4 Comparison of AULD and Partial AULD

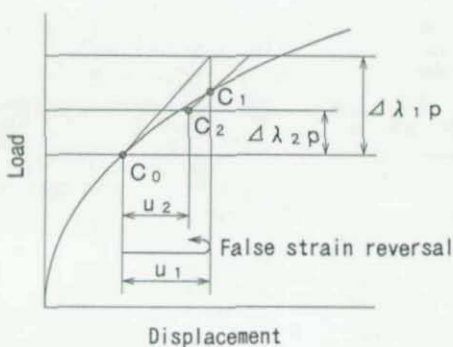


Fig. 5 A problem of AULD in elasto-plastic analysis

### 3.4 Other effective strategies

Other effective strategies introduced in this program for the analyses of spatial steel bridge structures are given as follows:

#### 1) Simplification of generating input data on residual stress

The input data on residual stress caused by welding can be generated automatically according to the residual stress distribution proposed by the second author through their experimental study<sup>11)</sup> only by designating the material type of steel.

#### 2) Restarting function of calculation

This program has a function of restarting calculation. Even if a calculation is interrupted for a reason unexpected before an unknown ultimate load, it can be resumed from that state by changing the load increment.



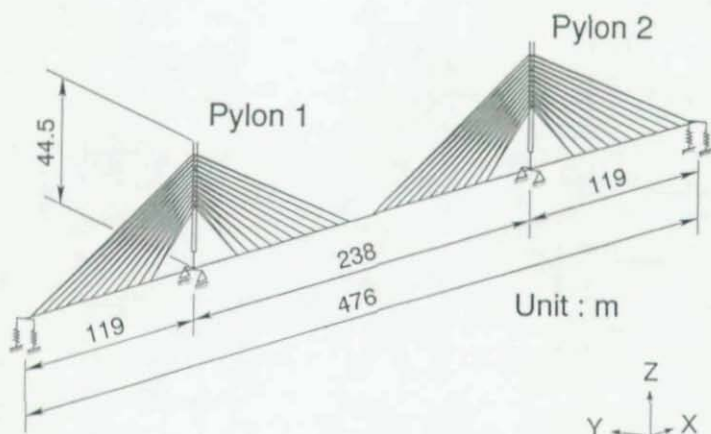


Fig. 6 Analytical model of a cable stayed bridge

#### 4. PRACTICAL EXAMPLE OF A CABLE STAYED BRIDGE

##### 4.1 Analytical model<sup>(2)</sup>

An actual example of a multi-cable type cable stayed bridge is analyzed by the system to verify the efficiency of the strategies mentioned above. In this model shown in Fig. 6, elasto-plastic box-sectional beam elements, which can simulate the elasto-plastic and finite displacement behavior of steel members subjected to compression, bending and torsion, are used for the pylons because the purpose of the analysis is to evaluate the load carrying capacity of the pylons. While elastic beam elements and rod elements are adopted to the main girder and cables respectively because it is sufficient to consider only elastic finite displacement behavior for these members. The load condition is described by:

$$1.0(D1+PS+D2)+0.7(D1+D2)+\alpha L \quad (3)$$

where

- D1 : pre-dead load (the weight of main girder, deck plates and pylons)
- D2 : post-dead load (the weight of pavement etc.)
- PS : prestressing load of cables
- $\alpha$  : load parameter to control load levels
- L : live load provided by JSHB<sup>(3)</sup>

First, the expected configuration of the completion model subjected to  $1.0(D1+PS+D2)$  is generated and then the load  $0.7(D1+D2)$  is applied to the model. Finally, the live load  $\alpha L$  is gradually increased until or after the ultimate load.

##### 4.2 Residual stress distribution in the cross sections of the pylons

The residual stress distribution shown in Fig. 7 is automatically introduced into the cross sections of the pylons.

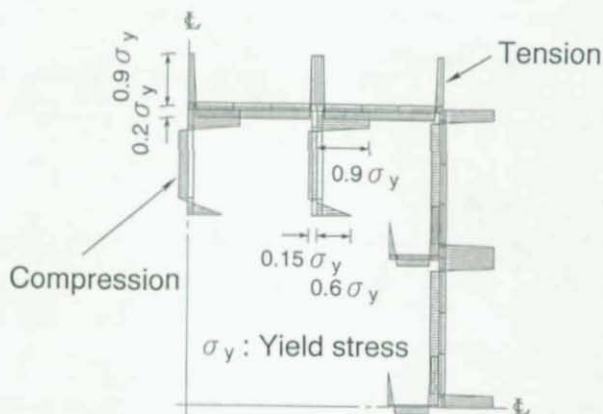


Fig. 7 Residual stress distribution of cross section of pylon

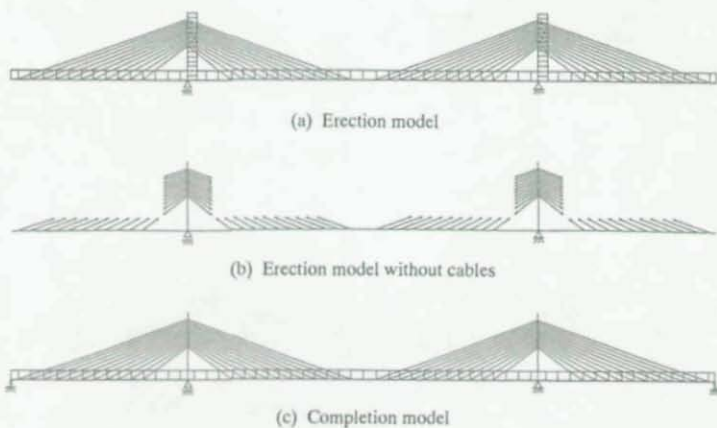


Fig. 8 Models for pre-processing analysis

#### 4.3 Pre-processing analyses

Pre-processing linear elastic analyses are carried out for evaluating the expected initial configuration of the analytical model subjected to the dead load,  $(D1+D2)$  and the prestressing load, PS, as shown in Fig. 8. As the results, stress resultants of each element

a) in the erection model without spring supports in the both ends of the main girder, subjected to the pre-dead load, D1,

b) in the erection model without cables subjected to external forces equivalent to the prestressing load, PS, and

c) in the completion model subjected to the post-dead load D2 are evaluated and then these stress resultants are introduced as the initial ones into the completion model together with the dead load (D1+D2) as the initial load and with the prestressing forces PS. The expected initial configuration of the completion model can be generated like this because these initial stress resultants are balanced with the initial load (D1+D2) and the prestressing load PS.

#### 4.4 Results of the analysis

Fig. 9 shows the relationships between the load parameter and deflection of the top of the Pylon 2. While it may be difficult to evaluate exactly the ultimate load by judging from the gradient of the load-deflection curve in the case of load increment method, it can be seen that the ultimate load can be accurately obtained in the case of arc-length method using the under-relaxation method simultaneously. However, converged solutions are not obtained in this example if only the arc-length method is used.

Fig. 10 shows that the ultimate load can be predicted through the extrapolation of a load-c.s.p. curve plotted from the numerical results by the load increment method shown in Fig. 9. As compared Fig. 9 with Fig. 10, it can be seen that this prediction method of ultimate load is very effective. And it is possible by using a load-c.s.p. diagram to know how close the final load level obtained is to an unknown ultimate load and to ascertain accuracy of the ultimate load obtained by an ordinary load increment method. Fig. 11 illustrates the deformation of the whole bridge at the ultimate state. In the ultimate state the out-of-plane deformation of Pylon 2 is predominant. The deformation and plastic area of Pylon 2 are shown in Fig. 12 which is very useful to understand the failure mode of a spatial steel structures.

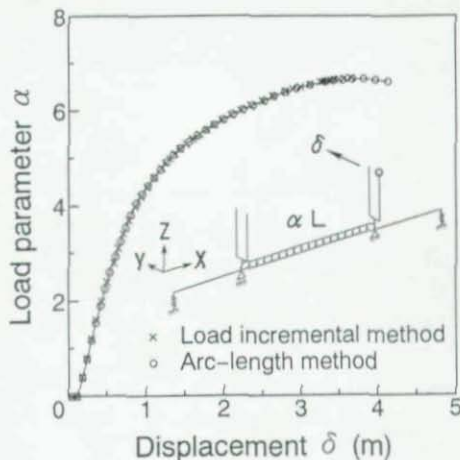


Fig. 9 Comparison of load incremental method with arc-length method

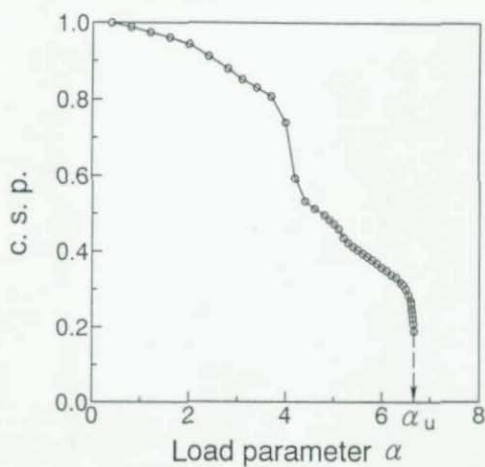


Fig. 10 Prediction of ultimate load by c.s.p.

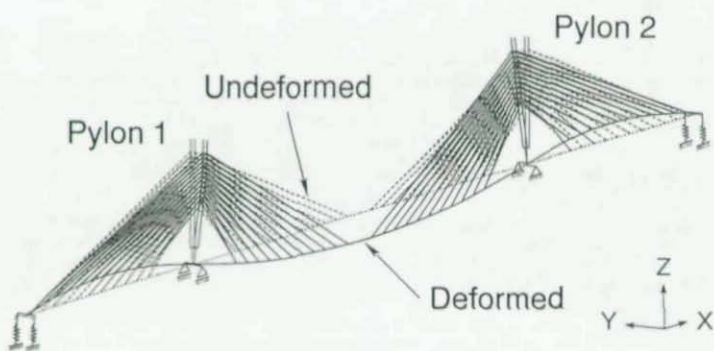


Fig. 11 Deformation of the bridge at ultimate state

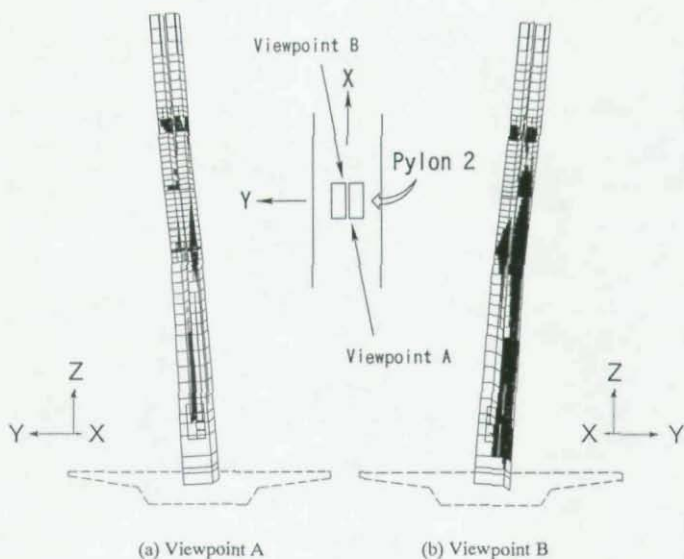


Fig. 12 Deformation and plastic area of Pylon 2 at ultimate state

## 5. CONCLUSION

The efficiency of the strategies such as pre-processing analysis, arc-length method, current stiffness parameter, under-relaxation method and post-processing which are used in EPASS for the accurate evaluation of ultimate load, labor-saving in making input data and processing output data, as well as reduction of computation time in the elasto-plastic and finite displacement analysis for calculating the load carrying capacity of big and complicated steel bridge structures, has been verified in this paper.

## REFERENCES

- 1) Komatsu, S. and Sakimoto, T. : Nonlinear Analysis of Spatial Frames Consisting of Members with Closed Cross-Sections, Proc. of JSCE, No.252, pp.143-157, August 1976.
- 2) Maeda, Y. and Hayashi, M. : In-Plane and Out-of-Plane Instability of a 297m Span Steel Arch Bridge, Transportation Research Record 664, Bridge Engineering, Vol.1, pp.246-254, September 1978.
- 3) Kitada, T., Ohminami, R., Nibu, M. and Tanaka, K. : Exploitation of Computer Program to Analyze Ultimate Strength of Steel Bridges Using Cable Members, Proc. of Symposium on Computational Methods in Structural Engineering and Related Fields, Vol.13, pp.89-94, July 1989 (in Japanese).
- 4) Crisfield, M. A. : A Fast Incremental/Iterative Solution Procedure that Handles "Snap-through", Computers & Structures, Vol.13, pp.55-62, 1981.
- 5) Bellini, P. X. and Chulya, A. : An Improved Automatic Incremental Algorithm for the Efficient Solution of Nonlinear Finite Element Equations, Computers & Structures, Vol.26, No.1, pp.99-110, 1987.



- 6) Bergan, P. G., Holand, I. and Soreide, T. H. : Use of the Current Stiffness Parameter in Solution of Nonlinear Problems, *Energy Methods in Finite Element Analysis* (ed. Glowinski, R., Rodin, E. Y. and Zienkiewicz, O. C.), pp.265-282, John Wiley & Sons, 1979.
- 7) Haisler, W. E. and Stricklin, J. A. : Displacement Incrementation in Non-Linear Structural Analysis by the Self-Correcting Method, *International Journal for Numerical Methods in Engineering*, Vol.11, pp.3-10, John Wiley & Sons, 1977.
- 8) Jetteur, P., Cescotto, S. and deGoyet, V. : Improved Nonlinear Finite Elements for Oriented Bodies Using an Extension of Marguerre's Theory, *Computers & Structures*, Vol.17, No.1, pp.129-137, 1983.
- 9) Wong, M. B. and Tin-Loi, F. : Geometrically Nonlinear Analysis of Elastic Framed Structures, *Computers & Structures*, Vol.34, No.4, pp.633-640, 1990.
- 10) Stricklin, J. A., Haisler, W. E., MacDougall, H. R. and Stebbins, F. J. : Nonlinear Analysis of Shells of Revolution by the Matrix Displacement Method, *Journal of American Institute of Aeronautics and Astronautics*, Vol.6, No.12, pp.2306-2312, 1968.
- 11) Komatsu, S., Ushio, M. and Kitada, T. : An Experimental Study on Residual Stresses and Initial Deformations of Stiffened Plates, *Proc. of JSCE*, Vol.265, pp.25-35, September 1977 (in Japanese).
- 12) Kitada, T., Nakai, H., Kamei, M. and Wakabayashi, Y. : Ultimate Load Capacity of a Cable-Stayed Steel Bridge with Multiple Cables, *Proc. of Int. Sym. for Innovation in Cable-Stayed Bridge*, Fukuoka, Japan, pp.41-52, April 1991.
- 13) Japan Road Association : Specification for Design of Highway Bridges, Part2, Steel Bridges, 1990 (in Japanese).



## THE EFFECTS OF FRAME GEOMETRICAL IMPERFECTIONS ON INELASTIC BUCKLING

E. D'AMORE<sup>1</sup>, A. DE LUCA<sup>1</sup>, M. DE STEFANO<sup>2</sup>

1. University of Reggio Calabria, ITALY

2. University of Napoli "Federico II", ITALY

### Summary

In this paper the effects of column and frame imperfections are evaluated. In particular, following the procedure already presented in previous studies, different amounts of frame out-of-plumb are considered in the analysis together with the equivalent column imperfections. The results obtained by means of advanced inelastic analysis of frames subjected to vertical joint loads have allowed to make a preliminary evaluation of the sensitivity of frame inelastic buckling to the magnitude of frame out-of-plumb.

The concept of frame equivalent global imperfection has been then introduced and it has been proved how the introduction of these equivalent frame imperfections allows to account for all imperfections including residual stresses, column out-of-camber, frame out-of-plumb. Extensive parametric analyses have been carried out to assess adequacy of such an approach for frames characterized by different number of stories, bays and for a very wide range of column and frame slenderness.

### Introduction

The effects of geometrical and mechanical imperfections on the behavior of steel structures are nowadays well known and all current codes provide specifications to account for them. Steel frames present global imperfections in addition to those affecting the column due to unavoidable inaccuracies of the construction process. In recent years some codes [1,2,3] have considered the effects of frame imperfections by means of an equivalent initial sway at the top of the frame.

In particular, when second-order inelastic analysis is used for evaluating the buckling load of frames, the European code EC3 [1] requires that the column mechanical and geometrical imperfections be accounted for by means of an equivalent geometrical imperfection. This is intended to implicitly represent both the residual stresses due to thermal and forming processes and the initial camber. The column equivalent imperfection is defined as a function of the buckling curve of the considered profile; the EC3 design values of the initial bow imperfection  $v_0/L$  are reported in Figure 1.

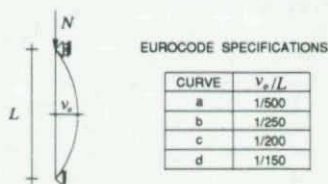


*Figure 1. Eurocode equivalent column imperfection.*

In addition to the member (column) imperfections, the unavoidable global imperfections arising from the erection process must be considered in the analysis. For this purpose, the EC3 specifies an initial out-of-plumb given by:

$$\phi = k_c k_s \phi_0 \quad (1)$$

being:

$$\phi_0 = 1/200,$$

$$k_c = (0.5 + 1/n_c)^{1/2} \leq 1 \text{ where } n_c = \text{number of columns at a single story,}$$

$$k_s = (0.2 + 1/n_s)^{1/2} \leq 1 \text{ where } n_s = \text{number of stories.}$$

On the other hand, the EC3 itself introduces a frame erection tolerance expressed by:

$$\phi = 0.0035/n_s^{1/2} \quad (2)$$

which is also reported as a function of  $n_s$ .

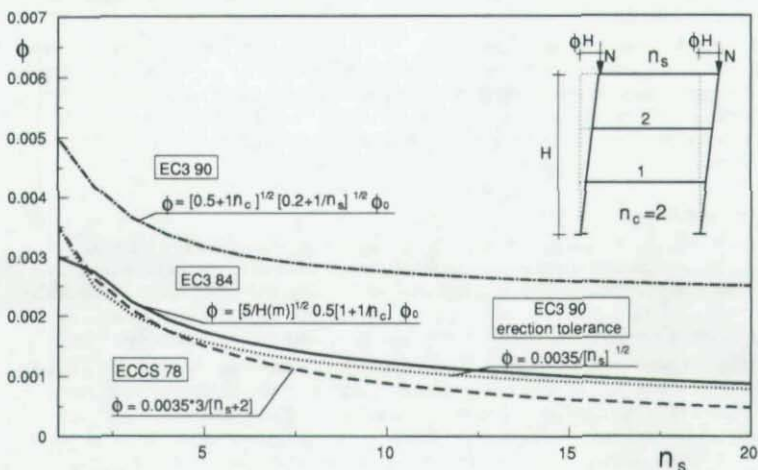


Figure 2. Frame imperfection  $\phi$  according to various formulations.

The EC3 requires to perform global inelastic analysis of frames affecting the initial geometry with both column and frame imperfections. This requirement leads to uncertainty in the combination of the two types of imperfection. The influence of variation in the pattern of imperfections is an issue dealt with in previous papers [4]. It has been demonstrated in [4] that inelastic buckling of frames under vertical loads is affected to a small degree by the assumed combination of local and global imperfections. In fact, results obtained considering four types of imperfection pattern have shown that the variation in the inelastic buckling load is marginal, being the maximum scatter with respect to the mean value not greater than 10%.

Furthermore the authors believe that, following the suggestions of the EC3 and therefore considering simultaneously both member and frame imperfections (given by Equation (1)), the resulting imperfections provides a too large value, especially if compared to the analogous values provided by other specifications. In fact, from the comparison among the global imperfections given by various codes, plotted in Figure 2 as a function of number of stories, it can be concluded that the frame erection tolerance suggested by EC3 is much smaller than the frame imperfection, as well as smaller than the imperfection suggested both by the ECCS Recommendations and by one of the previous Draft of the EC3 itself [5]. Equation (1) also leads to values of the global imperfection  $\phi$  clearly larger than those found on existing structures [6].

In this paper, feasibility of the concept of 'equivalent' frame imperfection  $\phi_{eq}$  is investigated in order to simplify second-order inelastic frame analysis. The equivalent imperfection  $\phi_{eq}$  is defined as the value of frame imperfection, to be assumed without any column imperfection, which leads to the same inelastic buckling load  $\alpha_c N$  of the frame as the one predicted by introducing both column and frame imperfection (Figure 3).

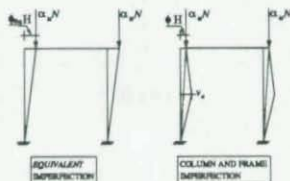


Figure 3. Development of concept of 'equivalent' frame imperfection  $\phi_{eq}$ .

#### Model for frame analysis

The computational model used herein has been already presented in [4]. The procedure is able to account for both geometrical and mechanical nonlinearities. In particular, a special column element allows to consider all plastic effects arising from residual stress distributions and lack of straightness by introducing an appropriate plastic hinge at mid-height of the column. Plastic hinges, with modifications to account for cross section strength surface, are adopted throughout the frame at joint locations.

$P-\delta$  effects are incorporated into the model by affecting the element stiffness coefficients by the Livesley functions, depending on the element axial force.  $P-\Delta$  are also introduced into the model by adding a geometric term to the stiffness matrix of each element and by formulating the equilibrium equations on the updated frame configuration. Accuracy of the model in representing all geometric and material nonlinearities has been demonstrated elsewhere.

#### Parametric analysis

An extensive parametric analysis has been carried out by using the above described model. Figure 4 reports geometry and shapes of beams and columns for one-bay frames having number of stories ranging between three and twelve (A1, B1, C1 and D1) that have been analyzed. Furthermore, three-bay frames have been studied, whose geometry is also represented in Figure 4 (A3, B3, and C3). Used shapes belong to European Standards.



Shape	A cm <sup>2</sup>	W cm <sup>3</sup>	Z cm <sup>3</sup>
IPE 600*	156	3070	3070
HE 300 M	303	3480	4078
HE 360 M	319	4300	4990
HE 450 M	335	5500	6330
HE 600 M	364	7660	8772

\* All beams are IPE 600

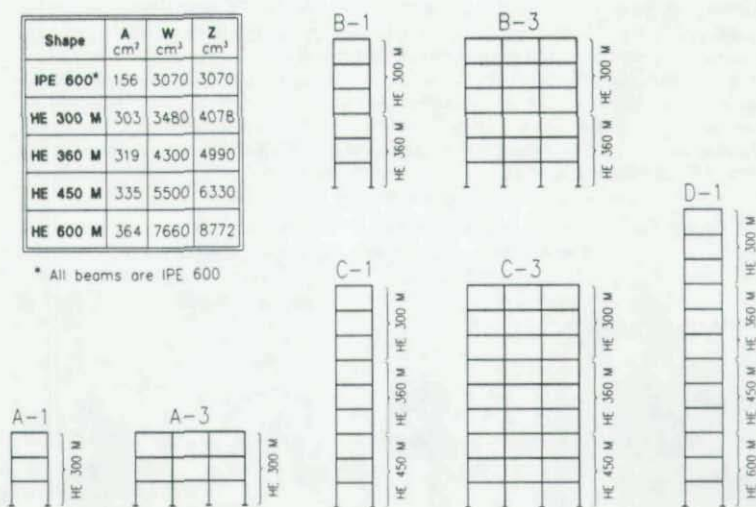


Figure 4. Properties of frames analyzed in the parametric analysis

In previous papers [4] it has been demonstrated that the frame slenderness  $\lambda_y$ , defined as:

$$\lambda_y = \sqrt{\frac{\alpha_y}{\alpha_c}} \quad (3)$$

where  $\alpha_y$  represents the squash multiplier of vertical loads, assumed to be applied at joint locations, and  $\alpha_c$  denotes the elastic buckling multiplier of vertical loads, is the most influential parameter on the ultimate frame capacity  $\alpha/\alpha_c$ , where  $\alpha_c$  is the ultimate multiplier of axial loads. The global slenderness  $\lambda_y$ , which is a direct generalization of the column nondimensional slenderness  $\lambda$ , is seen to influence inelastic buckling of frames in the same manner as  $\lambda$  affects inelastic buckling of a single column both from qualitative and from quantitative stand-point. The present analysis is conducted by considering values of  $\lambda_y$  and  $\lambda$  that virtually cover the whole available parametric range.

For what concerns combination of local and global imperfections, the frame initial geometry has been affected by the distribution of local and global imperfections that previous studies [4] have shown to give the largest reductions in  $\alpha/\alpha_c$  among those examined. However, as previously underlined, this is not a major issue, since variation in the imperfection pattern produces slight change in the frame buckling load.

#### Inelastic frame analysis with local and global imperfections

A preliminary investigation has been conducted in this paper in order to establish the influence of global imperfections suggested by EC3 and of the coupling of local and global imperfections.

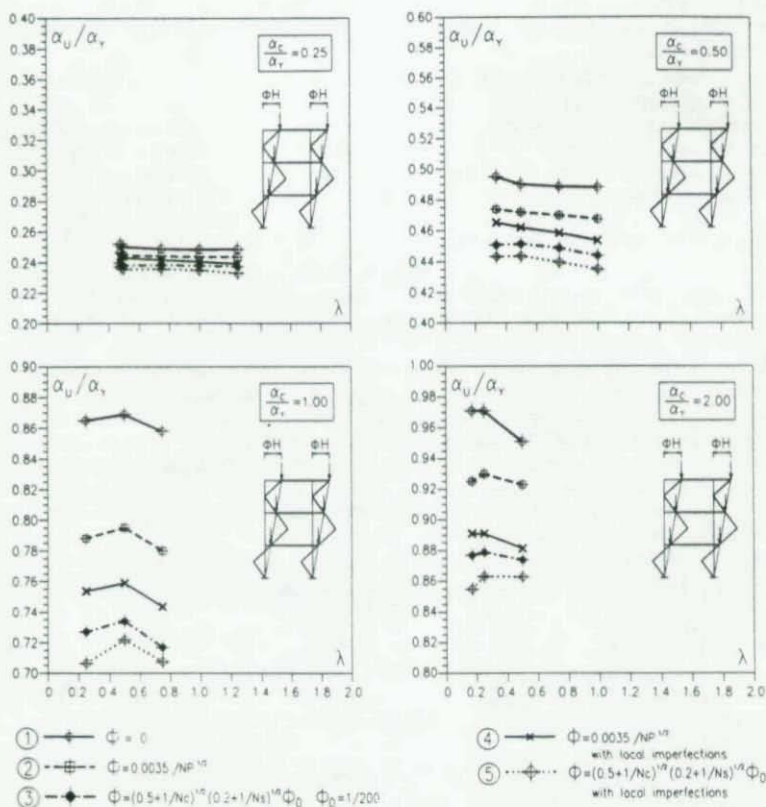


Figure 5. Variation in the frame ultimate buckling load with column and frame slenderness.

Figure 5 reports the ratio  $\alpha_U/\alpha_v$  as a function of  $\lambda$  and  $\lambda_v$  for a three-story one-bay frame. Each picture contains five curves corresponding to the various formulations used for defining imperfections. In particular, curves refer to:

- 1) 'perfect' frames ( $\Phi=0$ ,  $v_j/L=0$ )
- 2) global imperfection provided by Equation (2) alone
- 3) global imperfection provided by Equation (1) alone
- 4) local imperfection  $v_j/L$  in addition to the global imperfection of Equation (2).
- 5) local imperfection  $v_j/L$  in addition to the global imperfection of Equation (1)

Four values have been chosen for  $\alpha_c/\alpha_v$ :  $\alpha_c/\alpha_v=0.25$ , 0.50, 1.00 and 2.00, the first value referring to slender frames, the last to stocky frames.

Trends of the curves, confirming previous results [4], show that the column slenderness is almost unaffacting the frame inelastic buckling load, while, as expected, parameter  $\lambda_y$ , i.e. the ratio  $\alpha_u/\alpha_y$ , is very influential.

It can be observed that, for  $\alpha_u/\alpha_y=0.25$ , curves of  $\alpha_u/\alpha_y$  present values close to  $\alpha_u/\alpha_y$  itself, since  $\alpha_u/\alpha_y$  is larger than 0.23 for all analyzed imperfections. Therefore, frame behavior is essentially elastic up to buckling, which presents a sway mode. As  $\alpha_u/\alpha_y$  increases, buckling is affected by larger inelasticity and values of  $\alpha_u/\alpha_y$  are far smaller than  $\alpha_u/\alpha_y$ . As a matter of fact, it should be noticed that  $\alpha_u$  cannot exceed the value of the squash load multiplier  $\alpha_y$ , implying that the ratio  $\alpha_u/\alpha_y$  cannot exceed the unity, even if  $\alpha_u/\alpha_y$  is much larger than unity. Namely, if one looks at curves corresponding to  $\alpha_u/\alpha_y=2.00$ , maximum values of  $\alpha_u/\alpha_y$  are approximately equal to 0.98, thus implying that frames buckle with a non-sway mode.

For the smallest considered values of  $\alpha_u/\alpha_y$ , curves of ultimate frame load lie into a rather narrow band, whereas the various introduced combinations of local and global imperfections are seen to influence  $\alpha_u/\alpha_y$  to a greater degree for increasing values of  $\alpha_u/\alpha_y$ . Therefore, stocky frames seem to be more sensitive to the assumed imperfection.

The presence of imperfections obviously leads to a reduction in  $\alpha_u/\alpha_y$  with respect to values computed for the "perfect" frames. Moreover, it appears that the formulation expressed by Equation (1) for the global imperfection  $\phi$ , associated with the column imperfection  $v_u/L$ , always results in the minimum values of  $\alpha_u/\alpha_y$ . The most reasonable formulation, given by the combination of the erection tolerance specified by EC3 with the local imperfection  $v_u/L=1/250$ , leads to intermediate values of  $\alpha_u/\alpha_y$ . These values are even larger than those obtained by only considering the global imperfection provided by Equation (1). Therefore, it can be concluded that values proposed by EC3 through Equation (1) for  $\phi$  are over-conservative if it is considered in addition to the column equivalent imperfection  $v_u/L$ .

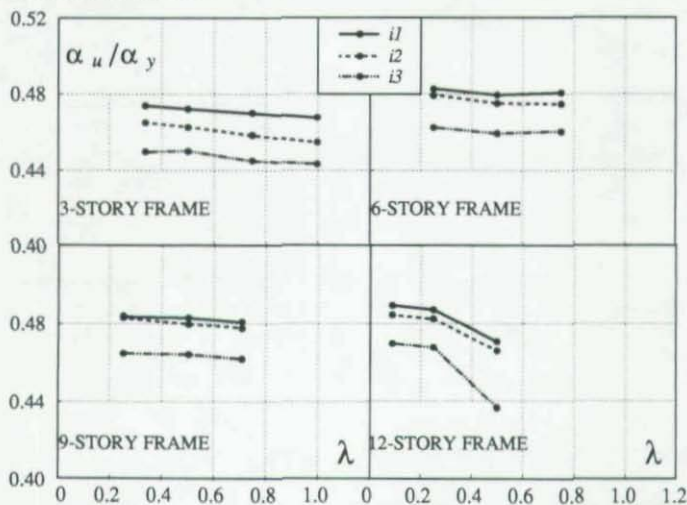


Figure 6. Results obtained for different values of imperfections ( $i_1, i_2, i_3$ ) on 3, 6, 9 and 12 story frames.

A further numerical investigation is conducted in order to define influence of frame topology on variation in the ultimate frame load. Figure 6 displays results obtained for one-bay frames A1, B1, C1 and D1 considering the most significant combinations of local and global imperfections among those examined in Figure 5. In particular, initial geometry of frames is modified by the following imperfections:

*i1*) erection out-of-plumb provided by Equation (2)

*i2*) combination of column imperfection and frame erection imperfection.

*i3*) frame imperfection provided by Equation (1)

Results are provided for frames characterized by  $\alpha_u/\alpha_s=0.5$  and by values of  $\lambda$  that cover the available parametric range. Both values and trends of curves of  $\alpha_u/\alpha_s$  are virtually unaffected by number of stories, as well as by column slenderness. In fact,  $\alpha_u/\alpha_s$  is always included between 0.44 and 0.49, with maximum values that slightly increase with number of stories. The same variation in the inelastic buckling load with imperfection type is found for all considered frames. In particular, adoption of frame imperfection given by Equation (1) always leads to values of  $\alpha_u/\alpha_s$  smaller than those provided by curves related to the combination *i2*.

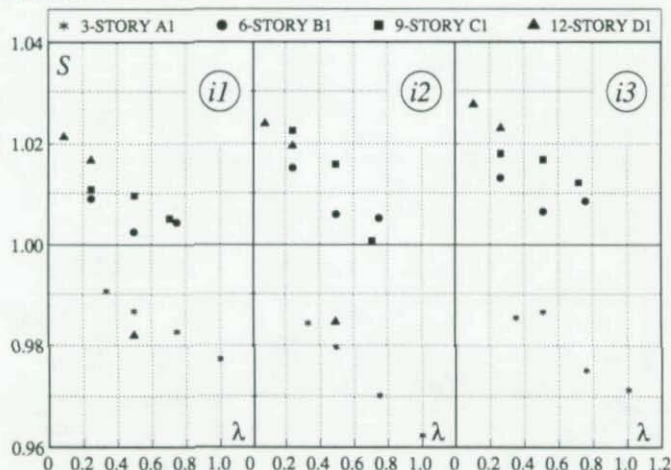


Figure 7. Scatter  $S$  of the ultimate frame multiplier with respect to mean value  $\mu$  as imperfection type varies.

Figure 7 furnishes more information about the scatter of  $\alpha_u/\alpha_s$  with respect its mean value  $\mu$  due to variation in number of stories, as the type of imperfection changes. A measure of the scatter can be given by parameter  $S$ , defined as:

$$S = 1 + \frac{\alpha_u/\alpha_s - \mu}{\mu} \quad (4)$$

Examination of Figure 7 evidences that for all considered imperfections parameter  $S$  is very close to unity, as number of stories and column slenderness vary. Similar results can be achieved when different values of  $\alpha_u/\alpha_s$  are selected. Furthermore, Figure 7 shows that maximum scatter in  $\alpha_u/\alpha_s$  is achieved for 12-story frames, for which, in any case,  $S$  is included between 0.95 and 1.03.



Thus, the frame ultimate load is mainly dependent on the frame slenderness  $\alpha_s/\alpha_y$ , even considering various types of imperfection and different number of stories and bays. The increase in the global imperfection  $\phi$  provided by Equation (1) with respect to that given by Equation (2) always causes a reduction in the frame inelastic buckling load. Furthermore, the addition of local imperfections to the global ones also results in a reduction of  $\alpha_s/\alpha_y$ , thus leading to an effect similar to that due to an increment of the global imperfection  $\phi$ . Therefore, it is of interest to define variation in the frame ultimate load  $\alpha_s/\alpha_y$  with magnitude of  $\phi$ , without considering local imperfections, in order to verify the possibility of introducing only a global imperfection to account also for local imperfections.

#### Inelastic frame analysis with 'equivalent' global imperfections

The analysis of inelastic buckling of frames affected only by global imperfections is carried out in order to assess feasibility of development of the concept of 'equivalent' global imperfection. As already mentioned, the equivalent global imperfection  $\phi_{eq}$  can be defined as the value of global imperfection which leads to the same value of the ultimate load multiplier as the one predicted by introducing both column imperfection  $v_j/L$  and frame imperfection  $\phi$  significative of the erection tolerance.

This requires analysis of sensitivity of the frame buckling load to the magnitude of the global imperfection  $\phi$ . Table 1 contains values of the ratio  $\alpha_s/\alpha_y$  obtained for a three-story frame characterized by various values of column and frame slenderness. The global imperfection  $\phi$  has been varied between zero ('perfect' frame) and 0.00808, the latter value being four times as the value of erection imperfection  $\phi$  proposed by EC3 for  $n_s=3$  through Equation (2).

**Table 1.** Values of the inelastic buckling load for a three-story one-bay frame.

$\alpha_s/\alpha_y$	$\bar{\lambda}$	$\phi=0$	$\phi=0.00202$	$\phi=0.00404$	$\phi=0.00606$	$\phi=0.00808$
		$\alpha_s/\alpha_y$	$\alpha_s/\alpha_y$	$\alpha_s/\alpha_y$	$\alpha_s/\alpha_y$	$\alpha_s/\alpha_y$
0.25	0.48	0.25	0.2465	0.2382	0.2305	0.2233
	0.50	0.25	0.2448	0.2448	0.2292	0.2212
	0.75	0.2487	0.2441	0.2369	0.2302	0.2239
	1.00	0.2484	0.2436	0.2365	0.2296	0.2232
	1.25	0.2485	0.2434	0.2357	0.2285	0.2217
0.50	0.34	0.4951	0.4740	0.4458	0.4217	0.4011
	0.50	0.4903	0.4721	0.4467	0.4246	0.4054
	0.75	0.4888	0.4701	0.4410	0.4217	0.4023
	1.00	0.4884	0.4676	0.4393	0.4155	0.3948
	1.25	0.4884	0.4676	0.4393	0.4155	0.3948
1.00	0.25	0.8650	0.7880	0.7135	0.6623	0.6207
	0.50	0.8690	0.7950	0.7221	0.6702	0.6291
	0.75	0.8580	0.7800	0.7047	0.6516	0.6097
2.00	0.17	0.9710	0.9251	0.8666	0.8181	0.7772
	0.25	0.8380	0.9300	0.8741	0.8270	0.7869
	0.50	0.9510	0.9230	0.8634	0.8143	0.7708

Again, Table 1 demonstrates that the ultimate multiplier  $\alpha_s/\alpha_y$  is almost insensitive to column slenderness  $\bar{\lambda}$ , whereas it varies significantly with the frame slenderness  $\lambda_p$ .



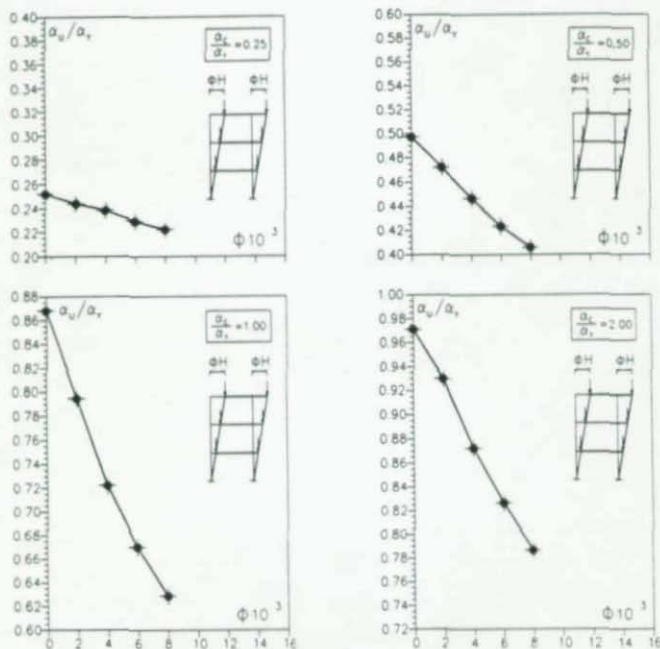


**Figure 8.** Sensitivity of the frame buckling load  $\alpha_u/\alpha_y$  to magnitude of global imperfection  $\phi$  for three-story one-bay frames.

Figure 8 reports variation in  $\alpha_u/\alpha_y$  with magnitude of  $\phi$ , as  $\alpha_u/\alpha_y$  ranges between 0.25 and 2.00 for a three-story one-bay frame. Although curves refer to a single value of  $\lambda$ , they are to be considered representative of all values of  $\lambda$  reported in Table 1 since variation in  $\alpha_u/\alpha_y$  with  $\lambda$  is negligible.

An almost linear variation in  $\alpha_u/\alpha_y$  with  $\phi$  is observed for all considered values of  $\alpha_u/\alpha_y$ , while the largest sensitivity can be found for  $\alpha_u/\alpha_y=1.00$ , i.e.  $\lambda_y=1.00$ . In fact, if  $\alpha_u/\alpha_y=1.00$ , the inelastic buckling load approximately reduces by 30% for  $\phi=0.00808$ , whereas it reduces by 10% for  $\alpha_u/\alpha_y=0.25$ .

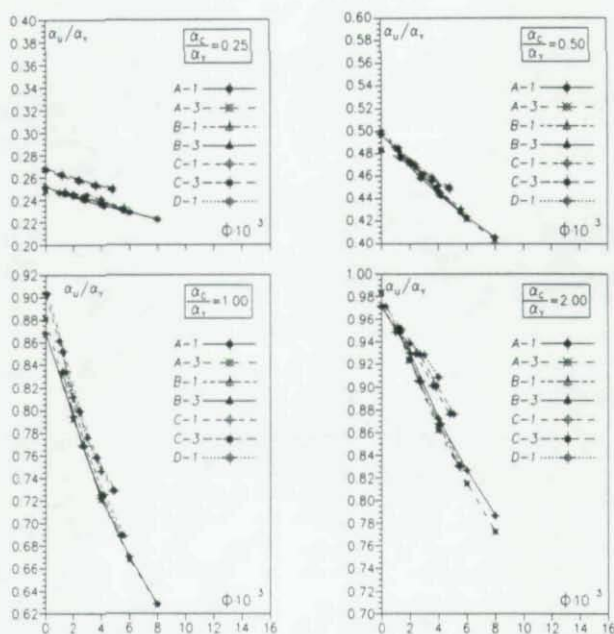


Figure 9. Sensitivity of ultimate multiplier to equivalent global imperfection for frames A1,A3,B1,B3,C1,C3,D1.

A further parametric analysis is conducted to define sensitivity of  $\alpha_u/\alpha_e$  to  $\phi$  for frames having larger number of stories and bays. Figure 9 collects all obtained results, which still refer to a single value of column slenderness, since, as before,  $\lambda$  is not influencing trends and values of curves. It appears that values computed for 3-story frames generally are slightly smaller than those computed as number of stories and bays increases. However, curves are included in very narrow bands both for slender ( $\alpha_c/\alpha_s=0.25$ ) and for stocky ( $\alpha_c/\alpha_s=2.00$ ) frames, presenting quite similar tendency for all values of  $\phi$ . This uniform behavior of curves is a crucial property for developing concept of equivalent imperfection.

Therefore, closeness of sensitivity curves reported in Figure 9, that overlap in many cases, is studied by evaluating parameter  $S$  as magnitude of  $\phi$  increases. Parameter  $S$  is represented for the examined cases in Figure 10; it can be found that  $S$  is always very close to unity, evidencing that almost no scatter in sensitivity curves arises from variation in number of stories and bays. Namely, Figure 10 shows that, for a given value of  $\phi$ , the variation in  $\alpha_u/\alpha_e$  with respect to the mean value is always less than 5%.

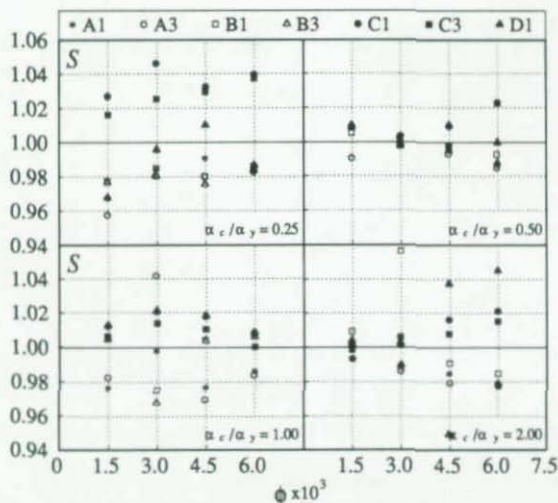


Figure 10. Scatter of  $S$  of ultimate frame multiplier to equivalent global imperfection for frames A1, A3, B1, B3, C1, C3, D1.

Therefore, since variation in  $\alpha_c/\alpha_y$  with  $\phi$  consists of a uniform reduction as  $\phi$  increases, without any significant change as number of stories and bays varies, the concept of amplifying the frame imperfection to account also for local imperfection appears to be practically suitable. In fact, the above analyses have demonstrated that an average sensitivity curve can be defined which represents all curves obtained by varying frame topology with an acceptable approximation. Once this average curve is assigned, the equivalent imperfection  $\phi_{eq}$  can be easily evaluated by selecting on the sensitivity curve the value of  $\phi$  which leads to the same inelastic buckling load as the actual combination of column and frame imperfections.

### Conclusions

In this paper, a parametric analysis has been carried out in order to investigate how inelastic buckling load is influenced by column and frame geometrical imperfections that current building codes introduce to account for actual geometrical and mechanical imperfections. It has been found that the frame imperfection suggested by EC3, combined to the column imperfection, is clearly over-conservative, since it provides the smallest values of the ultimate frame capacity among the selected imperfection types. This conclusion holds over the entire range of considered parameters: column and frame slenderness, number of stories and number of bays. Furthermore, it has been shown that variation in number of stories and bays virtually does not affect the frame ultimate multiplier of axial loads and its dependence on the type axial loads. A further analysis has been developed to evaluate sensitivity of the inelastic buckling load to magnitude of the frame imperfection. Sensitivity curves present quite similar trend and values despite of variation in column slenderness, number of stories and number of bays. Therefore, the concept of 'equivalent' frame imperfection, introduced herein, appears to be practically suitable since variation in the frame topology, i.e. variation in number of stories and frames, affects to a very little degree the sensitivity

curves, that are used to determine the equivalent imperfection.

The uniformity of the results obtained and the large parametric range analyzed suggest to propose a modification to the EC3 approach also in consideration of the fact that adoption of an equivalent frame imperfection is physically meaningful and allows to significantly simplify frame analysis.

#### References

- [1] CEN - European Committee for Standardization : "Eurocode 3 - Design of Steel Structures", February 1992.
- [2] Standards Australia: "AS4100 - 1990, Steel Structures", Standards Australia, Sydney, 1990.
- [3] ECCS European Recommendations for Steel Construction, European Convention of Structural Steelwork, Brussels, 1978.
- [4] De Luca, A., Mele E., Faella C.: "Advanced Inelastic Analysis: Numerical Results and Design Guide-lines for Rigid and Semirigid Sway Frames", Proc. of SSRC TG29 Workshop on *Plastic Hinge Based Methods for Advanced Analysis and Design of Steel Frames*, Pittsburgh, April 1992.
- [5] Commission of the European Communities: "Eurocode 3 - Design of Steel Structures", Edited Draft, 1984.
- [6] Alpsten, G.: "Geometrical Deviations of Steel Frames in Multi-Story Buildings - A Progress Report", Division of Steel Structures, Royal Institute of Technology, Stockholm, Report 1992.9, 1992.

#### Aknowledgements

This research is partially supported by the Italian Research Council (research grant CNR 92.02838.PF54)

#### APPENDIX: Notation

- $n_c$  = number of columns
- $n_s$  = number of stories
- $S$  = scatter of inelastic buckling load
- $v_0/L$  = column nondimensional imperfection
- $\alpha_u$  = ultimate multiplier of axial loads
- $\alpha_e$  = elastic buckling multiplier of axial loads
- $\alpha_s$  = squash multiplier of axial loads
- $\lambda$  = column nondimensional slenderness
- $\lambda_f$  = frame nondimensional slenderness
- $\mu$  = mean value
- $\phi$  = frame global imperfection
- $\phi_{eq}$  = equivalent frame imperfection

On A Computer Program, EPASS, to Analyse Ultimate Load  
Carrying Capacity of Spatial Steel Bridge Structures

by

Katsuhiro TANAKA\*, Toshiyuki KITADA\*\*, Mitsunori NIBU\*\*\*  
and Masato KANO\*\*\*

SUMMARY

This paper describes the outline of a computer program, EPASS, for analysing the ultimate load carrying capacity and elasto-plastic finite displacement behavior of spatial steel bridge structures composed of thin-walled box members and cable members. The main features of the program are as follows: (1) The elasto-plastic and finite displacement behavior of thin-walled box members subjected to compression, bending, and torsion can be simulated. (2) The inherent residual stress and initial deflection in steel bridge members are taken into consideration. (3) The non-linearity of cable members due to cable tension and deflection can be accounted. Several numerical examples are analysed for verifying the program, and then some numerical results of an actual Nielsen system bridge are shown.

1. INTRODUCTION

In recent year, many long span bridges with cable members, such as suspension bridges, cable-stayed bridges and Nielsen system bridges, are constructed in Japan. It is one of the most important problems in the design of these bridges to estimate their ultimate load carrying capacity. Some programs<sup>1),2)</sup> for analysing the load carrying capacity of steel bridge structures and several general purpose structural analysis programs, such as MARC and NASTRAN, have already developed. These programs may be, however, inconvenient for analysis of spatial bridge structures. A computer program, EPASS, has been, therefore, developed, which can analyse the load carrying capacity and elasto-plastic finite displacement behavior of spatial steel bridge structures composed of thin-walled box members and cable members.

This paper describes the outline of the EPASS. Firstly, the analytical assumptions for simulating the elasto-plastic and finite displacement behavior of steel members with box cross section are described, and then the analytical theory adopted in the program is formulated by a finite element method. Next, several numerical examples are analysed for verifying the program. Finally, a practical example of a Nielsen system bridge is analysed to examine the validity of the program.

---

\* Japan Information Processing Service Co., Ltd., Osaka, Japan.

\*\* Associate Professor, Department of Civil Engineering, Osaka City University, Osaka, Japan, Member-at-Large of SSRC.

\*\*\* Bridge & Computer Engineering Co., Ltd., Osaka, Japan.







## 2. OUTLINE OF THE PROGRAM

The main features of the program are as follows:





- (1) The elasto-plastic and finite displacement behavior of thin-walled box members subjected to compression, bending and torsion can be simulated.
- (2) The local buckling of plate elements is, however, assumed not to occur.
- (3) The inherent residual stress and initial deflection in steel bridge members are taken into consideration.
- (4) The non-linearity of cable members due to cable tension and deflection can be accounted.
- (5) The program copes with all the load combinations used in bridge design.
- (6) The initial configuration of a bridge subjected dead load and prestressing forces in cables can be easily realized in a computer.
- (7) The types of finite elements and connections can be used, as listed in Table 1.

A system using the EPASS is illustrated in Fig.1.

Table 1 Types of finite elements and connections in EPASS

Finite elements			
			
Elasto-plastic beam-column box element	Elastic beam-column element	Cable element	Spring element

Finite elements	Connections		
			
Elasto-plastic rod element	Rigid connection	Pin connection	Eccentric connection

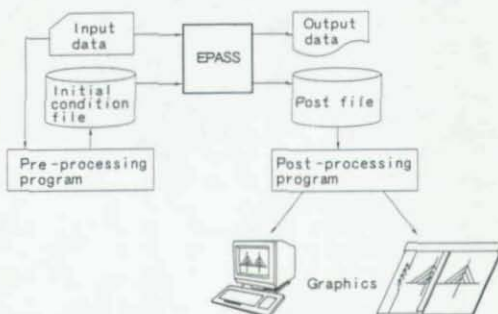


Fig.1 A system using EPASS

## 3.1 Analytical assumptions

The elasto-plastic and finite displacement behavior of three dimensional framed structures composed of thin-walled box members and cable members are formulated on the basis of the following assumptions:

- (1) The finite displacement behavior is formulated according to the Update Lagrangian Description method.
- (2) The cross section of beam-column elements keep plane after the displacement.
- (3) The shearing stress due to flexure and the warping stress by torsion can be neglected.
- (4) The torsional angle of cross section is small.
- (5) The elasto-plastic behavior of the thin-walled box members is formulated according to the assumption of constant shear flow along the box wall even after the partial yielding of cross section<sup>11</sup>.
- (6) The material of box members is assumed to be homogeneous, isotropic, perfectly elasto-plastic, and satisfying the von-Mises' yield criterion as well as Prandtl-Reuss' plastic flow rule.

## 3.2 Formulation using the principle of virtual work

The fundamental equation to derive the stiffness matrices of a finite element are obtained from the principle of virtual work as follows:

$$\iiint_V \delta \Delta \epsilon^T (D_e + D_p) \Delta \epsilon dV + \iiint_V \delta \Delta n^T \sigma dV = \delta \Delta u^T p - \iiint_V \delta \Delta \epsilon^T \sigma dV \quad (1)$$

where

- $\Delta u$ : incremental nodal displacement vector
- $\Delta \epsilon$ : linear terms of incremental strain vector
- $\Delta n$ : non-linear terms of incremental strain vector
- $D_e$ : stress-strain matrix in elastic range
- $D_p$ : stress-strain matrix needed in plastic range
- $\sigma$ : stress vector
- $p$ : nodal force vector including incremental nodal force

## 3.3 Relationship between incremental strains and incremental displacements

The local coordinate system is situated as shown Fig.2. The incremental displacements ( $\Delta u_p, \Delta v_p, \Delta w_p$ ) at a point P with the eccentricities  $\eta$  and  $\zeta$  from the shear center in the cross section of a box beam-column element, shown in Fig.3, can be expressed by the incremental displacements ( $\Delta u, \Delta v, \Delta w$ ) at the shear center and the incremental torsional angle  $\Delta \phi$  of the cross section as follows:

$$\left. \begin{aligned} \Delta u_p &= \Delta u - (\eta - \zeta \Delta \phi) \Delta v' - (\zeta + \eta \Delta \phi) \Delta w' \\ \Delta v_p &= \Delta v - \zeta \Delta \phi - \frac{1}{2} \eta \Delta \phi^2 \\ \Delta w_p &= \Delta w + \eta \Delta \phi - \frac{1}{2} \zeta \Delta \phi^2 \end{aligned} \right\} \quad (2)$$

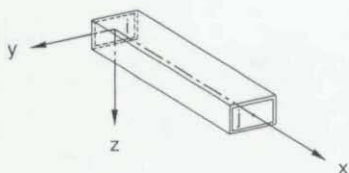


Fig. 2 Elasto-plastic beam-column box element and local coordinate system

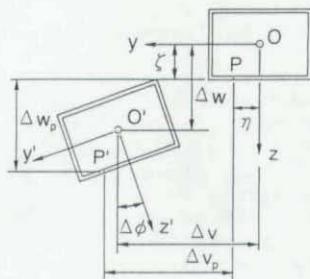


Fig. 3 Incremental displacements and torsional angle of cross section

in which the 'prime' notation means the differentiation with respect to  $x$ . The incremental normal strain  $\Delta \epsilon$  in the  $x$ -axis at a point  $P$  is given by:

$$\Delta \epsilon = \Delta u_p' + \frac{1}{2} (\Delta v_p')^2 + \frac{1}{2} (\Delta w_p')^2 \quad (3)$$

Substitution of Eq. 2 into Eq. 3 gives:

$$\Delta \epsilon = \Delta u' + \frac{1}{2} (\Delta v')^2 + \frac{1}{2} (\Delta w')^2 - \eta (\Delta v'' + \Delta w'' \Delta \phi) - \zeta (\Delta w'' - \Delta v'' \Delta \phi) + \frac{1}{2} (\eta^2 + \zeta^2) (\Delta \phi')^2 \quad (4)$$

### 3.4 Relationship between incremental stress and incremental strain

The elasto-plastic behavior of box beam-column elements subjected to axial force, bending moment, and torsional moment is alternatively formulated by exact and approximate methods. In the former method, the elasto-plastic behavior where normal stress and shearing stress interact, is formulated according to Ref. 1). In the latter method, the torsional behavior is assumed to be always elastic but yielding situation is checked by considering the combination of normal stress and shearing stress.

### 3.5 Equilibrium equations

Using Eq. (1) on the tangent stiffness matrix, the following equilibrium equations for the finite elements concerning the local coordinates system can be derived:

$$k \Delta u = p - f \quad (5)$$

where the stiffness matrix  $k$  is categorized into four groups as follows:

- 1) Elasto-plastic box and rod elements

$$k = k_e + k_p + k_o \quad (6)$$

- 2) Elastic beam-column elements

$$k = k_e + k_o \quad (7)$$

## 3) Cable elements

$$k = k_c \quad (8)$$

## 4) Spring elements

$$k = k_s \quad (9)$$

and

 $k_e$ : elastic stiffness matrix $k_p$ : plastic stiffness matrix $k_g$ : geometrical stiffness matrix $k_c$ : tangent stiffness matrix of catenary-cable element according to Ref.3). $k_s$ : stiffness matrix of spring element $P$ : nodal force vector for external loads $f$ : nodal force vector for internal forces

## 3.8 Solution Procedure

There are some effective strategies in the EPASS for the evaluation of the ultimate load carrying capacity and reduction of computation time as follows:

(1) Arc-length method<sup>4), 5)</sup>

It is possible for the arc-length method to trace the equilibrium path of a structure after the ultimate load state. The ultimate load can be, therefore, evaluated easily and accurately by the method. And automatic load increment scheme by the method is also useful.

(2) Current stiffness parameter<sup>6)</sup>

The current stiffness parameter in Ref.6) has been adopted to estimate the ultimate load level because the current stiffness parameter becomes equal to zero at the stationary points on a load-displacement curve.

## (3) Partial AULD (Approximate Updated Lagrangian Description)

The finite displacement behavior is formulated according to two kinds of ULD (Updated Lagrangian Description) methods. One is AULD<sup>7)</sup> and the other is Partial AULD. It may be advantageous to use the Partial AULD in the case of elasto-plastic analyses using the arc-length method.

## 4. NUMERICAL EXAMPLES

## 4.1 Verification of the program

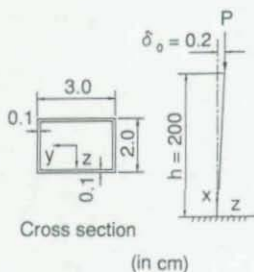
The several results of numerical examples analysed for verifying the EPASS are shown in this section.

## (1) The problem of the Elastica

In order to check the validity of the elastic finite displacement behavior by the EPASS, a cantilever column with initial deflection is analysed as shown in Fig.4. This model is composed of 20 finite elements and the critical buckling load is  $P_{cr} = 82.8 \text{ kgf}$ . The relationships between the load  $P$  and the displacements ( $u, w$ ) are shown in this figure. The numerical solutions obtained by the EPASS agree well with the theoretical results by Timoshenko and Gere<sup>8)</sup>.

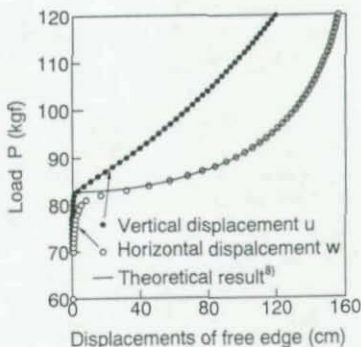
## (2) Elasto-plastic analysis of folded beam subjected to bending and torsion

Two cantilever beams connected at their free edges under a concentrated load is analysed as a numerical example to examine the validity of the elasto-plastic



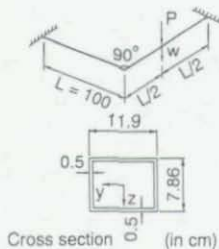
$$E = 2.1 \times 10^6 \text{ kgf/cm}^2$$

(a) Model



(b) Numerical result

Fig. 4 Analysis of elastica



$$E = 2.1 \times 10^6 \text{ kgf/cm}^2$$

$$\sigma_y = 4.032 \text{ kgf/cm}^2$$

$$M_{px} = 1.953 \times 10^5 \text{ kgf-cm}$$

$$M_{py} = 2.240 \times 10^5 \text{ kgf-cm}$$

(a) Model

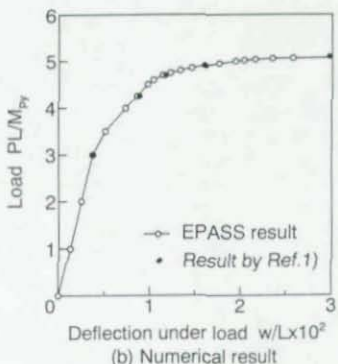


Fig. 5 Analysis of two cantilever beams connected at their free edges

behavior of box members subjected to bending and torsion. The relationships between the load  $P$  and deflection  $w$  at a loading point is shown in Fig. 5. The results of the exact method on elasto-plastic behavior are plotted in this figure, and the exact results agree with the results by Ref. 1). The variation of the bending and torsional moments at three nodal points are shown in Fig. 6. It can be seen from this figure that the numerical results by the EPASS vary well along the interaction curve of fully plastic state.

### (3) Elasto-plastic and finite displacement analysis of column

As an example for elasto-plastic and finite displacement analysis, a box column with initial deflection and residual stress is analysed. The results obtained by the EPASS are compared with the Euler's buckling load and the solutions given by Shulz<sup>9)</sup> in Fig. 7. These results agree with each other.



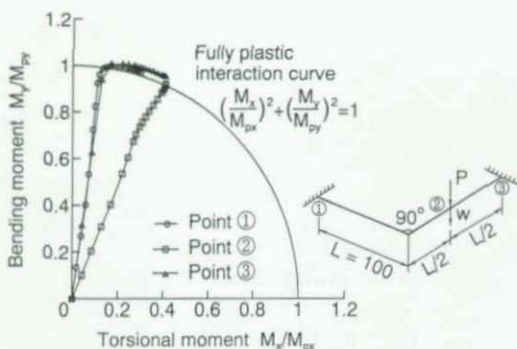


Fig. 6 Interaction between bending moment and torsional moment

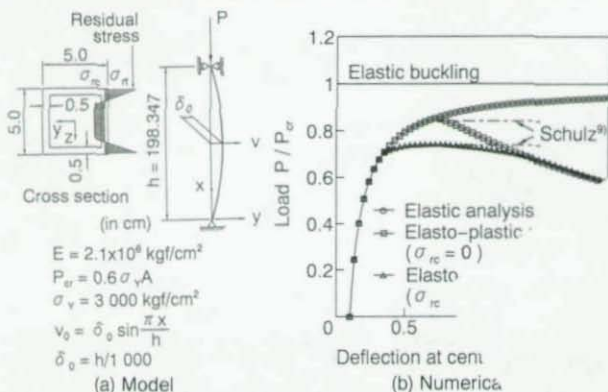


Fig. 7 Analysis of elasto-plastic column with residual stress

## (4) Cable element

The non-linearity of cable members is verified through the analysis of a sagging cable structure, shown in Fig. 8. In this figure,  $W$  is the weight per meter and  $L_0$  is the length of the cable without tension. The numerical results are plotted in Fig. 9 and they agree with the results by Goto<sup>33</sup>.

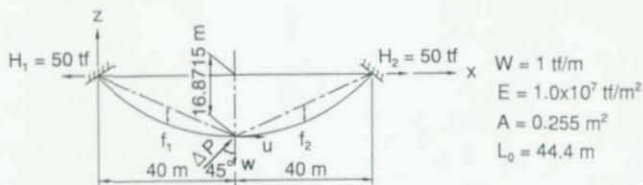


Fig. 8 Analytical model of a cable structure

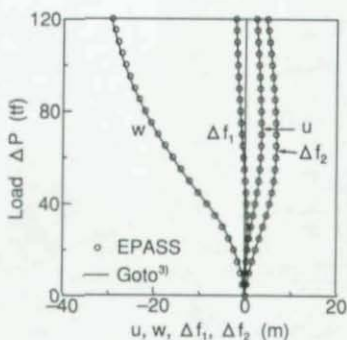


Fig.9 Displacements and sags of cable elements

#### 4.2 Actual Nielsen system bridge

A Nielsen system bridge shown in Fig.10 is taken up as a numerical example to examine the validity of applying the EPASS to the elasto-plastic and finite displacement analysis of actual bridge structures. In the analysis, the arch ribs and upper lateral bracings are regarded as the elasto-plastic beam-column box members, while the stiffening girders, floor beams and cables are treated as the elastic members. The horizontal and lateral initial deflection is introduced into the arch ribs by:

$$v_0 = -\delta_0 \sin 3\pi \frac{s}{l}, \quad \delta_0 = \frac{H}{1000} = 3.6 \text{ cm} \quad (10)$$

where  $H$  is the raise height,  $l$  the length of the arch ribs and  $s$  is the coordinate along the arch rib. The residual stress distribution, as shown in Fig.11, is considered in the cross section of the arch ribs according to Ref.10). The load combination of the dead load  $D$  in Fig.12 and live load  $L$  in Fig.13 is applied to the analytical model.

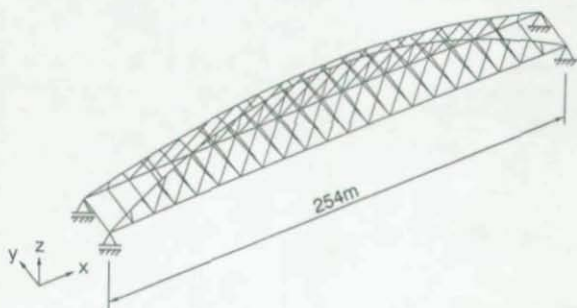


Fig.10 Analytical model of a Nielsen system bridge

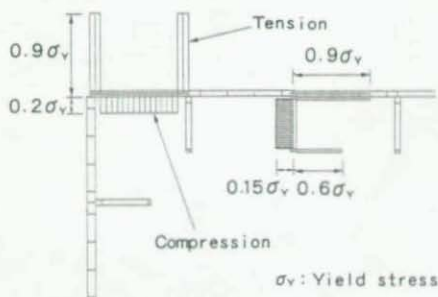


Fig. 11 Residual stress distribution of plate panel and stiffener in cross section of arch rib

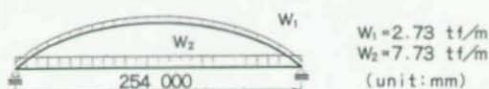


Fig. 12 Dead load intensity

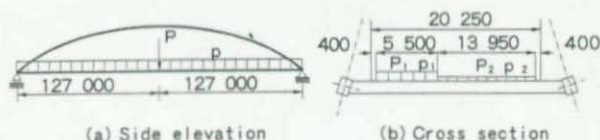


Fig. 13 Live load intensity

The elasto-plastic and finite displacement analysis is executed in the following manner. Firstly, the complete configuration is realized on the analytical model in the computer for the dead load of  $1.0D$ . Then, the live load of  $1.0L$  is applied to this model. Finally, the load combination of  $\alpha(D+L)$  ( $\alpha$ : load parameter) is gradually increased up to the ultimate state of the analytical model.

The displacement mode at the ultimate state is illustrated in Fig. 14. It can be observed from the figure that the out-of-plane deflection of the arch ribs is predominant near their central parts. Fig. 15 plots the relationships between the load parameter and horizontal displacements at three nodal points of the arch rib. It can be seen that these curves become nonlinear in the range over  $\alpha=0.9$  due to the influence of residual stress, and the ultimate state of the analytical model is very clear because the load parameter-displacement curves have been simulated after the ultimate state. Fig. 16 shows the distribution of plastic zone of the arch ribs at the ultimate state. This visual plastic zone is very useful to understand the failure mode of the arch ribs.

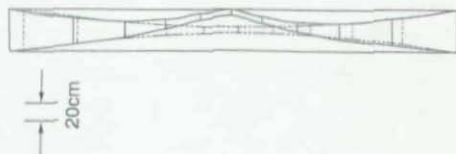
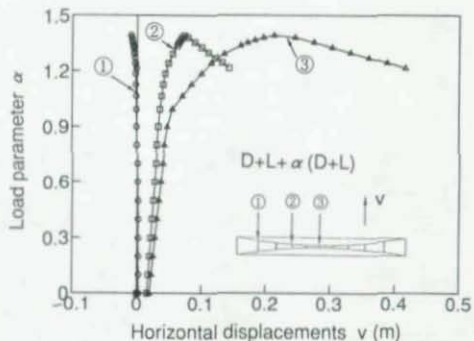
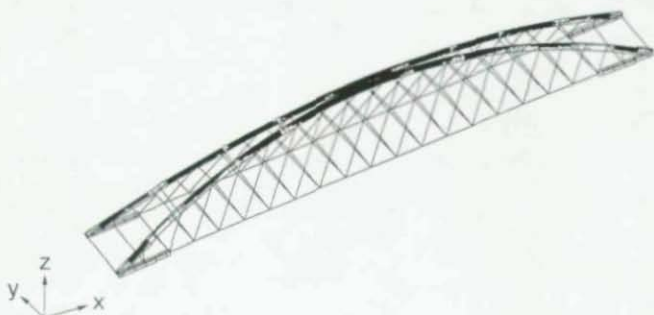
Fig. 14 Displacement mode at ultimate state ( $\alpha=1.39$ )

Fig. 15 Load parameter-displacement curves of arch rib

Fig. 16 Distribution of plastic zone at ultimate state ( $\alpha=1.39$ )

## 5. CONCLUSION

In the paper, a computer program, EPASS, to analyse the elasto-plastic and finite displacement behaviors of three dimensional framed structures composed of thin-walled box members and cable members have been presented. The outline of theory used in the EPASS, the several results of numerical examples analysed for verifying the EPASS, and the analytical results for an actual bridge have been

shown. The EPASS will be useful for the elasto-plastic and finite displacement analysis of spatial steel bridge structures.

#### REFERENCES

- 1) Komatsu, S. and Sakimoto, T.: Nonlinear Analysis of Spatial Frames Consisting of Members with Closed Cross-Sections, Proc. of JSCE, No.252, pp.143-157, August 1976.
- 2) Maeda, Y. and Hayashi, M.: In-Plane and Out-of-Plane Instability of a 297m Span Steel Arch Bridge, Transportation Research Record 664, Bridge Engineering, Vol.1, pp.246-254, September 1978.
- 3) Goto, S.: Tangent Stiffness Equation of Flexible Cable and Some Considerations, Proc. of JSCE, No.270, pp.41-49, February 1978 (in Japanese).
- 4) Crisfield, M.A.: A Fast Incremental/Iterative Solution Procedure that Handles "Snap-through", Computers & Structures, Vol.13, pp.55-62, 1981.
- 5) Bellini, P.X. and Chulya, A.: An Improved Automatic Incremental Algorithm for the Efficient Solution of Nonlinear Finite Element Equations, Computers & Structures, Vol.26, No.1, pp.99-110, 1987.
- 6) Bergan, P.G., Holand, I. and Soreide, T.H.: Use of the Current Stiffness Parameter in Solution of Nonlinear Problems, Energy Methods in Finite Element Analysis (ed. Glowinski, R., Rodin, E.Y. and Zienkiewicz, O.C.), pp.285-282, John Wiley & Sons, 1979.
- 7) Jetteur, P., Cescotto, S. and deGoyet, V.: Improved Nonlinear Finite Elements for Oriented Bodies Using an Extension of Marguerre's Theory, Computer & Structures, Vol.17, No.1, pp.129-137, 1983.
- 8) Timoshenko, S.P. and Gere, J.M.: Theory of Elastic Stability, McGraw-Hill, pp.76-82, 1961.
- 9) Schulz, G.: Die Traglastberechnung von Planmässig Mittig Belasteten Durchstäben aus Baustahl unter Berücksichtigung von Geometrischen und Strukturellen Imperfectionen, Dissertation eingereicht an der Technischen Hochschule in Graz, Juni 1968.
- 10) Komatsu, S., Ushio, M. and Kitada, T.: An Experimental Study on Residual Stresses and Initial Deformations of Stiffened Plates, Proc. of JSCE, No.285, pp.25-35, September 1977 (in Japanese).





J.P. JASPART, Ch. BRIQUET and R. MAQUOI  
Department MSM, University of Liège  
Quai Banning 6  
B-4000 LIEGE, BELGIUM

## 1. Introduction

Steel building frames are mainly constituted of beams subject to bending and beam-columns subject to combined bending and compression.

Several researches in the past have been devoted to the evaluation of the carrying capacity of beam-columns; they have led to the proposal of numerous interaction formulae which have been progressively introduced in national (LRFD, DIN, ...) and international codes.

The application of these different formulae to reference cases shows unfortunately a large discrepancy between the calculated values of the ultimate load, on one hand, and between the calculated values and results of numerical simulations, on the other hand.

Such a comparative study has been recently performed at the University of Liège; four interaction formulae have been considered: ECCS (1984), DIN 18800 (1988), LRFD (1986) and Eurocode 3 (1993). The present paper is aimed at presenting the results and the conclusions of this comparative study.

## 2. Beam-columns

The beam-columns considered in the present study are constituted of H or rectangular tubular cross-sections (figure 1.a). They are bent either uniaxially, about strong or weak axis, or biaxially. For simplicity, only plastic and compact cross-sections are considered, so avoiding local instability and coupling with global member instability.

The first order distribution of bending moments along the beam-column is linear and characterized by  $M$  and  $0.5 M$  values at the member extremities (see figure 1.b), whatever be the axis of bending.

As in braced frames, the transversal displacements of both beam-column extremities are assumed to be prevented.

Lastly, the buckling load of the beam-columns under pure compression is assumed to be lower about the weak axis than about the strong one (the beam-column extremities are hinged about X and Y axes). This last assumption may be expressed mathematically in the following way:

$$\bar{N}_y < \bar{N}_x \quad (I)$$

where  $\bar{N}$  represents the reduced compression normal force, defined as the ratio between the

ultimate buckling resistance  $N_u$  of the column under compression and its squash load  $N_p$ .

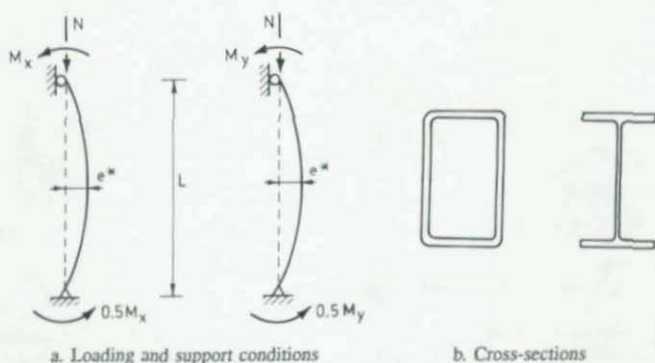


Figure 1 - Beam-columns considered

### 3. Numerical simulations

The numerical simulations of the behaviour till collapse of the beam-columns have been performed by means of the materially and geometrically non-linear finite element program FINELG which has been developed at the University of Liège and in which factors such as residual stresses and initial deformations may be accounted for.

Two different cross-sections are dealt with in this numerical study :

- a hot-rolled 200x100x6,3 rectangular tubular cross-section;
- a hot-rolled HE160B wide flange H section.

They are representative of the common practice in Europe. Both beam-columns are characterized by a reduced slenderness  $\bar{\lambda}$  equal to 1.5 about the weak axis and about 0.9 about the strong one. Mild steel (yield stress  $f_y = 235$  MPa) is used. A sinusoidal imperfection ( $e^* = L/1000$  in figure 1.a.) is assumed in the X and Y directions.

The numerical simulations performed for each profile are aimed at describing the evolution of the collapse load versus the  $N/M$  (normal force/bending moment) ratio in each of the four following situations :

- uniaxial bending about strong axis; lateral displacements prevented by an appropriate bracing system (figure 2.a.);
- uniaxial bending about strong axis; lateral displacements not prevented (figure 2.b.);
- uniaxial bending about weak axis (figure 2.c.);
- biaxial bending; bending moments  $M_x$  and  $M_y$  are such that  $M_x/M_{px} = M_y/M_{py}$  with  $M_{px}$  and  $M_{py}$  defined as the plastic moment resistances of the cross-section respectively about strong and weak axis (figure 2.d.).

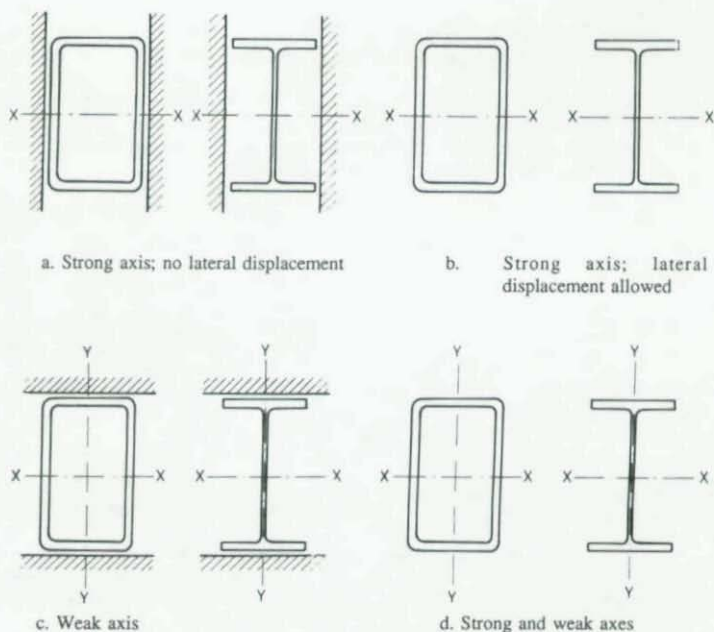


Figure 2 - Loading and support conditions for beam-columns under compression and uniaxial or biaxial bending.

#### 4. Interaction formulae

The collapse mode of a beam-column is highly dependent on the here above described loading and support conditions, as specified in figure 3.

Figure 3.a. is representative of a beam-column subject to uniaxial bending about weak axis or strong axis, with lateral displacements prevented. The in-plane instability under compression and bending is controlling for high and intermediate compression forces while the lack of resistance of the cross-section is predominant for low compression forces.

For beam-columns uniaxially bent about strong axis, the lateral displacements of which are not prevented, a supplementary collapse mode is controlling for low bending moments: the buckling instability about weak axis under pure compression (figure 3.b. for rectangular tubular cross-sections). For H sections, the lateral torsional buckling may obviously become predominant for high bending moments; for slender members, the instability controls then the collapse of the beam-column, whatever be the  $N/M$  ratio (dashed line in figure 3.c. where

$\bar{M}_{LT} = M_{LT}/M_p$ , with  $M_{LT}$  defined as the resistance moment for lateral torsional buckling in bending).

The collapse mode of beam-columns under biaxial bending is also seen to be highly dependent on  $N/M_x$ ,  $N/M_y$ , and  $M_x/M_y$  ratios characterizing the loading path (see figure 3.d.).

The diagrams reported in figure 3 are indicative ones. Depending on the flexural slenderness of the considered member, some collapse modes may be more or less predominant; the collapse of a very short column for instance will always be associated to the lack of resistance of the cross-section, whatever be the loading conditions.

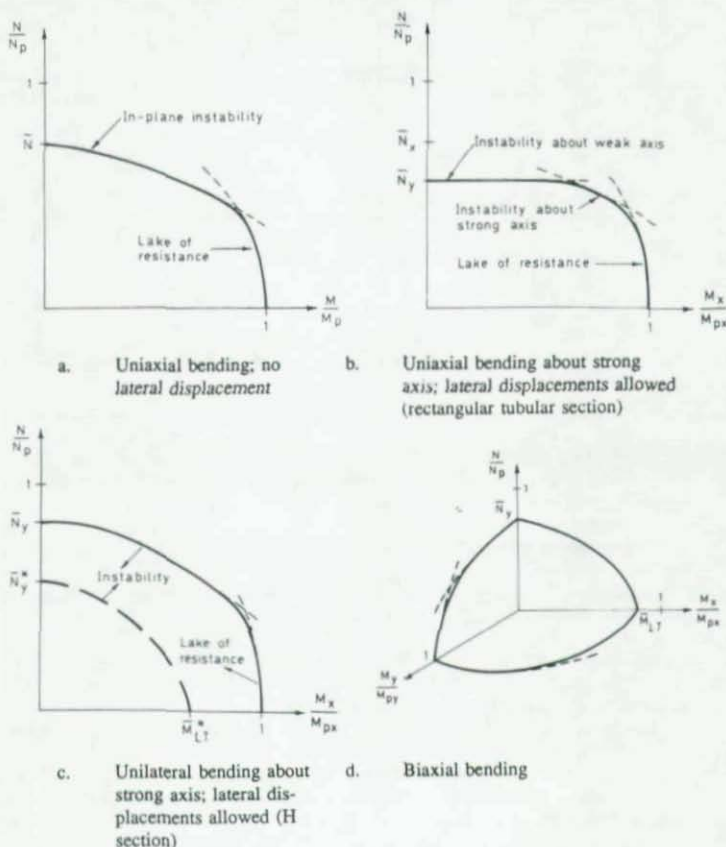


Figure 3 - Collapse modes of beam-columns



These different possible collapse modes have to be covered by the interaction formulae developed for design practice. The so-called ECCS [1], DIN 18800 [2], Eurocode 3 [3] and LRFD [4] ones are studied in the present paper; they correspond to four different ways to approach the problem, as clearly shown in table 1.

The 1985 ECCS proposal suggests the use of a specific formula for each possible collapse mode while in the DIN code, the stability and resistance checks are integrated into a single formula, except for beam columns subject to uniaxial bending about the strong axis and for which lateral torsional buckling is not likely to appear; for such beam-columns, the out-of-plane flexural buckling under pure compression has to be independently checked.

The EC3 European prestandard proposes a higher level of simplification by only distinguishing two cases according as the lateral torsional buckling is or not likely to occur. Lastly, the LRFD code suggests a single interaction curve which is aimed at covering all the possible collapse modes under compression and uniaxial or biaxial bending.

The interested reader is kindly asked to refer to original references for a more detailed description of each of these four design approaches.

### 5. Comparative study

The four design approaches described in table 1 are compared in figures 4.a. to 4.c. to the results of the numerical simulations on beam-columns constituted of a 200x100x6.3 rectangular tubular profile in which the instability by lateral torsional buckling is not likely to occur.

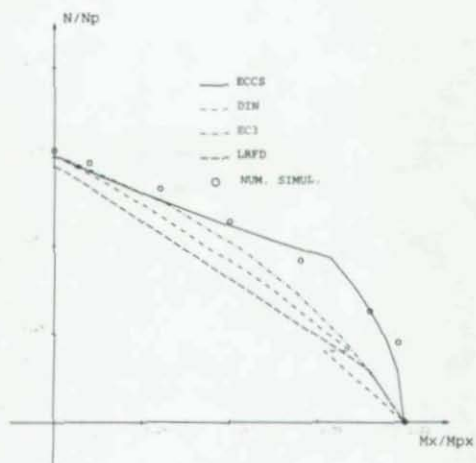
The following conclusions may be drawn :

- ECCS, DIN, EC3 and LRFD interaction formulae predict in a reasonable way the collapse load of beam-columns subject to uniaxial bending about strong axis and prevented to deform in the plane perpendicular to that of loading (figure 4.a.). For low N/M ratios where the resistance is controlling, DIN, EC3 and LRFD approaches leads generally to particularly conservative assessments of the ultimate resistance. This clearly results from the way in which the related formulae are "forced" to include the resistance verification. The ECCS approach provides the designer with accurate estimations of the collapse load, except in the transition zone from "instability mode" to "resistance mode" where the results are slightly overestimated. These conclusions may be extended to beam-columns subject to uniaxial bending about weak axis (figure 4.c.).
- LRFD and EC3 interaction formulae underestimate dramatically the ultimate resistance of the rectangular tubular beam-columns in case of uniaxial bending about strong axis, with allowed transversal displacements (figure 4.b.). The high level of interaction between the in-plane and out-of-plane instabilities predicted by these three formulae does not correspond at all to the actual behaviour in which the moment amplifications about strong and weak axis seem to be independent, except in a limited zone of transition from one collapse mode (buckling about weak axis) to another one (instability about strong axis or lack of resistance). In ECCS and DIN formulae, on the other hand, no coupling is considered; this explains the slightly unconservative results given by the ECCS approach in the transition zone.
- DIN, EC3 and LRFD design approaches provide similar ultimate carrying capacities over the whole range of normal forces and bending moments in case of combined

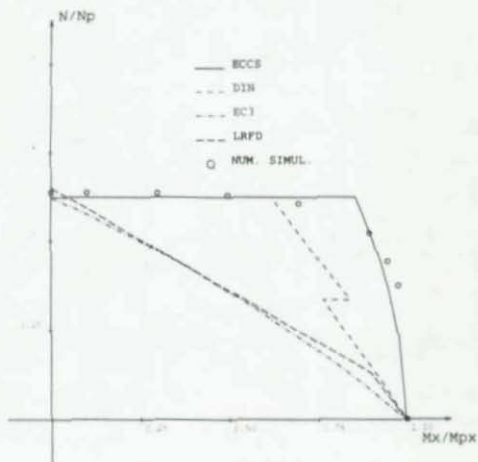
UNIAXIAL BENDING		BIAXIAL BENDING			
	Stability check in the plane of loading (I)	Resistance check for the end-sections	Stability check in the plane $\perp$ to the plane of loading	Stability check	Resistance check
ECCS	Lateral torsional buckling not likely to appear $\frac{N}{N_d} + \frac{1}{1 - \frac{N}{N_d} (\frac{M_1}{M_d})^2} \frac{C_m M_1}{M_d} K_{ed} \leq 1$	$\beta \frac{N}{N_p} \frac{M_1}{M_d} \leq 1$	$N < N_{ed}$	$\frac{C_m M_1}{M_d} + \frac{C_{ed} M_1}{M_{ed1}} \leq 1$	$\beta \frac{N}{N_p} \frac{M_1}{M_d} \leq 1$
	Lateral torsional buckling likely to appear $\frac{N}{N_d} + \frac{1}{1 - \frac{N}{N_d} (\frac{M_1}{M_d})^2} \frac{C_m M_1}{M_d} \leq 1$	$\beta \frac{N}{N_p} \frac{M_1}{M_d} \leq 1$			
DIN	Lateral torsional buckling not likely to appear $\frac{N}{N_d} + \frac{\beta_{ed} M_1}{M_d} \leq 1 - \Delta \alpha$		$N < N_{ed}$	$\frac{N}{\min(N_d, N_{ed})} + \frac{\beta_{ed} M_1}{M_d} k_1 + \frac{\beta_{ed} M_1}{M_d} k_2 \leq 1 - \Delta \alpha$	
	Lateral torsional buckling likely to appear $\frac{N}{N_d} + \frac{M_1}{K_{ed} M_d} k_1 \leq 1$			$\frac{N}{N_d} + \frac{M_1}{K_{ed} M_d} k_1 + \frac{M_1}{M_d} k_2 \leq 1$	

EC3	<p>Lateral torsional buckling not likely to appear</p> $\frac{N}{\min(N_d; N_{cr})} + \frac{k_1 M_1}{M_{pl}} + \frac{k_2 M_2}{M_{pl}} \leq 1$
	<p>Lateral torsional buckling likely to appear</p> $\frac{N}{N_{cr}} + \frac{k_{LT} M_1}{\chi_{LT} M_{pl}} + \frac{k_2 M_2}{M_{pl}} \leq 1$
LRFD	<p><math>\frac{N}{2\min(N_d; N_{cr})} + \frac{M_1^*}{M_d} + \frac{M_2^*}{M_{pl}} \leq 1</math> for <math>\frac{N}{\min(N_d; N_{cr})} &lt; 0.2</math></p> <p><math>\frac{N}{\min(N_d; N_{cr})} + \frac{8}{9} \left( \frac{M_1^*}{M_d} + \frac{M_2^*}{M_{pl}} \right) \leq 1</math> for <math>\frac{N}{\min(N_d; N_{cr})} \geq 0.2</math></p>

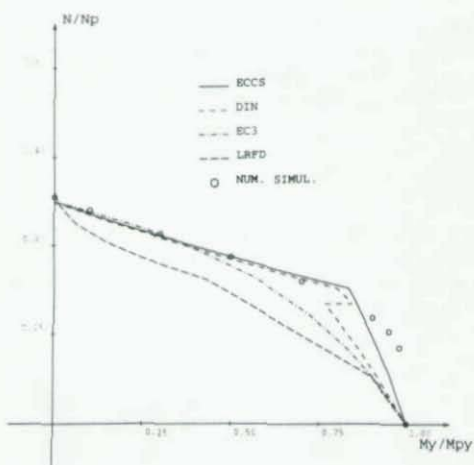
Table 1 - Four considered design approach



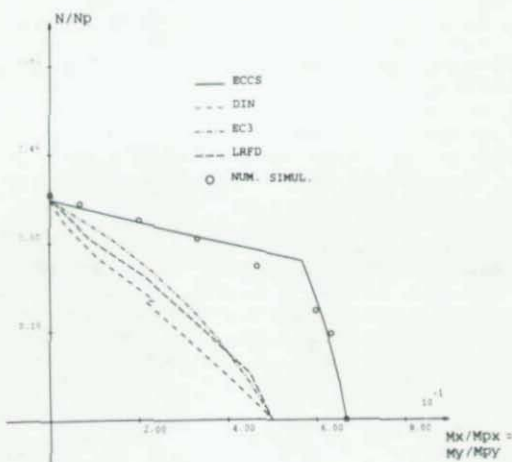
a. Uniaxial bending about strong axis; no lateral displacement



b. Uniaxial bending about strong axis; lateral displacements allowed



c. Uniaxial bending about weak axis



d. Biaxial bending

Figure 4 - Comparisons between numerical simulations and four considered design approaches for beam-columns constituted of a 200x100x6.3 rectangular tubular profile.



compression and biaxial bending. Unfortunately, these collapse loads are quite different from the actual ones, especially for intermediate and high bending moments (figure 4.d.). In these three approaches, the interaction formula for biaxial bending reduce to the following expression when the normal compression force in the column vanishes :

$$\frac{M_x}{M_{px}} + \frac{M_y}{M_{py}} \leq 1 \quad (2)$$

This linear expression differs considerably (see figure 5) from the following design criteria which is recommended in [5] for the evaluation of the plastic resistance of rectangular tubular cross-sections subject to biaxial bending :

$$\frac{3}{4} \left( \frac{M_x}{M_{px}} \right)^2 + \frac{M_y}{M_{py}} \leq 1 \text{ for } \frac{M_x}{M_{px}} \leq \frac{2}{3} \quad (3.a.)$$

$$\frac{3}{4} \left( \frac{M_y}{M_{py}} \right)^2 + \left( \frac{M_x}{M_{px}} \right) \leq 1 \text{ for } \frac{M_x}{M_{px}} > \frac{2}{3} \quad (3.b.)$$

The separate verification of the column stability and of the resistance in the most stressed cross-sections, on the other hand, allows a far better assessment of the maximum carrying capacity, as demonstrated by ECCS approach (figure 4.d.).

Similar conclusions may be drawn from the comparisons on beam-columns constituted of a hot-rolled HE160B profile : only the comparisons relative to beam-columns bent about strong axis, with lateral displacements allowed, are reported in this paper (figure 6). They present two particular features :

- The actual interaction between the out-of-plane flexural buckling of the beam-column and the lateral torsional buckling is seen to be more significant than the similar interaction between out-of-plane flexural buckling and in-plane instability in case of rectangular tubular cross-sections.
- The ECCS formula, as the DIN, EC3 and LRFD ones, underestimate, but less than the others, the actual carrying capacity. As a matter of fact, and contrary to what has been explained for rectangular tubular sections in which the lateral buckling is not likely to occur, the ECCS formula takes the coupling between out-of-plane buckling and lateral torsional buckling into consideration, but in a too conservative way. The necessity to check separately the instability and the resistance allows however, contrary to DIN, EC3 and LRFD approaches, a reasonable evaluation of the collapse load.

## 6. Conclusions

Some important conclusions have to be drawn from this comparative study in view of the improvement of the existing beam-column interaction formulae.

- LRFD and EC3 codes lead to too conservative assessments of the carrying capacity of beam-columns when the resistance is controlling (low N/M ratios). These two approaches are also too conservative when considering interaction between in-plane and out-of-plane instabilities.

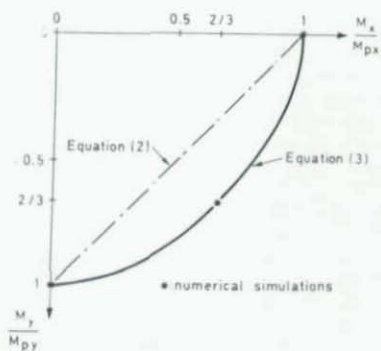


Figure 5 - Cross-section resistance under biaxial bending

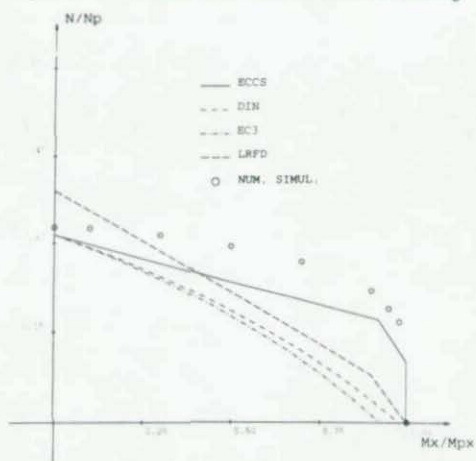


Figure 6 - Comparisons between numerical simulations and the four considered design approaches for a HE160B beam-column under uniaxial bending; lateral displacements allowed.

Simply replace  $\bar{N}_y$  by  $\bar{N}_x$  in the interaction formula proposed for in plane instability when the out-of-plane flexural buckling of the beam-column is likely to occur can not be considered as a consistent way to account for the actual amplification of the bending moment about strong and weak axes.

ECCS and DIN approaches consider also (and in a similar way) the interaction between in-plane and out-of-plane instabilities except when the lateral torsional

buckling is not likely to occur.

This results unfortunately in a non-smooth transition from one formula (with lateral torsional buckling) to the other (without lateral torsional buckling).

The ECCS formula is also characterized by a non-smooth transition from the case of bending about strong axis (collapse by lateral torsional buckling) to that of combined compression and uniaxial bending under strong axis (spatial instability).

#### 7. References

- [1] ECCS TC 8.1./8.2. *Working documents on beam-columns, not published, 1985.* (content introduced in the "Steel Structures" course of Prof. R. MAQUOI, Department MSM, University of Liège, 1988).
- [2] DIN 18800 Teil 1, Stahlbauten, Bemessung und Konstruktion, Beuth Verlag GMBH, Berlin, March 1988.
- [3] Eurocode 3 : Design of Steel Structures. Part 1.1. : General rules and rules for buildings, European prestandard ENV 1993-1-1, February 1992.
- [4] LRFD, Manual of Steel Construction, AISC, First Edition, 1986.
- [5] "Construction with hollow steel sections", British Steel Corporation, First Edition, December 1984.

## A STUDY ON ULTIMATE STRENGTH OF STIFFENED PLATES IN STEEL BRIDGES SUBJECTED TO BIAXIAL IN-PLANE FORCES

Tomiyasu FURUTA\*, Toshiyuki KITADA\*\* and Hiroshi NAKAI\*\*

\* Division of Long Span Bridges, Yokogawa Construction Co. Ltd.  
1-46-13, Nishigawara, Kita-ku, Tokyo 114, Japan.

\*\* Department of Civil Engineering, Osaka City University,  
Sugimoto 3-3-138, Sumiyoshi-ku, Osaka 558, Japan.

### ABSTRACT

This paper deals with the ultimate strength of longitudinally stiffened plates subjected to biaxial in-plane forces. Firstly, the residual stress and initial deflections of steel plates with the closed cross-sectional stiffeners are predicated. Then, the ultimate strength of the stiffened plates is investigated through elasto-plastic and finite displacement analyses. Also formulated are the interaction curves on the longitudinal and transverse ultimate stresses of stiffened plates. An approximate interaction curve for the ultimate stresses, which is the function of the ultimate longitudinal and transverse compressive stresses of the stiffened plates subjected to longitudinal and transverse compressions separately, is proposed for predicting the ultimate stresses of the unstiffened and stiffened plates subjected to biaxial in-plane forces. Finally, the test results carried out in the study are compared with the approximate interaction curve for the ultimate stresses.

### 1. INTRODUCTION

Recently, the number of plate elements to be designed as the unstiffened or stiffened plates subjected to biaxial in-plane forces ( hereafter called as the biaxially loaded plates or stiffened plates ), as illustrated in Fig.1, are gradually increasing in Japan in accordance with the increase of length of span or clear width of steel bridges. However, the current Japanese Specifications for Highway Bridges<sup>1)</sup> ( JSHB ) does not codify any design criteria for the biaxially loaded plates. Accordingly, in designing such a plate, the buckling stability must be investigated through a theoretical or experimental study for checking the safety against their ultimate limit state in the case where the transverse compression as well as the longitudinal in-plane stress

are predominated significantly. It is, therefore, preferable to establish promptly a rational design method for the biaxially loaded plates.

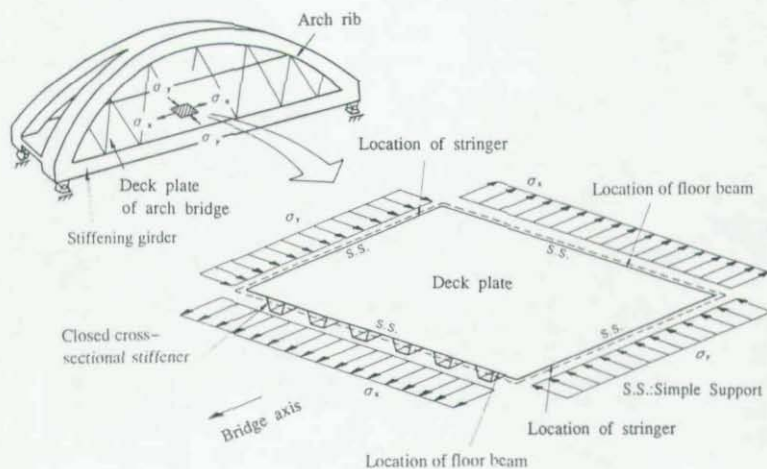


Fig.1 Example of biaxially loaded plate in steel bridges

For the reason mentioned above, an approximate method for predicting the ultimate longitudinal and transverse stresses of biaxially loaded stiffened plates, namely an interaction curve has been proposed by the authors<sup>2-4)</sup> based on the elasto-plastic and finite displacement analysis by considering initial deflection and residual stress through the check of validity in comparison with the tests results<sup>5,6)</sup> in this paper.

Thus, an approximate method, theoretical results and experimental results are briefly predicated.

## 2. INITIAL IMPERFECTIONS OF PLATES WITH CLOSED CROSS-SECTIONAL STIFFENERS

### 2.1 Residual Stress

The distribution of longitudinal residual stress in the closed cross-sectional stiffeners and



the transverse residual stress in the plate panels between stiffeners or under stiffeners were measured for three full scale stiffened plate specimens<sup>7)</sup>, because of the lack of these data. By arranging these data, a pattern of the residual stress distribution in the analytical models, which enable to investigate the influence of initial deflection and residual stress on the ultimate stresses of stiffened plates, is proposed. The measured distribution of the transverse residual stress,  $\sigma_{xy}$ , along the longitudinal direction of a plate panel in the three test specimens is shown in Fig.2.

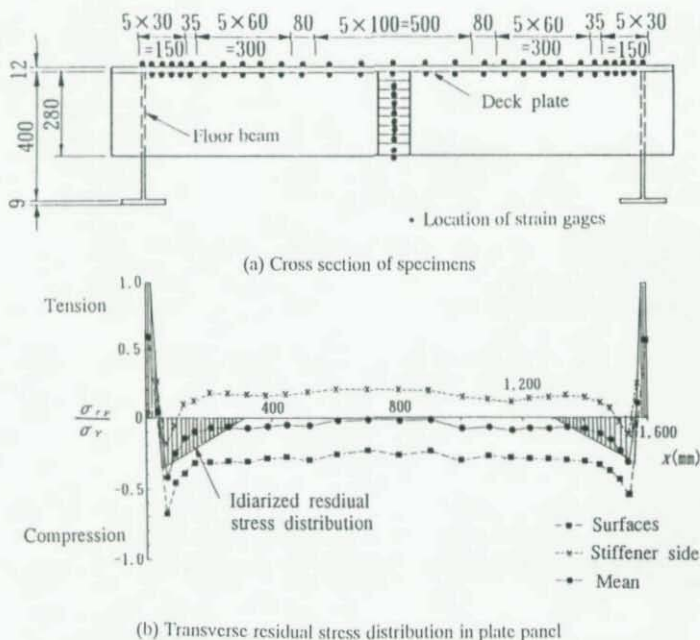


Fig.2 Transverse residual stress distribution in plate panel  
(dimensions in mm)

This figure reveals that the transverse bending residual stress is predominant, whereas the transverse in-plane residual stress, which is the average of the values at the surfaces of the plate panel, is negligible small values except the parts near the floor beams.

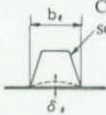
## 2.2 Initial Deflections

Numerous data on initial deflections of plate panels and stiffeners were also measured for the steel deck plates of two actual bridges. These initial deflections are arranged on the basis of statistical approach. Then, the measured initial deflections are compared with the tolerance in JSHB. Table 1 shows the maximum tolerances of initial deflection in plate panels and longitudinal stiffeners.

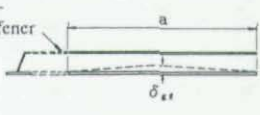
Table 1. Maximum values of initial deflection

Initial deflection	Measured locations	Deck plate $t=14\text{mm}$			Deck plate $t=12\text{mm}$	
		L/4	L/2	3L/4	L/2	L/5
$\delta_{\epsilon \max} / b_{\epsilon} / 150$		0.562	0.586	0.633	0.267	0.319
$\delta_{\epsilon \max} / a / 1,000$		0.768	0.683	0.928	0.236	0.859



(a) Initial deflection of plate panel



(b) Initial deflection of stiffener

Remark; L: Span length of bridges

It is observed from this table that the maximum values of initial deflection of plate panels and stiffeners are smaller than the allowable values of JSHB,  $b_{\epsilon} / 150$  and  $a / 1,000$ , respectively.

## 3. APPROXIMATE METHOD FOR PREDICTING ULTIMATE STRESSES

The ultimate stresses,  $\sigma_{xm}$  and  $\sigma_{ym}$  of biaxially loaded plates and stiffened plates can be predicted by using the approximate interaction curve as proposed in Ref.2), if the ultimate longitudinal and transverse compressive stresses,  $\sigma_{x(m)}$  and  $\sigma_{y(m)}$ , which respectively designate the ultimate stresses of these plates under longitudinal and transverse compressions, can be obtained separately.

### 3.1 Approximate Interaction Curve for Ultimate Stresses of Biaxially Loaded Stiffened Plates

The ultimate stresses of biaxially loaded stiffened plates are estimated through the elasto-plastic and finite displacement analysis of analytical models, shown in Fig.3, on the basis of a finite element method by considering both the initial deflections and residual stress. Then, the interaction curves on the ultimate stresses of biaxially loaded stiffened plates are derived through these analytical results.

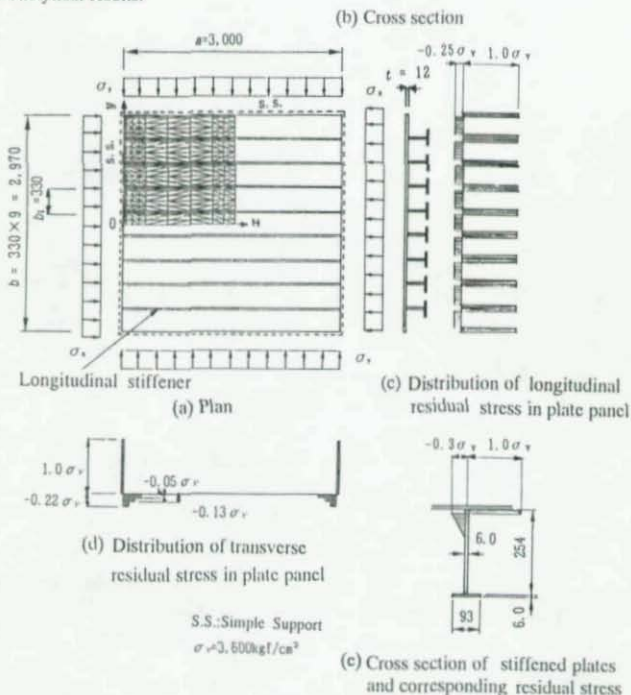


Fig.3 Analytical model (dimensions in mm)

The stress paths obtained from the elasto-plastic and finite displacement analyses are indicated in Fig.4 together with the von Mises' yield criteria and the approximate interaction curve for the ultimate stresses as is proposed in Ref.2).

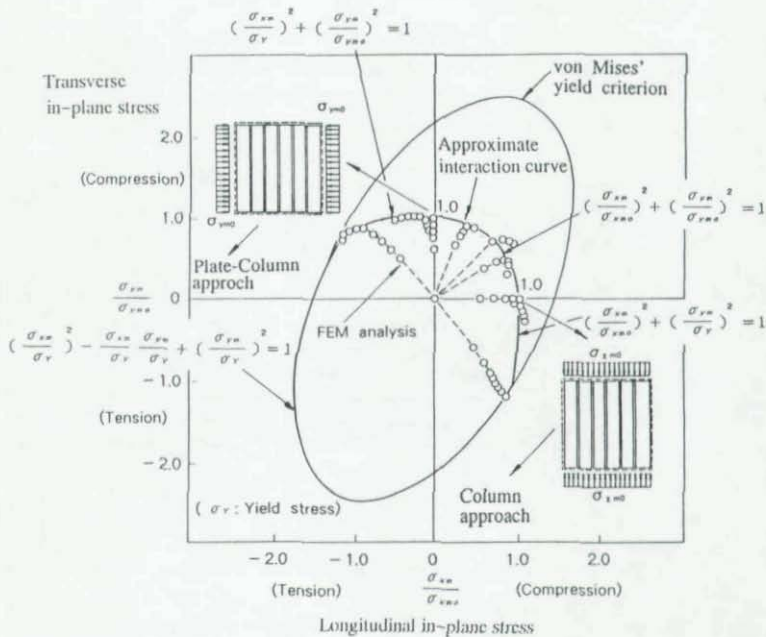


Fig.4 Approximate interaction curve for ultimate stresses

It can be seen from this figure that the ultimate limit states of the stress paths are well enveloped by the approximate interaction curve for ultimate stresses. Thus, a design method of the biaxially loaded unstiffened and stiffened plates is proposed by using the approximate interaction curve for ultimate stresses.

### 3.2 Approximate Method for Predicting Ultimate Longitudinal Compressive Stress

The ultimate longitudinal compressive stress of the stiffened plates can be obtained by using the column model approach as is proposed in Ref.8).

For this analysis, Fig.5 illustrates how to set the equivalent column for the column

approach from an original stiffened plate of which buckling mode does not have nodes at the location of the transverse stiffeners, because of the insufficient stiffness of the transverse stiffeners.

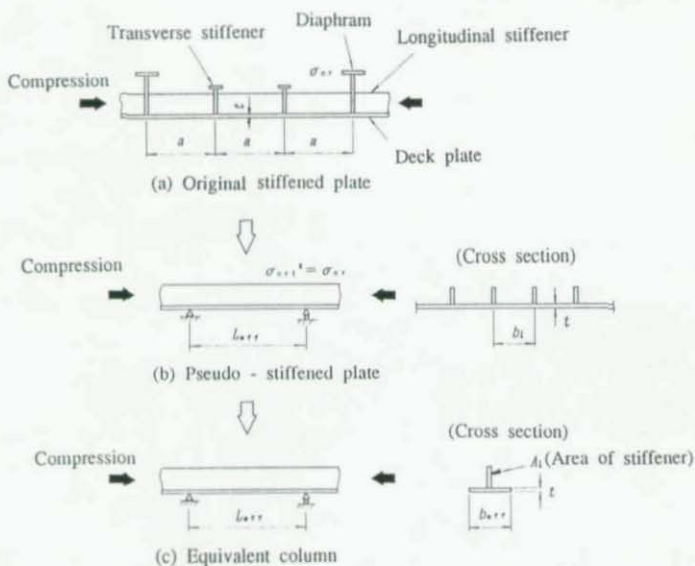


Fig.5 Original stiffened plate, pseudo - stiffened plate and equivalent column

In this figure,  $\sigma_{cr}$  and  $\sigma_{cr1}^*$  are the elastic buckling stresses of the original stiffened plate and pseudo-stiffened plate, respectively.

### 3.3 Approximate Method for Predicting Ultimate Transverse Compressive Stress

The ultimate transverse compressive stress of stiffened plates,  $\sigma_{ult}$ , can be estimated by the following equation.



$$\sigma_{y_{mo}} = \beta_r \frac{\sigma_{y_{ml}} + \sigma_{y_{mc}}(\alpha-1)}{\alpha} \quad \text{----- (1)}$$

where

$\sigma_{y_{ml}}$ : the ultimate stress of the side parts of a compression plate panel between longitudinal stiffeners, which can be obtained through the ultimate plate strength curves as proposed in Ref.10) by referring Figs.6 and 7.

$\sigma_{y_{mc}}$ : the ultimate stress of the middle part of the plate panel, which can be calculated by the ultimate column strength curve in JSHB<sup>1)</sup> multiplied by 0.9 by referring in Figs.6 and 7. This coefficient, 0.9, is to adjust the difference of initial deflections tolerance between columns and plate panels in JSHB.

$\alpha$ : The aspect ratio of the plate panel.

$\beta_r$ : The coefficient to obtain the transverse ultimate stress of stiffened plates with insufficient stiffeners.

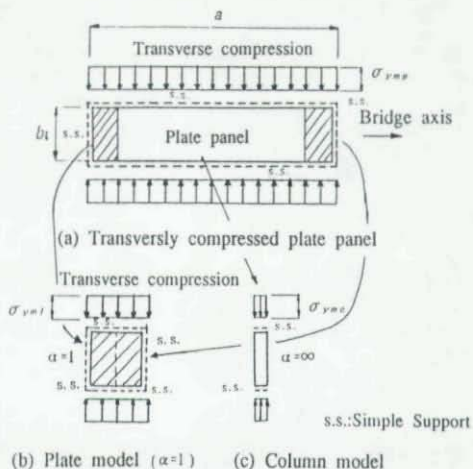


Fig.6 Models for predicting ultimate transverse compressive stress of unstiffened plates

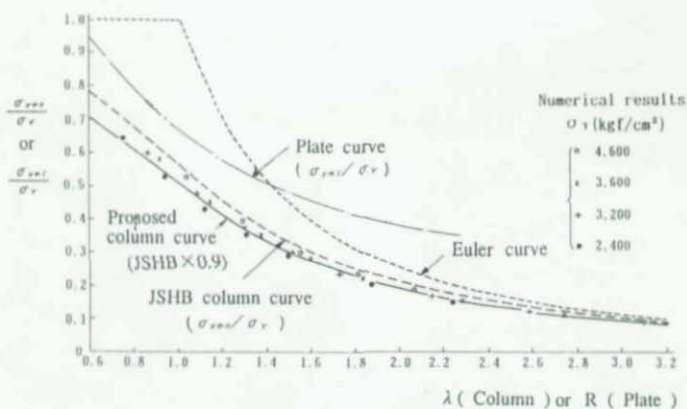


Fig.7 Ultimate strength curve for of transversely compressed plates

The coefficient,  $\beta_s$ , can be evaluated by using the ultimate strength curve as illustrated in Fig.8, which is derived through the elasto-plastic and finite displacement analysis for the steel deck plates with opened cross-sectional stiffeners.

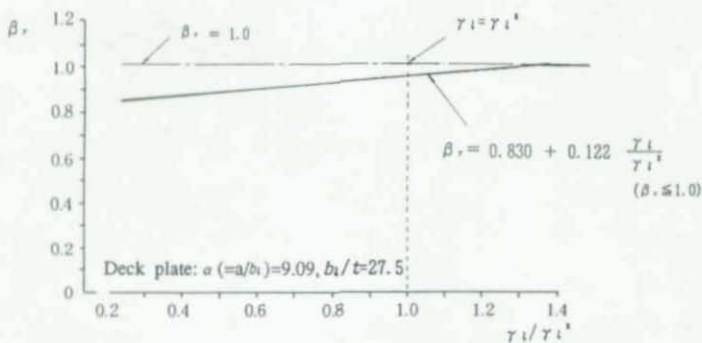


Fig.8 Variation of ultimate transverse strength of stiffened plates due to relative stiffness of a stiffener to plate panel

In this figure,  $\gamma_1$  and  $\gamma_1^*$  is the relative stiffness of a stiffener to plate panel and their minimum required value as is decided by the elastic linear buckling theory, respectively.

#### 4. EXPERIMENTAL STUDY

Experimental studies were conducted as reported in Refs.(5) and (6) in order to check the validity of the approximate interaction curves for ultimate stresses.

For the experimental study, an experimental apparatus, illustrated in Fig.9, was newly developed for these experimental studies. Ten stiffened plate specimens on scale 1/3 corresponding to that of the steel deck plate in an actual bridge were tested by using this experimental apparatus.

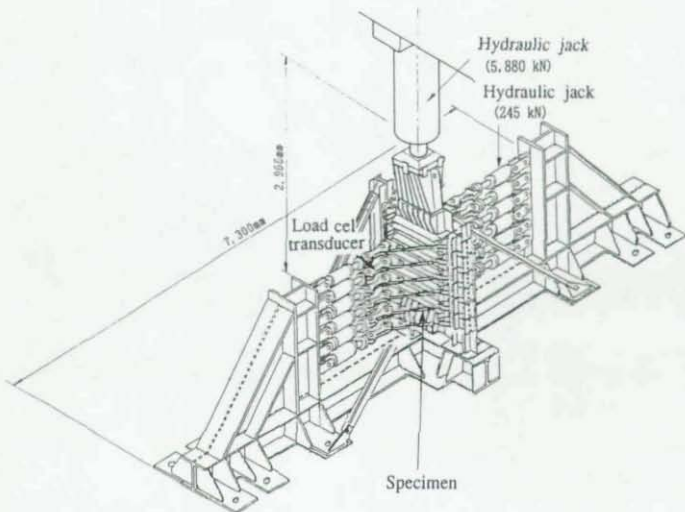


Fig.9 Experimental apparatus for stiffened plate specimens subjected enable to apply biaxial compressions

In Fig.10, the test results are compared with the approximate interaction curve for ultimate stresses. It is recognized from this figure that the approximate interaction curve well coincide with the experimental results and falls within the safety region. Thus, the experimental results reveal the validity of the approximate interaction curve.

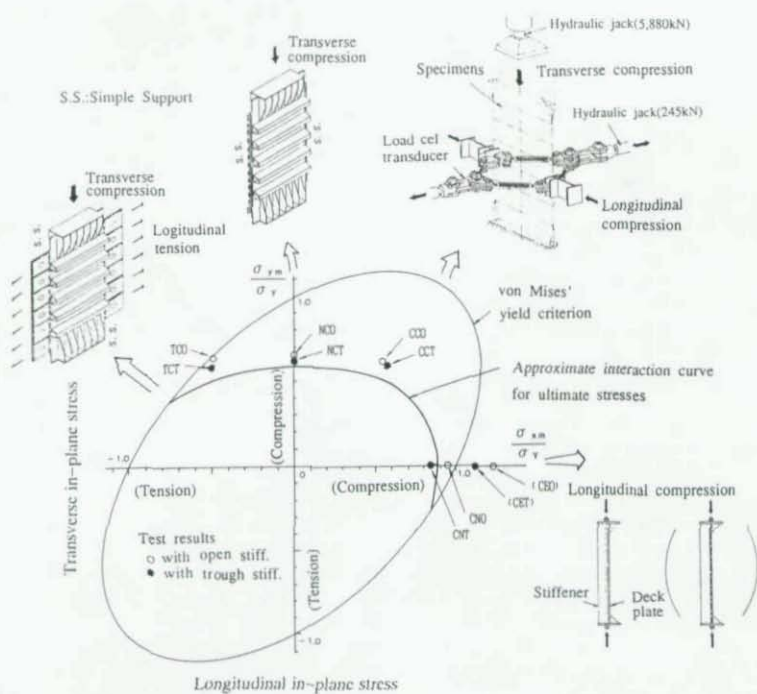


Fig.10 Comparison of experimental results with approximate interaction curve for ultimate stresses

## 5. CONCLUSION

In this paper, a method using the approximate interaction curve has been proposed for predicting the ultimate stresses of unstiffened and stiffened plates subjected to biaxial in-plane forces. The validity of the analytical method has been checked by the experimental study by using the special apparatus developed for this study.

## REFERENCES

- 1) Japanese Road Association: Japanese Specifications for Highway Bridges, Part II, Steel Bridges, Maruzen, Feb. 1990 ( in Japanese ).
- 2) Kitada, T., H. Nakai and T. Furuta: Ultimate Strength and Interaction Curve of Stiffened Plates Subjected to Biaxial In-plane Forces, Proc. of JSCE ( Japan Society of Civil Engineers ), Structural Eng./Earthquake Eng., No.437/1-17, pp.113s-1221, Oct.1991.
- 3) Furuta, T., T. Kitada and H. Nakai: Ultimate Strength of Stiffened Plates Subjected to Biaxial In-Plane Forces, Proc. of Annual Technical Session, SSRC, pp.269-280, Minneapolis, Minnesota, U.S.A., April 26-27, 1988.
- 4) Kitada, T., H. Nakai, T. Furuta and H. Suzuki: Ultimate Strength of Stiffened Plates Subjected to Biaxial In-plane Forces, Journal of Structural Engineering, JSCE, Vol.34A, pp.203-214, May 1988 ( in Japanese ).
- 5) Kitada, T., H. Nakai and T. Furuta: Experimental Study on Ultimate Strength of Stiffened Plates Subjected to Longitudinal Tension and Transverse Compression, Journal of Constructional Steel Research, Elsevier, Vol.19, No.2, pp.61-68, 1991.
- 6) Kitada, T., H. Nakai and T. Furuta: Experimental Study on Ultimate Strength of Stiffened Plates Subjected to Biaxial In-Plane Compressions, Proc. of JSCE, No.437/1-17, pp.156-168, Oct.1991 ( in Japanese ).
- 7) Kitada, T., H. Nakai and T. Furuta: A Study on Initial Deflections and Residual Stresses in Steel Plates with Closed Cross-Sectional Stiffeners, Proc. of JSCE, No.428/1-15, pp.127-136, April 1991 ( in Japanese ).
- 8) Nakai, H., Y. Taido, T. Kitada and H. Hayashi: A Design Method for Orthogonally Stiffened Plates with or without Stringers Subjected to Uni-axial Compression, Proc. of JSCE, Structural Eng./Earthquake Eng., Vol.2, No.2, pp.55-64, Oct.1985.
- 9) Furuta, T., T. Kitada and H. Nakai: A Design Method of Stiffened Steel Plates Subjected to Biaxial In-Plane Forces, Proc. of International Conference on Steel and Aluminum Structures, pp.481-490, Singapore, 22-24 May 1991.
- 10) Komatsu, S. and T. Kitada: A Study on the Ultimate Strength of Compression Plate with Initial Imperfections, Proc. of JSCE, No.270, pp.1-14, Feb. 1978( in Japanese ).



## Stiffening Effect of Lateral Bracing of Steel Arch Bridges on Their In-Plane Strength

Shigeru KURANISHI  
Professor of Tohoku University, Sendai, Japan

### Synopsis

The strength of steel arch bridge structures as a whole structure is achieved by appropriate proportioning of their lateral bracing system. The effect of the rigidity of the lateral bracing system on the in-plane ultimate strength is discussed being based on the results obtained from the finite displacements and elastic and plastic numerical analysis. The required rigidity of lateral bracing to get sufficient in-plane strength of arch bridge structure and resist to the lateral loading and the approximate estimation of their in-plane strength under the lateral loads are proposed in this paper.

### 1. Introduction

In the case where the form of arch axis is of the funicular curve, the arch rib is subjected to only the pure compression. As a fundamental structural system, arch bridges composed usually of main twin arch ribs and lateral bracing system connecting them each other. As a bridge structure, it is subjected to in-plane like dead and live loads and lateral loads like wind loads and/or forces by earthquake. The load carrying capacity of arches is generally governed by the in-plane and out-of-plane buckling strength even under the in-plane loading. Therefore, their spatial strength are affected by the strength and rigidity as a spatial structural system, loading condition, axial form, boundary conditions at the supports, variation of cross section, structural imperfections, material properties etc.

Concerning the out-of-plane strength, the rigidity of lateral bracing system plays rather a main role of the strength. Because, as a built-up-column which consist of twin shafts of arch ribs, it has sufficient flexural buckling strength if considered rather low slenderness ratio come from the rib distance or width for traffic. Consequently, the buckling strength is affected greatly by the connecting rigidity of the lateral bracing, i.e. the shear rigidity of them and the structure system can resist the loads only in corporation of the arch ribs and lateral bracing system. A certain number of studies are already carried out being taken notice of the influence of the rigidity of lateral bracing. Wastlund<sup>1)</sup> studied the effect of bending rigidity of Veerendalle type of cross beams bracing on bifurcation lateral buckling. Kuranishi<sup>2)</sup> discussed the effect of cross beams which resist to the torsional deformation of arch ribs on lateral buckling and proposed required rigidity of the cross beams to get sufficient lateral buckling strength. Kuranishi and Yabuki<sup>3)</sup> studied numerically the ultimate spatial strength paying attention to the shear rigidity as a whole structure and bending rigidity of cross beams which are composing the lateral bracing system. They<sup>3)</sup> also discussed the effect of lateral loads on the in-plane strength. Sakimoto and Komatsu<sup>4)</sup> proposed an evaluation formula of the lateral strength from the result of the numerical ultimate strength analysis for arch bridges with a certain numbers of bracing pattern which are subjected vertical loads.

This paper is treating the lateral buckling strength as a system of twin arch ribs and bracing which subjected to combined loads of vertical loads and the specified lateral loads like wind load. From the results obtained here, a required rigidity of lateral bracing is proposed. In addition, an approximate estimation formula of the in-plane strength under lateral loads is

presented.

## 2. Analysis

### 2.1 Analytical model

The basic arch bridge structures analyzed here are two-hinged steel arch bridge of parabolic form and composed of twin arch ribs of box cross sections and truss type of lateral bracing as shown Fig. 1. The effect of posts, hangers and stiffening girders is neglected. The proportion of the cross section of the rib and residual stress distribution over the cross section is shown in Fig. 2. Namely,  $H/t_w = 190$ ,  $B/H = 0.6$ ,  $A_c/A_w = 0.9$ ,  $t/H = 0.400$ ,  $k/H = 0.320$  and  $GJ_r/EI_r = 0.321$  where  $H$ ,  $B$ ,  $t_w$ ,  $r$ ,  $k$ ,  $GJ_r$  and  $EI_r$  are depth, width, radius of gyration of area, core radius, torsional rigidity and flexural rigidity of arch rib respectively. The rigidity of the lateral bracing system is modeled by diagonal linear springs continuously connected at the ribs and the spring constant is given by

$$K_s = \mu_s \times 1.2 \frac{EA_s}{c} \times \left(\frac{d}{L_s}\right)^2 \dots\dots (1)$$

where  $E$ ,  $A_s$ ,  $c$  and  $d$  are Young's modulus, cross sectional area of rib, panel length and diagonal distance in a panel respectively. The rigidity of bracing is evaluated here as shear rigidity as a whole in the plane including two ribs. This shear rigidity is defined as a ratio to the flexural rigidity of two arch ribs as a whole referred to Ref.3 as follows:

$$\mu_s = \frac{GA_{eq}}{2EA_s} \times \left(\frac{L_s}{b}\right)^2 \dots\dots (2)$$

where  $G$ ,  $b$  and  $A_{eq}$  are shear modulus, distance between arch ribs and equivalent shear rigidity of a plate to the shear rigidity of bracing as a whole. Namely,  $A_{eq}$  for warren type bracing is

$$A_{eq} = \frac{E}{G} \times \frac{2A_b b^2 c}{d^3} \dots\dots (3a)$$

for K type of bracing

$$A_{eq} = \frac{E}{G} \times \frac{A_b b^2 c}{d^3} \dots\dots (3b)$$

where  $A_b$  is cross sectional area of diagonal member of bracing.

The cross beams which are transversely connecting the twin ribs are modeled by rotational springs (twist spring for arch ribs) and axial springs. The rotational spring coefficient  $K_c$  is given by the following equation.

$$K_c = \frac{6EI_b}{b} = \frac{6GJ_{rc}}{L^2} \times \mu_c \dots\dots (4)$$

where  $EI_b$ : flexural rigidity of a cross beam,  $b$ : distance of the arch ribs,  $GJ_r$ : torsional rigidity of a rib and  $L$ : span length.  $\mu_c$  is a parameter which is presenting the effect of the flexural

rigidity of cross beams on the torsional rigidity of ribs and given by

$$\mu_T = \frac{E I_b}{G J_a} \times \frac{L^2}{b c} \dots\dots\dots (5)$$

The axial spring  $K_E$  is work to keep the distance between the ribs and given by

$$K_E = \frac{E A_b}{c} \dots\dots\dots (6)$$

where  $A_b$  is cross sectional area of a cross beam.  $\mu_T$  is taken as 10 referring to Ref.3 which guarantees to be able to avoid the torsional buckling of arch.

## 2.2 Analytical Method

The FEM adopted here to analyze the spatial ultimate strength is same as the method used in Ref.3. In the analysis, the geometrical and material non-linearity is considered. Each element as a spatial frame element has 6 freedom at each nodal point and is neglected the warping effect. The stress-strain relationship in each incremental stage is assumed to follow the Prandtl-Reuss's law basing on the Von Mises' yield criterion.

The chief assumption adopted here is as follows:

1. The line which pass through the centers of gravity of cross section makes the axial line of member. The axial line of arch is formed by the short straight members.
2. All the members have closed cross sections and have not initially torsional crookedness about the axial line.
3. All the members behave as Bernoulli-Euler beam. Only St.Venant's torsional rigidity is considered here.
4. Steel is of the ideal elastic-plastic material and has not strain-hardening property. In the unloading pass, equivalent stress-strain relationship follows the elastic unloading pass.
5. The ultimate load is determined by the divergence of the vertical or horizontal displacements in which the equilibrium state is not determined in the iterative analysis. The accuracy of the convergence in the iterative process is under 0.5% in the ratio of the load intensity to the imbalanced residual force.

## 2.3 Load and loading method

In the analysis, the lateral load  $p$  is initially applied and then the vertical load is applied and increased to the ultimate state. The lateral loads which simulate wind loads are determined according to the Japanese Specification for Highway Bridges. Namely,  $40.6 \text{ MN/m}^2$  of wind load is applied on the exposed surface of the windward members and half of it on the leeward members when the structure is not applied by live loads. When the structured applied by live loads, the value is estimated as half. So,  $p$  presents the lateral wind load density and  $0.5 p$  means the half wind loading in the case of live load application. The most unfavorable way of vertical loading against arch is asymmetrical loading. Generally speaking, for uniformly distributed vertical loads, the parabolic arch has the highest strength. The problem treated here is how much rigidity of the lateral bracing system is required to get enough strength as whole. So, considering the purpose of this theme, uniformly distributed loads over arch span is taken up and expressed non-dimensionally by the ratio to the yield load which produces yielding at the springing of arch.

## 2.4 Structural parameters

The structural parameters adopted here are as follows:

$\lambda_i$  (in-plane slenderness ratio of arch rib): 200–300

$\lambda_{out}$  (out-of-plane slenderness ratio of arch structure): 20–60

$\mu_b$  (parameter expressing relative rigidity of bracing to the lateral flexural rigidity of arch structure): 0.01–1.0

$\mu_T$  (parameter expressing the flexural rigidity of cross beams to the torsional rigidity of arch rib): 10

rise-span ratio: 0.15

initial deflection to the lateral direction at the crown:  $L/1000$

yield point\* 313 MN/m<sup>2</sup>

Young's Modules: 206 GN/m<sup>2</sup>

The span length is fixed here to 200m and lateral loads like the wind load is depending on the dimension of the structure. This means that the effect of the lateral loading on the strength is affected by their dimension, namely the results is only valid for the arch bridge of the span length. But, the span length of about 200m is usual as arch bridges and the results obtained here may be applicable to the almost same span of bridges or modifying it. If the arch bridge has far longer span, the effect of lateral bracing will be individually checked at its designing.

## 3. Analytical Result

### 3.1 General behavior

Generally, arches deflect to the vertical and lateral directions under vertical and vertical-lateral loadings and reach to the ultimate state as shown in Fig. 3. When the rigidity of the bracing is low, the deflections produced by vertical loads change abruptly from the planar phase to spatial one on the way to the ultimate state. On the contrary, if the arch has rather high rigid bracing, the lateral deflections are very small to the ultimate state. In addition of lateral loading, the fundamental feature of the deflections is almost same, but the spatial deflections become significant and they increase gradually until the ultimate state.

Fig. 4 is an example for the case  $\lambda_i = 200$  and  $\lambda_{out} = 30$  and represents the effect of the lateral bracing rigidity on the in-plane load carrying capacity. In the figure, solid line shows the case for the vertical loading and dotted line is for combined loadings. The ordinate is the non-dimensional vertical load intensity and the abscissa is the shear rigidity parameter of lateral bracing system.

As seen in the figure, the curves have turning points. At the left side of the turning point, namely when the lateral rigidity is weak, the arch collapses spatially. At the right side of the turning point, the collapse is in-plane one. Referring the other cases, it is concluded that when the out-of-plane flexural rigidity becomes higher and the in-plane flexural rigidity becomes low, the turning point goes to left and vice versa. At the right side, the load carrying capacity is governed by the in-plane strength of the arch ribs.

Under the lateral loading, the load carrying capacity becomes lower at the right side of the turning point under the influence of the increment of stresses by the lateral loads and subsequent early yielding. If the turning point is located to the right side, the required rigidity of the lateral bracing becomes higher. In addition, the effect of the cross beams is checked by taking  $\mu_T = 0.0$ . The result shows that  $\mu_T$  gives little affect on the load carrying capacity.

### 3.2 Required lateral rigidity

Under the uniformly distributed vertical loads, the arch buckles at the following axial force



per one rib.

$$P_{E,i} = \frac{\pi^2 EI_i}{(k_i \times L_s)^2} \dots\dots(7)$$

where  $k_i$  = an in-plane effective length coefficient of an arch rib for the curvilinear length and  $I_i$  = radius of gyration of an arch rib cross section about horizontal line. The buckling axial forces of a column of two shaft braced by diagonal and cross members is given by

$$P_s = \frac{P_{E,out}}{1 + \frac{P_{E,out}}{GA_{eq}}} \dots\dots(8)$$

where  $GA_{eq}$  = shearing rigidity as a whole given by the lateral bracing system and it is expressed by using the already introduced parameter  $\mu_r$  as follows:

$$GA_{eq} = 24 \mu_s EA_s \left(\frac{b}{L_s}\right)^2 \dots\dots(9)$$

where  $P_{E,out}$  is the buckling axial force of a column of which cross section consists of the cross section of two arch ribs and given by

$$P_{E,out} = \frac{\pi^2 EI_{out}}{(k_{out} L_s)^2} \dots\dots(10)$$

where  $k_{out}$  is an out-of-plane effective length coefficient for the curvilinear length and  $I_{out}$  is moment of inertia as a whole of the arch about the vertical axis.

Then the critical value at which the arch buckles to the in-plane or out-of-plane is

$$P_k = 2P_{E,in} \dots\dots\dots(11)$$

Rearranged by Eq.(8) to (10), we get the critical value for the rigidity parameter  $\mu_{rcr}$  as follows:

$$\mu_{rcr} = \frac{\pi^2}{48} \times \frac{1}{\left(\frac{k_i \lambda_i}{k_{out} \lambda_{out}}\right)^2 - 1} \dots\dots\dots(12)$$

Fig. 5 shows the correlation between the critical values which are given approximately by Eq.(11) and the values which are obtained by this numerical analysis. They have so good agreement each other as to be used for the required minimum rigidity parameter to get its in-plane load carrying capacity.

Fig. 5 shows the correlation between the critical values for no-lateral loading in the abscissa and corresponding values of it for combined loading, namely for 0.5p case, in the ordinate. Judging from this figure, the critical rigidity parameter for combined loading should be double of the value given by Eq.(15) as shown in a solid line in Fig. 6.

### 3.3 In-plane load carrying capacity



## 3.3.1 By curve fitting method

From the results obtained through this analysis, the in-plane load carrying capacity can be approximated being taken the capacity as constant in the in-plane buckling range of the  $q_{\max} - \mu_s$  relation curve and to be linear to  $\log \mu_s$  in the spatial buckling range of the figure. Namely, under no lateral load,

for  $\mu_s < \mu_{scr}$

$$q_{\max} = \frac{680}{\lambda_i \times \sqrt{\lambda_{out}}} \times \log 100 \mu_s + \frac{10\theta - 2\lambda_{out}}{\lambda_i} + 0.12, \dots (13)$$

for  $\mu_s \geq \mu_{scr}$

$$q_{\max} = \frac{680}{\lambda_i \times \sqrt{\lambda_{out}}} \times \log 100 \mu_{scr} + \frac{10\theta - 2\lambda_{out}}{\lambda_i} + 0.12, \dots (14)$$

When lateral loads are applied:

for  $\mu_s < \mu_{scr}$

$$q_{\max} = \frac{470}{\lambda_i \times \sqrt{\lambda_{out}}} \times \log 100 \mu_s + \frac{120 - 2\lambda_{out}}{\lambda_i} - 0.02, \dots (15)$$

for  $\mu_s \geq \mu_{scr}$

$$q_{\max} = \frac{470}{\lambda_i \times \sqrt{\lambda_{out}}} \times \log 100 \mu_{scr} + \frac{120 - 2\lambda_{out}}{\lambda_i} - 0.02, \dots (16)$$

The comparison of the approximate estimation by Eq.13 to Eq.16 with the analytical results is illustrated in Fig. 7. It is seen that there is a good agreement.

## 3.3.2 Approximation of the lateral deflection and its correlation with the in-plane buckling strength.

When the arch is not subject to lateral loads, the stress caused in the two arch ribs is same and they will buckle in the same manner. But, when the arch is subjected to lateral loads, the stress of the leeward arch rib will become higher than that of the windward rib and the leeward rib will be stressed higher and buckle. Those effect may be estimated by the lateral deflection at the arch crown. Therefore, firstly an approximate formula will be here introduced and the relation between the deflection and buckling strength will be discussed.

The lateral deflection at the arch crown is caused by the bending under the influence of the shear deformation and the torsion of the arch. The non-dimensional out-of-plane bending deflection  $(w/L_s)_B$  at the crown is expressed approximately as follows:

$$\left(\frac{w}{L_s}\right)_B = \alpha \times \frac{D^3 L_s^3}{E I^2 A_s} \times \left(\frac{1}{\mu_s}\right)^B, \dots (17)$$

Expressed in logarithm form

where  $p =$  lateral load intensity,  $b =$  distance between the two arch rib axes and  $A_s =$  cross

$$\log \left( \frac{w_c}{L_s} \right)_B = \log \left( \alpha \times \frac{PL_y^3}{EB^2A_a} \right) - \beta \log \mu_s, \dots (18)$$

sectional area of an arch rib.

There is the relationship between the rigidity of lateral bracing  $\mu_s$  and the lateral deflection  $w_c$  shown in Fig. 8. From this figure, we can have the values of  $\alpha$  and  $\beta$ . Finally, we get the lateral deflection as follows:

$$\left( \frac{w_c}{L_s} \right)_B = \frac{PL_y^3}{6.4 EB^2A_a} \times \left( \frac{1}{\mu_s} \right)^{0.9}, \dots (19)$$

Next, the deflection by torsion can be estimated by subtracting the bending deflection given by Eq.19 from the total lateral deflection calculated by the spatial analysis. Judging the calculated relationship between the deflection by torsion and the in-plane and out-of-plane bending rigidities, the deflection seems to be proportional to the third power of the in-plane slenderness ratio, the second power of the out-of-plane slenderness ratio and the rise-span ratio as shown in Fig. 9, Fig.10 and Fig.11 as example. Then, we have

$$\left( \frac{w_c}{L_s} \right)_T = \gamma \times \frac{f}{L} \times \frac{PL_y^3}{GJ} \times \left( \frac{L_s}{b} \right)^2, \dots (20)$$

where  $\gamma$  is determined the calculated results.

Then, the lateral deflection by torsion is given by

$$\left( \frac{w_c}{L_s} \right)_T = \frac{1}{360000} \times \frac{f}{L} \times \frac{PL_y^3}{GJ} \times \left( \frac{L_s}{b} \right)^2, \dots (21)$$

Finally, The total lateral deflection is obtained by the combination of Eq.20 and Eq.21.

Fig. 11 shows the relationship between the total lateral deflection at the crown and the buckling strength expressed non-dimensionally. The in-plane buckling strength decreases as increasing of the lateral deflection and the reduction factor of the in-plane buckling strength is expressed in the safer side as follows:

$$\frac{q_{max}}{q_i} = \frac{1}{1+2(w/b)}, \dots (22)$$

The correlation is shown in Fig. 12. This reduction factor is applicable only to the case of the application of uniformly distributed vertical loads in the strict sense. But, it may be applicable to the other loading case, for example to anti-symmetrical loading, being considered a characteristic common to the action of lateral loads on the in-plane load carrying capacity. But, the proof is not done here.

#### 4. Conclusion

For the purpose of determining the required rigidity of lateral bracing system to get a sufficient in-plane load carrying capacity of steel arch bridge structure, a numerical analysis

is carried out. In the analysis, the structural parameters concerning the in plane and out-of-plane flexural rigidity of the arch ribs and the lateral bracing system are varied. From the result, the following conclusion is driven.

1. The in-plane load carrying capacity for vertical loads is governed by the shearing rigidity parameter  $\mu_s$ , as a whole of the lateral bracing system if the parameter  $\mu_s$  is less than a critical value and not affected if the parameter is greater than the critical value.
2. Under the action of lateral loads, the load carrying capacity becomes less than the case of non-lateral loading.
3. To get the in-plane load carrying capacity even under lateral loading, the parameter  $\mu_{ser}$  should be increased. In the range of the structural parameters taken up in this analysis, the multiple factor is about 2.
4. The parameter  $\mu_{ser}$  can be approximately estimated by the critical shear rigidity of a built-up-column at which the buckling mode changes from in-plane to out-of-plane one and vice versa.
5. The reduction of the in-plane load carrying capacity under the influence of the lateral loading can be estimated approximately as the influence of the lateral displacement.

#### Acknowledgement

The calculation carried out in this paper is owing to former graduated student Mr.Okuder and Associate Researcher Dr.Nakazawa.

#### References

- 1)Wastlund,G : Stability of Compressed Steel Members and Arch Bridges, J.Strct.Div.,ASCE, No.ST6,pp.47-71,1960
- 2) Kuranishi,S: On Torsional Buckling of Arch Brdige, Proc. of JSCE, No.191,pp.109-116, 1961( in Japanese)
- 3)Kuranshi,S. & Yabuki,T.: The Influence of Rigidity of Lateral Bracing on the Ultimate Strength of Steel Arch Bridge, Proc. of JSCE, No.305,pp.47-58, 1981( in Japanese)
- 4)Sakimoto,T. & Komatsu,S.: Ultimate Strength of Steel Arches under Lateral Loads, Proc. of JSCE, No.292,pp.83-94,1979
- 5)Japanese Specifications for Highway Bridges, Japan Road Association, pp.277-291, 1973

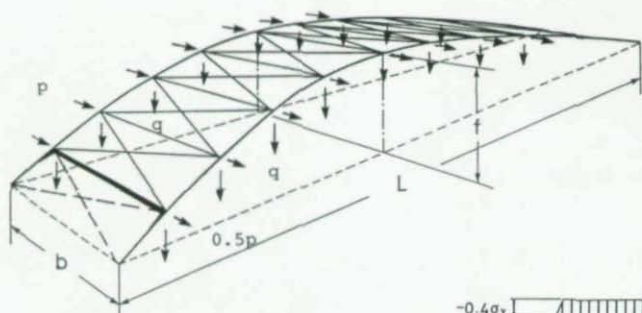


Fig. 1 Configuration and Loading

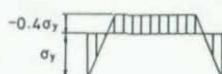
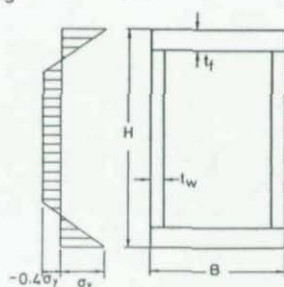


Fig. 2 Standard Cross Section and Residual Stresses



$$\frac{B}{H} = 0.6 \quad \frac{H}{t_w} = 190 \quad \frac{t_w}{t_f} = 15$$

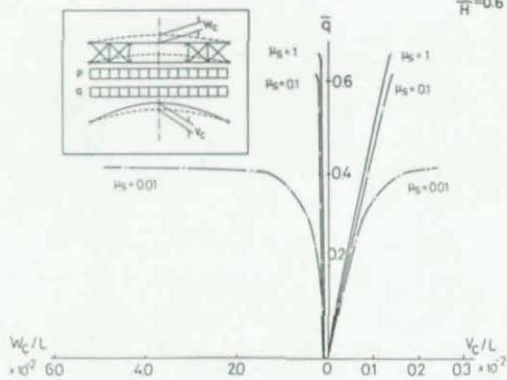


Fig. 3 Load-Deflection Curve under the Lateral Loading

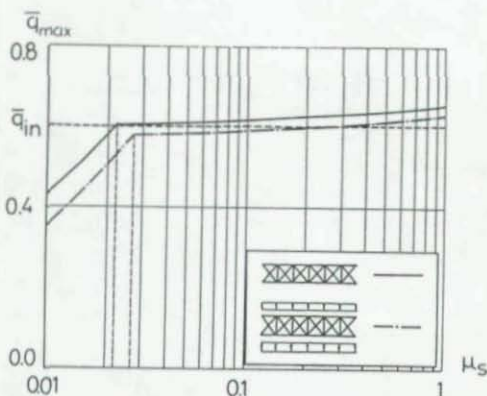


Fig. 4  
Effect of Shear Rigidity  
 $\mu_s$  on the In-Plane Load  
Carrying Capacity  
( $\lambda_{in} = 200$ ,  $\lambda_{out} = 30$ )

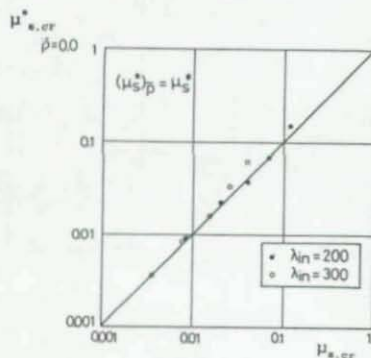


Fig. 5  
Correlation between the  
Proposed Critical Shear  
Rigidity and the Critical  
Shear Rigidity  
Obtained by the Analysis

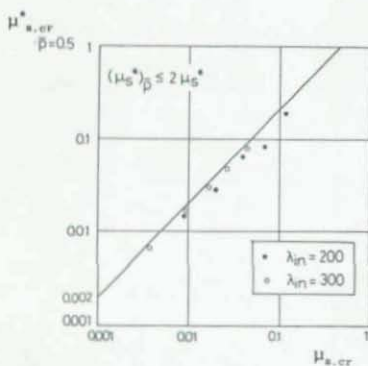


Fig. 6  
Correlation between the  
Proposed Critical Shear  
Rigidity and the Critical  
Shear Rigidity for  $p=0.5$   
(Laterally Loaded Case)



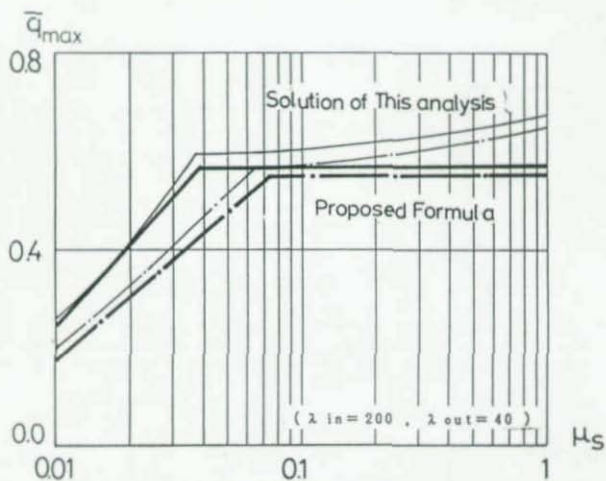


Fig. 7 Comparison of In-Plane Load Carrying Capacity by Porposed Formula and Analytical One

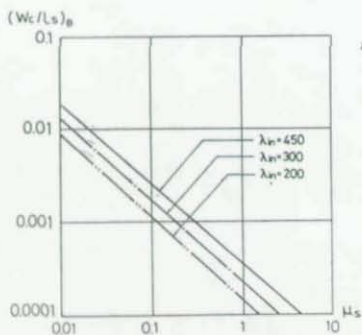


Fig. 8 Relationship between Flexual Displacement and Shear Rigidity  $\mu_s$

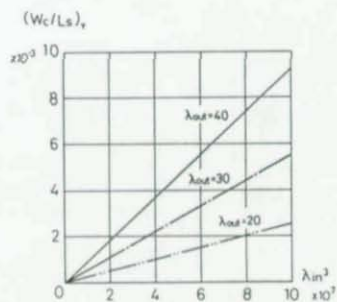


Fig. 9 Relationship between Torsional Displacement and In-Plane Slenderness Ratio

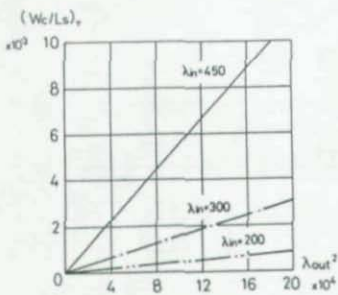


Fig. 10 Relationship between Torsional Displacement and Out-Of-Plane Slenderness Ratio

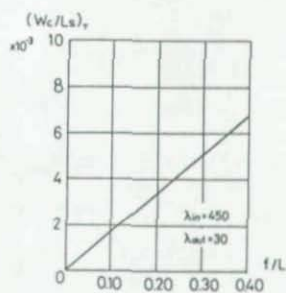


Fig. 11 Relationship between Torsional Displacement and Rise-Span Ratio

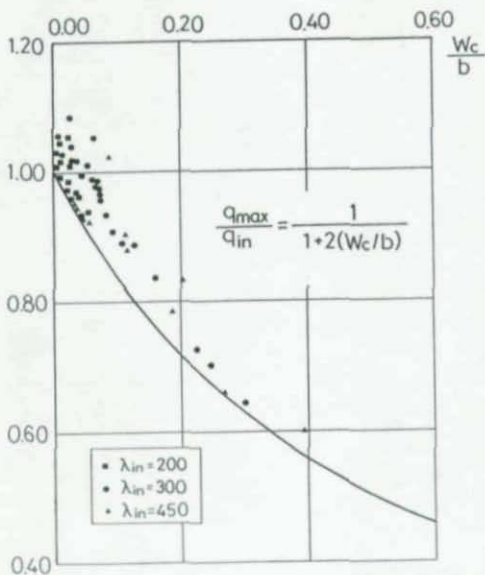


Fig. 12 Reduction of the In-Plane Load Carrying Capacity by the Lateral Deflection at the Arch Crown

**STRUCTURAL STABILITY RESEARCH COUNCIL**

**ATTENDEE ADDRESS LISTING**

**1993 Annual Technical Session  
Milwaukee, Wisconsin  
April 5-6, 1993**



Mr. Ahmad K. Abdelrazaq  
 Skidmore, Owings & Merrill  
 224 S. Michigan Ave., Suite 1000  
 Chicago, IL 60604

Dr. Ever Barbero  
 West Virginia University  
 315 Engineering Science Building  
 Morgantown, WV 26506-6101

Dr. Faisal Al-Mashary  
 Dept. of Civil Engineering  
 King Saud University  
 P. O. Box 800  
 Riyadh 11421, Saudi Arabia

Mr. Peter Bartnik (\*)  
 University of Wisconsin-Milwaukee  
 P. O. Box 784  
 Milwaukee, WI 53201

Mr. Joseph Ales (\*)  
 Dept. of Civil Engineering  
 University of Texas  
 Austin, TX 78712-1076

Mr. Christopher N. Baudhuin  
 C.R. Meyer & Sons Company  
 P. O. Box 2157  
 895 W. 20th Avenue  
 Oshkosh, WI 54903

Mr. Edmund R. Aller  
 NUCOR Corporation  
 P. O. Box 70  
 Waterloo, IN 46703

Dr. Lynn S. Beedle  
 Lehigh University  
 Structural Stability Research Council  
 13 E. Packer Avenue  
 Bethlehem, PA 18015

Mr. Donald Allison  
 Burns & McDonnell Engineering Co.  
 P. O. Box 419173  
 Kansas City, MO 64141

Prof. Peter C. Birkemoe  
 Department of Civil Engineering  
 University of Toronto  
 35 St. George St., GB 213  
 Toronto, Canada M5S 1A4

Mr. Robert C. Andren  
 Charles E. Pease Associates  
 110 W. Higgins Road  
 Park Ridge, IL 60068

Prof. Reidar Bjorhovde  
 University of Pittsburgh  
 Dept. of Civil Engineering  
 937 Benedum Hall  
 Pittsburgh, PA 15261

William F. Baker  
 Skidmore, Owings & Merrill  
 224 South Michigan Avenue  
 Suite 1000  
 Chicago, IL 60604

Mr. Gholamali Boolorchi (\*)  
 University of Wisconsin-Milwaukee  
 P. O. Box 784  
 Milwaukee, WI 53201

---

(\*) Student



Dr. Russel Q. Bridge  
Dept. of Civil Engineering  
The University of Sydney  
Sydney, NSW 2006, Australia

Mr. Nelson G. Chenaar  
Consulting Engineer  
11850 Edgewater Dr. #719  
Lakewood, OH 44107

Mr. Robert F. Brodowski  
O'Brien & Gere Engineers, Inc.  
5000 Brittonfield Parkway  
E. Syracuse, NY 13057

Dr. Mario De Stefano  
Istituto di Tecnica delle Costruzioni  
P.Le Tecchio, Universite di Napoli  
80125 Naples, Italy

Mr. Mark Broomell  
Webber/Smith Associates, Inc.  
1921 Wheatland Ave.  
Lancaster, PA 17603

Mr. Michael De Sautel  
Brander Construction Technology  
2357 W. Mason Street  
Greenbay, WI 54303

Mr. Rod Buchanan  
Frankfurt-Short-Bruza  
4108 Amon Carter Blvd. #200  
Fort Worth, TX 76155

Prof. Antonello De Luca  
Istituto di Tecnica delle Costruzioni  
P.Le Tecchio, Universita di Napoli  
80125 Naples, Italy

Ms. Liping Cai (\*)  
Dept. of Civil & Env. Engineering  
Rutgers University  
Piscataway, NJ 08855

Prof. Gregory G. Deierlein  
363 Hollister Hall  
Cornell University  
Ithaca, NY 14853

Mr. Steven Carter  
Donaldson Company, Inc.  
P. O. Box 1299  
Minneapolis, MN 55440

Mr. Samuel B. Dilcer  
Burns and Roe Industrial Services Co.  
700 Kinderkamack Road  
Oradell, NJ 07649

Prof. W. F. Chen  
School of Engineering  
Purdue University  
West Lafayette, IN 47907-1284

Mr. Jackson L. Durkee  
Consulting Structural Engineer  
217 Pine Top Trail  
Bethlehem, PA 18017

Mr. Chan Ho Chen  
LS Transit Systems  
1515 Broad Street  
Bloomfield, NJ 07003

Mr. Christopher J. Earles (\*)  
University of Minnesota  
425 13th Ave., #1602  
Minneapolis, MN 55414

---

(\*) Student

Dr. Mohamed Elgaaly  
Civil & Architectural Engrg. Dept.  
Drexel University  
Philadelphia, PA 19104

Dr. Duane S. Ellifritt  
College of Engineering  
University of Florida  
Gainesville, FL 32611

Dr. Samuel J. Errera  
1730 Maple Street  
Bethlehem, PA 18017

Dr. Hesham S. Essa  
Dept. of Structural Engineering  
Faculty of Engineering  
Ain Shams University  
Abbassia, Cairo, Egypt

Mr. Shu-Jin Fang  
Sargent & Lundy  
55 E. Monroe Street  
Chicago, IL 60603

Dr. David J. Fielding  
Consulting Structural Engineer  
8306 Shawnee Street  
Philadelphia, PA 19118-3907

Mr. Christopher Foley (\*)  
Marquette University  
1515 W. Wisconsin Avenue  
Milwaukee, WI 53233

Mr. Richard L. Forest  
Frankfurt Short Bruza Assoc.  
5701 N. Shartel, Suite 210  
Oklahoma City, OK 73118

Mr. Gerard F. Fox  
3 Whitehall Blvd.  
Garden City, NY 11530

Mr. David D. Frash  
Fanning/Howey Associates, Inc.  
3750 Priority Way South Dr., #110  
Indianapolis, IN 46240

Prof. Yuzuru Fujita  
President, The Japan Welding  
Engineering Society  
1-11 Kanda Sakuma-Cho, Chiyoda-ku  
Tokyo, Japan

Prof. Theodore V. Galambos  
122 C&ME Building  
University of Minnesota  
500 Pillsbury Drive SE  
Minneapolis, MN 55455-0220

Ms. Juliana E. Garner  
Pearson Engineering, Inc.  
P. O. Box 128  
Benton Harbor, MI 49023

Prof. Al Ghorbanpoor  
University of Wisconsin-Milwaukee  
C.E. Dept., P.O. Box 784  
Milwaukee, WI 53201

Prof. Luis Augusto Godoy  
Mechanical & Aerospace Engineering  
West Virginia University  
Morgantown, WV 26506-6101

---

(\*) Student

Prof. Subhash C. Goel  
Dept. of Civil & Environ. Engrg.  
The University of Michigan  
Ann Arbor, MI 48109

Mr. Anthony E. Goetz  
Frankfurt Short Bruza Assoc.  
5701 N. Shartel, Suite 210  
Oklahoma City, OK 73118

Dr. Arvind V. Goverdhan  
Stanley D. Lindsey & Associates  
300 Galleria Parkway, Suite 450  
Atlanta, GA 30339-3149

Mr. Robert G. Graham  
Steadfast Bridges  
201 40th St., N.E.  
P. O. Box 301  
Fort Payne, AL 35967

Mr. Edward A. Grebe  
2005 Two Tree Lane  
Wauwatosa, WI 53213

Mr. Kenneth E. Grebe  
Graef, Anhalt, Schloemer  
& Associates, Inc.  
345 North 95th Street  
Milwaukee, WI 53226

Mr. Stephen X. Gunzelman  
Brown & Root Representative  
10200 Bellaire Blvd.  
Houston, TX 77072-5299

Prof. Jerome F. Hajjar  
University of Minnesota  
Dept. of Civil & Mineral Engineering  
500 Pillsbury Drive, S.E.  
Minneapolis, MN 55455-0220

Mr. Dann H. Hall  
Bridge Software Development  
International, Ltd. (BSDI)  
562 Thomas Street, P.O. Box 287  
Coopersburg, PA 18036

Mr. Joseph P. Hartman  
Corps of Engineers  
20 Massachusetts Ave. NW  
Washington, DC 20314

Mr. Frank Hatfield  
Michigan State University  
Civil Engineering Dept.  
East Lansing, MI 48824-1226

Mr. Kirk A. Haverland  
C. R. Meyer & Sons Company  
P.O. Box 2157  
895 W. 20th Avenue  
Oshkosh, WI 54903

Mr. Todd Helwig (\*)  
University of Texas  
12166 Metric Blvd. #184  
Austin, TX 78758

Mr. Paul B. Hofland  
Nicol & Hofland Associates, Inc.  
1617 Wazee Street, Suite C  
Denver, CO 80202

---

(\*) Student

Mr. Michael J. Horne  
Graef, Anhalt, Schloemer  
& Associates, Inc.  
345 North 95th Street  
Milwaukee, WI 53226

Prof. Rola L. Idriss  
Dept. of Civil, Agricultural and  
Geological Engineering  
New Mexico State University  
Box 30001, Dept. 3CE  
Las Cruces, NM 88003-0001

Mr. Jerome S. B. Iffland  
Iffland Kavanagh Waterbury, P.C.  
1501 Broadway  
New York, NY 10036

Mr. John Imsdahl  
Donaldson Company, Inc.  
1400 West 94th Street  
P. O. Box 1299  
Minneapolis, MN 55440

Dr. Socrates A. Ioannides  
President  
Structural Affiliates International, Inc.  
2424 Hillsboro Road, Suite 202  
Nashville, TN 37212-5316

Dr. J. P. Jaspert  
MSM-Institut du Genie Civil  
Quai Banning, 6  
B-4000 Liege, Belgium

Mr. James Johnson  
Freeland Harris Consulting Engineers  
2410 Lexington Financial Center  
Lexington, KY 40507

Mr. Steven G. Judd  
Martin/Martin-Utah, Inc.  
455 E. 400 South St., Suite #400  
Salt Lake City, UT 84092

Mr. Richard Kaehler  
Computerized Structural Design, Inc.  
8989 N. Port Washington Road  
Milwaukee, WI 53217

Mr. Gary Karnthaler  
Wisconsin Electric Power Co.  
231 W. Michigan Avenue  
Milwaukee, WI 53201

Dr. Kenneth T. Kavanagh  
University of Western Australia  
Nedlands, Western Australia  
6009 Australia

Prof. Alan R. Kemp  
Dept. of Civil Engineering  
University of Witwatersrand  
P.O. WITS, 2050  
Johannesburg, South Africa

Prof. D. J. Laurie Kennedy  
Dept. of Civil Engineering  
University of Alberta  
Edmonton, Alberta  
Canada T6G 2G7

Prof. Toshiyuki Kitada  
Department of Civil Engineering  
Faculty of Engineering  
Osaka City University  
3-3-138, Sugimoto, Sumiyoshi-ku  
Osaka, 558 Japan

Prof. Sritiwat Kitipornchai  
The University of Queensland  
Dept. of Civil Engineering  
St. Lucia, Qld.  
Australia 4072

Dr. Laszlo Kollar  
Technical University of Budapest  
Dept. of Steel Structures  
Buegyetem rkp 3-9  
Budapest H-1521, Hungary

Mr. Kurt K. Konkol  
EXCELL Engineering, Inc.  
460 Cambellsport Drive  
Cambellsport, WI 53010

Ms. S. A. Korvink  
Rand Afrikaans University  
Laboratory of Materials  
P. O. Box 524  
Aucklandpark  
2006, South Africa

Mr. Ray Kowalik  
Burns & McDonnell Engineering Co.  
4800 E. 63rd Street  
Kansas City, MO 64130

Mr. Peter R. Krallitsch  
Peter R. Krallitsch & Assoc., Ltd.  
28 E. Jacoson Blvd., Suite 1707  
Chicago, IL 60604

Mr. James E. Kreis  
Red Mountain Engineers, Inc.  
P. O. Box 16115  
Santa Fe, NM 87506-6115

Mr. Ronald J. Kroon  
Martin Marietta Energy Systems  
P. O. Box 2003, Bldg. K1550-C  
Oak Ridge, TN 37831-7231

Prof. Shigeru Kuranishi  
Dept. of Civil Engineering  
Tohoku University  
Aoba, Sendai 980  
Japan

Dr. James C. LaBelle  
Computerized Structural Design, Inc.  
8989 N. Port Washington Road  
Milwaukee, WI 53217

Mr. Roger A. LaBoube  
University of Missouri-Rolla  
Associate Director, CCFSS  
209 Civil Engineering  
Rolla, MO 65401-0249

Dr. Samaan G. Ladkany  
University of Nevada, Las Vegas  
Dept. of Civil Engineering  
4505 Maryland Parkway  
Las Vegas, NV 89154

Mr. Stewart Lee  
Lane Bishop York Delahay, Inc.  
716 South 30th Street  
Birmingham, AL 35233

Mr. Stephen E. Long  
AVCA Corporation  
Consulting Engineers  
5855 Monroe Street  
Sylvania, OH 43560



Ms. Nadine Love-Filer  
 C. R. Meyer & Sons Company  
 P. O. Box 2157  
 895 W. 20th Avenue  
 Oshkosh, WI 54903

Dr. LeRoy A. Lutz  
 Computerized Structural Design, Inc.  
 8989 N. Port Washington Rd.  
 Milwaukee, WI 53217

Prof. Murty K.S. Madugula  
 Department of Civil & Env. Engrg.  
 University of Windsor  
 Windsor, Ontario  
 Canada N9B 3P4.

Mr. Michael P. Marinaro  
 American Consulting Engineers  
 4165 Millersville Road  
 Indianapolis, IN 46205

Mr. Peter Marshall  
 Shell Oil Company  
 P. O. Box 576  
 Houston, TX 77001

Mr. Michael D. Martello  
 Bergmann Associates  
 1 S. Washington Street  
 Rochester, NY 14614

Prof. Sheng-Taur Mau  
 Dept. of Civil & Env. Engrg.  
 University of Houston  
 Houston, TX 77204-4791

Prof. Federico M. Mazzolani  
 Facolta D'Ingegneria  
 Istituto di Tecnica delle Costruzioni  
 Universita di Napoli  
 P.Le Tecchio  
 80125 Naples, Italy

Mr. David McCloskey  
 McCloskey-Acevedo  
 P. O. Box 195361  
 Hato Rey, PR 00919-5361

Mr. Pat McCormick  
 Brander Construction Technology  
 2357 W. Mason Street  
 Green Bay, WI 54303

Mr. Clarence D. Miller  
 Chicago Bridge & Iron Technical  
 Services, Inc.  
 1501 N. Division Street  
 Plainfield, IL 60544

Mr. Majid Mobasser  
 Clark Dietz, Inc.  
 1817 S. Neil Street  
 Champaign, IL 61820

Mr. Thomas E. Montag  
 Segal, Inc.  
 P. O. Box 23158  
 Overland Park, KS 66223

Prof. Nicholas F. Morris  
 Manhattan College  
 Civil Engineering Department  
 Riverdale, NY 10471

---

(\*) Student

Mr. John William Norton  
American Buildings Co.  
P. O. Box 800  
Eufaula, AL 36072-0800

Mr. W. Allan Olson  
Arnold & O'Sheridan, Inc.  
4129 N. 124th Street  
Brookfield, WI 53005

Prof. Tetsuro Ono  
Department of Architecture  
Nagoya Institute of Technology  
Gokiso-Cho, Showa-ku, Nagoya  
466, Japan

Mr. John D. Papenfus  
Graef Anhalt Schloemer  
& Associates, Inc.  
345 N. 95th Street  
Milwaukee, WI 53226

Mr. Arvind M. Patel  
Eichleay Engineers  
8240 Gross Point Road  
Morton Grove, IL 60053

Mr. Pravin H. Patel  
246 Washington Street  
Tom's River, NJ 08753

Dr. Dahyabhai R. Patel  
Wright-Patterson Air Force Base  
39 E. Dixon Avenue  
Dayton, OH 45419

Mr. Conrad Paulson  
Wiss, Janney, Elstner Associates, Inc.  
29 North Wacker Drive, Suite 555  
Chicago, IL 60606

Dr. Paul Penserini  
Electricite de France  
Research and Development Division  
1 avenue du general de Gaulle  
92141 Clamart, Cedex, France

Mr. Kent D. Pierce  
Consulting Structural Engineer  
49 Timber Lane  
Brownsburg, IN 46112

Prof. Raymond H. Plaut  
Virginia Tech  
Civil Engineering  
Blacksburg, VA 24061-0105

Mr. Todd Poehlman  
CPR Associates, Inc.  
P. O. Box 3429  
De Pere, WI 54115

Prof. Dimos Polyzois  
Department of Civil Engineering  
University of Manitoba  
Winnipeg, Manitoba  
Canada R3T 2N2

Mr. Albert P. Popoli  
Popoli Engineering, Inc.  
920 Cross Lane  
Blue Bell, PA 19422

Mr. Alan T. Power  
 Alan T. Power Structural Engineer  
 220 S. Rock Blvd. #11  
 Reno, NV 89502

Mr. R. S. Prabhu  
 American Buildings Company  
 #1 State Docks Road  
 Eufaula, AL 36027

Mr. Thomas Price  
 NUCOR Corporation  
 P. O. Box 70  
 Waterloo, IN 46703

Prof. Helmut Prion  
 The University of British Columbia  
 Department of Civil Engineering  
 2324 Main Mall, Room 2010  
 Vancouver, BC  
 Canada V6T 1Z4

Mr. Jeffrey Steven Rabinovitch  
 University of Alberta, Edmonton  
 Department of Civil Engineering  
 220 Civil/Electrical Engrg. Bldg.  
 Edmonton, Alberta  
 Canada T6G 2G7

Mr. Rajkumar Rajagopalan  
 University of Nevada, Las Vegas  
 Civil & Environmental Engineering  
 Howard R. Hughes College  
 of Engineering  
 4505 Maryland Parkway  
 Las Vegas, NV 89154-4015

Mr. Richard Redwood  
 McGill University  
 817 Sherbrooke St., West  
 Montreal, Quebec  
 Canada H3A 2K6

Mr. Jeffrey Reep  
 Somerville Associates, Inc.  
 2100 Riverside Drive  
 Green Bay, Wisconsin 54301

Prof. James M. Ricles  
 Lehigh University  
 Structural Stability Research Council  
 13 E. Packer Avenue  
 Bethlehem, PA 18015

Mr. James E. Rinala  
 Marathon  
*Engineers/Architects/Planners*  
 2323 East Capitol Drive  
 P.O. Box 8028  
 Appleton, WI 54913-8028

Mr. Robert J. Riopelle  
 Riopelle Engineering Sales, Inc.  
 9406 N. 107th Street  
 Milwaukee, WI 53224

Mr. Richard B. Roe  
 Three I Engineering, Inc.  
 Consulting Engineers/Architects  
 P.O. Box 6562  
 2425 W. Indiana St  
 Evansville, IN 47719

Mr. Steven J. Roloff  
Arnold & O'Sheridan, Inc.  
2125 N. 124th Street  
Brookfield, WI 53005

Mr. Michael Schmidt  
Arnold & O'Sheridan, Inc.  
815 Forward Drive  
Madison, WI 53711

Mr. Anibal Salgado  
McCloskey-Acevedo  
P. O. Box 195361  
Hato Rey, Puerto Rico 00919-5361

Mr. Walter E. Schultz  
NUCOR Research & Development  
1601 West Omaha, Box 867  
Norfolk, NB 68702-0867

Mr. Walid Salman (\*)  
Civil Engineering Department  
Galbraith Building  
University of Toronto  
Toronto, Ontario  
Canada M5S 1A4

Mr. Mark Seng  
Hodge Design Associates  
329 Main Street, Suite 614  
Evansville, IN 47708

Dr. Charles G. Salmon  
University of Wisconsin-Madison  
614 South Segoe Road  
Madison, WI 53711

Mr. Maurice L. Sharp  
R. 1, Box 171AA  
Avonmore, PA 15618

Prof. Istvan Satjos  
Vorosvari u.27/X/29  
Budapest H-1035, Hungary

Mr. Donald R. Sherman  
Dept. of Civil Engineering  
University of Wisconsin-Milwaukee  
P. O. Box 784  
Milwaukee, WI 53201

Mr. Suresh C. Satsangi  
Butler Manufacturing Co.  
13500 Botts Road  
Grandview, MO 64030-2897

Mr. G. M. Singhvi  
Smith, Hinchman & Grylls  
Associates, Inc.  
150 W. Jefferson, Suite 100  
Detroit, MI 48226

Mr. Rolando Saylo  
Burns and Roe Industrial  
Services Co.  
700 Kinderkamack Road  
Oradell, NJ 07649

Mr. Robert Sinn  
Skidmore, Owings & Merrill  
224 S. Michigan Avenue, Suite 1000  
Chicago, IL 60604

---

(\*) Student

Mr. Paul D. Smith  
Gannett Fleming, Inc.  
150 Wood Road  
Braintree, MA 02184

Mr. Kamlesh N. Soni  
Peter Albrecht Corp.  
6250 Industrial Court  
Greendale, WI 53129-2432

Mr. Joseph P. Steigerwald  
Steigerwald Construction, Inc.  
5310 W. State Street  
Milwaukee, WI 53208

Dr. Lambert Tall  
Florida International University  
School of Engineering  
Miami, FL 33199

Mr. Katsuhiro Tanaka  
Japan Information Processing Service  
Company, Ltd.  
1-9-1 Edobori, Nishi-ku  
Osaka 550, Japan

Mr. J. Colin Taylor  
The Steel Construction Institute  
Silwood Park, Buckhurst Road  
Ascot, Berks SL5 7QN  
United Kingdom

Dr. Murray C. Temple  
University of Windsor  
Faculty of Engineering  
Windsor, Ontario  
Canada N9B 3P4

Mr. Mathew Tharaniyil (\*)  
Dept. of Civil Engineering  
University of Wisconsin-Milwaukee  
P. O. Box 784  
Milwaukee, WI 53201

Prof. Robert Tremblay  
The University of British Columbia  
2324 Main Mall  
Vancouver, B.C.  
Canada V6T 1Z4

Dr. Tony Tschanz  
Skiing Ward Magnusson  
Barkshire, Inc.  
1301 Fifth Avenue, Suite 3200  
Seattle, WA 98101-2699

Dr. G. J. van den Berg  
Rand Afrikaans University  
Laboratory of Materials  
P. O. Box 524  
Aucklandpark  
2006, South Africa

Mr. Todd L. Vinje  
Continental Bridge  
8301 State Highway 29N  
Alexandria, MN 56308

Prof. S. Vinnakota  
Marquette University  
1515 W. Wisconsin Avenue  
Milwaukee, WI 53233

(\*) Student



Prof. Andreas S. Vlahinos  
Department of Civil Engineering  
University of Colorado at Denver  
1200 Larimer Street, NC 3027  
Denver, CO 80204

Mr. Jeffery S. Volz  
C.T.L.  
5420 Old Orchard Road  
Skokie, IL 60077-1030

Mr. Marc Voss (\*)  
Marquette University  
1515 W. Wisconsin Avenue  
Milwaukee, WI 53233

Mr. Yang Wang (\*)  
Department of Civil Engineering  
University of Colorado at Denver  
1200 Larimer Street, NC 3027  
Denver, CO 80204

Mr. Dennis Waugh  
IIW Engineers & Surveyors  
4155 Pennsylvania Ave.  
Dubuque, IA 52002

Mr. Stephen M. Way  
Bergman Associates  
1 S. Washington Street  
Rochester, NY 14614

Mr. George Weatherford  
Central Soya Co., Inc.  
P. O. Box 2507  
Fort Wayne, IN 46801-2507

Michael A. West  
Computerized Structural Design, Inc.  
8989 N. Port Washington Road  
Milwaukee, WI 53217

Prof. Donald W. White  
School of Civil Engineering  
Purdue University  
1284 Civil Engineering Building  
W. Lafayette, IN 47907

Mr. P. Craig Williams  
The Haskell Company  
111 Riverside Avenue  
Jacksonville, FL 32202-4950

Mr. John M. Yadlosky  
HDR Engineering, Inc.  
3 Gateway Center  
Pittsburgh, PA 15222

Prof. Toshitaka Yamao  
Civil & Environmental Engineering  
Kumamoto University  
Kurokami 2-39-1  
Kumamoto 860, Japan

Dr. Chai H. Yoo  
Civil Engineering  
238 Harbert Engineering Center  
Auburn University, AL 36849

Prof. Wei-Wen Yu Yu  
University of Missouri-Rolla  
Dept. of Civil Engineering  
Rolla, MO 65401

---

(\*) Student

Dr. Joseph A. Yura  
University of Texas  
Dept. of Civil Engineering  
Austin, TX 78712

Dr. Ronald D. Ziemian  
Dept. of Civil Engineering  
Bucknell University  
221 Dana Engineering Building  
Lewisburg, PA 17837

---

(\*) Student

## NAME INDEX

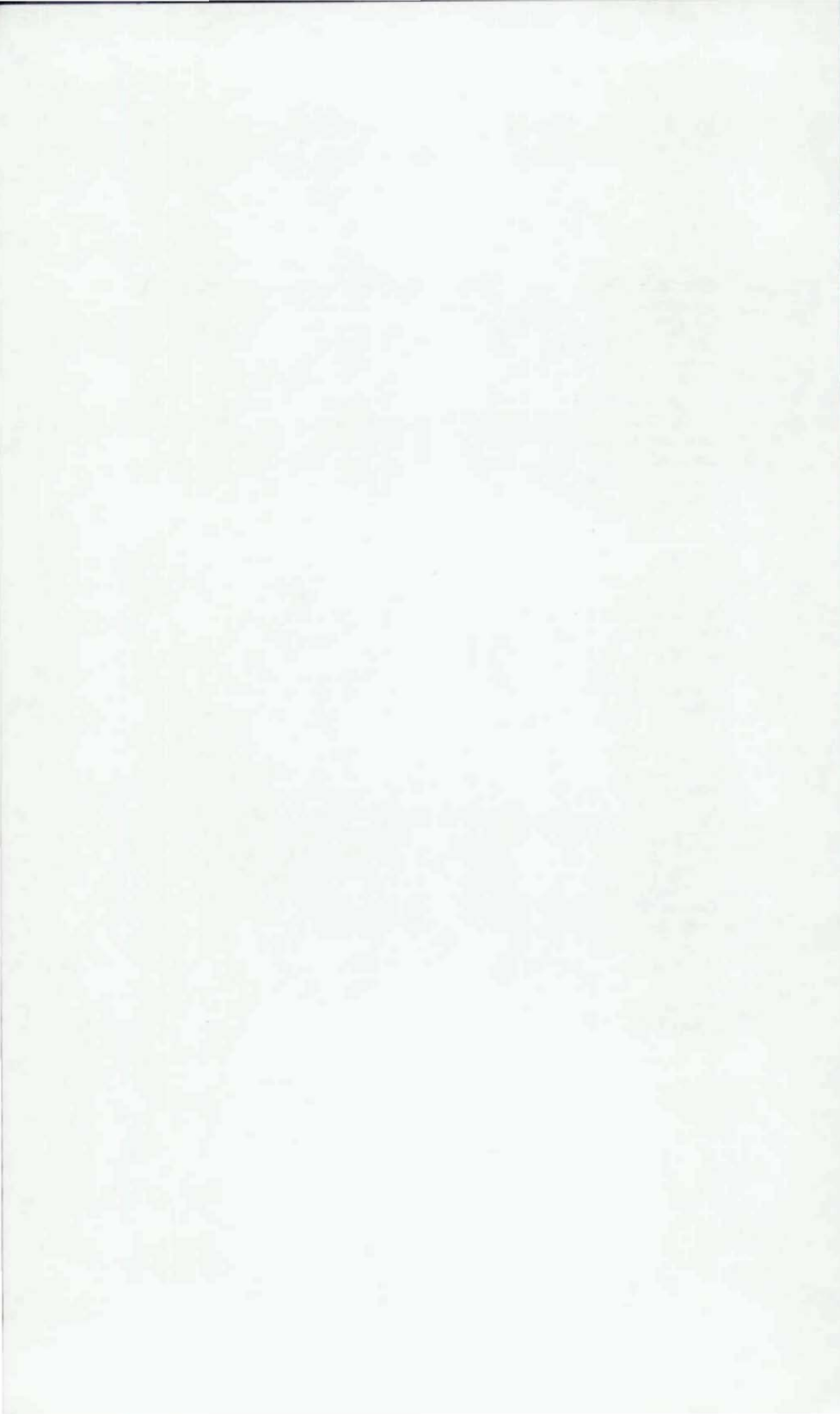
- Abdel-Ghaffar, M.; 321, 326  
 Abel, J.F.; 307  
 Adams; 201  
 Adams, A.M.; 195, 201, 202  
 Adluri, S.M.R.; 309, 310, 313, 315, 318  
 Akay, H.U.; 183  
 Al Sulaimami, G.; ; 282  
 Al-Bermami, F.G.A.; 307  
 Alameddine, F.; 260, 270  
 Alves, R.V.; 211, 221  
 Ang, A.H.S.; 282  
 Antonini, R.C.; 221  
 Antoniou, A.C.; 124  
 Aoki, T.; 59, 67  
 Aoshima, Y.; 307  
 Astaneh-Asl, A.; 52  
 Atsuta, T.; 307
- Baksai, R.; 170  
 Ballou, L.B.; 240  
 Basu, P.K.; 30, 44  
 Bathe, K.J.; 307  
 Batista, R.C.; 211, 221  
 Batoz, J.L.; 307  
 Beach, J.E.; 115, 124  
 Beaulieu, D.; 294  
 Bellini, P.X.; 342, 367  
 Berg, G.V.; 281  
 Bergan, P.G.; 308, 343, 367  
 Bernal, D.; 278, 282  
 Bernuzzi, C.; 26  
 Bertero, V.; 282  
 Birkemoe, P.C.; 240, 247  
 Birnstiel, C.; 307  
 Biswas, M.; 30, 44  
 Bjorhovde, R.; 27, 45, 326  
 Bleich, F.; 316, 318, 234  
 Bleich, H.H.; 318  
 Boehme, J.; 260, 270  
 Bolourchi, S.; 307  
 Bong, H.S.; 124  
 Braga, F.; 281  
 Bredenkamp, P.J.; 193  
 Briquet, Ch.; 369
- Brockenbrough, R.L.; 234  
 Brzoska, Z.; 234
- Cai, L.; 321, 327  
 Carlsen, C.A.; 124  
 Cescotto, S.; 343, 367  
 Chai, Y.H.; 270  
 Chan, S.C.; 221  
 Chan, S.L.; 295, 307, 308  
 Chen, W.F.; 27, 307, 326, 327  
 Cheng, J.J.R.; 45  
 Cherry, S.; 259  
 Christiano, P.; 221  
 Chulya, A.; 342, 367  
 Climenhaga, J.J.; 170  
 Colcea, E.; 77  
 Colson, A.; 283, 284, 294  
 Connor, J.J.; 221  
 Cosenza, E.; 27, 276, 282  
 Crisfield, M.A.; 308, 342, 367  
 Croll, J.G.A.; 221  
 Cujko, J.; 124
- D'Amore, E.; 345  
 Davids, A.J.; 67  
 De Luca, A.; 27, 281, 282, 345  
 De Stefano, M.; 345  
 deGoyet, V.; 343, 367  
 Dewolf, J.T.; 90  
 Dhatt, G.; 307  
 Driscoll, G.C.; 26  
 Drucker, D.C.; 161, 170, 171  
 Dubina, D.; 69, 77
- Ehsani, M.R.; ; 260, 270  
 El-Zanaty, M.H.; 321, 325, 326  
 Ellifritt, D.; 1  
 Epstein, H.I.; 221
- Faella, C.; 27, 281, 282  
 Faulkner; 117, 118, 119, 120, 123, 124  
 Frankland, J.M.; 118, 119, 120, 123, 124  
 Fraternali, F.; 276, 282  
 Frye, M. J.; 27  
 Fujieda, Y.; 152  
 Fujii, K.; 151, 152,

- Fukumoto, Y.; 67, 120,  
 124, 150  
 Furunishi, K.; 150  
 Furuta, T.; 381, 392  
 Galambos, T.V.; 44, 120, 124,  
 201, 202, 234, 306, 326  
 Galea, Y.; 294  
 Gaylord, C.H.; 45  
 Gaylord, E.H.; 45  
 Gere, J.M.; 240, 318  
 Gillum, T.; 254  
 Gladding, C.J.; 90  
 Glowinski, R.; 343  
 Goel, S.C.; 52  
 Goto, S.; 367  
 Green, P.S.; 115  
 Gregg, D.W.; 240  
 Gribbs, H.P.; 221  
 Grigoliuk, E.J.; 234  
 Gross, J.L.; 45  
 Guerra, C.A.; 278, 282  
  
 Haaijer, G.; 170  
 Haisler, W.E.; 343  
 Halasz, O.; 154, 160, 167, 170  
 Han, S.K.; 124  
 Hancock, G.J.; 67  
 Hanson, R.D.; 45, 281  
 Hardash, S.G.; 45  
 Harstead, G.A.; 307  
 Hartmann, A.J.; 181, 183  
 Hayashi, M.; 342, 367, 392  
 Hetrakul, N.; 90  
 Hirashima, M.; 151  
 Hiwatashi, S.; 150  
 Hoff, N.J.; 170  
 Hoffschild, T.E.; 259  
 Hoit, M.; 1  
 Holand, I.; 343, 367  
 Hori, T.; 124  
 Horne, M.R.; 164, 165,  
 159, 170  
 Hottigmoe, G.; 308  
 Hu, S.Z.; 45  
 Huber, M.T.; 234  
 Husid, R.; 281  
  
 Imai, F.; 151  
 Ivanyi, M.; 151, 153, 154,  
 155, 156, 159, 166, 167,  
 170, 171  
  
 Jagannathan, D.S.; 221  
 Jardine, L.J.; 240  
 Jaspert, J.P.; 369  
 Jetteur, P.; 343, 367  
 Johnson, B.G.; 234  
 Johnson, C.P.; 183  
 Johnson, P.; 170  
 Johnston, B.G.; 27  
  
 Kabanov, V.V.; 234  
 Kaliszky, S.; 162, 171  
 Kallo, M.; 167, 171  
 Kamei, M.; 343  
 Kanchanalai, T.; 326  
 Kano, M.; 333  
 Kashami, M.; 221  
 Kato, B.; 155, 170  
 Kawai, T.; 151  
 Kazinczy, G.; 153, 155,  
 160, 171  
 Ketter, R.L.; 179, 183  
 Kim, D.H.; 124  
 Kim, M.S.; 124  
 King, W.S.; 326  
 Kitada, T.; 141, 151, 152,  
 333, 342, 343, 367, 381,  
 392  
 Kitipornchai, S.; 296,  
 306, 307  
 Kniss, B.R.; 239, 240  
 Komatsu, S.; 342, 367,  
 392, 400  
 Korvink, S.A.; 79, 90  
 Kounadis, A.N.; 30,  
 Krakeland, B.; 308  
 Krawinkler, H.; 282  
 Kuranishi, S.; 150, 393, 400  
 Kurutz, M.; 162, 171

- LaBoube, R.A.; 103  
Ladkany, S.G.; 235, 239, 240  
Lampert, W.; 254  
Landolfo, R.; 282  
Lashkari, M.; 240  
Lay, M.G.; 171, 201, 202  
Lee, G.C.; 179, 181, 183  
Lee, H.W.; 296, 306, 307  
Lee, J.; 240  
Lee, S.Y.; 30  
LeMessurier, W.J.; 326  
Leon, R.T.; 260, 270  
Leu, K.C.; 307  
Liew, J.Y.R.; 326  
Logcher, R.D.; 221  
Lu, L.W.; 115, 119, 124  
Lui, E.M.; 326  
Lurkey, A.F.; 195, 201, 202
- MacDougall, H.R.; 343  
MacIntyre, J.; 252, 254  
Madugula, M.K.S.; 309, 310,  
313, 315, 318  
Maeda, Y.; 342, 367  
Maegawa, K.; 150  
Mahin, S.; 282  
Maier, G.; 161, 171  
Majid, K.; 171  
Makino, M.; 282  
Maquoi, R.; 369  
Maxwell, G.; 201, 202  
Mazzarella, O.; 282  
Mazzolani, F.M.; 27, 271,  
278, 282  
McGuire, W.; 307  
Medland, J.C.; 165, 170  
Meek, J.L.; 307  
Melchers, R.E.; 284, 294  
Mender, Z.K.; 223, 234,  
Merchant, W.; 170  
Mikami, I.; 150  
Mitani, I.; 282  
Miwa, S.; 124  
Monforton; 310, 313, 318  
Morrell, M.L.; 179, 181, 183  
Morris, G.A.; 27  
Morris, L.J.; 164, 170  
Morris, N.F.; 221  
Murayama, Y.; 141, 152
- Murray, D.W.; 326  
Murzewski, J.; 234  
Nakai, H.; 141, 150, 151,  
152, 343, 381  
Nakaoka, T.; 152  
Narayanan, R.; 27  
Nethercot, D.A.; 27, 181, 183  
Nibu, M.; 142, 333, 342  
O'Neal, W.C.; 240;  
Obaia, K.H.; 240  
Ohminami, R.; 150, 151,  
152, 342  
Ohmura, H.; 151  
Ohta, T.; 151  
Okamoto, T.; 122, 124  
Okiyama, H.; 282  
Omote, T.; 151  
Orbison, J.G.; 307  
Osgood, W.R.; 194, 202  
Oshio, M.; 343
- Packer, J.A.; 83, 90  
Pacoste, C.; 77  
Paik, J.K.; 124  
Palazzo, B.; 276, 282  
Pang, A.K.; 115, 119, 124  
Papp, F.; 170  
Parducci, A.; 281  
Park, Y.J.; 260, 282  
Parks, M.B.; 90, 202  
Penserini, P.; 283, 284, 294  
Pernetti, M.; 282  
Picard, A.; 294  
Piluso, V.; 271, 278, 281, 282  
Pilvin, P.; 294  
Poggi, C.; 27
- Polyzois, D.; 179  
Popov, E.P.; 195, 202  
Powell, G.H.; 282, 308  
Priestly, M.J.N.; 260, 270  
Prion, H.G.L.; 259, 260  
Przemieniecki, J.S.; 44
- Qing, L.; 179
- Rabinovitch, J.S.; 45  
Rajagopalan, R.; 235  
Ramberg, W.; 194, 202



- Ramm, E.; 308  
 Rashed, S.M.H.; 124  
 Ricles, J.M.; 115, 247, 254  
 Rijs, E.; 308  
 Rizzano, G.; 282  
 Rodin, E.Y.; 343  
 Roesset, J.M.; 282  
 Roller, B.; 161, 162, 163, 171  
  
 Sakimoto, T.; 59, 67,  
     342, 367, 400  
 Salman, W.A.; 247  
 Sankisa, K.K.; 309  
 Santaputra, C.; 82, 88, 89, 90  
 Schulz, G.; 367  
 Seible, F.; 270  
 Setti, P.; 27  
 Shan, M.Y.; 103  
 Simitzes, G.J.; 44  
 Simmons, J.; 308  
 Sivakumaran, K.S.; 90  
 Smith, C.V.; 44  
 Sohal, I.S.; 321, 326, 327  
 Soreide, T.H.; 308, 343, 367  
 Stallmeyer, J.E.; 45  
 Stebbins, F.J.; 343  
 Stricklin, J.A.; 343  
 Suetake, Y.; 151  
 Sun, C.K.; 281  
 Sun, Z.L.; 270  
 Suzuki, H.; 392  
 Szabo, J.; 161, 163, 171  
  
 Taido, Y.; 392  
 Tajima, T.; 151  
 Tanaka, K.; 151, 152, 333, 342  
 Tateishi, M.; 124  
 Thornton, W.A.; 45  
 Thurlimann, B.; 160, 171  
 Tiberi, T.; 115  
 Timoshenko, S.P.; 240, 318  
 Tin-Loi, F.; 343  
 Toma, S.; 327  
 Tomka, P.; 167, 171  
 Trahair, N.S.; 181, 183  
 Tuboura, N.; 67  
  
 Ueda, T.; 307  
 Usami, T.; 120, 124  
 Ushio, M.; 367  
  
 van den Berg, G.J.; 79, 193  
 van der Merwe, P.; 79, 193,  
     194, 202  
 Vinnakota, S.; 307  
 Vlahinos, A.S.; 29, 44  
 Von Mises; 395  
  
 Wakabayashi, Y.; 343  
 Wang, Y.C.; 29  
 Wastlund, G.; 400  
 White, D.W.; 326  
 Whitmore, R.E.; 45  
 Wight, J.K.; 260, 270  
 Will, K.M.; 183  
 Williams, G.C.; 45  
 Wing, B.A.; 90  
 Wong, M.B.; 343  
 Wood, R.H.; 27  
 Wu, C.L.; 240  
 Wu, D.L.; 240  
  
 Yabuki, T.; 400  
 Yam, M.C.H.; 45  
 Yamao, T.; 59, 67  
 Yao, T.; 307  
 Yasui, T.; 152  
 Yoda, T.; 151  
 Yokota, T.; 152  
 Yonezawa, H.; 150  
 Yoo, C.H.; 150  
 Yoshida, H.; 150  
 Yu, W.W.; 90, 103  
 Yura, J. A.; 27  
  
 Zandonini, R.; 26, 27  
 Zienkiewicz, O.C.; 240,  
     307, 343  
 Zohrei, M.; ; 282



## SUBJECT INDEX

- accelerogram; 279  
 analysis; 115, 119, 120, 122, 123, 247, 251, 252, 253  
   asymptotic (modal); 211, 212, 215, 216, 217, 221  
   advanced inelastic; 345  
   design; 13  
   eigenvalue; 212, 216, 217, 219, 220, 221  
   elastic stability; 29, 44  
   elasto-plastic; 238, 239, 333  
   finite displacement; 148, 358, 333  
   inelastic; 321  
 angle; 295, 296, 297, 305, 309, 310, 312, 313, 314, 315, 316, 317, 318, 319, 320  
 arc-length method; 334, 361  
 axial load; 247, 249, 250, 251, 252  
  
 beam category; 201, 204  
 beam-column; 322, 369, 370, 371, 372, 373, 377, 378, 379, 380  
 beam-column element; 299  
 beam-to-column joints; 271  
 bearing; 82  
 behavior mechanisms; 288  
 bending; 369, 370, 371, 372, 373, 374, 376, 377, 378, 379, 380  
 biaxial in-plane forces; 381  
 bifurcation; 211, 212, 213, 215, 216, 217, 219, 220, 221  
 bottom chord; 69, 70, 75  
 brace; 247, 248  
 braced frames; 29, 34, 44  
 bracing; 2, 3, 103, 104, 105  
 bridge:  
   box girder; 142  
   Japanese; 148  
   Nielsen system; 364  
   plate girder; 142  
   River Kizu; 148  
 buckling; 80, 103, 104, 105, 106, 107, 108, 109, 110, 213, 216, 220, 221, 236, 237, 238, 239, 292, 309, 310, 312, 313, 314, 315, 316, 317, 318,  
   curves; 226, 227, 228, 229, 230  
   flexural; 80  
   global; 59  
   interactive; 57  
   local; 59, 115, 118, 120, 122, 123, 314, 215  
   strength; 145, 391  
   sway; 29, 30, 34  
   tests; 309, 311  
   torsional; 30, 45  
 buildings; 1, 2  
  
 cable members; 358  
 canister; 235, 236, 237, 238, 239  
 central connector; 69  
 channel; 79  
 cold-formed; 79  
    $60\Delta$  angle; 309, 310, 312, 313, 314, 315, 316, 317, 318  
 collapse; 271  
 collapse mode; 371, 372, 373  
 column; 295, 303  
   approach; 387  
   imperfection; 345  
   slenderness; 348  
   -base connections; 283  
 combined stresses; 223, 225, 232  
 compression; 310, 369, 370, 371, 373, 378, 380  
 compression plate; 381  
 compressive strength; 103, 104, 106, 108  
 computation model; 75  
 computer program; 357  
 concentric and eccentric load; 60  
 concrete-filled tubes; 272  
 confinement; 272  
 crippling; 79  
 current stiffness parameter; 335  
 cyclic loading; 103, 105, 108, 110, 274  
 cyclic tests; 288  
  
 dent damage; 247, 248, 249, 253, 254

- design:  
 code; 313  
 curve; 295  
 method; 145  
 strength; 312, 313, 318
- diagonal; 75
- DIN; 369, 373, 374, 378, 379, 380
- doors; 2, 4
- double hull; 115, 116, 120, 122
- double-layer grid; 69, 70
- ductility; 106, 272, 273
- dynamic; 275
- EC3; 369, 373, 375, 378, 380
- ECCS; 369, 373, 374, 378, 379, 380
- effective length coefficient; 293
- effective slenderness; 13
- elastic critical load; 13
- end-one-flange; 81
- end-restraint capacity; 283
- equivalent frame imperfection; 355
- experiment; 143, 295
- experimental; 115, 116, 119, 120, 122, 247, 248, 252, 253, 254, 271  
 results; 324, 325  
 study; 60, 390
- external pressure; 231
- failure load; 313, 314
- finite element; 115, 119, 120, 121, 122, 123, 212, 236, 238, 239, 247, 248, 249, 250, 251, 252, 253, 254, 298, 333, 357
- flat width; 311, 314
- flexural; 80
- form factor method; 59  
 frame; 3, 4, 103, 104, 105, 278  
 imperfection; 345  
 instability; 24  
 slenderness; 348
- frames; 3, 4, 59, 103, 104, 105, 278  
 braced; 29, 34, 44  
 equivalent imperfection; 355  
 inelastic buckling; 352  
 semi-rigid sway; 13  
 slender and stocky; 354  
 space; 211, 213, 214, 215, 216, 217, 221
- square unit; 69
- three dimensional (3-D); 1, 3, 29, 30, 32, 33, 44, 359
- unbraced; 29, 34
- geometric imperfections; 60, 211, 212, 216, 220, 221, 295, 304
- geometrical nonlinearity; 296
- gradual yielding; 194
- grout; 247, 248, 249, 251, 253, 254
- gussett plates; 103, 104, 105, 106, 107, 108, 109, 110
- hangar; 2, 5
- hemispherical dome; 217, 218, 219
- high-strength low-alloy steel; 115, 116
- hollow structural steel sections; 271
- horizontally curved bridge; 141
- hot-rolled stainless steel section; 193
- hysteresis curves; 276
- impact; 235, 236, 237, 238
- imperfection pattern; 346
- imperfection sensitivity; 211, 212, 213, 217
- inelastic:  
 analysis; 321  
 buckling load; 347  
 column buckling; 15
- initial deflection; 384
- initial modulus; 194
- instability; 115, 116, 122, 211, 212, 216, 217, 220, 221, 247, 248, 251, 369, 371, 373, 378, 379, 380
- interaction formula; 224, 225, 228, 232, 369, 371, 373, 378, 379
- intermediate plastic hinge; 321
- isoparametric; 236
- joint nonlinearity; 14
- Lagrangian:  
 formulation; 296, 299  
 updated description method; 336, 359
- lattice dome; 211, 217, 220, 221

- limit curves; 228
- limit surface; 233
- load; 80
- load carrying capacity; 333
- loading condition; 14
- local buckling; 115, 118, 120, 121, 122, 123, 314, 325
- longitudinal compression; 231
- LRFD; 369, 373, 375, 378, 380
  
- material nonlinearity; 295, 298
- MDOF; 278
- mechanism; 69, 75
- member imperfection; 14
- member yielding; 16
- modeling; 288
- moment-rotation; 200
- monotonic tests; 288
  
- nonlinearity:
  - geometrical; 296
  - joint; 14
  - material; 295, 298
- non-linear; 211, 212, 213, 216, 218, 219, 220, 221, 235, 236, 238, 239
- normal force-moment interaction; 283
- nuclear waste; 235
- number of bays; 354
- number of stories; 351
- numerical simulation; 369, 370, 373, 377, 379
  
- out-of-flatness; 117, 118, 119
- offshore platforms; 247, 248
- orientation; 307
  
- P- $\Delta$  effect; 271
- perturbation method; 212
- plastic moment resistance; 195, 198, 199, 200
- plastic zone method; 324
- plate; 115, 118, 119, 120, 121, 122, 123
- post-bifurcation; 212, 216, 217, 219
  
- post-buckling; 117
- post-critical; 211, 212, 217, 220, 221
- practical design method; 386
- pre-critical; 211, 212, 217
- pre-processing analysis; 339
- prestressed high tensile bolt; 69
- prestressing load; 333
- proportional limit; 194
- pyramidal unit; 69, 70
  
- repair; 247, 248, 249, 254
- residual stress; 116, 117, 119, 333, 358, 383
- resistance; 370, 371, 372, 373, 374, 378, 379
- retrofit; 271
- rigid connector; 69
- rolled thin-walled column; 59
- rotation capacity; 195
  
- schifflerized angle; 309, 310, 311, 312, 313, 314, 315, 316, 317, 318, 319, 320
- SDOF; 273
- second order analysis; 321
- seismic; 271
- semi-rigid joints; 14
- semi-rigid sway frames; 13
- sensitivity of frame inelastic buckling; 352
- shell; 234, 236, 237, 238, 239
- slender and stocky frames; 354
- slenderness ratio; 59
- slope-deflection relation; 321
- softening behavior; 323
- space frame; 211, 213, 214, 215, 216, 217, 221
- space truss; 219, 220
- spatial steel bridge structure; 333
- spectrum; 275
- square frame unit; 69
- stability; 211, 213, 216, 217, 235, 236, 237, 273
  - criteria; 223, 224, 225, 226, 227, 228, 229, 230, 231, 232, 233, 234
  - cylindrical shells; 231
  - metal plates; 223



- stainless; 79
- state-of-the-art; 141
- steel; 1, 79, 271
  - bridge; 357
  - jacket; 272
  - structures; 103, 321
- stiffened plate; 143, 381
- stiffness matrix; 321
- strength; 247, 248, 251, 252, 254
- stress; 235, 237, 238
- stress-strain curves; 205, 206
- stub-column test; 60
- sway imperfection; 14
  
- tensile strength; 108, 110
- testing model; 71
- tests; 104, 105, 106, 107, 108, 109, 110
- thin-walled box members; 358
- thin-walled box columns; 115, 122
- three dimensional (3-D); 1, 3, 29, 30, 32, 33, 44
  - framed structure; 359
- torsion; 232
- torsional-flexural buckling; 310, 311, 312, 315, 316, 317
- transverse reinforcement; 272
  
- ultimate:
  - capacity; 295, 296, 297
  - limit strength; 290
  - load; 333
  - load carrying capacity; 357
  - longitudinal strength; 386
  - strength; 59, 60, 142, 381
  - transverse length; 388
- unbraced frames; 29, 34
- under-relaxation method; 336
- unilateral contact; 294
  
- web; 79
- width-to-thickness ratio*; 59
- wind; 1, 2, 5
  
- yield; 236, 237, 239
  - condition; 226
  - moment resistance; 195, 106, 197, 198
  - strength; 194





